Lecture Note 1

35. Overview of the topics and goals. Basic equations and linearization. Regular and irregular waves. (F:3-26)

Lecturing
Main 'hint' symbols used:
Hp: → Assumptions
[..] → Hint and examples
↑ → Information on topics not treated in detail
NB → Attention please
F: → Faltinsen's "sea loads" book

Background. (F:3-11)
The marine field is characterized by a broad variety of operating scenarios involving ships and ocean structures: ships with different type, size and speeds, ranging from small fishing vessels (say 10 m long) to large container ships (say 400 m long), and speed varying greatly from very small values up to high speed vessels (say with 60 knots speed); oil and gas platforms, freely-floating with suitable mooring or dynamic positioning or alternatively tensioned or fixed to the sea floor; floating airports, with very large horizontal dimensions with respect to the vertical ones; aquaculture plants; wave energy devices; wind energy devices.



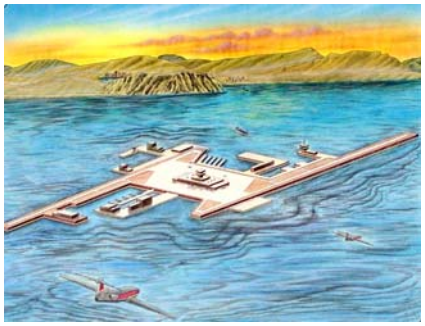

The activities involved are also various: transport, oil and gas production, infrastructures, sea food, renewable energy. The trends in terms of activities strategies are affected by many factors. Among them: the climate changes push toward greener alternative energy sources and greener transport, while the reduction in fuel availability at shallow and finite waters pushes toward deeper water exploitations (ocean space), new possible routes are opened by the planet warming involving arctic; the probability of extreme weather conditions seems to be increased.
All these factors may need upgrade of the existing marine design and operational criteria. In this framework it is crucial to characterize the behaviour of the specific marine unit in its environmental conditions to ensure that the activities can be performed successfully, which means in safety, effectively and efficiently (in terms of time/costs).

One must identify the relevant sea conditions: waves, current, wind, and investigate their induced loads and motions on the specific marine unit. This allows to establish and classify critical problems and may guide toward design or operation strategy changes.
The course will examine the sea loads with applications to displacement ships, supported by buoyancy and with Froude number $Fn=U/\sqrt{(gL)}<0.4$, and ocean platforms.
The steps will be:

1. to characterize the sea conditions (wave, current and wind),
2. to learn how to predict their induced loads and motions,
3. to learn how to identify critical problems and related criteria-response variables,
4. to learn how to minimize/control the response as required by regulations,

→ to learn how to design safe and effective operations.

Step 1: Sea conditions

Roughly speaking we will discuss the free-surface waves, i.e. perturbations propagating along the sea surface. The perturbation oscillate with certain amplitudes in time within a certain range of frequencies (periods), and in space within a certain range of wavelengths.
The currents will be characterized as steady incident water flows.
The winds will be characterized as steady plus fluctuating incident air flows.

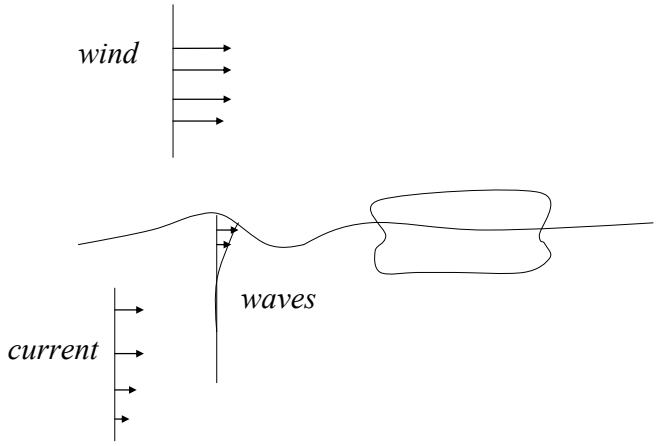

Step 2: Induced loads and motions

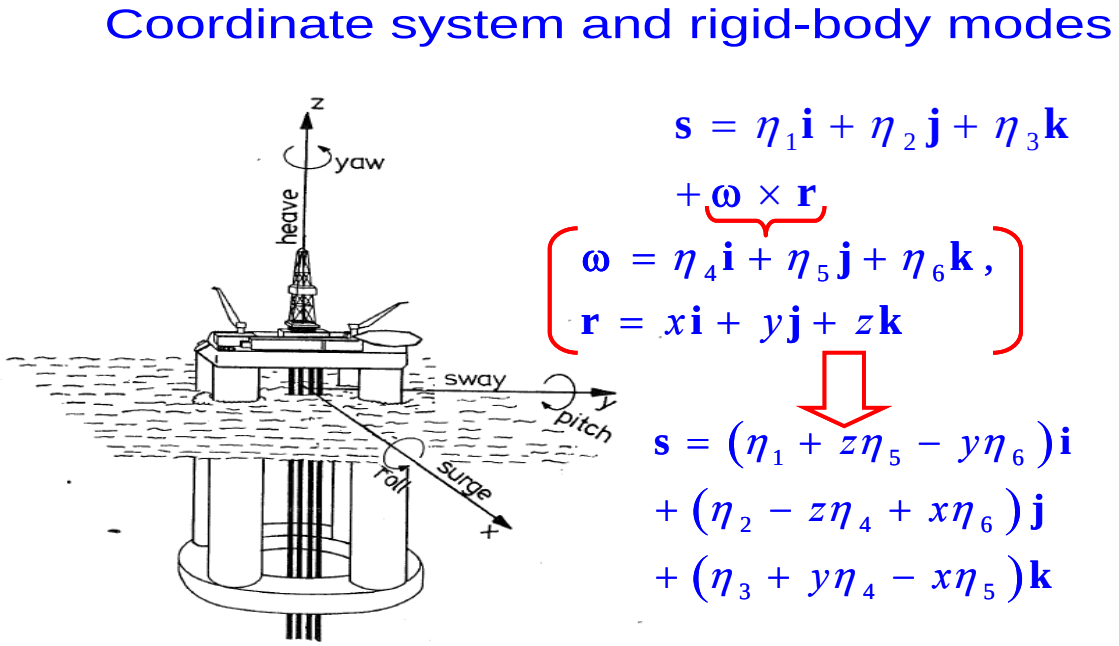

Fig. F:1.3

This requires a definition of the motions because different types of motions can be relevant for different marine units. In the seakeeping, the oscillatory translational and rotational motions are defined in the inertial reference frame Earth-fixed or translating with the vessel speed if any. They are respectively: surge, sway, heave, roll, pitch and yaw (Fig. 1.3 F). The rotational vector can also be indicated as $\boldsymbol{R}$. The i-th component of the cross vector $\boldsymbol{R}\times\boldsymbol{r}$ can be expressed as

$\left(\boldsymbol{R}\times\boldsymbol{r}\right)_i = \varepsilon_{ijk} R_j r_k$ with ε_{ijk} is the permutation tensor $\varepsilon_{ijk} =$ { 1 for 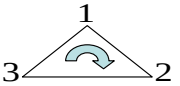 ; -1 for 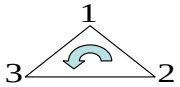 }

According to the involved fluid-vessel interactions, the relevant motion features may vary. We distinguish between:

1) wave-frequency motion,
2) high-frequency motion,
3) slow-drift motion and
4) mean drift motion.

The wave-frequency motion is mainly linearly excited in the wave-frequency range of significant wave energy in the sea spectrum. Typically we expect that the relevant incident-wave periods are much greater than 1 sec, corresponding to wavelength about 1.5 m, and much smaller than 1 min, corresponding to wavelength about 6km. The periods of interest are usually around O(10sec).
The other types of motions are caused by nonlinear effects because involve frequencies outside the excitation frequencies and non-zero mean values of the motionsor . What said for in terms of motions 1)-4) can be said for the induced loads.
We will examine greatly 1) and then discuss the causes and simplified predictions for 2)-4).

NB: Linear system=the output is proportional to the input, the output of a linear combination of inputs is a linear combination of the outputs to the single inputs→ linear superposition principle is valid. It means that: in transient conditions, small variations in the initial conditions result in small changes in the output and can not modify the qualitative behaviour of the output. In steady-state conditions, if the input oscillates with a given period, the output will oscillate with the same period.
Nonlinear system=the output depends nonlinearly on the input, so all features above are lost due to nonlinear interactions.

The relative importance of 1) to 4) types of response depends on the specific marine unit. In particular, the natural periods identify the resonance conditions in the different degrees of freedom. The marine units will have largest motion amplitude near resonance and the amplitude will depend on the damping level.
If the natural period of a certain degree of freedom (e.g. heave) is within the wave-frequency range then it can be excited, as 1), by linear wave-structure interactions and will dominate the behaviour. However, if the motions become large enough nonlinear effects may become relevant and excite high- and/or low-frequency motions, i.e. 2) and 3), and mean values of the response.
If the natural period is outside the wave-frequency range, it can only be excited by nonlinear effects. The natural periods vary greatly with the marine units type, as well as the physical mechanisms that excite them or damp out the related oscillation amplitudes. As an example Table F:1.1. examines the heave natural periods for a wide range of marine units.
We go from <1s for a high-speed vessel SES to >20s for semi-submersibles and high-speed vessel SWATH.
The value of the natural periods depends on the restoring sources.
In particular, the air-cushioning for the SES and elasticity of tethers result in small natural periods relative to relevant wave periods, the buoyancy connected with the waterplane area for the other units examined results in natural periods within the relevant wave periods ranges or greater.

The excitation mechanisms of the natural periods, i.e. resonance conditions, are linear (within the incident-wave frequency) or nonlinear (otherwise).
The amplitude of the motions at resonance depends on the damping mechanisms. The may be physical, provided by wave radiation and viscous effects, or artificial, provided by proper control systems. In general the higher the vessel speed the more control systems are require. The larger the amplitude the more important the nonlinear effects involved.

Natural heave periods

SES	TLP	Ship	Semi-sub	SWATH
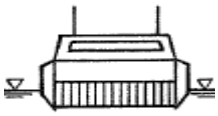	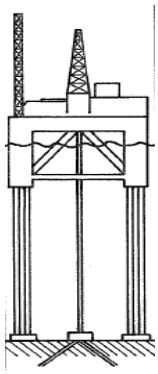	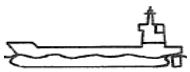	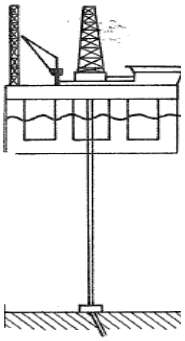	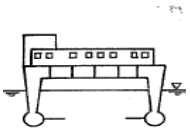
T_n<1s	T_n=2-4s	$T_n \approx \sqrt{L/1.5}$ $= 4-16s$	T_n>20s	T_n>20s

Table F:1.1

From Table F:1.1. in the vertical plane, typically the wave-frequency motions are relevant for conventional ships, i.e. $T_n = O(10\,\text{sec})$. High-frequency motions can be important for TLPs platforms: examples are the ringing and springing of TLPs due to resonance in the vertical motions. For such platforms the restoring forces are provided by the tethers and the mass forces of the platform. The natural periods for the vertical modes are 2-4 sec, i.e. smaller than relevant wave periods. It means they are excited by nonlinear effects as said.
Ringing is transient oscillations, while springing is steady-state oscillations. In terms of design, ringing is relevant for the tethers' extreme tension and springing for the tethers fatigue.
Low-frequency motions can be important for the semisubmersibles since the natural period is >20sec. Typically slow-drift and mean drift motion can be caused by nonlinear effects connected with wave, current or wind interactions with the marine unit. For mooring systems, they may more-easily occur in the horizontal plane since the restoring forces are given by the mooring lines and by masses forces of the involved platform. This leads to typical natural periods of 1-2 min.

Let us assume that we have a marine unit in a certain region of the sea, which can be characterized by waves, current, wind. The interaction with the vessel induces loads (and motions) on the body which depend on the relative dimensions and features of the factors involved. For example, focusing on ocean structures and assuming that D is the typical dimension of the structure and λ is a measure of the incoming-wave length. Fig. F:1.6 provides a qualitative hydrodynamic classification of the marine structures using a circular cylinder as representative of structural elements and examining the dominant loads.
Near the wave-breaking limit nonlinear effects become important. Above this limit waves can easily break during the interaction with the structure. Below this limit:
For $\lambda/D<\approx 5$ diffraction loads are important, i.e. those induced by the incident waves and their modification (diffraction) due to the structure.

For λ/D>≈5 (small-volume structures) the incident waves tend to be unaffected by the structure and long-wave approximation can be used, which means the induced loads are partially connected with the acceleration (mass loads) and partially with the velocity (viscous loads) of the incident waves at the center of the body, as the body was not there. Mass loads, i.e. proportional to acceleration (and so to the mass plus added mass term), are in general dominant as long as the incoming wave steepness H/D <≈10. If H/D <≈10, for sufficiently large λ/D viscous loads, i.e. connected with viscosity and flow separation and wake, varying as the squared power of the wave velocity, become dominant. As $\lambda/D \rightarrow \infty$ the wave behaves similarly as a slow-varying current.

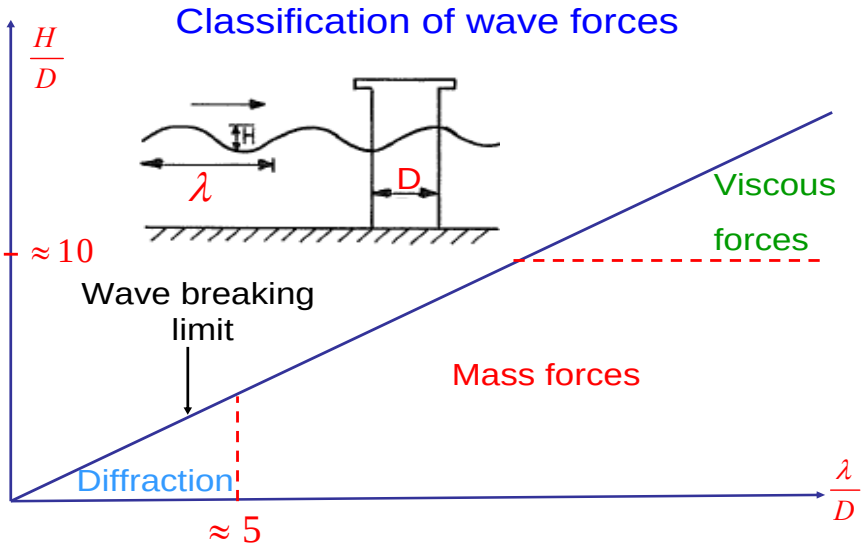

Fig. F:1.6

Step 3: Critical problems and related criteria-response variables

One has to identify the critical problems for the given vessel, find a way to predict their features and consequences and identify proper criteria-response variables associated with them. Minimization/control criteria of such variables can provide safe and successful design and operations. Recognized seakeeping and wave loads problems/response variables for ships are (Fig. F:1.4): local motions, accelerations, slamming, water on deck, breaking waves, sloshing, wave bending moment.

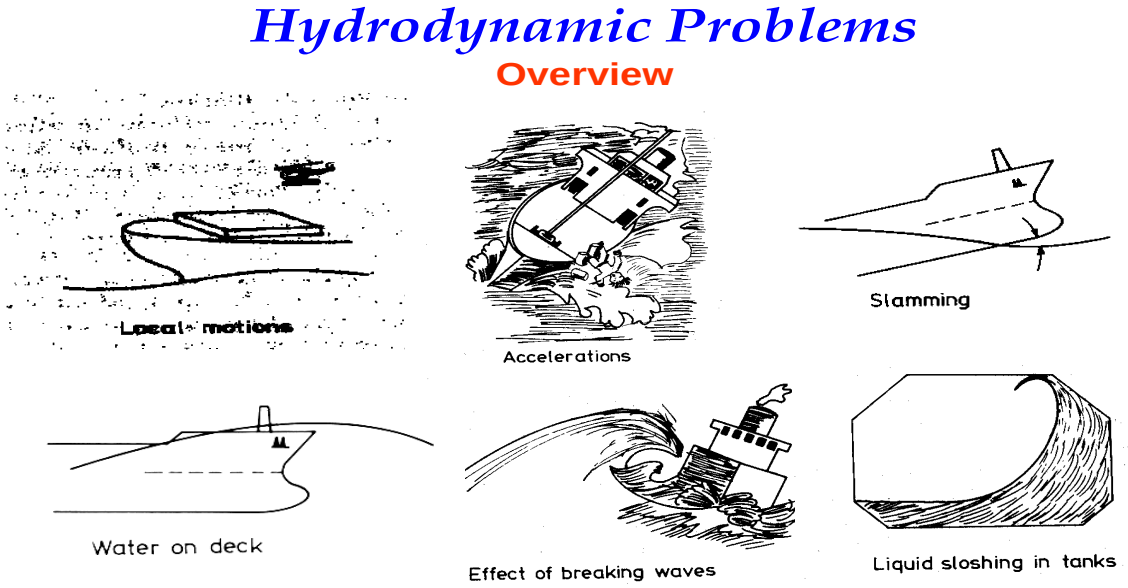

Fig. F:1.4

They may be dangerous for local/global safety, comfort and performance.
Generally speaking, the local water-vehicle relative motions represent important response variables, for example occurrence of slamming and water on deck phenomena can be assessed through them.
Also accelerations may be an important response variable because there are limits that must be satisfied to ensure comfort/proper onboard work conditions/safety. Such limits may vary according to the type of vessel and of work activities. In general. accelerations associated with longer periods are more difficult to stand with, so the limits for large ships are stricter than for smaller vessels for which typical natural periods are shorter.
Roll motion is of concern for different vessels, for example is relevant in terms of capsizing occurrence. Mechanisms to limit the roll amplitude are given by: bilge keels, anti-roll tanks and active fins.
Other causes of capsizing could be: breaking waves hitting the side of the vessel; following waves with phase velocity similar to the vessel speed inducing unstable route change (broaching).
Sloshing may be relevant any time there is a confinement of liquid (onboard tanks, ship decks with bulwark). It is a resonance phenomenon which is excited when the wave period is close to the natural period of the confinement region (i.e. the tank) and may lead to large fluid motions due to the limited damping associated with the fluid motion. Violent sloshing may lead to slamming, wave breaking and other complex scenarios which may be connected with high local pressures on the structures as well as large global loads. Both relevant for the design.
For large ships, another issue is the excitation of wave bending moment which may lead to whipping and springing, respectively, transient and steady-state elastic oscillations of the vehicle. They can be associated with linear and nonlinear excitation mechanisms.
Ship motions and induced sea loads may lead to voluntary and involuntary speed reduction of the vessel. The former is decided as operational strategy to ensure safety, comfort, operations on board. The latter is a consequence of reduced performance, for instance due to off-regime of the propeller in waves, added resistance in waves.

Step 4: Minimization/control criteria
The response variables of interest may vary according to the vessel type. The following figure documents the operational criteria used up-to-now for ships with different size, features and activities.

		Bottom slamming	Bow flare slamming	Deck wetness	Vertical accel.	Vertical motion	Roll	Propeller emerg.
								
Large oil/bulk carrier	laden			Yes				
	ballast	Yes						Yes
Large container vessel			Yes	Yes	Yes		Yes	
General cargo ship		Yes		Yes	Yes			Yes
Ro-Ro			Yes		Yes		Yes	Yes
Passenger vessel			Yes		Yes	Yes	Yes	

What are our tools? How can we predict motions/loads and take them under control?
The tools are: model and full scale experiments, analytical solutions, engineering tools (established methods like strip theory), and more general numerical solutions (Computational Fluid Dynamic, CFD, methods).
Experiments remain still the major tool. Analytical solutions when available are very useful. CFD approach is getting more and more popular.

Tool	Advantages	Disadvantages
Experiments	Complex geometries Visualization Local and global quantities	Cost Reliability Scaling (if with models)
Analytical solutions	Fast & cheap	Simplified models Simple geometries
Engineering tools	Relatively fast & cheap Well recognized reliability	Wide, but not enough, models Relatively simple geometries
CFD methods	Complex models Complex geometries Visualization Local and global quantities	Reliability Costs

Assumptions and basic equations. (F:13-17)
The water is considered continuous and with uniform density ρ. For the problems of interest the temperature is assumed uniform and constant and the fluid evolution can be fully described once estimated the velocity $\boldsymbol{V(r,t)}$ and pressure $p(\boldsymbol{r},t)$ fields. Assuming a Cartesian reference frame (x,y,z), alternative conventions are: $\mathbf{r}=(x,y,z)= x\boldsymbol{i}+y\boldsymbol{j}+z\boldsymbol{k}=x_1\boldsymbol{e_1}+ x_2\boldsymbol{e_2}+ x_3\boldsymbol{e_3}$, $\boldsymbol{V}= (u,v,w)=(u_1,u_2,u_3)$. In alternative to $\boldsymbol{r}$ we will also use $\boldsymbol{P}$.

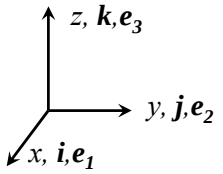

To solve the problem we need to identify:

Governing Equations + Boundary Conditions + Initial Conditions.

velocity ($\boldsymbol{V}$) and pressure (p) → we need 1 vectorial (3 scalar in3D) + 1 scalar equations.

<u>Governing Equations:</u>
1) Conservation of fluid mass → the fluid mass inside any volume Ω does not change in time
→ formally as mass =m=const
2) Conservation of fluid momentum → the fluid momentum changes inside Ω balance the forces acting on the volume and along its enclosing surface $\partial\Omega$
→ formally as $m\boldsymbol{a} = \boldsymbol{F}$ (Newton 2nd Law)

<u>Basic assumptions:</u>

The fluid is <u>inviscid</u> in <u>irrotational</u> motion and <u>incompressible</u>→ potential flow theory

- Inviscid:
  means zero viscosity μ=0, i.e. the tangential stresses are null.

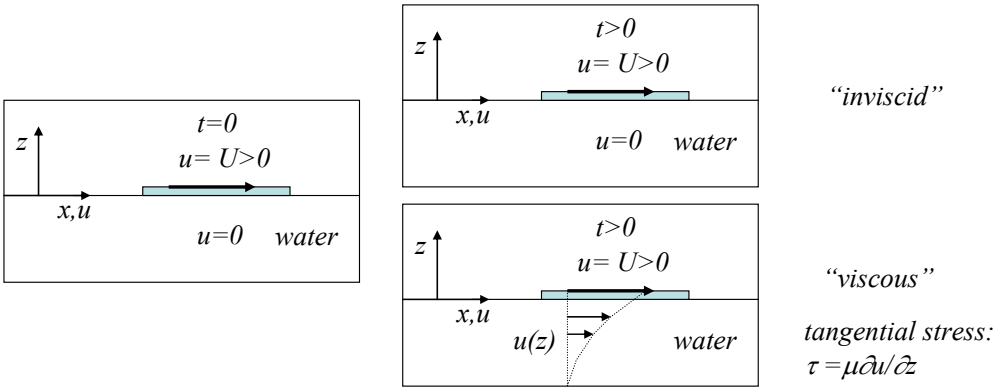

- Irrotational: means that locally the fluid does not tend to rotate → the vorticity **ω=0** → **ω=∇×V=0**

[For a rigid body **V=U+ω$_R$×r** → **ω**=2**ω$_R$**= twice the angular velocity]

- Incompressible: means that locally the fluid volume does not change

→ **∇·V=0** $\quad [\nabla \cdot \boldsymbol{V} = \frac{\partial u}{\partial x} + \frac{\partial v}{\partial y} + \frac{\partial w}{\partial z}\ ]$

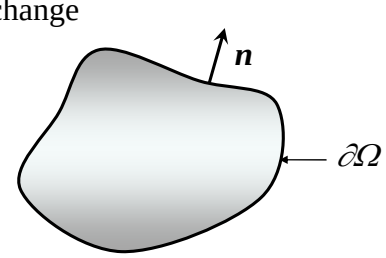

It means that the net flux across any ∂Ω is zero, i.e. the flux that enters in Ω ($\boldsymbol{V}\cdot\boldsymbol{n}$ <0) equals the flux going out from Ω ($\boldsymbol{V}\cdot\boldsymbol{n}$ >0).

<u>Consequences of the assumptions:</u>

$\nabla\times\boldsymbol{V}=\boldsymbol{0}$ → $\boldsymbol{V}$ can be written as the gradient of a scalar variable,

i.e. $\boldsymbol{V}=\nabla\phi = \frac{\partial\phi}{\partial x}\boldsymbol{i} + \frac{\partial\phi}{\partial y}\boldsymbol{j} + \frac{\partial\phi}{\partial z}\boldsymbol{k}$

with ϕ a scalar called velocity potential defined unless a constant.

The pressure can be obtained from the Bernoulli eq.:

$$p - p_a = \underbrace{-\rho g z}_{static} \underbrace{-\rho\frac{\partial\phi}{\partial t} - \frac{1}{2}\rho(\nabla\phi)^2}_{dynamic\ \ linear\ \ and\ \ quadratic}$$

NB: The dynamic linear part is very important from practical perspective, i.e. in terms of induced loads and motions.

Advantage: we need to find only ϕ (scalar) to solve for $\boldsymbol{V}$ and p
→ 1 scalar governing eq. instead of 1 vectorial and 1 scalar.

Problem for ϕ:

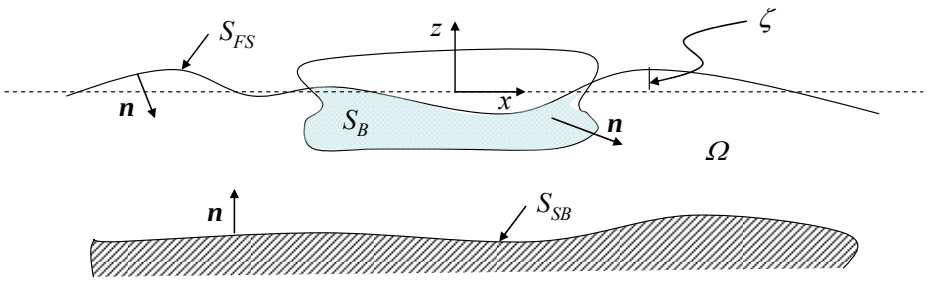

Governing eq:
$\nabla \cdot (\nabla \phi) = 0 \rightarrow \nabla^2 \phi = 0$ in Ω (F:2.3) Laplace eq.

Boundary conditions:

Sea-bottom kinematic condition: *impermeability condition*
$\frac{\partial \phi}{\partial n} = 0$ on S_{SF} (F:2.5)

Body kinematic condition: *impermeability condition*
$\frac{\partial \phi}{\partial n} = \underbrace{\boldsymbol{V_B}}_{\text{body velocity}} \cdot \boldsymbol{n}$ on S_B (F:2.6)

Free-surface kinematic condition: *fluid particles on S_{FS}, $z - \zeta(x,y,t) = 0$, remain there*
$\frac{D(z-\zeta)}{Dt} = 0 \rightarrow \frac{\partial \phi}{\partial z} = \frac{\partial \zeta}{\partial t} + \underbrace{\frac{\partial \phi}{\partial x}\frac{\partial \zeta}{\partial x} + \frac{\partial \phi}{\partial y}\frac{\partial \zeta}{\partial y}}_{\text{nonlinear}}$ on $z = \zeta(x,y,t)$ (F:2.10)

Free-surface dynamic condition: *pressure equal to ambient pressure p_a*
$g\zeta + \frac{\partial \phi}{\partial t} + \underbrace{\frac{1}{2}\left[\left(\frac{\partial \phi}{\partial x}\right)^2 + \left(\frac{\partial \phi}{\partial y}\right)^2 + \left(\frac{\partial \phi}{\partial z}\right)^2\right]}_{\text{nonlinear}} = 0$ on $z = \zeta(x,y,t)$ (F:2.11)

Far-field condition: *waves are outgoing*

Two conditions are necessary on S_{FS} because ζ is an unknown as ϕ.
The problem depends on time through conditions (F:2.6), (F:2.10) and (F:2.11) and is nonlinear due to (F:2.10) and (F:2.11).

Linearization of the problem
Assuming ε as measure of the problem nonlinearities, i.e. wave nonlinearities, the solution can be expressed as

$$\phi = \phi_1 \varepsilon + \phi_2 \varepsilon^2 + \phi_3 \varepsilon^3 + ...$$
$$\zeta = \zeta_1 \varepsilon + \zeta_2 \varepsilon^2 + \zeta_3 \varepsilon^3 + ...$$

substituting these expressions in the governing equation and boundary conditions and using Taylor expansion of the boundary conditions around the mean boundary configuration (i.e. body motions and free-surface deformations are expressed as power functions of ε) we can find the problems for each solution order.
Assuming ε small and neglecting terms $O(\varepsilon^n)$ with $n>1$, conditions (F:2.10) and (F:2.11) can be linearized and applied at the mean free surface $z=0$

NB: A consequence of linear theory is that the response (output), i.e. body-motion amplitude, is proportional to the excitation (input), i.e. incident-wave amplitude.

$$\frac{\partial \phi}{\partial z} = \frac{\partial \zeta}{\partial t} \quad \text{on } z=0 \quad \text{(F:2.12)}$$

$$g\zeta + \frac{\partial \phi}{\partial t} = 0 \quad \text{on } z=0 \quad \text{(F:2.13)}$$

Differentiating (F:2.13) with respect to time and substituting in (F:2.12), the combined free-surface condition is obtained:

$$\frac{\partial^2 \phi}{\partial t^2} + g\frac{\partial \phi}{\partial z} = 0 \quad \text{on } z=0 \quad \text{(F:2.14)}$$

In steady-state conditions, the solution oscillates with the incoming-wave frequency ω, and condition (F:2.14) becomes

$$-\omega^2 \phi + g\frac{\partial \phi}{\partial z} = 0 \quad \text{(F:2.15)}$$

Moreover space and time variables can be separated:

$$\phi(x,y,z,t) = \Re\left[\underbrace{\varphi(x,y,z)}_{space\ dependence}\ \underbrace{e^{i\omega t}}_{time\ dependence}\right]$$

NB: In linear conditions and steady-state conditions the 'response' (output) oscillates with the frequency of the 'disturbance' (input).

This means that it is possible to avoid the time dependence from the problem and solve a one-shot problem only dependent from ω (frequency domain analysis). In nonlinear conditions and/or in transient conditions the problem must be solved in time (time domain analysis).

The environmental conditions of interest are: waves, currents and wind. We are interested to estimate the loads (and motions) induced by them.

Environment
The marine vehicles are subjected generally to an environment made of incident waves (generated far from them), wind and current. So we must estimate the related induced loads (and motions).

Incident regular waves (F:17-23)
Hp: Incoming free-surface regular gravity linear waves propagating in deep-water conditions.
Incident: means generated far away

2D/planar waves: means propagating along a plane/direction
Free-surface waves: means propagating along the sea surface and null far from it
Gravity waves: means governed by gravity, i.e. λ>>1cm (surface tension negligible)
Regular: means oscillating with a certain frequency $\omega = 2\pi/T$ and then with a certain wavelength λ

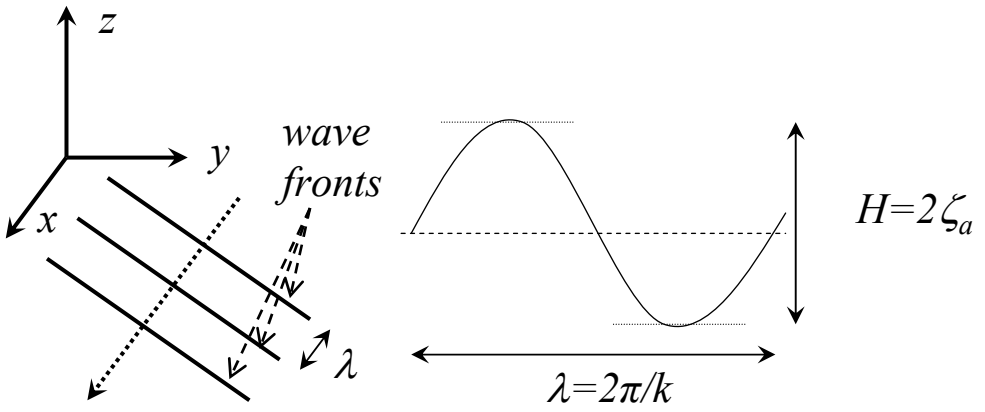

Propagating: means the wave fronts (surfaces with constant phase, e.g. phase=π/2 ←→ maximum wave elevation ←→ wave peaks) move with a certain speed, called phase velocity, c
Deep-water: means in a region with very large water depth, i.e. $h \to \infty$
Linear: means small ε
H/λ or $k\zeta_a = \pi H/\lambda$ are a measure of the 'steepness' of the waves, i.e. of the wave nonlinearities, so that can be used as parameter ε.

NB: Since the steepness is $\propto \zeta_a$ the nonlinearities are also expressed in powers of ζ_a however the steepness is more appropriate to express the nonlinearities within a perturbation method.

Hp: Waves propagating in x direction, with wavelength λ and amplitude ζ_a.

We want to find the solution for ϕ representing a wave in these conditions→We must find what features the waves must have to satisfy the problem:

$\nabla^2\phi = 0$ in Ω (a)

$-\omega^2\phi + g\dfrac{\partial\phi}{\partial z} = 0$ on $z=0$ (b)

$\phi, \nabla\phi \to 0 \quad as \quad z \to -\infty$ (c) [far field condition]

We do not find systematically the solution but we note that:
- Condition (c) is satisfied by e^{kz}
- Eq. (a) is satisfied by $e^{kz}\left[A\cos kx + B\sin kx\right]$
  → $k^2 e^{kz}\left[A\cos kx + B\sin kx\right] - k^2 e^{kz}\left[A\cos kx + B\sin kx\right] \equiv 0$
- Oscillation with frequency ω is ensured by $\cos(\omega t + \alpha)$ with α a phase
- So the solution could be written generally as
  $\phi = e^{kz}\left[A\cos kx + B\sin kx\right]\cos(\omega t + \alpha)$ (d)
- Substituting this in condition (b) we have a compatibility between space and time parameters:
  $\omega^2 = gk$ [dispersion relationship]
  i.e. waves with a certain length must oscillate with a certain period.

Expression (d) in general is not a propagating but a standing wave.

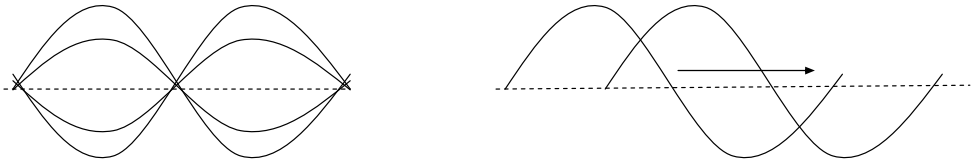

standing wave *propagating wave*

to have a propagating wave space and time variations must be combined as

$\phi = Ce^{kz}\cos(\omega t - kx + \gamma)$ (e)

In this way $\omega t - kx + \gamma$ = const → $kx = \omega t - \gamma$ -const indicates a wave front whose position x increases in time, i.e. the front propagates along the positive x with a speed

$c=dx/dt=\omega/k$ (phase speed).

$\phi = Ce^{kz}\cos(\omega t + kx + \gamma)$ is instead the solution for a wave propagating along the negative x.

Inserting (e) in the dynamic free-surface condition

$\zeta = -\frac{1}{g}\frac{\partial\phi}{\partial t}\Big|_{z=0} = \frac{C\omega}{g}\sin(\omega t - kx + \gamma)$ so $C\omega/g=\zeta_a$ → $C=\zeta_a g/\omega$

so the solution is found.

↑ For waves with a generic direction β with respect to x

→ $\omega t - kx + \gamma$ = const becomes $\omega t - \boldsymbol{k}\cdot\boldsymbol{r} + \gamma$ = const with $\boldsymbol{k}=(k\cos\beta, k\sin\beta)$ and $\boldsymbol{r}=(x,y)$

↑ For waves in finite water depth h

→ the z dependence e^{kz} becomes $\cosh k(h+z)/\cosh kz$h

→ the dispersion relation becomes $\omega^2 = gk\tanh kh$

Table F:2.1 gives the behaviour of the different variables in deep and water depth. They have in general maximum at different locations. Fig. F:2.1 shows this in terms of the wave elevation, pressure, velocity and acceleration along a wavelength and at a generic depth. We see that the dynamic pressure is negative under a trough and is positive under a crest. The same is true for u which then is in the wave-propagation direction under a crest and the opposite under a trough. The acceleration is greatest in magnitude under a node.

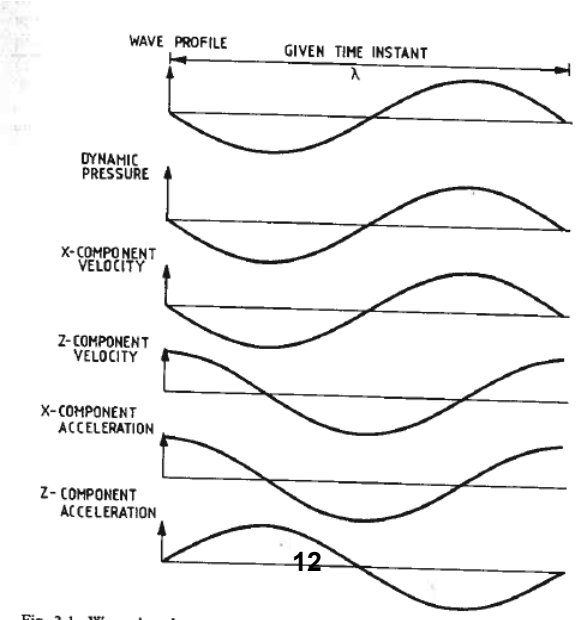

Fig. 2.1. Wave elevation, pressure, velocity and acceleration in long-crested sinusoidal waves propagating along the positive x-axis (see Table 2.1).

Fig. F:2.3 discusses the pressure behaviour according to linear theory. Since the pressure is given relative the atmospheric pressure it must go to zero at the free surface, which means that the static and dynamic contributions must balance each other. This is exactly satisfied at a crest but not at a trough, there a higher-order error, $O(\varepsilon^n)$ with $n>1$, is committed.

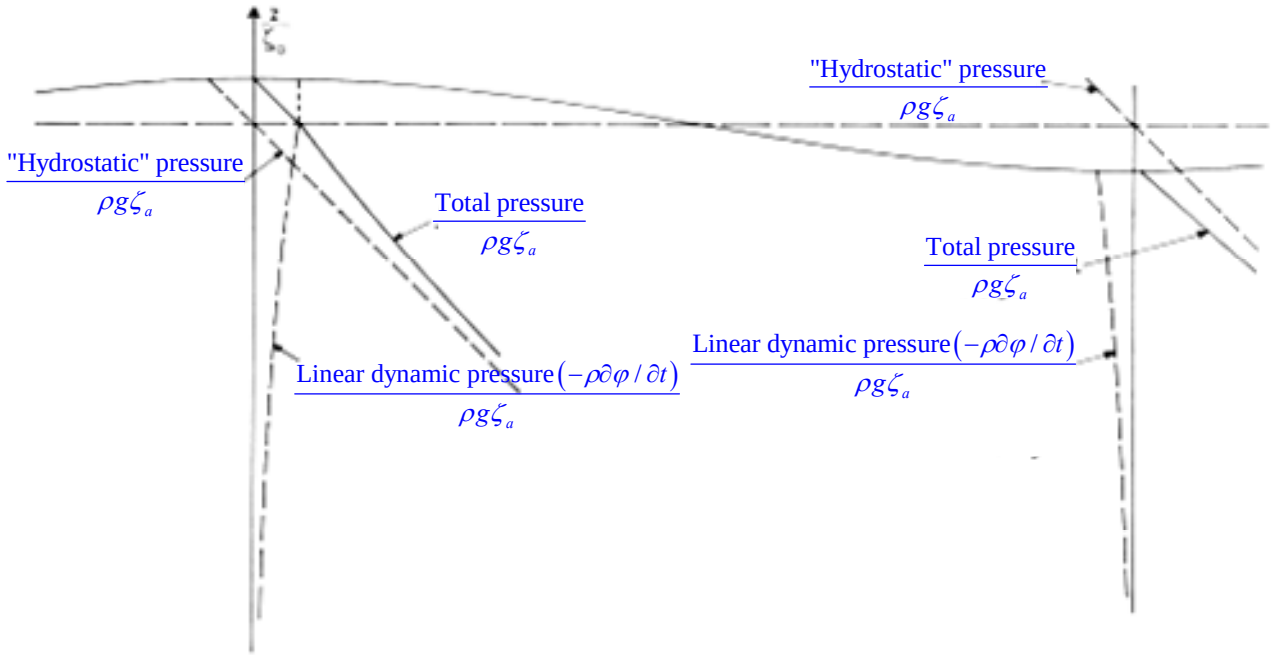

Fig. F:2.3

NB: At a fixed point the fluid velocity has zero mean value but if we follow the fluid particle in its motion consistent with linear theory, then the fluid particle is drifted in time in the wave-propagation direction with a velocity called Stokes drift velocity which is a second-order variable, i.e. $\zeta_a{}^2\omega k\exp(2kz_0)$, with z_0 the particle position when there are no waves, see Fig. F:2.4.

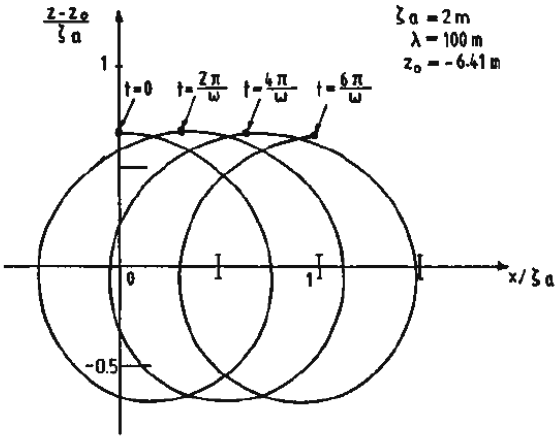

Fig. 2.4. Trajectory of a fluid particle in sinusoidal waves computed from first-order (linear) velocity potential (ζ_a = wave amplitude, λ = wavelength, z_0 = z-coordinate of fluid particle at rest.) (Ogilvie, 1983.)

The waves are associated with energy. The mean (potential and kinetic) wave energy in a wavelength and per unit width is

$$E = \frac{\rho g \zeta_a{}^2 \lambda}{2}$$

The mean wave-energy density is $\frac{E}{\lambda} = \frac{\rho g \zeta_a{}^2}{2}$

E travels with a speed $c_g = \partial\lambda/\partial T = \partial\omega/\partial k$ (group velocity) that is $c_g \underset{\omega^2=gk}{=} \frac{1}{2}\frac{\omega}{k}$ in deep water.

An important concept for practical application is the wave power, given by the wave-energy density multiplied by the wave-energy speed (group velocity):

$$P_W = \frac{\rho g \zeta_a{}^2}{2}\frac{g}{2\omega}$$

So we have three different velocities associated with the waves:

1) The fluid velocity $\nabla\phi$=associated with an orbital path, circular in deep water
2) The phase velocity c = of the propagating wave fronts
3) The group velocity c_g=of the wave energy

NB: Regular incident waves are far from being similar to how ocean waves appear in reality. However they can be useful to describe more general waves under the assumption of linear conditions due to superposition principle.

Incident long-crested irregular waves (F:23-27,29-31)
Long-crested=the wave energy is propagating in one dimension, i.e. 2D waves
Irregular= with energy within a certain range of frequencies

An important consequence of linear conditions is that superposition principle is valid, i.e. the problem can be split in its single elements.

In our case assuming an irregular wave with a wave spectrum $S(\omega)$ (see fig. F:2.5)

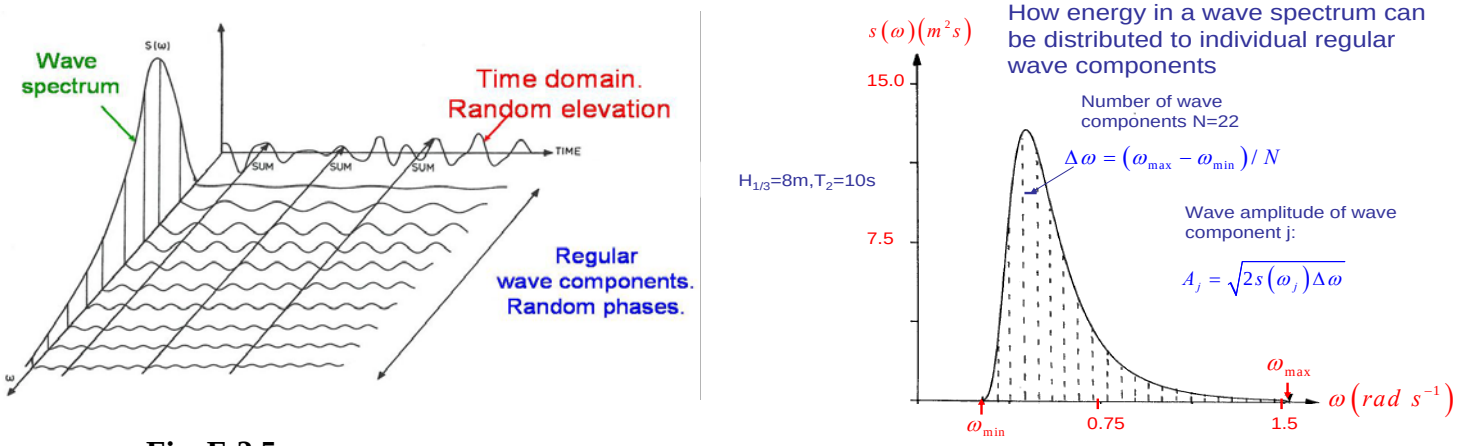

Fig. F:2.5

The energy in the spectrum can be split in a finite (large) number of regular wave components, i.e.

$$\zeta = \sum_{j=1}^{N} A_j \sin\left(\omega_j t - k_j x + \varepsilon_j\right) \quad (1)$$

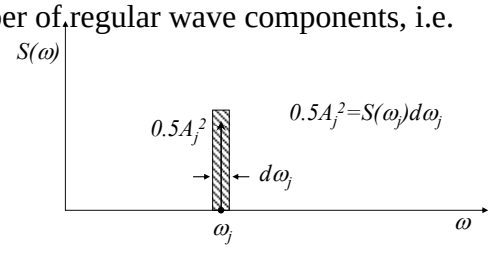

- $A_j \rightarrow \frac{1}{2} A_j^{\,2} = S(\omega)\Delta\omega$ to preserve the wave energy
- ε_j is a random phase to recover a statistic behaviour in time→ they are independent from each other
- ω_j and k_j are linked through the dispersion relation
- The wave elevation is Gaussian distributed
- The probability density function for the maxima of ζ can be approximated by a Rayleigh distribution.

Similarly we can obtain the velocity and other wave quantities.

So we can study the response to irregular waves as the sum of the responses to regular waves.

There are different recommendations in terms of $S(\omega)$ to describe properly ocean waves:
Examples are (see Fig. F:2.6)

- Pierson-Moskowitz (used for Mediterranean sea) and
- JONSWAP (used for the North sea).

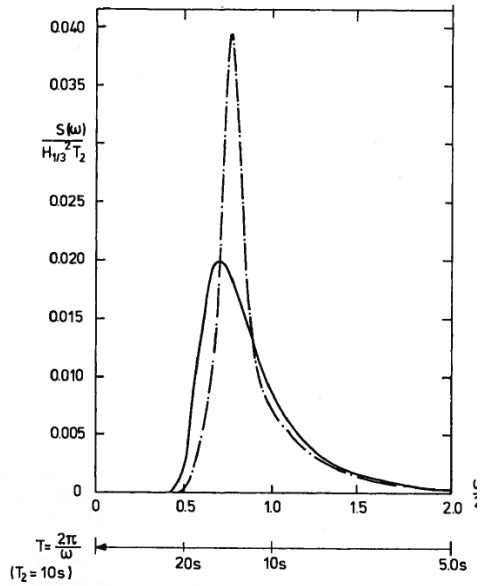

Fig. 2.6. Examples of wave spectra. ($H_{\frac{1}{3}}$ = significant wave height, T_2 = me wave period). Modified Pierson–Moskowitz spectrum ——— (see equation (2.24)), JONSWAP spectrum ——·——· (see equation (2.30)).

The features of the spectrum in terms of width, symmetry, nonlinearities, are given by the spectrum moments

$$m_k = \int_0^\infty \omega^k S(\omega) d\omega$$

m_0 is also known as variance σ^2 and its square-root (standard deviation) gives the deviation from the mean value of the spectrum.
As for the regular waves, we can define relevant wave periods and heights, i.e.

$T_1 = 2\pi m_0 / m_1$

$T_2 = 2\pi\sqrt{m_0 / m_2}$ (mean wave period)

T_0 (corresponding to the peak frequency of the spectrum, also known as modal period)

$H_{1/3}$ = significant wave height=mean of the one third highest waves $= 4\sqrt{m_0}$ for Gaussian distribution.

Marine Field: Scenarios

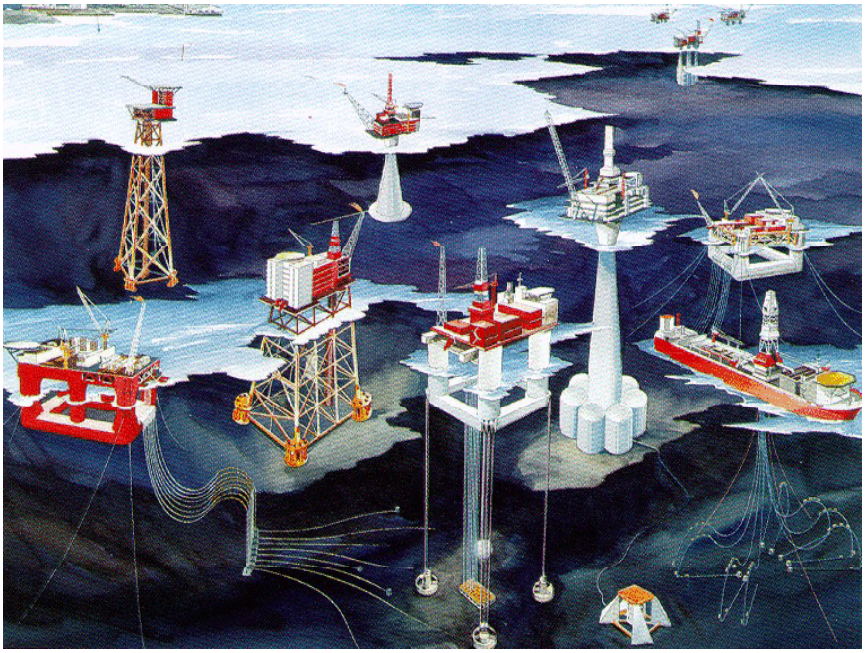

Very large floating structures (VLFS)

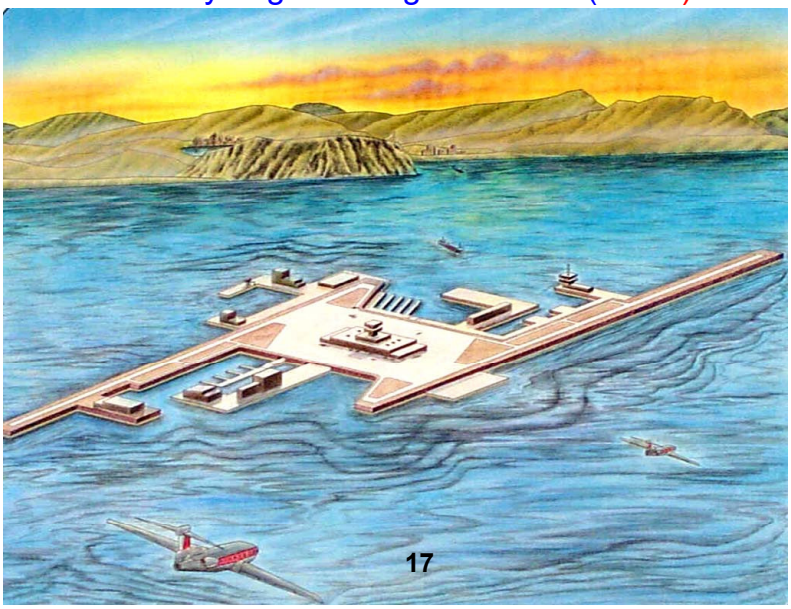

Aquaculture plants

Pelamis wave energy plant

Coordinate system and rigid-body modes

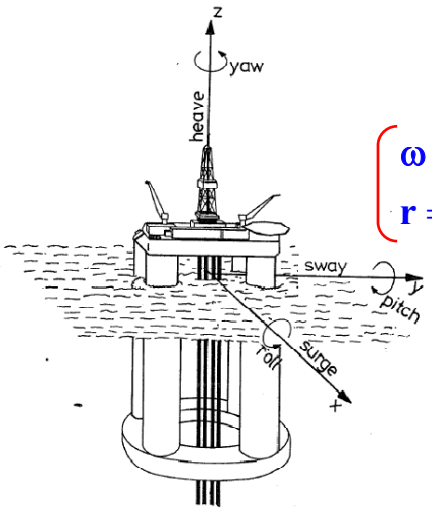

$$\mathbf{s} = \eta_1\mathbf{i} + \eta_2\mathbf{j} + \eta_3\mathbf{k}$$
$$+\boldsymbol{\omega}\times\mathbf{r}$$
$$\boldsymbol{\omega} = \eta_4\mathbf{i} + \eta_5\mathbf{j} + \eta_6\mathbf{k},$$
$$\mathbf{r} = x\mathbf{i} + y\mathbf{j} + z\mathbf{k}$$
$$\mathbf{s} = (\eta_1 + z\eta_5 - y\eta_6)\mathbf{i}$$
$$+(\eta_2 - z\eta_4 + x\eta_6)\mathbf{j}$$
$$+(\eta_3 + y\eta_4 - x\eta_5)\mathbf{k}$$

Natural heave periods

SES	TLP	Ship	Semi-sub	SWATH
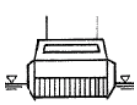	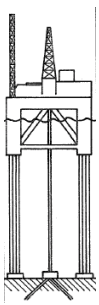		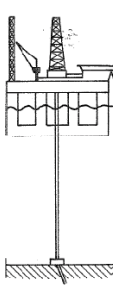	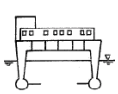
T_n<1s	T_n=2-4s	$T_n \approx \sqrt{L/1.5}$ =4–16s	T_n>20s	T_n>20s

Classification of wave forces

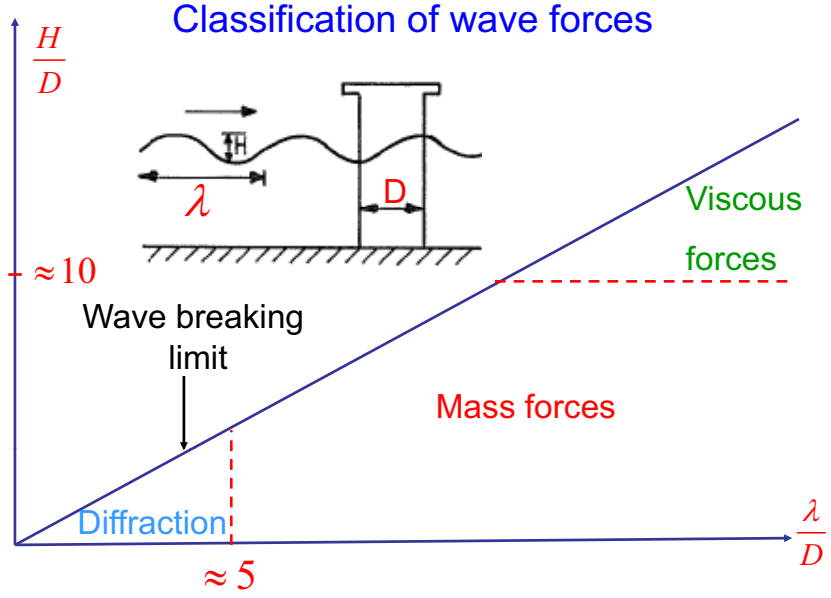

Hydrodynamic Problems

Overview

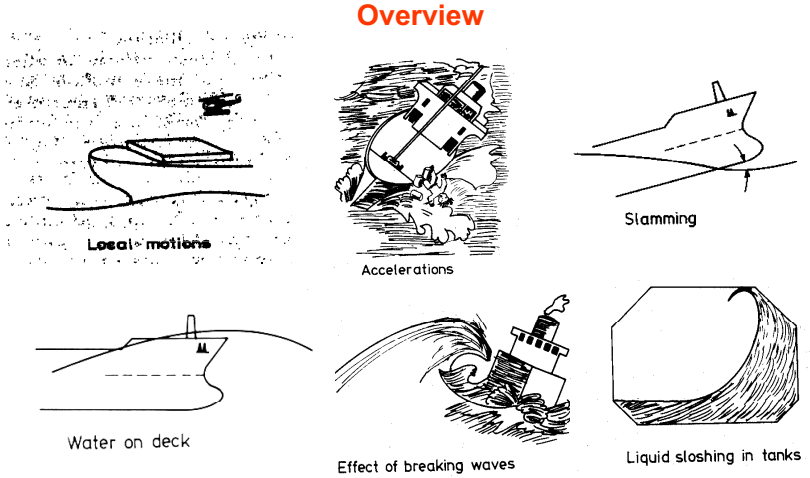

Operational criteria for ships

		Bottom slamming	Bow flare slamming	Deck wetness	Vertical accel.	Vertical motion	Roll	Propeller emerg.
Large oil/bulk carrier	laden			Yes				
	ballast	Yes						Yes
Large container vessel			Yes	Yes	Yes		Yes	
General cargo ship		Yes		Yes	Yes			Yes
Ro-Ro			Yes		Yes		Yes	Yes
Passenger vessel			Yes		Yes	Yes	Yes	

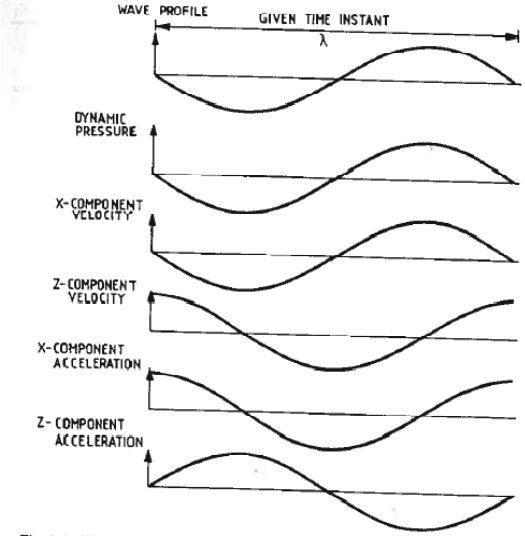

Fig. 2.1. Wave elevation, pressure, velocity and acceleration in long-crested sinusoidal waves propagating along the positive x-axis (see Table 2.1).

Pressure distribution in regular linear waves

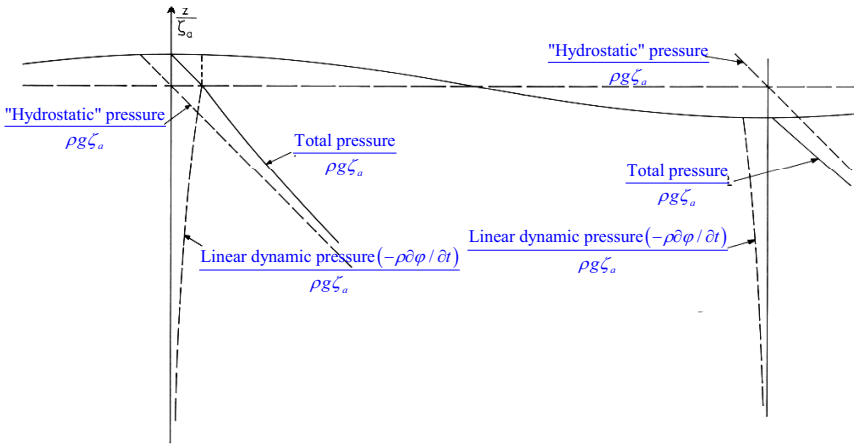

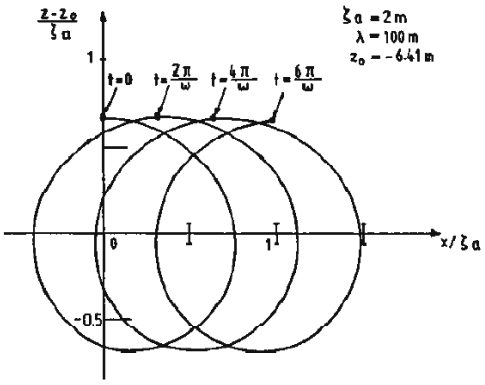

Fig. 2.4. Trajectory of a fluid particle in sinusoidal waves computed from first-order (linear) velocity potential (ζ_a = wave amplitude, λ = wavelength, z_0 = z-coordinate of fluid particle at rest.) (Ogilvie, 1983.)

How energy in a wave spectrum can be distributed to individual regular wave components

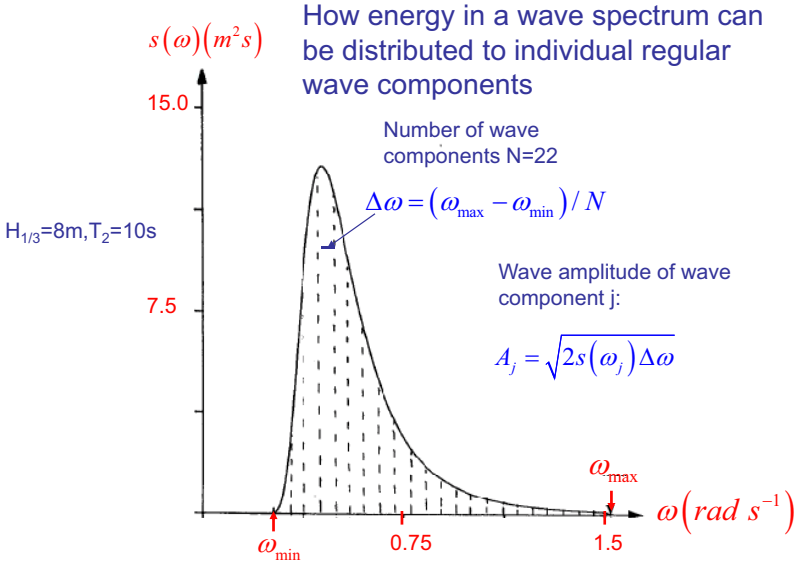

Number of wave components N=22

$$\Delta\omega = (\omega_{max} - \omega_{min}) / N$$

Wave amplitude of wave component j:

$$A_j = \sqrt{2s(\omega_j)\Delta\omega}$$

Time and frequency domain of waves

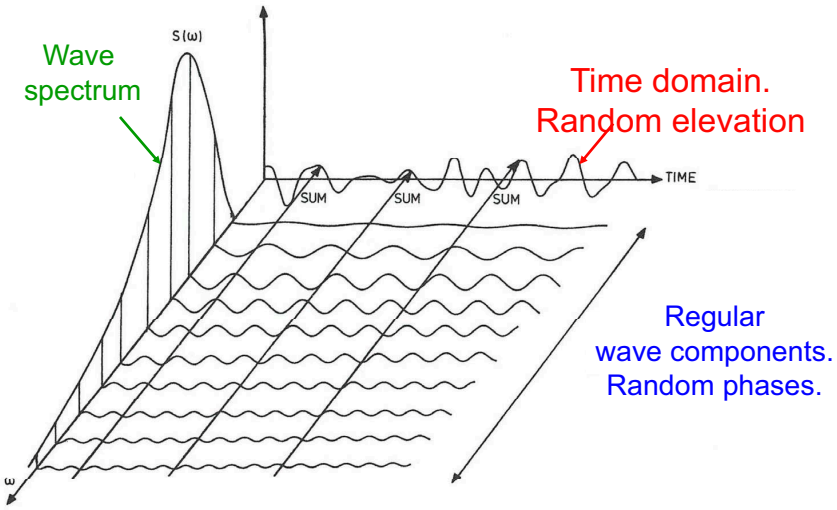

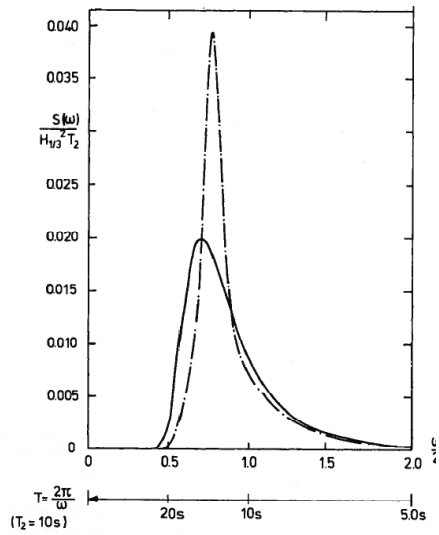

Fig. 2.6. Examples of wave spectra. ($H_{\frac{1}{3}}$ = significant wave height, T_2 = me wave period). Modified Pierson–Moskowitz spectrum ——— (see equation (2.24)), JONSWAP spectrum —·—·— (see equation (2.30)).

Lecture Note 2

36. Waves (continuation). Wind. Current. Radiation and diffraction problems. Excitation loads. Added-mass and damping: physical meaning, strip-theory. (F:27-34,39-49,58-66)

Incident long-crested irregular waves (F:27,29-31)

Summary: Long-crested irregular waves, superposition principle, periods, significant wave-height.

The peak values of the wave elevation are an important parameter to examine for safe design and operations. If a Gaussian distribution (spectrum bell shaped) is a good approximation for the wave process, the Rayleigh distribution is considered a good a approximation for the probability density function of the maxima (peak values), say A, of the wave elevation, i.e.

$$p(A) = \frac{A}{m_0}\exp\left(-\frac{A^2}{2m_0}\right) \quad \text{(F:2.32)}$$

The integration of it in a certain interval of maxima will provide the probability that the peak can have value in that interval.

The most probable largest value $A_{\max}$ during a 'short-term' time t is then

$$A_{\max} = \sqrt{2m_0 \log\frac{t}{T_2}} \quad \text{(F:2.35)}$$

The analysis so far considered is called as 'short-term' sea state. If the features of the spectrum change in time one talks about long-term sea state.

In this case the features of the sea state change in time, i.e. T_0 and $H_{1/3}$.

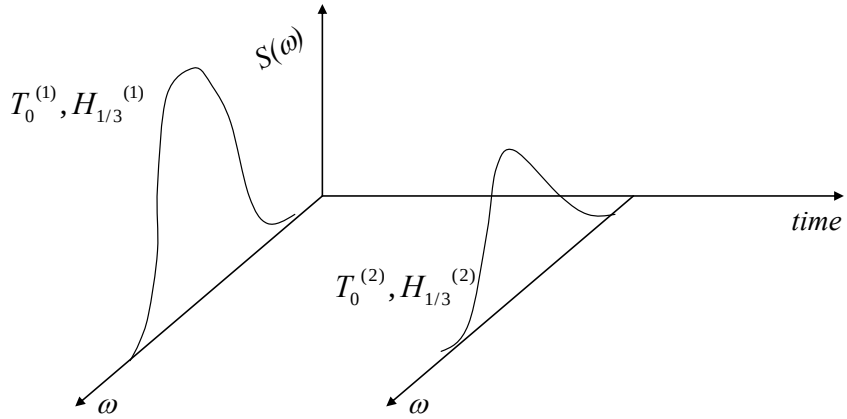

This means that different sea states can alternate, and the persistence of re-occurrence of a certain sea state will depend on its probability, the greater the probability, the longer one can expect that sea state. This means that we can sum up the short-term prediction for each sea state, weighted by the probability of the sea state, to get the long-term prediction. To find the probability that a certain combination (T_0 , $H_{1/3}$) occurs, joint probability, we need the scatter diagram. Table F:2.2 gives an example.

In the table, you see the ranges of periods and significant wave heights which have a probability of occurrence. The numbers in the table give the occurrence of T_0 and $H_{1/3}$ and the sum of all possible occurrences here is 100001, so the probability associated wit a certain occurrence is given by the occurrence divided by the sum of the occurrences.

Examples of application of table F:2.2:

1. The joint probability for $6m<H_{1/3}<7m$ and $T_1=9sec$ is $p_{ij} = \frac{27}{100001} \cong 0.00027$
2. If you want the probability for a certain $H_{1/3}$ for any value of the period, then you must sum all occurrences in the raw of that $H_{1/3}$ and divide by the sum. Similarly is you want the

probability for a certain T_0 for any value of the significant wave height, then you must sum all occurrences in the column of that T_0 and divide by the sum.
Ex., the probability for

- $H_{1/3} < 6m$ is $p_j = \frac{(8636 + 32155 + 25792 + 15442 + 9118 + 4839)}{100001} \cong 0.96$
- $H_{1/3} > 6m$ is $p_j = 1 - 0.96 = \frac{2329 + 1028 + 419 + 160 + 57 + 19 + 6 + 1}{100001} = 0.04$

  Hp: a certain criterion to be satisfied $H_{1/3}$ must be $<6m$. From the table the criterion is not satisfied for 4% of the time during a year.
- $3m < H_{1/3} < 6m$ is $p_j = \frac{(15442 + 9118 + 4839)}{100001} \cong 0.29$

Table 2.2. *Joint frequency of significant wave height and spectral peak period. Representative data for the northern North Sea*

Significant wave height (m) (upper limit of interval)	Spectral peak period (s)																			Sum
	3	4	5	6	7	8	9	10	11	12	13	14	15	16	17	18	19	21	22	
1	59	403	1061	1569	1634	1362	982	643	395	232	132	74	41	22	12	7	4	2	2	8636
2	9	212	1233	3223	5106	5814	5284	4102	2846	1821	1098	634	355	194	105	56	30	16	17	32 155
3	0	8	146	831	2295	3896	4707	4456	3531	2452	1543	901	497	263	135	67	33	16	15	25 792
4	0	0	6	85	481	1371	2406	2960	2796	2163	1437	849	458	231	110	50	22	10	7	15 442
5	0	0	0	4	57	315	898	1564	1879	1696	1228	748	398	191	84	35	13	5	3	9118
6	0	0	0	0	3	39	207	571	950	1069	885	575	309	142	58	21	7	2	1	4839
7	0	0	0	0	0	2	27	136	347	528	533	387	217	98	37	12	4	1	0	2329
8	0	0	0	0	0	0	2	20	88	197	261	226	138	64	23	7	2	0	0	1028
9	0	0	0	0	0	0	0	2	15	54	101	111	78	39	14	4	1	0	0	419
10	0	0	0	0	0	0	0	0	2	11	30	45	39	22	8	2	1	0	0	160
11	0	0	0	0	0	0	0	0	0	2	7	15	16	11	5	1	0	0	0	57
12	0	0	0	0	0	0	0	0	0	0	1	4	6	5	2	1	0	0	0	19
13	0	0	0	0	0	0	0	0	0	0	0	1	2	2	1	0	0	0	0	6
14	0	0	0	0	0	0	0	0	0	0	0	0	0	1	0	0	0	0	0	1
15	0	0	0	0	0	0	0	0	0	0	0	0	0	0	0	0	0	0	0	0
Sum	68	623	2446	5712	9576	12 799	14 513	14 454	12 849	10 225	7256	4570	2554	1285	594	263	117	52	45	100 001

NB: Table F:2.2 does not provide information on the duration of a certain sea state.

We have learned that for a regular wave the wave power is

$$P_W = \underbrace{\frac{\rho g \zeta_a^{\,2}}{2}}_{\substack{\text{mean}\\ \text{energy}\\ \text{density}}} \underbrace{\frac{\omega}{2k}}_{\substack{\text{group}\\ \text{velocity}}} \overset{\omega^2 = gk}{=} \underbrace{\frac{\rho g \zeta_a^{\,2}}{2}}_{\substack{\text{in}\\ N/m}} \underbrace{\frac{g}{2\omega}}_{m/s} \qquad in \quad W/m \equiv N/s$$

This can be extended for irregular waves:
In short-term perspective, assuming that the spectrum $S(\omega)$ is split in elementary interval wide $d\omega$ each regular-wave will contribute to the wave-power of the sea state with

$$\frac{\rho g A^2}{2} \frac{g}{2\omega} = \frac{\rho g 2S(\omega)d\omega}{2} \frac{g}{2\omega}$$

Summing all contributions, i.e. integrating from 0 to ∞ we find the power as

$$P_W = \frac{\rho g^2}{2} \int_0^\infty \frac{S(\omega)d\omega}{\omega} \quad (1)$$

So for instance for the Pierson-Moskovitz spectrum we have

$$P_W = 0.005535\rho g^2 H_{1/3}{}^2 T_1$$

In long-term perspective, the spectrum features, i.e. $H_{1/3}$ *and* T_1 will vary in time, so expression (1) contributes proportionally with the joint probability, say p_{ij}, of $H_{1/3}$ *and* T_1. Summing up all contributions the power will be

$$\bar{P}_W = \sum_i \sum_j P_W(H_{1/3}{}^{(i)}, T_1^{(j)}) p_{ij}$$

To evaluate the wave power on a long-term perspective we need then the scatter diagram. An example is given in the following figure.

Long-term statistics for available wave power in a specific area

We need to know the scatter diagram

	T_2 [seconds] →																
$H_{1/3}$ [m]	1	2	3	4	5	6	7	8	9	10	11	12	13	14	15	16	Sum
0.5	0	0	15	70	104	85	50	24	10	4	1	1	0	0	0	0	364
1	0	0	1	17	51	65	49	27	12	5	2	1	0	0	0	0	230
1.5	0	0	0	4	24	44	43	28	13	5	2	1	0	0	0	0	164
2	0	0	0	1	9	24	30	22	12	5	2	1	0	0	0	0	106
2.5	0	0	0	0	3	11	18	16	9	4	1	1	0	0	0	0	63
3	0	0	0	0	1	5	10	10	6	3	1	0	0	0	0	0	36
3.5	0	0	0	0	0	2	5	5	4	2	1	0	0	0	0	0	19
4	0	0	0	0	0	1	2	5	2	1	1	0	0	0	0	0	10
4.5	0	0	0	0	0	0	1	1	1	1	0	0	0	0	0	0	4
5	0	0	0	0	0	0	0	1	1	0	0	0	0	0	0	0	2
5.5	0	0	0	0	0	0	0	0	0	0	0	0	0	0	0	0	0
6	0	0	0	0	0	0	0	0	0	0	0	0	0	0	0	0	0
Sum	0	0	16	92	192	237	208	137	70	30	11	5	0	0	0	0	998

$$p_{ij} = \frac{24}{998} \quad for\ H_{1/3} = 2m, T_2 = 6s$$

$$\bar{P}_w = \sum_i \sum_j P_w(H_{1/3}, T_2) p_{ij} = 10.5 kW/m$$

Incident short-crested irregular waves (F:27-29)
Short-crested= the wave spectrum varies with direction θ, i.e. $S(\omega,\theta)$.

This mean that elementary waves in the spectrum have different propagation direction, and we can decompose the waves as

$$\zeta = \sum_{j=1}^{N} \sum_{k=1}^{K} A_{jk} \sin(\omega_j t - k_j x \cos\vartheta_k - k_j y \cos\vartheta_k + \varepsilon_{jk}) \quad (1)$$

- $A_{jk} \rightarrow \frac{1}{2} A_{jk}{}^2 = S(\omega_j, \vartheta_k)\Delta\omega_j \Delta\vartheta_k$ to preserve the wave energy
- ε_{jk} is a random phase to recover a statistic behaviour in time
- ω_j and k_j are linked through the dispersion relation

- θ_k is the direction relative to x of wave propagation

Wind (F:31-33)
Also the wind is typically described statistically with a spectrum that can vary in time and in space moving far from the sea level. One can identify

- a mean wind responsible for mean loads and
- gusts responsible for transient (even resonant) loads.

NB: A one-hour mean wind speed at 10 m above the sea level U_{10} for design of offshore structures in North Sea is 40m/s.

Current (F:33-34)
The 10th ISSC distinguishes 6 current contributions:

- U_t due to tides [depends on location]
- U_w due to local wind
- U_s due to Stokes drift (see eq. (F:2.21)) [can be relevant and is a Lagrangian contribution]
- U_m due to major ocean circulation
- $U_{set\text{-}up}$ due to set-up and storm phenomena
- U_d due to local density variations

NB: A total current velocity U for design of offshore structures in North Sea is 1m/s.

We will now discuss the "wave-frequency" loads/motions within the linear potential-flow theory, the sea environment is described by planar regular waves.

Loads
Under our assumptions of inviscid fluid, the forces and moments are obtained by integrating the pressure along the wetted surface of the body:

$$\boldsymbol{F} = \int_{S_B} p\boldsymbol{n}dS \qquad \boldsymbol{M} = \int_{S_B} p\boldsymbol{r}\times\boldsymbol{n}dS$$

NB: The normal vector is directed inside the body, in the opposite case there is '-' in the formula.

The linear loads are obtained integrating the pressure

$$p = \underbrace{-\rho\frac{\partial\phi}{\partial t}}_{dynamic=P_D} \underbrace{-\rho g z}_{hydrostatic}$$

The hydrostatic part must be integrated on the instantaneous body surface to include all linear terms, i.e. up to ~O(ζ_a), the dynamic part which is ~O(ζ_a), along the mean body wetted surface $S_{0,B}$. We now focus on P_D: Using the notation with the generalized normal vector

$$n_k = \begin{cases} n_k & for\ k = 1,2,3 \\ (\mathbf{r}\times\mathbf{n})_{k-3} & for\ k = 4,5,6 \end{cases}$$

we get the generalized forces

$$F_k(t) = -\rho\int_{S_{0B}} \frac{\partial\phi}{\partial t} n_k dS \qquad k = 1..6$$

(i.e. forces for k=1,2,3 and moments for k=4,5,6).

Radiation and diffraction problems (F:39-41)
Hp: Linear potential flow theory. Deep water. Regular incoming waves. Steady-state conditions. Zero forward speed.

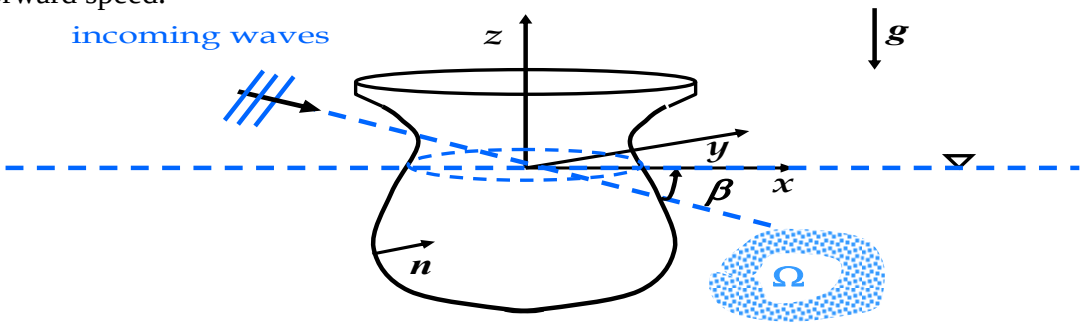

•Incoming waves:
For the incoming-wave velocity potential, we found the solution

$$\phi_0 = (g\zeta_a / \omega)e^{kz}\cos(\omega t - \mathbf{k}\cdot\mathbf{r}) = \Re\left\{\varphi_0(x,y,z)e^{i\omega t}\right\}$$

Here the additional phase was set to zero and we used $\underbrace{\exp(i\alpha)}_{A\in\mathbb{C}} = \underbrace{\cos\alpha}_{=\Re\{A\}} + i\underbrace{\sin\alpha}_{=\Im\{A\}}$.

Linearity+ steady state conditions → $\phi(x,y,z,t) = \Re\left\{\varphi(x,y,z)e^{i\omega t}\right\}$
→ the problem can be solved in φ as we have discussed previously [analysis in frequency domain]

Linearity → the superposition principle is valid and the potential can be decomposed in terms of the fundamental physical effects involved in the fluid-body interaction

Linear hydrodynamic loads

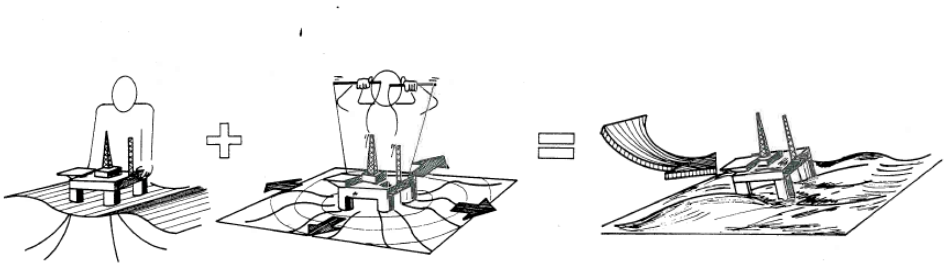

Excitation loads

Added mass
Damping
Hydrostatic restoring

Linear wave-induced motions, accelerations and structural loads

In this way the problem is split in two sub-problems:

• **Diffraction problem ("problem A" in F)**
Hp: the body is assumed fixed and interacting with incident waves.
The velocity potential is the sum

$$\phi(x,y,z,t) = \underbrace{\phi_0(x,y,z,t)}_{incident\ \ wave} + \underbrace{\phi_D(x,y,z,t)}_{diffraction}$$

NB: ϕ_D is alternatively indicated as ϕ_7.
Also another convention is widely used (Newman pg. 288):

$$\phi(x,y,z,t) = \underbrace{\underbrace{\phi_0(x,y,z,t)}_{incident\ \ wave} + \underbrace{\phi_S(x,y,z,t)}_{scattering}}_{diffraction}$$

The spatial potential satisfies

$$\frac{\partial(\varphi_o + \varphi_D)}{\partial n} = 0 \qquad \forall \mathbf{P} \in S_{0B}$$

Splitting the problem in the problems of the two potentials:

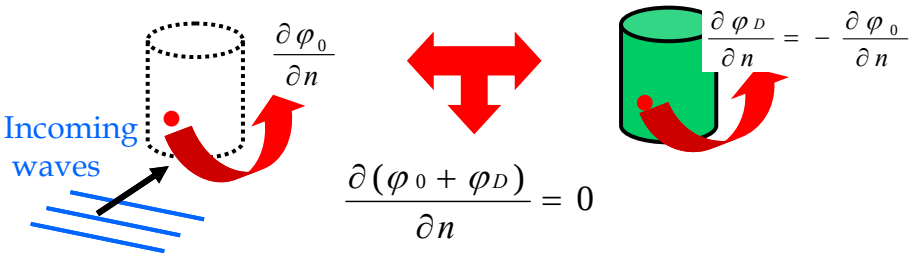

The flow due to φ_0 penetrates the body with normal velocity $\partial\varphi_0/\partial n$, i.e. like the body was not there. φ_D satisfies a problem where the body oscillates in the opposite way to the incident waves, i.e. as an elastic body with normal velocity $-\partial\varphi_0/\partial n$.
This causes hydrodynamic loads on the body called
wave excitation loads= Froude_Kriloff loads + diffraction loads:

$$F_{exc,k}(t) = \underbrace{-\int_{S_{0B}} \rho \frac{\partial \phi_0}{\partial t} n_k dS}_{Froude-Kriloff\ \ loads} \underbrace{-\int_{S_{0B}} \rho \frac{\partial \phi_D}{\partial t} n_k dS}_{diffraction\ \ loads} = \Re\left\{ \int_{S_{0B}} -i\omega e^{i\omega t} \rho(\varphi_0 + \varphi_D) n_k dS \right\} = \zeta_a \Re\{X_k(\omega,\beta)\}, k = 1..6$$

$|X_k(\omega,\beta)| = |F_{exc,k}| / \zeta_a$ is the transfer function for the excitation loads for a wave with frequency ω and direction β, i.e. loads amplitude per unit wave amplitude. Once known, it allows to know the magnitude of the loads for any wave amplitude (within linear theory).

- **Radiation problem ("problem B" in F)**

Hp: the body is forced to oscillate in its 6 degrees of freedom with frequency ω. No incident waves.

$$\eta_j(t) = \eta_{ja} \cos(\omega t) = \Re\{\eta_{ja} e^{i\omega t}\}$$

j=1..6: surge, sway, heave, roll, pitch, yaw, and η_{ja} is the oscillation amplitude in the j-th degree of freedom, as we have already learned.

NB: The motion calculations are made in an inertial reference frame, Earth-fixed or translating if there is forward speed.

Now $\phi(x,y,z,t) = \underbrace{\phi_R(x,y,z,t)}_{radiation}$ and can be split in 6 sub-problems as

$$\phi_R(x,y,z,t) = \Re\left\{ \sum_{j=1}^{6} \underbrace{\dot{\eta}_j}_{velocity\ \ in\ \ mode\ \ j} \underbrace{\varphi_j}_{potential\ \ per\ \ unit\ \ velocity} \right\}$$

φ_j is the velocity potential for the body oscillating with unitary speed in the j-th mode. It satisfies

$$\frac{\partial \varphi_j}{\partial n} = n_j \qquad \forall \mathbf{P} \in S_{0B}$$

with n_j the j-th component of the generalized normal vector.

The moving body generates waves (radiated waves) and so is subjected to hydrodynamic loads identified as added-mass, damping, and restoring terms:

$$F_{rad,k}(t) = -\int_{S_{0B}} \rho \frac{\partial \phi_R}{\partial t} n_k dS \qquad k = 1..6$$

$$= \sum_{j=1}^{6} \left\{ -A_{kj}\ddot{\eta}_j - B_{kj}\dot{\eta}_j \right\}, k = 1..6$$

with $A_{kj}(\omega) = \Re\left[\rho \int_{S_{0B}} \varphi_j n_k dS \right]$ and $B_{kj}(\omega) = -\omega \Im\left[\rho \int_{S_{0B}} \varphi_j n_k dS \right]$

Here the upper dots mean time derivatives.

$A_{kj}(\omega) \in \Re$ = **added-mass terms** → load contribution in phase with acceleration
$B_{kj}(\omega) \in \Re$ = **damping terms** → load contribution in phase with velocity

NB: We will analyse them more in detail later.

Radiation & Diffraction link: Haskind relations (v. Newman 1977)

$$\int_{S_{0B}} \varphi_D \underbrace{\frac{\partial \varphi_k}{\partial n}}_{=n_k} dS = \int_{S_{0B}} \varphi_k \underbrace{\frac{\partial \varphi_D}{\partial n}}_{=-\partial \phi_{0/\partial n}} dS \quad \text{(H)}$$

As a result of the Haskind relations, the excitation loads can be written in terms of φ_0 and φ_k (k=1,..6):

$$\Rightarrow F_{exc,k}(t) = \Re\left\{ \int_{S_{0B}} -i\omega e^{i\omega t} \rho (\varphi_0 + \varphi_D) n_k dS \right\} = \Re\left\{ \int_{S_{0B}} -i\omega e^{i\omega t} \rho \left(\varphi_0 \frac{\partial \varphi_k}{\partial n} - \varphi_k \frac{\partial \varphi_0}{\partial n} \right) dS \right\}$$

These two formulas are then alternative and in the second one, to estimate the diffraction loads one must know the incident waves and solve the radiation problem. It can be useful for check of the loads estimates.

NB: The second formula is useful when to find φ_k is easier than to find φ_D. For instance when for the radiation problem you can use the strip theory but not for the diffraction problem. If we want the pressure then we need to find φ_D.

Strip theory
It is very useful to estimate loads (motions) both for ships and elongated parts of ocean structures.
Basic Hp: The body is 'slender', i.e. elongated.

The body is split in strips dx along x. The loads are estimated for each strip and then integrated along x to provide the 3D loads.

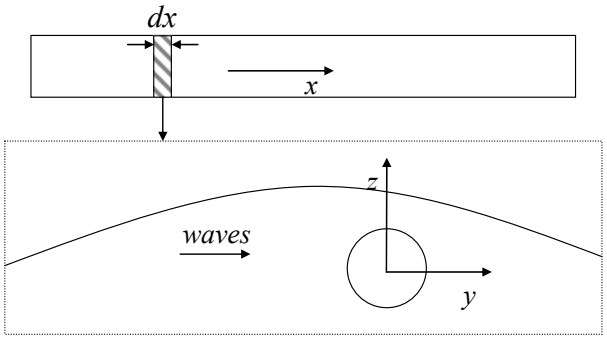

For the radiation problem: Strip theory can be justified for the zero-speed problem when the frequency of oscillation corresponds to a wavelength which is the order of the cross-sectional dimension in (*y,z*) plane, because in this case the flow variations occur mostly in the *(y,z)* plane→ the 3D problem can be approximated as the sum of 2D problems.
A strip theory cannot be rationally justified at forward speed as well as for longer wavelengths than mentioned above. However, the theory can give very satisfactory results and the difference between more theoretically correct and much more complicated linear theories are generally secondary.
For the diffraction problem: We cannot theoretically justify a strip theory for the same frequency range as we can for the radiation problem, i.e. for wave lengths comparable with the cross-sectional dimension. However, this frequency range is not of primary importance in the seakeeping problem, i.e. the motions and accelerations are small. We can instead handle the diffraction problem with wavelengths large relative to the cross-section in (*z,y*) plane by considering a fictitious "forced" motion against the incident wave motion in combination with strip theory →the 3D hydrodynamic problem can be approximated as the sum of 2D problems. In addition, it comes the Froude-Kriloff loads.

Long-wave approximation (F:60-62)
The excitation loads have a particular form in the case of long-wave approximation, or better small-volume structure approximation, which is of practical relevance in many circumstances.

Hp: Long waves: in case of an equivalent circular cylinder it means $\lambda >> D$ → $k << 1/D$
The waves propagate along *x* and the characteristic length *D* is in the plane *(x,y)*.

How much does it mean $\lambda >> D$?

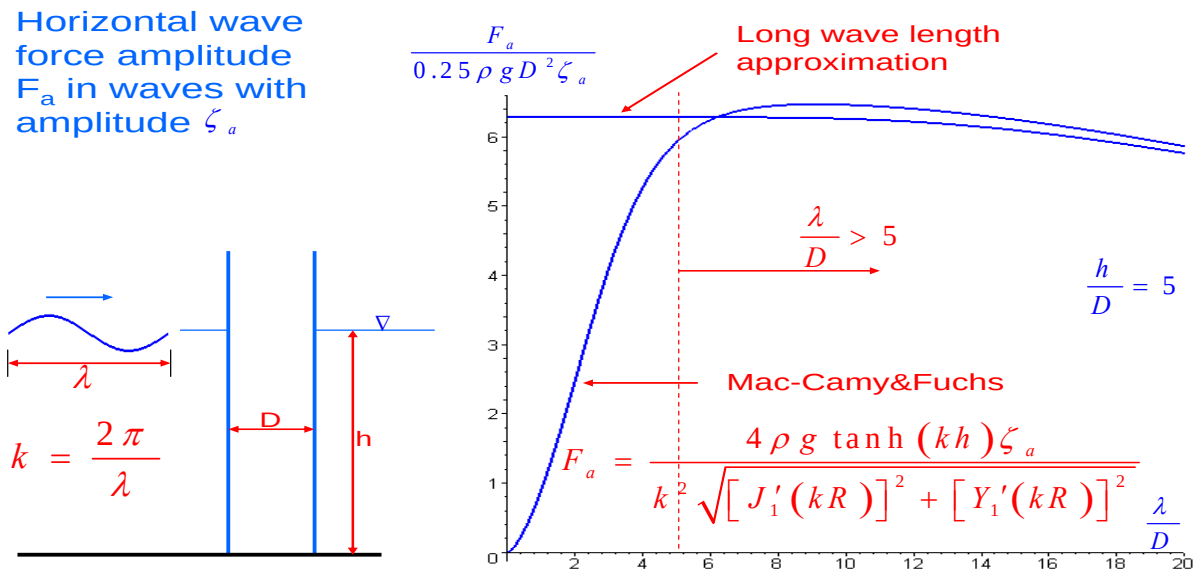

The figure above confirms that the long-wave approximation is good for $\lambda>5D$. For $\lambda<5D$ wave diffraction is important.

Example: 2D body in (y,z) plane with area $A=\Delta y(z_t-z_b)$. Long waves in y direction.

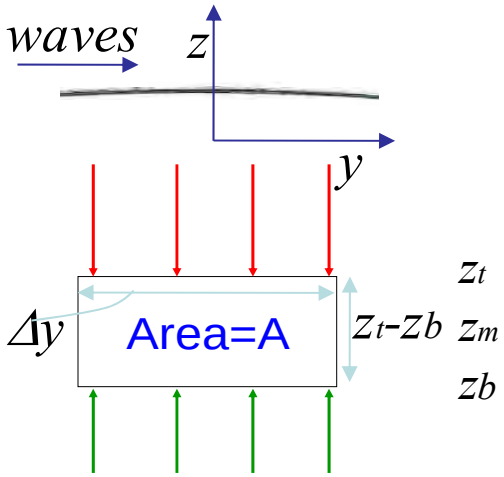

The vertical Froude-Kriloff force is

$$F_{FK,3}(t)=\int p_0 n_3 dl=-\int_t p_0 dl+\int_b p_0 dl=-\rho g\zeta\exp(kz_t)\Delta y+\rho g\zeta\exp(kz_b)\Delta y$$

$$\cong \underbrace{-\overbrace{gk}^{\omega^2}\zeta\exp(kz_m)}_{wave-vertical-acceleration}\ \rho\underbrace{\Delta y(z_t-z_b)}_{Area}=a_{03}(z_m)\rho A$$

$$=\bar{a}_{03}\rho A$$

Here a Taylor expansion around z_m has been used:

$$\exp(kz_t)\cong\exp(kz_m)+k\exp(kz_m)(z_t-z_m)$$

$$\exp(kz_b)\cong\exp(kz_m)+k\exp(kz_m)(z_b-z_m)$$

So the force is given by the incident-wave vertical acceleration at the geometrical center of the cross-section multiplied by the mass of water displaced by the boy.

NB: In the example the body is surrounded by water in the directions where FK force is estimated. These results cannot be used in the direction where this is not true, e.g. if the body is surface piercing or fixed to the sea floor.
If a 3D body is small and fully submerged the Froude-Kriloff forces can be approximated as

$$F_{FK,k}(t)=\bar{a}_{0k}\rho V \qquad k=1..3$$

with V the body volume.

For the incident waves the body is transparent, i.e. permeable. So in our 2D example:

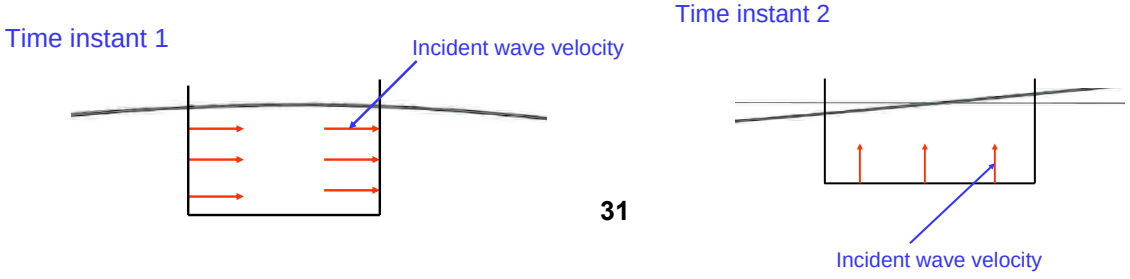

This means the wave-body interaction must generate a flow opposite to the incident wave motion to ensure the impermeability:

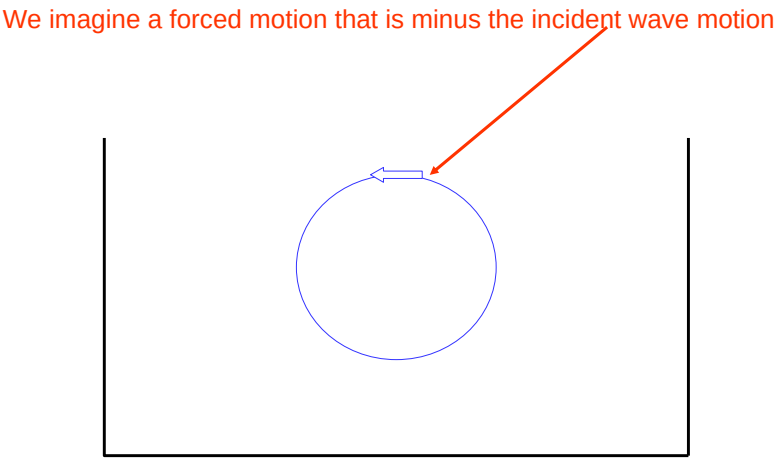

This causes the diffraction loads, as radiation loads due to the forced motion opposite to the incident waves to stop the flux across the body boundary. So they are associated with added-mass and damping terms respectively in phase with the opposite of the wave acceleration and with the opposite of the wave velocity.
Using the assumption $\lambda >> D$, for our 2D example we have:

$$F_{D,2}(t) = -A_{22}(-\bar{a}_{02}) - B_{22}(-\bar{u}_{02})$$
$$F_{D,3}(t) = -A_{33}(-\bar{a}_{03}) - B_{33}(-\bar{u}_{03})$$

NB: In the diffraction problem the body DOES NOT move: incident-waves plus diffraction flow give zero velocity at the body surface.

NB: Here we have velocity and acceleration opposite to those of the incident waves.
In the radiation problem they are the body velocity and acceleration.

The general expression for diffractions forces in long-wave approximation is

$$F_{D,k}(t) = \sum_{j=1}^{3}\left(\bar{a}_{0j}A_{kj} + \bar{u}_{0j}B_{kj}\right) \qquad k = 1..3$$

This shows in another way the link existing between the radiation and diffraction problems.

Another consequence of the long-wave approximation (small ω), is that the generated waves are small → the damping coefficients are small relative to the terms proportional to the acceleration, i.e.

So for small-volume structure the excitation forces can be expressed in general as

$$F_{exc,k}(t) \cong \int_S p_0 n_k dS + \sum_{j=1}^{3}\bar{a}_{0j}A_{kj} \qquad k = 1..3 \quad \text{(F:3.36)}$$

with the normal vector $\boldsymbol{n} = (n_1, n_2, n_3)$ pointing inside the body.

NB: Long-wave approximation means $\omega \to 0$ however in general is not good to estimate A_{kj} at $\omega=0$ because they may diverge. For example, A_{33} is infinite at $\omega=0$ for 2D surface-piercing bodies in deep water.

NB: If the body is elongated in one direction, in that direction the long-wave approximation is not valid but it might be valid to find the load components in other directions and then use a strip theory approach to find the 3D loads.

Examples:

1. For semisubmersible the length of the pontoons, say along *x*, is large but their cross-section, say in (*y,z*) plane, is small relative to incident waves of practical interest.
In this case, we can combine strip-theory and long-wave approximation. For instance for the force in *z* we have:

$$F_{D,3}(t) \cong \sum_{j=1}^{3} \int_x \bar{a}_{0j}(x,t) A_{3j}^{(2D)} dx$$

with $\bar{a}_{0j}$ estimated at the geometrical center of the cross-section and $A_{3j}^{(2D)}$ the 2D added-mass of the cross-section.

2. Vertical fixed circular cylinder in finite water (F:58-60).
Hp: Regular linear incident waves

$$\phi_0(x,z,t) = \frac{g\zeta_a}{\omega} \underbrace{\frac{\cosh(k(z+h))}{\cosh(kh)}}_{f(z)} \cos(\omega t - kx)$$

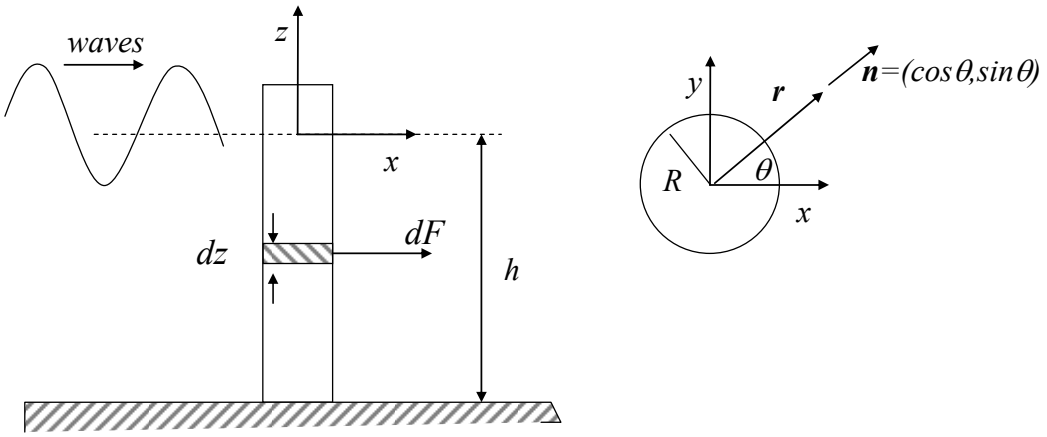

Fixed body → no radiation waves.
The Froude-Kriloff force is:

$$F_{FK,1}(t) = -\int_{S_{0B}} p_0 n_1 dS = \int_{S_{0B}} \rho \frac{\partial \phi_0}{\partial t} n_1 dS = -\int_{-h}^{0} \int_{0}^{2\pi} \rho g \zeta_a f(z) \sin(\omega t - kx) \cos(\vartheta) R d\vartheta dz$$

but for long waves: $kx << 1$ within the body cross-section

$$\rightarrow \quad \sin(\omega t - kx) = \sin \omega t \underbrace{\cos kx}_{\approx 1} - \cos \omega t \underbrace{\sin kx}_{\approx kx = kR\cos\theta}$$

so

$$F_{FK,1}(t) \cong \rho \pi R^2 \int_{-h}^{0} \underbrace{g\zeta_a k f(z) \cos(\omega t)}_{\bar{a}_{01}(z)} dz = \rho A \int_{-h}^{0} \bar{a}_{01}(z) dz$$

$\bar{a}_{01}(z)$ is the horizontal incident-wave acceleration in the center of the cross-section of the strip *z,* i.e

$$\bar{a}_{01}(z) = \frac{\partial}{\partial t}\left(\frac{\partial \phi_0}{\partial x}\right)_{x=0}(z).$$

The same approach could not be used for the vertical force because the cylinder is elongated, surface piercing and lays on the sea floor.

Added-mass and damping coefficients (F:41-45)

A_{kj} and B_{kj} =f(body geometry,
frequency,
vicinity of free surface,
water depth,
water confinement,
forward speed U)

Here we discuss some of them.

NB: A_{kj} does NOT represents a finite 'accelerated' mass added to the body mass, for some components the dimensions are not even those of a mass. In an inviscid fluid, the body oscillations cause instantaneously a disturbance everywhere in the fluid but with different intensity.

Example:
Asymptotic value for $\omega \to \infty$ and deep water for added mass and damping in heave of a half circle
Hp: $\eta_3 = \eta_{3a}\sin(\omega t)$ $\quad \phi_3 = \Re\{\dot{\eta}_3 \varphi_3\}$

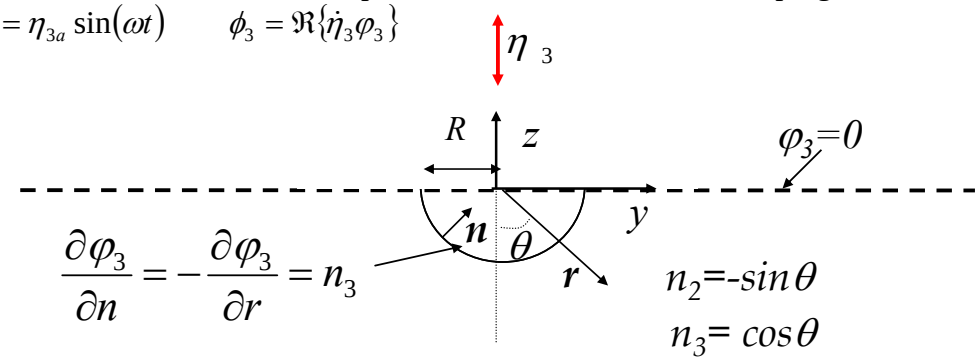

We want to find

$$A_{33} = \Re\left[\rho \int_{S_{0B}} \varphi_3 n_3 dS\right] \qquad B_{33} = -\omega\Im\left[\rho \int_{S_{0B}} \varphi_3 n_3 dS\right] \quad \text{(J)}$$

So we need to find φ_3. You can verify using polar coordinates that the solution is

$$\varphi_3 = \frac{R^2}{r}\cos\vartheta \Rightarrow \phi_3 = \frac{R^2}{r}\cos\vartheta\dot{\eta}_3$$

and tells that the fluid everywhere reacts instantaneously to the motion but with intensity reducing as *1/r* far from the body.

NB: You can verify the solution by substituting in the Laplace eq. and boundary conditions. Hint: use polar coordinates

The pressure is $p = -\rho \partial \phi_3 / \partial t = -\rho R^2 / r \cos\vartheta \ddot{\eta}_3$

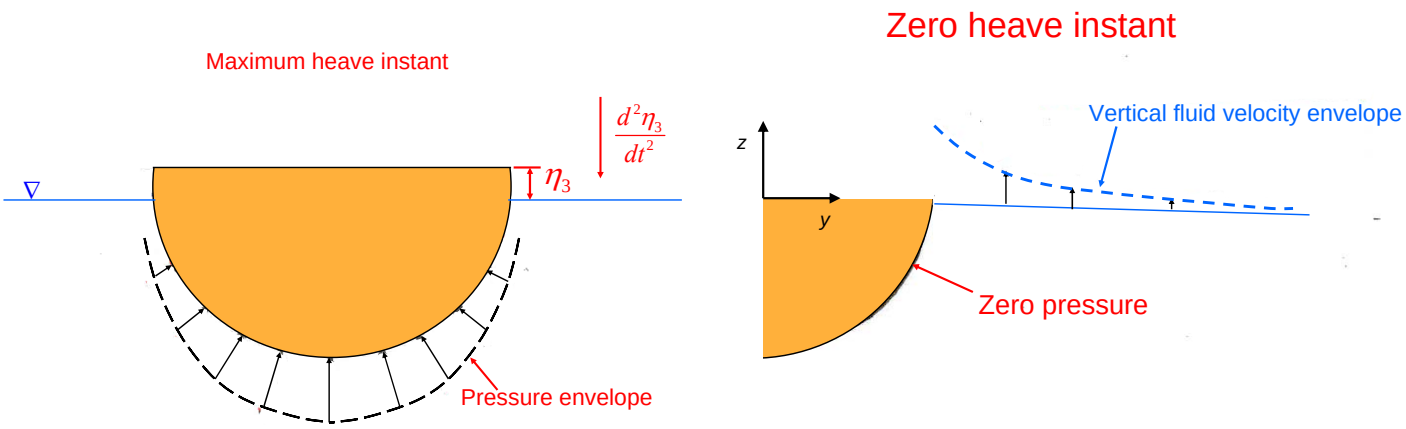

NB: Because $\phi_3 = 0$ on $z=0$, it means that is constant, i.e. $v=0$ and $w \neq 0$ → No radiated waves.
The problem is equivalent to a circle in infinite fluid.

$$A_{33} = \Re\left[\rho \int_{-\pi/2}^{\pi/2} \frac{R^2}{R} \cos\vartheta \cos\vartheta \underbrace{R d\vartheta}_{ds}\right] = \rho R^2 \frac{\pi}{2} = \frac{1}{2}\rho A$$

$$B_{33} = -\omega \Im\left[\rho \int_{-\pi/2}^{\pi/2} R^2 (\cos\vartheta)^2 d\vartheta\right] = 0$$

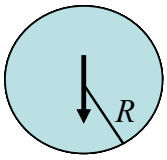

- B_{33} is zero because it is connected with the square power of the radiated waves (as we will see), which are zero.
- A_{33} corresponds to half of the value for a circle in infinite fluid (see Newman 1977) because we integrated in the half-circle.

Added-mass importance

The added-mass is relevant in reducing the body acceleration. We see this through an example.
Hp: A spherical air bubble immersed in infinite water is released at t=0. Bubble: volume=V, density= $\rho_0 = 1.21 kg/m^3$, water: density= $\rho = 998.2 kg/m^3$.

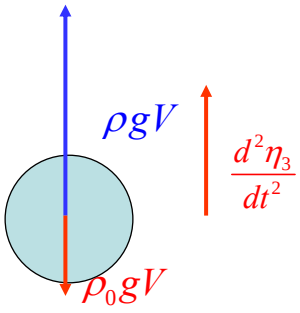

Once released, due to geometrical and load symmetry, the bubble starts to move along the vertical direction and upwards being its buoyancy $\rho g V$ much greater than its weight $\rho_0 g V$. If we consider only these forces, from the motion equation

$$\rho_0 V \ddot{\eta}_3 = (\rho - \rho_0) g V \Rightarrow \ddot{\eta}_3 = \frac{\rho - \rho_0}{\rho_0} g \approx 800 g$$

This acceleration is clearly unphysical. In reality, as we have seen for the half circular cylinder, the bubble motion causes a disturbance in the water. As a result a force is induced proportional but opposite to the body acceleration (at *t=0* the body velocity is zero so we can not have a damping effect initially):

$$F_3 = -A_{33}\ddot{\eta}_3 = -0.5\rho V\ddot{\eta}_3 .$$

The motion equation then gives

$$(\rho_0 V + 0.5\rho V)\ddot{\eta}_3 = (\rho - \rho_0)gV \Rightarrow \ddot{\eta}_3 = \frac{\rho - \rho_0}{\rho_0 + 0.5\rho} g \approx 2g$$

which is a more realistic acceleration.

Damping meaning: energy relations (F:45-49)

The damping coefficients are connected with the wave energy radiated from the body and so to the square power of the amplitude of the generated waves. We show this with an example.

Forced oscillatory heave with frequency ω and no coupling among the motions:

Hp: 2D symmetric body. No incident waves. Deep water dispersion relationship.

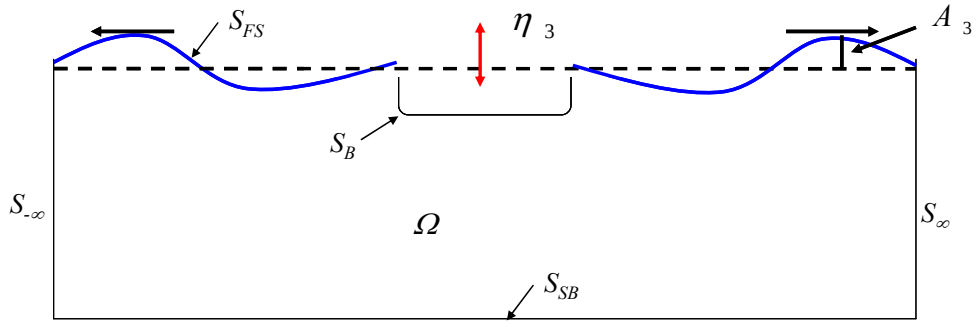

The motion is assumed as

$$\eta_3 = \eta_{3a}\cos(\omega t)$$

The energy inside the control volume Ω is periodic with period $T = 2\pi/\omega$

→ The rate of change of the energy in one period must be zero

→ The energy entering Ω in one period across S_B, due to the work done by the body, equals the energy leaving Ω in one period across $S_{FS} + S_{SB} + S_{-\infty} + S_\infty$.

The energy entering Ω in one period from the body:

$$E_B = \int_0^T \underbrace{F_3\dot{\eta}_3}_{power} dt$$

with the force obtained from the 1-dof equation for the heave motion

$$(m + A_{33})\ddot{\eta}_3 + B_{33}\dot{\eta}_3 + C_{33}\eta = F_3 \qquad (1)$$

involving the mass, added-mass, damping and restoring (like spring term).

It means

$$E_B = \omega^3 \eta_{3a}{}^2 (m + A_{33}) \underbrace{\int_0^T \cos(\omega t)\sin(\omega t)dt}_{=0} + \omega^2 \eta_{3a}{}^2 B_{33} \underbrace{\int_0^T [\sin(\omega t)]^2 dt}_{=T/2} - \omega \eta_{3a}{}^2 C_{33} \underbrace{\int_0^T \cos(\omega t)\sin(\omega t)dt}_{=0}$$

$$= B_{33}\omega^2 \eta_{3a}{}^2 \frac{T}{2}$$

The energy leaving Ω in one period across $S_{FS} + S_{SB} + S_{-\infty} + S_{\infty}$:

$S_{FS} + S_{SB}$: Fluid particles on such surfaces remain on them → Zero energy flux across them

$S_{-\infty} + S_{\infty}$: They are control surfaces → there is energy flux across them, with the same amount due to symmetry.

Across S_{∞} :

The energy leaving in one period is $\left(\frac{E_w}{\lambda} c_g T\right)_{S_{\infty}} = \frac{\rho g A_3^2}{2} \frac{1}{2} \frac{g}{\omega} T = \frac{\rho g^2 A_3^2}{4\omega} T$

with A_3 the amplitude of radiated waves due to the heave motion.

Then enforcing $E_B = \left(\frac{E_w}{\lambda} c_g T\right)_{S_{-\infty}+S_{\infty}}$

$$\Rightarrow B_{33} = \frac{\rho g^2}{\omega^3}\left(\frac{A_3}{\eta_{3a}}\right)^2 \qquad \text{(F:3.26)}$$

This proves that the damping coefficient is directly linked to the amplitude of waves generated by the body, so we see why for the previous asymptotic case ($\omega \to \infty$), i.e. without generated waves, B_{33} was zero.

Can A_{ij} and B_{ij} be negative?

From expression (3.26F) we see that the wave-induced (linear) damping B_{jj} can not be negative, while the added mass A_{jj} can be negative for certain frequencies and body shapes, e.g. for a catamaran. The cross-coupling terms can be negative.

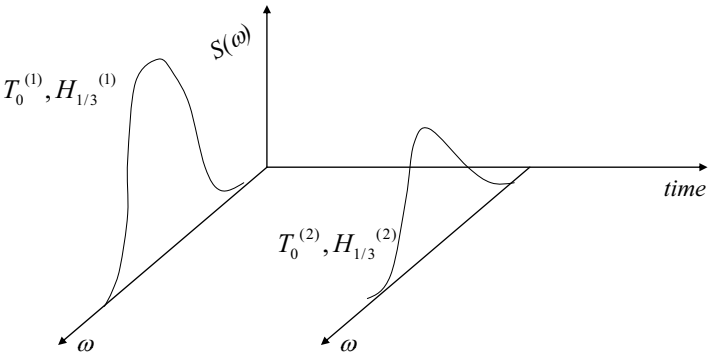

Table 2.2. *Joint frequency of significant wave height and spectral peak period. Representative data for the northern North Sea*

Significant wave height (m) (upper limit of interval)	Spectral peak period (s)																		
	3	4	5	6	7	8	9	10	11	12	13	14	15	16	17	18	19	21	22	Sum
1	59	403	1061	1569	1634	1362	982	643	395	232	132	74	41	22	12	7	4	2	2	8636
2	9	212	1233	3223	5106	5814	5284	4102	2846	1821	1098	634	355	194	105	56	30	16	17	32 155
3	0	8	146	831	2295	3896	4707	4456	3531	2452	1543	901	497	263	135	67	33	16	15	25 792
4	0	0	6	85	481	1371	2406	2960	2796	2163	1437	849	458	231	110	50	22	10	7	15 442
5	0	0	0	4	57	315	898	1564	1879	1696	1228	748	398	191	84	35	13	5	3	9118
6	0	0	0	0	3	39	207	571	950	1069	885	575	309	142	58	21	7	2	1	4839
7	0	0	0	0	0	2	27	136	347	528	533	387	217	98	37	12	4	1	0	2329
8	0	0	0	0	0	0	2	20	88	197	261	226	138	64	23	7	2	0	0	1028
9	0	0	0	0	0	0	0	2	15	54	101	111	78	39	14	4	1	0	0	419
10	0	0	0	0	0	0	0	0	2	11	30	45	39	22	8	2	1	0	0	160
11	0	0	0	0	0	0	0	0	0	2	7	15	16	11	5	1	0	0	0	57
12	0	0	0	0	0	0	0	0	0	0	1	4	6	5	2	1	0	0	0	19
13	0	0	0	0	0	0	0	0	0	0	0	1	2	2	1	0	0	0	0	6
14	0	0	0	0	0	0	0	0	0	0	0	0	0	1	0	0	0	0	0	1
15	0	0	0	0	0	0	0	0	0	0	0	0	0	0	0	0	0	0	0	0
Sum	68	623	2446	5712	9576	12 799	14 513	14 454	12 849	10 225	7256	4570	2554	1285	594	263	117	52	45	100 001

Table 2.2. *Joint frequency of significant wave height and spectral peak period. Representative data for the northern North Sea*

Significant wave height (m) (upper limit of interval)	Spectral peak period (s)																		
	3	4	5	6	7	8	9	10	11	12	13	14	15	16	17	18	19	21	22	Sum
1	59	403	1061	1569	1634	1362	982	643	395	232	132	74	41	22	12	7	4	2	2	8636
2	9	212	1233	3223	5106	5814	5284	4102	2846	1821	1098	634	355	194	105	56	30	16	17	32 155
3	0	8	146	831	2295	3896	4707	4456	3531	2452	1543	901	497	263	135	67	33	16	15	25 792
4	0	0	6	85	481	1371	2406	2960	2796	2163	1437	849	458	231	110	50	22	10	7	15 442
5	0	0	0	4	57	315	898	1564	1879	1696	1228	748	398	191	84	35	13	5	3	9118
6	0	0	0	0	3	39	207	571	950	1069	885	575	309	142	58	21	7	2	1	4839
7	0	0	0	0	0	2	27	136	347	528	533	387	217	98	37	12	4	1	0	2329
8	0	0	0	0	0	0	2	20	88	197	261	226	138	64	23	7	2	0	0	1028
9	0	0	0	0	0	0	0	2	15	54	101	111	78	39	14	4	1	0	0	419
10	0	0	0	0	0	0	0	0	2	11	30	45	39	22	8	2	1	0	0	160
11	0	0	0	0	0	0	0	0	0	2	7	15	16	11	5	1	0	0	0	57
12	0	0	0	0	0	0	0	0	0	0	1	4	6	5	2	1	0	0	0	19
13	0	0	0	0	0	0	0	0	0	0	0	1	2	2	1	0	0	0	0	6
14	0	0	0	0	0	0	0	0	0	0	0	0	0	1	0	0	0	0	0	1
15	0	0	0	0	0	0	0	0	0	0	0	0	0	0	0	0	0	0	0	0
Sum	68	623	2446	5712	9576	12 799	14 513	14 454	12 849	10 225	7256	4570	2554	1285	594	263	117	52	45	100 001

Table 2.2. *Joint frequency of significant wave height and spectral peak period. Representative data for the northern North Sea*

Significant wave height (m) (upper limit of interval)	Spectral peak period (s)																		
	3	4	5	6	7	8	9	10	11	12	13	14	15	16	17	18	19	21	22	Sum
1	59	403	1061	1569	1634	1362	982	643	395	232	132	74	41	22	12	7	4	2	2	8636
2	9	212	1233	3223	5106	5814	5284	4102	2846	1821	1098	634	355	194	105	56	30	16	17	32 155
3	0	8	146	831	2295	3896	4707	4456	3531	2452	1543	901	497	263	135	67	33	16	15	25 792
4	0	0	6	85	481	1371	2406	2960	2796	2163	1437	849	458	231	110	50	22	10	7	15 442
5	0	0	0	4	57	315	898	1564	1879	1696	1228	748	398	191	84	35	13	5	3	9118
6	0	0	0	0	3	39	207	571	950	1069	885	575	309	142	58	21	7	2	1	4839
7	0	0	0	0	0	2	27	136	347	528	533	387	217	98	37	12	4	1	0	2329
8	0	0	0	0	0	0	2	20	88	197	261	226	138	64	23	7	2	0	0	1028
9	0	0	0	0	0	0	0	2	15	54	101	111	78	39	14	4	1	0	0	419
10	0	0	0	0	0	0	0	0	2	11	30	45	39	22	8	2	1	0	0	160
11	0	0	0	0	0	0	0	0	0	2	7	15	16	11	5	1	0	0	0	57
12	0	0	0	0	0	0	0	0	0	0	1	4	6	5	2	1	0	0	0	19
13	0	0	0	0	0	0	0	0	0	0	0	1	2	2	1	0	0	0	0	6
14	0	0	0	0	0	0	0	0	0	0	0	0	0	1	0	0	0	0	0	1
15	0	0	0	0	0	0	0	0	0	0	0	0	0	0	0	0	0	0	0	0
Sum	68	623	2446	5712	9576	12 799	14 513	14 454	12 849	10 225	7256	4570	2554	1285	594	263	117	52	45	100 001

$H_{1/3}<6$

$H_{1/3}>6$

How to calculate available wave power

Regular waves

$$P_w = \frac{\rho g \zeta_a^2}{2} \cdot \frac{g}{2\omega}$$

Wave energy density

Wave energy propagation velocity

Short-term sea state

$$P_w = \frac{\rho g^2}{2} \int_0^\infty \frac{S(\omega)}{\omega} d\omega$$

Wave spectrum

Pierson- Moskowitz spectrum

$$P_w = 0.005535 \rho g^2 H_{1/3}^2 T_1$$

$H_{1/3}$ [m]	T_2 [seconds] → 1	2	3	4	5	6	7	8	9	10	11	12	13	14	15	16	Sum
0.5	0	0	15	70	104	85	50	24	10	4	1	1	0	0	0	0	364
1	0	0	1	17	51	65	49	27	12	5	2	1	0	0	0	0	230
1.5	0	0	0	4	24	44	43	28	13	5	2	1	0	0	0	0	164
2	0	0	0	1	9	24	30	22	12	5	2	1	0	0	0	0	106
2.5	0	0	0	0	3	11	18	16	9	4	1	1	0	0	0	0	63
3	0	0	0	0	1	5	10	10	6	3	1	0	0	0	0	0	36
3.5	0	0	0	0	0	2	5	5	4	2	1	0	0	0	0	0	19
4	0	0	0	0	0	1	2	5	2	1	1	0	0	0	0	0	10
4.5	0	0	0	0	0	0	1	1	1	1	0	0	0	0	0	0	4
5	0	0	0	0	0	0	0	1	1	0	0	0	0	0	0	0	2
5.5	0	0	0	0	0	0	0	0	0	0	0	0	0	0	0	0	0
6	0	0	0	0	0	0	0	0	0	0	0	0	0	0	0	0	0
Sum	0	0	16	92	192	237	208	137	70	30	11	5	0	0	0	0	998

$$p_{ij} = \frac{24}{998} \quad for\ H_{1/3} = 2m, T_2 = 6s$$

$$\overline{P_w} = \sum_i \sum_j P_w(H_{1/3}, T_2)\, p_{ij} = 10.5 kW/m$$

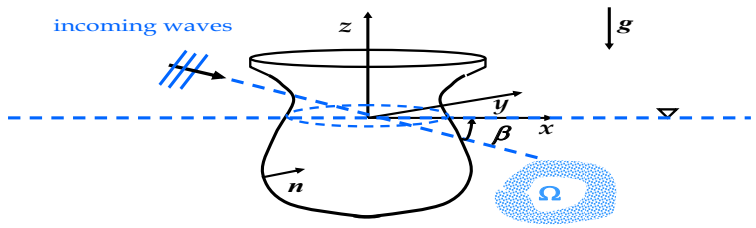

Linear hydrodynamic loads

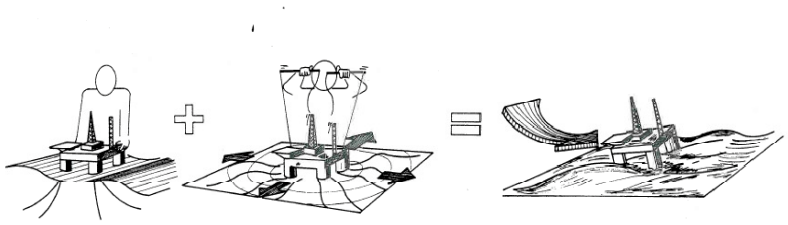

Excitation loads

Added mass
Damping
Hydrostatic restoring

Linear wave-induced motions, accelerations and structural loads

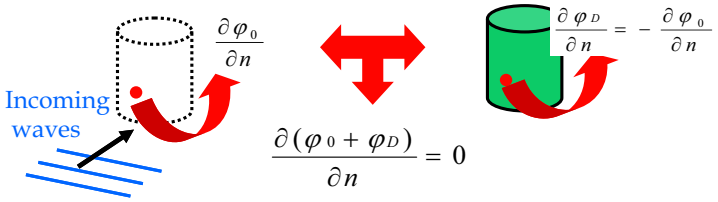

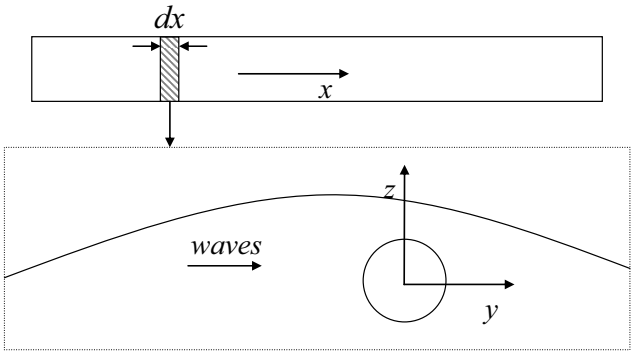

How much does it mean $\lambda >> D$?

Horizontal wave force amplitude F_a in waves with amplitude ζ_a

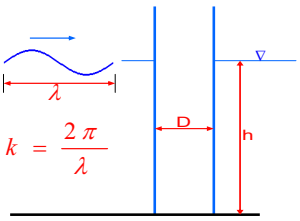

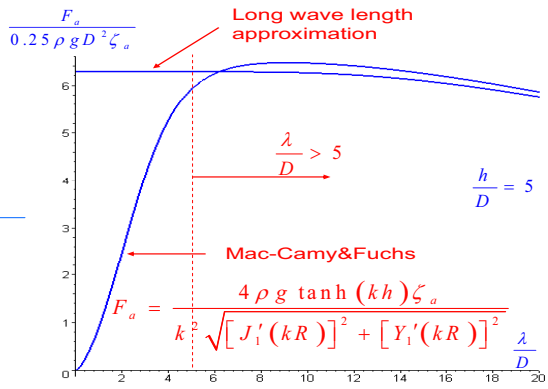

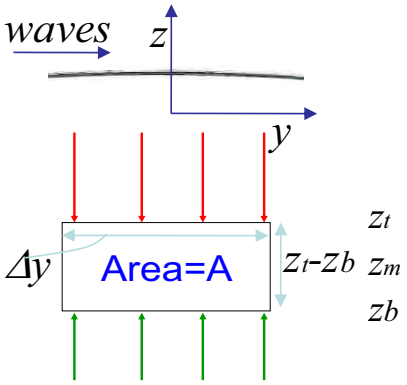

Time instant 1

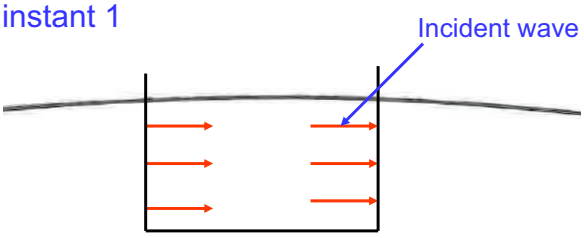

Time instant 2

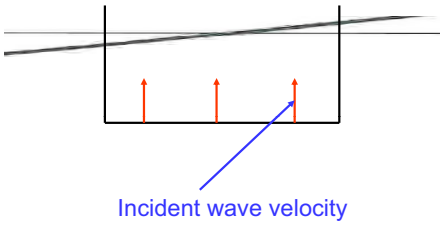

We imagine a forced motion that is minus the incident wave motion

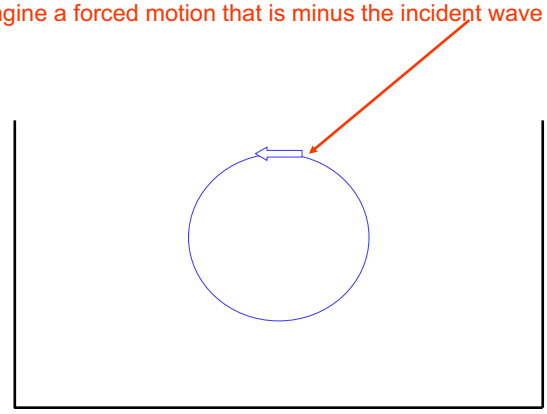

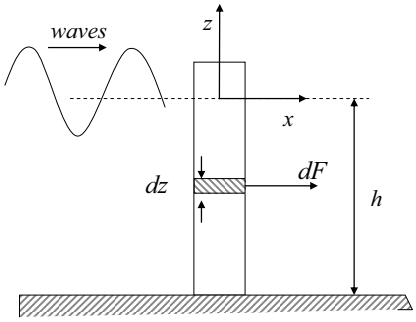

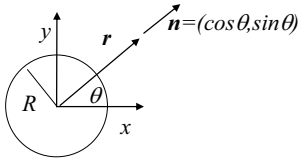

2. Vertical fixed circular cylinder in finite water (F:58-60).
Hp: Regular linear incident waves

$$\phi_0(x,z,t) = \frac{g\zeta_a}{\omega}\underbrace{\frac{\cosh(k(z+h))}{\cosh(kh)}}_{f(z)}\cos(\omega t - kx)$$

Fixed body → no radiation waves.

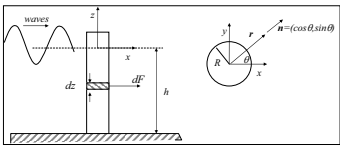

The Froude-Kriloff force is:

$$F_{FK,1}(t) = -\int_{S_{0B}} p_0 n_1 dS = \int_{S_{0B}} \rho\frac{\partial\phi_0}{\partial t} n_1 dS$$

$$= -\int_{-h}^{0}\int_{0}^{2\pi} \rho g\zeta_a f(z)\sin(\omega t - kx)\cos(\vartheta) R d\vartheta dz$$

$$\Rightarrow \sin(\omega t - kx) = \sin\omega t \underbrace{\cos kx}_{\approx 1} - \cos\omega t \underbrace{\sin kx}_{\approx kx = kR\cos\theta}$$

so $$F_{FK,1}(t) \cong \rho\pi R^2 \int_{-h}^{0} \underbrace{g\zeta_a kf(z)\cos(\omega t)}_{\bar{a}_{01}(z)} dz = \rho A \int_{-h}^{0} \bar{a}_{01}(z) dz$$

ρA = mass displaced water in the 2D

$\bar{a}_{01}(z)$ = horizontal incident-wave acceleration in the center of the cross-section of the strip z, i.e

$$\bar{a}_{01}(z) = \frac{\partial}{\partial t}\left(\frac{\partial\phi_0}{\partial x}\right)_{x=0}(z).$$

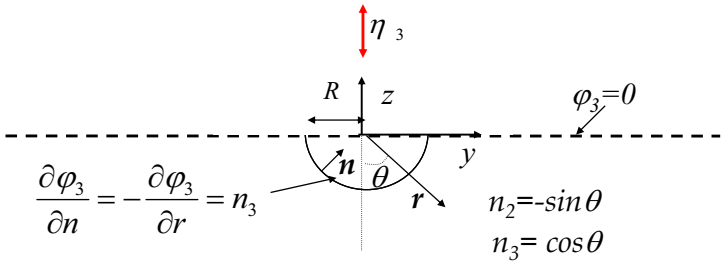

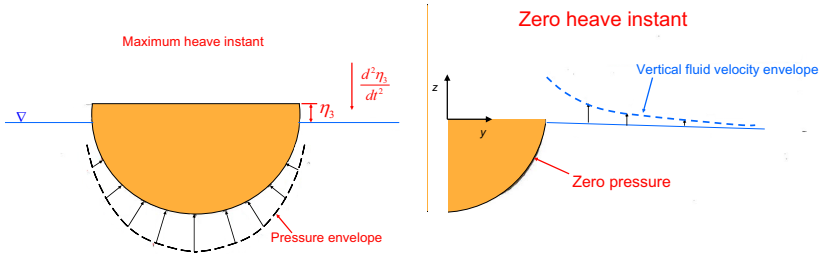

Hp: A spherical air bubble immersed in infinite water is released at t=0.
Bubble: volume=V, density=$\rho_0 = 1.21 kg/m^3$, water: density=$\rho = 998.2 kg/m^3$.

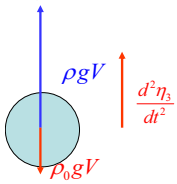

Considering only weight and buoincy

$$\rho_0 V\ddot{\eta}_3 = \underbrace{\rho gV}_{buoyancy} \underbrace{-\rho_0 gV}_{weight} \Rightarrow \ddot{\eta}_3 = \frac{\rho-\rho_0}{\rho_0} g \approx 800g$$

This acceleration is clearly unphysical.

In reality, the bubble motion causes a disturbance in the water. As a result a force is induced proportional but opposite to the body acceleration:

$$F_3 = -A_{33}\ddot{\eta}_3 = -0.5\rho V\ddot{\eta}_3.$$

The motion equation then gives

$$(\rho_0 V + 0.5\rho V)\ddot{\eta}_3 = (\rho-\rho_0)gV \Rightarrow \ddot{\eta}_3 = \frac{\rho-\rho_0}{\rho_0+0.5\rho} g \approx 2g$$

which is a more realistic acceleration.

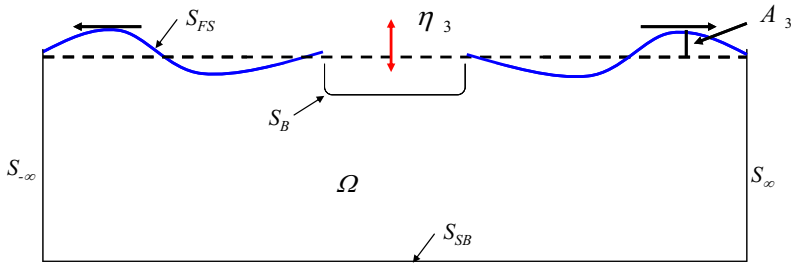

Hp: 2D body. No incident waves. Deep water dispersion relationship.

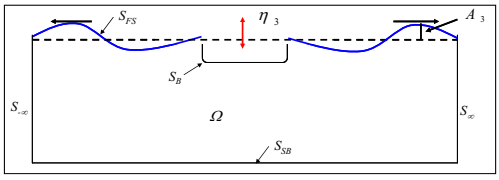

The motion is assumed as $\eta_3 = \eta_{3a}\cos(\omega t)$

•The energy entering Ω in T from the body: $E_B = \int_0^T \underbrace{F_3\dot{\eta}_3}_{power} dt$

with the force from the 1-dof heave motion

$$(m + A_{33})\ddot{\eta}_3 + B_{33}\dot{\eta}_3 + C_{33}\eta = F_3 \qquad (1)$$

It means $E_B = B_{33}\omega^2 {\eta_{3a}}^2 \frac{T}{2}$

• The energy leaving Ω in one period across $S_{FS}+S_{SB}+S_{-\infty}+S_{\infty}$:

$S_{FS}+S_{SB}$: Zero energy flux across them.

$S_{-\infty}+S_{\infty}$: Energy flux across them, identical due to symmetry.

S_{∞} : The energy leaving in T is $\left(\frac{E_w}{\lambda}c_g T\right)_{S_\infty} = \frac{\rho g A_3^2}{2}\frac{1}{2}\frac{g}{\omega}T = \frac{\rho g^2 A_3^2}{4\omega}T$

with A_3 the amplitude of radiated waves due to the heave.

Enforcing $E_B = \left(\frac{E_w}{\lambda}c_g T\right)_{S_{-\infty}+S_\infty}$

$$\Rightarrow B_{33} = \frac{\rho g^2}{\omega^3}\left(\frac{A_3}{\eta_{3a}}\right)^2 \qquad \text{(F:3.26)}$$

Reference Material

<u>On water waves</u>:

"Water Wave Mechanics for Engineers and Scientists"
by *Dean & Dalrymple*

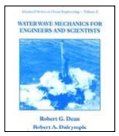

NB: In Sea Loads: $\mathbf{V} = \nabla\phi$
In WaterWave: $\mathbf{V} = -\nabla\phi$

<u>On Fluid Mechanics</u>:

"Fluid Mechanics" by *White*

Lecture Note 3

37. Strip-theory applications. Methods to estimate cross-sectional added mass and damping. Forward speed effects. Restoring loads. Response in regular waves and irregular sea states. (F: 37-39, 49-58, 66-68,262-265)

Added mass and damping using strip theory (F:50-51)
Generally added mass and damping coefficients of 3D bodies must be estimated solving 3D problems. But if

Hp: The body is 'slender', i.e. elongated and ω is large (small λ) → strip theory can be used

In the following, it is implicitly assumed no incident waves when dealing with the radiation problem.

Strip-theory applications: to a ship
Hp: Forced heave and pitch, zero forward speed $U=0$ (F:56)
Objective: find added-mass coefficients→Loads proportional to the body accelerations

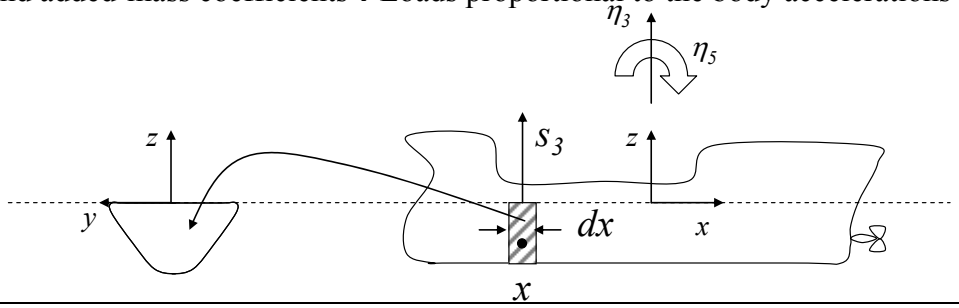

NB: typically 20 strips are considered, assuming that within each of them the ship cross-section is uniform

The local vertical displacement at location x is
$s_3 = \eta_3 + (\boldsymbol{R}\times\boldsymbol{r})_3 = \eta_3 + y\eta_4 - x\eta_5 = \eta_3 - x\eta_5 \Rightarrow \ddot{s}_3 = \ddot{\eta}_3 - x\ddot{\eta}_5$ (F:3.9)

For the strip dx, the heave force is
$$dF_3(x) = \underbrace{-A_{33}^{(2D)}(x)\ddot{s}_3}_{cross-section-solution}\, dx = -\ddot{\eta}_3 A_{33}^{(2D)}(x)dx + \ddot{\eta}_5 x A_{33}^{(2D)}(x)dx$$

Once evaluated $A^{2D}{}_{33}(x)$ we can integrate
$$F_3 = \int_L dF_3(x) = -\ddot{\eta}_3 \underbrace{\int_L A_{33}^{(2D)}(x)dx}_{A_{33}} + \ddot{\eta}_5 \underbrace{\int_L x A_{33}^{(2D)}(x)dx}_{-A_{35}} \underbrace{=}_{radiation\ \ load} - A_{33}\ddot{\eta}_3 - A_{35}\ddot{\eta}_5$$

The pitch moment (generalized force with k=5) can be calculated as torque (moment of force) as

$$dF_5 = (\mathbf{r}\times \underbrace{d\mathbf{F}}_{=(dF_1, dF_2, dF_3)})_2 = z dF_1 - x dF_3 = -x dF_3 = \ddot{\eta}_3 x A_{33}^{(2D)}(x)dx - \ddot{\eta}_5 x^2 A_{33}^{(2D)}(x)dx$$

and integrating
$$F_5 = \int_L dF_5(x) = \ddot{\eta}_3 \underbrace{\int_L x A_{33}^{(2D)}(x)dx}_{-A_{53}} - \ddot{\eta}_5 \underbrace{\int_L x^2 A_{33}^{(2D)}(x)dx}_{A_{55}} \underbrace{=}_{radiation\ \ load} - A_{53}\ddot{\eta}_3 - A_{55}\ddot{\eta}_5$$

Similar approach can be used for the damping coefficients.

In this way the 3D hydrodynamic coefficients are calculated in terms of 2D coefficients. We will discuss later the methods used to estimate the 2D coefficients.

NB: If U=0, added-mass and damping coefficients are symmetric, i.e. $A_{kj}=A_{jk}$ and $B_{kj}=B_{jk}$.

Strip-theory applications: to a deep-draught (D) buoy with circular cross-section
Hp: Forced sway and roll.

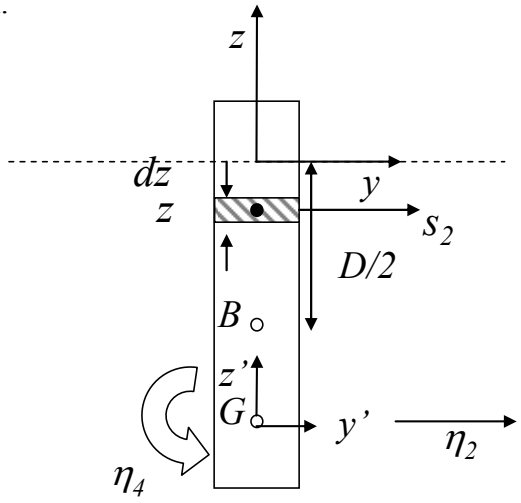

The local lateral displacement at location z is

$$s_2 = \eta_2 + (\boldsymbol{R}\times\boldsymbol{r'})_2 = \eta_2 + x'\eta_3 - z'\eta_4 = \eta_2 - z'\eta_4 \Rightarrow \ddot{s}_2 = \ddot{\eta}_2 - z'\ddot{\eta}_4 \quad \text{(F:3.9)}$$

with $z' = z + D/2 + BG \qquad z = 0 \Leftrightarrow z' = D/2 + BG \qquad z = -D \Leftrightarrow z' = -D/2 + BG$

For the strip $dz=dz'$, by definition the sway force proportional to the acceleration is

$$dF_2(z') = -A_{22}^{(2D)}(z')\ddot{s}_2 dz' = -\ddot{\eta}_2 A_{22}^{(2D)}(z')dz' + \ddot{\eta}_4 z' A_{22}^{(2D)}(z')dz'$$

In this case the 2D added mass is easy to be obtained because the related problem is equivalent to that of a circle in infinite fluid: $A_{22}^{(2D)}(z)=\rho A$, with ρ the water density and A the cross-section area (see example of the half-circle for $\omega\to\infty$).
We can then integrate to get

$$F_2 = \int_{-D/2+BG}^{D/2+BG} dF_2(z') = -\ddot{\eta}_2 \underbrace{\int_{-D/2+BG}^{D/2+BG} A_{22}^{(2D)}(z')dz'}_{A_{22}} + \ddot{\eta}_4 \underbrace{\int_{-D/2+BG}^{D/2+BG} z' A_{22}^{(2D)}(z')dz'}_{-A_{24}}$$

$$\underbrace{=}_{radiation} \underbrace{-A_{22}\ddot{\eta}_2 - A_{24}\ddot{\eta}_4}_{load}$$

The roll moment (generalized force with k=4) can be calculated as torque (moment of force) with respect to G, as

$$dF_4 = (\mathbf{r}'\times \underbrace{d\mathbf{F}}_{=(dF_1,dF_2,dF_3)})_1 = y'dF_3 - z'dF_2 = -z'dF_2 = \ddot{\eta}_2 z' A_{22}(z)^{(2D)}dz - \ddot{\eta}_4 z'^2 A_{22}^{(2D)}(z)dz$$

and integrating

$$F_4 = \int_{-D/2+BG}^{D/2+BG} dF_4(z') = \ddot{\eta}_2 \underbrace{\int_{-D/2+BG}^{D/2+BG} z' A_{22}^{(2D)}(z')dz'}_{-A_{42}} - \ddot{\eta}_4 \underbrace{\int_{-D/2+BG}^{D/2+BG} z'^2 A_{22}^{(2D)}(z')dz'}_{A_{44}}$$

$$\underbrace{=}_{radiation\ \ load} -A_{42}\ddot{\eta}_2 - A_{44}\ddot{\eta}_4$$

Let's see what is the value of the added-mass terms:

$$A_{22} = \int_{-D/2+BG}^{D/2+BG} A_{22}^{(2D)}(z')dz' = \rho AD$$

$$A_{24} = -\int_{-D/2+BG}^{D/2+BG} z' A_{22}^{(2D)}(z')dz' = -\rho A\left[z'^2/2\right]_{-D/2+BG}^{D/2+BG} = -\rho AD \cdot BG = A_{42}$$

$$A_{44} = \int_{-D/2+BG}^{D/2+BG} z'^2 A_{22}^{(2D)}(z')dz' = -\rho A\left[z'^3/3\right]_{-D/2+BG}^{D/2+BG} = \rho A\left[D \cdot BG^2 + D^3/3\right]$$

for A_{44} we used that
$(a+b)^3 - (a-b)^3 = (a^3 + 3a^2b + 3ab^2 + b^3) - (a^3 - 3a^2b + 3ab^2 - b^3) = 6a^2b + 2b^3$
with $a=D/2+BG$ and $b=-D/2+BG$

Similar approach can be used for the damping coefficients.
2D added-mass and damping coefficients are then useful also for practical '3D' cases.

How to estimate the cross-sectional added mass and damping?
There are two main ways used to estimate them, whose simplified description can be:

1) Source technique=it is a numerical method, i.e. it provides an approximated solution, for 2D and 3D problems.
   It uses source (sink) points, which are elementary solutions of the Laplace equation, with unknown strength. They are placed along the boundary *S* and used to express φ_j, so

   → also φ_j satisfies the Laplace equation and

   → only the boundary conditions must be satisfied. This is done in a finite number of points, say *N*, i.e. splitting *S* in *N* parts. This makes available the strengths of the sources and therefore φ_j everywhere in Ω.

   Example in 2D:

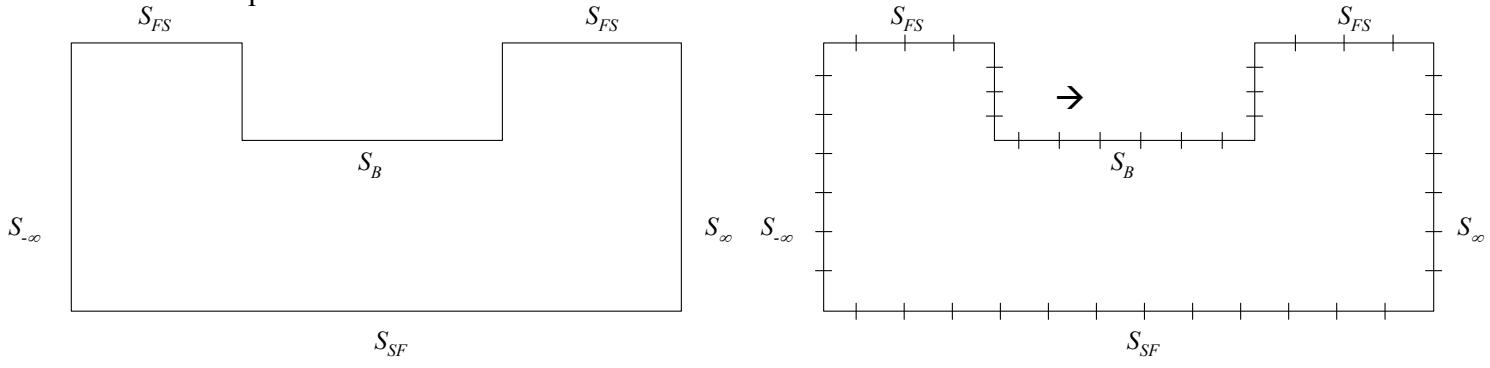

This means that the solution is not exact but has a certain order of accuracy. It is crucial to know the order of accuracy for engineering applications, as well as the rate to which the numerical solution converges to the physical one. Once found φ_j, o the load coefficients can be estimated. There are also other numerical methods, similar to the source technique, which can be applied.

NB: The source technique does not provide any solution for surface-piercing body at certain specific frequencies, called 'irregular frequencies'. This is linked to the method, not to a physical reason. John (1950) found that the smallest irregular frequency satisfies $\omega_{irr} \geq \sqrt{g/D}$, with D the vessel draft. So if the frequency range of interest for the motions of our structure contains only frequencies $\omega < \sqrt{g/D}$, irregular frequencies do not occur. This is typically the case for normal types of seakeeping calculations for ships. The problem of irregular frequencies can be avoided through method modifications.

2) Conformal mapping= it provides an analytical solution and applies to 2D problems. It transforms the cross-sectional geometry through a mapping law in another geometry for which the solution is known analytically. The transformation of such solution back to the plane of the original cross-section provides the physical solution.
Example, Joukowiski transformation from an airfoil to a circle:

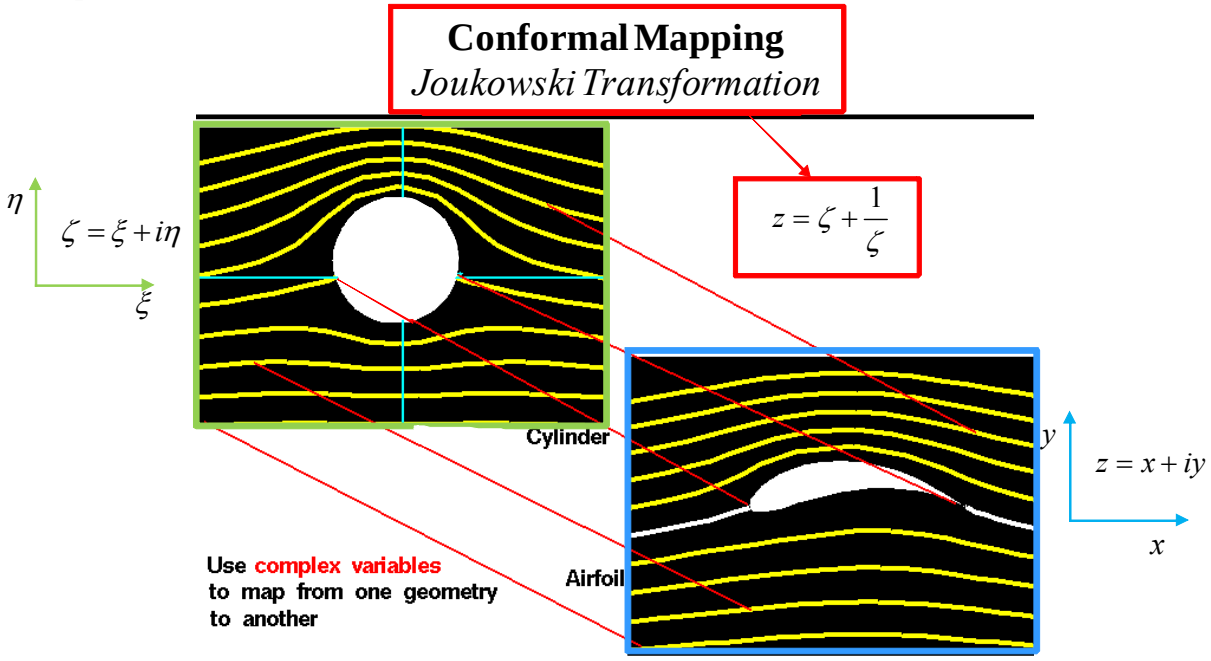

The Lewis-form technique is an approximate conformal mapping technique suitable for conventional ships. It transforms a ship cross-section into a circle. I It considers the beam-to-draft ratio B/D and the sectional area coefficient $\sigma=A/(BD)=C_B$ as the geometrical parameters sufficient to determine the added mass and damping coefficients of the cross-section.

Parameter analysis: influence of ω on A_{ij} and B_{ij} (F:49-50)
Added-mass and damping coefficients depend on the frequency. This can be understood with an example.

Hp: A 2D surface-piercing body forced to oscillate in heave with frequency ω in deep water.

The oscillations cause a perturbation ϕ_3 everywhere in the water and propagating (waves) along the free surface. Far from the body (far field), the waves are not affected explicitly by the body boundary condition but only by the free-surface boundary condition

$$-\omega^2 \phi_3^{FF} + g\frac{\partial \phi_3^{FF}}{\partial z} = 0 \qquad z = 0$$

i.e. they are in the form of the 'incident' regular waves:

$$\phi_3^{FF} = \frac{gA_3^{\pm}(\omega)}{\omega} e^{kz} \cos[\omega t + \varepsilon^{\pm}(\omega)] = \Re\left\{\varphi_3^{FF}(\omega) e^{i\omega t}\right\}$$

with the sign '-' and '+' in the amplitude and phase indicating, respectively, left and right location with respect to the body, and the term with the wave-number multiplied by the horizontal distance from the body is included in the phase.
The generated waves in the far field are implicitly affected by the body boundary condition through their amplitude and phase. These depend on the frequency because, as we learned, ω affects the body capability in generating waves and the wave speed.
If we use then the far-field solution φ_3^{FF} in the added-mass and damping definition as rough approximation,

$$A_{33} \cong \Re\left[\rho \int_{S_{0B}} \varphi_3^{FF}(\omega) n_3 dS\right] \qquad B_{33} \cong -\omega \Im\left[\rho \int_{S_{0B}} \varphi_3^{FF}(\omega) n_3 dS\right]$$

we clearly see that a dependence from ω must exist.
Figure F:3.6 discusses the frequency dependence for a surface-piercing half circle oscillating in heave and sway

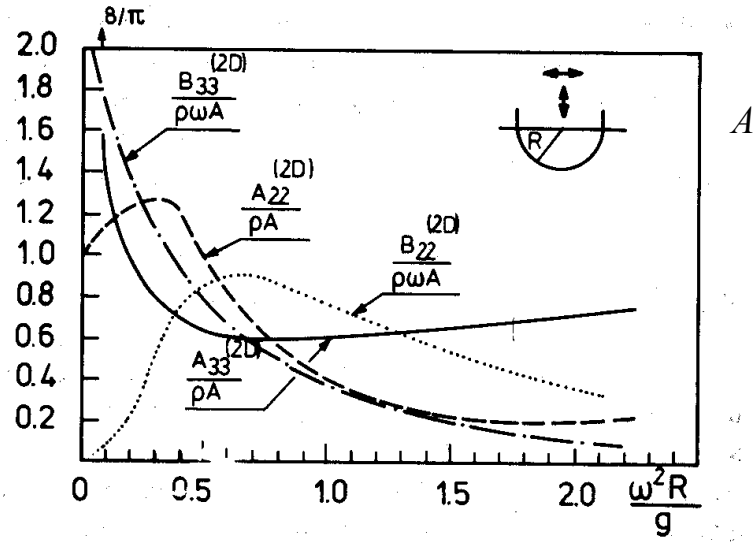

Fig. F:3.6

NB: B_{22} and B_{33} $\to 0$ as $\omega \to 0$ and $\omega \to \infty$ because in these case no waves are generated. A_{33} $\to \infty$ as $\omega \to 0$ and this is true for any 2D surface piercing body in deep water. But as $\omega \to 0$, finite water depth effects and 3D effects become important and make the added mass to be finite in reality.

Parameter analysis: influence of body shape on A_{ij} and B_{ij}

Added-mass and damping coefficients can be significantly affected by the body shape.

Example for the added-mass:

Hp: Forced heave of a surface-piercing rectangular cross-section with width B and draft D for $\omega \to \infty$.

Fig. F:3.8 examines this with Lewis technique to calculate added-mass in heave:

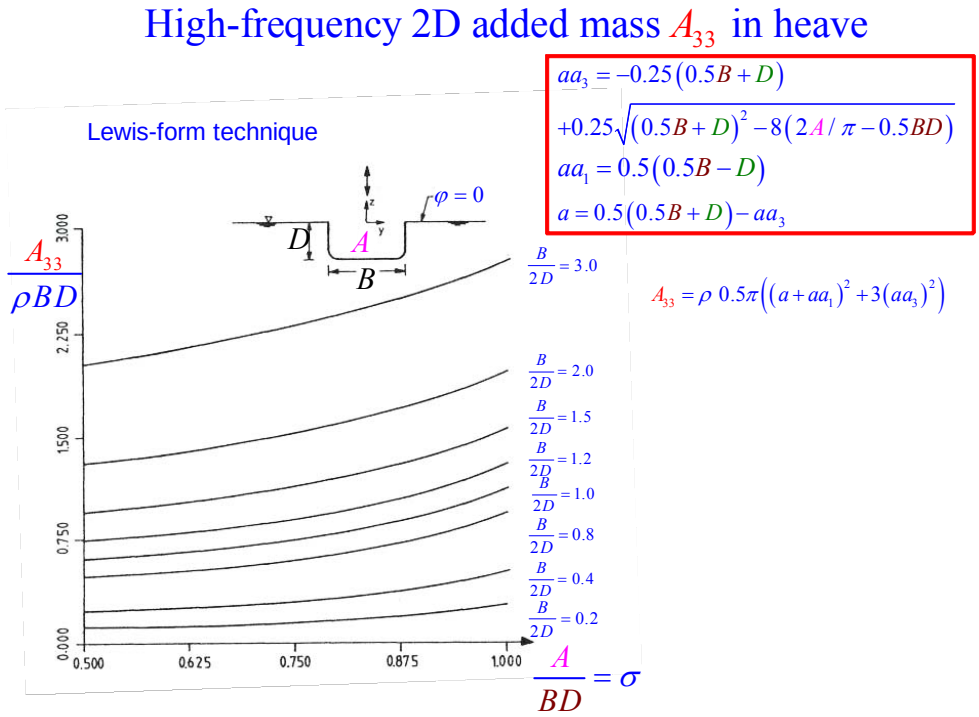

Fig. F:3.8

A_{33} increases as D/B reduces, i.e. as the structural mass in heave direction gets smaller. σ has a limited effect and A_{33} increases with it.

Forward speed effects (F:55-58)

The forward speed U causes an 'encounter' frequency, which means that the ship 'feels' an oscillation frequency different than the incident-wave frequency ω named encounter frequency ω_e.

Hp: 2D head incident regular waves. Deep water.

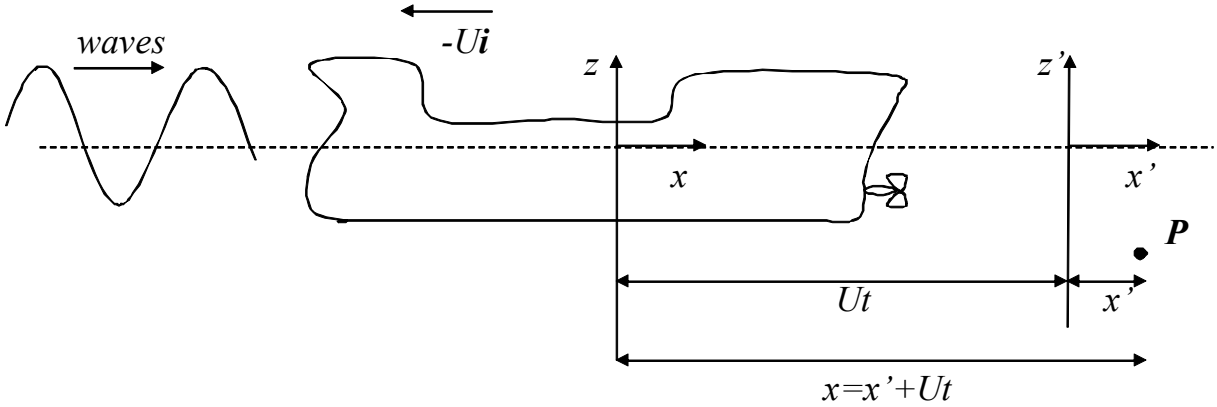

Here:

- (x,y,z) is the inertial reference frame translating with $-U\boldsymbol{i}$, i.e. where the motions are calculated

• (x',y',z') is the Earth-fixed reference frame

The incident-wave potential is

$$\phi_0(x',z',t) = \frac{g\zeta_a}{\omega} e^{kz'} \cos(\omega t - kx')$$

Because ϕ_0 is a scalar function it does not change with reference frame.
If we express (x',z') in terms of (x,z) we have

$$\phi_0(x',z',t) = \frac{g\zeta_a}{\omega} e^{kz} \cos\left[\omega t - k(x - Ut)\right] \underbrace{=}_{\text{using } k=\omega^2/g} \frac{g\zeta_a}{\omega} e^{kz} \cos\left[\underbrace{\left(\omega + \frac{\omega^2}{g}U\right)}_{=\omega_e} t - kx\right]$$

$$= \frac{g\zeta_a}{\omega} e^{kz} \cos(\omega_e t - kx) = \phi_0(x,z,t)$$

Here ω_e=encounter frequency characterizes the time oscillations in the case with forward motion. It implies an encounter period $T_e=2\pi/\omega_e$. ω_e depends on ω, U and the direction of incident wave relative to the forward motion.

NB: In the moving reference frame: $\frac{\partial}{\partial t} \underbrace{\rightarrow}_{becomes} \frac{\partial}{\partial t} + U\frac{\partial}{\partial x}$

Another way to introduce ω_e is given in the following figure:

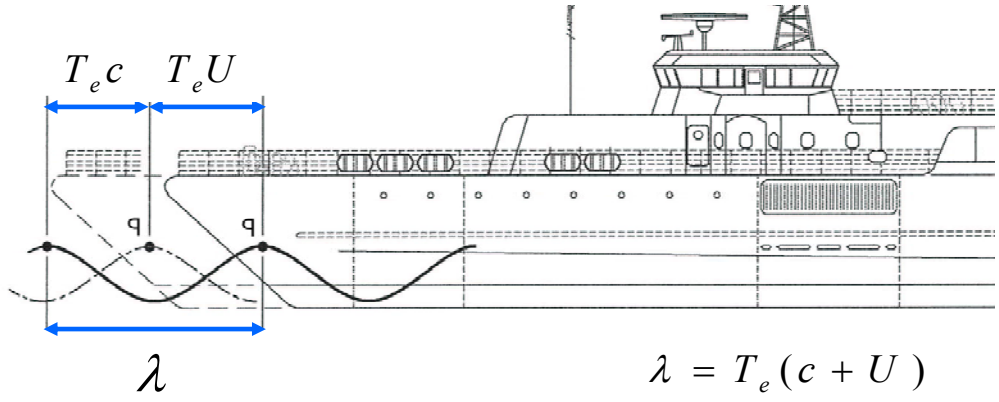

• For U=0 a wave front (e.g. wave crest) covers a distance=λ in T, i.e.

$$\lambda = cT = c(2\pi/\omega) \qquad \text{(A)}$$

with $c = \omega/k = g/\omega$ the phase speed in deep water.

• For $U\neq 0$, the relative wave front-ship speed is

$$u_{rel} = c + \underbrace{U}_{current}$$

and a wave front covers a distance=λ in $T_e \neq T$, i.e.

$$\lambda = u_{rel}T_e = u_{rel}(2\pi/\omega_e) \qquad \text{(B)}$$

Enforcing (A) and (B) to be the same, we have

$$c\frac{2\pi}{\omega} = (c+U)\frac{2\pi}{\omega_e} \Rightarrow \omega_e = \omega\left(1 + U\frac{\omega}{g}\right) \qquad \text{(F:3.28)}$$

If the waves propagate along the direction β with respect to the x axis, we have

$$\omega_e = \omega + \frac{\omega^2}{g} U \cos\beta \qquad \text{(F:3.29)}$$

It means, for instance, that $\omega_e > \omega$ for head waves (β=0 deg), as well as for bow waves, and $\omega_e < \omega$ for following waves (β=180 deg), as well as for quartering waves.

NB: If from eq. (F:3.29) $\omega_e < 0$ we must take the absolute value so that ω_e is always positive.

Parameter analysis: influence of forward speed on A_{ij} and B_{ij} (F:56-58)

The forward speed U affects the added-mass and damping coefficients. We examine this by studying the seakeeping problem with forward speed U in simplified conditions.

Hp: Linear potential-flow theory valid. Steady-state conditions. 'Slender' body.
Linear problem → superposition principle valid.

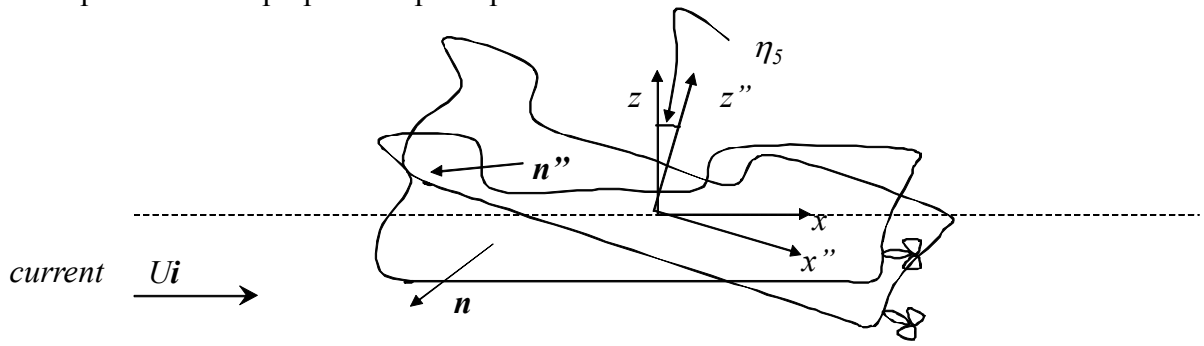

In this case:

- (x,y,z) is the inertial reference frame translating with $-U\boldsymbol{i}$, i.e. where the motions are calculated
- (x'',y'',z'') is the body reference frame

The body moves forward with constant speed $-U\boldsymbol{i}$ so generates waves and causes a local flow velocity. This is steady in (x,y,z), say $\nabla\phi_{steady}$, and counteracts the current $U\boldsymbol{i}$ seen by the body to ensure impermeability condition, i.e. $(\nabla\phi_{steady} + U\boldsymbol{i})\cdot\boldsymbol{n} = 0$ at $\forall \boldsymbol{P} \in S_{0B}$

The total velocity potential can then be split as the sum of

$$\phi_{tot}(\boldsymbol{r},t) = \overbrace{\underbrace{\phi_0(\boldsymbol{r},t) + \phi_D(\boldsymbol{r},t)}_{incident+diffraction} + \underbrace{\sum_{j=1}^{6}\phi_j(\boldsymbol{r},t)}_{radiation}}^{\phi:seakeeping-problem} + \overbrace{\underbrace{\phi_{steady}(\boldsymbol{r})}_{local\ steady} + \underbrace{Ux}_{current}}^{steady-forward-motion\ no-incident-waves}$$

Here ϕ_j is the radiation potential in j-th degree of freedom associated with velocity $\dot{\eta}_j$, i.e. not unitary.

In general the steady flow ϕ_{steady} will affect the unsteady flow ϕ, but
'Slender' body→ $|\nabla\phi_{steady}| << U$
→ the local steady flow does not interact with the unsteady flow, so the seakeeping can be solved separately.

NB: Care should be taken for Froude number $Fn = U/\sqrt{gL} >\approx 0.4$.

However the current affects the seakeeping problems in many ways. It causes:

1. Different frequency, i.e. we have ω_e instead of ω both for ϕ_D and each ϕ_j.
2. $\frac{\partial}{\partial t}$ becomes $\frac{\partial}{\partial t}+U\frac{\partial}{\partial x}$
   → the combined free-surface condition becomes

$$\left(\frac{\partial}{\partial t}+U\frac{\partial}{\partial x}\right)^2\phi_j+g\frac{\partial\phi_j}{\partial z}=0 \qquad j=D,1..6 \quad z=0,t\geq 0$$

3. A time-varying velocity component in *z* when the body has a pitch motion (*j*=5) and in *y* when the body has a yaw motion (*j*=6). They must be counteracted to ensure impermeability condition, i.e. the fluid velocity for these radiation problems are $\boldsymbol{V}=\nabla\phi_5+U\eta_5\boldsymbol{k}$ and $\boldsymbol{V}=\nabla\phi_6-U\eta_6\boldsymbol{j}$, respectively.

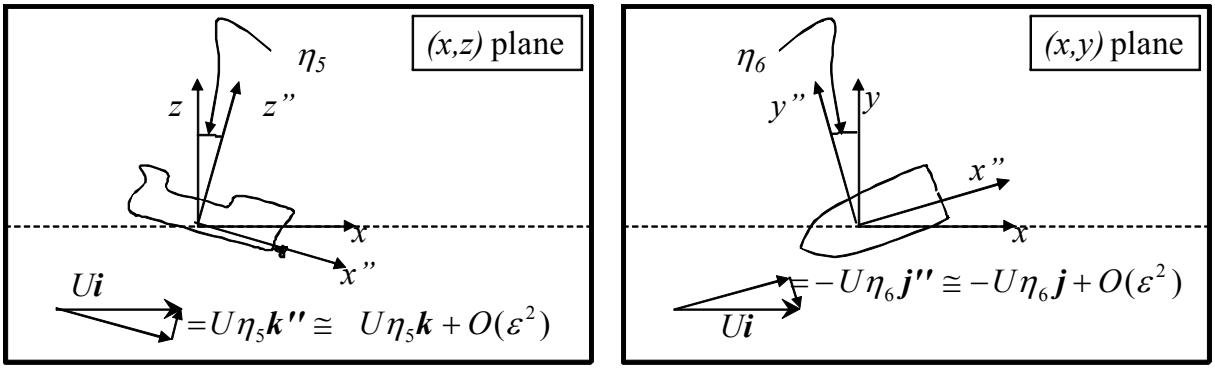

→ the body-boundary conditions for pitch and yaw are modified as

$$\frac{\partial\phi_5}{\partial n}\underbrace{+U\eta_5 n_3}_{additional-term}=\dot{\eta}_5 n_5 \qquad \frac{\partial\phi_6}{\partial n}\underbrace{-U\eta_6 n_2}_{additional-term}=\dot{\eta}_6 n_6 \quad \forall\mathbf{P}\in S_{0B}, t\geq 0$$

As a result of items 1-3 the radiation potentials depend on *U*. This is also true for the diffraction potential, as we can understand since it is linked to ϕ_j through the Haskind relations. This means that radiation and diffraction loads will depend on *U*. The Froude-Kriloff loads cannot depend on *U*, due to their definition, i.e. they are due to the incident-waves.

In the radiation problem:

- The dynamic pressure is given by

$$\underbrace{p-p_a}_{contribution\ j}=-\rho\left[\frac{\partial\phi_j(U)}{\partial t}+U\frac{\partial\phi_j(U)}{\partial x}\right] \qquad j=1..6 \qquad (1)$$

Here it has been emphasized that the solution ϕ_j depends on *U*.

- The added-mass and damping coefficients depend on *U* explicitly for the *U* term in the Bernoulli equation for *p* and indirectly for the variation in the boundary conditions. Moreover, because the vessel oscillates with ω_e, A_{kj} and B_{kj} must depend on ω_e.

Hp: If Froude number $Fn=U/\sqrt{gL}$ is small, say <0.2, or if the frequency is large, the effect of *U* is mainly in the body boundary condition and in the presence of the encounter frequency. In this case A_{kj} and B_{kj} can be expressed formally as power series of *U*, i.e.

$$A_{kj}\cong A_{kj}^{(0)}+A_{kj}^{(1)}U+A_{kj}^{(2)}U^2$$

$$B_{kj}\cong B_{kj}^{(0)}+B_{kj}^{(1)}U+B_{kj}^{(2)}U^2$$

with coefficients in the right-hand-side independent from *U,* i.e. obtained from the solution without forward speed. So using strip-theory we have:

$$
\begin{aligned}
&A_{33} \cong \int_L A_{33}^{(2D)} dx, \quad B_{33} \cong \int_L B_{33}^{(2D)} dx \\
&A_{35} \cong -\int_L x A_{33}^{(2D)} dx + \frac{U}{\omega_e^2} B_{33}, \quad A_{53} \cong -\int_L x A_{33}^{(2D)} dx - \frac{U}{\omega_e^2} B_{33} \\
&B_{35} \cong -\int_L x B_{33}^{(2D)} dx - U A_{33}, \quad B_{53} \cong -\int_L x B_{33}^{(2D)} dx + U A_{33} \\
&A_{55} \cong \int_L x^2 A_{33}^{(2D)} dx + \frac{U^2}{\omega_e^2} A_{33}, \quad B_{55} \cong \int_L x^2 B_{33}^{(2D)} dx + \frac{U^2}{\omega_e^2} B_{33}
\end{aligned}
\qquad \text{(F:3.30)}
$$

With $U \neq 0$, $A_{kj} \neq A_{jk}$ and $B_{kj} \neq B_{jk}$

Strip theory for ships

Theoretically: strip theory is good in head and bow waves but dangerous in following and quartering waves. The limitations are for ω_e that must be large to limit 3D effects.

Other limits of validity of strip theory are connected with:

- body geometry must be elongated→ e.g. there are limitation for ships with small length-to-beam ratio *L/B* (though the 18th ITTC says it can be used down to *L/B*=2.5).
- linearity must be valid → i.e. not good for high sea states
- steady-unsteady flow interaction is neglected

  → questionable for $Fn = U / \sqrt{gL} >\approx 0.4$.

In practice: strip theory gives good results in the important frequency-range of ship motions. When the ω_e becomes small, e.g. at forward speed and following and quartering sea, for the vertical motions there are some difficulties because the heave added mass goes to infinity. But the integrated effect is small because the added-mass force goes to zero, i.e. the acceleration goes to zero as ω_e^2, and the restoring terms dominate for vertical motions. However, there are some singular behaviours at forward speed when applying strip theory for estimating vertical shear force and vertical bending moment at small ω_e. For lateral motions one can justify strip theory also for small frequencies, in this case added mass does not diverge. For roll viscous effects are important for the motion. For surge, 3D effects are larger than for the other motions, but the added mass is small relative to the ship mass. This can be checked using an approximated but practical formula by Søding (1982), i.e.

$$A_{11} \approx 2.7 \rho \nabla^{5/3} / L^2$$

with ρ the water density, ∇ the displaced volume of water and *L* the ship length.

NB: The waves generated by an advancing vessel in waves are different than those predicted by strip theory. However this difference does not matter for the vessel response and strip theory can be used to estimate the response, within the mentioned limitations. In this framework an important parameter is the 'reduced frequency' $\tau = \omega_e U / g$. For $\tau > 1/4$ the group wave velocity is smaller than *U*, i.e. there are no waves moving upstream of the vessel. This fact occurs for $\tau < 1/4$. In the latter regime the frequency-domain approach has problems.

Restoring loads (F:58)

We assume that the mean buoyancy is balanced by body weight, i.e. $\rho g V = mg$, with V the displaced volume of water (also indicated as ∇).

Under these assumptions, the linear restoring loads are connected with the "hydrostatic" pressure $p = -\rho g z$ and caused by the change of the displaced volume, i.e. changes of the buoyancy, due to the rigid motions,.

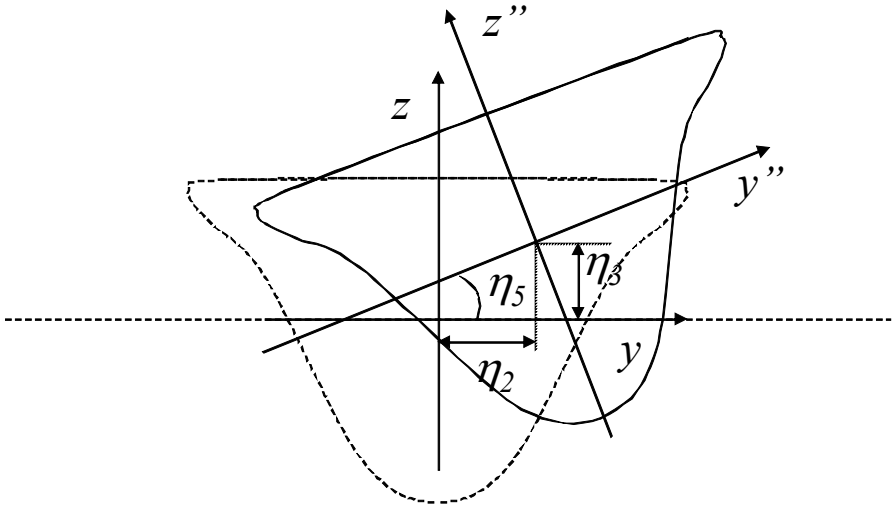

The generalized restoring loads (forces and moments) can be written as

$$F_{hydr,k}(t) = -\sum_{j=1}^{6} C_{kj}\eta_j \qquad k = 1..6 \qquad \text{(F:3.32)}$$

with C_{kj} the restoring coefficients. The restoring coefficients can be obtained estimating the variation of the buoyancy loads due to the rigid motions.

NB: C_{kj} >0 gives a stabilizing restoring load because counteracts the motion and tends to bring the system (body) in its original position. C_{kj} <0 is destabilizing.
The restoring loads are important in fixing the natural periods of the body motions, as we already discussed.

Examples of restoring loads

Example 1: Restoring coefficient in heave for a semisubmersible

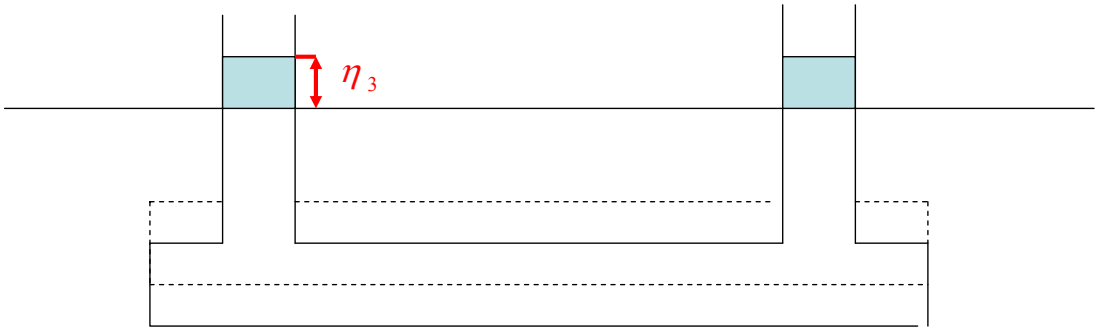

The restoring force associated with the heave motion is due to the change in displaced volume, i.e.

$$dF_{hydr,3} = \rho g dV = \rho g dS(-\eta_3)$$

$$\Rightarrow F_{hydr,3} = -\rho g \int_{A_w} dS\eta_3 = -\rho g A_w \eta_3 \underbrace{=}_{by-definition} -C_{33}\eta_3$$

$$\Rightarrow C_{33} = \rho g A_w$$

with A_w the total waterplane area.

NB: From this we understand that, for instance, C_{11}, C_{22} and C_{66} are zero, i.e. surge, sway and yaw do not cause a variation of the displaced volume→ no restoring loads in these directions.

Example 2: Restoring coefficient in pitch for a ship

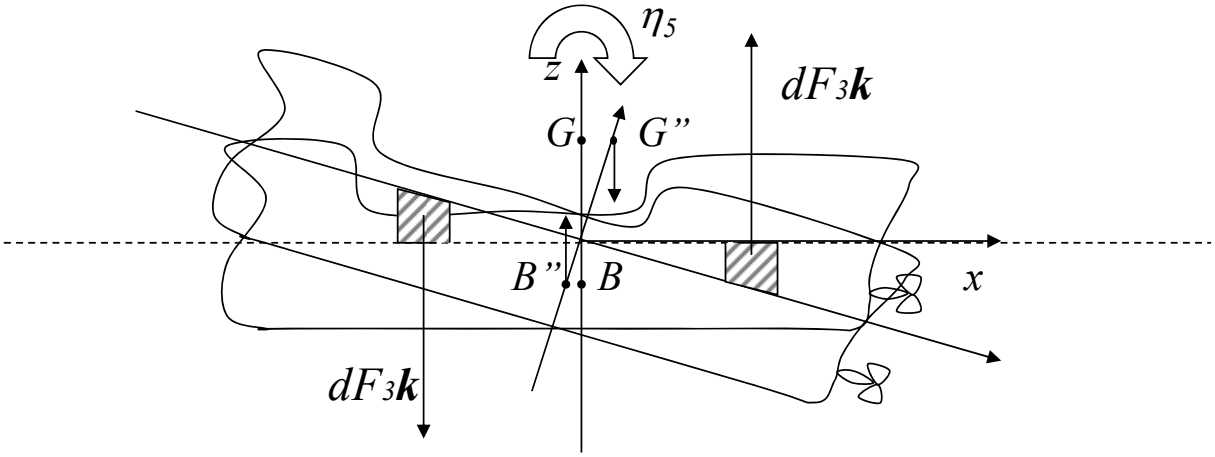

NB: The arrows in the figure do not give information about the magnitude of the forces

The restoring pitch moment $F_{exc,5}$ is characterized by two parts:

$$F_{exc,5} = M_a + M_b$$

- M_a is stabilizing and due to variation of buoyancy

$$dM_a = -x dF_3 = -x\rho g \underbrace{x\eta_5}_{\substack{displacement \\ in\ z\ direction}} dS \Rightarrow M_a = -\rho g \int_{A_W} x^2 dS\eta_5$$

with A_W the waterplane area.

- M_b is destabilizing

$$M_b = \rho g V \left(\int_m z dm / m - \int_V z dV / V \right) \eta_5 = \rho g V \left(z_G - z_B \right) \eta_5$$

with V and m the displacement and body mass, respectively, and z_G and z_B are the vertical position of center of mass (coincident with center of gravity for uniform gravitational field) and center of buoyancy, respectively.

So the restoring pitch moment is

$$F_5 = -\rho g V \left(\int_{A_W} x^2 dS / V + z_B - z_G \right) \eta_5 \underbrace{=}_{by-definition} -C_{55}\eta_5$$

$$\Rightarrow C_{55} = \rho g V\Big(\overbrace{\int_{A_W} x^2 dS}^{\geq 0} / V + z_B - z_G\Big) = \rho g V \underbrace{\overline{G}\overline{M}_L}_{\text{longitudinal metacentric height}}$$

$\underbrace{\qquad\qquad}_{\text{metacenter}}$

For a stable vessel, i.e. $C_{55} > 0 \rightarrow \overline{G}\overline{M}_L$ must be >0

→ It means that the metacenter must be higher than the center of mass.

Example 3: Restoring coefficient in surge due to a mooring line. (F:262-265)

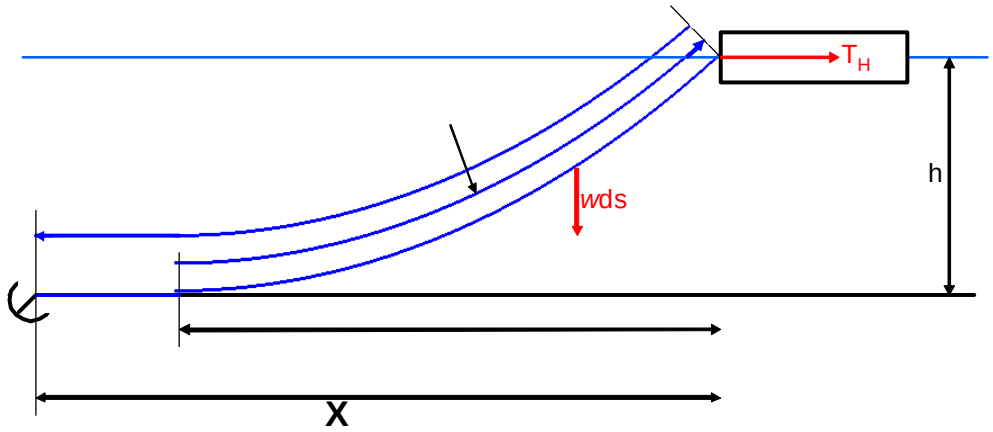

Hp: A vessel is moored as in the figure and oscillates in surge about its mean configuration in wave-current-wind environment.

Here: w= weight per unit length of the line in water

T_H =horizontal line tension, $(T_H)_M$ =value of the force in the mean configuration.

$X = l - l_s + x$ = distance from the anchor to the connection of the line to the vessel

Defining $a = T_H / w$:

$$\left.\begin{aligned} l_s &= a\sinh(x/a) \qquad (F:8.14) \\ h &= [a\cosh(x/a) - 1] \qquad (F:8.15) \end{aligned}\right\} \Rightarrow l_s^{\,2} = h^2 + 2ha \qquad (F:8.17)$$

$$\Rightarrow X = l - h\sqrt{1 + 2a/h} + a\cosh^{-1}(1 + h/a) = f(T_H) \qquad (F:8.21)$$

Due to the motion, the horizontal tension oscillates in time around $(T_H)_M$, i.e.

$$T_H = (T_H)_M - \left.\frac{dT_H}{dX}\right|_{X=(X)_M} \underbrace{\eta_1}_{by-definition} \underbrace{=}\; (T_H)_M - C_{11}\eta_1 \Rightarrow C_{11} = \left.\frac{dT_H}{dX}\right|_{X=(X)_M}$$

with η_1 the surge motion of the vessel point connected with the cable.

Procedure to estimate C_{11} (see figure F:8.4):

1. Find the "average" wave, current and wind horizontal force, i.e. $(T_H)_M$
2. $(T_H)_M$ into eq. (F:8.21) → $X = (X)_M$
3. From eq. (F:8.21) estimate $\dfrac{dT_H}{dX}$ at $X = (X)_M$, i.e. $\left.\dfrac{dT_H}{dX}\right|_{X=(X)_M}$ → C_{11}

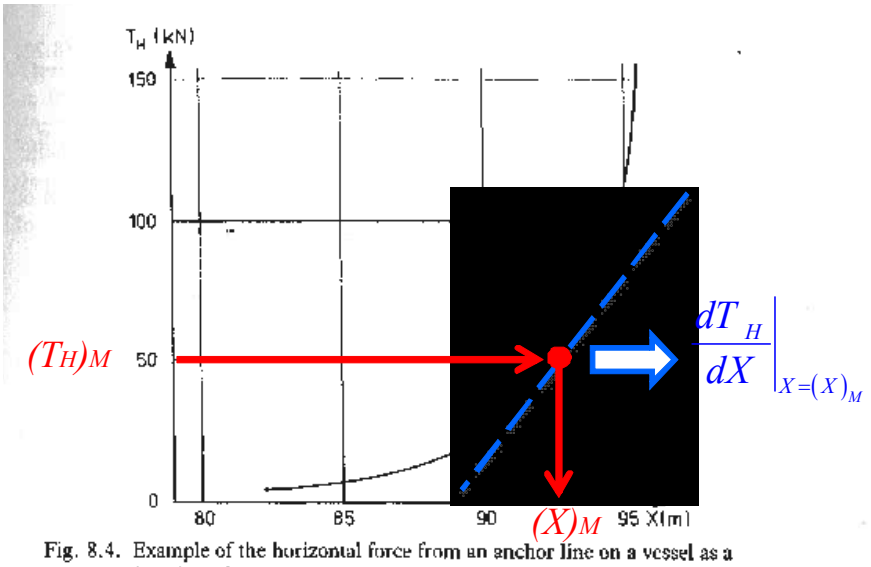

Fig. 8.4. Example of the horizontal force from an anchor line on a vessel as a function of the horizontal distance X between the anchor and the point where the anchor line is connected to the vessel. (The vessel and the anchor line configuration is shown in Fig. 8.3.) Water depth: 25 m. Weight per unit length of chain in water: 828 N m^{-1}. Chain length: 100 m.

Linear body motions in regular waves (F:66-68)

The body motions can be evaluated by solving the system

$$\sum_{j=1}^{6} M_{kj}\ddot{\eta}_j = F_k \quad k = 1..6$$

once estimated the loads F_k and known M_{kj}.

Hp: Zero forward motion. The body is stable in calm water→ $mg = \rho g V$, i.e. the weight of the body equals the weight of the displaced water in the mean position.

The loads F_k are only the result of wave-body interactions, i.e. <u>hydrodynamic loads</u>:

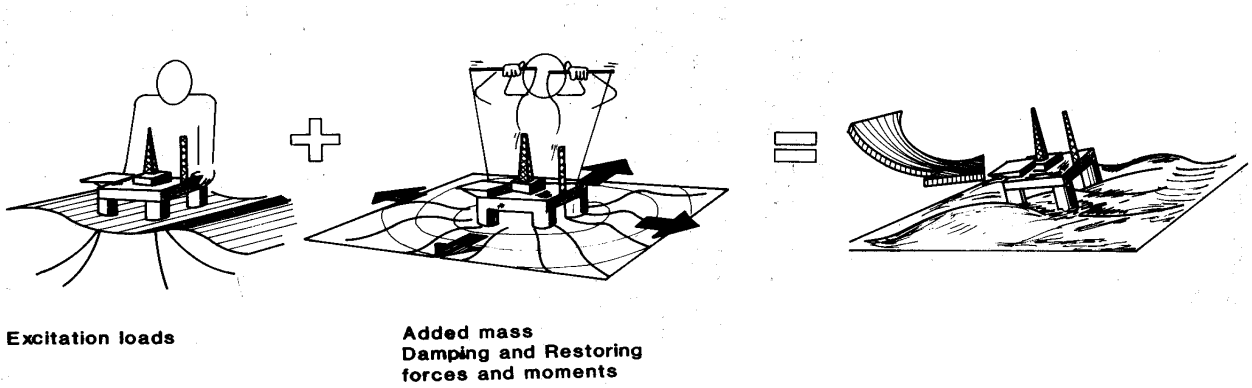

Fig. F:3.1

So that the body-motion system becomes

$$\Rightarrow \sum_{j=1}^{6}\left[-\omega^2(M_{kj} + A_{kj}(\omega)) + i\omega B_{kj}(\omega) + C_{kj}\right]\eta_{ja} = \zeta_a X_k(\omega,\beta)$$

Here η_{ja} and $X_k(\omega,\beta)$ are complex quantities.
Assuming that we solved for the excitation and radiation loads, to estimate the motions we only need to know M_{kj}, the mass matrix of the body.

The elements of M_{kj} involve:

- the body mass *m*,
- the moments of inertia $I_{3+i3+i} = \int_m (x_j{}^2 + x_k{}^2) dm$ with *i=1..3* and $j \neq k \neq i$
- the products of inertia $I_{3+i3+j} = \int_m x_i x_j dm$ with *i,j=1..3* and $j \neq i$
- the coordinates of the center of mass $x_{G,i} = \int_m x_i dm / m$

and are linked to the inertial force (the first 3 rows) and moment (the last 3 rows).

The elementary inertial force is $dF_i = dm\ddot{s}_i, i = 1..3$.
We examine the component in heave as an example, which will provide the 3rd row of M_{kj} :

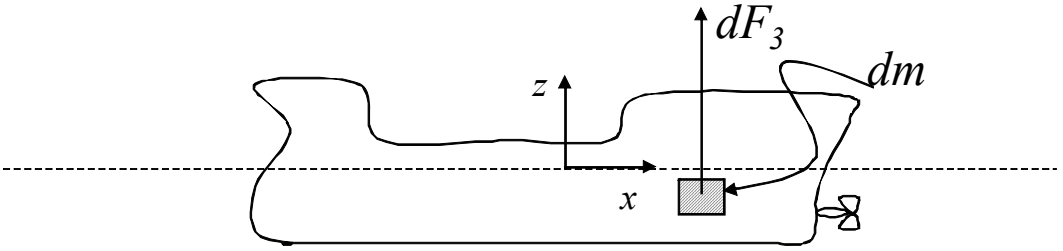

$$dF_3 = dm \quad \ddot{s}_3 = dm(\ddot{\eta}_3 - x\ddot{\eta}_5 + y\ddot{\eta}_4)$$

$$\Rightarrow F_3 = \int_m (\ddot{\eta}_3 + y\ddot{\eta}_4 - x\ddot{\eta}_5) dm = m\ddot{\eta}_3 + \ddot{\eta}_4 \underbrace{\int_m y dm}_{my_G} - \ddot{\eta}_5 \underbrace{\int_m x dm}_{mx_G}$$

$$\Rightarrow F_3 = 0\ddot{\eta}_1 + 0\ddot{\eta}_2 + m\ddot{\eta}_3 + my_G\ddot{\eta}_4 + mx_G\ddot{\eta}_5 + 0\ddot{\eta}_6$$

Now y_G is zero assuming a symmetry with respect to the *(x,z)* plane. Further, x_G can be set to zero choosing the *z* axis passing through *G*.
If this is so, the 3rd row of matrix M_{kj} is *[0,0,m,0,0,0]*.
Similarly can be done for the 1st and 2nd rows, using the other 2 force components.

The elementary inertial moment is

$$\boldsymbol{dM} = \boldsymbol{r} \times \underbrace{\boldsymbol{dF}}_{(dF_1, dF_2, dF_3)} = dm(\boldsymbol{r} \times \ddot{\boldsymbol{s}}) = \underbrace{\boldsymbol{i}(y\ddot{s}_3 - x\ddot{s}_2)dm}_{in\ roll} + \underbrace{\boldsymbol{j}(z\ddot{s}_1 - x\ddot{s}_3)dm}_{in\ pitch} + \underbrace{\boldsymbol{k}(x\ddot{s}_2 - y\ddot{s}_1)dm}_{in\ yaw}$$

Let's take the pitch component as an example. This will provide the 5th row of M_{kj}:

$$dM_2 = dF_5 = (z\ddot{s}_1 - x\ddot{s}_3)dm = [z(\ddot{\eta}_1 + z\ddot{\eta}_5 - y\ddot{\eta}_6) - x(\ddot{\eta}_3 + y\ddot{\eta}_4 - x\ddot{\eta}_5)]dm$$
$$= zdm\ddot{\eta}_1 + 0\ddot{\eta}_2 - xdm\ddot{\eta}_3 - xydm\ddot{\eta}_4 + (x^2 + z^2)dm\ddot{\eta}_5 - yzdm\ddot{\eta}_6$$

$$\Rightarrow F_5 = \int_m dF_5 = mz_G\ddot{\eta}_1 + 0\ddot{\eta}_2 - m\underbrace{x_G}_{Hp:=0}\ddot{\eta}_3 - \underbrace{I_{45}}_{=0\ symmetry\ (xz)}\ddot{\eta}_4 + I_{55}\ddot{\eta}_5 - \underbrace{I_{56}}_{=0\ symmetry\ (xz)}\ddot{\eta}_6$$

so the 5th row of M_{kj} is $[mz_G,0,0,0,I_{55},0]$.
Similarly can be done for the 4th and 6th rows, using the other 2 moment components.

The motions can then be found as:

$$\boldsymbol{H}(\omega,\beta) = \boldsymbol{\eta}_a / \zeta_a$$
$$= \left[-\omega^2 (\boldsymbol{M} + \boldsymbol{A}(\omega)) + i\omega \boldsymbol{B}(\omega) + \boldsymbol{C} \right]^{-1} \boldsymbol{X}(\omega,\beta)$$

Because the motions are linear in ζ_a , $\boldsymbol{H}(\omega,\beta)$ does not depend on ζ_a.
$|\boldsymbol{H}(\omega,\beta)|$ gives the Response Amplitude Operator (RAO), which is the transfer function of the body motions, i.e. response amplitude per unit wave amplitude.

NB: For sufficiently simple geometries, theoretical methods can provide analytical formulas for the different load terms and then for the response. In general (3D problems, generic body geometry), the diffraction-radiation problem, required to estimate the RAO, can not be solved analytically. Strip theory can be applied under certain assumptions (i.e. the problem is quasi 2D). Otherwise 3D numerical techniques must be applied, similar as discussed in connection with the source technique to find 2D added-mass and damping. Experiments can be used to measure directly the RAO.

Body motions in irregular sea state (F:37-39)
The procedure is the same as done for the incident irregular waves.

Hp: Short-term statistics→ we have a sea state with a certain spectrum *S(ω)* that does not change in time, i.e. T_0 and $H_{1/3}$ are constant. For simplicity, let assume wave propagation in *x* direction

The vessel response in a degree of freedom of interest (i.e. heave, pitch,..) can be obtained by splitting the spectrum in *N* regular-wave components, using an interval $\Delta\omega = (\omega_{MAX} - \omega_{MIN})/N$, each component with frequency ω_j, amplitude $A_j = \sqrt{2S(\omega_j)\Delta\omega}$, randomic phase ε_j, as already studied and then summing up the responses of the single regular-wave components. It means

$$\sum_{j=1}^{N} A_j \, |H(\omega_j)| \sin[\omega_j t + \delta(\omega_j) + \varepsilon_j] \quad \text{(F:3.4)}$$

with $|H(\omega)| = |\eta_a| / \zeta_a$ and $\delta(\omega_j)$ the phase angle of the response with respect to the corresponding incident wave, i.e. this is a deterministic phase while ε_j is a random phase equal to the random phase of the incident wave. The approximate variance of the response is

$$\sigma_r^2 \cong \sum_{j=1}^{N} |H(\omega_j)|^2 \frac{A_j^2}{2}$$

which becomes

$$\sigma_r^2 = \int_0^{\infty} |H(\omega)|^2 \, S(\omega) d\omega \quad \text{(F:3.5)}$$

in the limit for $N \rightarrow \infty$ and $\Delta\omega \rightarrow 0$. Assuming the response as a Gaussian process, the Rayleigh probability function can be used as approximation of the probability density function for the maxima (peak values) of the response, say R, i.e. probability of R is

$$p(R) = \frac{R}{\sigma_r^{\,2}} \exp\left(-\frac{R^2}{2\sigma_r^{\,2}} \right) \qquad \text{(F:3.6)}$$

The most probable largest value $R_{\max}$ during a 'short-term' time t is

$$R_{\max} \sqrt{2\sigma_r^{\,2} \log \frac{t}{T_r}} \qquad \text{(F:3.7)}$$

where T_r is the mean period for the response variable (e.g. motion, velocity, etc.). Due to the assumption of linear wave-induced motions and loads this can be written as T_2 , which is the mean incoming wave period.

Using short-term statistics results, by varying combinations of $H_{1/3}$ and T_0 (or T_1 or T_2), we can build up a long-term statistics.
Assuming a combination of M wave heights $H_{1/3}$ and K wave periods T_0, the long-term probability for the response r to be less than a value R is

$$P(R) = 1 - \sum_{j=1}^{M} \sum_{k=1}^{K} p_{jk} \exp\left(-\frac{R^2}{2\left(\sigma_r^{\,jk}\right)^2} \right) \qquad \text{(F:3.8)}$$

p_{jk} is the joint probability for the significant wave height and the modal period to be in the interval-numbers j and k, respectively.

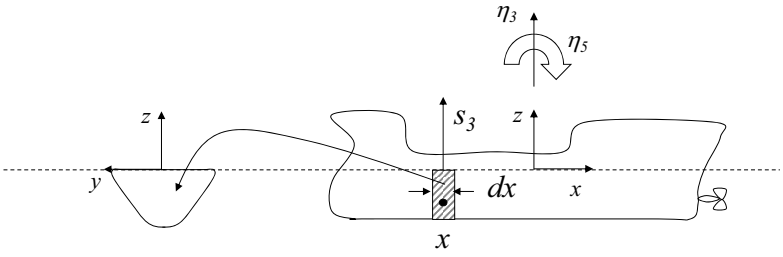

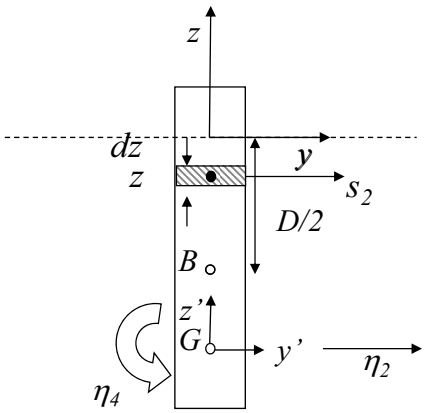

Strip-theory applications: to a deep-draught (*D*) buoy with circular cross-section
Hp: Forced sway and roll.

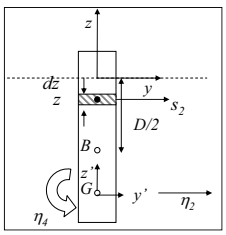

The local lateral displacement at location *z* is

$$s_2 = \eta_2 + (\boldsymbol{R}\times\boldsymbol{r}')_2 = \eta_2 + x'\cancel{\eta_3}^{=0} - z'\eta_4 = \eta_2 - z'\eta_4 \Rightarrow \ddot{s}_2 = \ddot{\eta}_2 - z'\ddot{\eta}_4 \quad \text{(F:3.9)}$$

with $z' = z + D/2 + BG$ $\quad z = 0 \Leftrightarrow z' = D/2 + BG$ $\quad z = -D \Leftrightarrow z' = -D/2 + BG$

For the strip *dz=dz'*, by definition the sway force proportional to the acceleration is

$$dF_2(z') = -A_{22}{}^{(2D)}(z')\ddot{s}_2 dz' = -\ddot{\eta}_2 A_{22}{}^{(2D)}(z')dz' + \ddot{\eta}_4 z' A_{22}{}^{(2D)}(z')dz'$$

We can then integrate to get

$$F_2 = \int_{-D/2+BG}^{D/2+BG} dF_2(z') = -\ddot{\eta}_2 \underbrace{\int_{-D/2+BG}^{D/2+BG} A_{22}{}^{(2D)}(z')dz'}_{A_{22}} + \ddot{\eta}_4 \underbrace{\int_{-D/2+BG}^{D/2+BG} z' A_{22}{}^{(2D)}(z')dz'}_{-A_{24}}$$

$$\underbrace{\qquad}_{\text{radiation}} \quad \underbrace{-A_{22}\ddot{\eta}_2 - A_{24}\ddot{\eta}_4}_{\text{load}}$$

The roll moment (generalized force with k=4) can be calculated as torque (moment of force) with respect to G, as

$$dF_4 = (\mathbf{r}' \times \underbrace{d\mathbf{F}}_{=(dF_1, dF_2, dF_3)})_1 = y' \cancel{dF_3}^{=0} - z' dF_2 = -z' dF_2 = \ddot{\eta}_2 z' A_{22}(z)^{(2D)} dz - \ddot{\eta}_4 z'^2 A_{22}^{(2D)}(z) dz$$

and integrating

$$F_4 = \int_{-D/2+BG}^{D/2+BG} dF_4(z') = \ddot{\eta}_2 \underbrace{\int_{-D/2+BG}^{D/2+BG} z' A_{22}^{(2D)}(z') dz'}_{-A_{42}} - \ddot{\eta}_4 \underbrace{\int_{-D/2+BG}^{D/2+BG} z'^2 A_{22}^{(2D)}(z') dz'}_{A_{44}}$$

$$\underbrace{=}_{radiation} \underbrace{-A_{42}\ddot{\eta}_2 - A_{44}\ddot{\eta}_4}_{load}$$

Let's see what is the value of the added-mass terms:

$$A_{22} = \int_{-D/2+BG}^{D/2+BG} A_{22}^{(2D)}(z') dz' = \rho A D$$

NB: Cross-section like circle in infinite fluid
→$A_{22}^{(2D)}(z)=\rho A$ (ρ=water density, A=area)

$$A_{24} = -\int_{-D/2+BG}^{D/2+BG} z' A_{22}^{(2D)}(z') dz' = -\rho A \left[z'^2/2 \right]_{-D/2+BG}^{D/2+BG} = -\rho A D \cdot BG = A_{42}$$

$$A_{44} = \int_{-D/2+BG}^{D/2+BG} z'^2 A_{22}^{(2D)}(z') dz' = -\rho A \left[z'^3/3 \right]_{-D/2+BG}^{D/2+BG} = \rho A \left[D \cdot BG^2 + D^3/3 \right]$$

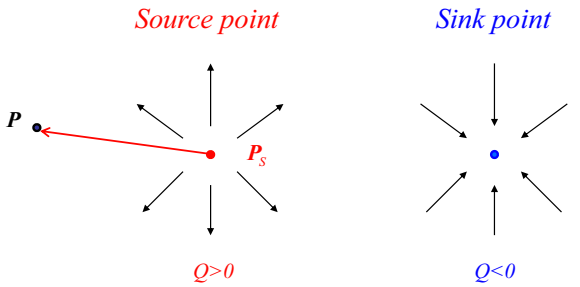

Strength Q is equal to the flux of the flow generated by the source

$$\text{2D: } \varphi_S(\boldsymbol{P}) = \frac{Q}{2\pi} \log(|\boldsymbol{P} - \boldsymbol{P}_S|)$$

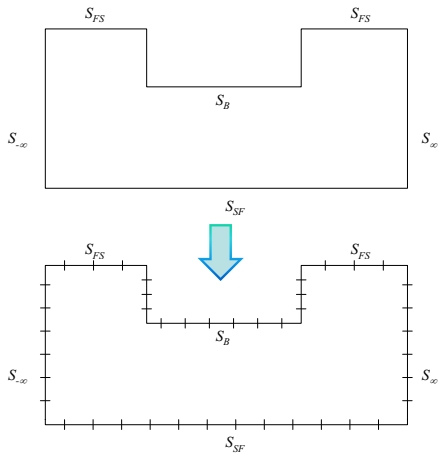

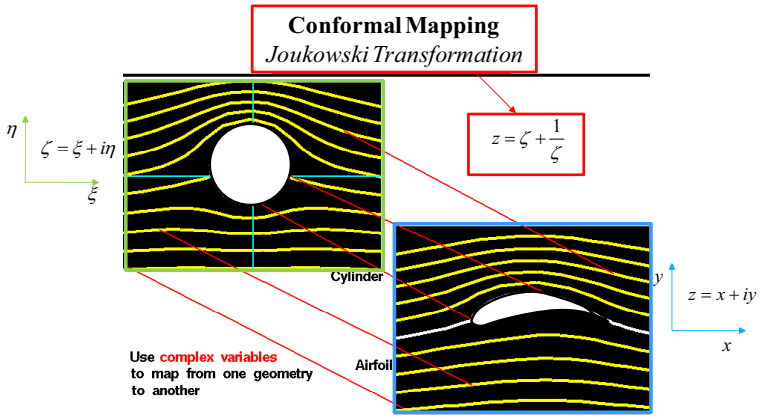

2D added mass and damping of hemicircle in deep water

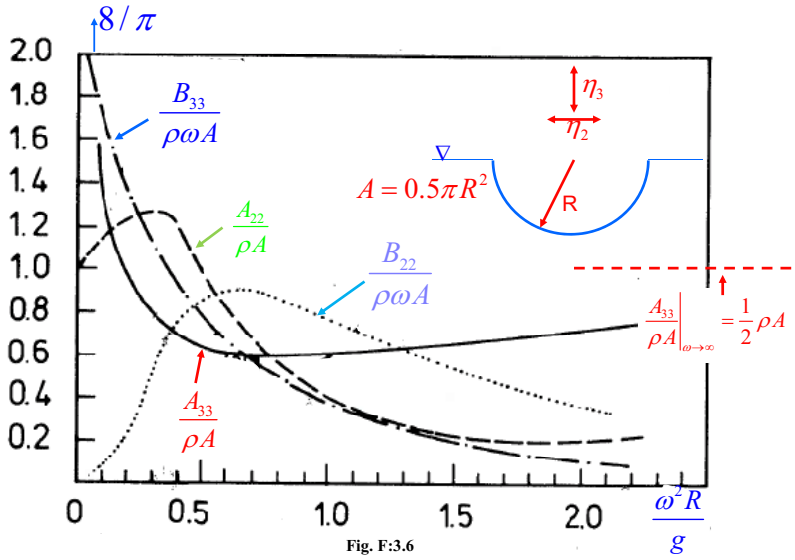

Fig. F:3.6

High-frequency 2D added mass A_{33} in heave

Lewis-form technique

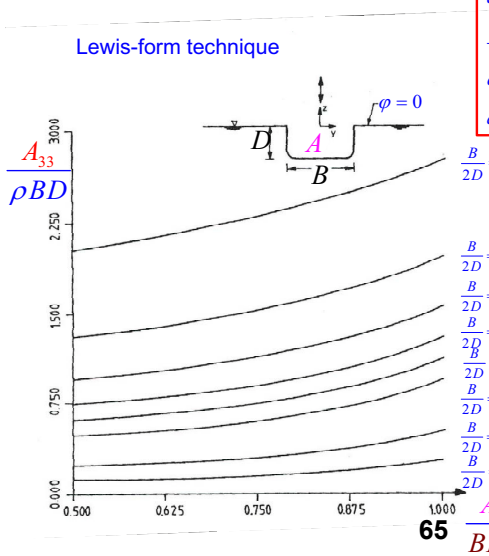

$$aa_3 = -0.25(0.5B + D) + 0.25\sqrt{(0.5B + D)^2 - 8(2A/\pi - 0.5BD)}$$

$$aa_1 = 0.5(0.5B - D)$$

$$a = 0.5(0.5B + D) - aa_3$$

$$A_{33} = \rho\, 0.5\pi\left((a + aa_1)^2 + 3(aa_3)^2\right)$$

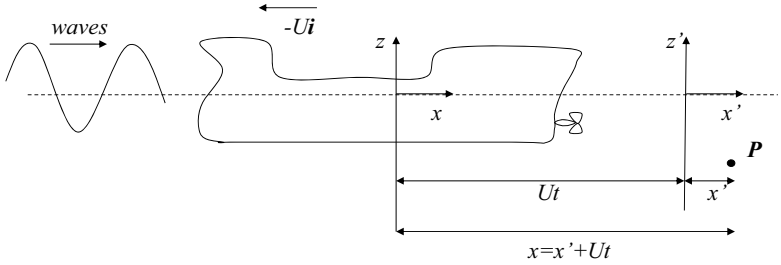
waves
-Ui
z
z'
x
x'
P
Ut
x'
x=x'+Ut

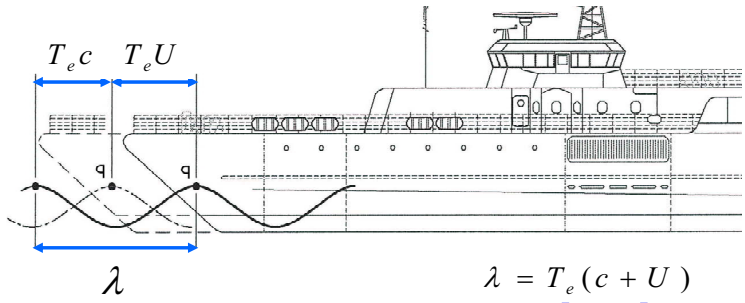
$T_e c$
$T_e U$
λ
$\lambda = T_e (c + U)$

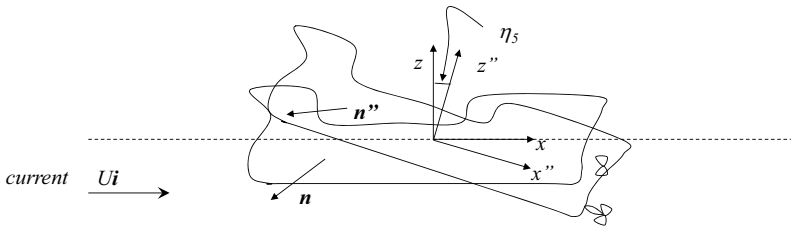
η_5
z
z''
n''
x
x''
n
current
Ui

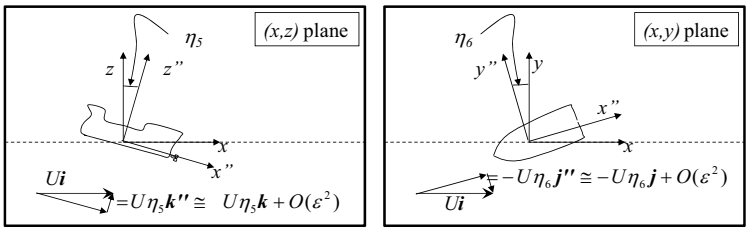

$$A_{33} \cong \int_L A_{33}^{(2D)} dx, \quad B_{33} \cong \int_L B_{33}^{(2D)} dx$$

$$A_{35} \cong -\int_L x A_{33}^{(2D)} dx + \frac{U}{\omega_e^2} B_{33}, \quad A_{53} \cong -\int_L x A_{33}^{(2D)} dx - \frac{U}{\omega_e^2} B_{33} \qquad A_{kj} \neq A_{jk} \quad k \neq j$$

$$B_{35} \cong -\int_L x B_{33}^{(2D)} dx - U A_{33}, \quad B_{53} \cong -\int_L x B_{33}^{(2D)} dx + U A_{33} \qquad B_{kj} \neq B_{jk} \quad k \neq j$$

$$A_{55} \cong \int_L x^2 A_{33}^{(2D)} dx + \frac{U^2}{\omega_e^2} A_{33}, \quad B_{55} \cong \int_L x^2 B_{33}^{(2D)} dx + \frac{U^2}{\omega_e^2} B_{33}$$

Wave systems at forward speed

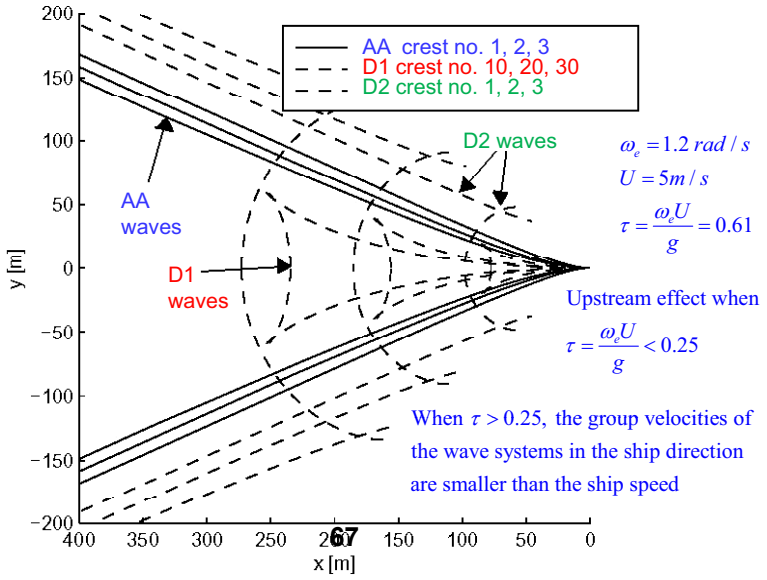

$\omega_e = 1.2\ rad/s$

$U = 5m/s$

$\tau = \frac{\omega_e U}{g} = 0.61$

Upstream effect when

$\tau = \frac{\omega_e U}{g} < 0.25$

When $\tau > 0.25$, the group velocities of the wave systems in the ship direction are smaller than the ship speed

Simplified estimates of wave angle

$$\tan\alpha = \frac{c_g t}{Ut}$$

$$c_g = \frac{g}{2\omega_e}$$

$$\tan\alpha = \frac{0.5gt/\omega_e}{Ut} = \frac{1}{2\tau}$$

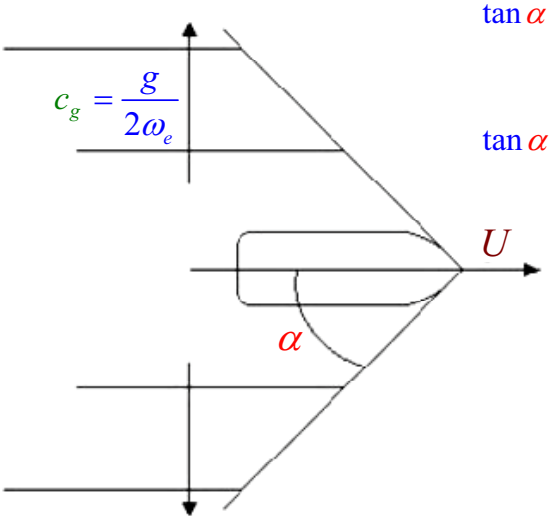

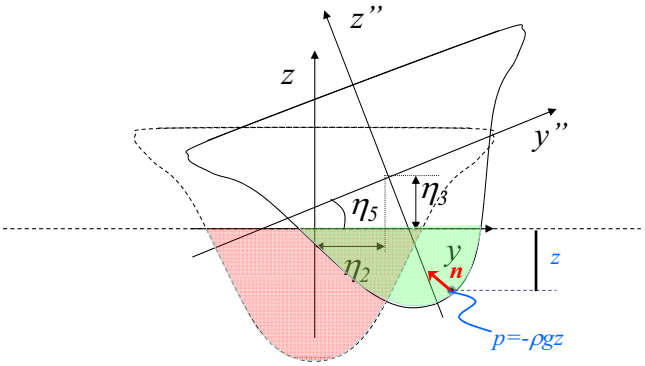

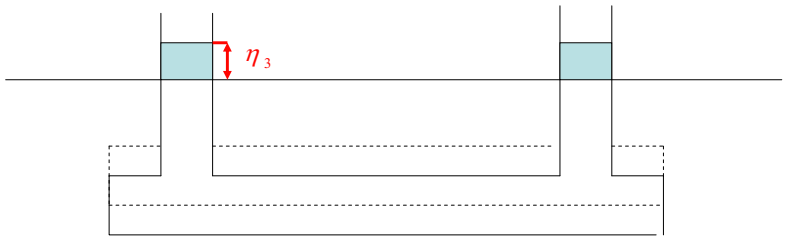

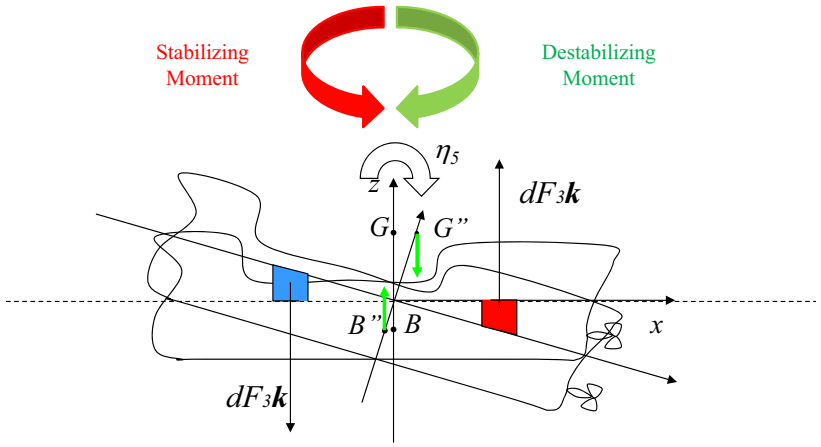

Example 2: Restoring coefficient in pitch for a ship

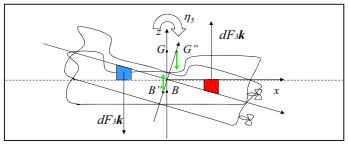

The restoring pitch moment $F_{exc,5}$ is characterized by two parts:

$F_{exc,5} = M_a + M_b$

- M_a is stabilizing and due to variation of buoyancy

$$dM_a = -xdF_3 = -x\rho g \underbrace{x\eta_5}_{\substack{displacement \\ in\ z\ direction}} dS \Rightarrow M_a = -\rho g \int_{A_W} x^2 dS\eta_5$$

with A_w the waterplane area.

- M_b is destabilizing

$$M_b = \rho g V \left(\int_m z dm / m - \int_V z dV / V \right) \eta_5 = \rho g V \left(z_G - z_B \right) \eta_5$$

with V and m the displacement and body mass, respectively, and z_G and z_B are the vertical position of center of mass (coincident with center of gravity for uniform gravitational field) and center of buoyancy, respectively.

So the restoring pitch moment is

$$F_5 = -\rho g V (\int_{A_W} x^2 dS / V + z_B - z_G) \eta_5 \underbrace{=}_{by-definition} -C_{55}\eta_5$$

$$\Rightarrow C_{55} = \rho g V (\underbrace{\overbrace{\int_{A_W} x^2 dS}^{\geq 0} / V + z_B - z_G}_{metacenter}) = \rho g V \underbrace{\overline{G}\overline{M}_L}_{\substack{longitudinal\ metacentric\ height}}$$

For a stable vessel, i.e. $C_{55} > 0 \rightarrow \overline{G}\overline{M}_L$ must be >0

→ It means that the metacenter must be higher than the center of mass.

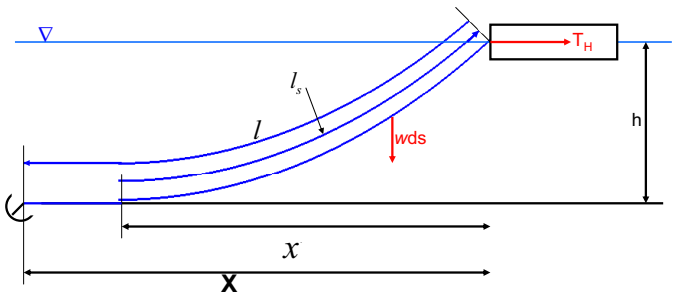

Example 3: Restoring coefficient in surge due to a mooring line. (F:258-265)

Hp: A vessel is moored as in the figure and oscillates in surge about its mean configuration in wave-current-wind environment.

η_1=surge at the cable-vessel connection

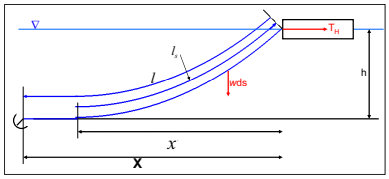

Here: w= weight per unit length of the line in water

T_H=horizontal line tension, $(T_H)_M$=value of the force in the mean configuration.

$X = l - l_s + x$ = distance from the anchor to the connection of the line to the vessel

Defining $a = T_H / w$:

$$\left.\begin{aligned} l_s &= a\sinh(x/a) \quad (F:8.14) \\ h &= [a\cosh(x/a) - 1] \quad (F:8.15) \end{aligned}\right\} \Rightarrow l_s^2 = h^2 + 2ha \qquad (F:8.17)$$

$$\Rightarrow X = l - h\sqrt{1 + 2a/h} + a\cosh^{-1}(1 + h/a) = f(T_H) \qquad (F:8.21)$$

$$\Rightarrow X = f(T_H)$$

Due to the motion, the horizontal tension oscillates in time around $(T_H)_M$, i.e.

$$T_H = (T_H)_M - \left.\frac{dT_H}{dX}\right|_{X=(X)_M} \eta_1 \underset{by-definition}{\equiv} (T_H)_M - C_{11}\eta_1$$

$$\Rightarrow C_{11} = \left.\frac{dT_H}{dX}\right|_{X=(X)_M}$$

$$Hp: \ (T_H)_M = 50KN$$

$X = f(T_H)$

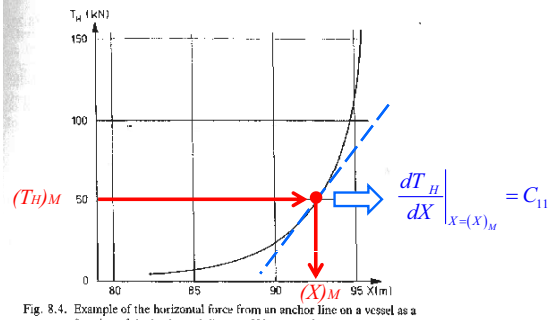

Fig. 8.4. Example of the horizontal force from an anchor line on a vessel as a function of the horizontal distance X between the anchor and the point where the anchor line is connected to the vessel. (The vessel and the anchor line configuration is shown in Fig. 8.3.) Water depth: 25 m. Weight per unit length of chain in water: 828 N m^{-1}. Chain length: 100 m.

Linear hydrodynamic loads

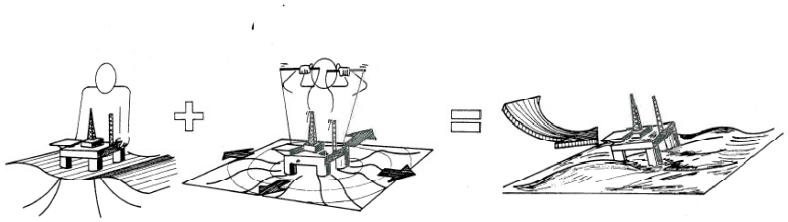

Excitation loads

Added mass
Damping
Hydrostatic restoring

Linear wave-induced motions, accelerations and structural loads

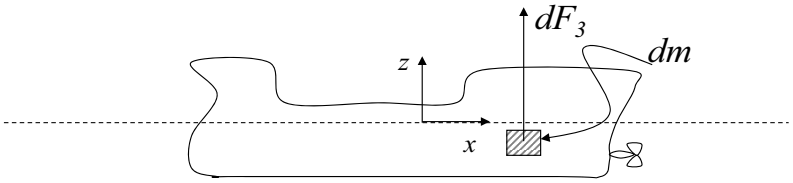

Lecture Note 4

38. Examples of response. (F: 76-79,89-91,99-100)

Examples involving ocean structures and vessels are given in the following.

1) Heave motion on a semisubmersible (F:76-79)

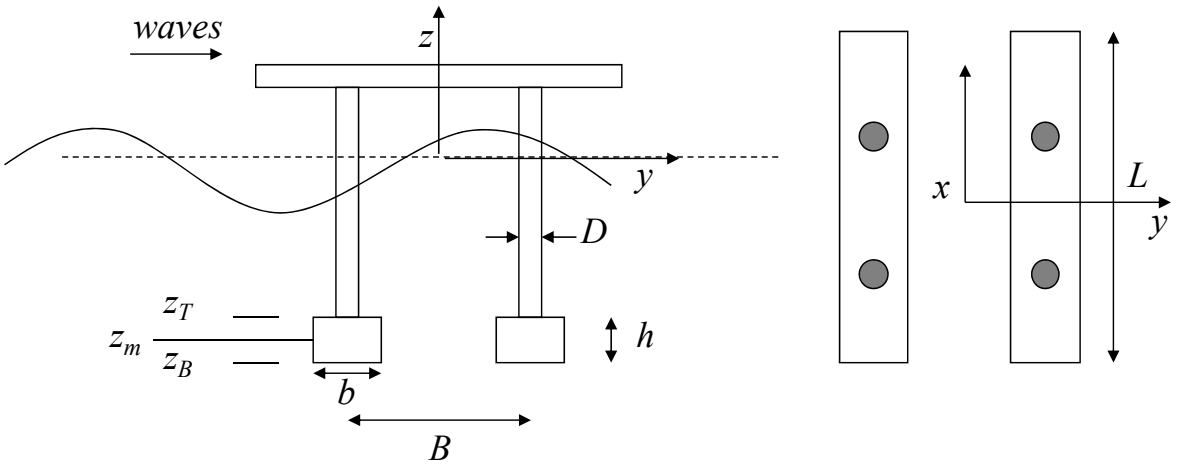

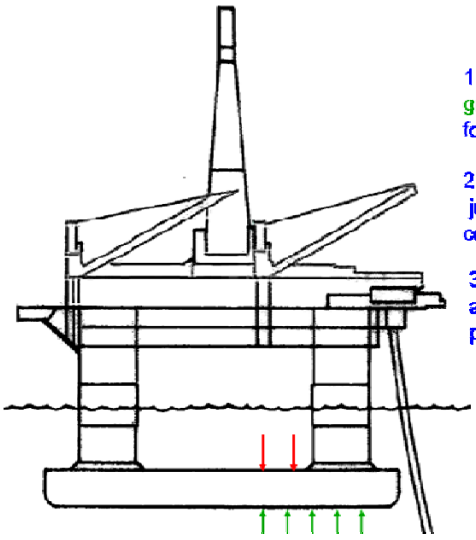

1.Difference between red and green pressure gives vertical force on the pontoons

2. Only green pressure at junctions between columns and pontoons

3. The loads mentioned in 1. and 2. are 180deg. out of phase

Small heave

Hp: 1. Regular beam waves.
2. Deep water.
3. Mass loads are dominant ($\lambda > 5D$, i.e. long-wave approximation).
4. Steady-state conditions.
5. Neglect coupling between degrees of freedom

Objective: Heave motion

Using **Hp** 1+2:

$$\phi_0 = \frac{g\zeta_a}{\omega} e^{kz} \cos(\omega t - ky)$$

$$\zeta_0 = \zeta_a \sin(\omega t - ky)$$

$$p_0 = \rho g \zeta_a e^{kz} \sin(\omega t - ky)$$

$$a_{03} = \frac{\partial^2 \phi_0}{\partial t \partial z} = -\underbrace{gk}_{=\omega^2} \zeta_a e^{kz} \sin(\omega t - ky) = -\omega^2 \zeta_a e^{kz} \sin(\omega t - ky)$$

Using **Hp** 3:
Because λ is large the wave-induced damping can be neglected in a first step approximation.

Using **Hp** 3+5:
The undamped equation of heave motion is

$$(m + A_{33})\ddot{\eta}_3 + C_{33}\eta_3 = F_{exc,3}(t) = F_{FK,3}(t) + F_{D,3}(t)$$

We need to know all terms to find η_3:

- The mass m of the platform is given by

Volume of the 2 pontoons: $V_p=2hbL$
Waterplane area of the 4 columns: $A_W=4\pi D^2/4=\pi D^2$
Volume of the wetted columns: $A_W(-z_T)$
→ Platform mass: $m=\rho\underbrace{(V_p-A_w z_T)}_{V}$

- The <u>restoring coefficient</u> is
  $C_{33}=\rho g A_W$

- The <u>excitation force</u> in vertical direction is associated to the pontoons and obtained as

Using **Hp** 3:

<u>Froude-Friloff force:</u>
Let's take the pontoon with center at $y=B/2$:

- The incident-wave pressure on the bottom side is
$$p_{0B}=\rho g\zeta_a e^{kz_B}\sin(\omega t-kB/2)\Rightarrow Force: F_{FK,B}=\underbrace{p_B Lb}_{uniform\ \ pressure,\ n_3=1}$$

- The incident-wave pressure on the top side is
$$p_{0T}=\rho g\zeta_a e^{kz_T}\sin(\omega t-kB/2)\Rightarrow Force: F_{FK,T}=\underbrace{-p_T(Lb-A_W/2)}_{uniform\ \ pressure,\ n_3=-1}$$

Here the wetted area is reduced of $A_w/2$ to account for the presence of the 2 columns on the pontoon.

The vertical force on the pontoon is
$$F_{FK,B}+F_{FK,T}=\rho g\zeta_a[e^{kz_B}-e^{kz_T}]\sin(\omega t-kB/2)Lb+\rho g\zeta_a e^{kz_T}\sin(\omega t-kB/2)A_W/2$$
Using Taylor expansion about $z=z_m$ + **Hp** 3, i.e. $kh<<1$:
$$e^{kz_B}=e^{kz_m-kh/2}\underset{kh<<1}{\cong}e^{kz_m}-\frac{kh}{2}e^{kz_m}$$
$$e^{kz_T}=e^{kz_m+kh/2}\underset{kh<<1}{\cong}e^{kz_m}+\frac{kh}{2}e^{kz_m}$$
$$\Rightarrow e^{kz_B}-e^{kz_T}\cong -e^{kzm}kh$$
$$\Rightarrow F_{FK,B}+F_{FK,T}\cong -\rho gk\zeta_a e^{kz_m}\sin(\omega t-kB/2)\underbrace{Lbh}_{V_p/2}+\rho g\zeta_a e^{kz_T}\sin(\omega t-kB/2)A_W/2$$
$$\underset{\mathbf{NB}}{=}\underbrace{\bar{a}_{03}\rho V_p/2}_{\substack{added\text{-}mass\ at\ geometrical\ center\\ multiplied\ by\ mass\ of\ displaced\ water\\ for\ a\ pontoont\ surrounded\ by\ water}}}+\rho g\zeta_a e^{kz_T}\sin(\omega t-kB/2)A_W/2$$
$$=\rho g\zeta_a e^{kz_m}\sin(\omega t-kB/2)[e^{k(z_T-z_m)}A_W-kV_p]/2$$

Similarly on the other pontoon we have
$$\Rightarrow F_{FK,B}+F_{FK,T}=\rho g\zeta_a e^{kz_m}\sin(\omega t+kB/2)[e^{k(z_T-z_m)}A_W-kV_p]/2$$

Knowing that

$$\left.\begin{aligned}\sin(\omega t - kB/2) &= \sin\omega t\cos\frac{kB}{2} - \cos\omega t\sin\frac{kB}{2}\\ \sin(\omega t + kB/2) &= \sin\omega t\cos\frac{kB}{2} + \cos\omega t\sin\frac{kB}{2}\end{aligned}\right\} sum\min g \quad up \Rightarrow 2\sin\omega t\cos\frac{kB}{2} \qquad (1)$$

The total force on the 2 pontoons is

$$F_{FK,3} = \left(F_{FK,B} + F_{FK,T}\right)_{tot} = \rho g\zeta_a e^{kz_m}\sin(\omega t)\cos(kB/2)[e^{k(z_T - z_m)}A_W - kV_p]$$

Diffraction force:

From the assumptions, the damping contribution is considered negligible. Further the added-mass of the structure in heave, A_{33}, is due to the 2 pontoons. So the vertical diffraction force acting on the two pontoons is

$$F_{D,3} = \frac{1}{2}A_{33}\underbrace{a_{03}\left(y = -\frac{B}{2}\right)}_{\text{at the geometrical center}} + \frac{1}{2}A_{33}\underbrace{a_{03}\left(y = \frac{B}{2}\right)}_{\text{at the geometrical center}} = -kg\zeta_a e^{kz_m}\sin(\omega t)\cos\left(\frac{kB}{2}\right)A_{33}$$

Here result from (1) has been used.

The total vertical excitation force is

$$F_{exc,3} = F_{FK,3} + F_{D,3}$$

which means

$$F_{exc,3} = \rho g\zeta_a e^{kz_m}\sin(\omega t)\underbrace{\cos(kB/2)}_{\text{phase difference between pontoons}}\underbrace{\left[e^{k(z_T - z_m)}A_W - k\left(V_p + \frac{A_{33}}{\rho}\right)\right]}_{\text{counteracting forces on the pontoons}} \qquad \text{(F:3.63)}$$

Using Taylor expansion about $\Delta z = 0$ + Hp 3:

$$\Rightarrow \rho g e^{k(z_T - z_m)}A_W \cong \rho g[1 + k(z_T - z_m)]A_W = \rho g A_W + \rho\underbrace{gk}_{=\omega^2}A_W(z_T - z_m)$$

so

$$\Rightarrow F_{exc,3} \cong \zeta_a e^{kz_m}\sin(\omega t)\cos(kB/2)[\rho g A_W - \rho\omega^2 A_W z_m + \underbrace{\rho\omega^2 A_W z_T - \rho\omega^2 V_p}_{=-\omega^2\rho(V_p - A_W z_T) = -\omega^2\rho V = -\omega^2 m} - \omega^2 A_{33}]$$

$$= \zeta_a e^{kz_m}\sin(\omega t)\cos(kB/2)[\rho g A_W - \rho\omega^2 A_W z_m - \omega^2(m + A_{33})]$$

Using **Hp** 4:

Because we neglect damping, the response will be in phase with the excitation force, i.e. we can assume $\eta_3 = \eta_{3a}\sin\omega t$. The steady-state equation of motion gives

$$[-\omega^2(m + A_{33}) + \rho g A_W]\eta_3 = F_{exc,3}$$

$$\Rightarrow \eta_3 = \frac{F_{exc,3}}{[-\omega^2(m+A_{33})+\rho g A_W]} = \frac{F_{exc,3}}{\left[\frac{-\omega^2(m+A_{33})}{\rho g A_W}+1\right]\rho g A_W} = \frac{F_{exc,3}}{\left[-\frac{\omega^2}{\omega^2{}_n}+1\right]\rho g A_W}$$

with ω_n the heave natural frequency $\omega_n = \sqrt{\frac{C_{33}}{(m+A_{33})}} = \sqrt{\frac{\rho g A_W}{(m+A_{33})}}$

The transfer function (RAO) is then:

$$\frac{|\eta_{3a}|}{\zeta_a} = \left|\frac{e^{kz_m}\cos(kB/2)[\rho g A_W - \rho\omega^2 A_W z_m - \omega^2(m+A_{33})]}{[-\frac{\omega^2}{\omega^2{}_n}+1]\rho g A_W}\right| = \left|\frac{e^{kz_m}\cos(kB/2)}{[1-\frac{\omega^2}{\omega^2{}_n}]}[1-\underbrace{\frac{\omega^2}{g}}_{=k} z_m - \frac{\omega^2}{\omega^2{}_n}]\right|$$

$$= \left|e^{kz_m}\cos(kB/2)[1-\frac{kz_m}{1-\frac{\omega^2}{\omega^2{}_n}}]\right|$$

There are circumstances for which $|\eta_{3a}|=0$→ i.e. no motion. This occurs if:

1) $kz_m = 1-\frac{\omega^2}{\omega^2{}_n}$ and/or 2) $\cos(kB/2)=0$

These can be relevant for the design and operations.

Condition 1) means:

$$\omega^2 = \omega^2{}_n(1-kz_m) = \omega^2{}_n \underbrace{+}_{\text{NB: } z_m=-|z_m|<0} \frac{\omega^2}{g}|z_m|\omega^2{}_n \Rightarrow \omega_c = \frac{\omega_n}{\sqrt{1-|\frac{z_m}{g}|\omega^2{}_n}} \quad (\text{F}:3.67)$$

this is the <u>cancellation frequency</u>. Because $\omega_c > \omega_n \Rightarrow T_c < T_n$, the cancellation period is lower than the natural (resonance) period.

Condition 2) means:

$\cos(kB/2)=0 \Rightarrow kB/2 = \pi/2 + n\pi$, $n = 0,1,2,..$

So using the dispersion relationship

$$\omega_{cn}{}^2 B/g = \pi + 2n\pi \Rightarrow \left(\frac{2\pi}{T_{cn}}\right)^2 \frac{B}{g} = \pi + 2n\pi \Rightarrow T_{cn} = \sqrt{\frac{4\pi B}{g(1+2n)}} \qquad n = 0,1,2,..$$

Assuming the case in figure F:3.20 as an example: T_n=22s and B=50m

From condition 1) we find T_c=*20.1s*

From condition 2) we find $T_{c0} = \sqrt{\frac{4\pi B}{g}} = 8.0s$ $\qquad T_{c1} = \sqrt{\frac{4\pi B}{3g}} = \frac{1}{\sqrt{3}}T_{c0} = 4.6s$

These periods are shown in the qualitative figure below based on linear potential-flow theory. The split in regions without and with incident waves is due to the fact that for periods T larger than: T_n=*22s* the wavelengths are $\lambda > gT_n{}^2/2\pi \cong 757m$ and we expect in practice a negligible energy for such long waves.

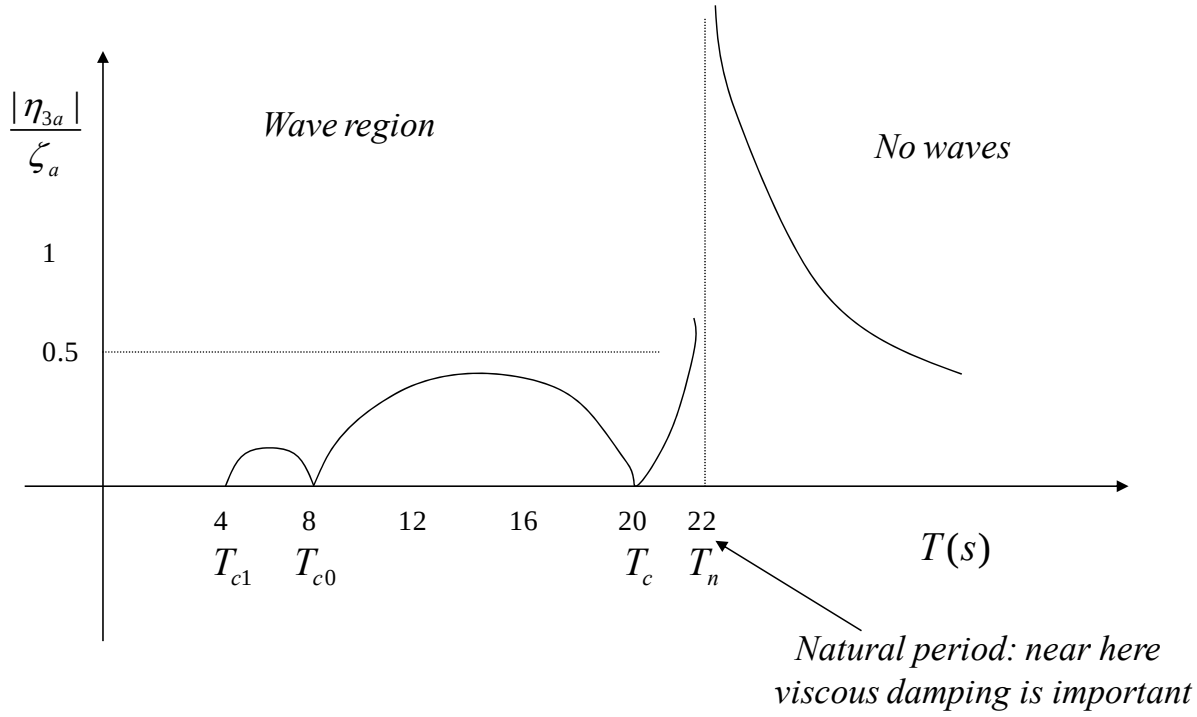

The figure confirms that cancellation effects occur for periods smaller than the natural period. The inviscid solution gives a very small damping near resonance because of the long-wave regime→ there, viscous damping matters. Similar results are given in Fig. F:3.19 for different natural frequencies: the greater $\omega_n^2 |z_m|/g$ the smaller the secondary peak in the response and the shorter the cancellation period T_c.

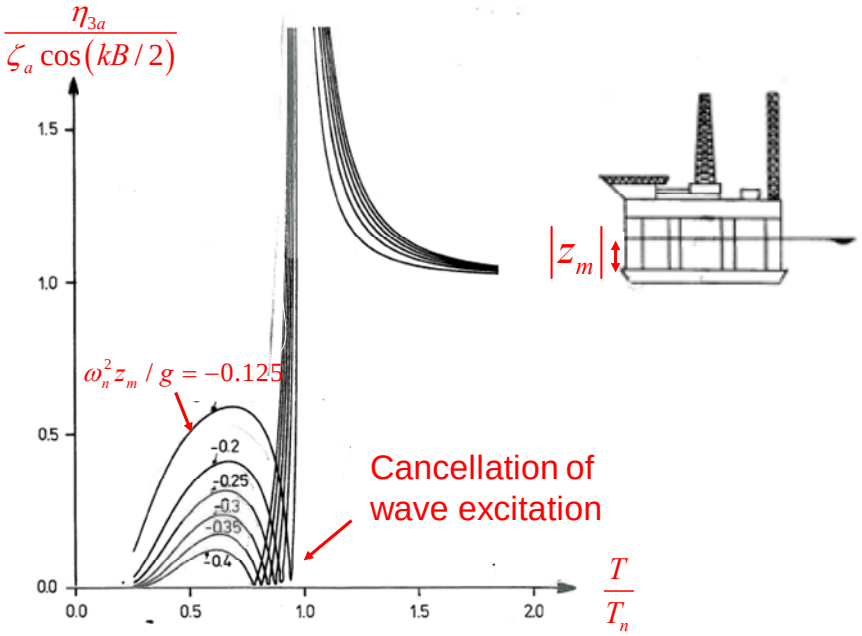

Fig. F:3.19

A semisubmersible:

- is designed to have natural period >20s to reduce the induced-wave motions
- as a result the resonance can only be caused by nonlinear effects. Slowly-varying excitation loads, connected with 2nd order effects, matter
- the long-wave theory is reliable for survival conditions

2) Linear sway and roll of a buoy

Hp: Linear problem. Deep-water regular incident waves in *y* direction. Strip theory + long-wave approximation. Steady-state conditions.

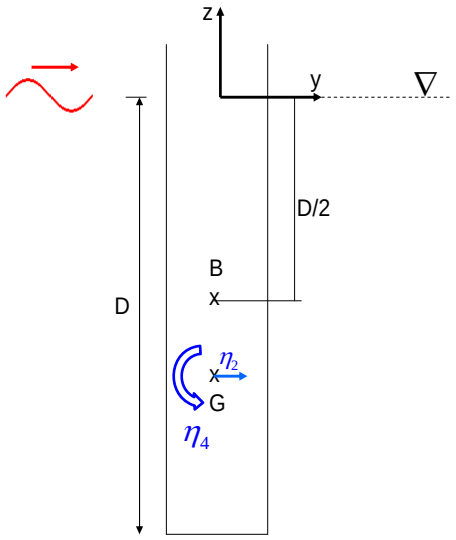

Using what learned before, the elementary excitation force in *y* direction is

$$dF_{exc,2} = (\underbrace{\rho A \bar{a}_{02}}_{F_{FK,2}^{(2D)}} + \underbrace{A_{22}^{(2D)}}_{\rho A} \underbrace{\bar{a}_{02}}_{F_{D,2}^{(2D)}})dz = 2\omega^2 \zeta_a e^{kz} \cos\omega t \rho A dz$$

with *A* the cross-section area. So integrating along the body we have

$$F_{exc,2} = \underbrace{2\rho g A \zeta_a (1 - e^{-kD})}_{F_{exc,2a}} \cos\omega t = F_{exc,2a} \cos\omega t$$

Similarly for the roll moment we find formally

$$F_{exc,4} = F_{exc,4a} \cos\omega t$$

Also in this case we neglect damping due to long-wave approximation. So in steady-state conditions the motions will be in phase with the corresponding excitation loads, i.e. $\eta_j = \eta_{ja} \cos(\omega t), \quad j = 2,4$, giving

$$\left.\begin{aligned} &(m + A_{22})\ddot{\eta}_2 + A_{24}\ddot{\eta}_4 = F_{exc,2a} \cos\omega t \\ &A_{42}\ddot{\eta}_2 + (I_{44} + A_{44})\ddot{\eta}_4 + C_{44}\eta_4 = F_{exc,4a} \cos\omega t \end{aligned}\right\} \underset{\text{steady state}}{\Rightarrow} \underbrace{\begin{bmatrix} -\omega^2(m + A_{22}) & -\omega^2 A_{24} \\ -\omega^2 A_{42} & -\omega^2(I_{44} + A_{44}) + C_{44} \end{bmatrix}}_{=MAT} \begin{Bmatrix} \eta_{2a} \\ \eta_{4a} \end{Bmatrix} = \begin{Bmatrix} F_{exc,2a} \\ F_{exc,4a} \end{Bmatrix}$$

with

$$A_{22} = \rho A D,\ A_{24} = -\rho A D \cdot BG = A_{42},\ A_{44} = \rho A \left[D \cdot BG^2 + D^3/3 \right],\ C_{44} = \rho g V \cdot \bar{G}\bar{M}_T$$

(*V* is the displaced volume) and the moment of inertia from its definition, i.e.

$$I_{44} = \int_m (y^2 + z^2) dm\,.$$

NB: Only the restoring term C_{44} is different than zero and has the same expression as C_{55} but with the transverse metacentric height $\bar{G}\bar{M}_T$ in place of the longitudinal one.

Enforcing the matrix determinant to be zero, i.e. *Det(MAT)*=0, we get the natural frequency as

$$\omega_n = \sqrt{\frac{(m+\rho AD)\rho g V \cdot \bar{G}\bar{M}_T}{(m+\rho AD)(I_{44}+A_{44})-(\rho AD \cdot BG)^2}}$$

NB: The coupling between roll and sway affects the natural frequency.

An important concept in this context is the **center of roll**: the point for which the horizontal displacement of the body is zero at any time, which identifies the axis about which the body rolls. It is important both for ships and ocean structures. For instance for a spar buoy, the center of roll is important for the attachment of a mooring line when located on the body, typically at the bottom part. However the center of roll may also be below the buoy, in this case physically the buoy moves as part of a "pendulum".
In general then the center of roll may not be on the body and may also not exist. Let's see this with an example (see Faltinsen's book "Hydrodynamics of high-speed marine vehicles", pg. 232):

Hp: A vessel/ocean platform with sway and roll motions due its interaction with incident waves:

$$\eta_2 = \eta_{2a}\sin(\omega t + \varepsilon_2) \qquad \eta_4 = \eta_{4a}\sin(\omega t + \varepsilon_4)$$

The horizontal displacement of a point of the platform is

$$s_2 = \eta_2 - z\eta_4 = \eta_{2a}\sin(\omega t + \varepsilon_2) - z\eta_{4a}\sin(\omega t + \varepsilon_4)$$

Using that $\sin(a+b) = \sin a\cos b + \cos a \sin b$
re-arranging and enforcing s_2 to be zero at any time, we have

$$s_2 = \underbrace{(\eta_{2a}\cos\varepsilon_2 - z\eta_{4a}\cos\varepsilon_4)}_{=0}\sin\omega t + \underbrace{(\eta_{2a}\sin\varepsilon_2 - z\eta_{4a}\sin\varepsilon_4)}_{=0}\cos\omega t = 0$$

which leads to the system

$$\begin{bmatrix} \cos\varepsilon_2 & -\cos\varepsilon_4 \\ \sin\varepsilon_2 & -\sin\varepsilon_4 \end{bmatrix} \begin{Bmatrix} \eta_{2a} \\ z\eta_{4a} \end{Bmatrix} = 0$$

so a non-trivial solution exists only if the matrix determinant is zero:

$$\Rightarrow -\cos\varepsilon_2\sin\varepsilon_4 + \sin\varepsilon_2\cos\varepsilon_4 = 0 \Rightarrow \tan\varepsilon_2 = \tan\varepsilon_4$$

NB: Phases ε_2 and ε_4 depend on ω, for advancing vessels on ω_e and U. So, in general they do not this condition. A concept similar to the center of roll exists also for the pitch motion.

3) Heave motion of a 2D section in regular beam waves

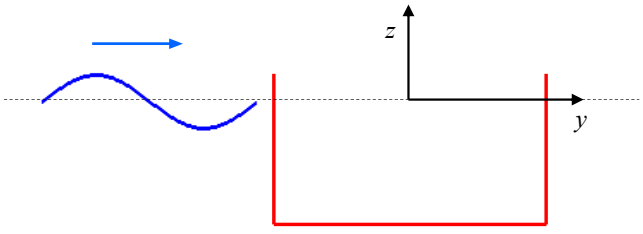

Hp: Linear problem. Deep water waves. Steady-state conditions.

The equation of motion is

$$(m + A_{33}^{(2D)})\ddot{\eta}_3 + B_{33}^{(2D)}\dot{\eta}_3 + C_{33}^{(2D)}\eta_3 = F_{exc,3a}^{(2D)}\cos(\omega t - \alpha_3) \quad (1)$$

At the undamped resonance

$$(m + A_{33}^{(2D)})\ddot{\eta}_3 + C_{33}^{(2D)}\eta_3 = 0 \Rightarrow [-\omega_{n3}^{\ 2}(m + A_{33}^{(2D)}) + C_{33}^{(2D)}]\eta_3 = 0$$

So the natural frequency is $\omega_{n3} = \sqrt{\dfrac{C_{33}^{(2D)}}{m + A_{33}^{(2D)}}}$

The heave amplitude at undamped resonance, from eq. (1), is then $\eta_{3a} = \dfrac{F_{exc,3a}^{(2D)}}{\omega_{n3} B_{33}^{(2D)}}$

Newman (1962) has derived the expression for the excitation loads per unit length on an infinitely long cylinder in beam sea. The amplitude of load depends on the corresponding damping coefficient for the cross-section:

$$F_{exc,ia}^{(2D)} = \zeta_a \sqrt{\frac{\rho g^2}{\omega} B_{ii}^{(2D)}} \qquad i = 2,3,4 \qquad \text{(F:3.45)}$$

So in our case we have

$$\eta_{3a} = \zeta_a \frac{g}{\omega_{n3}^{\ 3/2}} \sqrt{\frac{\rho}{B_{33}^{(2D)}}}$$

It means that the motion amplitude is larger for longer waves and for smaller damping level.

4) <u>Motions in marine operations: crane operations</u>

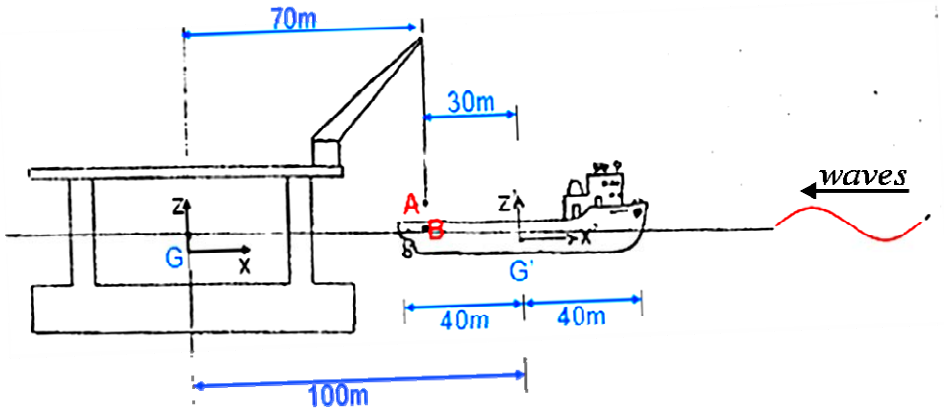

Hp: Transfer of equipment, personnel, etc. between semisubmersible and supply ship.
Regular deep-water head waves.

- Waves: T=10s, ζ_a=1m $\qquad \zeta_0 = \zeta_a \sin(\omega t + kx) = \zeta_a \sin(\omega t' + kx')$
  $\omega = 2\pi/T$, $\omega^2 = gk$
- Phase shift between center of (x,y,z) on the semisubmersible and $(x',y'z')$ on the supply ship: $\omega t' = \omega t + 100k = \omega t + 4.024$ (1)
- Semisubmersible: η_3=0.22sin(ωt) (m) , η_5=-0.0075cos(ωt) (rad)
- Supply ship: η_3=0.73sin($\omega t'$-0.0872) (m) , η_5=0.032sin($\omega t'$+1.4835) (rad)

Objective: Relative vertical motion between A and B

$s_3^A = \eta_3 - x\eta_5 = 0.22\sin(\omega t) - 70(-0.0075)\cos(\omega t) = 0.57\sin(\omega t + 1.17)$ (m)
$s_3^B = \eta_3 - x\eta_5 = 0.73\sin(\omega t' - 0.0872) - (-30)(0.032)\sin(\omega t' + 1.4835)$ (m)
$= 0.73\sin(\omega t + 3.94) \quad -(-30)(0.032)\sin(\omega t + 5.51) = 1.20\sin(\omega t - 1.4)$ (m)

Here, for s_3^B relation (1) has been used and the expressions have been rearranged using

$$A\sin(\alpha) + B\cos(\alpha) = \underbrace{\sqrt{A^2+B^2}}_{=C}\left(\underbrace{\frac{A}{\sqrt{A^2+B^2}}}_{=\cos(\beta)}\sin(\alpha) + \underbrace{\frac{B}{\sqrt{A^2+B^2}}}_{=\sin(\beta)}\cos(\alpha)\right) = C\sin(\alpha+\beta)$$

So the relative motion is: $s_3^A - s_3^B = 1.717\sin(\omega t + 1.54)$ (m)

Compared with the incident-wave amplitude ζ_a, the motion amplitudes of the two locations confirm the validity of linear theory. The amplitude of their relative motion is about twice ζ_a. This is important to account for to ensure safe and successful operations.

5) Motions and sea loads on a barge (F: ex. 3.1 pg. 89)

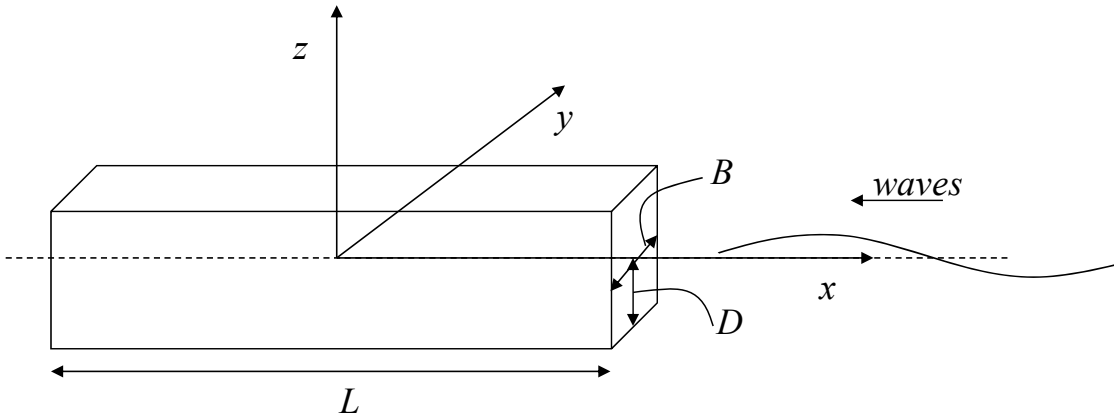

Hp: Floating barge with L=200m, B=30m, D=15m, with uniform density, and $U=0$.
Regular deep-water incident waves propagating in negative x axis, with λ=300m and $H=2\zeta_a$=20m
Linear potential flow theory theory.

For the incident waves we have:

$$\phi_0 = \frac{g\zeta_a}{\omega}e^{kz}\cos(\omega t + kx)$$
$$\zeta_0 = \zeta_a \sin(\omega t + kx)$$
$$p_0 = \rho g \zeta_a e^{kz}\sin(\omega t + kx)$$
$$a_{0i} = \frac{\partial^2\phi_0}{\partial t \partial x_i} \Rightarrow a_{03} = \frac{\partial^2\phi_0}{\partial t \partial z} = -\underbrace{gk}_{=\omega^2}\zeta_a e^{kz}\sin(\omega t + kx) = -\omega^2\zeta_a e^{kz}\sin(\omega t + kx)$$

Q: What is the vertical excitation force on the barge?

λ/D=300/15=20>>5 → long-wave approximation can be used
($L/D \cong 13$, $L/B \cong 7$)>>1 → the body is elongated so we can apply strip theory

Using the long-wave approximation and the strip theory:

$$F_{exc,3} = F_{FK,3} + F_{D,3}$$

with

$$F_{FK,3} \underbrace{=}_{\substack{\text{waves}\\ \text{along } x}} B\int p_0 \underbrace{n_3}_{\substack{\text{inside}\\ \text{the body}}} dl \underbrace{=}_{\substack{\text{contribution only}\\ \text{from bottom}}} \rho g\zeta_a B e^{-kD}\int_{-L/2}^{L/2} \sin(\omega t + kx)(\underbrace{n_3}_{=1})dx$$

$$= -\frac{1}{k}\rho g\zeta_a B e^{-kD}\left[\cos(\omega t + kL/2) - \cos(\omega t - kL/2)\right]$$

$$= \frac{2}{k}\rho g\zeta_a B e^{-kD}\sin\omega t \sin(kL/2)$$

$$F_{D,3} = \int_x \left[\underbrace{A_{31}^{(2D)}}_{\substack{=0:\ \text{symmetry}\\ (y,z)\ \text{plane}}} \bar{a}_{01} + A_{32}^{(2D)} \underbrace{\bar{a}_{02}}_{=0:\ \text{waves along } x} + A_{33}^{(2D)}\bar{a}_{03}\right]dx$$

$$= -\underbrace{A_{33}^{(2D)}}_{\text{section uniform}} gk\zeta_a e^{-kD/2}\int_{-L/2}^{L/2}\sin(\omega t + kx)dx$$

$$= -\frac{2}{k}A_{33}^{(2D)} gk\zeta_a e^{-kD/2}\sin\omega t \sin(kL/2)$$

$$\Rightarrow F_{exc,3} = \left\{\rho g\zeta_a B e^{-kD} - A_{33}^{(2D)} gk\zeta_a e^{-kD/2}\right\}\frac{2}{k}\sin\omega t \sin(kL/2)$$

For the force to be finite $k\neq 0$ which is not true if $\omega \to 0$. In the latter case $\bar{a}_{03} \to 0$ and

$$F_{exc,3} \cong \rho g\zeta_a B e^{-kD}\frac{2}{k}\sin(kL/2)\sin\omega t = \rho g\zeta_a BL \underbrace{e^{-kD}}_{\to 1 as\ k\to 0}\underbrace{\frac{\sin(kL/2)}{kL/2}}_{\to 1\ as\ kL/2\to 0}\sin\omega t \cong \rho g\zeta_a BL\sin\omega t$$

Q: Using $A_{33}^{(2D)}=0.8\rho BD$, no damping, what is the heave motion of the center of gravity?

We are looking for the steady-state solution and because the damping is zero, the response oscillates in phase with the excitation load:

$$\eta_3 = \eta_{3a}\sin(\omega t)$$

The equation of heave motion (without coupling with pitch and no damping) is:

$$[-\omega^2(m + A_{33}) + C_{33}]\eta_3 = F_{exc,3}$$

with $m=\rho LBD$ (using the equilibrium between the weight and buoyancy), $A_{33}=A_{33}^{(2D)}L = 0.8\rho BDL$, $C_{33}=\rho gLB$, we have:

$$\eta_3 = \frac{F_{exc,3a}\sin\omega t}{[-\omega^2(m + A_{33}) + C_{33}]} = \frac{\left\{\rho g\zeta_a B e^{-kD} - 0.8\rho BDgk\zeta_a e^{-kD/2}\right\}\frac{2}{k}\sin(kL/2)}{[-\omega^2(1+0.8)\rho BDL + \rho gBL]}\sin\omega t$$

$$= \frac{\left\{(\lambda/\pi)e^{-kD} - 1.6De^{-kD/2}\right\}\zeta_a \sin(kL/2)}{[-(2\pi/\lambda)(1.8)D + 1]L}\sin\omega t$$

$$= 4.9\sin(\omega t) \quad \text{(m)}$$

The heave is in phase with the incident wave at *x=0* and its amplitude is about half of the incident-wave amplitude.

Q: **How is the pitch motion?**

The equation of pitch motion (without coupling with heave and no damping) is:

$$[-\omega^2(I_{55}+A_{55})+C_{55}]\eta_5 = F_{exc,5}$$

Here the excitation moment is obtained by integrating between *–L/2* and *L/2*

$$dF_{exc,5}=-xdF_{exc,3} \rightarrow \quad F_{exc,5} \propto \cos(\omega t)$$

The full expression can be found in F:90.

The moment of inertia from its definition, i.e.

$$I_{55} = \int_m (x^2+z^2)dm\,.$$

The added-mass coefficient comes from the hydrodynamic moment proportional to the pitch acceleration

$$F_{rad,5} = \int_{-L/2}^{L/2} A_{33}^{(2D)}(\ddot{\eta}_3 - x\ddot{\eta}_5)xdx = \int_{-L/2}^{L/2} A_{33}^{(2D)}xdx\ddot{\eta}_3 - \int_{-L/2}^{L/2} A_{33}^{(2D)}x^2dx\ddot{\eta}_5 \underbrace{=}_{\substack{\text{radiation load}\\ \text{proportional to}\\ \text{acceleration}}} -A_{53}\ddot{\eta}_3 - A_{55}\ddot{\eta}_5$$

so, as we have already seen, we have

$$A_{55} = \int_{-L/2}^{L/2} A_{33}^{(2D)}x^2dx$$

The restoring coefficient comes from the restoring moment

$$F_{hyd,5} = \int_{-L/2}^{L/2} \rho gB(\eta_3 - x\eta_5)xdx = \int_{-L/2}^{L/2} \rho gBxdx\eta_3 - \int_{-L/2}^{L/2} \rho gBx^2dx\eta_5 \underbrace{=}_{\text{hydrostatic load}} -C_{53}\eta_3 - C_{55}\eta_5$$

so we obtain

$$C_{55} = \int_{-L/2}^{L/2} \rho gBx^2dx$$

Substituting these expressions in the pitch-motion equation, we can find

$$\eta_5 = \eta_{5a}\cos(\omega t) = -0.15\cos(\omega t) \quad \text{(rad)}\,.$$

The incident-wave steepness mid-ship (*x*=0) is:

$$\partial\zeta/\partial x\big|_{x=0} = k\zeta_a\cos(\omega t) = 0.21\cos(\omega t) \quad \text{(rad)}$$

so η_5 is in phase with the mid-ship steepness and its maximum is about 2/3 of maximum steepness $k\zeta_a$.

Both heave and pitch amplitude results confirm that linear theory is valid.

Q: What is the vertical acceleration in the bow (*x=L/2)*?

NB: this is the most critical region in head sea waves.

$$s_3{}^B = [\eta_3 - (L/2)\eta_5] = \eta_{3a}\sin(\omega t) - (L/2)\eta_{5a}\cos(\omega t)$$
$$\Rightarrow \ddot{s}_3{}^B = -\omega^2\left[\eta_{3a}\sin(\omega t) - (L/2)\eta_{5a}\cos(\omega t)\right] = \ddot{s}_{3a}{}^B\sin(\omega t + \varepsilon)$$

The magnitude $|\ddot{s}_{3a}{}^B| = \omega^2\sqrt{\eta_{3a}{}^2 + (L/2)^2\eta_{5a}{}^2} = 0.34g$ so it is limited in this case.

Q: There is any danger of water exit or water on deck in the studied conditions?

NB: Water exit=bottom out of water. Water on deck=shipped water, a criterion for this is "water exceeding the freeboard".

To answer this question we need to estimate the relative vertical motion, i.e. between ship and waves, at the bow (where the motions are largest in head waves):

$$\left[s_3 - \zeta\right]_{x=L/2} = \eta_3 - (L/2)\eta_5 - \zeta_a\sin(\omega t + kL/2) = 9.86\sin\omega t + 6.72\cos\omega t$$
$$\Rightarrow \left[s_3 - \zeta\right]_{a,x=L/2} = \sqrt{9.86^2 + 6.72^2} = 11.93\text{ m}$$

Water exit: The draft is $D = 15\text{ m} > \left[s_3 - \zeta\right]_{a,x=L/2}$ so there is no risk of water exit according to linear theory.

Water on deck: The freeboard must be at least $f = 12\text{ m} > \left[s_3 - \zeta\right]_{a,x=L/2}$ or greater to avoid water on deck.

6) Wave-induced accelerations of cargo and equipments (see Faltinsen's book "Hydrodynamics of high-speed marine vehicles", pg. 232-233):

The wave-induced motions are estimated in the inertial reference frame (*x,y,z*) fixed or moving with the forward speed of the vessel. It is important to keep this in mind when estimating the loads acting on objects on the deck of the vessel which may risk for instance to lose grip in waves. An example is given in the figure below:

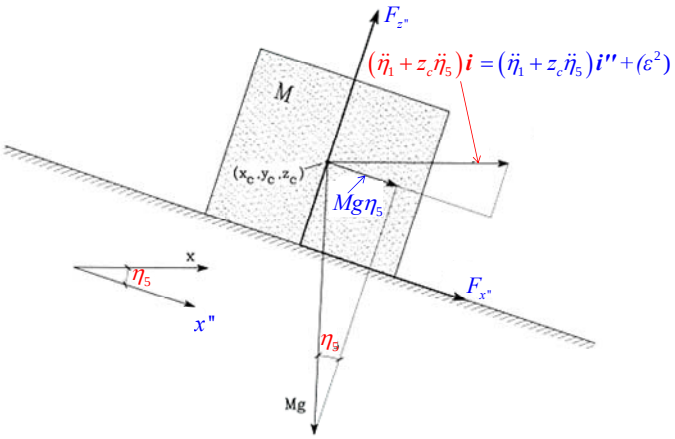

Hp: An object, with mass *M* and center of gravity (x_c,y_c,z_c) in the (*x,y,z*) reference frame, is on the deck. The ship is oscillating in surge, heave and pitch due to its interaction with head incident waves.

Objective: Find the equation of object motions in the body-fixed reference frame (*x'',y'',z''*).

The object is subjected to external forces $F_{x''}$ and $F_{z''}$ due the contact with the deck (e.g. deck friction, fastening, etc.). Moreover the ship motions cause additional forces.

Along *x''*: The pitch motion causes a time-varying component associated with the object weight $Mg\eta_5\boldsymbol{i}''$. Moreover, the object center of gravity has an acceleration along x which is the same along x'' within linear theory, i.e. $\left(\ddot{\eta}_2 + z_c\ddot{\eta}_5\right)\boldsymbol{i} = \left(\ddot{\eta}_2 + z_c\ddot{\eta}_5\right)\boldsymbol{i}'' + (\varepsilon^2)$ so we have

$$M\left(\ddot{\eta}_2 + z_c\ddot{\eta}_5\right) = Mg\eta_5 + F_{x''} \qquad (1)$$

Along *z''*: With similar procedure we have

$$M\left(\ddot{\eta}_3 - x_c\ddot{\eta}_5\right) = -Mg + F_{z''} \qquad (2)$$

Equation (1) is useful to guarantee suitable fastening of the object. From equation (2) we see that for the object to not leave the deck $F_{z''}$ must be positive.

7) Fluid motion in a moonpool (F:99-100, exercise 3.6)

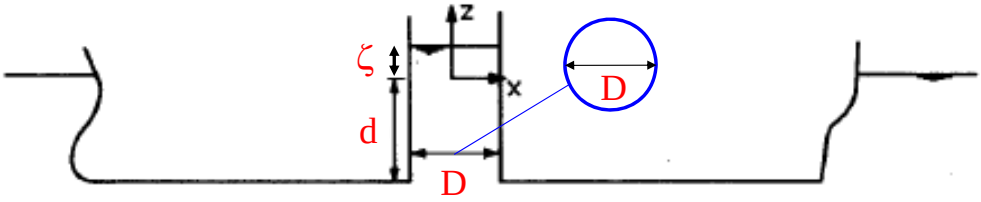

A moonpool is an opening in the ship used in oil field to provide access for the well drilling.

Hp: -The ship motions are known.
-The moonpool has a horizontal cross-section uniform and circular with diameter D.
-The internal fluid motion is only vertical with uniform velocity $d\zeta/dt$ and acceleration $d^2\zeta/dt^2$, ζ being the free surface elevation relative to the mean free-surface level in the sea (the mean free-surface level from the ship bottom is the dradt d).

Objective: We analyse occurrence of piston-mode (1D oscillations in z) resonance in the moonpool using linear theory.

Q: What is the fluid acceleration?
Within potential-flow theory, the fluid-momentum equation is given by the Euler equation:

$$\underbrace{\rho\frac{d^2\zeta}{dt^2}}_{\substack{local\text{-}flow\\ inertia\ force}} = \underbrace{-\frac{\partial p}{\partial z} - \rho g}_{\substack{external\ forces:\\ pressure\ gradient\ and\ gravity}} \qquad (1)$$

This gives directly the fluid acceleration $\frac{d^2\zeta}{dt^2} = -\frac{1}{\rho}\frac{\partial p}{\partial z} - g$ (F:3.85).

Q: Equation (1) is local in the fluid, what does it give its integration from z=-d to z=ζ within linear theory?

$$\int_{-d}^{\zeta}\left(\underbrace{\rho\frac{d^2\zeta}{dt^2}}_{uniform} = -\frac{\partial p}{\partial z} - \rho g\right)dz \Rightarrow \underbrace{\rho\frac{d^2\zeta}{dt^2}}_{second\ order}\zeta + \rho\frac{d^2\zeta}{dt^2}d = -\left[\underbrace{p_a}_{atmospheric} - \underbrace{p}_{z=-d}\right] - \rho g(\zeta + d)$$

$$\underbrace{\Rightarrow}_{\substack{using\ linear\\ Bernouilli\ eq.\ for\ p}} \rho\frac{d^2\zeta}{dt^2}d = -\left[p_a - p_a + \rho\left.\frac{\partial\phi}{\partial t}\right|_{z=-d} + \rho g(-d)\right] - \rho g(\zeta + d)$$

$$\Rightarrow \frac{d^2\zeta}{dt^2}+\frac{g}{d}\zeta=-\frac{1}{d}\frac{\partial\phi}{\partial t}\bigg|_{z=-d} \qquad \text{(F:3.86)}$$

This equation is like a mass-spring system forced by the right-hand-side excitation load. The natural frequency of the system is obtained from the homogenous equation:

$$\frac{d^2\zeta}{dt^2}+\frac{g}{d}\zeta=0 \underbrace{\Rightarrow}_{\text{steady state}} \left[-\omega_n{}^2+\frac{g}{d}\right]\zeta=0 \Rightarrow \omega_n=\sqrt{\frac{g}{d}} \Rightarrow T_{n0}=2\pi\sqrt{\frac{d}{g}} \qquad \text{(F:3.87)}$$

So the resonance condition is characterized by a period T_{n0} which only depends on d and increases with square root of it. This is because the moonpool beam (diameter D) is assumed small relative to the draft d.

Molin (2001) has studied the piston-mode (1D oscillations) of a moonpool. The main geometrical parameters are in the figure below :

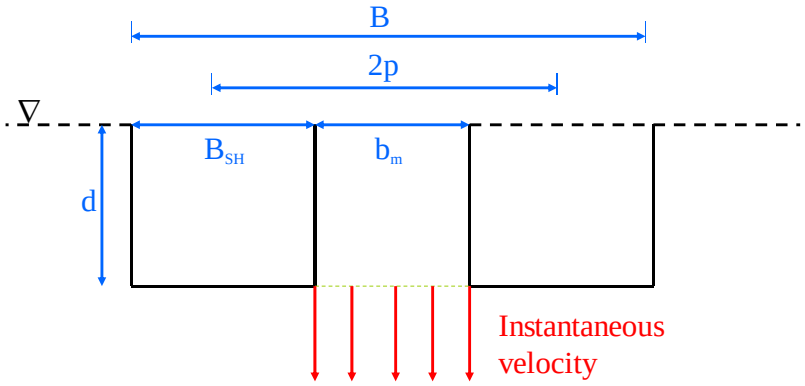

In this case also other body dimensions, i.e. b_m/d and $B/2b_m$, matter for the natural period, which becomes

$$T_n=\underbrace{2\pi\sqrt{\frac{d}{g}}}_{T_{n0}}\underbrace{\sqrt{1+\frac{1}{\pi}\frac{b_m}{d}\left(1.5+\ln\frac{B}{2b_m}\right)}}_{\text{additional term}}$$

This expression reduces to T_{n0} from Faltinsen's formula (F:3.87) if $b_m/d\to 0$. The additional term leads to T_n greater than T_{n0} if $\ln(B/2b_m)>-1.5$ which means if the side-hull beam B_{SH} is sufficiently wide relative to the moonpool width.

The parameter b_m/d, by itself would tend to increase the natural period, but its increase may cause 3D effects in the moonpool flow.

The ratio between the resonant moonpool amplitude and the amplitude of the heave motion, $\zeta_a{}^{moonpool}/\eta_{3a}$, is given in the figure below, as a function of B_{SH}/b_m and shows a nearly linear trend for a given d/b_m and h/b_m with h the water depth.

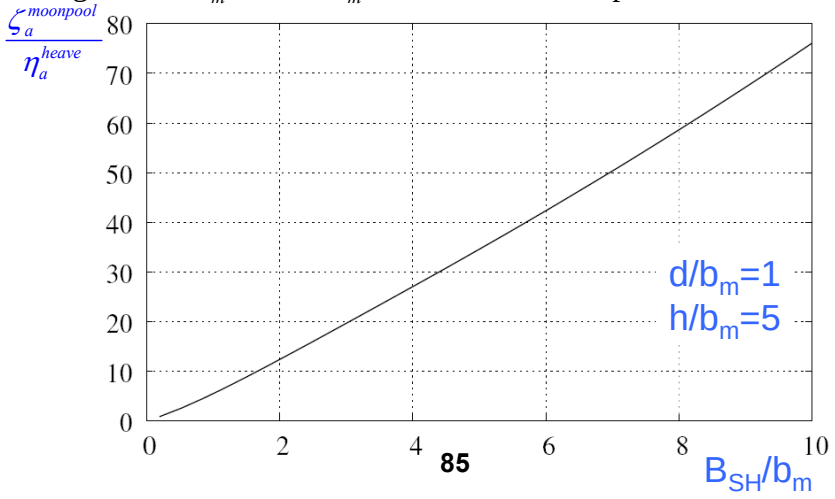

From the results, $\zeta_a^{moonpool} / \eta_{3a}$:

- increases with increasing the side-hull beam B_{SH}
- increases with decreasing moonpool width b_m
- less sensitive to draft *d* and water depth *h* (not shown here)

The resonant mass flux in the moonpool is larger than the heave mass flux and their ratio increases with B_{SH} / b_m. The trend is faster than linear for small B_{SH} / b_m and tends to a linear behaviour as B_{SH} / b_m gets large. This is shown in the figure below:

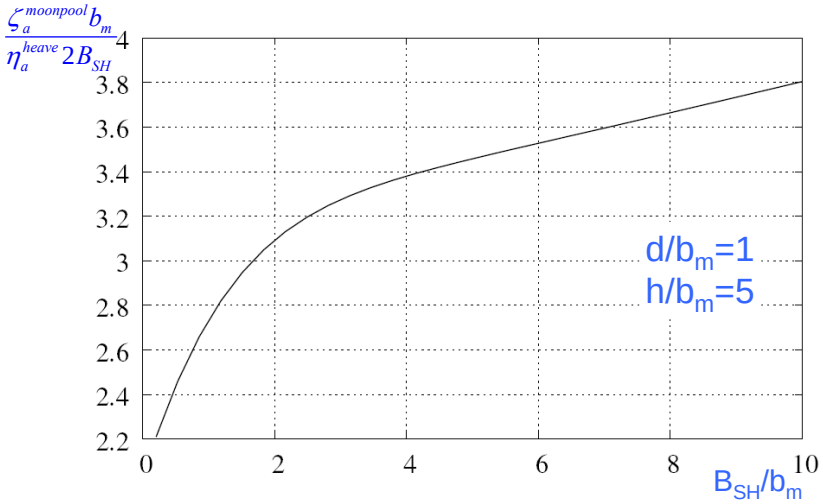

The resonance of piston-type mode is also relevant in the case of a vessel (like an LNG tanker) near a terminal. In particular in the region between the two marine units (see example in the figure below:

8) <u>Mathieu-type instability in roll</u>
The roll motion of a marine structure can be subjected to a Mathieu-type instability.
Hp: 1D roll motion problem

The restoring term depends on the transverse metacentric height $\bar{G}\bar{M}_T$, so if $\bar{G}\bar{M}_T$ changes in time also the restoring term will. In this case, the equation of motion becomes
$(I_{44} + A_{44})\ddot{\eta}_4 + B_{44}\dot{\eta}_4 + C_{44m} \cdot f(t)\eta_4 = 0$
with C_{44m} the restoring term corresponding to the mean transverse metacentric height, say $\bar{G}\bar{M}_{Tm}$. The function *f(t)* accounts for the time variation of the restoring term. Dividing by $I_{44} + A_{44}$ and writing explicitly *f(t)*, we have

$$\ddot{\eta}_4 + 2\xi\omega_n\dot{\eta}_4 + \omega_n^2\underbrace{\left[1+\frac{\delta\bar{G}\bar{M}_T}{\bar{G}\bar{M}_{Tm}}\sin(\omega_e t+\beta)\right]}_{f(t)=\text{time-varying part of restoring term}}\eta_4 = 0$$

with $\xi = B_{44}/[2(I_{44}+A_{44})\omega_n]$ the fraction of the damping relative to the critical damping and $\omega_n = \sqrt{C_{44m}/(I_{44}+A_{44})}$ is the natural frequency. $\delta\bar{G}\bar{M}_T$, ω_e and β are, respectively, the amplitude of the variation of $\bar{G}\bar{M}_T$, its frequency and its phase relative to the roll motion. When *f(t)* becomes negative the restoring term is destabilizing. We talk about Mathieu instability and its existence plane in terms of $\frac{\delta\bar{G}\bar{M}_T}{\bar{G}\bar{M}_{Tm}}\left(\frac{\omega_n}{\omega_e}\right)^2$ and $\left(\frac{\omega_n}{\omega_e}\right)^2$ is given in the figure below:

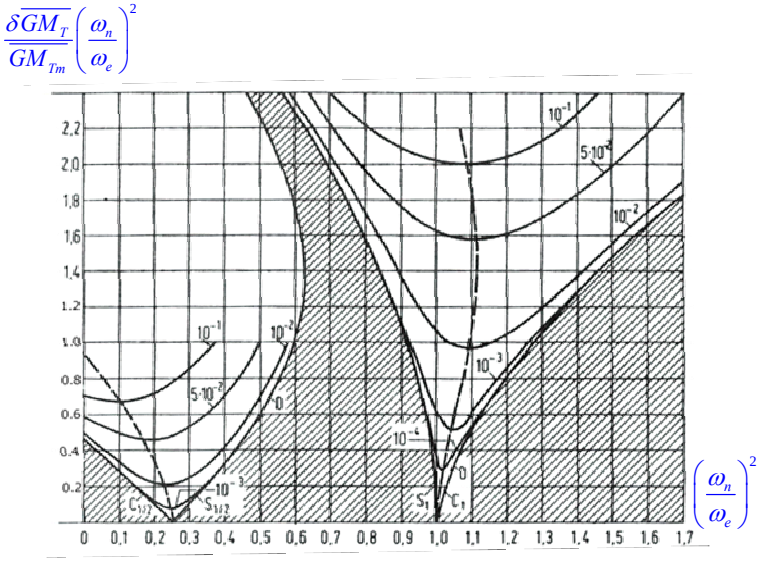

The white regions mean instability, those in grey stable conditions.
Mathieu-type instability can be for instance excited for a spar platform by second-order effects responsible for the variation distance between the center of buoyancy and the center of gravity which is the dominating restoring contribution for such platforms due to the limited waterplane area.

9) <u>RAO from linear seakeeping model tests.</u>
The **RAO** $|\boldsymbol{\eta}_a|/\zeta_a$ can also be estimated experimentally. The used techniques are mainly two and use a physical wavemaker to generate the incident waves:

1) Regular-wave technique=each test generates regular-incident waves at a given ω with amplitude so that $k\zeta_a$ is small (linear theory) and the RAO is measured. ω is varied to study the whole relevant range for body motions.
2) Transient-test technique=one test generates regular waves with different frequencies, first the shortest, slower, then increasing progressively λ. The generated waves will 'meet' in a prescribed point of the basin (i.e. at the ship location). This involves a focusing process and leads to a very concentrated disturbance of the free surface, wave packet. Its interaction with the body causes a response which can be splits in the different frequency components to provide the RAO as in 1).

Technique 2) has the advantage that you can find one-shot the RAO for all ω values of interest, it has no problems of wave reflections from the tank sides and high repeatability. But it has problems to study irregular waves.

Piston mode

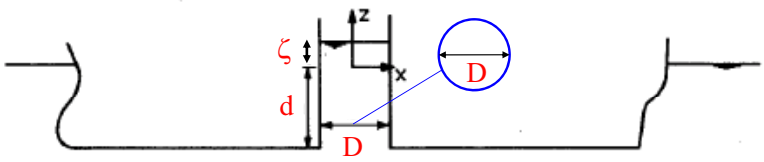

Piston mode resonance

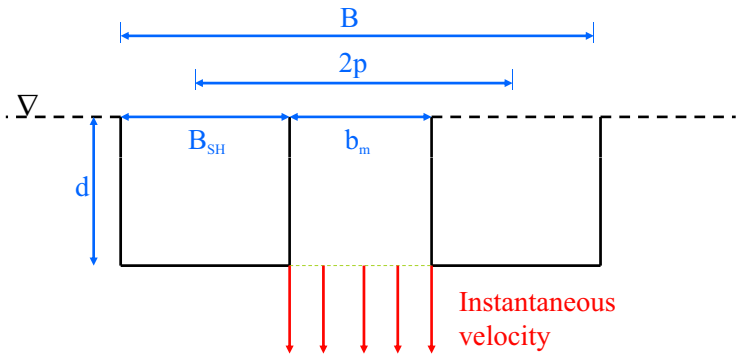

Resonant moonpool amplitude divided by heave amplitude

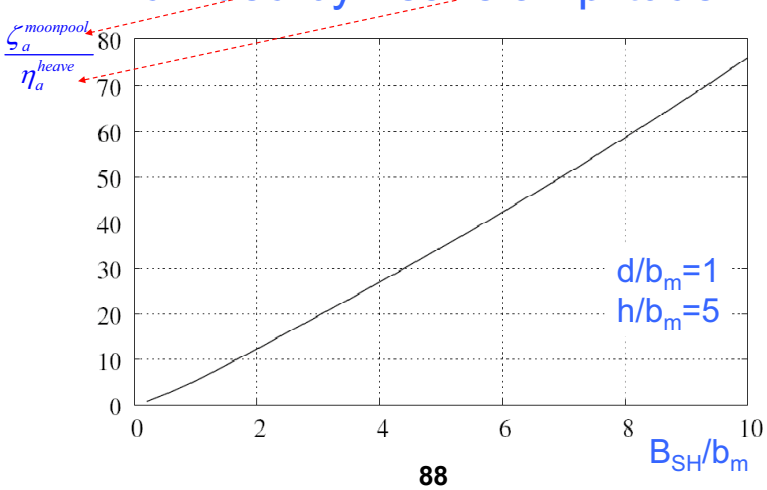

Resonant mass-flux in moonpool divided by heave mass-flux

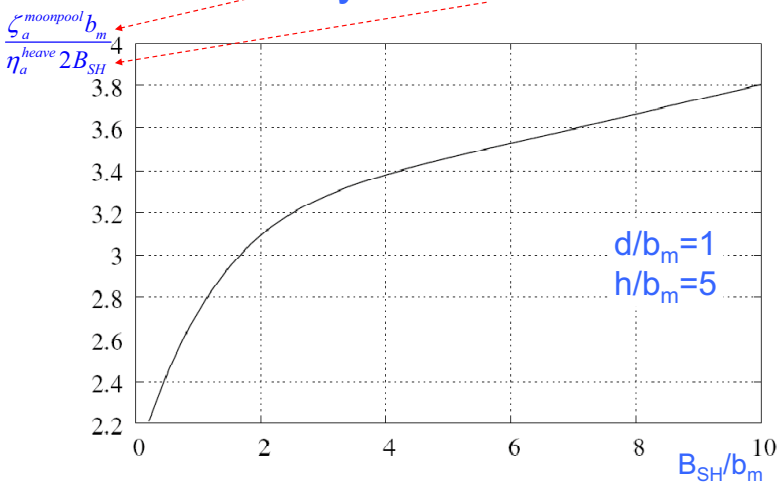

Resonant fluid motion

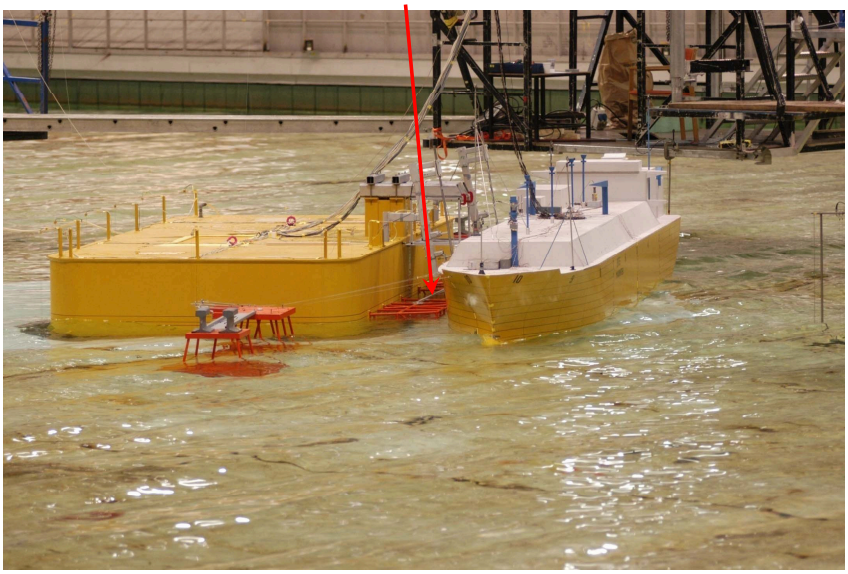

Mathieu instability

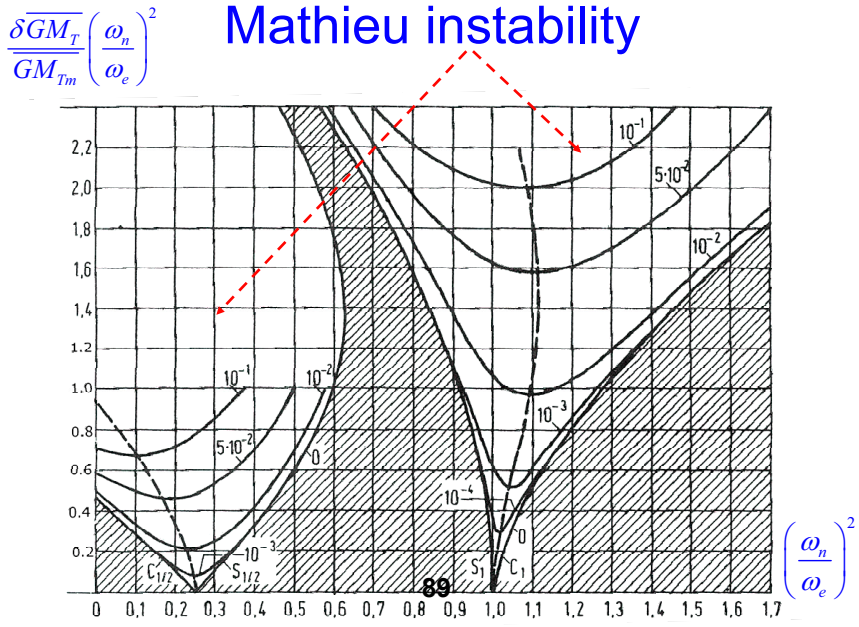

Consequence of Mathieu type instability in roll

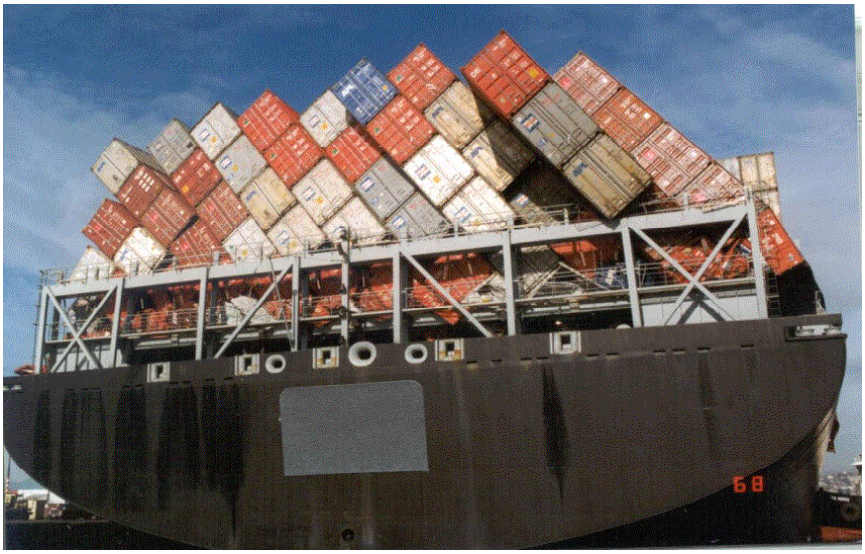

Transient Tests

(wave packets)

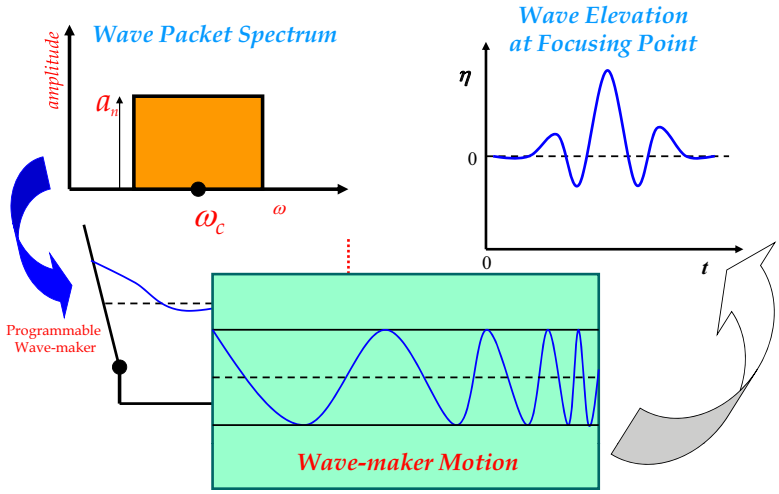

Transient Tests

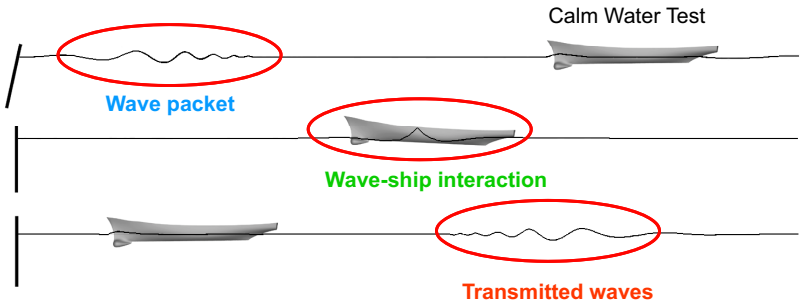

- *One Shot Test*
- *High repeatability*
- *No reflections from the ends*
- *No statistical estimation*

Linear Seakeeping Model Tests

Tests in regular waves

Transient tests

SEA LOADS BOOK

(in Korean and Chinise)

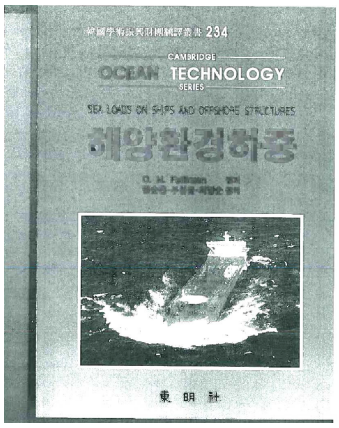

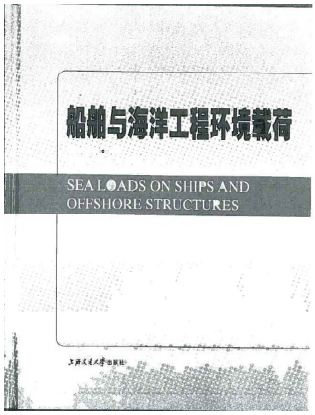

Lecture Note 5

39. Minimization of heave, pitch and roll motion. Second-order effects: mean values, difference and sum-frequency effects. Mean wave induced loads from direct pressure integration and conservation of fluid momentum. (F:81-89,131-133,142-143)

Minimization of heave and pitch ship motions (F:81-85)

The wave induced damping terms in heave and pitch are in general large, i.e. the vessel capability in generating waves in heave and pitch is high.

This fact is particularly important near the resonance to keep the motions limited. Other important aspects that affect the motions features are cancellation effects of the motions and dependence of motions from geometry and operational conditions, i.e. without or with forward motion.

We discuss this in a simplified way, the aim is to show general trends.

Hp: - Linear regular deep-water head sea long waves

→ Long-wave approximation valid, i.e. cross-section small relative to the wavelength

- The ship is elongated and has uniform box-shaped cross-sections (i.e. like a barge), symmetry about *(x,z)* and *(y,z)*, U=0

→ Due to elongation, strip theory can be applied

→ Due to uniform cross sections, added mass A_{33}, damping B_{33}, and restoring C_{33}, are uniformly distributed along L, i.e. $dA_{33}=A_{33}dx/L$, $dB_{33}=B_{33}dx/L$, $dC_{33}=C_{33}dx/L$

→ Due to fore-aft symmetry, heave and pitch motions are uncoupled

- The mass m is uniformly distributed along L, i.e. $dm=mdx/L$

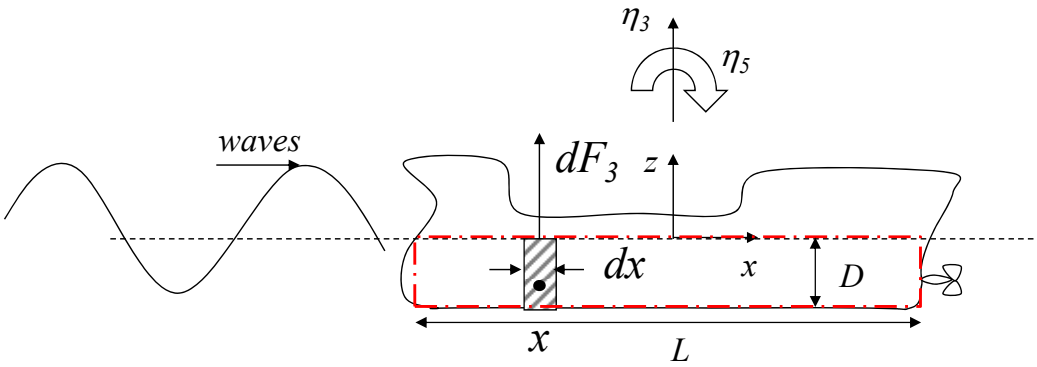

Ship and its approximated barge (dash-dotted red line)

For the linear regular deep-water head sea waves we have:

$$\zeta_0 = \zeta_a \sin(\omega t - kx)$$

$$p_0 = \rho g \zeta_a e^{kz} \sin(\omega t - kx)$$

$$a_{03} = \frac{\partial^2 \phi_0}{\partial t \partial z} = -\omega^2 \zeta_a e^{kz} \sin(\omega t - kx)$$

- Heave motion

Using long-wave approximation + strip theory + symmetry about *(x,z)* and *(y,z)* + head waves, the excitation force in heave is:

$$F_{exc,3HS} \cong \int_{S_{0B}} -p_0 n_3 dS + \int_L A_{33}^{(2D)} \overline{a}_{03} dx \quad \text{(normal vector pointing inside the fluid)}$$

Using that the cross-section is box shaped and uniform (i.e. like a barge), we have

$$F_{exc,3HS} = \underbrace{\zeta_a \left[\rho g e^{-kD} - \omega^2 A_{33}^{(2D)} e^{-kD/2} \right]}_{=F_0/L} \int_{-L/2}^{L/2} \sin(\omega t - kx) dx = \frac{2F_0}{kL} \sin\left(\frac{kL}{2}\right) \sin \omega t$$

NB:

$$\int_{-L/2}^{L/2} \sin(\omega t - kx) dx = \frac{1}{k} \left[\cos(\omega t - kx) \right]_{-L/2}^{L/2} = \left[\cos \omega t \cos kx + \sin \omega t \sin kx \right]_{-L/2}^{L/2} = 2 \sin\left(k \frac{L}{2}\right) \sin \omega t$$

The result says that in head sea the wave loads along the ship can counteract each other and cancel the total wave excitation loads, this occurs for

$\sin(kL/2)=0$ → for $kL/2=n\pi$ → $\lambda/L=1/n$ with $n=0,1,..$

$n=0$ means no waves, $n=1$ means $\lambda/L=1$, i.e. at the resonance.

NB: This means that, without forward speed, the cancellation effect on the heave motion in head-sea conditions may be dominant around the natural frequency for heave and pitch.

Let's now estimate the excitation force in heave induced by beam waves with the same parameters as the head waves assumed here:

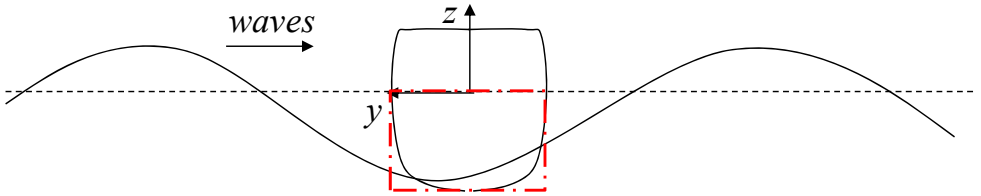

Ship cross-section and its approximation (dash-dotted red line)

The incident waves are:

$\zeta_0 = \zeta_a \sin(\omega t + ky)$

$p_0 = \rho g \zeta_a e^{kz} \sin(\omega t + ky)$

$a_{03} = \frac{\partial^2 \phi_0}{\partial t \partial z} = -\omega^2 \zeta_a e^{kz} \sin(\omega t + ky)$

So, using valid the same assumptions, we have:

$$F_{exc,3BS} \cong \int_{S_{0B}} -p_0 n_3 dS + \int_L A_{33}^{(2D)} \overline{a}_{03} dx \underset{y=0}{=} \underbrace{\zeta_a \left[\rho g e^{-kD} - \omega^2 A_{33}^{(2D)} e^{-kD/2} \right]}_{=F_0/L} \underbrace{\int_{-L/2}^{L/2} dx}_{L} \cdot \sin(\omega t) = F_0 \sin(\omega t)$$

It means that the heave-force amplitudes in head and beam waves with identical parameters are linked as

$$|F_{exc,3HS}| = \frac{2}{kL} \left| \sin\left(\frac{kL}{2}\right) \right| |F_{exc,3BS}| \quad \text{(F:3.70)}$$

Due to the linearity, the motion amplitude is proportional to the excitation-force amplitude:

$$|\eta_3| \propto |F_{exc,3}| \Rightarrow |\eta_{3HS}| = \frac{2}{kL} \left| \sin\left(\frac{kL}{2}\right) \right| |\eta_{3BS}| \quad \text{(F:3.71)}$$

NB: Because the term $|\sin(kL/2)/(kL/2)| < 1$ and tends to 1 for $kL/2 \to 0$, the response in heave is in general smaller in head sea than in beam sea with the same parameters.

- Pitch motion

We can use the same approach as for the heave. In head-sea waves the excitation moment is:

$$dF_{exc,5HS} = -xdF_{exc,3HS} = -\frac{F_0}{L}x\sin(\omega t - kx)dx$$

$$\Rightarrow F_{exc,5HS} = -\frac{F_0}{L}\int_{-L/2}^{L/2} x\sin(\omega t - kx)dx = -\frac{F_0}{L}\left[\frac{L}{k}\cos\left(k\frac{L}{2}\right) - \frac{2}{k^2}\sin\left(k\frac{L}{2}\right)\right]\cos\omega t$$

NB: $$\int_{-L/2}^{L/2} x\sin(\omega t - kx)dx = \int_{-L/2}^{L/2}\left[\sin(\omega t)\underbrace{x\cos(kx)}_{antisym\Rightarrow \text{int}egral=0} - \cos(\omega t)\underbrace{x\sin(kx)}_{sym\Rightarrow \text{int}egral\neq 0}\right]dx$$

$$= -\cos(\omega t)\left[-\frac{x}{k}\cos(kx) + \frac{1}{k^2}\sin(kx)\right]_{-L/2}^{L/2} = \left[\frac{L}{k}\cos\left(k\frac{L}{2}\right) - \frac{2}{k^2}\sin\left(k\frac{L}{2}\right)\right]\cos\omega t$$

and the uncoupled pitch motion equation gives:

$$\Rightarrow (I_{55} + A_{55})\ddot{\eta}_{5HS} + B_{55}\dot{\eta}_{5HS} + C_{55}\eta_{5HS} = F_{exc,5HS} \Rightarrow \eta_{5HS} = \frac{12}{L^2}\frac{F_{exc,5HS}}{-\omega^2(m + A_{33}) + i\omega B_{33} + C_{33}}$$

NB: $I_{55} = \int_m (x^2 + z^2)dm \cong \frac{m}{L}\int_{-L/2}^{L/2} x^2dx = \frac{mL^2}{12}$, $K_{55} \underset{\substack{strip\\theory}}{=} \int K_{33}x^2dK_{33} = \frac{K_{33}}{L}\int_{-L/2}^{L/2} x^2dx = \frac{K_{33}L^2}{12}$

with $K = A,\ B,$ C

The I_{55} contribution with z^2 can be neglected because it is connected with the draft D while the term in x^2 is connected with the ship length L and we assume L/D large.

The pitch amplitude in head sea is then

$$|\eta_{5HS}| = \frac{12}{L^2}\left|\frac{\frac{F_0}{L}\left[\frac{2}{k^2}\sin\left(k\frac{L}{2}\right) - \frac{L}{k}\cos\left(k\frac{L}{2}\right)\right]}{\sqrt{[-\omega^2(m + A_{33}) + C_{33}]^2 + \omega^2 B_{33}{}^2}}\right| \qquad (1)$$

This can be related to the heave amplitude in beam sea obtained from

$$(m + A_{33})\ddot{\eta}_{3BS} + B_{33}\dot{\eta}_{3BS} + C_{33}\eta_{3BS} = F_{exc,3BS} \Rightarrow |\eta_{3BS}| = \left|\frac{F_0}{\sqrt{[-\omega^2(m + A_{33}) + C_{33}]^2 + \omega^2 B_{33}{}^2}}\right|$$

by expressing F_0 in eq. (1) in terms of $|\eta_{3,BS}|$, we have

$$|\eta_{5HS}| = \frac{12}{L}\left|\frac{2}{L^2k^2}\sin(k\frac{L}{2}) - \frac{1}{Lk}\cos(k\frac{L}{2})\right||\eta_{3BS}| \qquad \text{(F:3.72)}$$

- With forward motion

Hp: We account only for the change in frequency due to U,

i.e. $\omega_e = \omega + \omega^2 U / g$ (head sea waves).

The natural frequency ω_n is considered identical with and without speed

→ at $U \neq 0$ resonance is caused by longer waves because the encounter frequency is greater than the incoming-wave frequency.

If we use the last assumption in the expressions of $|\eta_{3HS}|$ and $|\eta_{5HS}|$, we have:

→ The cancellation effect on heave and pitch excitation loads appears less pronounced at $U\neq 0$

→ Heave and pitch at resonance may be greater within a certain limits of increasing Froude number.

Example.

Hp: A ship with L=95m. Deep-water head sea waves.

T_n=7.8s is the period at resonance condition→ $\omega_n = 2\pi / T_n = 0.805 rad/s$

Obj: Find the incident wave length at natural oscillation frequency ω_n.

At U=0m/s → $\omega = \omega_n \rightarrow \lambda = 2\pi g / \omega_n^{\,2} \cong 95$ m i.e. L/λ=1

So there is heave cancellation.

At U=10m/s → $\omega_e = \omega + \dfrac{\omega^2}{g} U = \omega_n = 0.805 rad/s$

$$\Rightarrow \omega = \frac{-0.5 + \sqrt{0.25 + 4\pi U/(gT_n)}}{2U/g} \cong 0.527 rad/s$$

$$\Rightarrow \lambda_U = \frac{2\pi g}{\omega^2} \cong 222 m$$

So for U=10m/s at resonance L/λ_U=95/222=0.428 giving $\sin(k_U L/2) = \sin(\pi L/\lambda_U) \cong 0.975$.

This means that the cancellation effect is much reduced relative to zero forward speed.

To find the heave and pitch amplitude at resonance in head sea we need to know the amplitude of the heave motion at resonance in beam waves. This can be estimated assuming negligible 3D effects (i.e. studying the heave motion of the cross-section) and using the Newman's (1962) excitation vertical force on an infinitely long cylinder in beam sea (already discussed in the example of a 2D cross-section in beam waves):

$$|F_{exc,3BS}^{(2D)}| = \zeta_a \sqrt{\frac{\rho g^2}{\omega_3} B_{33}^{(2D)}}$$

So we have:

$$|\eta_{3BS}| = \zeta_a \frac{g}{\omega_{n3}^{3/2}} \sqrt{\frac{\rho}{B_{33}^{(2D)}}} \qquad \text{(F:3.74)}$$

with ω_{n3} the undamped natural (circular) frequency in heave and $B_{33}^{(2D)}$ the cross-sectional 2D damping in heave. $B_{33}^{(2D)}$ depends on ω_{n3}.

Using the Lewis-form technique to find the damping coefficient, the heave amplitude at resonance can be obtained, as reported in figure F:3.22 (given qualitatively below).

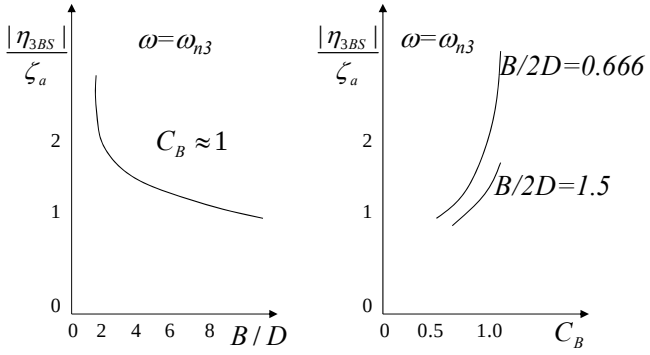

Fig. F:3.22

$|\eta_{3BS}|$ increases decreasing the beam-to-draft ratio *B/D* and increasing the sectional area coefficient $\sigma=A/(BD)$ which in this case (box-shaped uniform cross-sections) is equal to the block coefficient, i.e. $\sigma=C_B$. These results can be transferred to the heave and pitch amplitude in head sea.

NB: The results obtained must be read as trends, i.e. considering large variations of the examined parameters. Making small changes may not show this behaviour since there are other parameters that matter: heave and pitch natural periods depend on the hull geometry and the cancellation effects in heave and pitch will vary from hull to hull.

The RAO discussed here can be inserted in a statistical analysis assuming a spectrum $S(\omega)$. The analysis suggests that the vertical motions in head sea conditions depend on the ship length *L* and we expect that they decrease as *L* increases. Also this must be interpreted as a trend, i.e. it applies considering large variations in length. The vertical motions may also depend on other hull parameters than those considered here. Other aspects that could be relevant for the motions are: bulb, transom stern, pitch radius of gyration, U-form or V-form of the vessel. In the used simplified model, heave and pitch coupling is not accounted for due to the fore-aft symmetry of the vessel. In general the coupling matters for the motion amplitude.

Minimization of roll motion. (F:85-89)
The wave induced roll damping can be limited in particular when the considered geometry has a limited capability in generating waves while rolling, e.g. cross-sections close to circular. In such conditions viscous damping becomes important associated with flow separation (we will see this later) which takes away a portion of the motion energy. When the vessel hull does not ensure sufficient roll damping, additional mechanisms are needed to ensure proper damping. Typical means used for ships are:

1) Bilge keels: due to the presence of a geometrical singularity, flow separation is ensured. The roll stabilization is obtained by causing flow separation and then modifying the pressure distribution on the bilge keel and around the hull. This provides a load proportional to the square power of the roll velocity which acts as a damping for roll motion, i.e. it is proportional to $\dot{\eta}_4|\dot{\eta}_4|$.

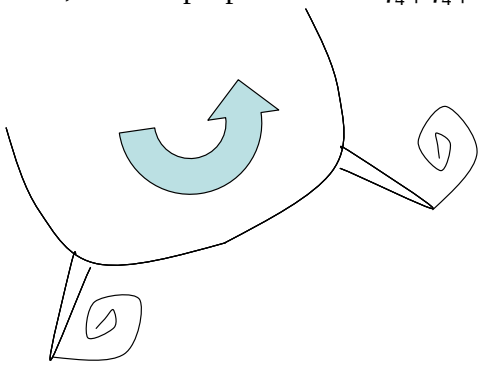

2) Passive anti-roll tanks: they cause a roll moment, say M_{AT}, counteracting the roll velocity. Both free-surface and U-tube tanks are used with this scope (see Fig. F:3.23). A detailed description can be found in Faltinsen's book "Sloshing", from pg. 82).

For them to work best, the tank natural period, say T_N, must be close to the roll natural period, say T_{n4}. In this way the tank moment is almost 180° out-of-phase to the roll velocity (i.e. 90° out-of-phase to the roll motion).

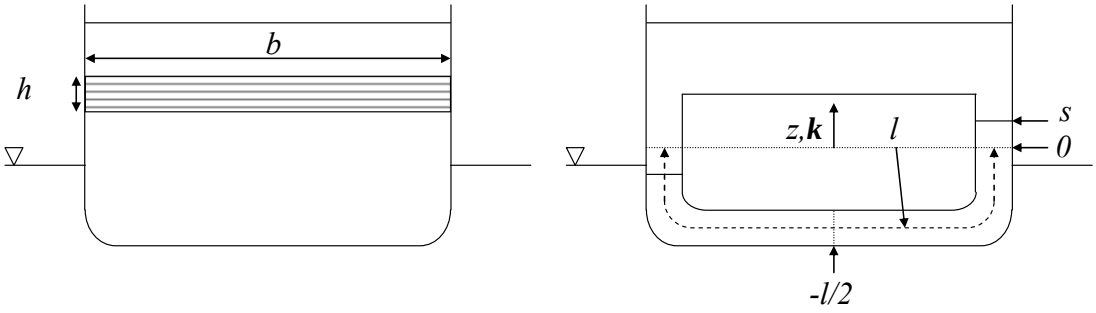

Fig. F:3.23

In particular, fig. F:3.24 shows a free-surface tank at zero roll motion (maximum roll speed). In this condition a hydraulic jump forms in the middle and the related pressure distribution causes a maximum tank moment against the roll speed.
Some designers set $T_{4n} = T_N$, while others use T_N 6-10% smaller than T_{4n}.

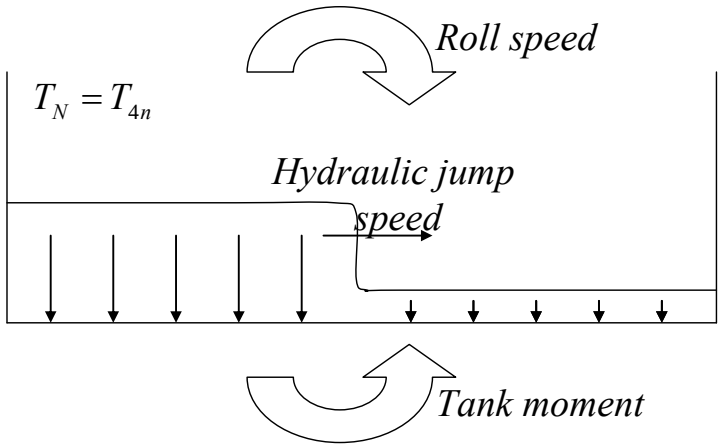

Fig. F:3.24

The damping effect is greater the tank causes a reduction, $\delta\bar{G}\bar{M}_T$, of the transversal metacentric height relative to the case without tank, $\bar{G}\bar{M}_T$, in the range $0.15 \le \delta\bar{G}\bar{M}_T / \bar{G}\bar{M}_T \le 0.3$.

Free-surface tank:
The highest natural period T_1 is connected with a wavelength $\lambda=2b=2\pi/k$, so using the dispersion relationship in finite water depth $\omega^2 = gk\tanh kh$ we have

$$T_1 = 2\pi / \sqrt{g(\pi / b)\tanh((\pi / b)h)} \qquad \text{(F:3.75)}$$

Because the water depth is typically small relative to *b*, shallow-water conditions apply, i.e. $h/b \to 0$, so $\tanh(\pi h / b) \approx \pi h / b$ and

$$T_N \cong 2b / \sqrt{gh} \qquad \text{(F:3.76)}$$

The following figure shows the effect of the water depth h and the width of the tank b on the tank highest natural period T_1 according to formula (F:3.75). For a given h, T_1 increases as b increases. For a given b, T_1 decreases as h increases.

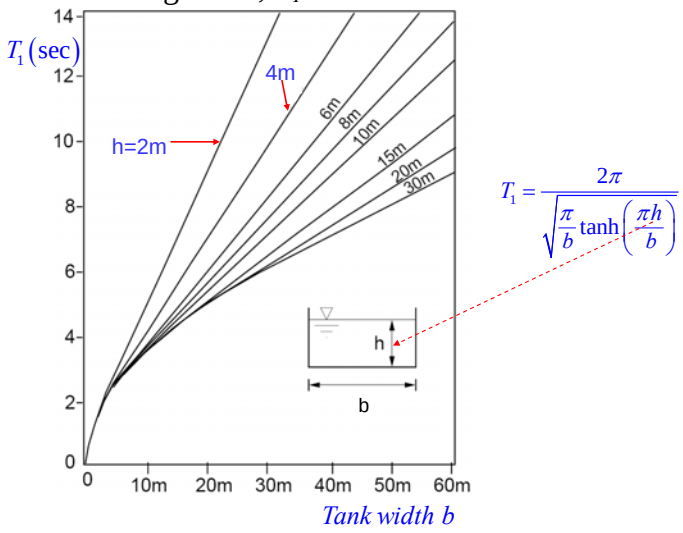

Due to the possibility to change the natural period by changing h, this type of anti-roll tank is well suited for ships operating with a wide range of metacentric heights.
The ideal would be to have a linear moment from the anti-roll tank. The moment given by a free-surface tank is instead nonlinear, as shown in the figure below:

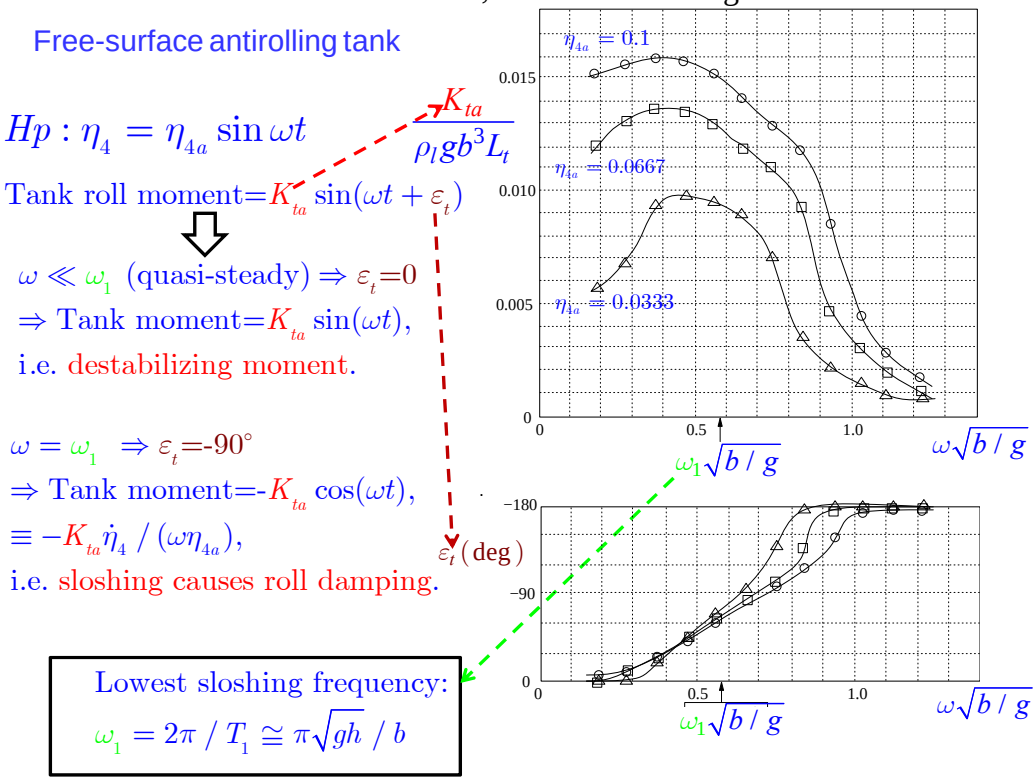

The figure also proves as in quasi-steady conditions a sloshing tank is destabilizing for the roll motion, while it causes roll damping when the roll motion frequency is equal to the natural sloshing frequency.

U-tube tank:
Assuming a constant cross-section area A, the natural period can be obtained following the same approach as done for the piston-mode in a moonpool and assuming linear conditions:

$$\int_{-l/2}^{s}\left(\rho\underbrace{\frac{d^2s}{dt^2}}_{uniform}=-\frac{\partial p}{\partial s}-\rho g\frac{\mathbf{s}\cdot\mathbf{k}}{|\mathbf{s}|}\right)ds$$

$$\Rightarrow \rho\underbrace{\frac{d^2s}{dt^2}}_{second\ order}s+\rho\frac{d^2s}{dt^2}\frac{l}{2}=-\left[\underbrace{p_a}_{atmospheric}-\underbrace{p}_{s=-l/2}\right]-\rho g[(1)s+(0)\frac{l}{2}]$$

$$\underbrace{\Rightarrow}_{\substack{from\ linear\\ Bernouilli}}\rho\frac{d^2s}{dt^2}\frac{l}{2}=-\left[p_a-p_a+\rho\frac{\partial\phi}{\partial t}_{s=-l/2}\right]-\rho gs$$

$$\Rightarrow\frac{d^2s}{dt^2}+\frac{2g}{l}s=-\frac{2}{l}\frac{\partial\phi}{\partial t}_{s=-l/2}\Rightarrow \text{natural period}: T_N=2\pi\sqrt{\frac{l}{2g}}\qquad\text{(F:3.77)}$$

An alternative approach can be based on the fact that at undamped resonance the sum of the kinetic energy

$$K=\frac{1}{2}\rho lA\left(\frac{ds}{dt}\right)^2$$

and the potential energy

$$P=2A\rho g\frac{s^2}{2}$$

in the tank is constant, i.e.

$$\frac{d(K+P)}{dt}=0\Rightarrow\left(l\frac{d^2s}{dt^2}+2gs\right)\rho A\frac{ds}{dt}=0\Rightarrow l\frac{d^2s}{dt^2}+2gs=0\Rightarrow\text{natural period}: T_N=2\pi\sqrt{\frac{l}{2g}}$$

A change of the natural frequency for sloshing is not so easy for a U-tube tank. If the metacentric height for the vessel may vary of a factor greater than 2 for different loading conditions, it is common to use two U-tube tanks. Side valves are used to control the fluid motion inside the tank. These can be part of an automatic control system. The U-tube tanks can provide a quasi-linear moment unless flow separation occurs. In the latter case the behaviour is nonlinear. The figure below shows an example of a U-tube tank on a patrol boat. The use of the anti-roll tank (curve: Stabilized) reduces the roll motion at the resonance with respect to the case without anti-roll tank (curve: Unstabilized). It also shows two side effects: existence of two natural frequencies and increase of the motion at smaller frequencies.

Passive U-tube anti-rolling tanks on 53m long patrol boat

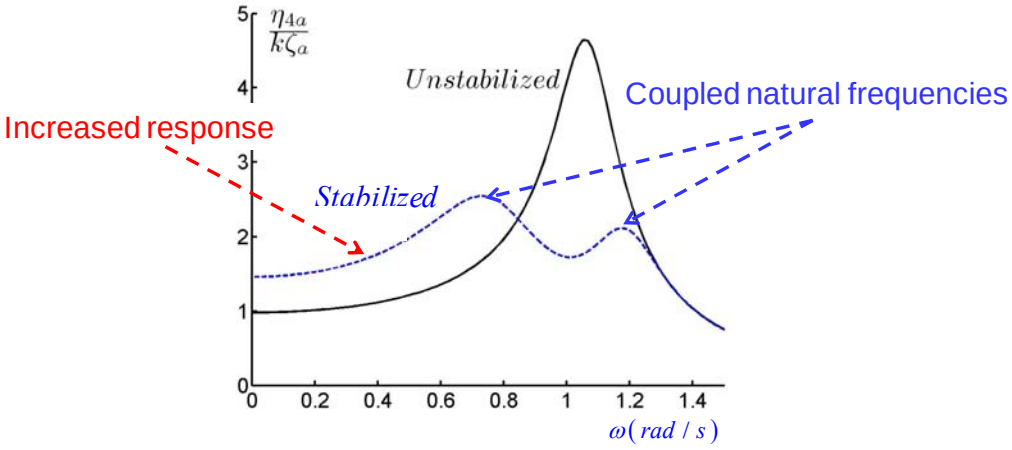

A major problem for the passive anti-roll tanks is saturation, e.g. when the ship motions are very large tank roof impacts can occur reducing the tank ability of producing roll moment.
Both free-surface and U-tube tanks may provide damping in a wider frequency range (i.e. not only at the resonance frequency) if damping is increased in the fluid inside the tank, i.e. introducing screens or other internal obstacles.

Using T_{n4} and $\delta\bar{G}\bar{M}_T / \bar{G}\bar{M}_T$ allows to design the tank

If we want to design a free-surface tank, we need to define the proper value for h, b and L_T, with L_T the tank length. The width b can be taken as the ship beam B, h can be obtained from $T_{n4} = T_N \cong 2b/\sqrt{gh} \Rightarrow h = \left(2b/T_{n4}\right)^2 / g$ and the length L_T and vertical position relative to $z=0$ can be estimated by enforcing the ratio $\delta\bar{G}\bar{M}_T / \bar{G}\bar{M}_T$ within $0.15 \le \delta\bar{G}\bar{M}_T / \bar{G}\bar{M}_T \le 0.3$. Similar approach must be made to design a U-tube tank.

The figure below shows how to design a U-tube and a free-surface tank to damp the motions of a tall building as a function of the building height H:

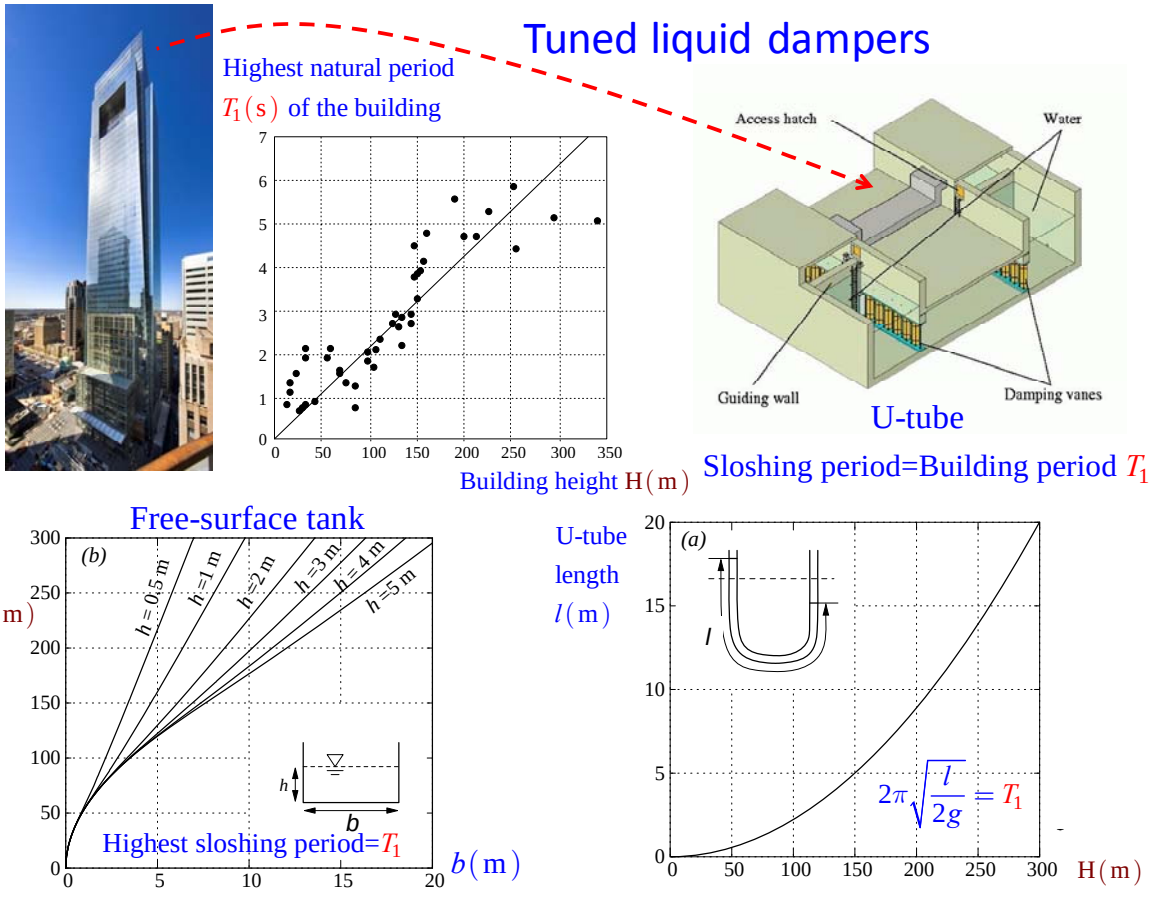

Summary: Environment. Assumptions. Linear wave loads. Diffraction and radiation problems. Excitation loads. Added-mass, damping and restoring coefficients. Parameter analysis. Response. Minimization of vertical motions.

Second-order effects: mean, difference and sum wave-frequency effects (F:131-133)
Up to now we have examined the linear response to linear wave systems. This means that we retained all terms *O(1)* and proportional to $\varepsilon=k\zeta_a$. As the incident waves become steeper, i.e. $k\zeta_a$ increases, also higher order terms must be retained for a suitable estimate of the loads and motions. Using the perturbation approach, i.e. expressing the solution as

$$\phi = \overbrace{\tilde{\phi}_1\varepsilon}^{\phi_1} + \overbrace{\tilde{\phi}_2\varepsilon^2}^{\phi_2} + \tilde{\phi}_3\varepsilon^3 + ...$$
$$\zeta = \underbrace{\tilde{\zeta}_1\varepsilon}_{\zeta_1} + \underbrace{\tilde{\zeta}_2\varepsilon^2}_{\zeta_2} + \tilde{\zeta}_3\varepsilon^3 + ...$$

We can proceed including terms $O(\varepsilon^2)$ (second-order terms) and examining their effects. In this way we are satisfying a bit better the conditions:

- we enforce better the impermeability of the body in its instantaneous configuration,
- the pressure to be atmospheric on the instantaneous free surface and
- the normal fluid velocity at the free surface to be closer to the free-surface normal velocity.

In other words, the problem is still approximated but with a smaller error, i.e. $O(\varepsilon^3)$.

NB: It is more difficult to estimate second-order loads than linear loads, both experimentally and numerically, because they are typically small relative to the first-order contributions
→ they are more sensitive to the specific conditions (geometry, waves, first-order motion, etc).

Hp: Let assume that we have a regular incident wave or a wave spectrum $S(\omega)$.
Objective: we want to examine the response (motions/loads) accurate to the second order.

First-order solution: the response has zero mean value and oscillates with the frequency of the incident waves, i.e. superposition principle is valid.

Second-order effects cause on the response:
1) a mean value → constant (drift)
2) a difference-wave frequency oscillatory behaviour → $(\omega_i - \omega_j)$ long period
3) a sum wave-frequency oscillatory behaviour → $(\omega_i + \omega_j)$ short period

For a regular incident wave: $\omega_i = \omega_j = \omega$
→ the 2nd order effects caused are a mean value and a sum wave-frequency behaviour.
For a sea state with $S(\omega)$: ω_i and ω_j are two generic regular components of $S(\omega)$
→ all 2nd order effects are caused.

NB: Among effects 1)-2)-3): the sum wave-frequency effects are more challenging to be estimated, due to the fast time variations involved. The slow-drift effects are easier to estimate but require longer time analysis, especially when extreme values must be estimated and a statistics must be built for them, this is of concern in model tests.

From where mean, difference and sum effects come from?

Hp: Regular deep-water incident wave with amplitude ζ_a, frequency ω and propagating in x.

The first-order incident wave velocity potential is:

$$\phi_{01} = \frac{g\zeta_a}{\omega} e^{kz} \cos\left(\omega t - kx + \varepsilon\right)$$

In the subscript of ϕ_{01}, the first index '0'=incident wave, the second index indicates the order of approximation.

The wave-induced loads can be obtained by integrating the pressure along the wetted surface of the body. This is given by the Bernoulli eq.:

$$p = -\rho\left[\frac{\partial\phi}{\partial t} + \frac{1}{2}\nabla\phi\cdot\nabla\phi + gz\right] \quad (1)$$

We can assume $\phi = \phi_1(\omega) + \phi_2(2\omega)$, i.e. the solution of the wave-body interaction accurate to the second order (**NB**: It has been emphasized that ϕ_1 and ϕ_2 oscillate in time with ω and 2ω, respectively). This means that the pressure correct to the second order is

$$p = \underbrace{-\rho g z - \rho\frac{\partial\phi_1}{\partial t}}_{O(\zeta_a)} \underbrace{-\rho\frac{\partial\phi_2}{\partial t} - \rho\frac{1}{2}\nabla\phi_1\cdot\nabla\phi_1}_{O(\zeta_a{}^2)}$$

and in general we need to solve the linear and second-order problems to find the velocity potential, i.e. we need to estimate both ϕ_1 and ϕ_2.

The contributions from $\nabla\phi_1\cdot\nabla\phi_2 \propto \zeta_a{}^3$ and $\nabla\phi_2\cdot\nabla\phi_2 \propto \zeta_a{}^4$ to the square-velocity term must be neglected. We now examine the features of this second-order term using the contribution $\left(\partial\phi_1/\partial x\right)^2$ at $x=0$:

Squaring the linear velocity component along x

$$\left.\frac{\partial\phi_1}{\partial x}\right|_{x=0} = A\cos(\omega t + \varepsilon)$$

we have

$$\left(\partial\phi_1/\partial x\big|_{x=0}\right)^2 = A^2\cos^2(\omega t+\varepsilon) = \underbrace{A^2/2}_{\text{constant term}} + \underbrace{A^2\cos[2(\omega t+\varepsilon)]/2}_{\text{sum-frequency term}}$$

NB: $\cos^2(\omega t+\varepsilon) = \{1+\cos[2(\omega t+\varepsilon)]\}/2$

It means that we have a mean load and a sum-frequency load effect.

The second-order term due to $\partial\phi_2/\partial t$ gives a sum-frequency load effect and zero mean value because $\partial\phi_2/\partial t \propto \sin(2\omega t)$.

Hp: Two incident wave components of a sea state with spectrum $S(\omega)$, wave 1 and wave 2, with amplitudes ζ_{a1} and ζ_{a2}, frequencies ω_1 and ω_2 and propagating in x.

The first-order incident-wave velocity potentials are

$$\phi_{01}{}^{(1)} = \frac{g\zeta_{a1}}{\omega_1} e^{k_1 z}\cos\left(\omega_1 t - k_1 x + \varepsilon_1\right) \qquad \phi_{01}{}^{(2)} = \frac{g\zeta_{a2}}{\omega_2} e^{k_2 z}\cos\left(\omega_2 t - k_2 x + \varepsilon_2\right)$$

Here the apex indicates the wave.

Now the velocity potential accurate to the second order is

$$\phi = \phi_1 + \phi_2 = \phi_1{}^{(1)}(\omega_1) + \phi_1{}^{(2)}(\omega_2) + \phi_2(\omega_1,\omega_2)$$

with ϕ_2 involving a combined effect from the two incident waves. We analyse as before the contribution of $\left(\partial\phi_1 / \partial x\right)^2$ to the square-velocity term at *x=0*:

Squaring the linear velocity component along *x*

$$\left.\frac{\partial\phi_1}{\partial x}\right|_{x=0} = \underbrace{A_1\cos(\omega_1 t+\varepsilon_1)}_{\text{due to interaction with wave 1}} + \underbrace{A_2\cos(\omega_2 t+\varepsilon_2)}_{\text{due to interaction with wave 2}}$$

we have

$$\left(\partial\phi_1/\partial x\big|_{x=0}\right)^2 = A_1^{\,2}\cos^2(\omega_1 t+\varepsilon_1) + A_2^{\,2}\cos^2(\omega_2 t+\varepsilon_2) + 2A_1A_2\cos(\omega_1 t+\varepsilon_1)\cos(\omega_2 t+\varepsilon_2)$$

NB: • $\cos^2(\omega t+\varepsilon) = \{1+\cos[2(\omega t+\varepsilon)]\}/2$

• $\cos(\omega_1 t+\varepsilon_1)\cos(\omega_2 t+\varepsilon_2) = \{\cos[(\omega_1+\omega_2)t+\varepsilon_1+\varepsilon_2] + \cos[(\omega_1-\omega_2)t+\varepsilon_1-\varepsilon_2]\}/2$

$$\Rightarrow \left(\partial\phi_1/\partial x\big|_{x=0}\right)^2 = \underbrace{(A_1^{\,2}+A_2^{\,2})/2}_{\text{constant term}} + \underbrace{A_1^{\,2}\cos[2(\omega_1 t+\varepsilon_1)]/2 + A_2^{\,2}\cos[2(\omega_2 t+\varepsilon_2)]/2 + A_1A_2\cos[(\omega_1+\omega_2)t+\varepsilon_1+\varepsilon_2]}_{\text{Sum-frequency terms}} + \underbrace{A_1A_2\cos[(\omega_1-\omega_2)t+\varepsilon_1-\varepsilon_2]}_{\text{Difference-frequency term}}$$

So the second-order body interaction with a sea state with spectrum $S(\omega)$, involves mean loads and loads oscillating in time as $\omega_i \pm \omega_j$.

What is the practical relevance of second-order loads?

Mean (drift) loads resulting from second-order effects are important in many contexts:

- design of mooring systems
- design of thrusters systems
- towing
- offshore loading
- submarines
- capsizing of semisubmersibles
- added resistance in waves

If the two wave frequencies involved are very similar, the sum-frequency effect is of an oscillation period almost half of the incident-wave period and the difference effect is of an oscillation period almost zero, i.e. very slowly-varying loads.

The slowly-varying loads can cause resonance in surge, sway and yaw of a moored structure, for which relevant periods are *O(1-2min)*.

The high-frequency loads can cause resonance in heave, pitch and roll of TLPs, for which relevant periods are *O(2-4sec)*.

We will now discuss the three second-order effects 1)-2)-3) in terms of loads. Most of the discussion is in terms of forces but similarly can be done for the moments.

The forces of a marine structure can be estimated in two ways:

1) The direct pressure integration: integrating the pressure along the instantaneous wetted surface of the body

$$\boldsymbol{F} = \int_{S_B} p\mathbf{n}dS = -\rho \int_{S_B} \left(\frac{\partial \phi}{\partial t} + \frac{1}{2} |\nabla \phi|^2 + gz \right) \mathbf{n}dS = \qquad (1)$$

with **n** pointing inside the body

NB: We are assuming zero viscosity otherwise the tangential stresses should also be considered.

2) The conservation of the fluid momentum: given a certain fluid volume (material/fixed/etc.), the fluid momentum may vary in time because of the forces acting in the volume, like the gravity, or on its enclosing surface, normal and tangential (zero for zero viscosity) stresses, and of the net flux of fluid momentum through its enclosing surface, i.e.

$$\frac{d}{dt}\left(\int_\Omega \rho \mathbf{V} d\Omega \right) = \boldsymbol{F}_S + \boldsymbol{F}_V - \underbrace{\int_S \rho \mathbf{V}(V_n - U_n) dS}_{\mu=0} = -\int_S p\mathbf{n}dS - \int_\Omega \rho g \mathbf{k} d\Omega - \int_S \rho \mathbf{V}(V_n - U_n) dS$$

$\underbrace{\quad}_{if\ >0 \Leftrightarrow\ flux\ leaving\ \Omega}$

with ***n*** pointing out of the fluid volume, ***k*** the unit vector vertical and upwards and U_n the normal velocity of the boundary surface (U_n =0 for a control surface and $U_n = V_n$ for a solid or free surface). If Ω is a fluid volume enclosed by our marine structure, a part of the free surface and a remaining control surface, then from (1) we know that the force on the body can be expressed as

$$\boldsymbol{F} = -\frac{d}{dt}\left(\int_\Omega \rho \mathbf{V} d\Omega \right) - \int_{S-S_B} p\mathbf{n}dS - \int_\Omega \rho g \mathbf{k} d\Omega - \int_S \rho \mathbf{V}(V_n - U_n) dS \qquad (2)$$

Expression (2) is formally more complicated than (1) and involves volume integrals, but there are circumstances where, when the mean loads are of interest, the integrals simplify and may reduce to an integral on a 'far-field' control surface that can be estimated more simply and correctly than that in (1). Expression (1) involves terms that counteract each other and may make it difficult to estimate accurately the loads. Further, approach (2) offers an important physical interpretation of the mean loads, as we will see (i.e. Maruo's formula).

NB: Expressions (1) and (2) are 'exact', i.e. no perturbation process has been introduced, the latter must be considered when we want to estimate explicitly the second-order effects.

Mean wave (drift) forces: direct pressure integration. (F:142-143)
The sources of second-order terms in the loads are:

- **The pressure:** Its expression up to the 2nd order is

$$p = \underbrace{-\rho g z - \rho \frac{\partial \phi_1}{\partial t}}_{O(\zeta_a)} \underbrace{-\rho \frac{\partial \phi_2}{\partial t} - \rho \frac{1}{2} \nabla \phi_1 \cdot \nabla \phi_1}_{O(\zeta_a{}^2)}$$

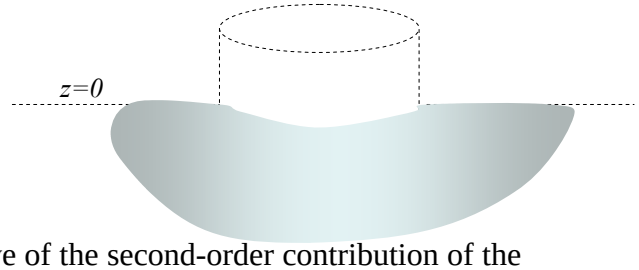

It involves two second-order terms: the time derivative of the second-order contribution of the velocity-potential and the square power of the first-order velocity. Only the latter causes mean forces.

- **The body motions:** The body motions contribute

in two ways to the second-order effects, (a) their first-order value modifies the linear dynamic pressure and causes (if rotational motions) a time variation of the normal vector, (b) their second-order value modifies the hydrostatic pressure. These second-order effects cause mean forces.

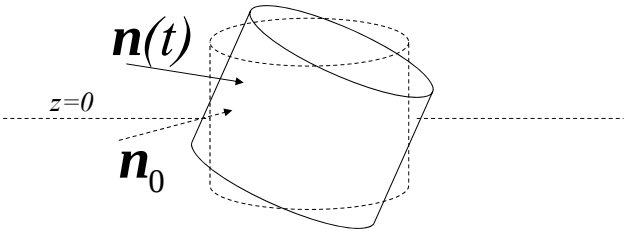

- **The body wetted surface:** The free-surface evolution results in the time variation of the body wetted surface and this has a contribution to the second-order effects. These second-order effects cause mean forces.

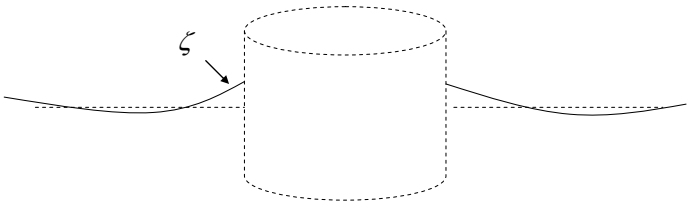

For example the mean value coming from second-order effects in the variation of the wetted surface of the body is shown in Fig. F:5.1:

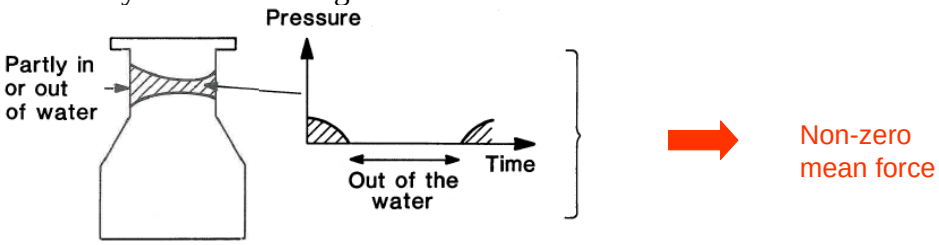

Fig. F:5.1

The different second-order effects come out when we use the perturbation technique to estimate the loads up to the second order. The second-order contribution to the forces can be formally written as the sum of five terms:

$$F_2 = I_1 + I_2 + I_3 + I_4 + I_5$$

They can be interpreted as:

I_1=correction of local flow acceleration, it is the only one connected to ϕ_2, i.e. to $-\rho\partial\phi_2/\partial t$

I_2=quadratic term of the velocity

I_3=pressure correction due to changes in the body wetted surface

I_4=pressure correction due to body motions

I_5=change of the first-order force direction due to body rotations

F_2 has mean value different than zero connected with I_2-I_5.

I_1 has zero mean value because $\partial\phi_2/\partial t \propto \sin(2\omega t)$ has zero mean value.

NB: ϕ_2 does not contribute to the mean (drift) forces so to evaluated the mean loads we do not need to find ϕ_2, but just to solve the problem for the first-order velocity potential ϕ_1.

The mean loads are due to the **body capability in generating waves,** i.e. by its capability in diffracting the incident waves and irradiating waves.
It means that the mean loads are relevant for large structures and are negligible for small vessels (relative to the incident waves).

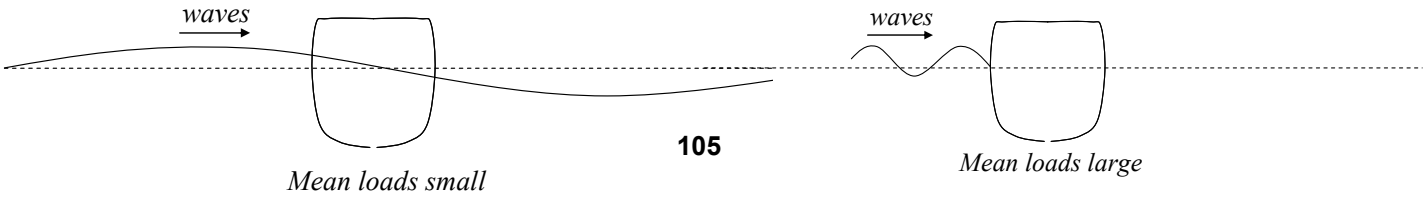

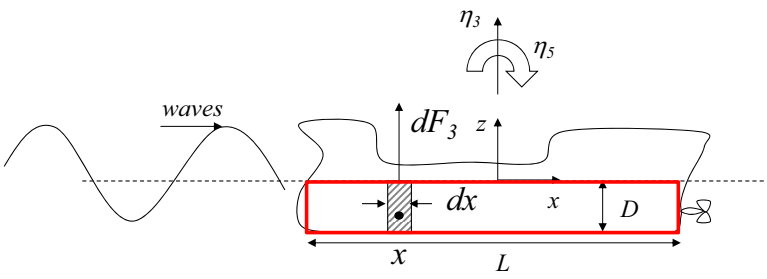
η3
η5
waves
dF3
z
dx
x
D
x
L

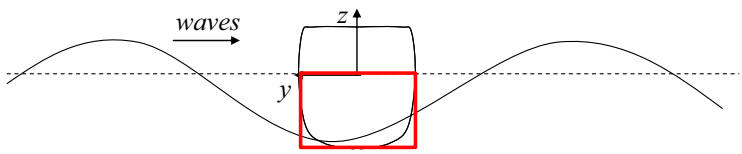
waves
z
y

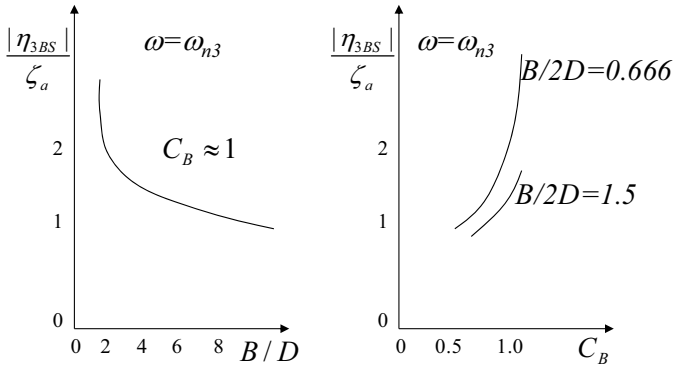
|η3BS|
ζa
ω=ωn3
CB ≈1
2
1
0
0 2 4 6 8 B / D
|η3BS|
ζa
ω=ωn3
B/2D=0.666
B/2D=1.5
2
1
0
0 0.5 1.0 CB

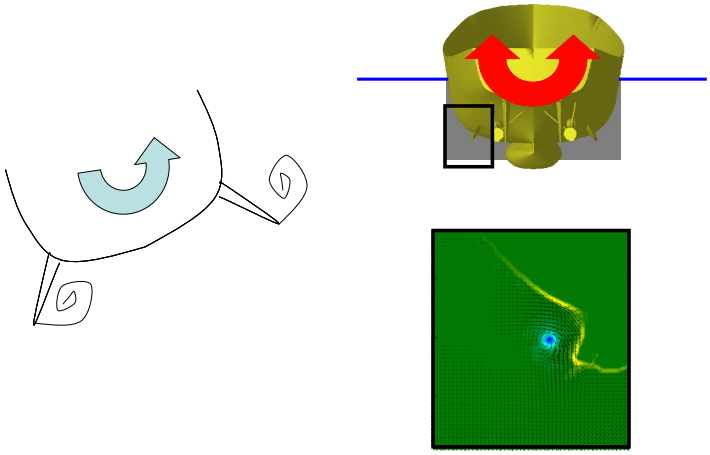

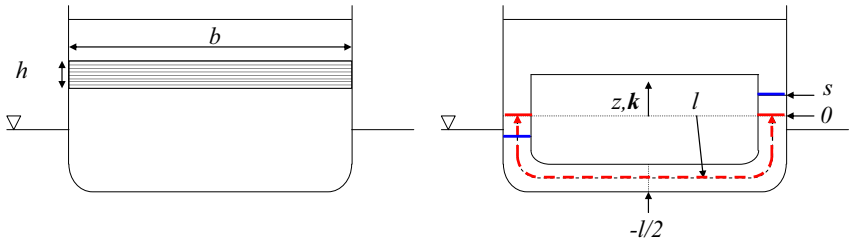
Free-surface tank
U-tube tank
b
h
z,k
l
s
0
-l/2

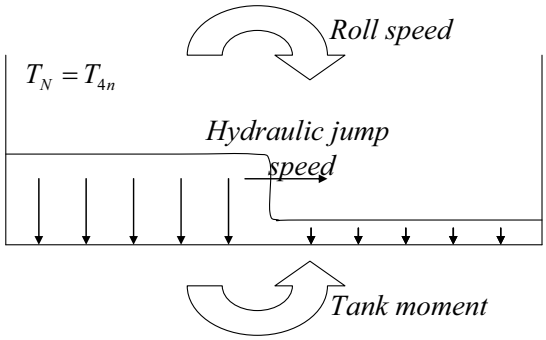
Roll speed
$T_N = T_{4n}$
Hydraulic jump speed
Tank moment

Free-surface tank: Natural sloshing period ≈ Natural roll period

Why a free-surface tank causes a maximum damping when
the forcing frequency is equal to the natural sloshing period?

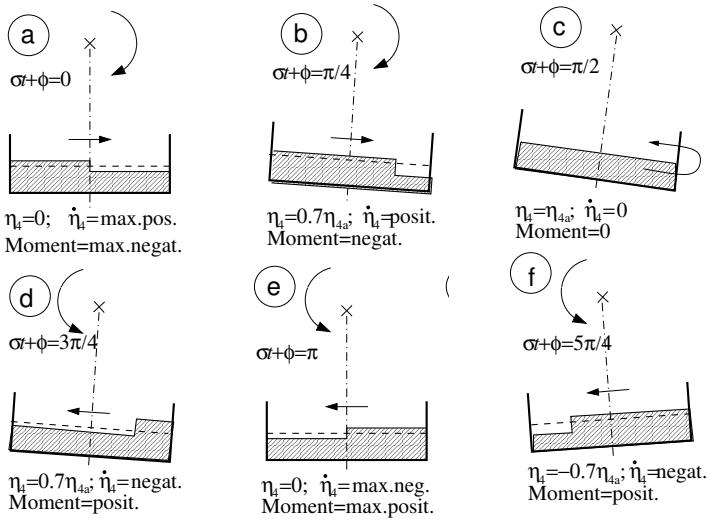

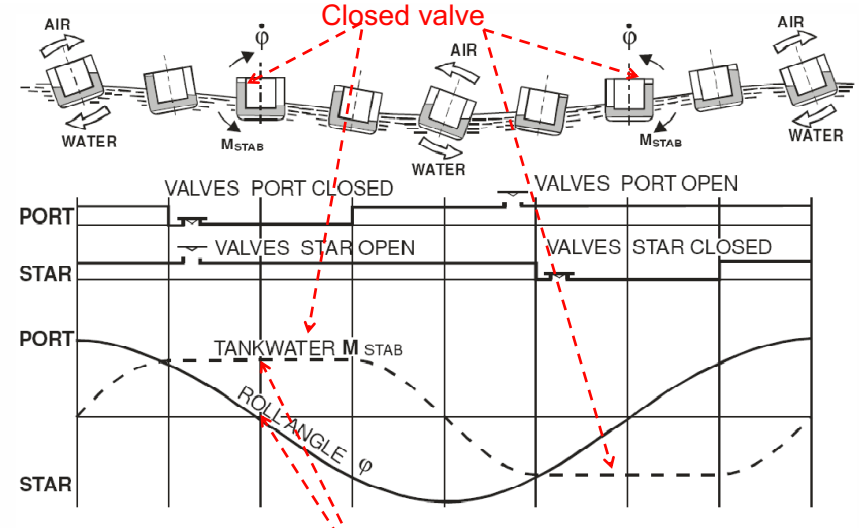

ROLL PERIOD ≈ NATURAL PERIOD OF TANK

Roll is 90° out of phase with tank moment ⇒ Max damping

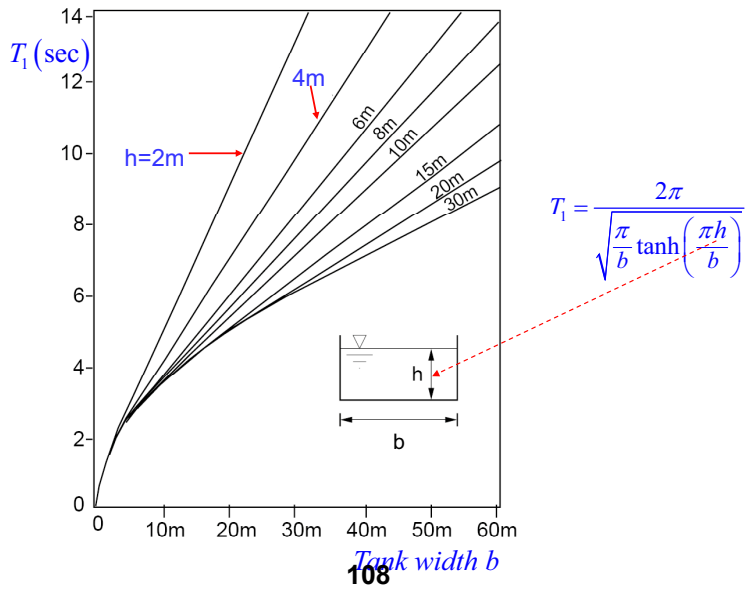

$$T_1 = \frac{2\pi}{\sqrt{\frac{\pi}{b}\tanh\left(\frac{\pi h}{b}\right)}}$$

Free-surface antirolling tank

$Hp: \eta_4 = \eta_{4a} \sin \omega t$

Tank roll moment $= K_{ta} \sin(\omega t + \varepsilon_t)$

$\omega \ll \omega_1$ (quasi-steady) $\Rightarrow \varepsilon_t = 0$

$\Rightarrow$ Tank moment $= K_{ta} \sin(\omega t)$,

i.e. destabilizing moment.

$\omega = \omega_1 \Rightarrow \varepsilon_t = -90^\circ$

$\Rightarrow$ Tank moment $= -K_{ta} \cos(\omega t)$,

$\equiv -K_{ta} \dot{\eta}_4 / (\omega \eta_{4a})$,

i.e. sloshing causes roll damping.

Lowest sloshing frequency:

$\omega_1 = 2\pi / T_1 \cong \pi\sqrt{gh} / b$

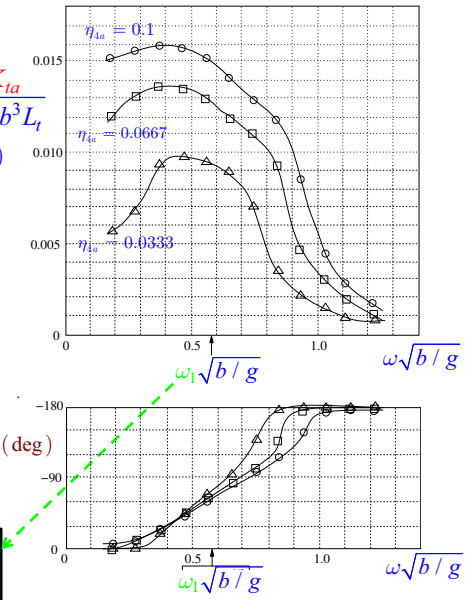

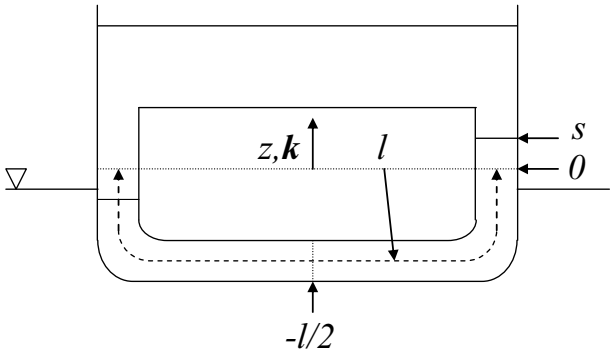

Passive U-tube anti-rolling tanks on 53m long patrol boat

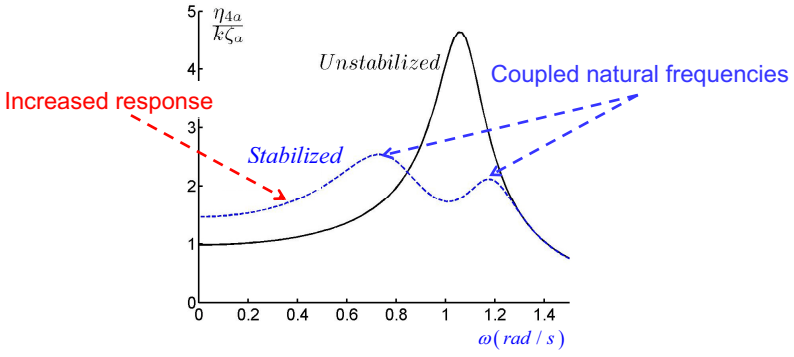

Tuned liquid dampers

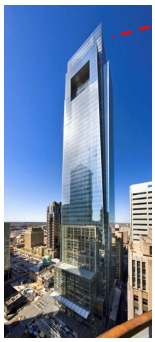

Highest natural period T_1(s) of the building

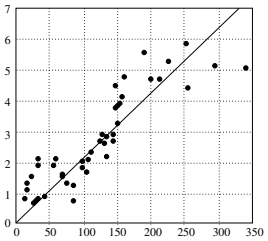

Building height H(m)

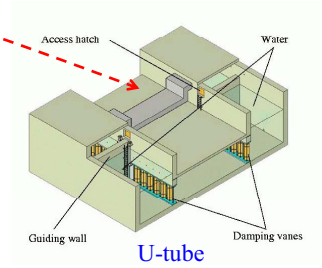

U-tube

Sloshing period=Building period T_1

Free-surface tank

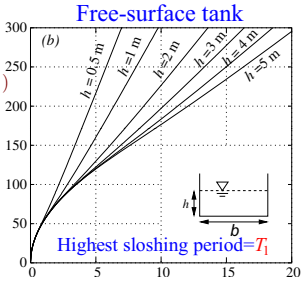

Highest sloshing period=T_1 b(m)

U-tube length l(m)

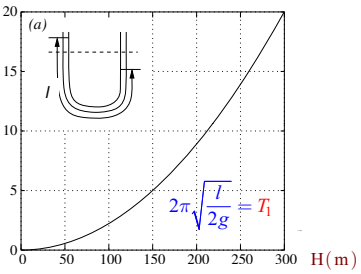

$2\pi\sqrt{\frac{l}{2g}} = T_1$

Summary

Environment. Assumptions. Linear wave loads. Diffraction and radiation problems. Excitation loads. Added-mass, damping and restoring coefficients. Parameter analysis. Response. Minimization of vertical motions.

Coordinate System and Rigid-Body Modes

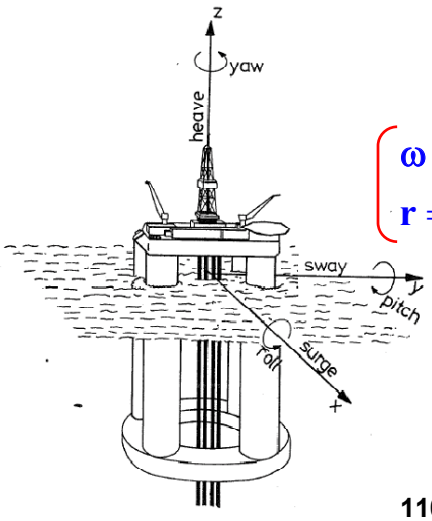

$$\mathbf{s} = \eta_1\mathbf{i} + \eta_2\mathbf{j} + \eta_3\mathbf{k}$$

$$+\boldsymbol{\omega}\times\mathbf{r}$$

$$\boldsymbol{\omega} = \eta_4\mathbf{i} + \eta_5\mathbf{j} + \eta_6\mathbf{k},$$

$$\mathbf{r} = x\mathbf{i} + y\mathbf{j} + z\mathbf{k}$$

$$\mathbf{s} = (\eta_1 + z\eta_5 - y\eta_6)\mathbf{i}$$

$$+(\eta_2 - z\eta_4 + x\eta_6)\mathbf{j}$$

$$+(\eta_3 + y\eta_4 - x\eta_5)\mathbf{k}$$

Environment

- 2D Regular, short-term and long-term long-crested and short-crestes waves
- Wind
- Current

Scatter Diagram: Sea State Probability

Table 2.2. *Joint frequency of significant wave height and spectral peak period. Representative data for the northern North Sea*

Significant wave height (m) (upper limit of interval)	Spectral peak period (s)																		
	3	4	5	6	7	8	9	10	11	12	13	14	15	16	17	18	19	21	22	Sum
1	59	403	1061	1569	1634	1362	982	643	395	232	132	74	41	22	12	7	4	2	2	8636
2	9	212	1233	3223	5106	5814	5284	4102	2846	1821	1098	634	355	194	105	56	30	16	17	32 155
3	0	8	146	831	2295	3896	4707	4456	3531	2452	1543	901	497	263	135	67	33	16	15	25 792
4	0	0	6	85	481	1371	2406	2960	2796	2163	1437	849	458	231	110	50	22	10	7	15 442
5	0	0	0	4	57	315	898	1564	1879	1696	1228	748	398	191	84	35	13	5	3	9118
6	0	0	0	0	3	39	207	571	950	1069	885	575	309	142	58	21	7	2	1	4839
7	0	0	0	0	0	2	27	136	347	528	533	387	217	98	37	12	4	1	0	2329
8	0	0	0	0	0	0	2	20	88	197	261	226	138	64	23	7	2	0	0	1028
9	0	0	0	0	0	0	0	2	15	54	101	111	78	39	14	4	1	0	0	419
10	0	0	0	0	0	0	0	0	2	11	30	45	39	22	8	2	1	0	0	160
11	0	0	0	0	0	0	0	0	0	2	7	15	16	11	5	1	0	0	0	57
12	0	0	0	0	0	0	0	0	0	0	1	4	6	5	2	1	0	0	0	19
13	0	0	0	0	0	0	0	0	0	0	0	1	2	2	1	0	0	0	0	6
14	0	0	0	0	0	0	0	0	0	0	0	0	0	1	0	0	0	0	0	1
15	0	0	0	0	0	0	0	0	0	0	0	0	0	0	0	0	0	0	0	0
Sum	68	623	2446	5712	9576	12 799	14 513	14 454	12 849	10 225	7256	4570	2554	1285	594	263	117	52	45	100 001

Classification of Motions/Loads

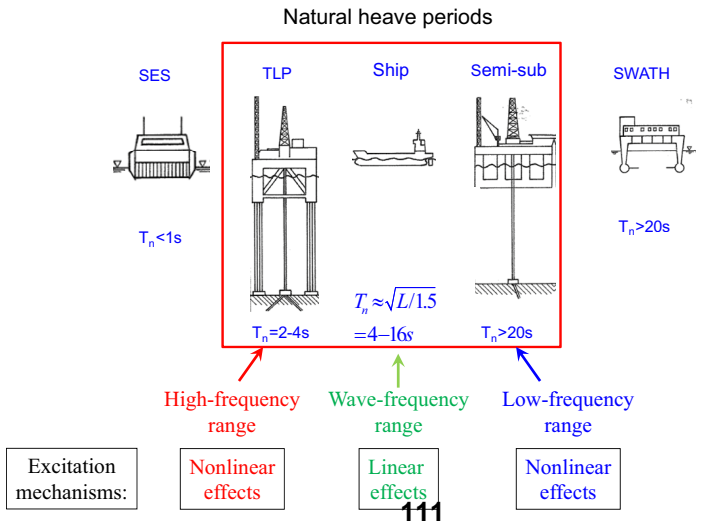

Classification of wave forces

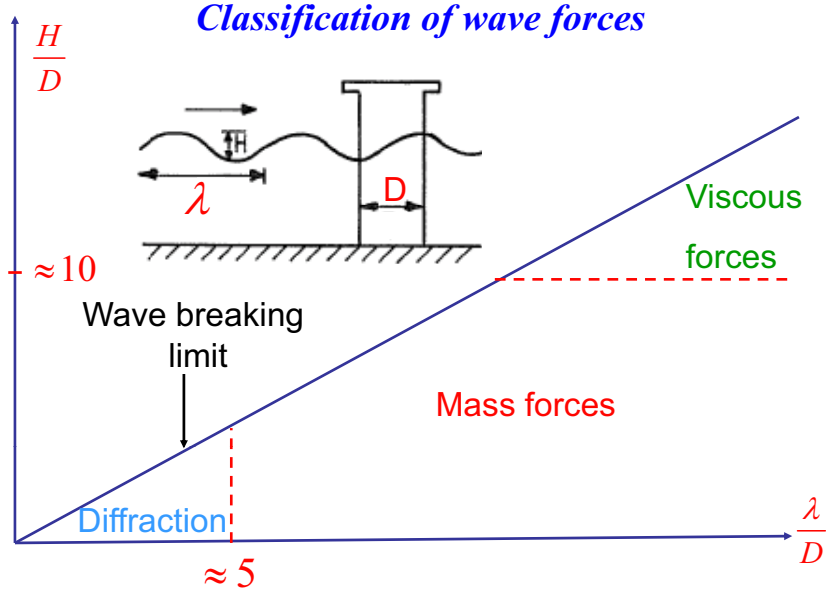

Basic Assumptions and Problem

Potential flow theory:

Inviscid → zero tangential stresses

Irrotational → $V = \nabla\phi$

Incompressible → $\nabla^2\phi = 0$

⇩

$\underbrace{p}_{\text{Bernoulli eq.}}$ and V from scalar function ϕ

Problem: Gouverning eq. +B.C.+I.C.

Linearity:

Small parameter ε, i.e. wave steepness

⇩

Solution in { Time domain; Frequency domain }

2D Regular Linear Incident Waves

Pressure: hydrostatic and dynamic parts

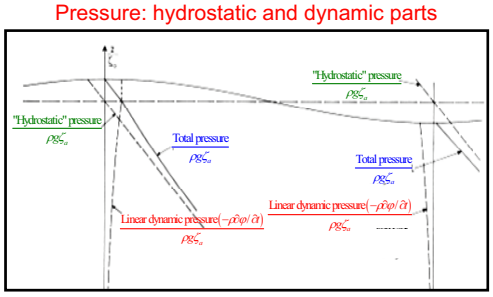

Phases of wave variables

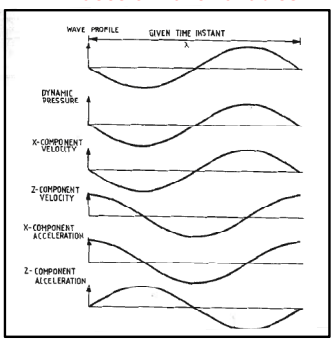

Stokes-drift velocity (Lagrangian)

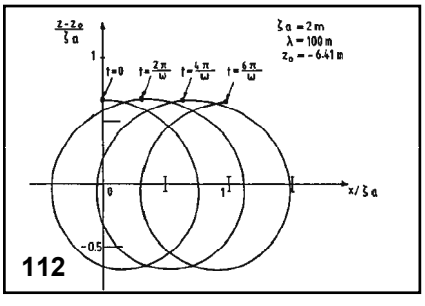

How energy in a wave spectrum can be distributed to individual regular wave components

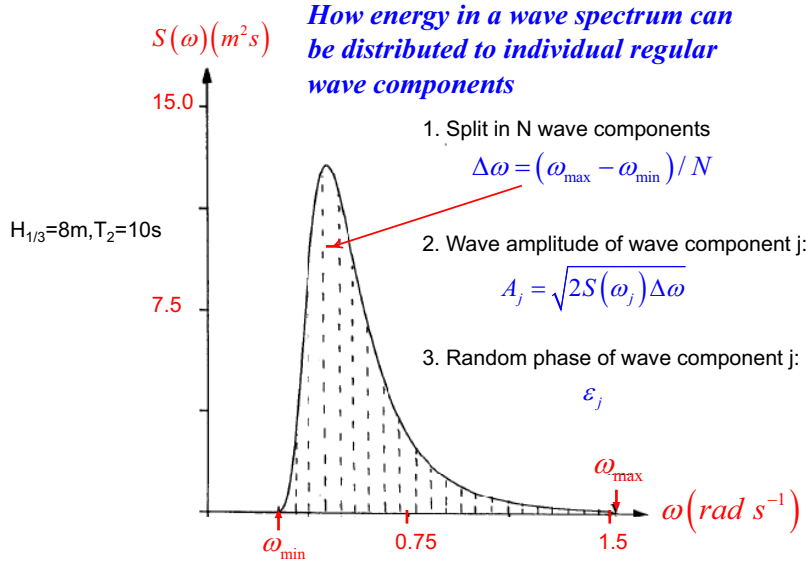

1. Split in N wave components

$$\Delta\omega = (\omega_{max} - \omega_{min})/N$$

2. Wave amplitude of wave component j:

$$A_j = \sqrt{2S(\omega_j)\Delta\omega}$$

3. Random phase of wave component j:

$$\varepsilon_j$$

Time and Frequency Domain of Waves

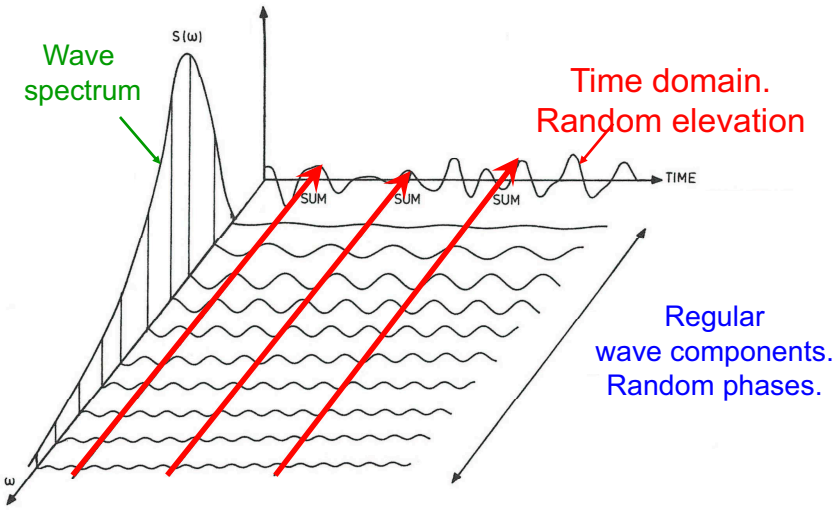

From Regular → Short-Term → Long-Term

Example: available wave power

Regular waves $P_w = \frac{\rho g \zeta_a^2}{2} \cdot \frac{g}{2\omega}$ ← Wave energy propagation velocity

↑ Wave energy density

Short-term sea state $P_w = \int_0^\infty \frac{\rho g^2}{2} \frac{S(\omega)}{\omega} d\omega$ ← Wave spectrum

Long-term analysis $\overline{P}_w = \sum_i \sum_j p_{ij} P_w(T_0^{(i)}, H_{1/3}^{(j)})$

↑ Probability of sea state $T_0^{(i)}, H_{1/3}^{(j)}$

Scatter Diagram: Sea State Probability

Table 2.2. *Joint frequency of significant wave height and spectral peak period. Representative data for the northern North Sea*

Significant wave height (m) (upper limit of interval)	Spectral peak period (s)																		
	3	4	5	6	7	8	9	10	11	12	13	14	15	16	17	18	19	21	22	Sum
1	59	403	1061	1569	1634	1362	982	643	395	232	132	74	41	22	12	7	4	2	2	8636
2	9	212	1233	3223	5106	5814	5284	4102	2846	1821	1098	634	358	194	105	56	30	16	17	32 155
3	0	8	146	831	2295	3896	4701	4456	3531	2452	1543	901	497	263	135	67	33	16	15	25 792
4	0	0	6	85	481	1371	2400	2960	2796	2163	1437	849	458	231	110	50	22	10	7	15 442
5	0	0	0	4	57	315	898	1564	1879	1696	1228	748	398	191	84	35	13	5	3	9118
6	0	0	0	0	3	39	207	571	950	1069	885	575	309	142	58	21	7	2	1	4839
7	0	0	0	0	0	2	27	136	347	528	533	387	217	98	37	12	4	1	0	2329
8	0	0	0	0	0	0	2	20	88	197	261	226	138	64	23	7	2	0	0	1028
9	0	0	0	0	0	0	0	2	15	54	101	111	78	39	14	4	1	0	0	419
10	0	0	0	0	0	0	0	0	2	11	30	45	39	22	8	2	1	0	0	160
11	0	0	0	0	0	0	0	0	0	2	7	15	16	11	5	1	0	0	0	57
12	0	0	0	0	0	0	0	0	0	0	1	4	6	5	2	1	0	0	0	19
13	0	0	0	0	0	0	0	0	0	0	0	1	2	2	1	0	0	0	0	6
14	0	0	0	0	0	0	0	0	0	0	0	0	0	1	0	0	0	0	0	1
15	0	0	0	0	0	0	0	0	0	0	0	0	0	0	0	0	0	0	0	0
Sum	68	623	2446	5712	9576	12 799	14 513	14 454	12 849	10 225	7256	4570	2554	1285	594	263	117	52	45	100 001

Linear Wave-Induced Body Motions

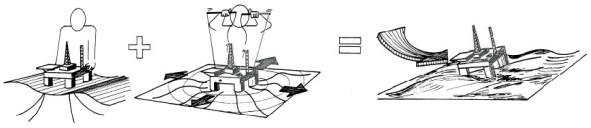

Problem Decomposition:

Diffraction + Radiation = Wave-body interaction

Haskind Relations

Excitation loads: Froude-Kriloff + Diffraction

Added mass, Damping, Hydrostatic restoring

Linear wave-induced motions, accelerations and structural loads

Hydrodynamic loads

Response

Hydrodynamic Loads: Diffraction Problem

Hp: Fixed body in incident waves

Froude-Kriloff loads

Diffraction loads

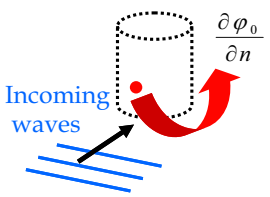

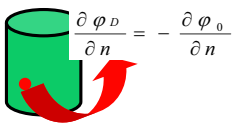

$$\frac{\partial(\varphi_0 + \varphi_D)}{\partial n} = 0$$

Due to incident-wave pressure, as the body was not there

Due to flow motion against incident waves to ensure impermeability

Dynamic pressure integrated on the mean wetted body surface

Hydrodynamic Loads: Radiation Problem

Hp: Body forced to oscillate in its 6 d.o.f. without incident waves

From linear dynamic pressure:

$$\underbrace{p}_{\text{contribution } j} = -\rho\left[\frac{\partial \phi_j}{\partial t} + \underbrace{U\frac{\partial \phi_j}{\partial x}}_{\text{due to forward motion}}\right] \quad j = 1..6$$

Integrated on the mean wetted body surface

From "hydrostatic" pressure:

$$p = -\rho g z$$

Integrated on the instantaneous wetted body surface

Added mass loads — Damping loads

$$F_{rad,k}(t) = = \sum_{j=1}^{6} \left\{-A_{kj}\ddot{\eta}_j - B_{kj}\dot{\eta}_j\right\}, k = 1..6$$

Restoring loads

$$F_{hydr,k}(t) = \sum_{j=1}^{6}\left\{-C_{kj}\eta_j\right\} \quad k = 1..6$$

Added-Mass and Damping

	Meaning	Parameter dependence
Added-mass coefficients	• Do NOT represent a finite 'accelerated' mass added to the body mass • Affect the body acceleration	A_{kj} and B_{kj} =f(body geometry, frequency, vicinity of free surface, water depth, water confinement, forward speed U)
Damping coefficients	• Connected to the square power of the amplitude of body generated waves ex. Heave: $B_{33} = \frac{\rho g^2}{\omega^3}\left(\frac{A_3}{\eta_{3a}}\right)^2$	

→Encounter frequency
→ $\partial/\partial t + U\partial/\partial x$
→ Different B.C.

Estimation

- In general solving a 3D problem for φ_j .
- If strip-theory valid: from $A_{ij}^{(2D)}$ and $B_{ij}^{(2D)}$

$A_{ij}^{(2D)}$ and $B_{ij}^{(2D)}$ from: - Source technique - Conformal mapping

Strip Theory

→the 3D problem as the sum of 2D problems.

For radiation problem : theoretical/practical applicability in terms of frequency
For diffraction problem: theoretical/practical applicability in terms of frequency
For ships: theoretical/practical applicability in terms of ω_e, Fn, body slenderness,...

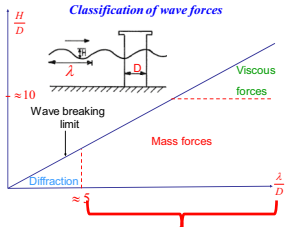

Long-Wave Approximation

Special forms for Excitation loads, e.g.

$$F_{exc,k}(t) \cong \int_S p_0 n_k dS + \sum_{j=1}^{3}(\bar{a}_{0j}A_{kj} + \bar{u}_{0j}B_{kj}) \quad k = 1..3$$

Further approximation for small submerged geometries — small

Strip theory combined with Long-wave approximation

Response & Response Amplitude Operator (RAO)

- **In**: Regular waves, short-term and long-term seas
- **As**: Motions, relative motions, accelerations, loads…
- **Relevant phenomena**:
  - Resonance for ships, ocean structures, fluid (piston mode, sloshing)
  - Instability (Mathieu-type instability for roll)
  - Wave-induced accelerations on equipments
- **Experimental RAO**:
  - Regular-wave tests
  - Transient tests
- **Minimization of vertical motions**

Hp: Two incident wave components of a sea state with spectrum $S(\omega)$, wave 1 and wave 2, with amplitudes ζ_{a1} and ζ_{a2}, frequencies ω_1 and ω_2 and propagating in x.

The first-order incident-wave velocity potentials are

$$\phi_{01}^{(1)} = \frac{g\zeta_{a1}}{\omega_1} e^{k_1 z} \cos(\omega_1 t - k_1 x + \varepsilon_1) \qquad \phi_{01}^{(2)} = \frac{g\zeta_{a2}}{\omega_2} e^{k_2 z} \cos(\omega_2 t - k_2 x + \varepsilon_2)$$

Here the apex indicates the wave.
Now the velocity potential accurate to the second order is

$$\phi = \phi_1 + \phi_2 = \phi_1^{(1)}(\omega_1) + \phi_1^{(2)}(\omega_2) + \phi_2(\omega_1, \omega_2)$$

with ϕ_2 involving a combined effect from the two incident waves. We analyse as before the contribution of $(\partial\phi_1 / \partial x)^2$ to the square-velocity term at $x=0$:
Squaring the linear velocity component along x

$$\left.\frac{\partial \phi_1}{\partial x}\right|_{x=0} = \underbrace{A_1 \cos(\omega_1 t + \varepsilon_1)}_{\text{due to interaction with wave 1}} + \underbrace{A_2 \cos(\omega_2 t + \varepsilon_2)}_{\text{due to interaction with wave 2}}$$

we have

$$\left(\partial\phi_1 / \partial x|_{x=0}\right)^2 = A_1^2 \cos^2(\omega_1 t + \varepsilon_1) + A_2^2 \cos^2(\omega_2 t + \varepsilon_2) + 2A_1 A_2 \cos(\omega_1 t + \varepsilon_1)\cos(\omega_2 t + \varepsilon_2)$$

NB: • $\cos^2(\omega t + \varepsilon) = \{1 + \cos[2(\omega t + \varepsilon)]\} / 2$

• $\cos(\omega_1 t + \varepsilon_1)\cos(\omega_2 t + \varepsilon_2) = \{\cos[(\omega_1 + \omega_2)t + \varepsilon_1 + \varepsilon_2] + \cos[(\omega_1 - \omega_2)t + \varepsilon_1 - \varepsilon_2]\} / 2$

$$\Rightarrow \left(\partial\phi_1 / \partial x|_{x=0}\right)^2 = \underbrace{(A_1^2 + A_2^2)/2}_{\text{Constant-term}} + \underbrace{A_1^2 \cos[2(\omega_1 t + \varepsilon_1)]/2 + A_2^2 \cos[2(\omega_2 t + \varepsilon_2)]/2 + A_1 A_2 \cos[(\omega_1 + \omega_2)t + \varepsilon_1 + \varepsilon_2]}_{\text{Sum-frequency term}} + \underbrace{A_1 A_2 \cos[(\omega_1 - \omega_2)t + \varepsilon_1 - \varepsilon_2]}_{\text{Difference-frequency term}}$$

So the second-order body interaction with a sea state with spectrum $S(\omega)$, involves mean loads and loads oscillating in time as $\omega_i \pm \omega_j$.

The sources of second-order terms in the loads

The pressure:

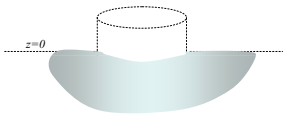

mean value=0 | mean value≠0

$$p = -\rho g z - \rho \frac{\partial \phi_1}{\partial t} \underbrace{-\rho \frac{\partial \phi_2}{\partial t}}_{O(\zeta_a)} \underbrace{-\rho \frac{1}{2} \nabla \phi_1 \cdot \nabla \phi_1}_{O(\zeta_a^2)}$$

First order | Second order

The body motions:

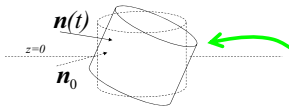

mean value≠0

(a) their 1st-order value modifies the linear dynamic pressure and causes (if rotational motions) a time variation of the normal vector,

(b) their 2nd-order value modifies the hydrostatic pressure.

A major contribution to vertical mean wave force on a Spar platform in survival condition:

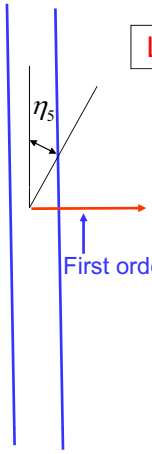

Linear Solution

First order "horizontal" hydrodynamic force= $M \frac{d^2\eta_1}{dt^2}$

A major contribution to vertical mean wave force on a Spar platform in survival condition:

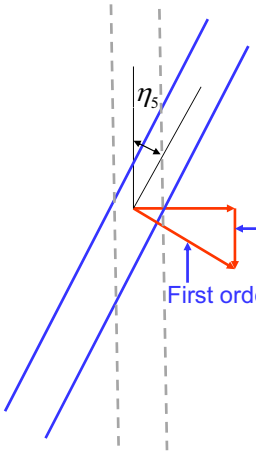

Second-order force

$M \frac{d^2\eta_1}{dt^2} \eta_5$ ⇒ Mean vertical force

First order "horizontal" hydrodynamic force= $M \frac{d^2\eta_1}{dt^2}$

The sources of second-order terms in the loads

The pressure:

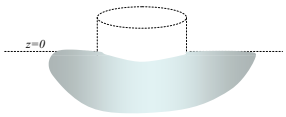

mean value=0 | mean value≠0

$$p = \underbrace{-\rho g z - \rho \frac{\partial \phi_1}{\partial t}}_{O(\zeta_a)} \underbrace{-\rho \frac{\partial \phi_2}{\partial t} - \rho \frac{1}{2} \nabla \phi_1 \cdot \nabla \phi_1}_{O(\zeta_a^{\,2})}$$

First order | Second order

The body motions:

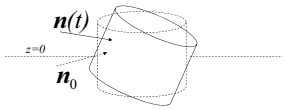

mean value≠0

(a) their 1st-order value modifies the linear dynamic pressure and causes (if rotational motions) a time variation of the normal vector,
(b) their 2nd-order value modifies the hydrostatic pressure.

The body wetted surface:

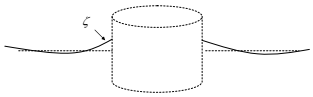

mean value≠0

The free-surface evolution causes a time variation of the body wetted surface and this has a contribution to the 2nd -order effects.

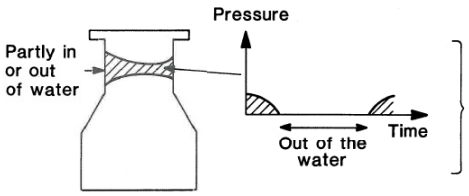

➡ Non-zero mean force

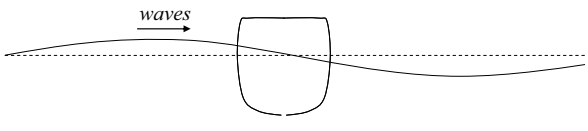

Mean loads small

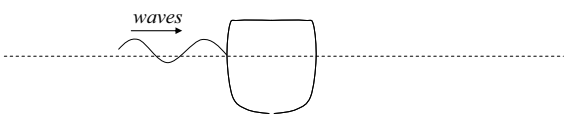

Mean loads large

Lecture Note 6

40. Drift loads from body capability in generating waves. Maruo's formula. Conservation of fluid momentum. Direct-pressure integration versus conservation of fluid momentum. Added resistance in waves. Viscous effects on mean wave forces. (F: 134-141,143-155)

Drift loads from body capability in generating waves.
If the waves are very short relative to the structure, they only see a vertical wall.

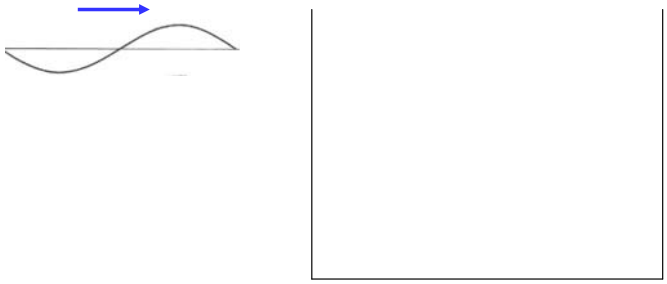

We can then estimate the mean force due to the wave-structure interaction by approximating the problem as the problem of an incident wave interacting with an infinitely long vertical wall.

Hp: 2D deep-water incident regular beam waves interacting with an infinitely long vertical (fixed) wall.
Obj: Mean wave (drift) force in sway.

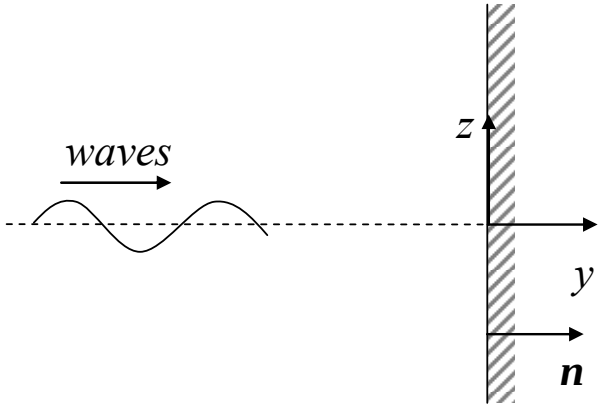

Incident-wave first-order velocity potential:

$$\phi_{01} = \phi_0 = \frac{g\zeta_a}{\omega} e^{kz} \cos(\omega t - ky)$$

As in general, without current and without forward motion, ϕ_2 does not contribute to the mean loads, we only need to find the first-order wave-wall interaction solution ϕ_1 to estimate the mean force.

NB: ϕ_2 could contain a space-dependent term constant in time. In the case of current or forward motion such term could contribute to the drift loads through the pressure additional term $-\rho U \partial\phi_2 / \partial x$.

The problem is a diffraction problem because the body does not move, so it can only diffract (reflect) the incident waves. We need to find ϕ_D, its problem is:

$$\begin{cases} \textit{Laplace eq.}: \nabla^2\phi_D = 0 \quad \forall \boldsymbol{P} \in \Omega \qquad \Rightarrow \phi_D \propto A\cos(k_1 y) + B\sin(k_1 y) \\ \textit{FS B.C.}: -\omega^2\phi_D + g\dfrac{\partial \phi_D}{\partial z} = 0 \qquad z = 0 \Rightarrow \omega^2 = gk_1 = gk \\ \textit{Wall B.C.}: \left.\dfrac{\partial \phi_D}{\partial n}\right|_{y=0} = \left.\dfrac{\partial \phi_D}{\partial y}\right|_{y=0} = -\left.\dfrac{\partial \phi_0}{\partial y}\right|_{y=0} = -\omega\zeta_a e^{kz}\sin(\omega t) \quad \Rightarrow \phi_D = \dfrac{g\zeta_a}{\omega}e^{kz}\cos(\omega t + ky) \\ \textit{Far field}: \phi_D \to 0 \qquad as \quad z \to -\infty \qquad \text{satisfied as } \phi_D \propto e^{kz} \end{cases}$$

The solution is then:

$$\phi_D = \frac{g\zeta_a}{\omega}e^{kz}\cos(\omega t + ky)$$

The total first-order solution is

$$\phi_1 = \phi_0 + \phi_D = \frac{g\zeta_a}{\omega}e^{kz}\cos(\omega t - ky) + \frac{g\zeta_a}{\omega}e^{kz}\cos(\omega t + ky) = 2\frac{g\zeta_a}{\omega}e^{kz}\cos\omega t\cos ky\,,$$

with wave elevation $\zeta_1 = \zeta_a\sin(\omega t - ky) + \zeta_a\sin(\omega t + ky) = 2\zeta_a\sin\omega t\cos ky$.

This is a standing (non propagating) wave with amplitude twice the incident wave amplitude:

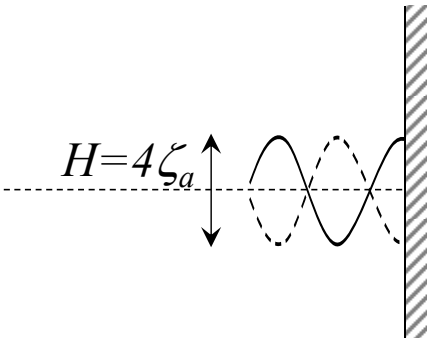

To find the mean horizontal force, we need to integrate the pressure along the wall, retain all force terms proportional to $\zeta_a{}^2$ and find the mean value of their sum. The pressure accurate to the second order is

$$p = \underbrace{-\rho g z - \rho\frac{\partial \phi_1}{\partial t}}_{O(\zeta_a)} \underbrace{-\rho\frac{\partial \phi_2}{\partial t} - \rho\frac{1}{2}\nabla\phi_1\cdot\nabla\phi_1}_{O(\zeta_a{}^2)} \qquad (1)$$

The first two terms in eq. (1) are linear so their contribution to the second-order horizontal force is obtained integrating from 0 to ζ_1 along the wall.

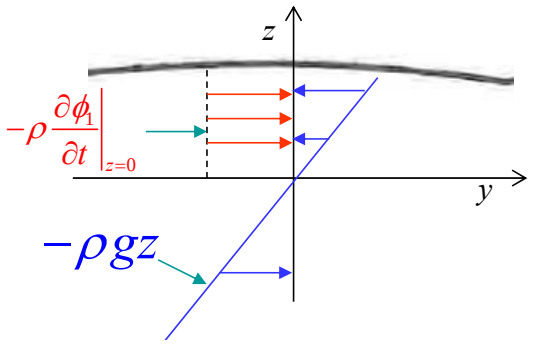

The second two terms in eq. (1) are $\propto \zeta_a{}^2$ so their contribution to the second-order horizontal force is obtained integrating from -∞ to 0 along the wall. Among these second-order pressure terms, only the square power of the velocity contributes to the mean value of the horizontal force. $\partial\phi_2/\partial t$ does not contribute to the force mean value because, as ϕ_2, it is periodic with frequency 2ω so $-\rho\int_{-\infty}^{0}\frac{\partial\phi_2}{\partial t}n_2 dz$ has zero mean value.

The second-order contribution to the horizontal force with non-zero mean value is:

$$F_2=\left[-\rho\int_{-\infty}^{0}\frac{1}{2}\nabla\phi_1\cdot\nabla\phi_1\underbrace{n_2}_{=1}dz-\rho\int_{0}^{\zeta_1}\left(\left.\frac{\partial\phi_1}{\partial t}\right|_{z=0}+gz\right)\underbrace{n_2}_{=1}dz\right]_{y=0}$$

$$\underbrace{=}_{y=0}-\rho\int_{-\infty}^{0}\frac{1}{2}\left(\left.\frac{\partial\phi_1}{\partial z}\right|_{y=0}\right)^2dz-\rho\left[\left.\frac{\partial\phi_1}{\partial t}\right|_{z=0}z+g\frac{z^2}{2}\right]_0^{\zeta_1}$$

$$=-2\rho\omega^2\zeta_a{}^2(\cos\omega t)^2\left[\frac{1}{2k}e^{2kz}\right]_{-\infty}^{0}-\rho\underbrace{(-2g\zeta_a\sin\omega t)}_{\partial\phi_1/\partial t|_{z=0}}\underbrace{(2\zeta_a\sin\omega t)}_{\zeta_1}-2\rho g\zeta_a{}^2(\sin\omega t)^2$$

$$=-\rho g\zeta_a{}^2(\cos\omega t)^2+2\rho g\zeta_a{}^2(\sin\omega t)^2$$

$$=-\rho g\zeta_a{}^2[1+\cos(2\omega t)]/2+2\rho g\zeta_a{}^2[1-\cos(2\omega t)]/2$$

The mean value of F_2 is then

$$\bar{F}_2=-\rho g\zeta_a{}^2/2+2\rho g\zeta_a{}^2/2=\rho g\zeta_a{}^2/2\,.$$

NB: This formula shows that the force is proportional to the square power of the reflected wave amplitude, in this case this amplitude coincides with the incident wave amplitude, i.e. it is the largest possible value of the reflected wave amplitude. This means that this is the maximum possible value for $\bar{F}_2$ without current and without forward speed.

Mean wave (drift) forces: Conservation of fluid momentum. (F:135-137)

$$\boldsymbol{F}=-\frac{d}{dt}\underbrace{\left(\int_{\Omega}\rho\boldsymbol{V}d\Omega\right)}_{=\boldsymbol{M}}-\int_{S-S_B}p\boldsymbol{n}dS-\int_{\Omega}\rho g\boldsymbol{k}d\Omega-\int_{S}\rho\boldsymbol{V}(V_n-U_n)dS \qquad (1)$$

Here the normal vector points outside the fluid domain Ω.

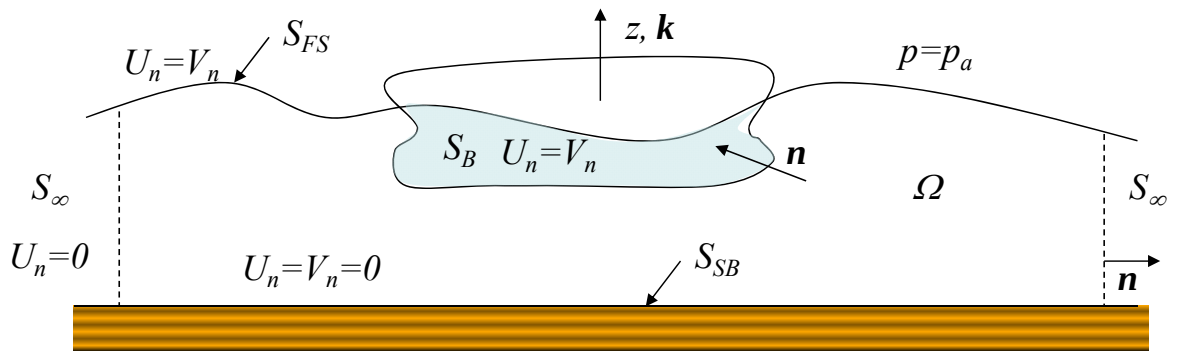

Hp: The 3D fluid domain Ω is enclosed by the surface S made by the body, a control surface S_∞, i.e. fixed and transparent for the fluid, and the portion of free surface and of the flat sea floor limited by such surface. The boundary conditions are given in the following figure.

The pressure appears in equation (1) in the term $\boldsymbol{F} + \int_{S-S_B} p\mathbf{n}dS$, i.e. in the term

$\int_S p\mathbf{n}dS = \int_\Omega \nabla p d\Omega$ (using the Gauss theorem, see eq. (F:5.6))

The free-surface pressure is equal to the atmospheric pressure p_a which is uniform and constant so its gradient is zero, i.e.

$$\int_S p_a \mathbf{n}dS = \int_\Omega \nabla p_a d\Omega = 0 \Rightarrow \int_S (p - p_a)\mathbf{n}dS = \int_S p\mathbf{n}dS$$

It means that if we express the pressure relative to p_a, i.e. p-p_a, the results for the force do not change. This has the advantage that on the free surface we have

$$\int_{S_{FS}} (p - p_a)\mathbf{n}dS = 0$$

So the contribution from the free surface to the mean force will be zero. From now on, the symbol p will then indicate p-p_a. Time averaging expression (1) over one period of oscillation T we can get the mean force. The mean value of $d\boldsymbol{M}/dt$ is zero because it is periodic with period T, So, in terms of force components, the mean value from eq. (1) reduces to:

$$\overline{F_i} = \overline{-\int_{S_\infty} (pn_i + \rho V_i V_n)dS - \int_{S_{SB}} pn_i dS - \int_\Omega \rho g \underbrace{\delta_{i3}}_{\substack{=0\ i\neq 3 \\ =1\ i=3}} d\Omega} \qquad i = 1,2,3$$

The right-hand-side must be intended as a mean-value expression. The mean vertical force component depends on a volume integral associated with the gravity, which can be transformed in a surface intergral, i.e. $\int_\Omega \rho g\mathbf{k}d\Omega = \int_S \rho g z\mathbf{n}dS$.

For the mean horizontal force components: the gravity term does not contribute and the term connected with the sea bottom (second term) is also zero because S_{SB} has a vertical normal vector. It implies that the horizontal force components are given by the integral along the control surface, i.e.

$$\overline{F_i} = -\overline{\int_{S_\infty} (pn_i + \rho V_i V_n)dS} \quad i = 1,2 \quad \text{(F:5.9)}$$

Formula (F:5.9) was derived by Maruo. Newman derived a similar formula for the mean wave-drift yaw moment starting from the conservation of fluid angular momentum.
Formula (F:5.9) is valid also in 2D, in this case the control surface has two parts $S_{-\infty}$ and S_∞, respectively upstream and downstream of the body.

NB: Despite the control surface has been named as S_∞, there are no restrictions on its location, i.e. it can be close to the body. The location and shape is chosen to make easier the load estimation. It is a great advantage of this method when compared with the direct-pressure integration method.

Maruo derived a simpler expression for the horizontal mean wave-drift force under additional assumptions, which shows more explicitly the fact that the drift loads are due to the body capability in generating waves.

Maruo's formula. (F:137-141)
Hp: 2D incident regular beam-sea waves in deep water. No current. No forward motion.
Obj: Find mean wave (drift) force in sway $\overline{F}_2$.

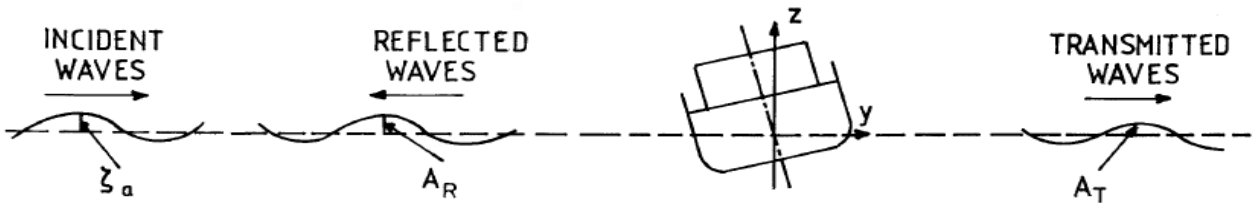

The first-order incident-wave velocity potential is

$$\phi_{01} = \phi_0 = \frac{g\zeta_a}{\omega} e^{kz} \cos(\omega t - ky)$$

Diffraction waves will be generated by the body presence. Radiation waves will be generated by body motions. As a result we have:

Upstream of the body:

- incident waves
  (propagating in positive y direction)
  → amplitude = ζ_a
- reflected waves =diffraction +radiation waves
  (propagating in negative y direction)
  → amplitude =A_R, 1st-order velocity potential: $\phi_R = \frac{gA_R}{\omega} e^{kz} \cos(\omega t + ky + \varepsilon)$

Downstream of the body:

- transmitted waves = incident+ diffraction + radiation waves
  (propagating in positive y direction)

→ amplitude =A_T, 1st-order velocity potential: $\phi_T = \frac{gA_T}{\omega} e^{kz} \cos(\omega t - ky + \delta)$

Applying eq. (F:5.9) in this 2D case to find the mean wave force along y, we have:

$$\overline{F}_2 = -\int_{S_{-\infty}} \{pn_2 + \rho V_2 \mathbf{V}\cdot\mathbf{n}\}\, dz - \int_{S_\infty} \{pn_2 + \rho V_2 \mathbf{V}\cdot\mathbf{n}\}\, dz \underset{\mathbf{n}=n_2\mathbf{j}}{=} -\int_{S_{-\infty}} \{p + \rho V_2^2\} \underbrace{n_2}_{=-1}\, dz - \int_{S_\infty} \{p + \rho V_2^2\} \underbrace{n_2}_{=1}\, dz$$

$$= +\int_{S_{-\infty}} \left\{ p + \rho \left(\frac{\partial(\phi_0 + \phi_R)}{\partial y} \right)^2 \right\} dz - \int_{S_\infty} \left\{ p + \rho \left(\frac{\partial \phi_T}{\partial y} \right)^2 \right\} dz$$

When integrating, it is convenient to split $S_{\pm\infty}$ in two parts:

- $S0_{\pm\infty}$: between $z=-\infty$ and $z=0$
  → the second-order pressure terms provide the second-order contribution
- $S1_{\pm\infty}$: between $z=0$ and $z=\zeta$

→ the first-order pressure terms provide the second-order contribution

So introducing the Bernoulli equation for the pressure, we have:

$$\bar{F}_2 = \underbrace{\int_{S0_{-\infty}} \left\{ -\frac{\rho}{2}\left(\frac{\partial(\phi_0+\phi_R)}{\partial z}\right)^2 + \frac{\rho}{2}\left(\frac{\partial(\phi_0+\phi_R)}{\partial y}\right)^2 \right\} dz}_{=0}$$

$$+ \underbrace{\int_{S0_{\infty}} \left\{ \frac{\rho}{2}\left(\frac{\partial\phi_T}{\partial z}\right)^2 - \frac{\rho}{2}\left(\frac{\partial\phi_T}{\partial y}\right)^2 \right\} dz}_{=0}$$

$$+ \int_{S1_{-\infty}} \left\{ -\rho g z - \rho \frac{\partial(\phi_0+\phi_R)}{\partial t}\bigg|_{z=0} \right\} dz + \int_{S1_{\infty}} \left\{ \rho g z + \rho \frac{\partial\phi_T}{\partial t}\bigg|_{z=0} \right\} dz$$

$$\Rightarrow \bar{F}_2 = -\frac{\rho g}{4}\left(\zeta_a{}^2 + A_R{}^2\right) + \frac{\rho g}{2}\left(\zeta_a{}^2 + A_R{}^2\right) + \frac{\rho g}{4} A_T{}^2 - \frac{\rho g}{2} A_T{}^2$$

which means

$$\bar{F}_2 = \frac{\rho g}{4}(\zeta_a{}^2 + A_R{}^2 - A_T{}^2) \qquad \text{(F:5.14)}$$

This can be generalized for finite water depth h (Longuett-Higgins, 1977) as:

$$\bar{F}_2 = \frac{\rho g}{4}(\zeta_a{}^2 + A_R{}^2 - A_T{}^2)\left(1 + \frac{2kh}{\sinh(2kh)}\right)$$

which coincides with expression (F:5.14) in the limit for

$kh \to \infty$, i.e. $\dfrac{2kh}{\sinh(2kh)} \to 0$

Hp: The average energy flux is zero through the body surface

→ This means that body can not be an active wave-power device.

The reason for this is that a wave-power device must absorb energy which means that there is an energy flux through its surface. This can be achieved by combining in a suitable way its motions, as for instance shown in the figure below, examining a symmetric body and addressing what is the condition to have a perfect absorber:

To absorb waves means to generate waves

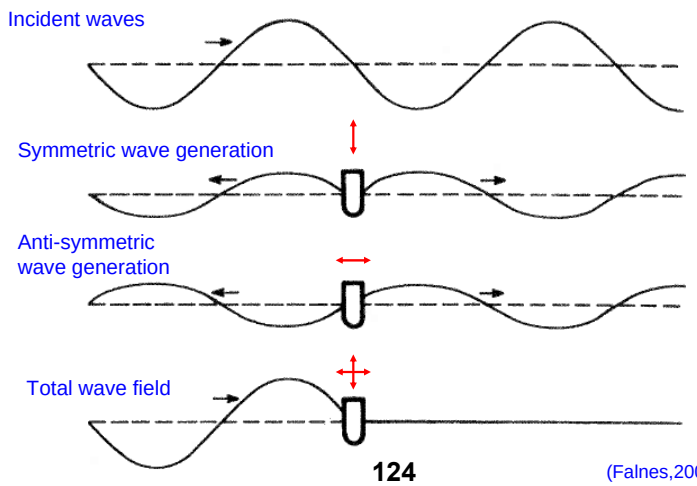

(Falnes,2002)

The assumption that there is zero energy flux through the body surface implies that (a) there is no work done on the body during one period of oscillation. Moreover, (b) the variation of the energy has zero mean value, i.e. $\overline{dE}/dt = 0$. (a) +(b) lead to

$$\zeta_a^{\,2} = A_R^{\,2} + A_T^{\,2} \quad (1)$$

It means that the mean incident-wave energy is split in the reflected and transmitted wave energy. As a result the mean wave drift force becomes

$$\overline{F}_2 = \frac{\rho g}{2} A_R^{\,2} \qquad \text{(F:5.16)}$$

This is known as **Maruo's formula**. It is consistent with the formula obtained using the direct pressure integration for the 2D example of an incident wave interacting with an infinitely long vertical wall. Indeed such example corresponds to the asymptotic value of the Maruo's formula for $\omega \to \infty$, i.e. short waves relative to the structure. In this case there are no transmitted waves, i.e.

$$A_R = \zeta_a \quad (2) \Rightarrow \overline{F}_2 = \frac{\rho g}{2} \zeta_a^{\,2} \quad (3)$$

Using relation (1) above we see that (2) is the largest value for the reflected wave amplitude. This confirms that (3) is the largest value of the mean drift force without current and without forward speed.

Formula (F:5.16) states that drift loads are due to the body capability in generating waves:

- radiated waves connected with body motions and
- diffracted waves connected with the body presence.

So the mean-wave (drift) force is smaller for submerged bodies and reduces as the submergence depth, say *d*, increases. Moreover it is smaller for geometries which generate smaller waves.

Ogilvie (1963) showed that $A_R=0$ for all frequencies and all *d* in the case of a submerged horizontal circular cylinder fixed or moving in circular orbits.

A typical behaviour of the drift force for a 2D surface piercing body in deep-water beam sea waves is as given in fig. F:5.5:

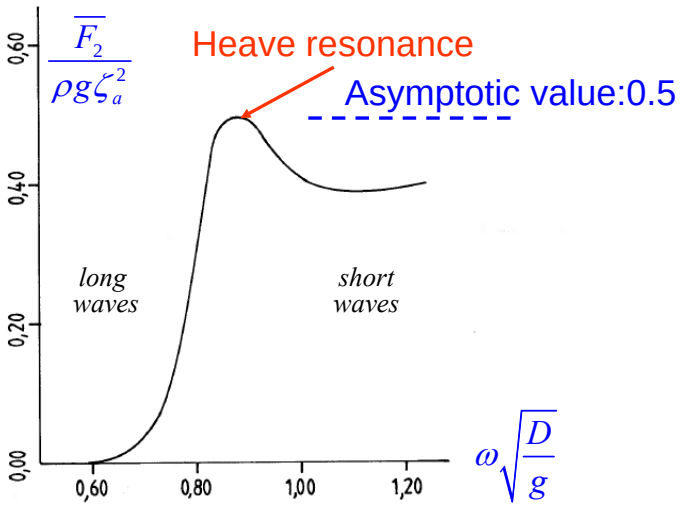

Fig. F:5.5

- It goes to zero as the waves get longer

→ the body follows the waves, i.e. it does not generate much waves.

- It has a local maximum at the heave resonance when the vertical motions are largest. In this region the relative vertical motions matter
  → radiation waves are important.
- It increases again as the waves get shorter
  → diffraction waves become important
  → the asymptotic value for $\omega \to \infty$ is the value in the case of an infinite vertical wall.

Maruo (1960) has derived an extension of formula (F:5.16) for drift forces of 3D bodies under the following assumptions.
Hp: 3D body. Regular incident waves. Zero current. Zero forward speed. Conservation of energy, i.e. viscous effects are neglected.

$$\overline{F}_1 = \frac{\rho g}{4}\int_0^{2\pi} A^2(\theta)(\cos\beta - \cos\theta)d\theta \qquad \text{(F:5.17)}$$

$$\overline{F}_2 = \frac{\rho g}{4}\int_0^{2\pi} A^2(\theta)(\sin\beta - \sin\theta)d\theta \qquad \text{(F:5.18)}$$

Here β is the incident-wave direction with respect to the x direction and $A(\theta)/\sqrt{r}$ is the amplitude of waves generated by the body at large horizontal radial distance $r = \sqrt{x^2 + y^2}$ from it. These waves include the waves radiated by body motions and diffracted by body presence. The angle θ is defined by $x = r\cos\theta, y = r\sin\theta$. Also these expressions confirm that drift forces are connected with the body ability of generating waves.

NB: In beam and head waves the drift force is in the direction of the incident waves but in a general wave heading the force direction can be different than the incident wave direction.

Maruo's 3D formulas do not show which wave directions are responsible for greater drift forces. This is discussed in figure F:5.6, which examines the influence of the wavelength and wave direction on the transverse drift force on a ship.

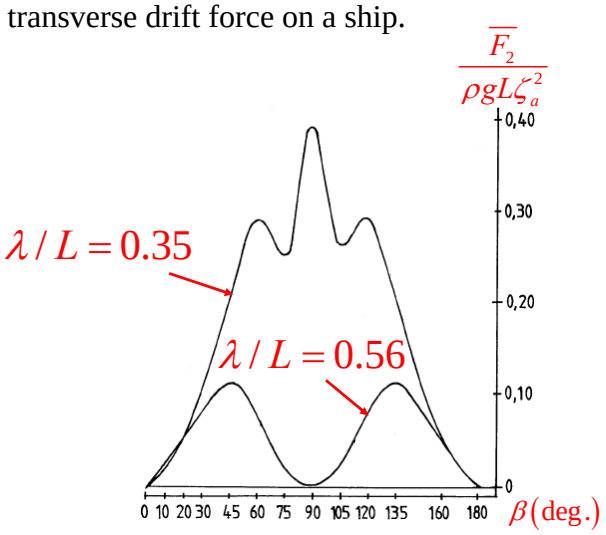

Fig. F:5.6

Here β=0° means head sea waves. Two wavelengths are considered. The maximum value of the transverse drift force occurs at the smallest λ, in particular in beam sea. For the largest λ

the force is almost zero in beam sea and largest for wave headings 45° and 135°. This is because for this wavelength the ship follows better the incident waves if they are at 90° (beam sea), i.e. the generated waves are small.

NB: This confirms that, the wave headings which result in greater wave generation correspond to higher wave-drift force.

What is the importance of $\overline{F}_2$ for a 2D surface-piercing body with respect to the horizontal force caused by a current U_c in calm water (i.e. without incident waves)?
As we will see later in the course, the force associated with the current is proportional to the square power of the current speed and can be expressed as

$$F_c = \frac{1}{2}\rho C_D D U_c^{\,2}$$

Here C_D is the drag coefficient for the current flow and D is the body draught. So we have

$$\frac{\overline{F}_2}{F_c} = \frac{0.5\rho g A_R^{\,2}}{0.5\rho C_D D U_c^{\,2}} = \frac{g A_R^{\,2}}{C_D D U_c^{\,2}} \qquad (1)$$

Example.
Hp: U_c =1m/s, D=10m and C_D =1
→ $\overline{F}_2 / F_c = A_R^{\,2}$ (with the reflected wave amplitude given in metres).

So the wave-drift force is rather important for large volume structures like ships, causing reflected waves with large amplitude.

NB: Expression (1) of the force ratio assumes that there is no interaction between waves and current. In reality:

- the current affects the waves
  → so A_R will be affected
- the wave-current interaction modifies the flow separation around the body
  → so C_D will be affected

Figure below examines the longitudinal drift force for a TLP in regular waves propagating along the positive x axis, without and with current. The trend and maximum value of the force as a function of the incident-wave period change introducing the current and depend on the current direction. This is because the current affects the body capability in generating waves.

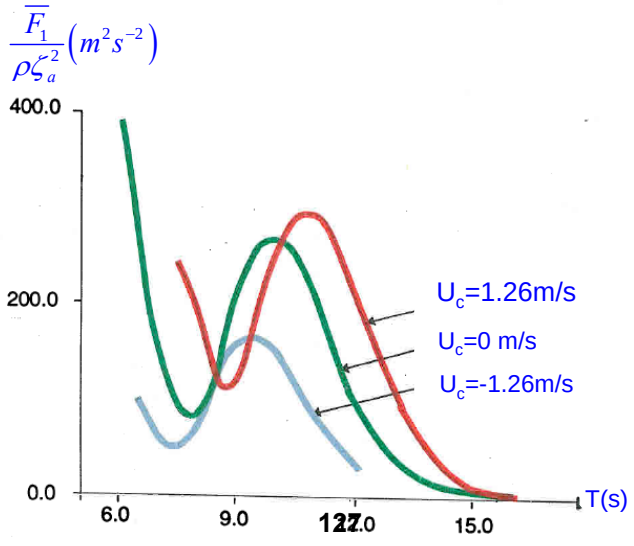

Methods to estimates the mean loads: direct-pressure integration *versus* conservation of fluid momentum.

As we have discussed, the direct-pressure integration (DPI) and the conservation of fluid momentum (CFM) offer two alternative ways to evaluate the drift forces. The figure below shows a comparison between numerical results using the two methods for the vertical mean force on a vertical cylinder.

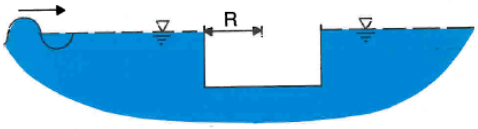

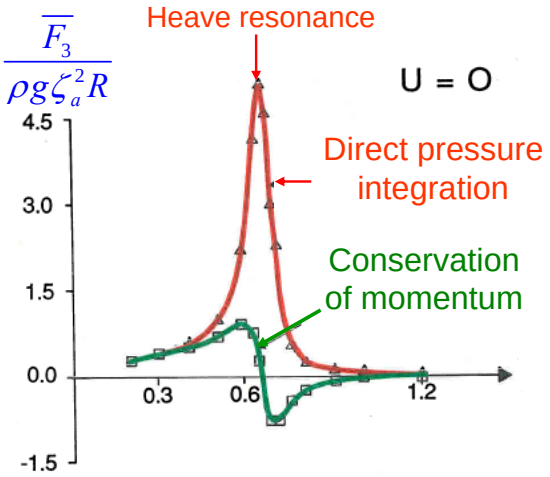

Large differences occur near the zone where the mean force should change sign according to CFM. This is due to errors associated with cancellation effects of load contributions when using DPI. Estimation through DPI involves different terms which counteract each other. This may lead to accuracy problems. It also involves a greater sensitivity of the force values to the approximation made for the body geometry. Geometrical singularities represent a source of numerical errors in this context. This discussion does not mean that one must not use the DPI method but only that one must be careful when applying it and one must make sure that the results obtained are converged, i.e. they do not depend on the numerical parameters.

Extension of the asymptotic value of Maruo's 2D formula for ω→ ∞

Faltinsen has generalized the asymptotic value of the Maruo's 2D formula for short waves (i.e. $\omega \to \infty$) to 3D structures with vertical sides.

Hp: 3D body with vertical sides at the water-plane. Regular incident short waves. No current. No forward speed.

Assuming that the body geometry is as in figure F:5.8:

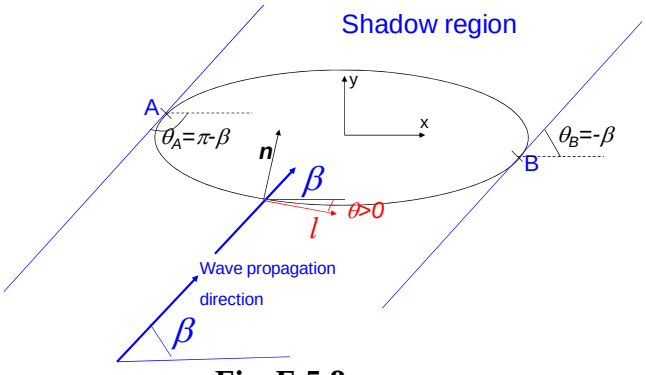

Fig. F:5.8

we have:

$$\bar{F}_i = \underbrace{\frac{\rho g \zeta_a^{\,2}}{2}}_{original} \underbrace{\int_{L_1} [\sin(\theta+\beta)]^2 n_i dl}_{non\ shadow\ part} \qquad i = 1,2,6 \quad \text{(F:5.21)}$$

Here $n_1 = \sin\theta$, $n_2 = \cos\theta$ and $n_6 = x\cos\theta - y\sin\theta$ and the integration is along the non-shadow part of the body (i.e. the part exposed to the incident waves) with length L_1 along the waterline. This formula is valid for the horizontal force components and the yaw-drift moment integrated along the water-plane non-shadow curve.

Some examples of applications. (F:144-145)

1) Infinitely long horizontal cylinder ($L \to \infty$) with generic heading β:

- $\theta = 0$ deg, $n_1 = 0 \quad n_2 = 1 \quad n_6 = x$

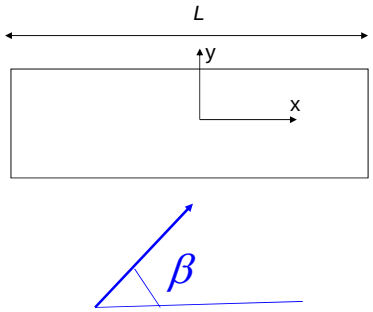

$$\bar{F}_1 = 0$$

$$\bar{F}_2 = \frac{\rho g \zeta_a^{\,2}}{2} \underbrace{\sin\beta\,|\sin\beta|}_{>0\ if\ 0<\beta<\pi} L \qquad \text{(It means that } \bar{F}_2 \to \infty \text{ if } L \to \infty\text{)}$$

$$\bar{F}_6 = \frac{\rho g \zeta_a^{\,2}}{2} (\sin\beta)^2 \int_{-L/2}^{L/2} x dx = \frac{\rho g \zeta_a^{\,2}}{2} (\sin\beta) 2\left[x^2/2\right]_{-L/2}^{L/2} = 0$$

So the only mean load is the horizontal force component normal to the cylinder surface. If β=90° → $\sin\beta\,|\sin\beta| = 1$. This is the maximum value of the drift force and gives

$$\frac{\bar{F}_2}{L} = \frac{\rho g \zeta_a^{\,2}}{2}$$

for the force per unit length, i.e. 2D force. In this way we recovered the Maruo's 2D formula for $\omega \to \infty$ and we have again the confirmation that this is the maximum value we can have for the drift force, i.e. wave right against an infinitely extended body, without current and without forward speed.

2) Structure with circular water-plane area of radius r:

- $n_1 = \sin\theta \quad n_2 = \cos\theta \quad n_6 = (-r\sin\theta)\cos\theta - (-r\cos\theta)\sin\theta = 0$

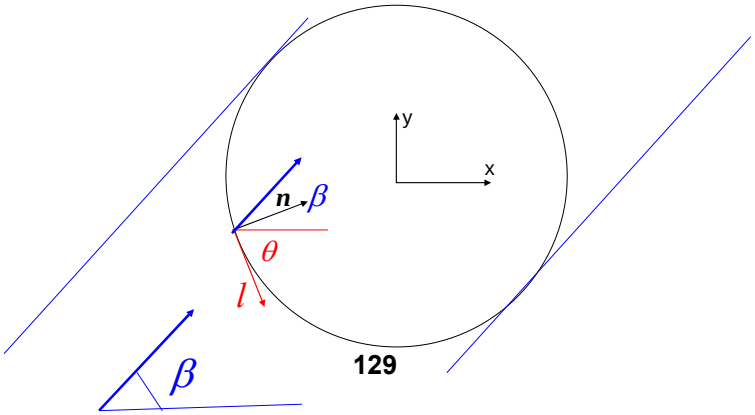

$$\bar{F}_1 = \frac{\rho g \zeta_a^{\,2}}{2} \int_{-\beta}^{\pi-\beta} \left[\sin(\theta+\beta)\right]^2 \sin\theta r d\theta = \frac{2}{3}\rho g r \zeta_a^{\,2} \cos\beta$$

$$\bar{F}_2 = \frac{\rho g \zeta_a^{\,2}}{2} \int_{-\beta}^{\pi-\beta} \left[\sin(\theta+\beta)\right]^2 \cos\theta r d\theta = \frac{2}{3}\rho g r \zeta_a^{\,2} \sin\beta$$

$$\bar{F}_6 = 0$$

So, due to the radial symmetry of the body: the moment must be zero and the two mean loads are identical and 90 degree out-of-phase from each other.

3) Structure with circular water-plane area consisting of 2 circular ends of radius r and a parallel part of length $2l$:

- In the circular part: $n_1 = \sin\theta \quad n_2 = \cos\theta \quad n_6 = (\pm l - r\sin\theta)\cos\theta - (-r\cos\theta)\sin\theta$
  $= \pm l\cos\theta$
- In the linear part: $n_1 = 0 \quad n_2 = 1 \quad n_6 = x$

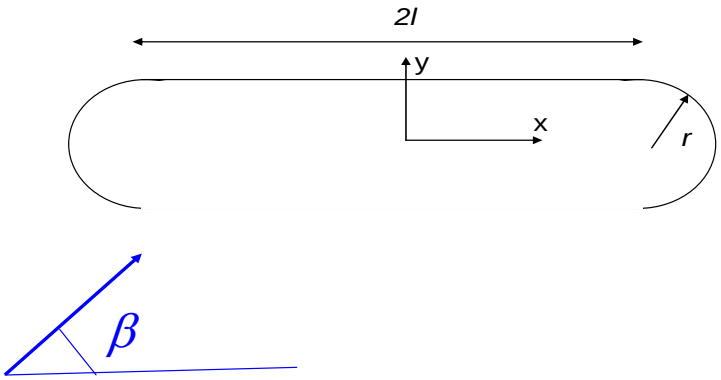

$$\bar{F}_1 = \frac{\rho g \zeta_a^{\,2}}{2}\left\{\underbrace{\int_{-\beta}^{\pi-\beta} \left[\sin(\theta+\beta)\right]^2 \sin\theta r d\theta}_{circular} + \underbrace{0}_{linear}\right\} = \frac{2}{3}\rho g r \zeta_a^{\,2}\cos\beta$$

$$\bar{F}_2 = \frac{\rho g \zeta_a^{\,2}}{2}\left\{\underbrace{\int_{-\beta}^{\pi-\beta} \left[\sin(\theta+\beta)\right]^2 \cos\theta r d\theta}_{circular} + \underbrace{\sin\beta\,|\sin\beta|\,2l}_{linear}\right\} = \rho g \zeta_a^{\,2}\left\{\frac{2}{3} r\sin\beta + l\sin\beta\,|\sin\beta|\right\}$$

$$\bar{F}_6 = \frac{\rho g \zeta_a^{\,2}}{2}\left\{\underbrace{lr\int_{-\beta}^{0} \left[\sin(\theta+\beta)\right]^2 \cos\theta d\theta - lr\int_{0}^{\pi-\beta} \left[\sin(\theta+\beta)\right]^2 \cos\theta d\theta}_{two\ semicircles} + \underbrace{0}_{linear}\right\} = -\frac{\rho g l r \zeta_a^{\,2}}{3}\sin 2\beta$$

The geometry comes from combining the geometries in examples 2) and 3). As a result: the forces are given by simply summing the forces for those two geometries. A moment is caused by the fact that the radial symmetry of the circle is broken by the elongated central part. This is equal to zero if the wave direction is parallel or normal to the central part.

Added resistance in waves. (F:145-150)

The wave-drift force represents an additional resistance in the case of a vessel advancing with forward speed U in waves. It is then called added resistance in waves and usually indicated as R_{AW}.

Hp: Blunt ship forms with vertical sides at the waterplane. Small Froude number, i.e. Fn<~0.2. Head sea regular deep-water waves (in this case it means $\beta=0$ deg). Small wavelengths, i.e. λ/L<~0.5.

The mean horizontal force due to second-order effects in the wave-body interactions is

$$\bar{F}_1 = \frac{\rho g}{2}\zeta_a^{\,2}\left(1+\frac{2\omega U}{g}\right)\int_{L_1}\left[\sin(\theta)\right]^2 n_1 dl \quad \text{(F:5.22)}$$

Here ω is the (circular) frequency of the waves, i.e. $\omega^2 = gk = 2g\pi/\lambda$, and L_1 is the non-shadow part of the body.

Formula (F:5.22) is sensitive only to the bow part of the vessel and increases as the body becomes blunter, i.e. greater wave reflection. This is analysed by figure F:5.10 in terms of the variation of added resistance with respect to a reference value F_0.

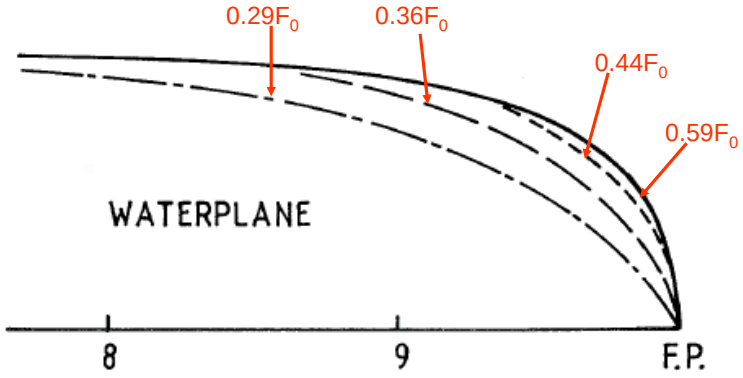

Fig. F:5.10

From expression (F:5.22) and substituting $R_{AW} = \bar{F}_1$, we have:

$$\Rightarrow \frac{R_{AW(Fn\neq 0)}}{R_{AW(Fn=0)}} = 1+\frac{2\omega U}{g}$$

Using this formula:

If we choose for instance λ/L=0.5 (i.e. limit of validity)

→ $R_{AW(Fn\neq 0)} = (1+7Fn)R_{AW(Fn=0)}$

which means an important effect of the forward speed.

Also the effect of a current is important for drift loads in the case of large marine structure

→A current of 1 m/s could increase the drift forces of 50% (shown by Zhao et al. 1988)

For a ship at moderate Fn the added resistance in head sea waves is typically as in the figure F:5.11:

- For λ/L<0.5 the added resistance in waves is dominated by the bow-wave reflection, i.e. eq. (F:5.22) can be used.
- In the resonance region, i.e. around λ/L=1, the wave generation connected with ship motions governs. It means that R_{AW} depends strongly on the relative vertical motion between vessel and waves.
- For longer waves the added resistance in waves becomes negligible.

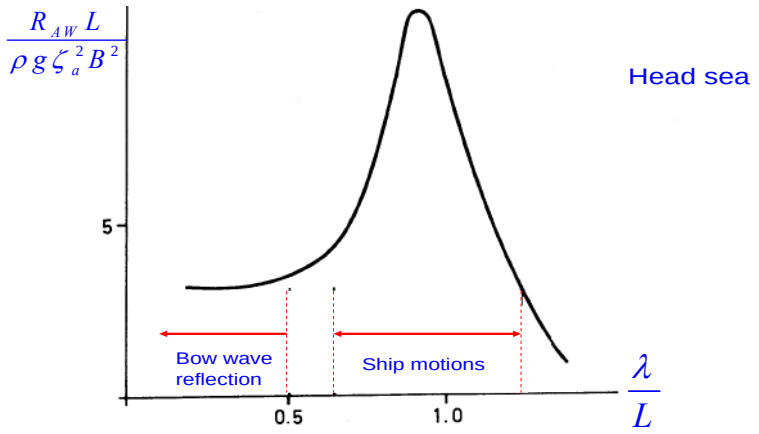

Fig. F:5.11

The drift loads are also affected by confined waters. This means that when performing experiments in a tank, the tank-wall effects influence the loads. Figure below examines this for the longitudinal drift force on a hemisphere in regular waves and with forward speed.

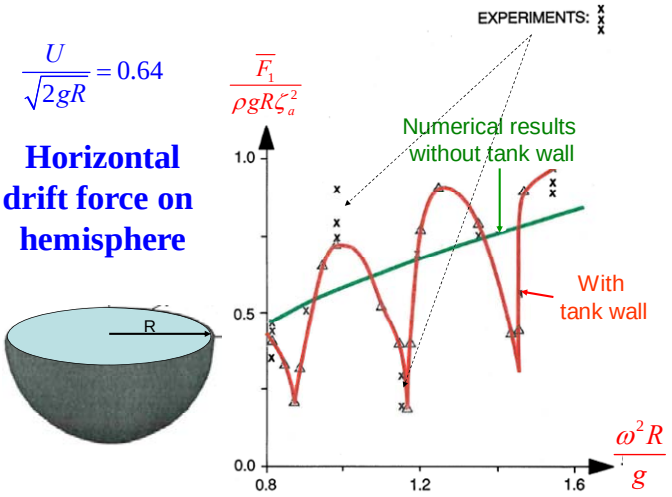

Both measurements and numerical results modelling the tank walls show a more complex behaviour of the drift force in terms of the frequency, with respect to the numerical results not modelling the tank walls.

From what discussed we have learned that:

Hp: A regular incident wave with frequency ω, direction β and amplitude ζ_a

The induced mean wave (drift) loads are $\overline{F}_i(\omega,\beta) \propto \zeta_a^2$.

It means that $\overline{F}_i(\omega,\beta)/\zeta_a^2$ is independent on the wave amplitude and represents then the transfer function for the mean-wave drift loads for a given regular wave with frequency ω and direction β. So to mean drift loads caused by a wave with these parameters and amplitude A will be:

$$\left[\frac{\overline{F}_i(\omega,\beta)}{\zeta_a^2}\right] A^2$$

The drift loads in regular waves can be used to estimate the drift loads in irregular long-crested waves with a spectrum $S(\omega)$ and propagating in β direction.

Approximating the spectrum as N wave components with amplitude

$$A_j^{\,2} = 2S(\omega_j)(\omega_{\max} - \omega_{\min}) / N ,$$

the velocity potential can be written as

$$\phi_1 = \sum_{j=1}^{N} \frac{gA_j}{\omega_j} e^{k_j z} \cos(\omega_j t - k_j x \cos\beta - k_j y \sin\beta + \varepsilon_j)$$

So for the regular wave component with ω_j, β and A_j the drift loads are given by

$$\left(\bar{F}_i(\omega_j, \beta) / \zeta_a^{\,2}\right) A_j^{\,2}$$

and summing up for all N wave components of the wave spectrum, the mean-wave loads associated with the sea state are obtained, i.e.

$$\bar{F}_i^s = \sum_{j=1}^{N} \overbrace{\underbrace{\left(\frac{\bar{F}_i(\omega_j, \beta)}{\zeta_a^{\,2}}\right) A_j^2}_{\text{contribution from } j\text{-th wave}}}^{\text{independent on wave amplitude}} \qquad i = 1,..,6 \quad \text{(F:5.27)}$$

which becomes

$$\bar{F}_i^s = 2\int_0^{\infty} S(\omega) \frac{\bar{F}_i(\omega, \beta)}{\zeta_a^{\,2}} d\omega \qquad i = 1,..,6 \quad \text{(F:5.28)}$$

for $N \to \infty$. $\bar{F}_i(\omega, \beta) / \zeta_a^{\,2}$ can be calculated independently from the spectrum for any combination of ω_j and β and then used to estimate the mean wave drift loads for the specific spectrum.

The added resistance $R_{AW} = \bar{F}_1^{\,s}$ in short waves can be obtained as

$$R_{AW} = \frac{\rho g}{16} H_{1/3}^{\,2} \left(1 + Fn \frac{4\pi}{T_1} \sqrt{\frac{L}{g}}\right) \int_{L_1} \left[\sin(\theta)\right]^2 n_1 dl \quad \text{(F:5.30)}$$

with $H_{1/3}$ significant wave height and $T_1 = 2\pi \frac{m_0}{m_1}, m_1 = \int_0^{\infty} \omega S(\omega) d\omega.$

It means that $R_{AW} \propto H_{1/3}^{\,2}$ and it reduces as T_1 increases.

If the wave elevation can be considered as a Gaussian process: $H_{1/3} = 4\sqrt{m_0}, = 4\int_0^{\infty} S(\omega) d\omega$

NB: To use formula (F:5.30) one must require that there is no significant waves energy for λ/L>~0.5.

Example of application of formula (F:5.30)

Hp: One-parameter Pierson-Moskowitz spectrum

The condition that there must be no significant waves energy for λ/L>~0.5, in this case means → $H_{1/3}$ must be <0.0065L

- If L=300m → $H_{1/3}$ must be <1.95m
  This occurs about 40% of the time in the North Atlantic.
- If L=100m → $H_{1/3}$ must be <0.65m
  This occurs less than 4% of the time in the North Atlantic.

This confirms that this formula is relevant for large volume structures.

Viscous effects on mean wave forces (F:152-155)
When the wavelength is large relative to the cross-dimensional lengths of the structure, the wave generation capability of the structure is small. Hence the wave drift loads due to potential flow effects are small. However, if the wavelength is large and the wave amplitude is sufficiently large, then viscous effects can cause important wave drift loads. The reason is that their contribution to drift loads is of higher order than second order in terms of wave amplitude.
In general we may say that wave drift forces are due to

- the body capability in generating waves (inviscid effects)
- viscous effects

Practical example where viscous effects are important:
A semisubmersible in incident waves long relative to the cross-sections of the semisubmersible.

Hp: Head regular waves in deep water. Wavelength large compared with the cross-sectional dimensions of the platform length and wave amplitude large. Small platform motions.
Obj: Discuss mean wave force in *x* direction.

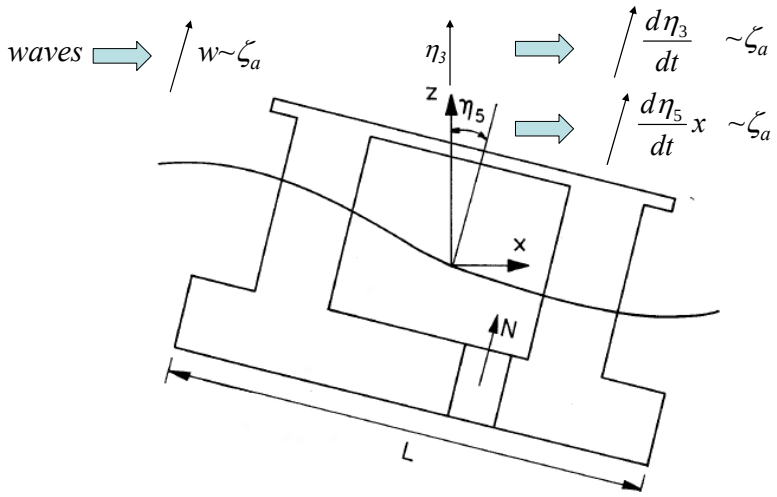

In the following we use the cross-flow principle for the flow around pontoons and columns of the platform to express the drag force contributions from the pontoons and columns. We decompose the forces into components in the Earth-fixed coordinate system and time average over one wave period. In this way we find non-zero mean wave loads proportional to $\zeta_a^{\,3}$.

Pontoons contribution:
The drag force normal (i.e. in the ***N***-direction) to the pontoons can be found as

$$F_N = -\underbrace{2}_{2\ pontoons}\int_{-L/2}^{L/2} b\frac{\rho}{2}C_D V_{RN}\,|V_{RN}|\,dl \propto \zeta_a^{\,2} \quad (1)$$

Here b is the transversal size of the pontoon, C_D the drag coefficient and V_R is the relative velocity between a body strip and the incident waves in ***N*** direction. This can be approximated as

$$V_{RN} \underset{\substack{\text{Hp: small}\\ \text{motions}}}{\approx} \underbrace{\frac{d\eta_3}{dt} - x\frac{d\eta_5}{dt}}_{\substack{\text{velocity due}\\ \text{to motions}}} - \underbrace{w}_{\text{wave velocity}}$$

because the motions are small and the error committed is of higher order than ζ_a.

The absolute value in (1) is due to the fact that the force is directed as V_R, i.e. it acts as a damping force. The incident-wave vertical velocity w is $w = \omega\zeta_a e^{kz}\cos(\omega t - kx)$.

The pitch motion causes a force component along x:

$$F_x = F_N\eta_5 \propto \zeta_a^3 \quad \text{with} \quad \overline{F}_x \neq 0$$

This then gives a mean (drift) force due to third-order effects associated with viscous effects, as shown in the figure below.

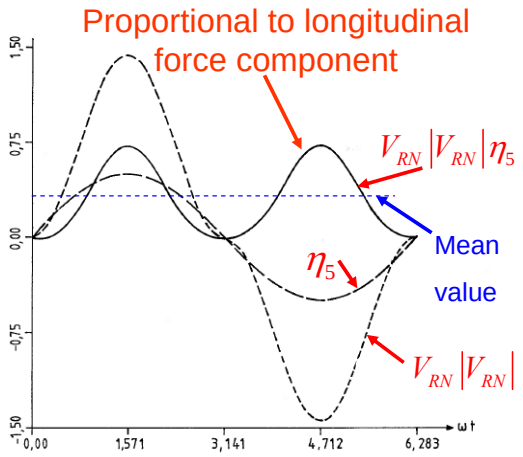

Columns contribution:

There will be a similar contribution to the horizontal mean force due to the columns. We will here limit ourselves to consider only the contribution from the time varying wetted surface. Further, if we for simplicity neglect the longitudinal platform velocity we can write the horizontal force per column as

$$F_x = \frac{\rho}{2} C_D D \int_{-h}^{\zeta} u\,|u|\,dz \qquad (1)$$

with D the column diameter, h the column draft and a u the horizontal incident-wave velocity. Because waves are long compared with the cross-sectional dimensions, we can take u in the expression (1) as $u = \omega\zeta_a e^{kz}\sin(\omega t - kx_0)$, with x_0 at the center of the column.

NB: According to expression (1) the magnitude of the force per unit length is largest at the free surface. This is unphysical because the force per unit length must go to zero at the free surface. The vertical position of the maximum magnitude must be found experimentally. Typically it is around the 25% of the wave amplitude down in the fluid from the free surface.

Introducing the expression of u in the force and integrating, we have:

$$F_x = \frac{\rho}{2} C_D D \omega^2 \zeta_a^2 \sin(\omega t - kx_0) \left| \sin(\omega t - kx_0) \right| \left[\int_{-h}^{0} e^{2kz} dz + \int_{0}^{\zeta(x_0)} dz \right]$$

$$= \frac{\rho}{2} C_D D \omega^2 \zeta_a^2 \left[\frac{1}{2k} (1 - e^{-2kh}) \underbrace{\sin(\omega t - kx_0) \left| \sin(\omega t - kx_0) \right|}_{odd*even \Rightarrow mean\ value = 0} + \zeta_a \underbrace{\sin^2(\omega t - kx_0) \left| \sin(\omega t - kx_0) \right|}_{even*even \Rightarrow mean\ value \neq 0} \right]$$

So only the integration near the free surface can provide a mean value. The mean force is

$$\bar{F}_x = \frac{\rho}{2T\omega} C_D D \omega^2 \zeta_a^3 \left\{ \int_{-kx_0}^{\pi - kx_0} \sin^3 \underbrace{\gamma}_{\gamma = \omega t - kx_0} d\gamma - \int_{\pi - kx_0}^{2\pi - kx_0} \sin^3 \gamma d\gamma \right\}$$

$$= \frac{\rho}{4\pi} C_D D \omega^2 \zeta_a^3 \left\{ \left[\frac{1}{12} \cos 3\gamma - \frac{3}{4} \cos \gamma \right]_{-kx_0}^{\pi - kx_0} - \left[\frac{1}{12} \cos 3\gamma - \frac{3}{4} \cos \gamma \right]_{\pi - kx_0}^{2\pi - kx_0} \right\}$$

$$= \frac{\rho}{4\pi} C_D D \omega^2 \zeta_a^3 \left\{ \left[-\frac{2}{12} \cos 3kx_0 + \frac{6}{4} \cos kx_0 \right] - \left[\frac{2}{12} \cos 3kx_0 - \frac{6}{4} \cos kx_0 \right] \right\}$$

$$= \frac{\rho}{4\pi} C_D D \omega^2 \zeta_a^3 \left\{ -\frac{1}{3} \cos 3kx_0 + 3 \cos kx_0 \right\}$$

This expression depends on the horizontal location of the column center.
For instance if $x_0=0$:

$$\bar{F}_x = \frac{\rho}{4\pi} C_D D \omega^2 \zeta_a^3 \left\{ -\frac{1}{3} + 3 \right\} = +\frac{2\rho}{3\pi} C_D D \omega^2 \zeta_a^3$$

while if $x_0=\pm\lambda/2$:

$$\bar{F}_x = \frac{\rho}{4\pi} C_D D \omega^2 \zeta_a^3 \left\{ \frac{1}{3} - 3 \right\} = -\frac{2\rho}{3\pi} C_D D \omega^2 \zeta_a^3$$

NB: This means that, depending on the phase angles between platform motions and wave motions, viscous effects can create a force that causes the platform to move against the waves. This is not possible according to Maruo's formula based on potential flow theory.

Summarizing: <u>The main parameters affecting the drift loads are</u>:

- wave amplitude:
  - potential flow → $\propto \zeta_a^2$
  - viscous effects → $\propto \zeta_a^3$
- wavelength
- wave direction
- structural form
- difference between restrained and moving body
- current → <50%
- forward motion
- confined waters, e.g. wall effects when performing experiments

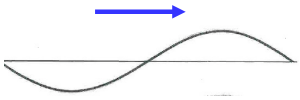

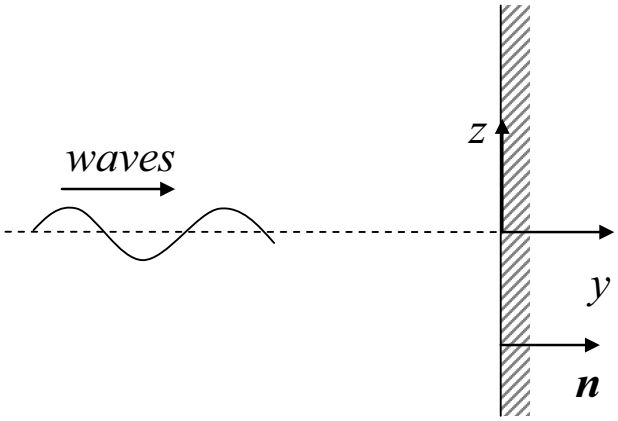
waves
z
y
n

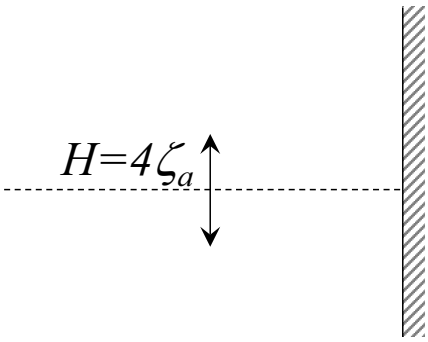
H=4ζa

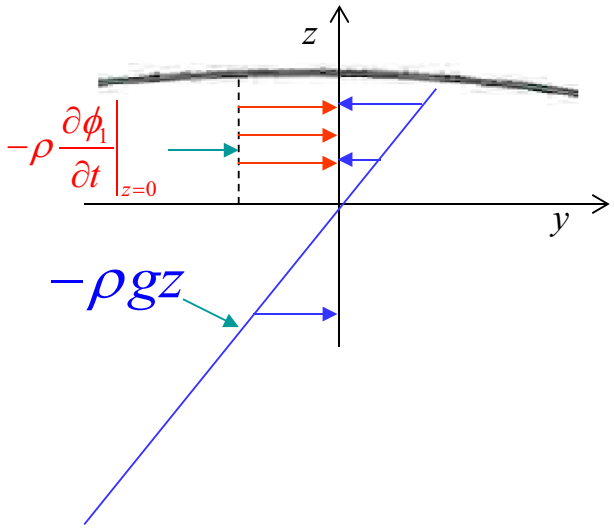

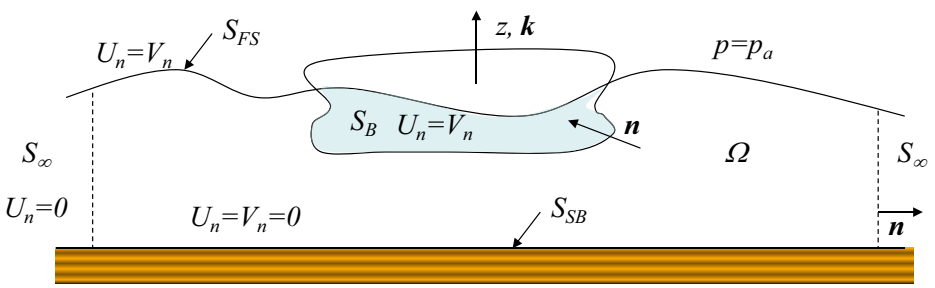

Example of S_∞

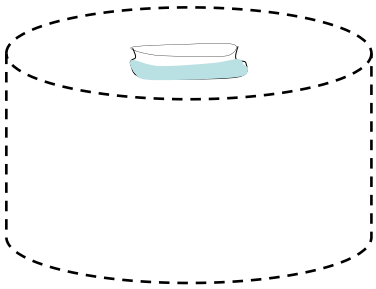

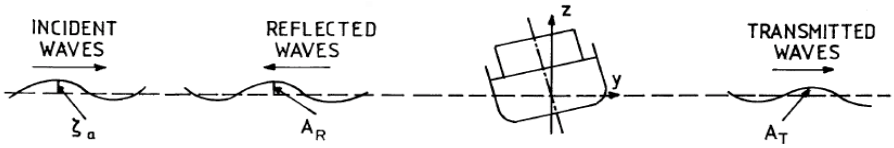

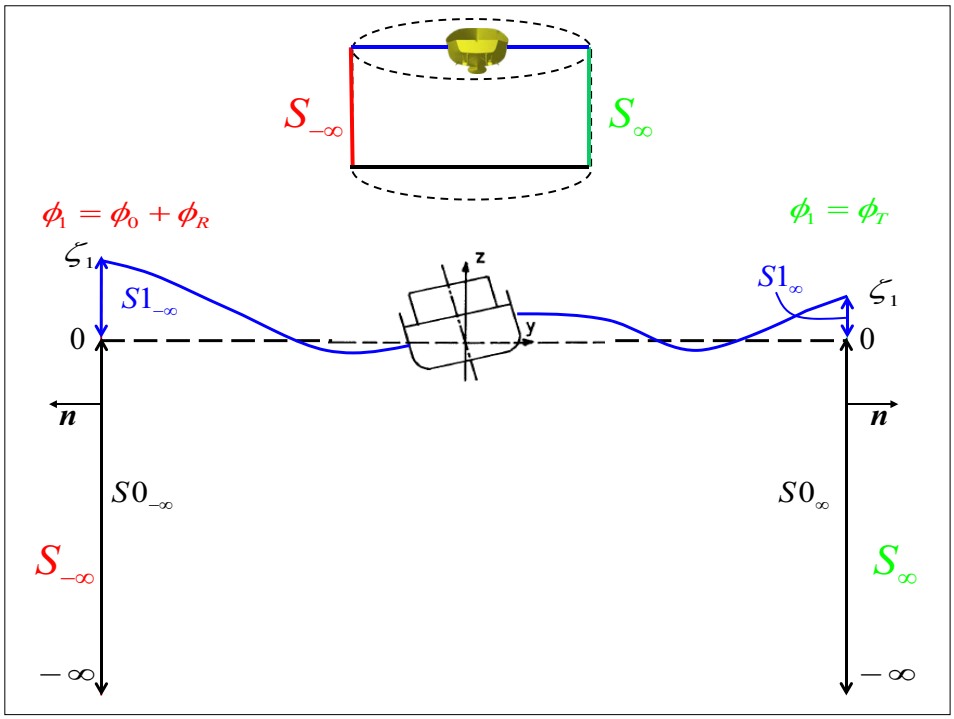

$$\bar{F}_2 = -\int_{S_{-\infty}} \left\{ p + \rho \left(\frac{\partial(\phi_0 + \phi_R)}{\partial y} \right)^2 \right\} \underbrace{n_2}_{=-1} dz - \int_{S_{\infty}} \left\{ p + \rho \left(\frac{\partial \phi_T}{\partial y} \right)^2 \right\} \underbrace{n_2}_{=1} dz$$

So introducing the Bernoulli equation for the pressure, we have:

$$\bar{F}_2 = \underbrace{\int_{S0_{-\infty}} \left\{ -\frac{\rho}{2} \left(\frac{\partial(\phi_0 + \phi_R)}{\partial z} \right)^2 + \frac{\rho}{2} \left(\frac{\partial(\phi_0 + \phi_R)}{\partial y} \right)^2 \right\} dz}_{=0}$$

$$+ \underbrace{\int_{S0_{\infty}} \left\{ \frac{\rho}{2} \left(\frac{\partial \phi_T}{\partial z} \right)^2 - \frac{\rho}{2} \left(\frac{\partial \phi_T}{\partial y} \right)^2 \right\} dz}_{=0}$$

$$+ \int_{S1_{-\infty}} \left\{ -\rho g z - \rho \left. \frac{\partial(\phi_0 + \phi_R)}{\partial t} \right|_{z=0} \right\} dz + \int_{S1_{\infty}} \left\{ \rho g z + \rho \left. \frac{\partial \phi_T}{\partial t} \right|_{z=0} \right\} dz$$

$$= -\frac{\rho g}{4} \left(\zeta_a^{\,2} + A_R^{\,2} \right) + \frac{\rho g}{2} \left(\zeta_a^{\,2} + A_R^{\,2} \right) + \frac{\rho g}{4} A_T^{\,2} - \frac{\rho g}{2} A_T^{\,2}$$

To absorb waves means to generate waves

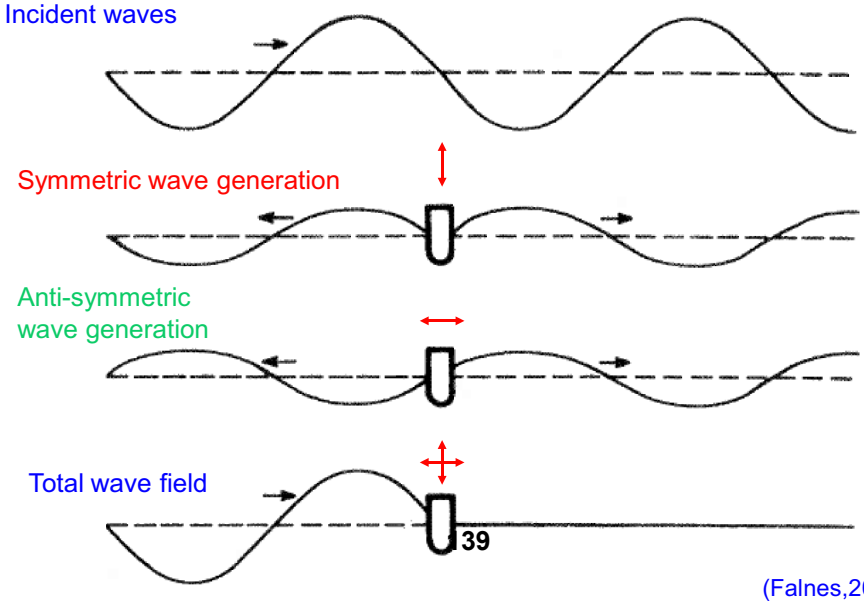

(Falnes,2002)

Studies on Absorbers by Maeda et al. (1981)

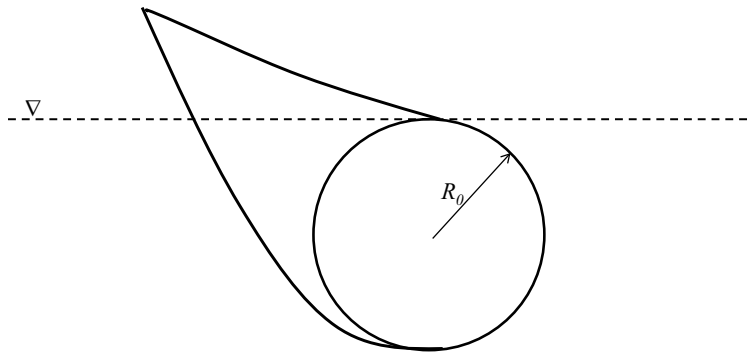

2D Drift Force (U_c=0, U=0)

a =wave amplitude
V_g=group velocity
=$g/(2\omega)$
K =wave number
= ω^2/g

$$\frac{F_D}{\frac{1}{2}\rho g a^2} = \frac{F_D}{\frac{1}{2}\rho g a^2 V_g \frac{2K}{U}}$$

Maximum drift force:
(non wave-power devices)

$$\frac{F_D}{\frac{1}{2}\rho g a^2} = 1$$

Perfect wave-power device:

$$\frac{F_D}{\frac{1}{2}\rho g a^2} = \frac{1}{2}$$

Maeda et al. (1981)

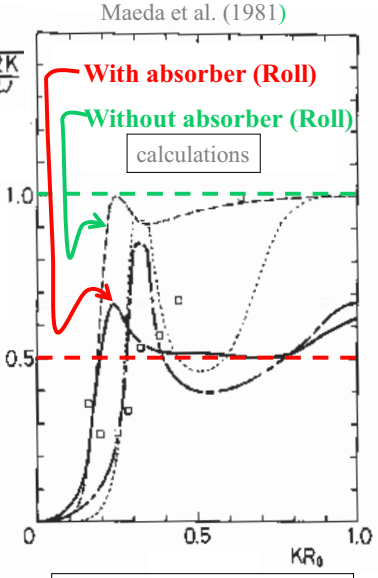

R_0=body dimension length

2D Drift Force (U_c=0, U=0)

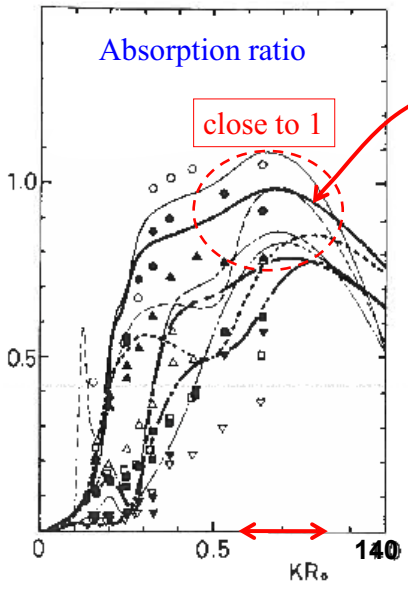

Maeda et al. (1981)

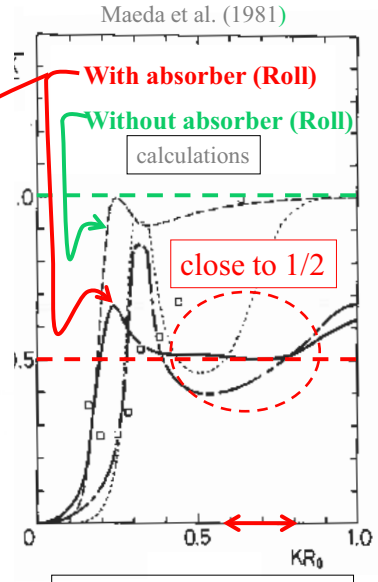

R_0=body dimension length

2D drift force in beam sea. Deep water.

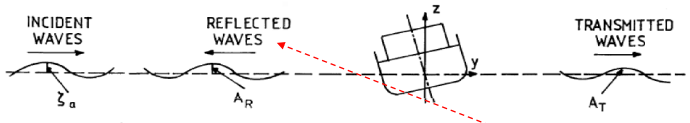

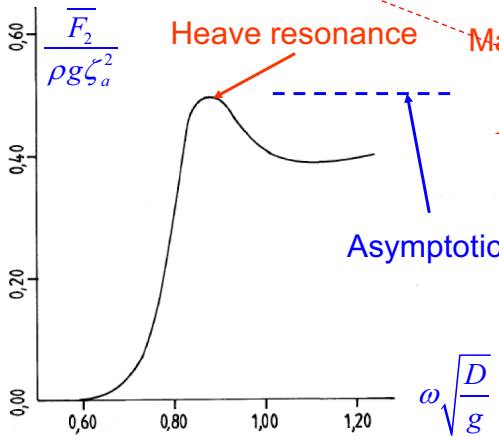

Heave resonance

Maruo's formula:

$$\overline{F}_2 = \frac{\rho g}{2} A_R^2$$

Asymptotic value:0.5

Transverse drift force on a ship as a function of wave length and heading

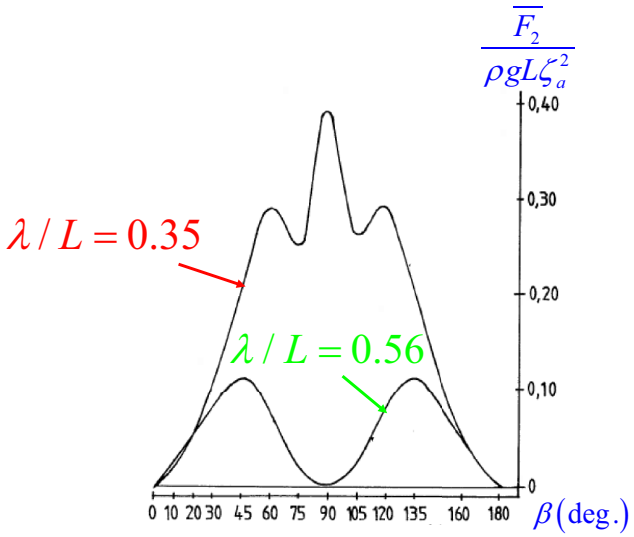

Drift force on a TLP

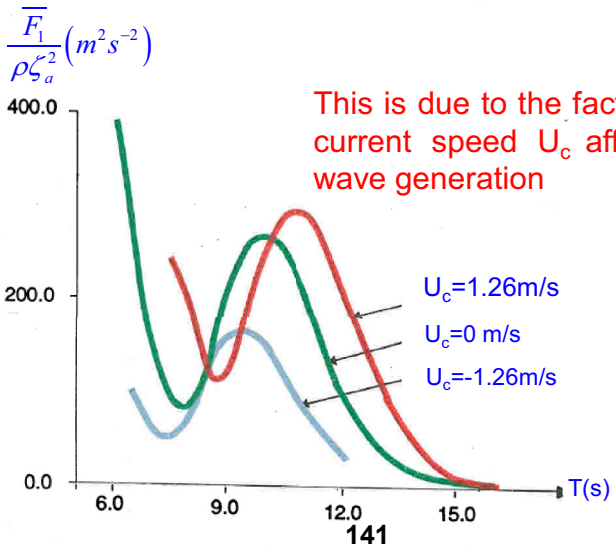

This is due to the fact that the current speed U_c affects the wave generation

U_c=1.26m/s

U_c=0 m/s

U_c=-1.26m/s

Vertical mean wave force on a vertical cylinder

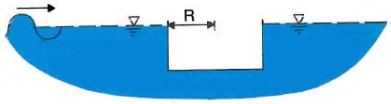

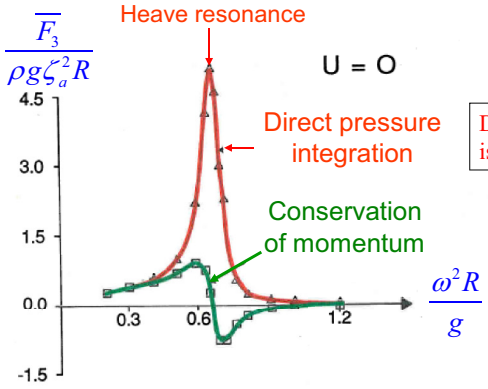

Direct pressure integration is numerically sensitive

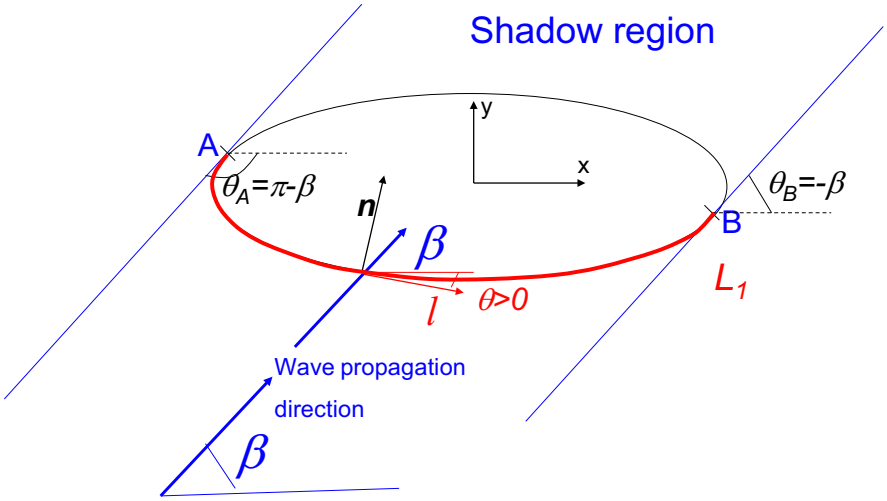

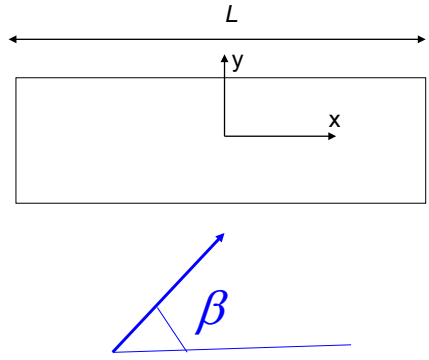

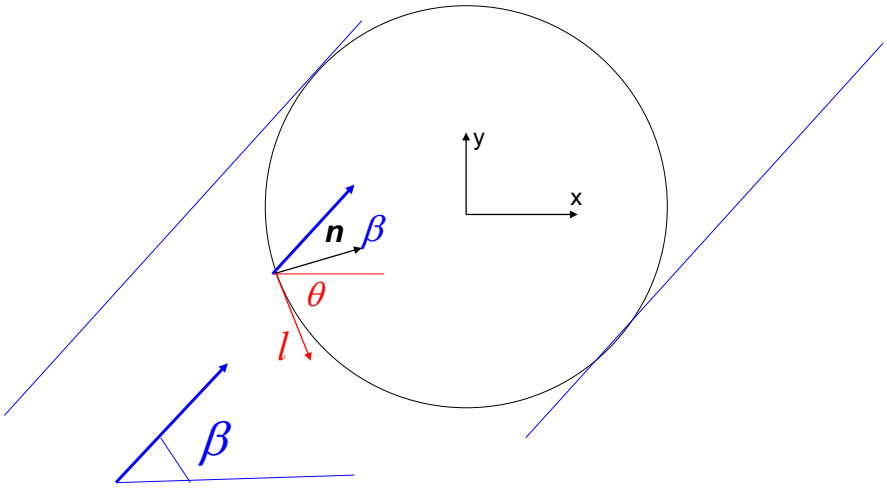

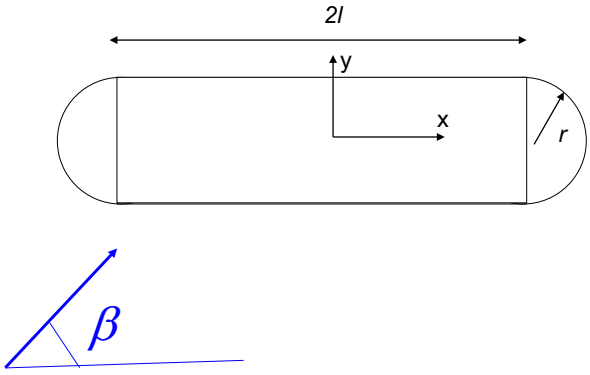

Circular part

$n_1 = \sin\theta \quad n_2 = \cos\theta$

$n_6 = (\pm l - r\sin\theta)\cos\theta - (-r\cos\theta)\sin\theta$

$= \pm l\cos\theta$

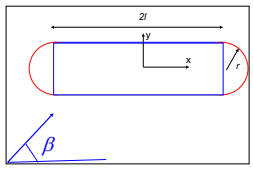

Linear part

$n_1 = 0 \quad n_2 = 1 \quad n_6 = x$

$$\bar{F}_1 = \frac{\rho g \zeta_a^{\,2}}{2}\left\{\underbrace{\int_{-\beta}^{\pi-\beta}\left[\sin(\theta+\beta)\right]^2 \sin\theta r d\theta}_{circular} + \underbrace{0}_{linear}\right\} = \frac{2}{3}\rho g r \zeta_a^{\,2}(\cos\beta)$$

$$\bar{F}_2 = \frac{\rho g \zeta_a^{\,2}}{2}\left\{\underbrace{\int_{-\beta}^{\pi-\beta}\left[\sin(\theta+\beta)\right]^2 \cos\theta r d\theta}_{circular} + \underbrace{\sin\beta\,|\sin\beta|\,2l}_{linear}\right\} = \rho g \zeta_a^{\,2}\left\{\frac{2}{3}r(\sin\beta) + l\sin\beta\,|\sin\beta|\right\}$$

$$\bar{F}_6 = \frac{\rho g \zeta_a^{\,2}}{2}\left\{\underbrace{lr\int_{-\beta}^{0}\left[\sin(\theta+\beta)\right]^2 \cos\theta d\theta - lr\int_{0}^{\pi-\beta}\left[\sin(\theta+\beta)\right]^2 \cos\theta d\theta}_{two\ \ semicircles} + \underbrace{0}_{linear}\right\} = -\frac{\rho g l r \zeta_a^{\,2}}{3}\sin 2\beta$$

Drift force in head sea and small wave lengths

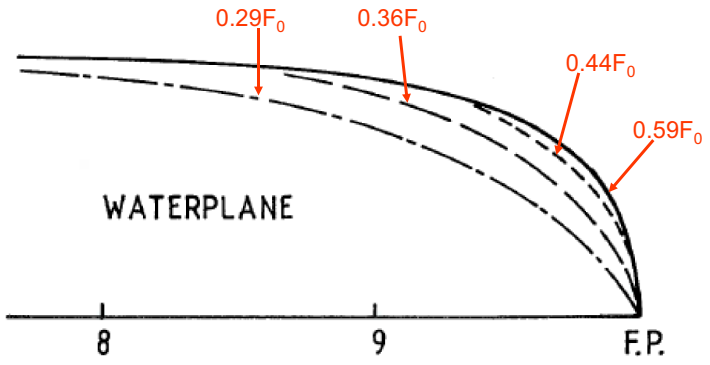

Non-dimensional added resistance of a ship

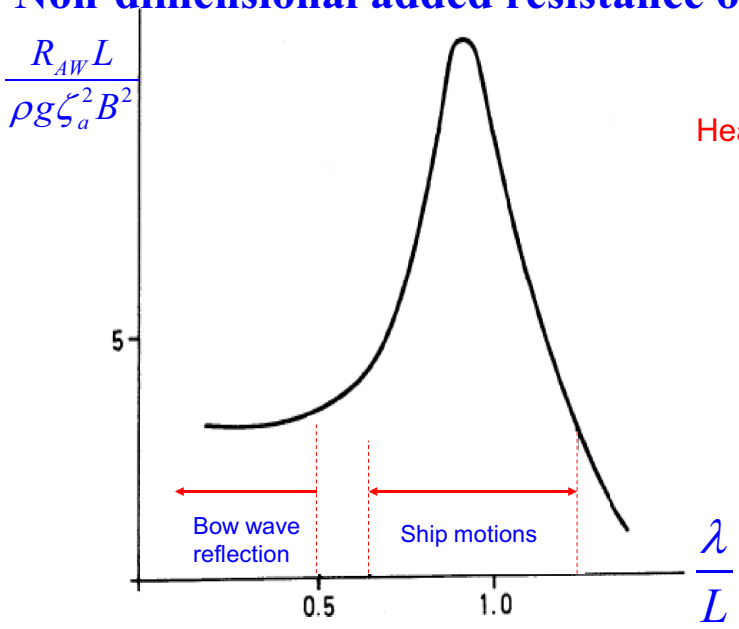

$$\frac{U}{\sqrt{2gR}} = 0.64$$

Horizontal drift force on hemisphere

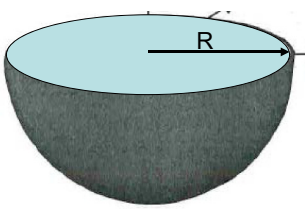

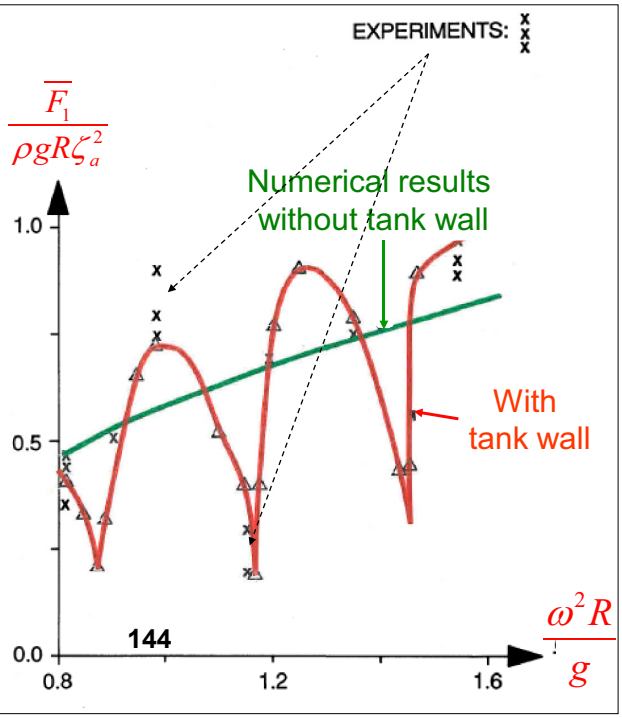

No significant wave energy must be for λ>~0.5L

$$R_{AW} = \frac{\rho g}{16} H_{1/3}{}^2 \left(1 + Fn \frac{4\pi}{T_1}\sqrt{\frac{L}{g}}\right) \int_{L_1} [\sin(\theta)]^2 n_1 dl \quad \text{(F:5.30)}$$

Hp: A one-parameter Pierson-Moskowitz spectrum

→ Expression (F:5.30) can be used if $H_{1/3}$ <0.0065L

- For L=300m →$H_{1/3}$ <1.95 m (in the North Atlantic ~40% of the time)
- For L=100m →$H_{1/3}$ <0.65 m (in the North Atlantic <4% of the time)

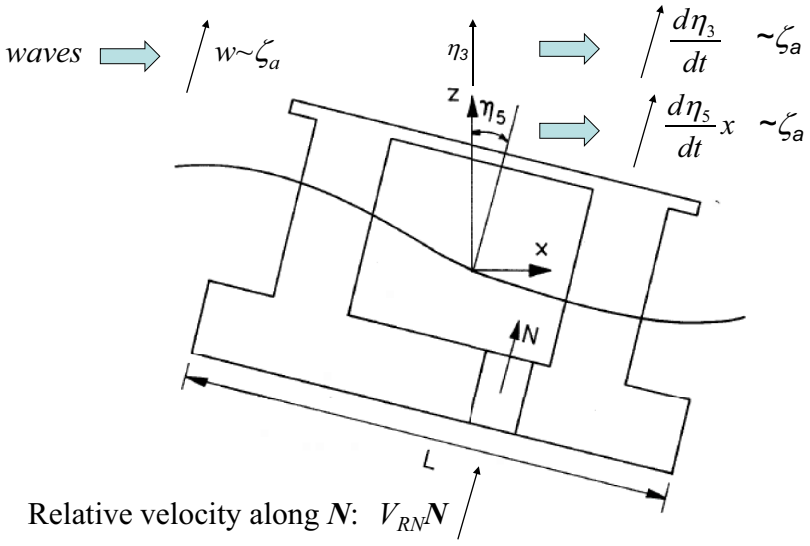

Relative velocity along ***N***: V_{RN}***N***

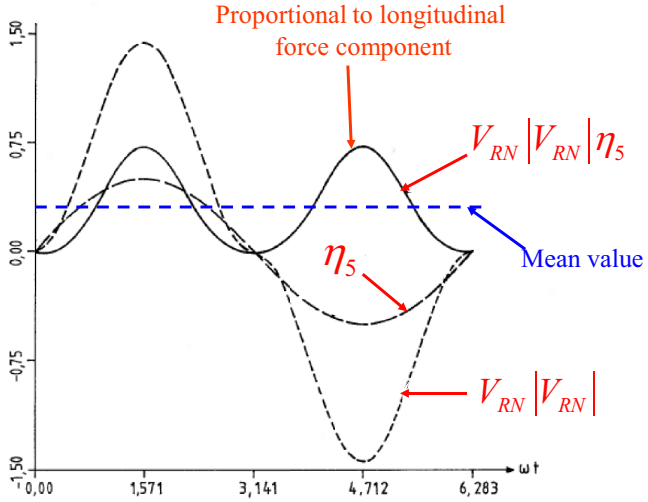

Force per unit length

- From cross-flow principle
- More physical behaviour

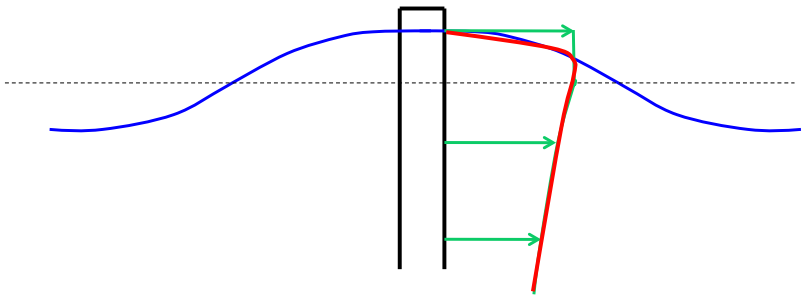

Lecture Note 7

41. Slow-drift motions. Slow drift motions in irregular waves. Wave-drift damping. Eddy-making damping: equivalent linearization. (F: 155-166)

Slow drift motions: general. (F:155-157)
Slow-drift motions are resonance oscillations excited at frequencies low compared with the incoming-wave frequencies due to nonlinear interactions. Such motions are caused by slowly-varying drift loads connected with second-order difference-frequency effects.

From where do these loads come from?
Hp: An incident irregular wave.
This will induce a slowly varying drift force on a marine structure like in the figure below. We can approximate locally the irregular wave as a regular wave, with a certain period and amplitude. This will cause a mean-drift force due to second order effects. At a following time, we can approximate the irregular wave as a regular wave with different frequency and amplitude. This will cause a different mean-drift force. As a result, the mean-drift force will slowly vary in time and its envelope gives the slowly-varying drift force caused by the irregular wave.

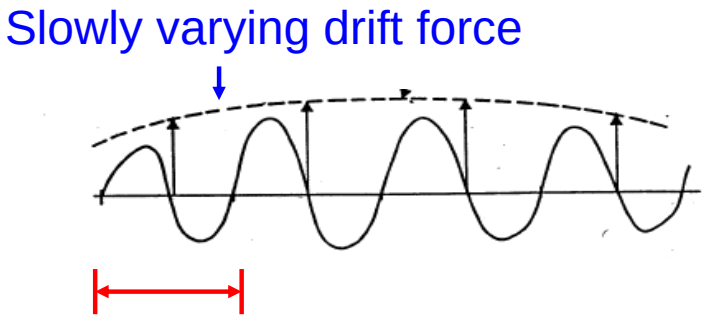

The period associated with the slowly-varying drift loads is of concern when it is close to the resonance period for the considered marine structure.
For example:

- For a freely-floating structure with small waterplane area, restoring terms in vertical plane are small so natural periods are large, e.g. *O*(30 s), and slowly-varying drift (slow-drift) motions can occur in the vertical plane → heave, roll and pitch
  An example is a spar buoy platform.
- For a moored structure, the restoring provided by the mooring lines leads to large resonance periods for the horizontal motions, e.g. *O*(1-2 min), slow-drift motions can occur in the horizontal plane → surge, sway and yaw
- For a structure with small waterplane area and moored, the slow-drift motions can occur both in the horizontal and vertical plane

Large periods mean low frequencies so
→ wave-radiation linear damping is small
→ large amplification of the motions occurs near resonance
In this case viscous damping becomes important. In addition there is a wave-drift damping which is not the same as the wave-radiation linear damping. We will later discuss the main damping mechanisms involved.
An example of motion amplification is shown below for the transverse motion around a period *O*(1-2 min). This leads to large slowly varying motions.

Transverse motion amplitude

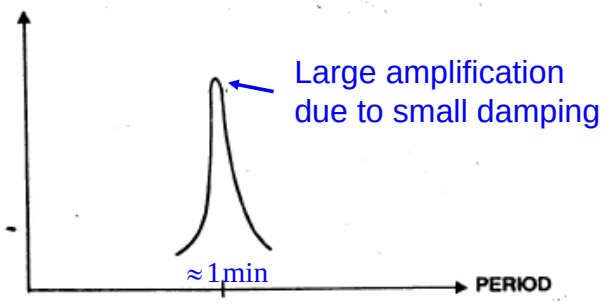

The slowly-varying motions can be connected with a wave-current-wind environment (see sketch in figure below) and are relevant for stationary marine structures that are moored or kept in position by a dynamic-positioning system. Considering the use of mooring lines as in the figure below, the control forces due them counteract the mean forces connected with the wave-current-wind environment, while these control forces are small compared with wave-induced first order forces, i.e. they can not counteract the first order forces. Due to the presence of the mooring lines the moored system will have natural periods in the horizontal plane which are large compared with the incident-wave period range. Such periods can be excited by second-order difference-frequency effects.

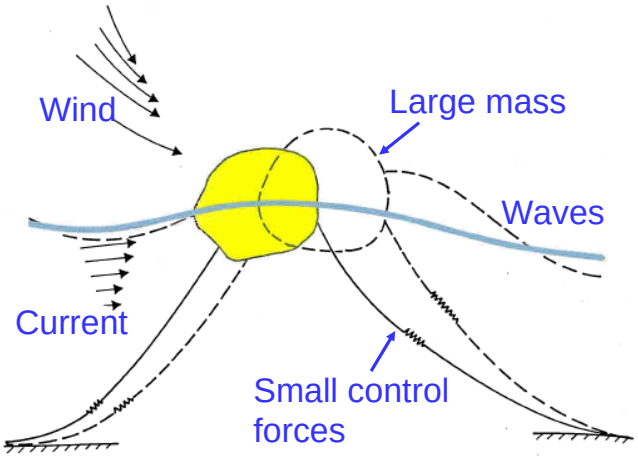

The slow-drift motions are critical for instance for the design of mooring lines and risers. Figure below shows how the anchor line force can become relevant when the horizontal motion of a moored ship becomes large in irregular waves. This occurs when the ship motions show a slowly-varying drift behaviour relative to the incident waves.

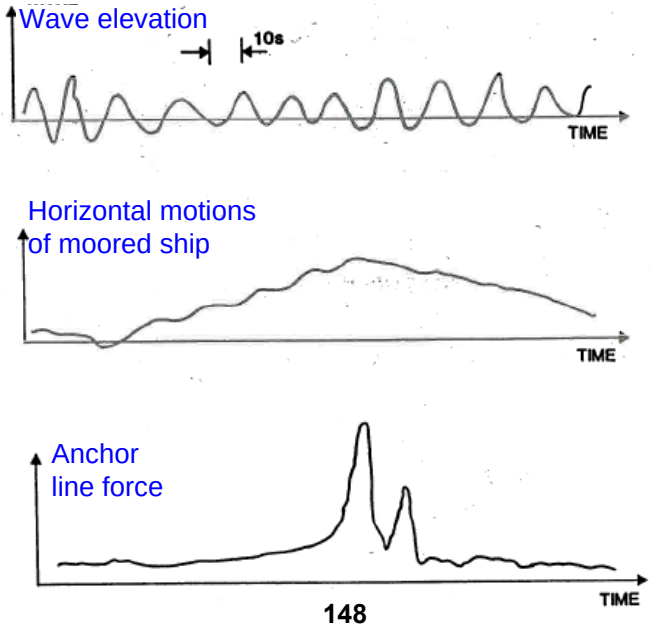

Figure below shows the results from full-scale model tests on the wave-energy ship Kaimei, i.e. used to extract energy through a system of oscillating water columns where the air inside the columns is compressed and expanded by the change of the internal water level and drives the motion of air turbines.
In irregular waves, the anchor line force showed a slow-drift behaviour with period much higher than the incident wave-frequency range. The peaks of the force appeared dangerously close to the ultimate force for the designed anchor line.

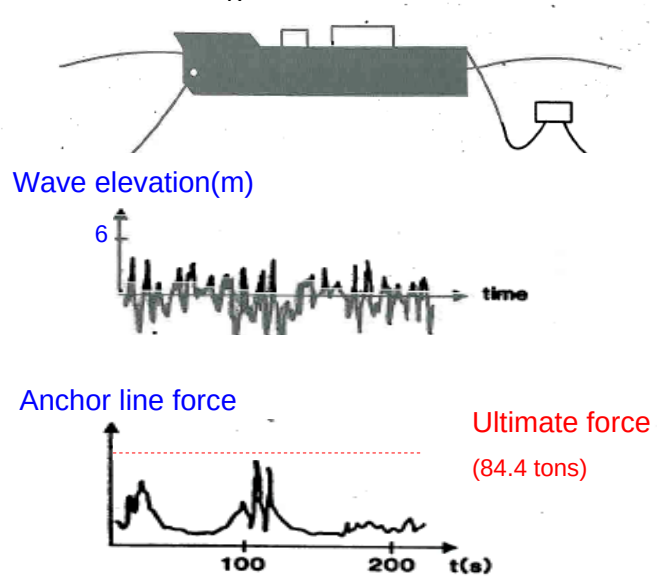

Figure F:5.17 confirms that slow-drift motions are relevant in the horizontal plane also for a TLP.

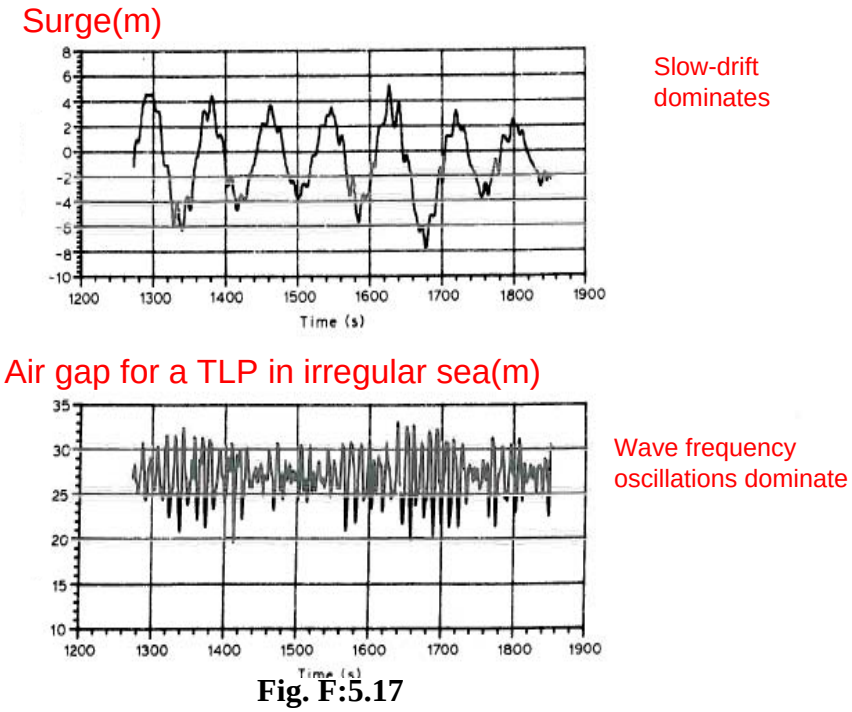

Fig. F:5.17

The case refers to irregular waves with $H_{1/3} = 7m, T_0 = 12s$. In these conditions, the surge motion is clearly dominated by a slow-drift behaviour (T=O(100s)). The air gap (i.e. the relative vertical motion between the underside of the platform deck and the waves) is within the incident-wave frequency range. It means that the surge motion is dominated by second-order effects and the air gap by first-order effects.

How large the slow-drift motion amplitude can be?
Obj: Discuss slowly-varying motions versus linear motions.

Examples
1. Turret-moored production ship, i.e. designed to be weather varying so to work with head or almost head sea waves:

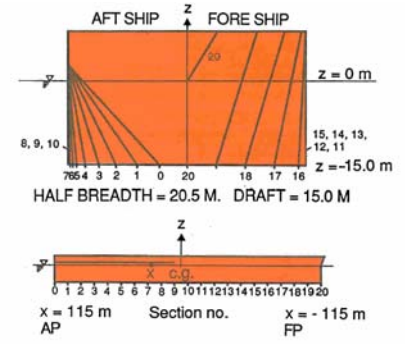

10deg. heading
$H_{1/3}$=15.5m, T_2=13.5s

	Slow-drift	Combined 1. and 2.order
Surge	17.5m	22.2m
Sway	7.0m	7.8m
Yaw	13.6deg.	13.7deg.

2. Deep-draft moored floater:

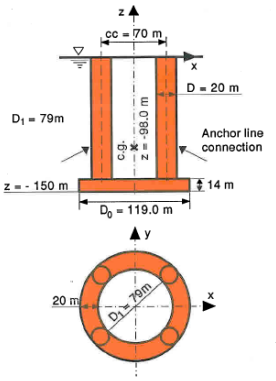

Head sea, $H_{1/3}$=15.5m , T_2=13.5s

	Slow-drift	Combined 1. and 2.order
Surge	5.1m	9.2m
Heave	0.74m	0.95m
Pitch	2.1deg.	2.9deg.

NB: Both results show that the second-order effects (slow-drift motions) are relevant when compared with the first-order effects. This is due to resonance at periods large compared with the incident-wave periods caused by the presence of mooring lines. In these conditions the slow-drift motions dominate on the linear motions.

Slow-drift motions can then be larger than the linear motions. However, because they are slowly varying motions, their velocities and accelerations are small compared with linear velocities and accelerations.

Another example of marine unit where first-order effects could be limited or negligible while second-order effects matter is a submerged bridge:

- linear wave effects go to zero very quickly (exponentially) with the submergence in the case of deep water (as we have learned)
- second-order slowly-varying wave effects go to zero more slowly than linear wave effects (as we will see later)

So the slow-drift response of the submerged bridge, caused by second-order difference-frequency effects, can be relevant and must be estimated. The main damping mechanism in this case is connected with the viscous damping. The main restoring mechanisms are due to the tethers and to the elasticity properties of the bridge.

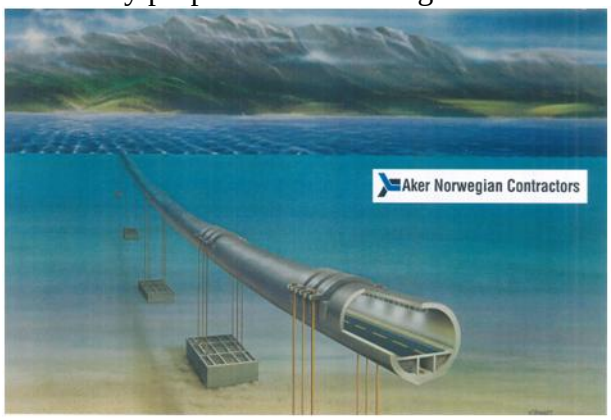

Slow drift motions in irregular waves. (F:155-157)
For a single body in open sea, slow-drift motions can not be caused by body interactions with a regular wave, because a single regular wave with frequency ω can only cause two types of second-order effects: a mean value and a sum-frequency oscillation behavior with frequency 2ω. Second-order difference-frequency effects responsible for slow-drift motions on a single body in open sea need at least two waves with different frequencies to be caused. In general slow-drift motions are caused by irregular waves.

How we can estimate the slow-drift loads F_i^{SV} ?

Hp: Two incident deep-water regular waves propagating in x direction, with first-order velocity potentials

$$\phi_{01}{}^{(1)} = \frac{g\zeta_{a1}}{\omega_1} e^{k_1 z} \cos\left(\omega_1 t - k_1 x + \varepsilon_1\right) \text{ and } \phi_{01}{}^{(2)} = \frac{g\zeta_{a2}}{\omega_2} e^{k_2 z} \cos\left(\omega_2 t - k_2 x + \varepsilon_2\right)$$

The expression for slow-drift excitation loads can be obtained as done for the mean-drift loads, i.e. 1) direct pressure integration or 2) conservation of fluid momentum (angular momentum for the moments).

In general the second-order velocity potential ϕ_2 contributes to the slow-drift loads, so first and second order problems must be solved to estimate these loads. We know how to find the linear solution, we will discuss the second-order problem later while in the following we assume that it has been solved.

NB: In general, to find an accurate solution of the ϕ_2 problem is not straightforward because the second-order solution is usually small, i.e. smaller than first-order solution, and goes to zero slowly moving far from the body.

We then assume that we estimated the slow-drift loads caused by the body interaction with the two regular waves. They are second-order difference-frequency effects so they can be formally written as

$$F_i^{SV} = C_{12}^{ic} \cos[(\omega_2 - \omega_1)t + (\varepsilon_2 - \varepsilon_1)] + C_{12}^{is} \sin[(\omega_2 - \omega_1)t + (\varepsilon_2 - \varepsilon_1)] \quad i = 1,..,6$$

with the amplitudes C_{12}^{ic} and $C_{12}^{is} \propto \zeta_{a1}\zeta_{a2}$ i.e.

$C_{12}^{ic} = \zeta_{a1}\zeta_{a2}T_{12}^{ic}$ and $C_{12}^{is} = \zeta_{a1}\zeta_{a2}T_{12}^{is}$.

Here T_{12}^{ic} and T_{12}^{is} do not depend on the wave amplitudes and therefore are the transfer functions of the slow-drift loads, i.e. second-order transfer functions. They depend on

$T_{12}^{ic}, T_{12}^{is} = f(\omega_1, \omega_2,$ wave direction, body geometry,..)

NB: In the superscripts '*ic*' and '*is*', '*i*' indicates the load component, '*c*' and '*s*' refer to the coefficient of the cosine and sine function, respectively.

We can then write:

$$F_i^{SV} = \zeta_{a1}\zeta_{a2}T_{12}^{ic}\cos[(\omega_2-\omega_1)t+(\varepsilon_2-\varepsilon_1)] + \zeta_{a1}\zeta_{a2}T_{12}^{is}\sin[(\omega_2-\omega_1)t+(\varepsilon_2-\varepsilon_1)]$$

If we have a sea state with spectrum *S(ω)* of *N* incoming regular-wave components with amplitudes

$$A_j = \sqrt{2S(\omega_j)\Delta\omega}$$

The second-order loads become

$$F_i^{SV} = \sum_{j=1}^{N}\sum_{k=1}^{N} A_j A_k \left\{T_{jk}^{ic}\cos[(\omega_k-\omega_j)t+(\varepsilon_k-\varepsilon_j)] + T_{jk}^{is}\sin[(\omega_k-\omega_j)t+(\varepsilon_k-\varepsilon_j)]\right\} \quad \text{(F:5.39)}$$

This expression includes both the mean- and slow-drift (difference-frequency) contributions. To see this we take *N*=2 and omit the phases for simplicity:

$$\begin{aligned}
F_i^{SV} &= A_1A_1[T_{11}^{ic}\overbrace{\cos(\omega_1-\omega_1)t}^{=1} + T_{11}^{is}\overbrace{\sin(\omega_1-\omega_1)t}^{=0}] \\
&+ A_1A_2[T_{12}^{ic}\cos(\omega_2-\omega_1)t + T_{12}^{is}\sin(\omega_2-\omega_1)t] \\
&+ A_2A_1[T_{21}^{ic}\underbrace{\cos(\omega_1-\omega_2)t}_{=\cos(\omega_2-\omega_1)t} + T_{21}^{is}\underbrace{\sin(\omega_1-\omega_2)t}_{=-\sin(\omega_2-\omega_1)t}] \\
&+ A_2A_2[T_{22}^{ic}\cos(\omega_2-\omega_2)t + T_{12}^{is}\sin(\omega_2-\omega_2)t] \\
&\Downarrow \\
&= (A_1^2T_{11}^{ic} + A_2^2T_{22}^{ic}) \ : \text{mean drift} \\
&+ A_1A_2\left[(T_{12}^{ic}+T_{21}^{ic})\cos(\omega_2-\omega_1)t + (T_{12}^{is}-T_{21}^{is})\sin(\omega_2-\omega_1)t\right] \ : \text{slow drift}
\end{aligned}$$

Generalizing to *N* incident regular-wave components of the spectrum, the mean-drift term is

$$\overline{F}_i^{SV} = \sum_{j=1}^{N} A_j^2 T_{jj}^{ic} \quad \text{(F:5.41)}$$

this is the same as the formula already discussed in connection with the mean-drift loads in irregular waves, i.e.

$$\overline{F}_i^{s} = \sum_{j=1}^{N} \frac{\overline{F}_i(\omega_j,\beta)}{\zeta_a^{\,2}} A_j^2 \quad \text{(F:5.27)} \quad \Rightarrow T_{jj}^{ic} = \frac{\overline{F}_i(\omega_j,\beta)}{\zeta_a^{\,2}}$$

So the second-order transfer function of the slow-drift load in *i* direction, T_{jj}^{ic}, connected with the wave with frequency ω_j, is equal to the second-order transfer function of the mean-drift load in *i* direction connected with the same wave.

NB: It means that the second-order transfer function T_{jj}^{ic} depends only on the first-order solution in regular waves, as far as there is no current and no forward speed.

Newman approximation (F:157-158)

The Newman's approximation concerns the second-order transfer functions and implies that

$$\underbrace{\underbrace{T_{jk}^{ic} = T_{kj}^{ic}}_{\text{Newman's definition}} = \frac{1}{2}(T_{jj}^{ic} + T_{kk}^{ic})}_{\text{Newman's approximation}} \quad \text{and} \quad \underbrace{\underbrace{T_{jk}^{is} = -T_{kj}^{is}}_{\text{Newman's definition}} = 0}_{\text{Newman's approximation}} \qquad \text{(F:5.42+5.43)}$$

This approximations allows to simplify greatly expression (F:5.39), as we will see. Newman's approximation corresponds to taking the values of the second-order transfer functions along the line $\omega_j = \omega_k$. Indeed in this case j=k and expressions (F:5.42+5.43) are satisfied. In reality we are not on the line $\omega_j = \omega_k$ but we can be near to this line if ω_j and ω_k are close, i.e. if $\mu = \omega_k - \omega_j$ is small. The Newman's approximation is a good approximation if:

1) we are interested to small $\mu = \omega_k - \omega_j$, e.g. for the horizontal motions of moored systems for which the natural periods are O(1-2min);
2) T_{jk}^{ic} and T_{kj}^{ic} do not change much with the frequency, so that they can be approximated using the same expression as if we were along the line $\omega_j = \omega_k$.

If conditions 1) and 2) are satisfied, we have also that

$$\underbrace{0.5(T_{jj}^{ic} + T_{kk}^{ic})}_{\text{arithmetic average}} \cong \underbrace{\sqrt{T_{jj}^{ic} T_{kk}^{ic}}}_{\text{geometric average}}$$

because $T_{jj}^{ic} \cong T_{kk}^{ic}$. This means that the geometric average can also be used to approximate T_{jk}^{ic} and T_{kj}^{ic}.

An example when the Newman's approximation is valid is given in figures F:5.18 and F:5.19 showing, respectively, the calculated second-order transfer functions T_{jk}^{ic} and T_{jk}^{is} for the difference-frequency horizontal force on a 2D circular cross-section with the axis in the mean free surface and radius R.

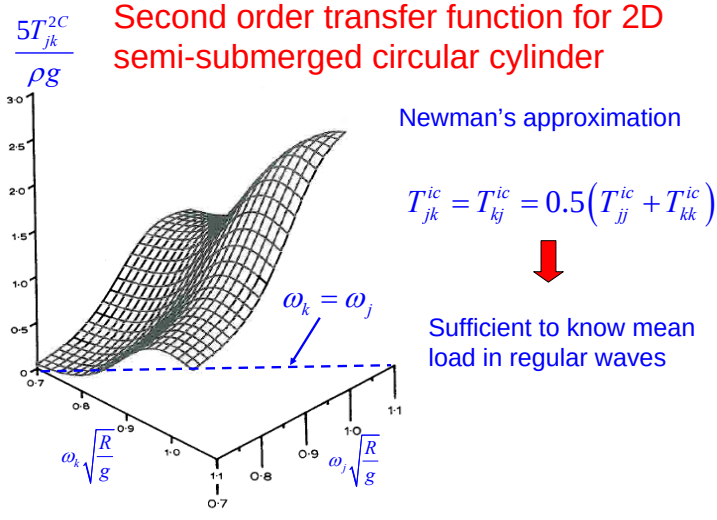

Fig. F:5.18

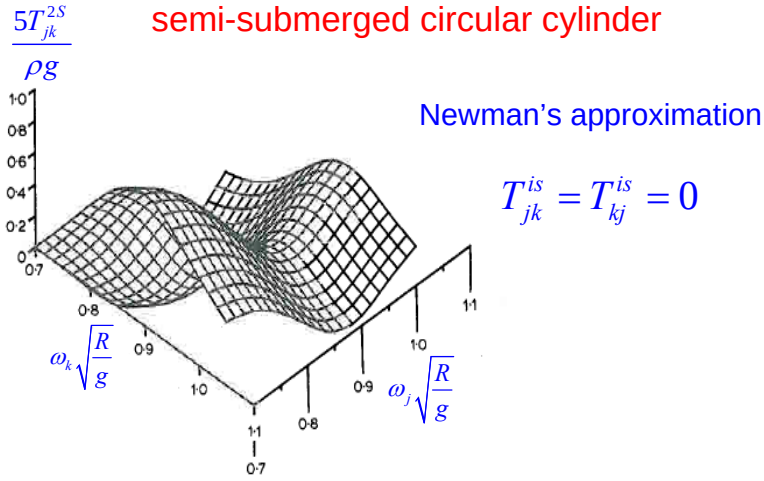

Fig. F:5.19

NB: Newman's approximation does not represent a good approximation for instance when ω_j is close to the resonance frequency in heave and the heave damping is small. In this case:
→ large motions occur

→ the second-order transfer functions have pronounced maxima along the line $\omega_j = \omega_k$, i.e. they change greatly near this line (**NB**: This is because along the line $\omega_j = \omega_k$ we have T_{jj}^{ic} which is equal to $(\overline{F}_i(\omega_j, \beta) / \zeta_a{}^2)$ and this is large for large motions)

In general the Newman's approximation is less good for vertical motions because the natural periods involved are large but not as for the horizontal motions, i.e. they are *O*(30 s).

Introducing the Newman's approximation in expression (F:5.39) and using the geometric average leads to:

$$\Rightarrow F_i^{SV} \cong \sum_{j=1}^{N}\sum_{k=1}^{N} A_j A_k \sqrt{T_{jj}^{ic} T_{kk}^{ic}} \cos[(\omega_k - \omega_j)t + (\varepsilon_k - \varepsilon_j)]$$

Important consequence of Newman's approximation:

To find F_i^{SV} there is no need to calculate the second-order velocity potential ϕ_2. This is because the terms T_{jj}^{ic} are transfer functions of mean-drift loads, so they depend only on the first-order solution in regular waves as long as there is no current and no forward motion. This means a great reduction in terms of computational costs.

An additional simplification of the slow-drift load expression is obtained introducing a sum-frequency term in the slow-drift loads expression. This term <u>is not physical</u> but provides a much simpler formula and, being a high-frequency contribution, it does not affect the slow-drift response that we want to estimate:

$$F_i^{SV} = \sum_{j=1}^{N}\sum_{k=1}^{N} A_j A_k \sqrt{T_{jj}^{ic} T_{kk}^{ic}} \left\{ \underbrace{\cos[(\omega_k - \omega_j)t + (\varepsilon_k - \varepsilon_j)]}_{\textit{original difference-frequency term}} + \underbrace{\cos[(\omega_k + \omega_j)t + (\varepsilon_k + \varepsilon_j)]}_{\textit{additional sum-frequency term}} \right\}$$

$$= \sum_{j=1}^{N}\sum_{k=1}^{N} A_j A_k \sqrt{T_{jj}^{ic} T_{kk}^{ic}} \{ \cos(\omega_j t + \varepsilon_j)\cos(\omega_k t + \varepsilon_k) + \sin(\omega_j t + \varepsilon_j)\sin(\omega_k t + \varepsilon_k) + \cos(\omega_j t + \varepsilon_j)\cos(\omega_k t + \varepsilon_k) - \sin(\omega_j t + \varepsilon_j)\sin(\omega_k t + \varepsilon_k) \}$$

$$= 2\sum_{j=1}^{N}\sum_{k=1}^{N} A_j A_k \sqrt{T_{jj}^{ic} T_{kk}^{ic}} \cos(\omega_j t + \varepsilon_j)\cos(\omega_k t + \varepsilon_k)$$

$$= 2\sum_{j=1}^{N} A_j \sqrt{T_{jj}^{ic}} \cos(\omega_j t + \varepsilon_j) \sum_{k=1}^{N} A_k \sqrt{T_{kk}^{ic}} \cos(\omega_k t + \varepsilon_k)$$

$$\Rightarrow F_i^{SV} = 2\sum_{j=1}^{N} \left[A_j \sqrt{T_{jj}^{ic}} \cos(\omega_j t + \varepsilon_j) \right]^2 \quad \text{(F:5.44)}$$

In this way we need to sum only *N* terms instead of N^2 needed in the previous expression and in expression (F:5.39).

Pinkster's formula (F:159-160)

Pinkster's formula provides the spectral density of the low-frequency part of the loads, i.e. connected with the difference-frequency oscillation behaviour.

We can start considering the contribution to F_i^{SV} given by two wave components of the wave spectrum $S(\omega)$ with frequencies ω_j and ω_k. Using the Newman's approximation

$$T^{ic}_{jk} = T^{ic}_{kj} = 0.5(T^{ic}_{jj} + T^{ic}_{kk}) \quad \text{and} \quad T^{is}_{jk} = -T^{is}_{kj} = 0$$

We have

$$\Rightarrow F^{SV}_{i,jk} = \underbrace{A_j A_k \left[T^{ic}_{jj} + T^{ic}_{kk} \right]}_{=(F^{SV}_{i,jk})_0} \cos[\underbrace{(\omega_k - \omega_j)}_{=\mu} t + \varepsilon_k - \varepsilon_j] \quad (1)$$

NB: To obtain eq. (1) we used that $\cos[(\omega_k - \omega_j)t + \varepsilon_k - \varepsilon_j] = \cos[(\omega_j - \omega_k)t + \varepsilon_j - \varepsilon_k]$

The frequency μ has a small value because it is the difference of two frequencies and we are interested to long periods near the low-frequency resonance.
As an example: If the period of interest is T =90s → $\mu = 2\pi / 90 = 0.07$ rad/s

Obj: Find the spectral density of the low-frequency part of the loads, i.e. $S_F(\mu)$.

The wave amplitudes are related to the wave spectrum given in the figure below by $A_j = \sqrt{2S(\omega_j)\Delta\omega}$ and $A_k = \sqrt{2S(\omega_k)\Delta\omega} = \sqrt{2S(\omega_j + \mu)\Delta\mu}$.

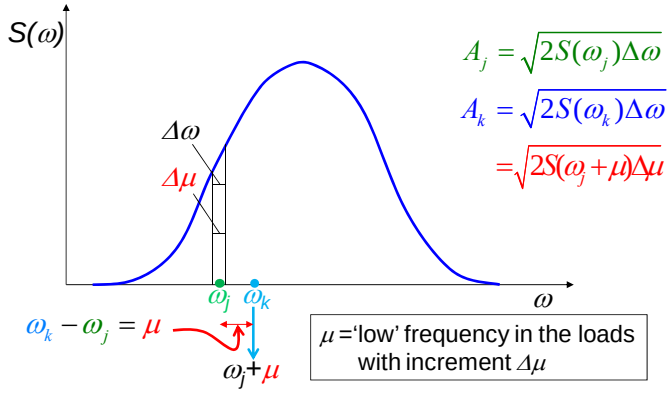

Let's study $\mu = n\Delta\omega$, then k becomes $k=j+n$, with $n = 1, 2, ..$
So index j is connected with the incident-wave frequency ω and index n is connected with the low frequency μ.
Because μ is small, we can approximate $T^{ic}_{jj}(\omega_j)$ and $T^{ic}_{(j+n)(j+n)}(\omega_j + \mu)$ with the value at mean position $\omega_j + \mu/2$, i.e. $T^{ic}(\omega_j + \mu/2)$.

The slow-drift loads due to the spectrum become then

$$F^{SV}_i = \sum_n \sum_{j=1}^{N} \underbrace{\left\{ 2A_j A_{j+n} \left[T^{ic}(\omega_j + \mu/2) \right] \right\}}_{=(F_{i,(j)(j+n)})_0} \cos(\mu t + \varepsilon_{j+n} - \varepsilon_j)$$

We know that the load amplitude $(F_{i,jn})_0$ is linked to the slow-drift load spectrum by

$$S_F(\mu)\Delta\mu = \sum_{j=1}^{N} \frac{1}{2} \left(F_{i,(j)(j+n)} \right)_0^2 = \frac{1}{2} \sum_{j=1}^{N} 4A_j^2 A_{j+n}^2 \underbrace{[T^{ic}(\omega_j + \mu/2)]^2}_{=\frac{\bar{F}_i(\omega_j+\mu/2)}{\zeta_a^2}} \quad (2)$$

Substituting the expressions of the wave amplitudes in terms of the wave spectrum (see above) and letting $N \to \infty$, we have

$$S_F(\mu) = 8 \int_0^{\infty} S(\omega) S(\omega + \mu) \left[\frac{\bar{F}_i(\omega + \mu/2)}{\zeta_a^2} \right]^2 d\omega \quad \text{(F:5.45)}$$

This is the spectral density for the low-frequency part of the loads and is linked to the significant-wave height as follows

$$S_F(\mu) = 8\int_0^\infty \underbrace{S(\omega)}_{\propto H_{1/3}^2}\underbrace{S(\omega+\mu)}_{\propto H_{1/3}^2}\underbrace{\left[\frac{\bar{F}_i(\omega+\mu/2)}{\zeta_a^{\,2}}\right]^2}_{\neq f(H_{1/3}^2)} d\omega \quad \propto H_{1/3}^4$$

Hp: One degree of freedom motion.
Obj: Find the amplitude of the slow-drift response $x = x_0 e^{i(\mu t+\varepsilon)}$.

The motion equation is

$$m\ddot{x} + b\dot{x} + cx = F_i(t) = F_{i0}e^{i\mu t}$$

with *m* the mass term, *b* the damping term, *c* the restoring term and $F_i(t)$ the slow-drift excitation force.

$$\Rightarrow (-\mu^2 m + i\mu b + c)x_0 e^{i\varepsilon} = F_{i0}$$

So the response amplitude is

$$x_0 = \frac{1}{\sqrt{(-m\mu^2 + c)^2 + \mu^2 b^2}} F_{i0} = |H(\mu)|\, F_{i0} \quad (1)$$

with $|H(\mu)|$ the response transfer function also named as Response Amplitude Operator (RAO).

The amplitude of the force and of the response can be expressed in terms of their corresponding spectral densities as

$$F_{i0}^2 = 2S_F(\mu)d\mu$$

and

$$x_0^2 = 2S_x(\mu)d\mu$$

So using the link (1) above, we have

$$S_x(\mu) = |H(\mu)|^2\, S_F(\mu).$$

The variance of the response is

$$\sigma_x^{\,2} = \int_0^\infty S_x(\mu)d\mu = \int_0^\infty S_F(\mu)\frac{1}{(c-\mu^2 m)^2 + b^2\mu^2}d\mu \quad \text{(F:5.47)}$$

If the response variable *x* is the surge, the term *m* would be in general $m = (M + A_{11})$, with *M* and A_{11} the ship mass and added mass in surge, $b = B_{11}$ and $c = C_{11}$.

NB: As we have seen previously, the variance is an important parameter. Its square-root, i.e. the standard deviation, gives a measure of the response deviation from its mean value, so it is directly linked to the most probable largest value of the response.

We are interested to the slow-drift resonance, i.e. the frequency μ is in the vicinity of resonance. Let then $\mu_n = \sqrt{c/m}$. If we assume that the damping term *b* is small, i.e. small relative to the critical damping $2m\mu_n$, then the major contribution to the variance comes from the resonance, i.e. $S_F(\mu) \approx S_F(\mu_n)$, because at resonance the response is largest.

The figure below shows this circumstance by plotting the spectrum of the slow-drift force and the other factor of the integrand in (F:5.47), together with the incident wave spectrum. The damping is small near the resonance. As a result, it is apparent that the variance of the slow-drift motion is mostly affected by the contribution near μ_n while it does not have basically contribution from the incident-wave frequency range and from elsewhere.

Then we can approximate $\sigma_x^{\,2}$ as follows

$$\sigma_x^{\,2} \cong S_F(\mu_n)\int_0^{\infty} \frac{1}{(c-\mu^2 m)^2 + b^2\mu^2} d\mu = S_F(\mu_n)\frac{\pi}{2bc} \quad \text{(F:5.48)}$$

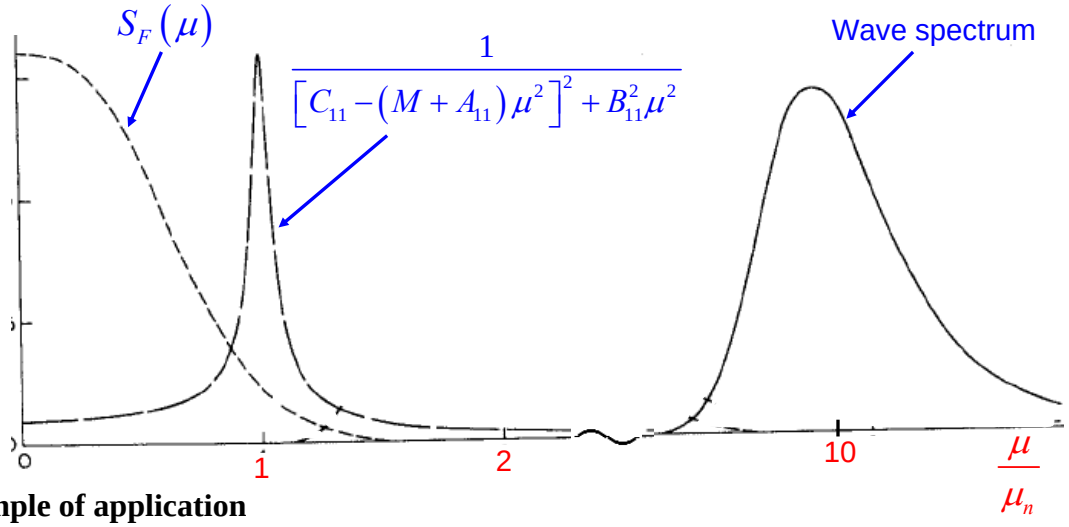

Example of application

Hp: A moored tanker.

Obj: Find the standard deviation σ_x of the slow-drift surge motion using formula (F:5.48).

To estimate σ_x we need $S_F(\mu_n)$, b and c. The steps to do are the following:

1. The restoring term $c = C_{11}$ is given by the mooring system characteristics (we have seen how to find this through an example of a moored vessel).
2. μ_n is the resonance frequency, i.e. $\mu_n = \sqrt{c/m} = \sqrt{C_{11}/(M+A_{11})}$. So we need to calculate the added-mass in surge, for instance using the 3D source technique.
3. The slow-drift spectrum $S_F(\mu)$ for surge can be obtained once known the drift forces in regular waves (see Pinkster's formula). The drift forces can be estimated using a numerical solver and applying the conservation of fluid momentum or direct-pressure integration. Then $S_F(\mu_n)$ becomes available.
4. The damping term b is given by skin friction, eddy-making damping, wave-drift damping and anchor-line damping. The wave-drift damping dominates for high sea states, for example,
   Hp: A ship long L=235m.
   For $H_{1/3}$=8.1m the wave-drift damping represents the 85% of the total damping, while it is negligible for $H_{1/3}$=2.8m.
   In the case of sway, both eddy-making and wave-drift damping are important.

Slow-drift damping

The main sources of slow-drift damping are connected with nonlinear phenomena and can be listed as:

1. wave-drift damping
2. viscous hull damping
3. viscous anchor-line damping

Wave-drift damping (F:161-164)
It is due to the body interaction with incident waves. For a marine vehicle/platform, it can be quantified for instance doing free-decay model tests of the vehicle/platform in calm water and in regular waves. In the latter case it is found that the decay is faster, and so the damping-level is higher. The additional damping is a wave-drift damping and is due to the interaction between the rapid oscillating behaviour of the incident waves and the slow-drift motion connected with the free decay.
Figure F:5.20 documents this in terms of surge decay for a TLP in two cases: (a) in calm water and (b) in regular waves. The results show that, once filtered the incident-wave frequency from the measurements in waves, the decay of the motion appears clearly stronger with respect to the case in calm water.

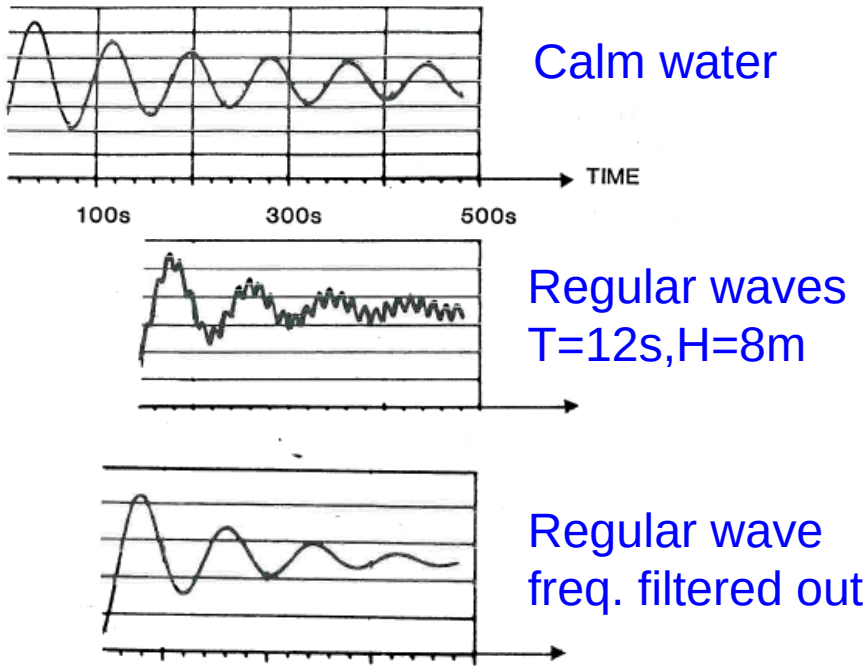

Let's consider the surge-motion case.
The second-order difference-frequency effects of the body-irregular wave interaction cause a slow-drift surge speed in the vessel. This interacts with the rapid oscillation behaviour of the incident waves causing a wave-drift damping. This is because an average force (a mean-drift force) is caused which acts as a damping force to the motion.
We can interpret the slow-drift surge speed induced as a quasi-steady forward and backward speed, say U.
If we then split the spectrum in elementary regular incident waves, we can study the vessel with such quasi-steady speed in incident head-sea regular waves.
We need then to find the mean-drift force in surge. This coincides with the added-resistance in waves. For instance for $L>>\lambda$, i.e. $\lambda<\sim 0.5L$, in head sea we have

$$R_{AW} = \bar{F}_1 = \frac{\rho g \zeta_a^{\,2}}{2}\left(1+\frac{2\omega U}{g}\right)\int_{L_1}\left[\sin(\theta)\right]^2 n_1 dl \qquad \text{(F:5.22)}$$

The U-term in the formula can be interpreted as a damping of the form $B_{11}^{WD}U$, so the coefficient B_{11}^{WD} will be

$$B_{11}^{WD} = \rho\omega\zeta_a{}^2 \int_{L_1} [\sin(\theta)]^2 n_1 dl \qquad \text{(F:5.49)}$$

This is the slow-drift damping coefficient, proportional to $\zeta_a{}^2$ and is due to the interaction between the slow-drift motion in surge and the rapid oscillation behaviour of the waves.

NB: Formula (F:5.49) is valid for small wavelengths compared to the ship length, Zhao et al. (1988) developed a numerical method to evaluate the wave-drift damping for any λ.

NB: If we consider the slow-drift surge speed U as it is, i.e. oscillating with low frequency, then we find that the damping has also a slowly-varying behaviour. This aspect is not discussed in the lecture in further detail.

An example of the procedure to find numerically B_{11}^{WD} is given in fig. F:5.22.

Hp: - A vertical circular cylinder that is free in surge in linear motions. Incident regular waves in deep water.

- The slow-drift surge speed is interpreted as quasi-steady forward and backward current with values U_1=U and U_2=-U, positive value means a speed in the wave direction.
- Using this quasi-steady approach one can express the wave-drift damping as a power series of the current speed. Here we estimate the first term of this series, i.e. a term like $B_{11}^{WD}U$ with B_{11}^{WD} independent from the current speed. This has the same form as the damping force providing the wave-drift damping for small wavelengths given by eq. (F:5.49).

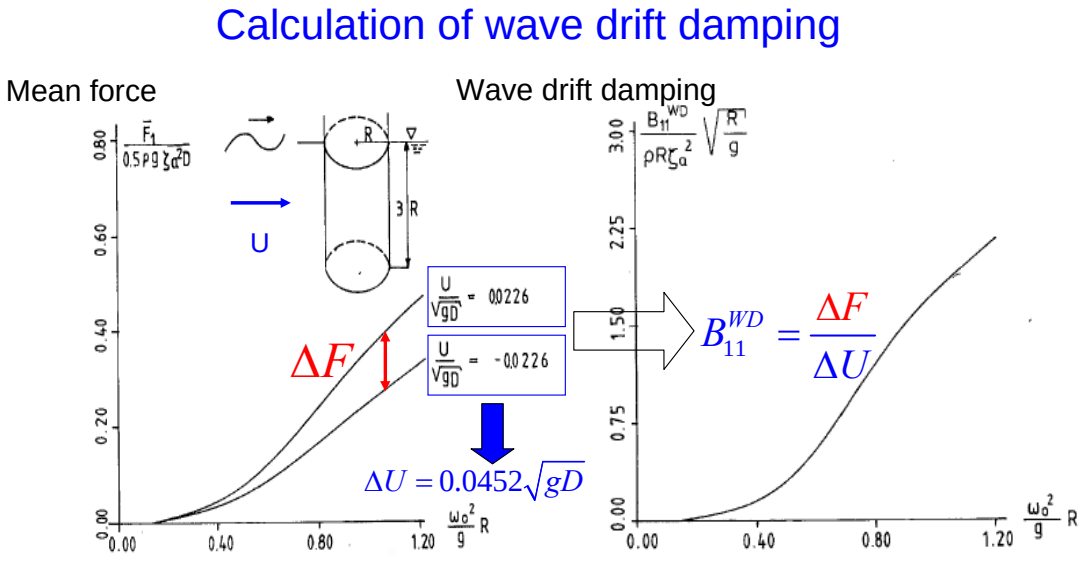

Fig. F:5.22

The procedure to find B_{11}^{WD} is:

1. We calculate the mean-drift force in surge $\bar{F}_1$ for U_1 and U_2 and varying the incident wave frequency.

2. We estimate the variation ΔF of the mean force connected with the velocity variation $\Delta U = U_2 - U_1$ for every incident frequency.
3. We then use the fact that this force variation is a damping force, i.e. $\Delta F = B_{11}^{WD} \Delta U \quad \Rightarrow \quad B_{11}^{WD} = \Delta F / \Delta U$.

The damping curve in figure F:5.22 shows an important increase with the square power of the incident-wave frequency.

Being a second-order effect, also the wave-drift damping is not easy to estimate. Fig. F:5.21 shows the wave-drift damping in surge measured for two ship hulls in head regular waves. Also the wave-drift expression (F:5.49) valid for small wavelengths compared with the ship length is reported. One must note that the experiments can show easily large scatter in the measurements. This means that high accuracy is required when doing model tests.

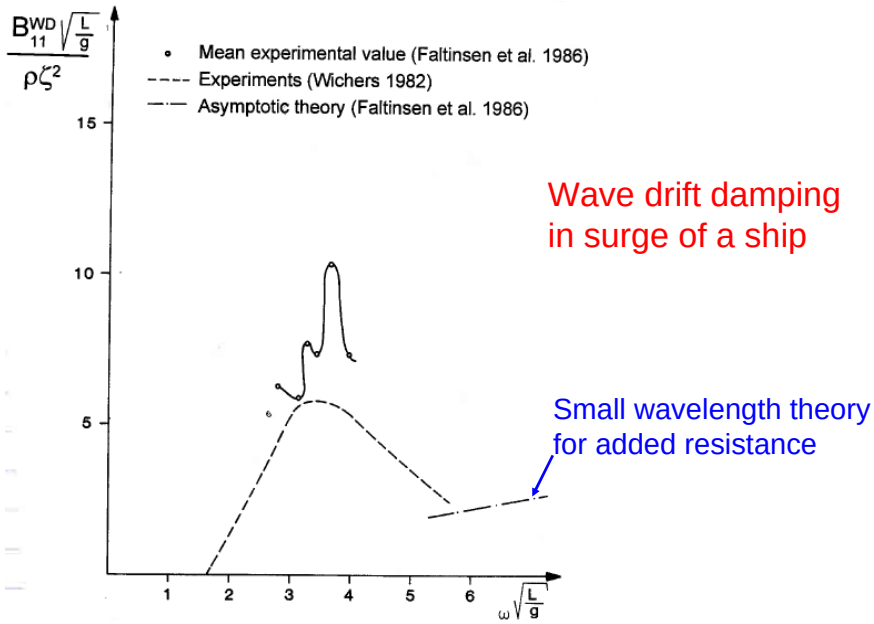

Fig. F:5.21

Tank-wall effects can cause bias in the estimation of the wave-drift damping. An example is given in the figure below. The case refers to a hemisphere in regular waves along x direction. Both model tests and numerical results accounting for the side walls of the tank show a wave-drift damping reducing as the incident-wave period increases, with an oscillatory behaviour which leads to negative values of B_{11}^{WD}. The negative values are connected with the presence of the walls which can cause exchange of energy from the fluid to the body, while the wave-drift damping in open waters is positive.

hemisphere

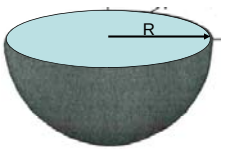

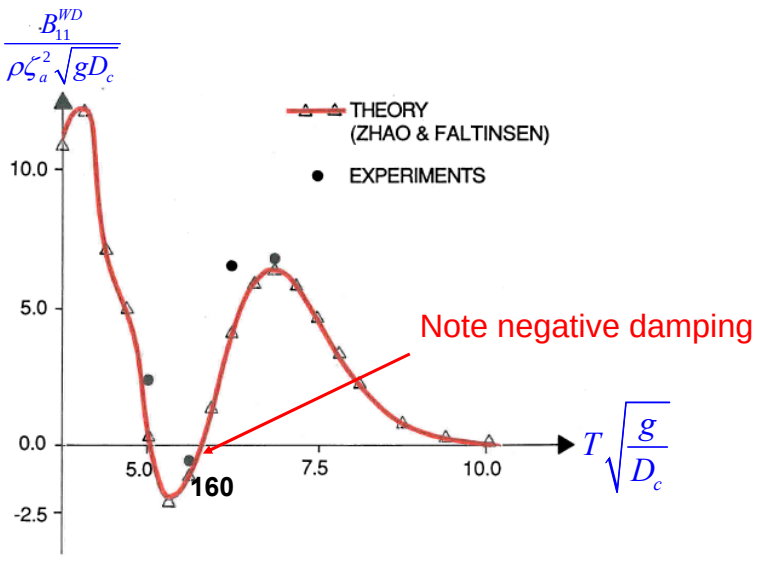

The wave-drift damping associated with a given spectrum $S(\omega)$ can be obtained using a formula similar to that for the mean-drift force. So if for the mean-drift force in surge we have

$$\bar{F}_1^s = 2\int_0^\infty S(\omega)\left(\frac{\bar{F}_1(\omega,\beta)}{\zeta_a{}^2}\right)d\omega \qquad \text{(F:5.28)}$$

for the wave-drift damping in surge we will have

$$B_{11}{}^{WDs} = 2\int_0^\infty S(\omega)\left(\frac{B_{11}{}^{WD}(\omega,\beta)}{\zeta_a{}^2}\right)d\omega$$

NB: $B_{11}^{WD} \propto H_{1/3}^2$ because it is proportional to $\zeta_a{}^2$ in the case of regular waves with amplitude ζ_a. Since the spectrum of slow-drift force $S_F \propto H_{1/3}^4$, then from expression (F:5.48): $\sigma_x{}^2 = S_F(\mu_n)\pi/(2bc)$, with $b = B_{11}^{WD} \Rightarrow \sigma_x \propto \sqrt{S_F/b} \propto H_{1/3}$. This is unexpected since we talk about second-order variables, i.e. we would expect a dependence on $H_{1/3}$ to the square power.

The probability density function of the extreme values of the slowly-varying response can be approximated by a Rayleigh distribution. Strictly speaking this requires that the response is a Gaussian narrow-banded process. In this case, the most probable largest value of the response in a storm of duration *t* is

$$x_{\max} = \sigma_x\sqrt{2\log\left(\frac{t}{T_N}\right)} \qquad \text{(F:5.50)}$$

with T_N the natural period of the slow-drift response.

If , for instance, *t*=5h and T_N =100s → $x_{\max} = 3.22\sigma_x$

Børresen has proposed a pragmatic formula to estimate the most probable largest value of the response, accounting for first- and second-order effects. It is based on Rayleigh distribution for the extreme values of both the first-order and the slowly-varying second-order response and on summing them up, i.e.

$$x_{\max} = \sigma_x{}^{1.order}\sqrt{2\log\left(\frac{t}{T_{r1}}\right)} + \sigma_x{}^{2.order}\sqrt{2\log\left(\frac{t}{T_{r2}}\right)}$$
$$\cong 4\sigma_x{}^{1.order} + 3\sigma_x{}^{2.order}$$

The approximated expression is obtained considering typical duration *t* of a storm, typical mean period of the first-order response T_{r1} and typical slowly-varying period of second-order response, T_{r2}. For instance *t*=*O*(5h), T_{r1} can be approximated as the mean incident-wave period T_2, e.g. *O*(10 s), and T_{r2}=T_{N2}=*O*(100s).

Formula (F:5.50) gives a rough estimate of the most probable largest value. An improvement can be obtained with a better hydrodynamic and statistical analysis. In particular, an improved statistical analysis means that one should consider several long-time random realizations of the wave spectrum and estimate from them a proper distribution of the extremes, i.e. with several samples of extreme values.

The procedure to be used for the estimation of the most probable largest value of the motion is examined in the figure below in terms of the slow-varying motions.

The figure shows 4 random-time realizations of the same process. The differences in the time histories are due to different random phases, necessary to reproduce a random process. The procedure is the following:

1) The extreme value (absolute maximum) recorded in each time series is stored;
2) The most probable largest value is found as the mean among the stored maxima of the motion.

We understand that in reality we need more realizations to build a proper statistical analysis and have a proper estimation of the most probable largest value, as well as of other statistical quantities. As mentioned above, this implies the need for long-time simulations and model tests, which could be impractical or too expensive.

The standard deviation is less sensitive to the use of different random-time realizations than the extreme values and so it can be estimated more easily.

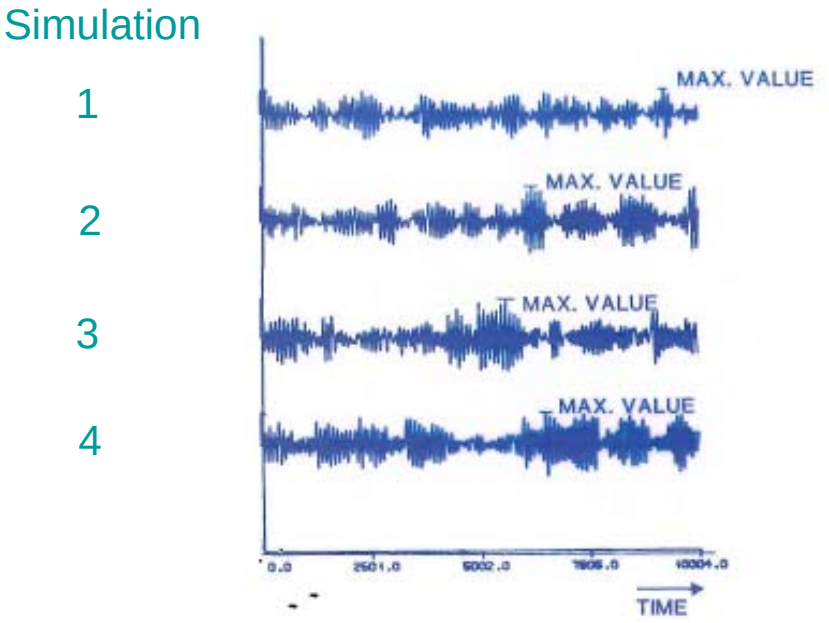

Eddy-making damping: equivalent linearization (F:164-166)

Eddy-making damping is connected with vortex shedding. It is nonlinear, i.e. it behaves as the square power of speed, i.e. as $B_D \dot{y}|\dot{y}|$. It means that in general the response must be found in time domain. If we want to use the more efficient frequency-domain approach, we need to linearize the eddy-making damping.

Let's see how to perform the linearization in the case of slow-drift sway motion. The uncoupled 1D motion is:

$$(M + A_{22})\ddot{y} + B_D \dot{y}|\dot{y}| + C_{22} y = F_2^{SV}(t) \quad \text{(F:5.51)}$$

Here M and A_{22} are the ship mass and added mass in sway and C_{22} is the restoring term, for instance connected with the mooring system. F_2^{SV} is the slow-drift excitation force in sway. The damping coefficient is $B_D = 0.5\rho C_D A$, with ρ the water density, C_D the drag coefficient and A the frontal area of the submerged structure against the motion.

We can find an equivalent linear damping B^e by

1) assuming that the slow-drift response is a Gaussian process (not always true) and
2) enforcing that the linearization must ensure an energetic equivalence, i.e. that the energy taken from the system by the linear damping is the same as the energy taken from the system by the nonlinear damping.

This gives

$$B^e = 4 B_D \sigma_{\dot{y}} / \sqrt{2\pi} \qquad \text{(F:5.52)}$$

so that

$$(M + A_{22})\ddot{y} + B^e\dot{y} + C_{22}y = F_2^{SV}(t)$$

Using the approximation of the response standard deviation given by

$$\sigma_y^{\,2} \cong S_F(\mu_n)\frac{\pi}{2B^eC_{22}} \quad \text{(F:5.48)}$$

and the fact that, as the response slowly oscillates with frequency μ,

$$|\dot{y}| = \mu|y| \;\Rightarrow\; |\dot{y}|^2 = \mu^2|y|^2 \;\Rightarrow\; S_{\dot{y}}(\mu) = \mu^2 S_y(\mu) \;\Rightarrow\; \sigma_{\dot{y}}^{\,2} = \mu^2\sigma_y^{\,2}$$

we have

$$\sigma_{\dot{y}}^{\,2} \cong \mu_n^{\,2}S_F(\mu_n)\frac{\pi}{2B^eC_{22}} = \mu_n^{\,2}S_F(\mu_n)\frac{\pi\sqrt{2\pi}}{8B_D\sigma_{\dot{y}}C_{22}}$$

$$\Rightarrow \sigma_{\dot{y}} = \left(\mu_n^{\,2}S_F(\mu_n)\frac{\pi\sqrt{2\pi}}{8B_DC_{22}}\right)^{1/3} \quad \text{(F:5.54)}$$

This shows that $\sigma_{\dot{y}} \propto B_D^{\,-1/3}$, so $\sigma_y \propto B_D^{\,-1/3}$, where B_D is like a drag force damping coefficient. σ_y is not affected much from the damping, i.e. 100% increase damping causes only about 20% decrease.

NB: $S_F \propto H_{1/3}^4$ and $\sigma_y \propto S_F^{\,1/3} \Rightarrow \sigma_y \propto H_{1/3}^{\,4/3}$

Slow-drift damping from mooring lines

The mooring lines contribute to the slow-drift damping. An example is shown below for the case of a mooring line to a ship surging in irregular waves.

The results show an important contribution to the damping in the region of small frequencies, i.e. periods larger than the incident wave-period range. While the effect of the mooring line is negligible for the surge response within the wave-period range.

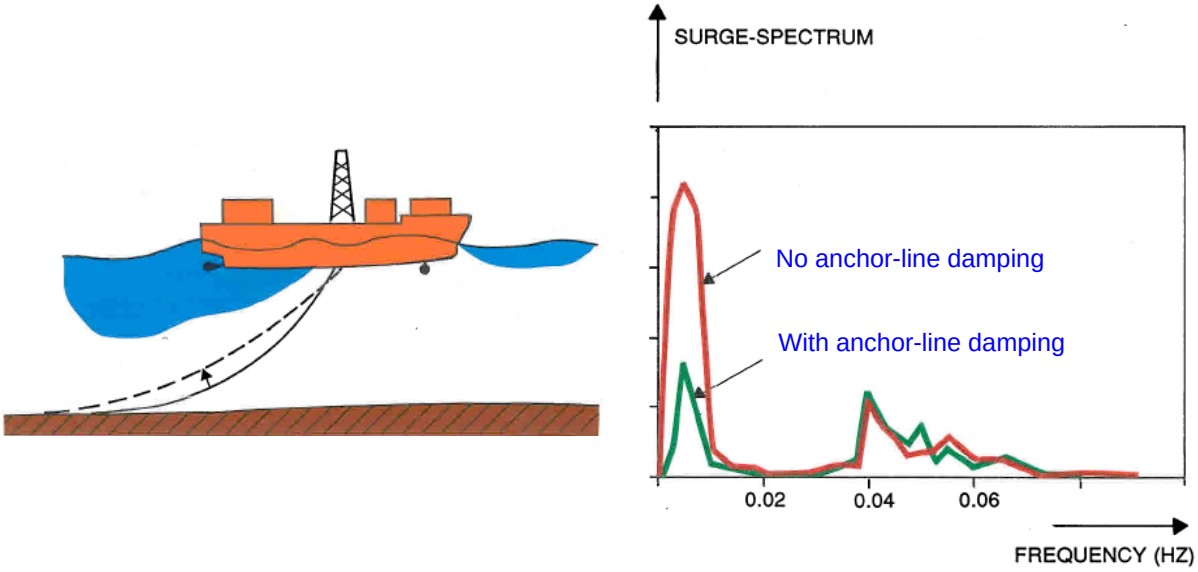

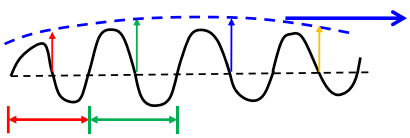

Approximate regular wave ⇨ Drift force in regular waves

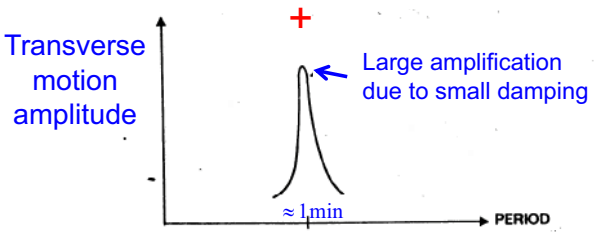

=

Large slowly varying motions

Moored offshore platforms

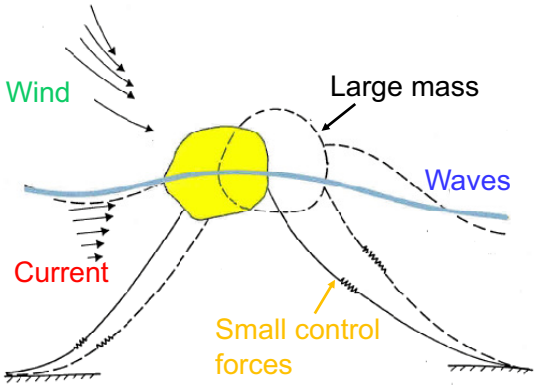

Slow-drift motions are important mooring line design

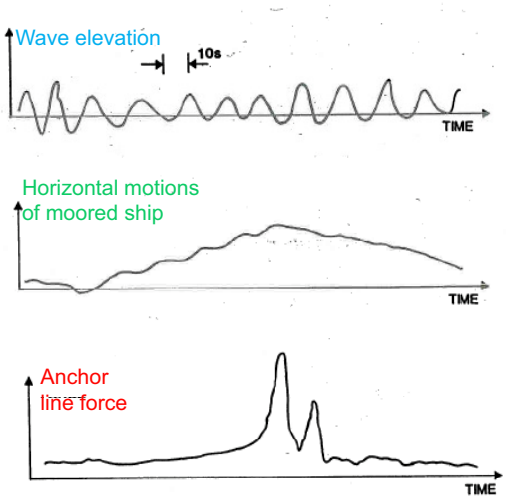

Full scale test of the wave energy ship Kaimei

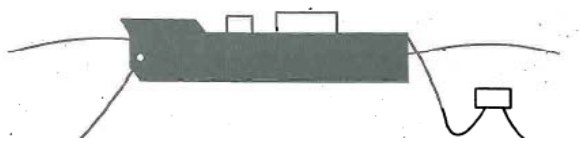

Wave elevation(m)

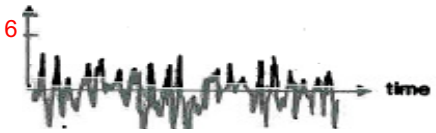

Anchor line force

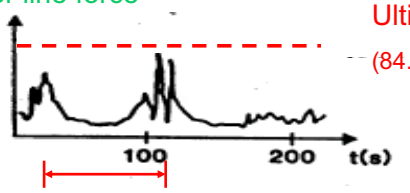

Ultimate force

(84.4 tons)

TLP in irregular sea with: $H_{1/3} = 7m,\ T_0 = 12s$

Surge(m)

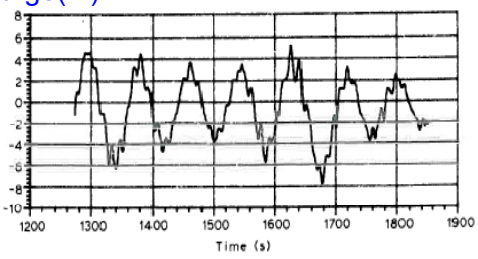

Slow-drift dominates

$T = O(100s)$

Air gap for a TLP in irregular sea(m)

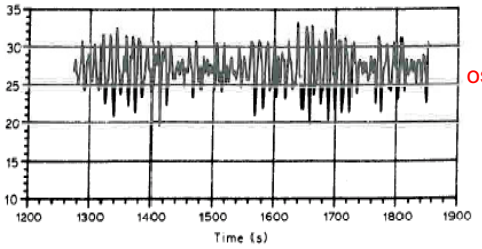

Wave frequency oscillations dominate

Extreme motions of turret-moored production ship

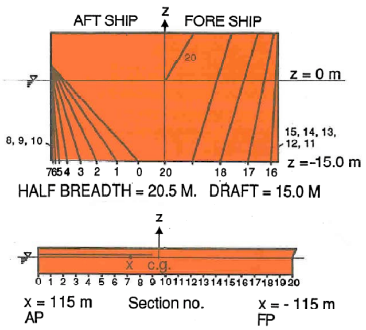

10deg. heading

$H_{1/3}$=15.5m, T_2=13.5s

	Slow-drift	Combined 1. and 2.order
Surge	17.5m	22.2m
Sway	7.0m	7.8m
Yaw	13.6deg.	13.7deg.

Extreme motions of deep-draft floater

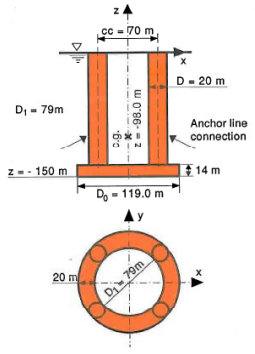

Head sea, $H_{1/3}$=15.5m , T_2=13.5s

	Slow-drift	Combined 1. and 2.order
Surge	5.1m	9.2m
Heave	0.74m	0.95m
Pitch	2.1deg.	2.9deg.

Is the fact that second order motions are larger than first order motions contradictory?

Submerged floating bridge

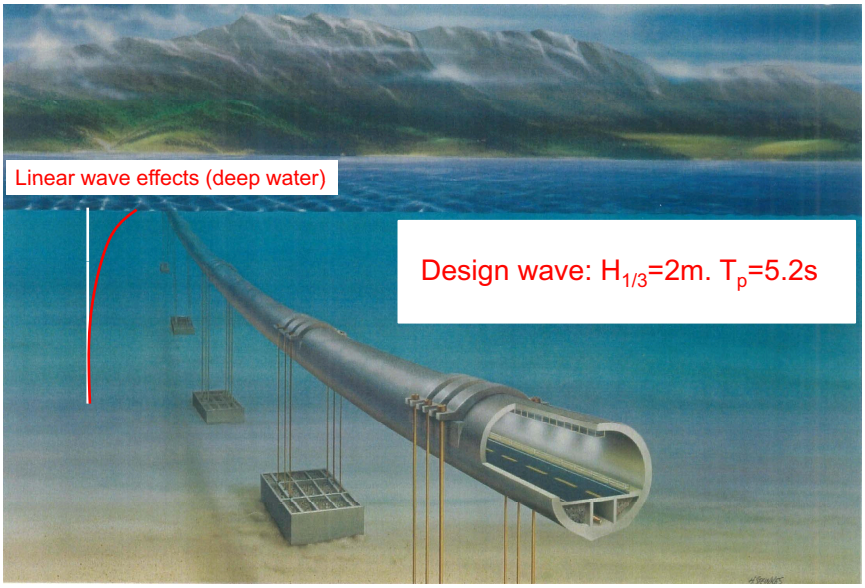

Slow-Drift Loads

$$F_i^{SV} = \sum_{j=1}^{N}\sum_{k=1}^{N} A_j A_k \{ \; T_{jk}^{ic} \cos[(\omega_k - \omega_j)t + (\varepsilon_k - \varepsilon_j)] + T_{jk}^{is} \sin[(\omega_k - \omega_j)t + (\varepsilon_k - \varepsilon_j)]\}$$

Second order transfer function for 2D semi-submerged circular cylinder

$\frac{5T_{jk}^{2C}}{\rho g}$

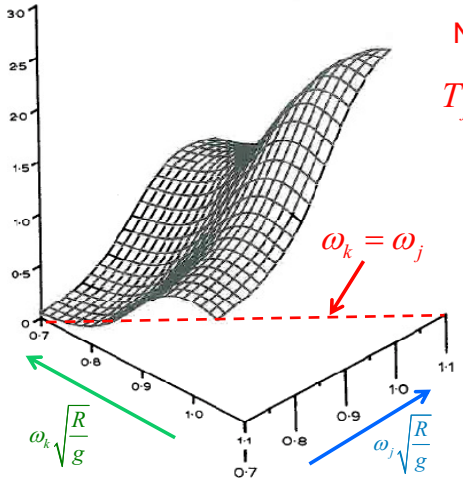

Newman's approximation

$$T_{jk}^{ic} = T_{kj}^{ic} = 0.5\left(T_{jj}^{ic} + T_{kk}^{ic}\right)$$

Second order transfer function for 2D semi-submerged circular cylinder

$\frac{5T_{jk}^{2S}}{\rho g}$

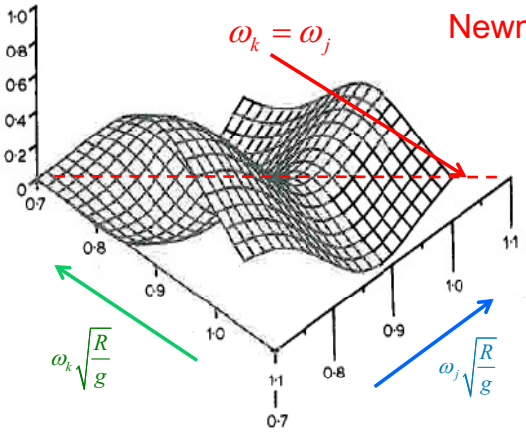

Newman's approximation

$$T_{jk}^{is} = T_{kj}^{is} = 0$$

$$F_i^{SV} = \sum_{j=1}^{N}\sum_{k=1}^{N} A_j A_k \sqrt{T_{jj}^{ic} T_{kk}^{ic}} \left\{ \underbrace{\cos[(\omega_k - \omega_j)t + (\varepsilon_k - \varepsilon_j)]}_{\text{original difference - frequency term}} + \underbrace{\cos[(\omega_k + \omega_j)t + (\varepsilon_k + \varepsilon_j)]}_{\text{additional sum - frequency term}} \right\}$$

$$= \sum_{j=1}^{N}\sum_{k=1}^{N} A_j A_k \sqrt{T_{jj}^{ic} T_{kk}^{ic}} \{ \cos(\omega_j t + \varepsilon_j)\cos(\omega_k t + \varepsilon_k) + \sin(\omega_j t + \varepsilon_j)\sin(\omega_k t + \varepsilon_k)$$

$$+ \cos(\omega_j t + \varepsilon_j)\cos(\omega_k t + \varepsilon_k) - \sin(\omega_j t + \varepsilon_j)\sin(\omega_k t + \varepsilon_k)\}$$

$$= 2\sum_{j=1}^{N}\sum_{k=1}^{N} A_j A_k \sqrt{T_{jj}^{ic} T_{kk}^{ic}} \cos(\omega_j t + \varepsilon_j)\cos(\omega_k t + \varepsilon_k)$$

$$= 2\sum_{j=1}^{N} A_j \sqrt{T_{jj}^{ic}} \cos(\omega_j t + \varepsilon_j) \sum_{k=1}^{N} A_k \sqrt{T_{kk}^{ic}} \cos(\omega_k t + \varepsilon_k)$$

$$\Rightarrow F_i^{SV} = 2\sum_{j=1}^{N}\left[A_j \sqrt{T_{jj}^{ic}} \cos(\omega_j t + \varepsilon_j)\right]^2$$

Sum of N terms instead of N^2 terms

Newman's approximation:

$$T_{jk}^{ic} = T_{kj}^{ic} = 0.5\left(T_{jj}^{ic} + T_{kk}^{ic}\right) \qquad T_{jk}^{is} = T_{kj}^{is} = 0$$

$$F_i^{SV} \cong \sum_{j=1}^{N}\sum_{k=1}^{N} A_j A_k \underbrace{\frac{1}{2}(T_{jj}^{ic} + T_{kk}^{ic})}_{\text{arithmetic average}} \cos[(\omega_k - \omega_j)t + (\varepsilon_k - \varepsilon_j)]$$

Contribution from ω_j and ω_k:

$$F_{i,jk}^{SV} = \frac{1}{2} A_j A_k (T_{jj}^{ic} + T_{kk}^{ic}) \cos[(\omega_k - \omega_j)t + (\varepsilon_k - \varepsilon_j)]$$
$$+ \frac{1}{2} A_j A_k (T_{jj}^{ic} + T_{kk}^{ic}) \cos[(\omega_j - \omega_k)t + (\varepsilon_j - \varepsilon_k)]$$
$$= A_j A_k (T_{jj}^{ic} + T_{kk}^{ic}) \cos[\underbrace{(\omega_k - \omega_j)}_{=\mu} t + (\varepsilon_k - \varepsilon_j)]$$

Slow-drift effects in the wave spectrum

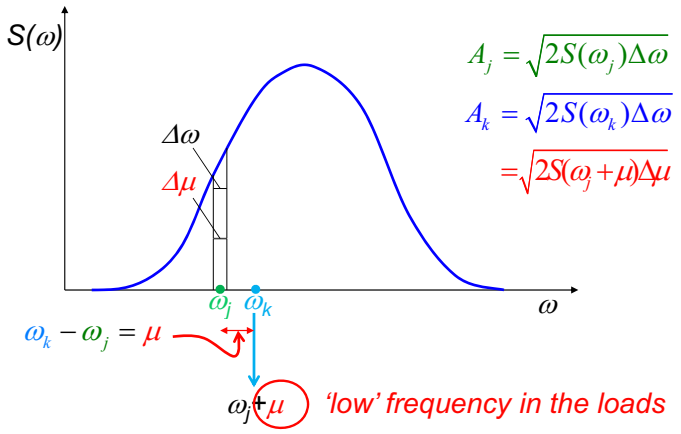

'low' frequency in the loads

$\Delta\mu$: low frequency increment

$$\sigma_x^2 = \int_0^\infty S_F(\mu) \frac{1}{\left[C_{11} - (M + A_{11})\mu^2\right]^2 + B_{11}\mu^2} d\mu$$

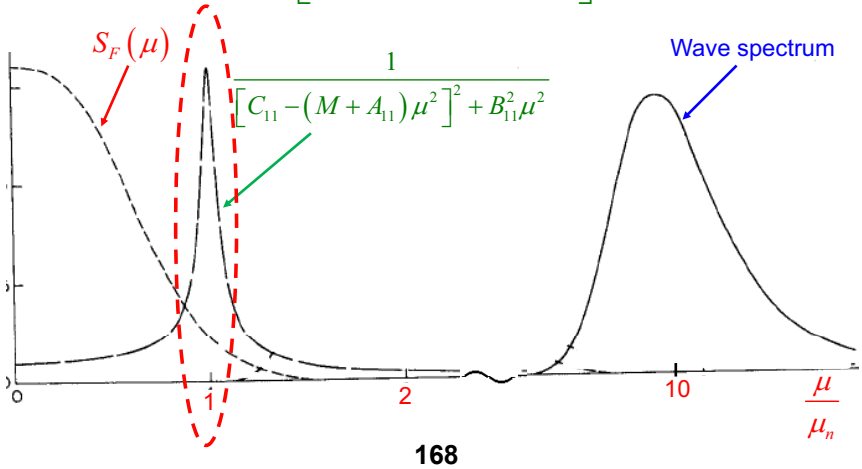

Free-decay test in surge of TLP

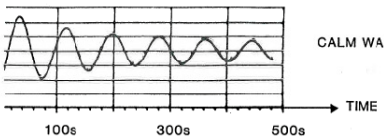

Calm water

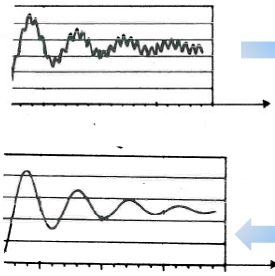

Regular waves
T=12s,H=8m

The regular wave frequency filtered out

Note:Larger damping

Wave drift force damping

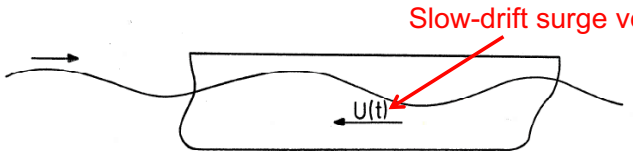

Average force depends on U(t)

⇩

Damping contribution

Mean force

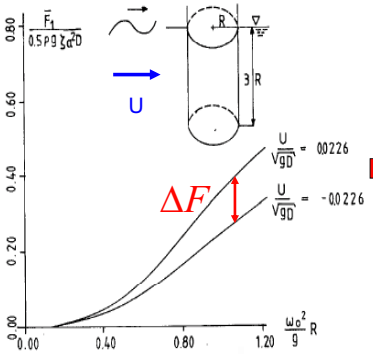

Calculation of wave drift damping

$$\Delta U = 0.0452\sqrt{gD}$$

Wave drift damping:

$$B_{11}^{WD} = \frac{\Delta F}{\Delta U}$$

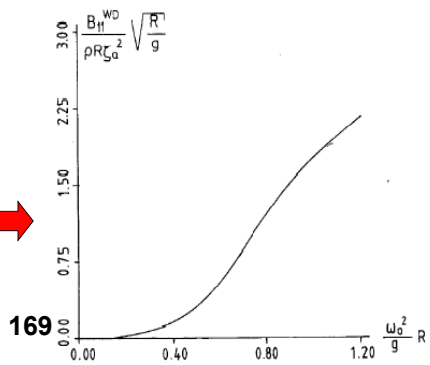

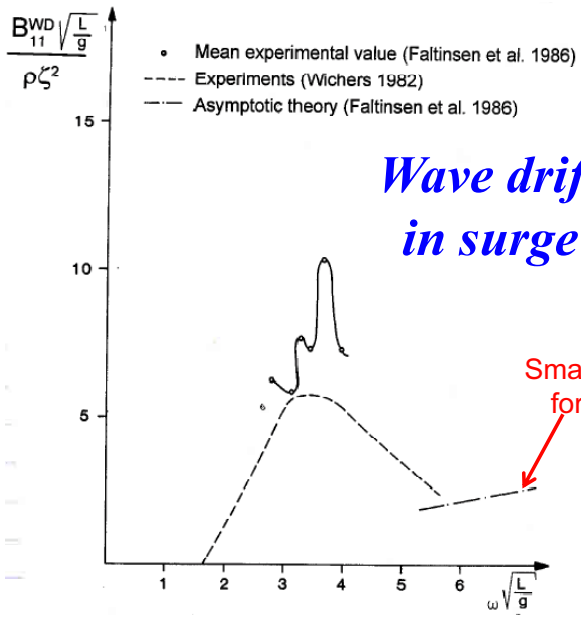

Wave drift damping in surge of a ship

Small wavelength theory for added resistance

Wave-drift damping

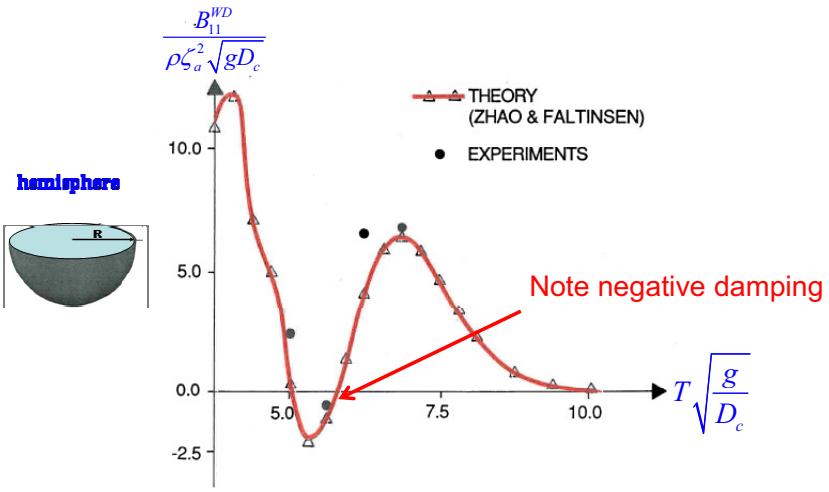

Note negative damping

Extreme values of slowly varying motions

Simulation

1

2

3

4

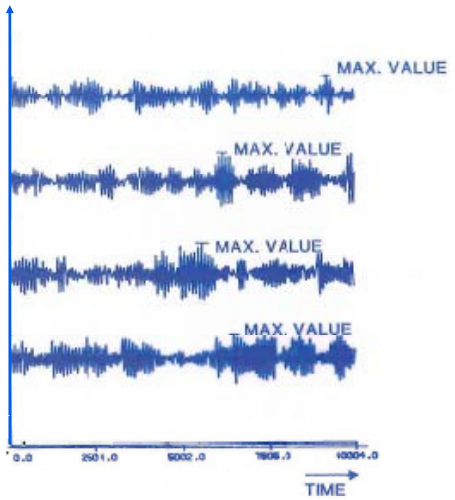

Slow-drift damping contribution from a mooring line

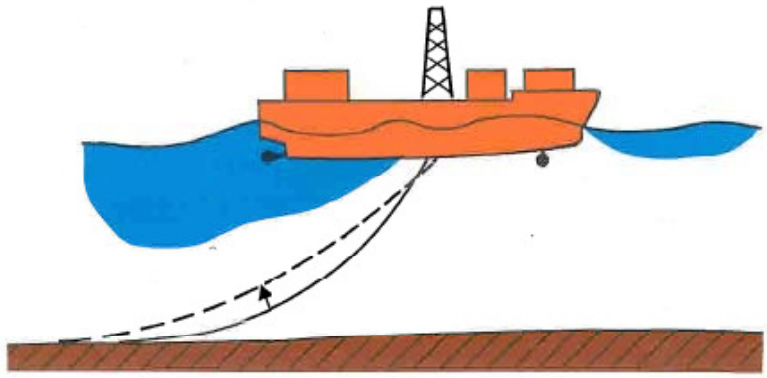

Influence of anchor-line damping on surge

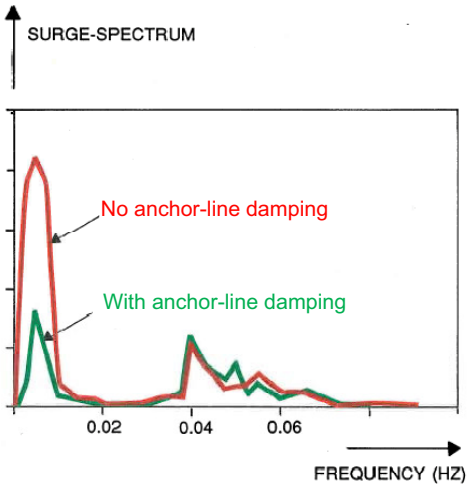

Auxiliary information

Dear all, I will update this file if necessary and put information I was asked about from some of you, in case it might be useful for others.

- **Derivation of added-mass and damping expressions:**

$$F_{rad,k}(t) = -\int_{S_{0B}} \rho \frac{\partial \phi_R}{\partial t} n_k dS = \Re\left\{ \omega^2 e^{i\omega t} \sum_{j=1}^{6} \eta_{ja} \rho \int_{S_{0B}} \varphi_j n_k dS \right\}, k = 1..6$$

$$= \sum_{j=1}^{6} \left\{ \underbrace{\omega^2 \eta_{ja} e^{i\omega t}}_{-\ddot{\eta}_j} \underbrace{\Re\left[\rho \int_{S_{0B}} \varphi_j n_k dS \right]}_{A_{kj}} - \underbrace{i\omega \eta_{ja} e^{i\omega t}}_{\dot{\eta}_j} \underbrace{i\omega \; i\Im\left[\rho \int_{S_{0B}} \varphi_j n_k dS \right]}_{B_{kj}} \right\}$$

$$= \sum_{j=1}^{6} \left\{ -A_{kj} \ddot{\eta}_j - B_{kj} \dot{\eta}_j \right\}, k = 1..6$$

NB: $\phi_R(x, y, z, t) = \Re\left\{ \sum_{j=1}^{6} \dot{\eta}_j \varphi_j(x, y, z) \right\} = \Re\left\{ \sum_{j=1}^{6} i\omega \eta_{ja} e^{i\omega t} \varphi_j \right\}$

42. Slowly varying oscillations due to wind. Slow-drift models. Sum-frequency effects. Current and wind loads. (F: 166-169,174-177)

Slowly varying oscillations due to wind (F:166-168)
The wind can also cause slowly-varying oscillations of marine structures, this is due to wind gust with high energy content at periods of *O*(1-2min).

Hp: A wind speed $U(t)=\overline{U}+u'(t)$ with $\overline{U}$ the mean value and $u'(t)$ the gust velocity, i.e. changing randomly in time, and with amplitude $|u'|<<|\overline{U}|$.

The horizontal force induced by the wind in its direction can be written in the form of a drag force, i.e.

$$F_D=\frac{1}{2}\rho_{air}C_D A U^2(t)=\frac{1}{2}\rho_{air}C_D A[\overline{U}^2+(u')^2+2\overline{U}u']\cong \underbrace{\frac{1}{2}\rho_{air}C_D A\overline{U}^2}_{\text{mean drag}=\overline{F}_D}+\underbrace{\rho_{air}C_D A\overline{U}u'}_{\text{fluctuating drag}=F_D'}$$

with *A* the frontal area of the structure against the wind and C_D the drag coefficient. So for the fluctuating part we have

$$F_D'=\underbrace{\left(\rho_{air}C_D A\overline{U}\right)}_{\substack{\text{transfer function}\\ \text{from } u' \text{ to } F_D'}}u'$$

The gust spectral density is usually given in frequency f (Hertz) instead of in circular frequency $\omega=2\pi f$ (rad/s), i.e. $S^W(f)$. $S^W(f)$ and $S^W(\omega)$ are linked by

$$S^W(\omega)d\omega=S^W(f)df$$

implying the same energy content. This means that

$$S^W(\omega)d\omega=S^W(\omega)2\pi df=S^W(f)df\Rightarrow S^W(\omega)=\frac{1}{2\pi}S^W(f).$$

The wind-gust spectrum is linked to the power spectrum of F_D' as

$$S_F{}^W(f)=\left(\rho_{air}C_D A\overline{U}\right)^2 S^W(f)$$

We can then use the same procedure as in waves to estimate the slow-drift response *x* due to wind, i.e. assuming one degree of freedom:

$$m\ddot{x}+b\dot{x}+cx=F_D'(t)$$

NB: The air density ρ_{air} is very small, i.e. 1.21 Kg/m^3 at 20 degrees Celsius → the added mass connected with the marine structure in air is negligible.

So we can have evaluate the variance of the response, obtaining similarly as in eq. (F:5.48):

$$\sigma_x{}^2\cong S_F{}^W(\omega_N)\frac{\pi}{2bc}=S_F{}^W(f_N)\frac{1}{4bc}$$

here the link between $S^W(f)$ and $S^W(\omega)$ has been used.

The standard deviation of the surge motion can be connected with the mean offset $\bar{x}$ due to the steady wind, for example assuming the Harris wind spectrum (not recommended for frequencies lower than 0.01Hz)

$$S^W(f) = 4k\tilde{f}\bar{U}_{10}{}^2 / \left(2+\tilde{f}^2\right)^{5/6}$$

with $\bar{U}_{10}$ the one hour mean wind speed at 10 m above the sea level, k the surface drag coefficient (in this framework the surface is the free surface) for example 0.003, and $\tilde{f} = Lf / \bar{U}_{10}$ with f the frequency and L a characteristic length, for example 1800m, we have

$$\sigma_x = \sqrt{0.038\tilde{f}_N} / \left[\sqrt{p}\left(2+\tilde{f}_N{}^2\right)^{5/6}\right]\bar{x}$$

with p the ratio between the damping b and the critical damping $2m\omega_N$.

Assuming $\bar{U}_{10} = 40m/s$, T_N=100s and b the 10% of the critical damping
→ σ_x is 30% of the offset $\bar{x}$.

Limitations of slow-drift models

Typically slow-drift models, used to estimate slow-drift loads and motions, are based on the perturbation approach and therefore neglect the influence of 2nd order motions on 1st order motions.

In reality there are circumstances where second-order effects can influence linear motions, for instance:

- A slow-drift yaw motion changes the incident-wave heading and this affects the 1st order response if the slow-drift yaw motion is sufficiently large.
- A slow-drift sway motion causes a frequency of encounter effect on the 1st order roll in beam waves, i.e. $\omega_e = \omega + kV(t)$ with $V(t)$ the slow-drift sway speed. This means that $\omega_e(t)$. If we are close to the roll natural frequency, then $\omega_e(t)$ may go in and out of resonance causing motion amplification. The consequence of this is examined in the figure below considering free-decay model tests in regular beam waves near the roll resonance.

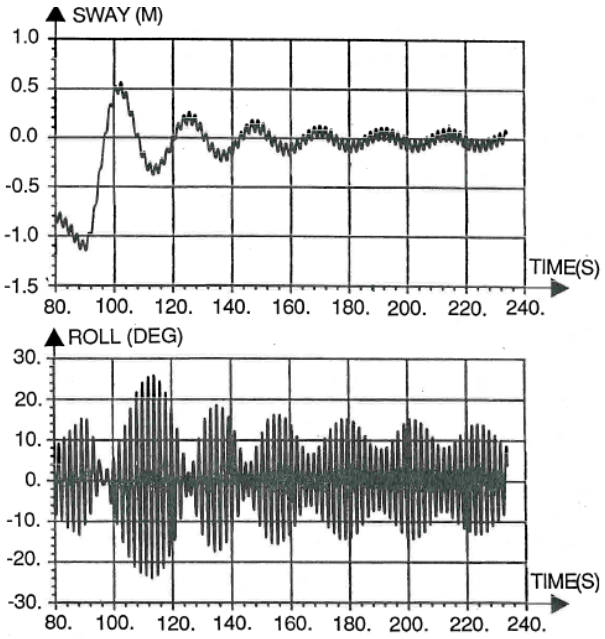

From the model tests the slow-drift sway connected with the free decay tests induces an envelope in the roll motion modulating the high-frequency behaviour corresponding to the encounter frequency. Such envelope is evident even when the sway motion reduces drastically.

Sum-frequency effects (F:168-169)

Using the square velocity term in the Bernoulli equation for the pressure we have seen that there are 3 contributions connected with sum-frequency effects connected with wave frequencies ω_j and ω_k: i.e. $2\omega_j, 2\omega_k, \omega_j + \omega_k$.

In general the sum-frequency effects depend on the second-order wave-body interaction velocity potential ϕ_2, which in some circumstances may represent the major contribution.

Examples of: Sum-frequency loads in deep-water conditions

1. A vertical offshore structure with deep draft *D*, e.g. a buoy, in waves. Zero current.
   In deep water:
   → the linear velocity dies out exponentially with *z*
   → the square-velocity term in the pressure dies out also exponentially with *z*

The vertical force is connected with the pressure at the bottom of the platform, i.e. at *z*=-*D*. There, the square-velocity term in the pressure is small and the major sum-frequency contribution comes from the second-order velocity potential which dies out less quickly than the linear velocity potential, as we will see.

2. A modified Wigley hull in head-sea regular waves. No forward speed. No ship motions. Figure below shows the amplitude of the vertical second-order sum-frequency force as a function of the incident wavelength-to ship length ratio. From the results, the ϕ_2 contribution is much larger than the contribution from the square-velocity term in the pressure (**NB**: The latter contribution for the force is opposite in sign with respect to the second-order potential term, this is why the total force is smaller than the contribution from ϕ_2.).

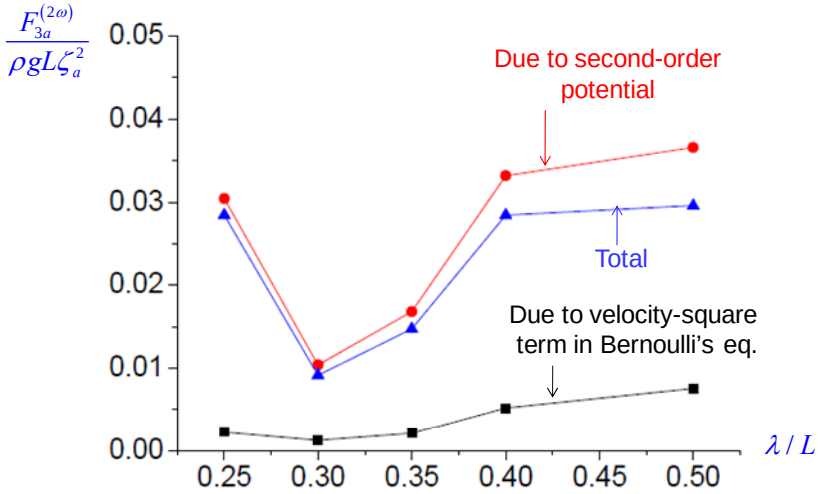

In the following we briefly analyse the ϕ_2 related problem.

Hp: Deep water conditions.

ϕ_2 satisfies the Laplace eq. and inhomogeneous free-surface and body-boundary conditions which depend on the first-order solution ϕ_1.

For example the combined free-surface condition is obtained by Taylor expansion around the mean free surface, *z*=0, of the nonlinear combined free-surface condition, keeping only the terms $O(\zeta_a{}^2)$ and reads

$$\frac{\partial^2\phi_2}{\partial t^2}+g\frac{\partial\phi_2}{\partial z}=-\frac{\partial}{\partial t}\left[\left(\frac{\partial\phi_1}{\partial x}\right)^2+\left(\frac{\partial\phi_1}{\partial y}\right)^2+\left(\frac{\partial\phi_1}{\partial z}\right)^2\right]+\frac{1}{g}\frac{\partial\phi_1}{\partial t}\frac{\partial}{\partial z}\left[\frac{\partial^2\phi_1}{\partial t^2}+g\frac{\partial\phi_1}{\partial z}\right] \quad \text{on } z=0 \quad \text{(F:5.62)}$$

$$= Source\ term(\phi_1)$$

So the first-order solution acts as a disturbance, i.e. a sort of pressure distribution, on the free surface. In equation (F:5.62) the effect of current and forward speed is neglected and so it is done in the next discussion.

Let's examine the second-order velocity potential solution with the following assumption.
Hp: The linear solution is

$$\phi_1=\frac{gA_1}{\omega_1}e^{k_1z}\cos(\omega_1t-k_1x+\delta_1)+\frac{gA_2}{\omega_2}e^{k_2z}\cos(\omega_2t-\mathrm{A}k_2x+\delta_2) \quad \text{(F:5.63)}$$

This represents for
A= +1→ two 2D (long-crested) waves propagating in the same direction
A= - 1→ two 2D (long-crested) waves propagating in opposite directions

A particular second-order solution, satisfying the Laplace equation and the combined free-surface boundary condition eq. (F:5.62), is

$$\mathrm{A}=+1\Rightarrow\phi_2=\frac{2A_1A_2\omega_1\omega_2(\omega_1-\omega_2)}{-(\omega_1-\omega_2)^2+g\,|\,k_1-k_2\,|}e^{|k_1-k_2|z}\sin[(\omega_1-\omega_2)t-(k_1-k_2)x+(\delta_1-\delta_2)] \quad \text{(F:5.64)}$$

$$\mathrm{A}=-1\Rightarrow\phi_2=\frac{2A_1A_2\omega_1\omega_2(\omega_1+\omega_2)}{-(\omega_1+\omega_2)^2+g\,|\,k_1-k_2\,|}e^{|k_1-k_2|z}\sin[(\omega_1+\omega_2)t-(k_1-k_2)x+(\delta_1+\delta_2)] \quad \text{(F:5.65)}$$

From this solution we see two things:

1. A sum-frequency effect occurs if the waves propagate in opposite direction and a slow-drift effect otherwise.
2. ϕ_2 (and therefore the pressure contribution $-\rho\partial\phi_2/\partial t$) goes to zero slowly as $z\to-\infty$ when ω_1 and ω_2 are close because then also k_1 and k_2 are close (**NB**: Remember the application to the slowly-varying motion of a submerged floating bridge.). It does not decay at all if $\omega_1=\omega_2$. In the latter case both the dependence on x and z disappear (Longuett-Higgins 1953). This is true both in the case of difference- and of sum-frequency effects.
   If $\omega=\omega_1=\omega_2$ and A=+1→ $\phi_2=0$.
   If $\omega=\omega_1=\omega_2$ and A=-1→ ϕ_2 is of the form $\phi_2=-\omega A_1A_2\sin(2\omega t+\delta_1+\delta_2)$. This does not decay with z. A similar effect occurs in 3D. This behaviour means that the pressure term $-\rho\partial\phi_2/\partial t$ does not give any force on a fully submerged body, because its gradient is zero. It is instead relevant for surface-piercing bodies. As an example this gives a sum-frequency vertical force contribution from the column bottom of a TLP.

We can interpret the two waves in ϕ_1 has incident waves. In this case we see that the second-order incident-wave potential in deep water connected with a wave with frequency ω is zero.
We can also interpret the two waves in ϕ_1 as connected with the wave-body interaction problem: assuming a 2D body in deep water.
The interaction between incident regular waves and waves reflected from the body is an example of sum-frequency effect. In this case $\omega_1=\omega_2$ and A=-1.
In the transmitted waves, the interaction of the waves generated by the body with the incident waves is an example of difference-frequency effect. In this case $\omega_1=\omega_2$ and A=+1 and there is no second-order effect in the downstream far field in deep water.

NB: In 3D the waves generated by the body propagate in different directions, the interaction with the incident waves along the incident-wave direction is affected by the interactions in other directions → second-order effects in 3D are different than in 2D.

Newman (1990) has shown that approximating the source term in the combined free-surface condition with its far-field behaviour (i.e. far from the body), ϕ_2 goes to zero as the inverse of the depth instead of exponentially for large depths.

Examples of sum-frequency effects for offshore structures

Example of consequence of 2nd order sum-frequency effects is the **springing** on Tension Leg Platforms (TLP):

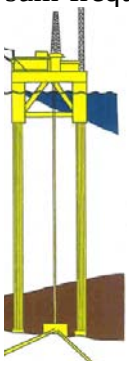

This is a steady-state resonant elastic motion of the platform in the vertical plane.
Sum-frequency effects can cause resonant vertical motions, because the natural period is T_n= O(2-4 sec) and the effects go to zero slowly with the depth as the 2nd order potential goes to zero slowly.

Example of consequence of 3rd and 4th order sum-frequency effect is the **ringing** for instance on TLPs and gravity based monotowers:

This is a transient resonant elastic motion of the platform caused in survival conditions. Survival conditions correspond to large incident-wave periods connected with high waves. If we assume for instance incident waves with mean period T_2=O(15 sec) and bending moment natural period of the monotower T_n= O(5 sec), then resonance can be caused by 3rd order effects, i.e. oscillations with frequency 3ω. Because of the high waves 3rd and 4th order can be relevant. The figure below shows the ringing caused by irregular waves on a TLP:

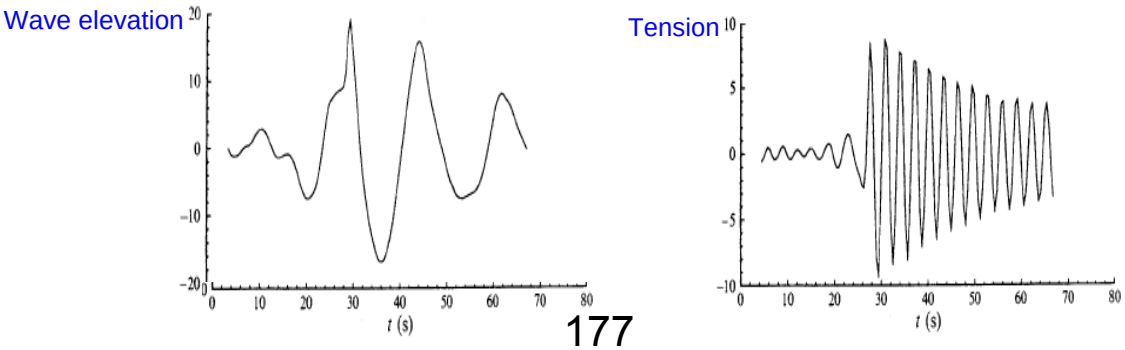

It is apparent the high-frequency behaviour of the tension measured with respect to the incident wave time history.

The figure below shows the ringing caused by irregular waves on a gravity-based monotower (Farnes et al. 1993).

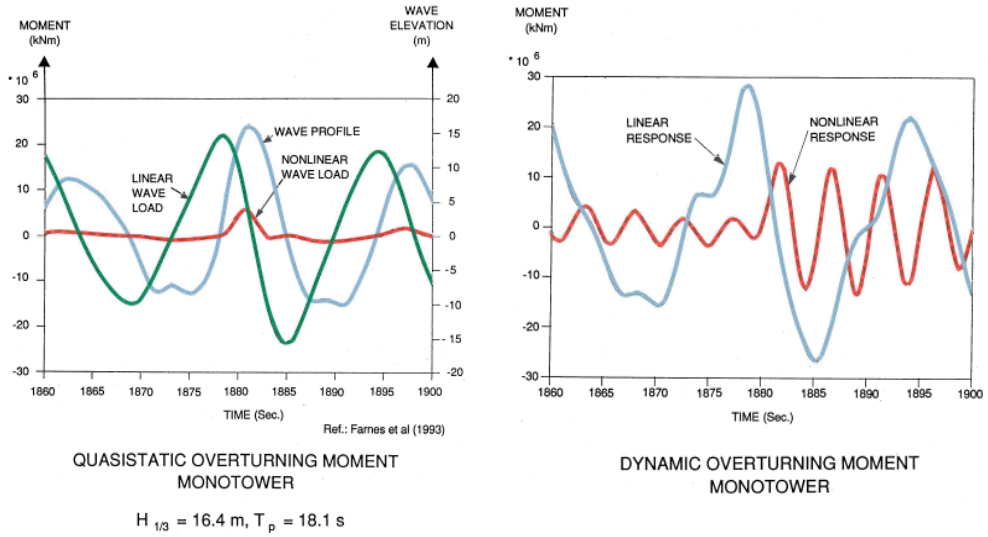

A quasi-static approach is used to calculate the excitation linear and nonlinear wave loads, i.e. the monotower is assumed rigid and fixed. Then the response is estimated assuming the monotower free to dynamically interact with incident waves. The results in terms of loads show a dominance of the first-order wave effects with respect to the nonlinear effects. The dynamic overturning moment of the monotower highlights that the nonlinear response is of similar importance as the linear one.

What can cause ringing?

In survival conditions, high waves can reach the monotower, partially rising along it and partially propagating around it (see figures below). Waves from the opposite sides of the monotower will later collide against each other on the back of the cylindrical structure and then hit the mono-tower. The nonlinear effects involved in such a wave evolution are at least of the 3rd order. They can excite transient elastic resonant oscillations.

Therefore ringing can be caused by transient nonlinear phenomena due to higher-order wave-body interactions and associated with high-frequency behaviour near the elastic resonance period of the platform.

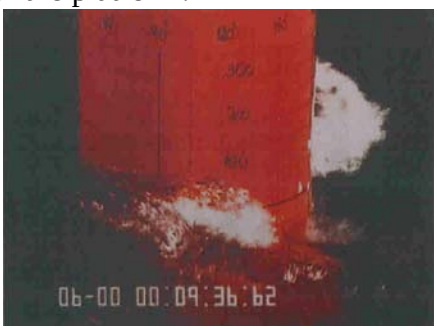

Side view

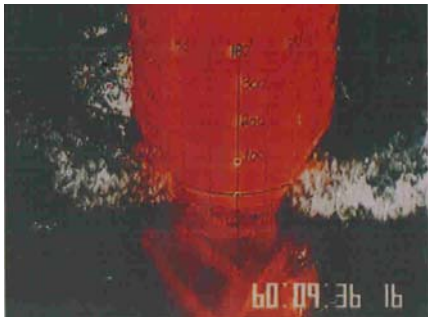

Back view

Summary: Second-order effects. Mean (drift) loads. Maruo's formula. Slow-drift loads and damping. Newman approximation. Pinkster formula. Slow-drift effects due to wind. Sum-frequency effects due to second- and higher-order effects.

Current and wind loads. (F:174)
The general sea environment is characterized by wave, wind and current. Current corresponds to a steady water flow. Wind corresponds to an air flow with a steady component plus a slowly-varying fluctuating part (gust). Current is relevant for second-order drift effects. Waves and current are relevant environment for small-volume structures like jackets and risers. Current and winds may matter for all marine structures exposed to them and result in viscous effects.
In the following we assume no waves and discuss the current and wind loads. There are similarities between the current and mean wind loads, though water and air have different properties and therefore current and wind speed can be rather different, i.e. Design values in North Sea are: wind speed $=O(40m/s)$, current speed $=O(1\ m/s)$.

Several parameters can affect the flow past a body and the resulting loads and motions:

- Reynolds number=$Rn = \rho UD / \mu = UD / \nu$
  (U=characteristic free-stream velocity, D=characteristic body length, ρ the fluid density, μ and ν the dynamic and kinematic viscosity, respectively)
- Roughness number=k/D
  (k=characteristic dimension of body roughness)
- Body form
- Free-surface effects
- Sea-floor effects
- Nature and direction of the ambient flow
- Reduced velocity$= U / f_n D$
  (with f_n the natural frequency of the structure)

The Reynolds number measures the importance of kinetic energy relative to the tangential (shear) stresses connected with viscous effects. In practical cases for offshore structures, at full scale Rn may be large, i.e. $O(10^7)$. For ships at forward speed it is $O(10^9)$.
Examples:
In water (ν=1.05·10^{-6} m^2/s at 20 ^{o}C):
- Current speed U=1m/s and a column of a semi-submersible with D=15m
  → Rn=1.4·10^7

In air (ν=1.50·10^{-5} m^2/s at 20 ^{o}C):
- Wind speed U=40m/s and a structure with characteristic length D=20m
  → Rn=5.3·10^7

But at model scale, as well as for full-scale structures with smaller characteristic lengths (e.g. jackets, risers, pipelines), the Reynolds number can be much smaller.
Examples:
In water (ν=1.05·10^{-6} m^2/s at 20 ^{o}C):
1) Model tests by Froude scaling the semi-submersible to 1:50, i.e. U=0.14m/s, D=0.3m
   → Rn=4.0·10^4
2) Full-scale pipeline with D=1m in a current with speed U=1m/s
   → Rn=9.5·10^5

Different values of the Reynolds number may correspond to different flow regimes leading to different loads on the structure.
In this framework, viscous effects matter in connection with tangential (shear) stresses in the boundary layer along the structure and in connection with flow separation. These aspects are discussed in the following.

A simple and relevant example is represented by the problem of the flow past a circular cylinder because it shows fundamental features that can characterize more general geometries. Here we assume a current as environmental condition and start with the features of the separated flow of a circular cylinder in steady ambient flow.

Steady ambient flow past a (fixed) circular cylinder (F:174-177)

Hp: Non-separated flow and high value of *Rn*

→ viscous effects negligible

→ potential flow theory is valid

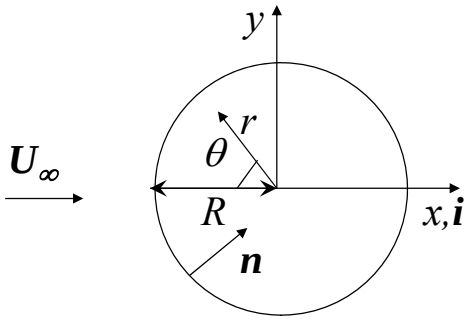

$$\mathbf{n} = (\cos\theta, -\sin\theta)$$
$$x = -r\cos\theta,\ y = r\sin\theta$$

The total velocity potential is $\phi_{tot} = U_\infty x + \phi$ with ϕ the flow associated to the body-current interaction which must satisfy the problem:

$$\begin{cases} \nabla^2\phi_{tot} = 0 \Rightarrow \nabla^2\phi = 0 \equiv \dfrac{\partial^2\phi}{\partial r^2} + \dfrac{1}{r}\dfrac{\partial\phi}{\partial r} + \dfrac{1}{r^2}\dfrac{\partial^2\phi}{\partial\theta^2} = 0 \qquad \forall \boldsymbol{P} \in \Omega \\ \dfrac{\partial\phi_{tot}}{\partial n} = 0 \Rightarrow \dfrac{\partial\phi}{\partial n} = -U_\infty \boldsymbol{i}\cdot\boldsymbol{n} = -U_\infty\cos\theta \qquad \forall \boldsymbol{P} \in S_B \\ \phi \to 0 \qquad r \to \infty \end{cases}$$

This problem is satisfied by a dipole singularity in *x* direction placed at the center of the cylinder, i.e. $\phi = \gamma \boldsymbol{i}\cdot\boldsymbol{r}/r^2 = -\gamma\cos\theta/r$. The unknown strength γ is found enforcing the impermeability condition along the body:

$$\begin{cases} \dfrac{\partial^2\phi}{\partial r^2} + \dfrac{1}{r}\dfrac{\partial\phi}{\partial r} + \dfrac{1}{r^2}\dfrac{\partial^2\phi}{\partial\theta^2} = \gamma\cos\theta\left[-\dfrac{2}{r^3} + \dfrac{1}{r^3} + \dfrac{1}{r^3}\right] \equiv 0 \qquad \forall \mathbf{P} \in \Omega \\ \dfrac{\partial\phi}{\partial n} = -\dfrac{\partial\phi}{\partial r}\bigg|_{r=R} = -\dfrac{\gamma}{R^2}\cos\theta = -U_\infty\cos\theta \qquad \forall \mathbf{P} \in S_B \Rightarrow \gamma = R^2 U_\infty \\ \phi \to 0 \qquad r \to \infty \ \text{ satisfied} \end{cases}$$

So the solution is

$$\phi_{tot} = -U_\infty\left(r + \frac{R^2}{r}\right)\cos\theta$$

which means that the tangential velocity on the body is

$$U_e = \left[\frac{1}{r}\frac{\partial\phi_{tot}}{\partial\theta}\right]_{r=R} = 2U_\infty\sin\theta$$

and has a maximum at $\theta=\pi/2$.

The pressure on the body can be obtained from the steady Bernoulli equation:

$$p+\frac{1}{2}\rho U_e^2 = p_0+\frac{1}{2}\rho U_\infty^2 \Rightarrow p-p_0=\frac{1}{2}\rho U_\infty^2[1-4(\sin\theta)^2]$$

with p_0 the ambient pressure. We can define the pressure coefficient as

$$C_p=\frac{p-p_0}{\frac{1}{2}\rho U_\infty^2}=1-4(\sin\theta)^2$$

$C_p=1$ at $\theta=0,\pi$ (stagnation points)

$C_p>0 \quad if \quad U_e<U_\infty$

$C_p<0 \quad if \quad U_e>U_\infty$

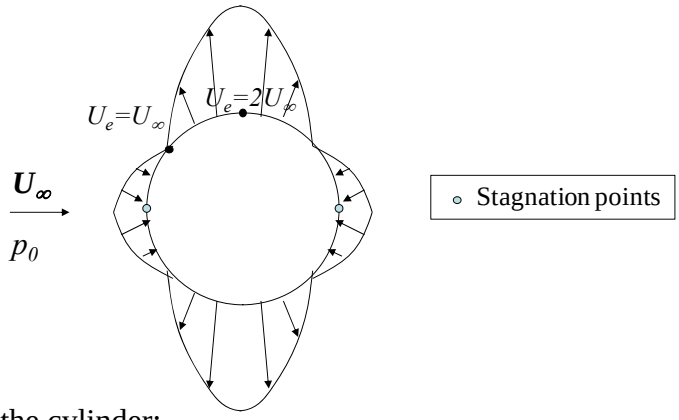

Under these assumptions there is no force on the cylinder:

$$F_x=\oint(p-p_0)n_1 dl=\frac{1}{2}\rho R U_\infty{}^2\int_0^{2\pi}[1-4(\sin\theta)^2]\cos\theta d\theta=0$$

and similarly in y direction. This is the **D'Alembert's paradox**:
A body in an infinite potential steady flow is not subjected to any force.

NB: In general a moment exists for a body in an infinite potential steady flow: the Munk's moment, we will later discuss it.

Actually in the real case the flow separates in the back side of the cylinder, say for $\theta>=\theta_0$. Flow separation occurs when the flow is not able to follow the body. In this case the flow follows another streamline (called separation streamline) and the pressure along the body part with separated flow remains almost uniform and smaller than p_0, this implies that

$C_p<1$ at $\theta=\pi$

This is shown in fig. F:6.2 in terms of the time-average pressure coefficient on the cylinder for different Reynolds numbers:

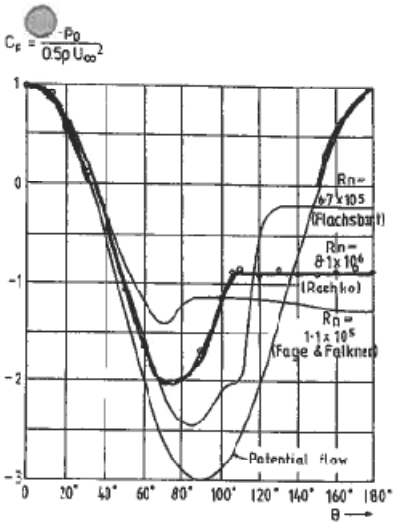

Fig. 6.2. Average pressure distribution p around a smooth circular cylinder in steady incident flow. (Rn = $U_\infty D/\nu$, D = cylinder diameter, U_∞ = incident flow velocity, θ defined in Fig. 6.1, p_0 = ambient pressure.) (Roshko, 1961.)

- For $Rn \rightarrow \infty$ the pressure on the back of the cylinder recovers the pressure on the front, i.e. there is zero drag force.
- As Rn reduces the pressure, downstream of a certain angle θ, becomes nearly uniform and remains smaller than the ambient pressure, this leads to a non-zero drag force.

So, flow separation causes a horizontal force, i.e. in the current direction (while the force along y is still zero due to pressure symmetry). A rough estimation can be obtained assuming the flow as potential for $-\pi/2 \le \theta \le \pi/2$ and the pressure uniform $p=p_B<p_0$ (p_B is called 'base pressure') for the other angular positions along the cylinder, as shown in the figure below.

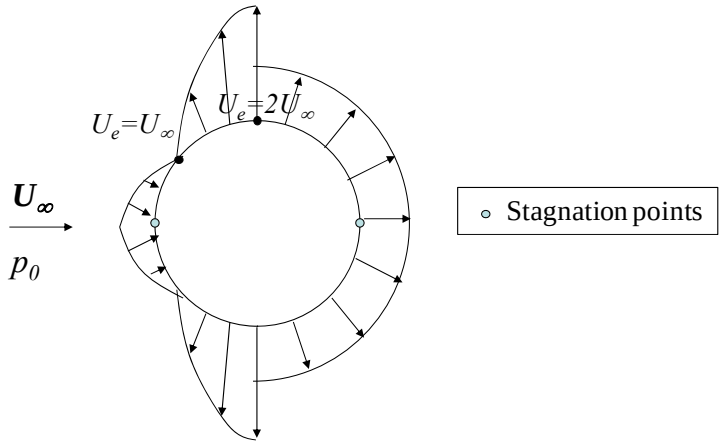

This is based on the fact that the major contribution to the drag force comes from integrating the pressure forces in the vicinity of $\theta = 0$ and $|\theta| = \pi$. It involves errors near $\theta = \pm\pi/2$.
Under these assumptions:

$$F_x = \frac{1}{2}\rho R U_\infty^2 \int_{-\pi/2}^{\pi/2} [1-4(\sin\theta)^2]\cos\theta d\theta + R\int_{\pi/2}^{3\pi/2} \underbrace{[p_B - p_0]}_{\equiv \rho U_\infty^2 Q/2}\cos\theta d\theta \quad \text{(F:6.5)}$$

$$= \frac{1}{2}\rho \underbrace{2R}_{D} U_\infty^2 \left[-\frac{1}{3} - Q\right]$$

Here Q gives an average measure of the pressure loss due to flow separation and must be obtained empirically, i.e. from experiments. The drag coefficient can be defined as

$$C_D \equiv \frac{F_x}{\frac{1}{2}\rho D U_\infty^2} = -\frac{1}{3} - Q \qquad \text{(F:6.6)}$$

This expression gives results in qualitative agreement with experiments.
For example integrating the time-average pressure coefficient along the cylinder given in fig. F:6.2 for $Rn=1.1\cdot10^5$ it gives Q=-1.25 and from expression (F:6.6) we have C_D=0.92 which is in qualitative agreement with accepted experiments.

The Reynolds number is a very important parameter for the drag coefficient because the flow has different regimes according to Rn.
For sufficiently small Rn the flow is in laminar conditions, for large Rn the flow becomes turbulent:

- Laminar = the flow is well organized
- Turbulent = the flow is characterized by a mean (organized) component and a fluctuation about the mean component.

Example:

Hp: A group of people. We ask them to march in order at the same speed $\bar{U}$.

- If $\bar{U}$ is small, they are able to do so
  → this corresponds to a laminar flow
- If $\bar{U}$ is higher, someone can have problems
  → this corresponds to disturbances in the flow
- If $\bar{U}$ is sufficiently high, people will march in average with $\bar{U}$ but each of them can go slightly faster or slower
  → this corresponds to turbulent flow, with speed $U = \bar{U} + u'$, u' being a fluctuation around the mean value $\bar{U}$.

The transition from laminar to turbulent conditions is connected with flow instability and the speed associated with the transition (flow instability) is called critical speed.
If the day is windy then the speed at which the organized march is lost, i.e. the critical speed, is smaller than without wind. This means that the ambient flow is important.

Going back to the circular cylinder: The *Rn* is important for the location of the separation point and for the transition from laminar to turbulent flow. We also understand that the flow tends to be laminar in the upstream part of the cylinder while it tends to become turbulent moving downstream due to its acceleration for increasing θ.

Relative damping for turret-moored ship

	Operational condition		Design condition	
Organization number	Surge	Sway-yaw	Surge	Sway-yaw
4	2%		4%	
5	2%	5%	2%	5%
14	1%		1%	
20	10%		10%	

Relative damping for deep-draft floater

Organization number	Operational condition	Design condition
4	15.0%	30.0%
5	1.2%	1.7%
14	1.0%	1.0%
20	10.0%	10.0%

Free decay test in regular beam waves close to roll resonance

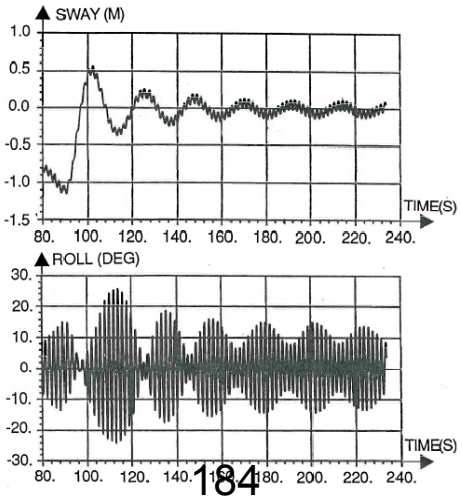

Second-order sum-frequency vertical force amplitude $F_{3a}^{(2\omega)}$ on modified Wigley hull in head sea. Zero speed. No ship motions.

Importance of second-order potential

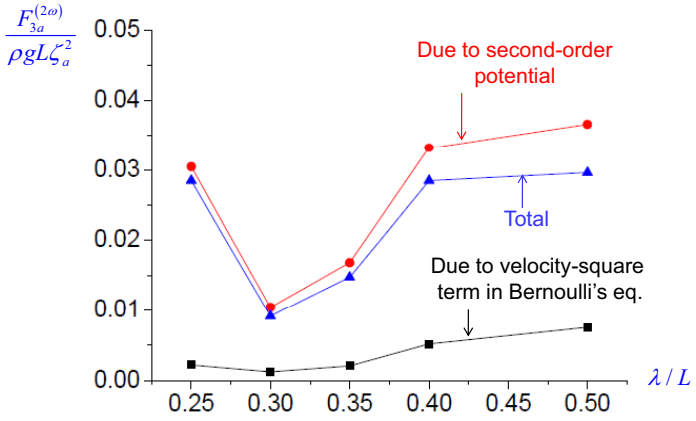

First and second-order solutions

Free-surface boundary condition

$$\frac{\partial^2 \phi_1}{\partial t^2} + g\frac{\partial \phi_1}{\partial z} = 0 \qquad \text{on } z = 0$$

$$\frac{\partial^2 \phi_2}{\partial t^2} + g\frac{\partial \phi_2}{\partial z} = \textit{Source term}(\phi_1) \qquad \text{on } z = 0$$

Springing of Tension Leg Platforms (TLP)

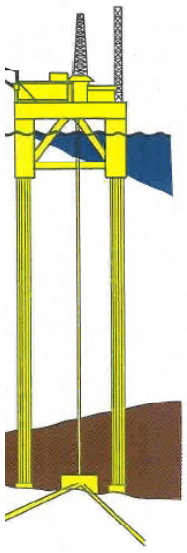

Resonant vertical motions due to sum-frequency nonlinear wave loads

Resonance period T_n=2-4s

The second-order sum-frequency potential decays slowly with depth

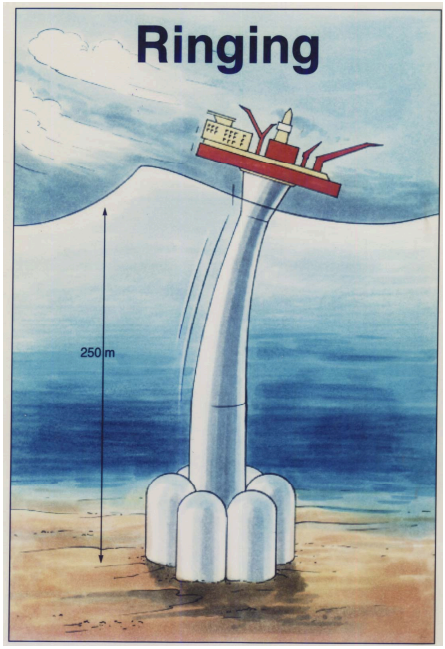

A third and fourth order wave load effect in survival conditions

Ringing measurements for TLP

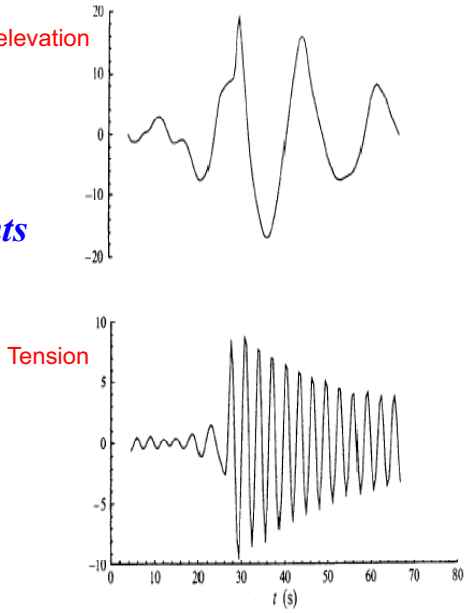

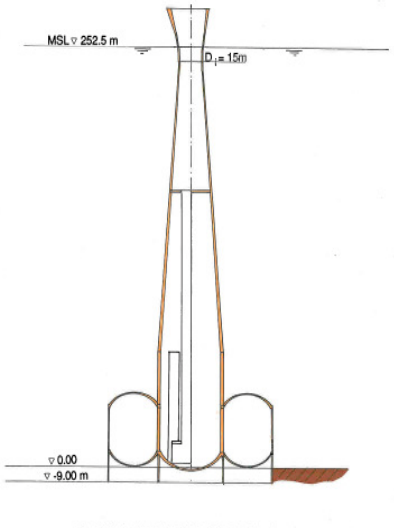

GRAVITY BASED MONOTOWER

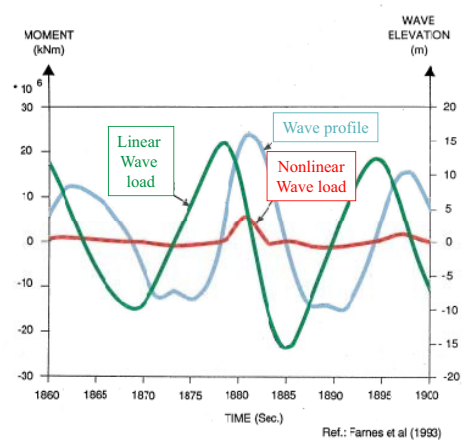

QUASISTATIC OVERTURNING MOMENT
MONOTOWER

$H_{1/3}$ = 16.4 m, T_p = 18.1 s

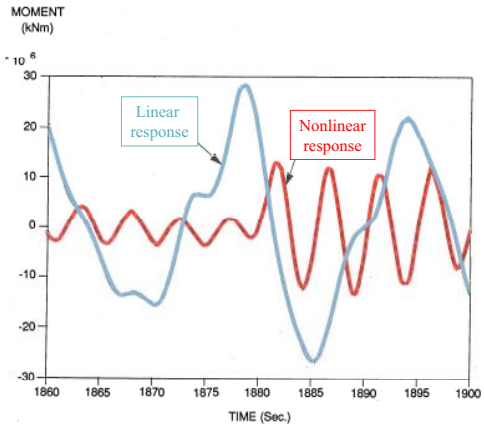

DYNAMIC OVERTURNING MOMENT
MONOTOWER

$H_{1/3}$ = 16.4 m, T_p = 18.1 s

Ref.: Farnes et al (1993)

Ringing of monotower in survival condition

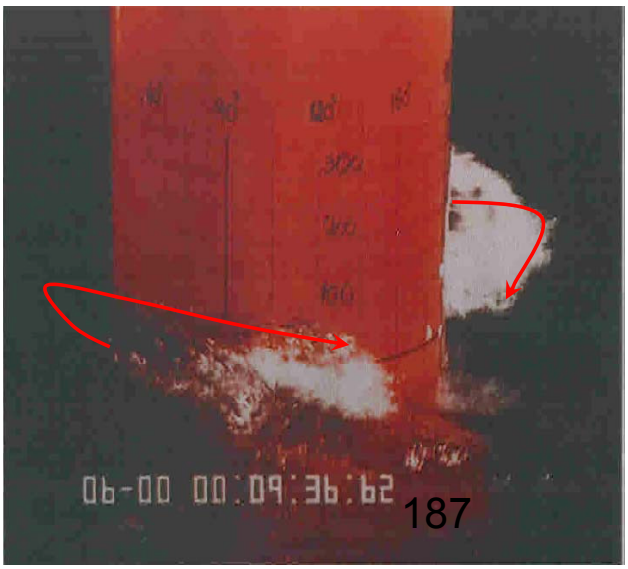

Steep local waves propagating on the two sides of the cylinder

The waves start on the upstream hull side when there is a wave trough

Ringing of monotower in survival condition

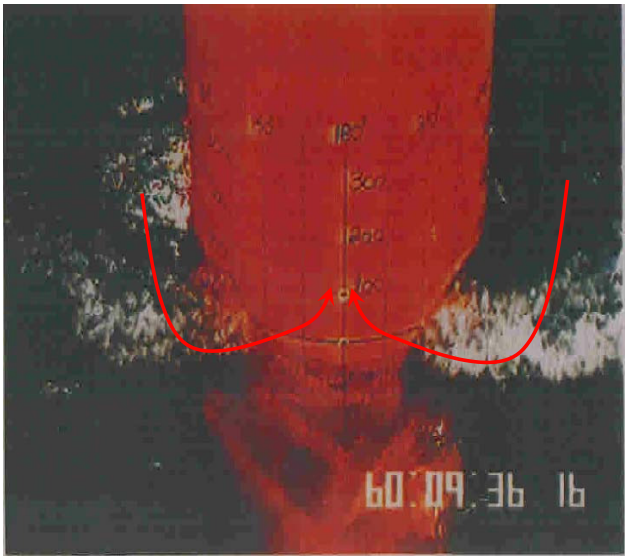

The two steep propagating waves will later collide

⬇

Big splash

Summary

Second-order effects. Mean (drift) loads. Maruo's formula. Slow-drift loads and damping. Newman approximation. Pinkster formula. Slow-drift effects due to wind. Sum-frequency effects due to second- and higher-order effects.

Solution accurate to the second order

ε = wave steepness

Solution of wave-body interaction problem:

$$\phi = \overbrace{\tilde{\phi}_1 \varepsilon}^{\phi_1} + \overbrace{\tilde{\phi}_2 \varepsilon^2}^{\phi_2} + \tilde{\phi}_3 \varepsilon^3 + \ldots\ldots$$

$$= \phi_1 + \phi_2 + O(\varepsilon^3)$$

First-order solution:

has zero mean value and oscillates with the frequency of the incident waves (if U_c=0 & U=0), i.e. superposition principle valid.

Second-order solution:

1) Mean value → constant (drift)
2) Difference-frequency oscillations → $(\omega_k-\omega_j)$, i.e. long period
3) Sum-frequency oscillations → $(\omega_k+\omega_j)$, i.e. short period

Second-order effects

A regular incident wave with frequency ω:
$\omega=\omega_k=\omega_j$ → a mean value and sum-frequency oscillations with 2ω.

Example, from square-velocity term in the pressure:

$$\left(\partial\phi_1/\partial x|_{x=0}\right)^2 = \underbrace{A^2/2}_{\text{constant term}} + \underbrace{A^2\cos[2(\omega t+\varepsilon)]/2}_{\text{sum - frequency term}}$$

An irregular incident wave with spectrum *S(ω)*:
All second-order effects are caused.

Second-order loads Relevance: Practical examples

Mean-wave (drift) loads:

- Design of mooring and thruster systems, towing
- Offshore loading
- Submarines
- Capsizing of semisubmersibles
- Added resistance in waves (involuntary speed loss)

Difference-frequency (slow-drift) loads:

- Vertical motions of structures with small waterplane area, $T_n=O(30\text{s})$
- Horizontal motions of moored structures, $T_n=O(1\text{-}2\text{min})$

Sum-frequency 2nd and higher-order loads:

- Vertical motions of TLPs, $T_n=O(2\text{-}4\text{s})$
- Springing of TLPs, ringing of TLPs and gravity-based monotowers

How to estimate the second-order loads?

Direct Pressure Integration (DPI):
Integrate pressure from Bernoulli equation along the body surface

Conservation of Fluid (angular for moments) Momentum (CFM):
Use the conservation in a fluid domain enclosed by the body, free-surface, sea bottom and control surfaces.

DPI versus CFM:
The general form of CFM is more complicated. Convenient in some cases, e.g. horizontal drift loads. The advantage is to integrate along a control surface that can be chosen smooth.
With DPI involves terms counteracting each other, this can lead to accuracy problems. Difficulties with body geometric singularities.

Direct pressure integration: Source of 2nd order effects

Second-order Force (U_c=0, U=0)

$$\boldsymbol{F}_2 = \text{Mean-drift forces} + \text{Low-drift forces} + \text{Sum-frequency forces}$$

$$= \underbrace{I_1}_{\substack{\text{correction of local}\\ \text{flow acceleration}}} + \underbrace{I_2}_{\substack{\text{square-velocity in}\\ \text{the pressure}}} + \underbrace{I_3}_{\substack{\text{pressure correction}\\ \text{due to wetted-surface}\\ \text{changes}}}$$

$$+ \underbrace{I_4}_{\substack{\text{pressure correction}\\ \text{due to body motions}}} + \underbrace{I_5}_{\substack{\text{rotation of } I^{st} \text{ order force}\\ F_1 \text{ due to body motions}}}$$

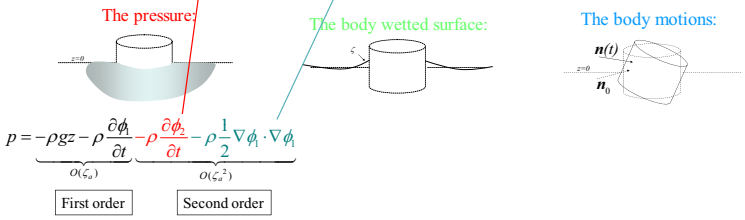

$$p = \underbrace{-\rho g z - \rho \frac{\partial \phi_1}{\partial t}}_{O(\zeta_a)} \underbrace{-\rho \frac{\partial \phi_2}{\partial t} - \rho \frac{1}{2} \nabla \phi_1 \cdot \nabla \phi_1}_{O(\zeta_a^2)}$$

First order | Second order

Second-order loads

In general they require to find the solution of the wave-body interaction problem accurate to the second order, i.e. $\phi = \phi_1 + \phi_2$

NB: In general, to find ϕ_2 numerically is not straightforward: it involves smaller and higher frequencies requiring a well-refined and sufficiently-large computational grid.

Mean-drift loads:

If U_c=0 and U=0, they do not depend on ϕ_2. If $U_c \neq 0$ or $U \neq 0$, ϕ_2 can contribute through the additional pressure term $-\rho U \partial \phi_2 / \partial x$.

Slow-drift loads:

In general they depend also on ϕ_2. If Newman's approximation is valid and U_c=0 and U=0, no dependence on ϕ_2.

Sum-frequency loads:

In general they depend also on ϕ_2.

Mean-wave (drift) loads

Using potential flow theory, they are due to the body capability in generating waves, i.e. in diffracting incident waves and irradiating waves → Relevant for large structures (relative to the incident waves)

- 3D horizontal forces (from CFM, by Maruo):

$$\bar{F}_i = -\overline{\int_{S_\infty} (p n_i + \rho V_i V_n) dS} \quad i = 1,2$$

- 2D drift force (from CFM, by Maruo):

$$\bar{F}_2 = \frac{\rho g}{4} \left(\underbrace{\zeta_a}_{\text{incident waves}}^2 + \underbrace{A_R}_{\text{reflected waves}}^2 - \underbrace{A_T}_{\text{trasmitted waves}}^2 \right)$$

NB: For a perfect absorber: $\bar{F}_2 = \frac{\rho g}{4} \zeta_a^2$

Mean-wave (drift) loads

Hp: Zero average energy flux through the body surface, i.e. the body is not an absorber.

$$\rightarrow \zeta_a^{\,2} = A_R^{\,2} + A_T^{\,2}$$

• 2D drift-force Maruo's formula:

$$\bar{F}_2 = \frac{\rho g}{2} A_R^{\,2} \underset{\text{as } \omega \to \infty}{\rightleftharpoons} \bar{F}_2 = \frac{\rho g}{2} \zeta_a^{\,2}$$

Maximum value of the force if U_c=0 and U=0, because ζ_a is the maximum value of A_R.

• Extension to 3D bodies (by Maruo):

$$\bar{F}_1 = \frac{\rho g}{4} \int_0^{2\pi} A^2(\theta)(\cos\beta - \cos\theta) d\theta$$

$$\bar{F}_2 = \frac{\rho g}{4} \int_0^{2\pi} A^2(\theta)(\sin\beta - \sin\theta) d\theta$$

Mean-wave (drift) loads

• Extension of Maruo's asymptotic formula to 3D bodies (by Faltinsen):

$$\bar{F}_i = \underbrace{\frac{\rho g \zeta_a^{\,2}}{2}}_{\textit{original}} \underbrace{\int_{L_1} [\sin(\theta+\beta)]^2 n_i dl}_{\textit{non shadow part}} \qquad i = 1,2,6$$

• Added-resistance in head waves (by Faltinsen):
Relevant assumptions: short waves and small *Fn*.

$$\bar{F}_1 = \frac{\rho g}{2} \zeta_a^{\,2} \left(1 + \frac{2\omega U}{g}\right) \int_{L_1} [\sin(\theta)]^2 n_1 dl$$

Incident-wave frequency

• Mean-drift loads in irregular waves and due to viscous effects

Mean-wave (drift) loads

Using potential flow theory, we found that

For small wavelengths: they are dominated by diffraction effects.
Near the resonance: they are dominated by radiation effects.
For large wavelengths: they become negligible.

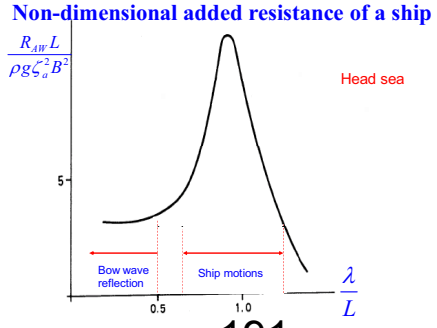

Mean-wave (drift) loads

Main parameters:

- wave amplitude:
  - potential flow → $\propto \zeta_a^{\,2}$
  - viscous effects → $\propto \zeta_a^{\,3}$
- wavelength
- wave direction β
- structural form
- difference between restrained and moving body
- current → <50%
- forward motion
- confined waters, e.g. wall effects when performing experiments

Slow-drift loads

Connected with a wave-wind-current environment.

For a single body in open sea can not be caused by body interaction with a regular wave. In general they are connected with irregular waves.

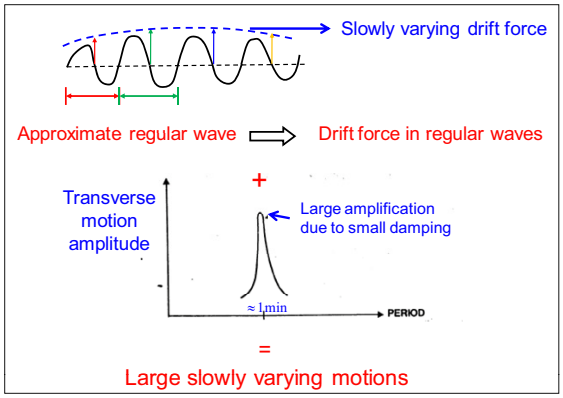

Slow-drift motions

• Relevant for design of mooring lines and risers

•They can be larger than linear motions but the linear velocities and accelerations are larger than slow-drift values

•They are caused by slowly-varying loads:

$$F_i^{SV} = \sum_{j=1}^{N}\sum_{k=1}^{N} A_j A_k \left\{T_{jk}^{ic}\cos[(\omega_k-\omega_j)t+(\varepsilon_k-\varepsilon_j)] + T_{jk}^{is}\sin[(\omega_k-\omega_j)t+(\varepsilon_k-\varepsilon_j)]\right\}$$

with $T_{jk}^{ic}, T_{jk}^{ic} = f(\phi_2)$ for $j \neq k$ and $T_{jj}^{ic} = \dfrac{\bar{F}_i(\omega_j,\beta)}{\zeta_a^{\,2}} \neq f(\phi_2)$ if $U_c = 0$, $U = 0$

Slow-drift loads using Newman's approximation

$$\underbrace{\underbrace{T_{jk}^{ic} = T_{kj}^{ic}}_{\text{Newman's definition}} = \frac{1}{2}(T_{jj}^{ic} + T_{kk}^{ic})}_{\text{Newman's approximation}} \quad \text{and} \quad \underbrace{\underbrace{T_{jk}^{is} = -T_{kj}^{is}}_{\text{Newman's definition}} = 0}_{\text{Newman's approximation}}$$

$$F_i^{SV} = 2\sum_{j=1}^{N}\left[A_j\sqrt{T_{jj}^{ic}}\cos(\omega_j t + \varepsilon_j)\right]^2$$

This formula is independent on ϕ_2 if $U_c = 0$ and $U = 0$

Slow-drift loads and response

- Pinkster formula for the spectral density of low frequency part of the loads (based on Newman's approximation):

$$S_F(\mu) = 8\int_0^\infty S(\omega)S(\omega+\mu)\left[\frac{\bar{F}_i(\omega+\mu/2)}{\zeta_a^{\,2}}\right]^2 d\omega \quad \propto H_{1/3}{}^4$$

- Variance of the response:

$$\sigma_x{}^2 \cong S_F(\mu_n)\frac{\pi}{2bc}$$

- Most probable largest value (using Rayleigh distribution):

$$x_{\max} = \sigma_x\sqrt{2\log\left(\frac{t}{T_N}\right)}$$

Slow-drift damping

Three main sources are:

1) Wave-drift damping
2) Viscous hull damping
3) Viscous anchor line damping

Wave-drift damping:

Connected with the interaction of a slow-drift motion with rapid oscillations of incident waves. It is important in high sea, because $B^{WD} \propto H_{1/3}{}^2$.
We discussed how to find it.

Eddy-making damping:

It is connected with vortex shedding and nonlinear, i.e. $B_D\dot{y}|\dot{y}|$.
We discussed equivalent linearization.

Standard deviation of the response:

Using $\sigma_r{}^2 \cong S_F(\mu_n)\pi/(2bc)$

$$\begin{cases} \text{If } b = B^{WD} \rightarrow \sigma_r \propto H_{1/3} \\ \text{If } b = B_D \rightarrow \sigma_r \propto H_{1/3}{}^{4/3} \end{cases}$$

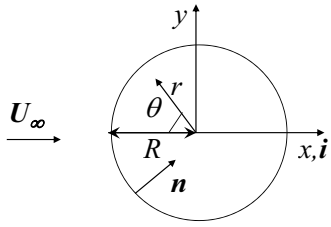

$$\mathbf{n} = (\cos\theta, -\sin\theta)$$
$$x = -r\cos\theta,\ y = r\sin\theta$$

Source point *Sink point*

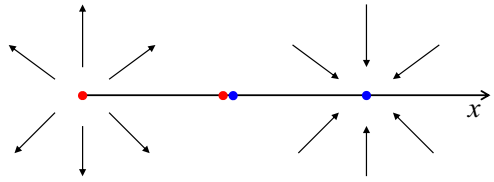

$$\text{2D: } \phi(x,y) = \frac{Q}{2\pi}\log(r)$$

Dipole along x

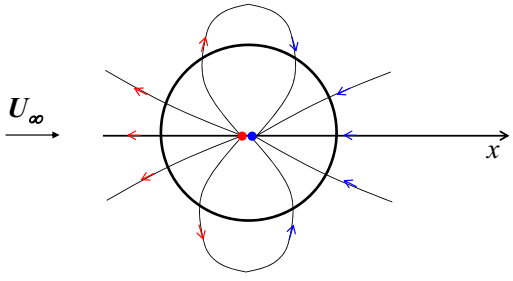

$$\text{2D: } \phi(x,y) = \frac{\gamma}{2\pi}\frac{x}{r^2} = -\frac{\gamma}{2\pi}\frac{\cos\theta}{r}$$

Found enforcing impermeability condition

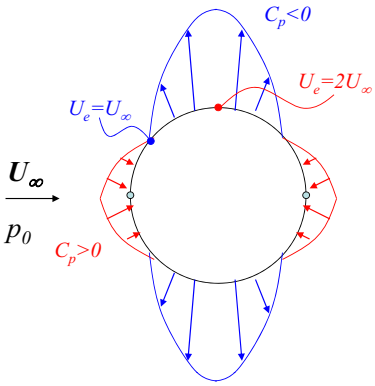

Stagnation points

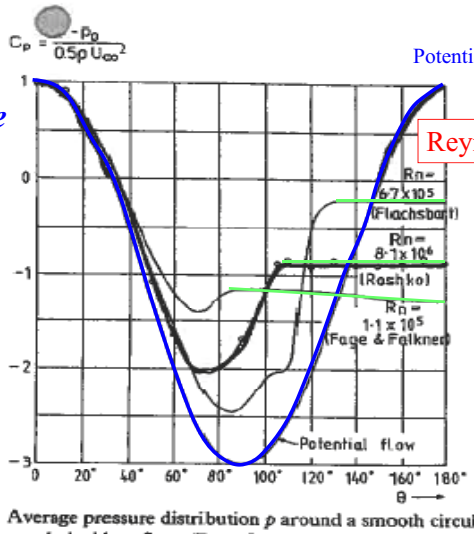

Potential-flow solution

Time-average pressure Coefficient

Reynolds Number

Fig. 6.2. Average pressure distribution p around a smooth circular cylinder in steady incident flow. (Rn = $U_\infty D/\nu$, D = cylinder diameter, U_∞ = incident flow velocity, θ defined in Fig. 6.1, p_0 = ambient pressure.) (Roshko, 1961.)

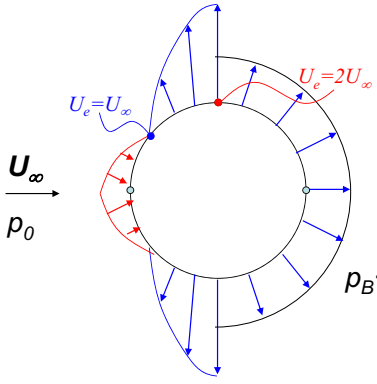

Stagnation points

43. Current and wind loads. Boundary-layer. Wake. Current loads on ships. (F: 177-190)

Boundary layer and Flow regimes (F:177-181)

Let's assume a current U_∞ past a fixed 2D body and take local coordinates with x,u as position and velocity along the body surface and y,v as position and velocity normally to the body ($y=0$ on the body).

In the potential-flow theory the body is impermeable and a tangential velocity, say $u=U_e$, exists along the body: free-slip condition (see the potential-flow solution for the circular cylinder). In reality the fluid velocity must go to zero at the body surface, i.e. it must be equal to the body velocity. This is called no-slip condition. So u must go from U_e to zero within a certain distance, say $\delta(x)$, from the body.

The layer of fluid with thickness $\delta(x)$ is called boundary layer (BL) and there viscous effects are important, even if viscosity is small. The reason is that the shear/tangential stresses, of the form $\tau = \mu \partial u / \partial y$, can be large because the normal gradient brings u from 0 to U_e within the distance $\delta(x)$. So the smaller the boundary layer thickness the larger the shear stresses. This fact gives another contribution to the drag force on the body. In general we have: a friction/shear force due to tangential stresses along the body surface and a pressure force due to the pressure losses caused by flow separation.

NB: The friction/shear force is dominant for streamlined bodies while the pressure force due to viscous effects is more relevant for blunt bodies with separation.
For example, in the case of a ship usually the frictional component is more important than the pressure loss, because the form is typically as much as possible streamlined. However ships in manoeuvring can be associated with relevant flow separation and therefore loss in pressure in this case is greater than normally.

The thickness $\delta(x)$ of the boundary layer can be defined in many ways. The reason is that u tends to U_e asymptotically, i.e. as $y \to \infty$. One possible definition is: at any location x, δ is the distance $y=\delta(x)$ where the tangential velocity u becomes the 99% of the tangential velocity just outside the boundary layer $U_e(x)$.

For a laminar boundary layer of a circular cylinder, the velocity u at $\theta=80°$ appears as in fig. F:6.4.

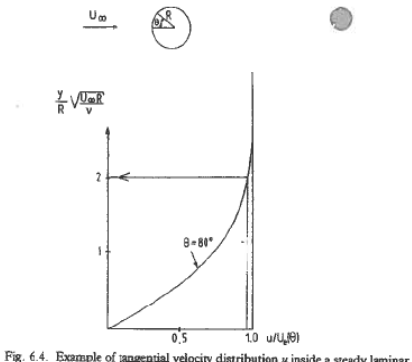

Fig. 6.4. Example of tangential velocity distribution u inside a steady laminar boundary layer flow around a circular cylinder. The results are for one angular position θ and are presented as a function of the y-coordinate normal to the body surface ($y=0$ is at the body surface). $U_e(\theta)$ = tangential potential flow velocity just outside the boundary layer at the same angular position θ.

In this case: $u=0.99U_e$ at $\frac{y}{R}\sqrt{\frac{U_\infty R}{\nu}} \underbrace{=}_{\text{by BL thickness definition}} \frac{\delta}{R}\sqrt{\frac{U_\infty R}{\nu}} \cong 2 \Rightarrow \delta \cong 2\frac{\sqrt{2}}{\sqrt{Rn}}R$.

So if $Rn = U_\infty D/\nu = 1\cdot 10^5 \Rightarrow \delta \cong 0.01R$ at this location and it decreases increasing Rn in laminar conditions.

In isothermal conditions, the governing equations of the flow evolution inside BL are the conservation of fluid mass (for incompressible flow) and the Navier-Stokes (NS) equations. Let us study the boundary layer along a 2D body long L assuming laminar flow.
In terms of orders of magnitude, we have that: $u = O(U_\infty)$, $x = O(L)$ and $y = O(\delta)$

Assuming steady conditions, inside the boundary layer, we have:

1. From the continuity equation, the normal velocity and its variation along the body surface are small → $v = O(\delta)$, $\partial v/\partial x = O(\delta)$
2. Introducing 1. in the NS equation in y direction, the normal derivative of the pressure can be neglected → $\partial p/\partial y \cong 0$
   → This means that the pressure is equal to the pressure of the flow just outside the BL. There, the flow is inviscid and does not 'see' the BL, so p can be obtained from the Euler eq. in x direction applied along the body, i.e.
   $\rho U_e \partial U_e/\partial x = -\partial p/\partial x$ (1)
3. So the conservation of the fluid mass and the NS equation in x direction represent the equations governing the flow evolution in the BL:
   $\partial u/\partial x + \partial v/\partial y = 0$
   $$\rho u \partial u/\partial x + \rho v \partial u/\partial y = -\partial p/\partial x + \mu\left(\underbrace{\partial^2 u/\partial x^2}_{\text{it can be neglected because much smaller than } \partial^2 u/\partial y^2} + \partial^2 u/\partial y^2\right) \quad (2)$$
   with BC conditions: $u=0$ and $v=0$ at $y=0$ and $u=U_e$ at $y=\infty$. p is given by eq. (1)
   (**NB**: The integration is up to $y=\infty$ because u tends to U_e asymptotically.)

Condition for flow separation:
Using the tangential velocity profiles (see figure below for a 2D body) we can determine the condition for flow separation along a body.

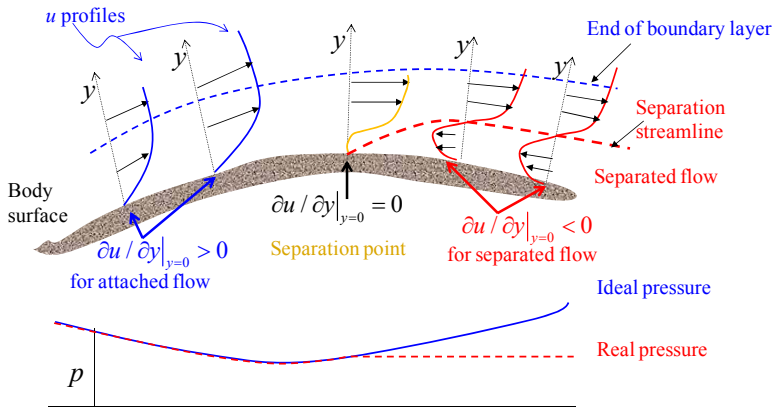

In the region where the flow is attached to the body

$$\left.\frac{\partial u}{\partial y}\right|_{y=0} > 0$$

while, in the region where flow separation has occurred, the fluid motion near the body is reversed creating vortices so that

$$\left.\frac{\partial u}{\partial y}\right|_{y=0} < 0 .$$

This suggests that the separation point (SP) can be defined as the point on the body with

$$\left.\frac{\partial u}{\partial y}\right|_{y=0} = 0 \qquad \text{(F:6.8)}$$

This means that the separation point is an extreme point for the velocity u. Starting from the separation point, the flow will follow the separation streamline instead of the body surface.
When there is flow separation, somewhere in the boundary layer there must be a minimum of u due to the reversed flow, i.e.

$$\partial^2 u / \partial y^2 > 0$$

This means that the separation point must be connected with a minimum of u on the body surface, i.e.

$$\left.\frac{\partial^2 u}{\partial y^2}\right|_{y=0} > 0$$

Applying the NS equation in x direction on the body surface, i.e. at y=0, in steady conditions gives:

$$\mu \partial^2 u / \partial y^2 \big|_{y=0} = \partial p / \partial x \big|_{y=0}$$

This tells that we have separation only if

$$\partial p / \partial x \big|_{y=0} > 0$$

which means if there is an adverse pressure gradient, i.e. the pressure increases.

NB: As a result, there is no separation in the case of a uniform free-stream velocity U_∞ with zero angle of attack past a flat plate with zero thickness. In this case the potential flow solution is uniform, i.e. U_e=U_∞ → $\partial U_e / \partial x = 0$ along the plate, so using the Euler equation (1) we find $\partial p / \partial x = 0$, i.e. the pressure never increases.

For the circular cylinder, if we assume a laminar boundary layer and potential-flow tangential velocity U_e for the flow external to the BL, the separation condition tells that separation occurs at ±100°.
In reality the separation in laminar conditions occurs at about ±80°, this is because the potential-flow solution $U_e = 2U_\infty \sin\theta$ is not a good representation of the velocity outside the boundary layer along the whole cylinder, i.e. at any θ. It is a good approximation only within $-\pi/4 \le \theta \le \pi/4$ for values of Rn of practical interest.
Moreover the flow in the boundary layer is laminar before the separation only up to a certain Rn. For larger Reynolds numbers, the flow becomes turbulent before the separation.

Flow regimes:
According to the value of Rn we can distinguish four flow regimes. Assuming a smooth circular cylinder:

1) $Rn <\approx 2\cdot 10^5$ subcritical flow regime
2) $\approx 2\cdot 10^5 < Rn <\approx 5\cdot 10^5$ critical flow regime
3) $\approx 5\cdot 10^5 < Rn <\approx 3\cdot 10^6$ supercritical flow regime
4) $Rn >\approx 3\cdot 10^6$ transcritical flow regime

In the subcritical regime (1): the boundary layer is always laminar.
In the supercritical and transcritical regimes (3 and 4): the boundary layer is turbulent upstream of the separation point.

Figure below shows the boundary-layer conditions for a value of Rn in the transcritical regime.

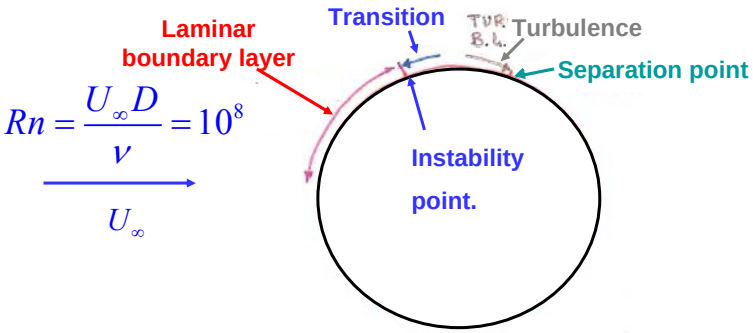

In this case, more than the global Reynolds number $Rn = UD/\nu$, it is important the local Reynolds number $Rn_x = U_\infty x/\nu$, with x the distance along the body starting from θ=0°. As we move downstream along the body, Rn_x increases, as well as δ. Flow instability occurs at the location x where $Rn_x = Rn_{crit}$. Downstream of the critical point disturbances appear in the flow which amplify and after a transition zone (which corresponds to a range of Rn_x) the flow becomes turbulent at the location x where $Rn_x = Rn_{tr}$.

NB: The boundary layer thickness depends differently on the global and local Reynolds numbers Rn and Rn_x. We have seen in laminar conditions that δ decreases by increasing Rn, while it increases increasing Rn_x.

In terms of the global Reynolds number:
As Rn increases → the point where instability occurs moves upstream and in particular at θ smaller than the separation point.
As Rn reduces → the instability point moves closer to the separation point until we reach the condition when the flow remains laminar in the boundary layer before separation.
The distance between the instability point and the separation point is measured experimentally.

In laminar flow the (laminar) viscosity μ leads to an exchange of fluid momentum between fluid layers through viscous (laminar) shear stresses, inside the BL this occurs normally to the body surface, i.e. along y. The turbulence leads to a greater exchange of fluid momentum. This can be seen as another viscosity in the flow, connected with turbulent stresses, which is added to the laminar viscosity, leading to a greater effective viscosity.
As a result, the turbulent flow leads to
→ a greater thickness δ of the boundary layer
→ a larger normal gradient of the tangential velocity at the body, $\partial u / \partial y\big|_{y=0}$
→ then to higher tangential stresses
This is shown by the figure below giving the velocity profiles in laminar and turbulent BLs for a flat plate.

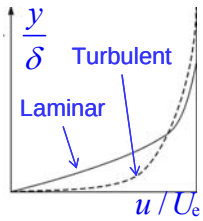

As we said, separation can not occur for a flat plate.

For a circular cylinder, as well as for a generic body geometry, a larger $\partial u / \partial y\big|_{y=0}$ means that for a turbulent flow the condition for flow separation, i.e. $\partial u / \partial y\big|_{y=0} = 0$, occurs with a spatial delay with respect to a laminar flow.
This means that, if the flow becomes turbulent upstream of the separation point, the location of the separation point changes, with respect to the location with laminar flow upstream of the separation point, and moves downstream along the body. For example, for a circular cylinder, the separation point moves from ±80°to ±120°.

Important general consequences of turbulence are:

1) higher friction drag contribution due to
   - the greater velocity gradients and
   - the greater effective viscosity due to larger fluid-momentum exchange
2) lower pressure drag contribution because the BL remains attached in a larger portion of the body

NB: The position of the separation point is the most important scale effect for the pressure drag because typically Froude scaling is used and the *Rn* at model scale is then smaller than at full scale. As a result, the flow regimes at model and full scales can be different.

Going back to the circular cylinder, we understand now the behaviour of the drag coefficient in the different Reynolds regimes. If we limit ourselves to a smooth cylinder (see figure below):

- In the laminar regime, the drag coefficient is mainly due to pressure loss for the separation.
- In the critical regime, there is a drop in drag coefficient due to the delay in the separation.
- In the supercritical and transcritical regimes, the drag coefficient tends to increase due to the increase in the frictional stresses.

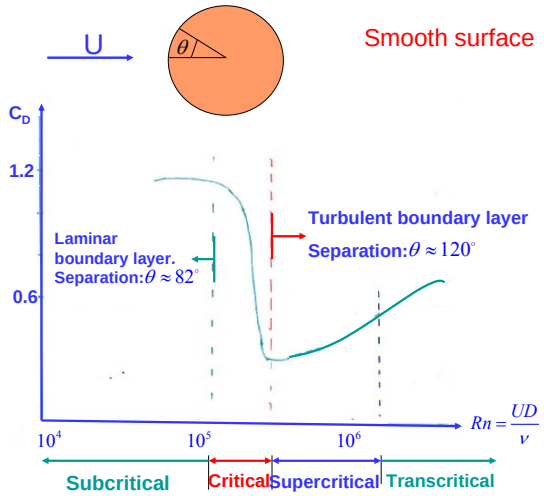

A smooth cylinder means that the surface roughness *k* is zero. Experimental values of C_D also including the effect of the roughness are given in fig. F:6.3.
The results show that *k/D* affects the drag coefficient. In general each curve shows a drop of the drag for a given $Rn=Rn_{crit}$. This corresponds to the critical zone where the separation point location shifts suddenly downstream. As *k/D* increases, the laminar value of the drag coefficient tends to increases due to a greater frictional effect, the C_D drop in the critical zone becomes then less marked and occurs at lower *Rn*, i.e. Rn_{crit} becomes smaller, because the

roughness represents a flow disturbance and so supports the flow instability, i.e. the flow becomes earlier turbulent.

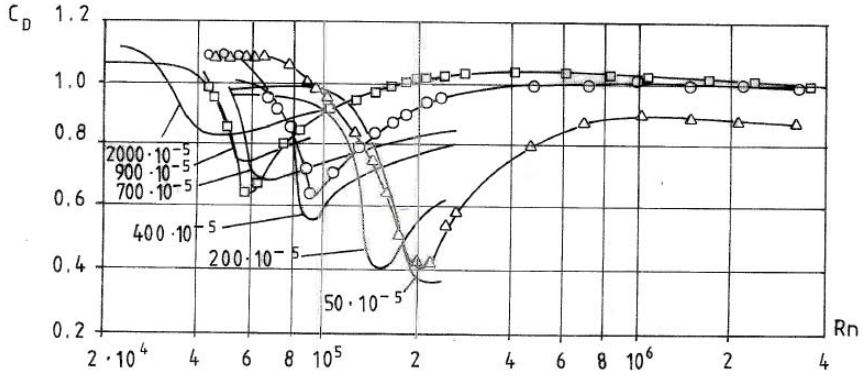

Fig. F:6.3

NB: The separation process studied here occurs because of viscous effects, but inviscid separation may also occur, which means that the flow detachment from the body is not due to viscous phenomena. This may happen:

a) when there is a geometrical singularity and the flow is not able to follow the body surface

b) when the pressure along the body tends to become smaller than the ambient pressure, e.g. during water entry (we will later discuss this phenomenon).

Wake behaviour (F:181-184)

In the boundary layer the vorticity $\boldsymbol{\omega} = \nabla \times \boldsymbol{V}$ is non-zero → the flow is rotational.

For a 2D body, the vorticity component in the direction normal to the flow-motion plane is:

$$\omega_z = \partial v / \partial x - \partial u / \partial y \cong -\partial u / \partial y \neq 0$$

At the separation point, a flux of vorticity is shed from the body in the form of vortices (leading to vortex sheets, i.e. free-shear layers) also indicated as wake. Inside the shear layers the flow is then viscous and rotational. This vorticity flux is given by

$$\int_0^\infty \omega_z u dy \cong -\int_0^\infty \partial u / \partial y u dy = -\frac{1}{2} U_s^2$$

where U_s is the tangential velocity just outside of the BL at the separation point location. This flux is equal to the time rate of change of the circulation

$$\Gamma = \oint_C \boldsymbol{V} \cdot \boldsymbol{dl}$$

in the wake. Here C is a closed line that intersects a separation point (in the example in figure below this is point B) and does not intersect any vortex sheet.

A,B = separation points

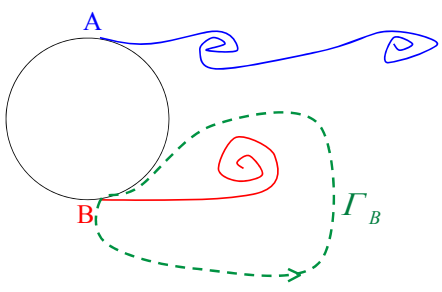

Assuming that Γ is positive when anti-clockwise, we have

$$\frac{\partial \Gamma_A}{\partial t} = -\frac{1}{2} U_{sA}^{\ 2} \qquad \frac{\partial \Gamma_B}{\partial t} = \frac{1}{2} U_{sB}^{\ 2} \qquad \text{(F:6.14+6.15)}$$

for the time derivatives of the circulations connected with vortex shedding from separation points A and B, respectively. At time t=0 the circulation is zero → $\Gamma_A(0)$ and $\Gamma_B(0)$ are zero and expressions (F:6.14+6.15) tell how Γ_A and Γ_B evolve in time.
From the Kelvin's theorem (see i.e. Newman 1977): In an inviscid fluid under conservative forces (e.g. gravity), the circulation along a material curve, i.e. moving with the fluid, remains constant. So if it is initially zero (irrotational flow) it will remain zero at any time.
→This means that as Γ was zero around the cylinder at t=0, it will remain zero along any closed curve which surrounds the cylinder and does not intersect the vortex sheets.

NB: The free shear layers released from the body become easily unstable, i.e. turbulent. So even when the boundary layer detaches as laminar, the flow downstream the separation is typically turbulent.

Vortex shedding (F:184-187)
In the starting process of a separated flow around a circular cylinder the vortices are released symmetrically from separation points A and B, but due to instabilities the vortices are shed alternatively from the two separation points.
Von Karman studied the stability of vortex shedding considering idealised vortex streets, i.e. the body does not appear in the problem like it was far away. The results of the analysis are valid for a generic blunt body.
The vortices are modelled as point vortices with strength $|\Gamma|$ which travel in two parallel rows distant h with opposite sign of vorticity. Vortices in the same row are distant l from each other. He found that only two solutions are possible:

1) One with vortices travelling in couple
2) The other with vortices travelling symmetrically staggered

Configuration 1) is unstable, 2) is also unstable except for when

$$\frac{h}{l} = \frac{1}{\pi} \cosh^{-1} \sqrt{2} = 0.28 \quad \text{(F:6.16)}$$

This solution is shown in figure F:6.9.

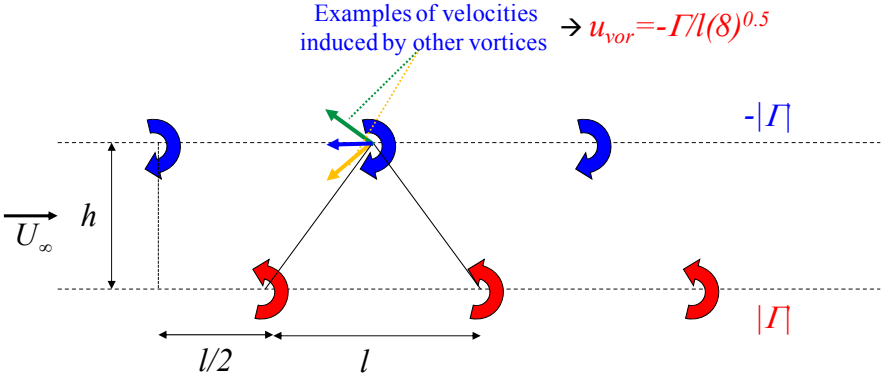

Fig. F:6.9

The vortices in the body reference frame move with speed

$$u_{tot\ vor} = U_\infty \underbrace{-\frac{\Gamma}{l\sqrt{8}}}_{\substack{\text{induced by the} \\ \text{other vortices}}}$$

It means that the period of shedding is given by the following relationship

$$\underbrace{T_v}_{=1/f_v}\left(U_\infty - \frac{\Gamma}{l\sqrt{8}}\right) = l \qquad \text{(F:6.18)}$$

i.e. as the time interval for a vortex to cover the distance l and so the time interval between two following vortex shedding from the same separation point. Here f_v is the shedding frequency.

To estimate T_v we need to know Γ and l which depend on the body geometry, not included in the Von Karman's problem formulation.

In the case of the circular cylinder we can set as a first approximation that $h=D$ and approximate the vortex velocity as $u_{tot\ vor} \cong U_\infty$, i.e. neglecting the velocity reduction due to the other vortices. Then combining (F:6.16) and (F:6.18) we have:

$$T_v U_\infty = \frac{D}{0.28}$$

This is usually expressed in terms of a non-dimensional parameter called Strouhal number

$$St = \frac{f_v D}{U_\infty} \qquad \text{(F:6.20)}$$

St gives the ratio between the cylinder diameter and the distance covered by the current during a shedding period.

In the examined case we find *St*=0.28 which is consistent with the vortex shedding in transcritical regime. In subcritical conditions a better approximation is given using $h \cong 1.2D$ and $u_{tot\ vor} = U_\infty - \Gamma/(l\sqrt{8}) \cong 0.85U_\infty$ as the vortex velocity. This means that the vortex rows spread outwards with respect to the body transverse dimension and the velocity reduction due to the other vortices in the row matters. This leads to *St*=0.2

An important practical consequence of a vortex shedding is that if there is a cylinder in the wake of another cylinder then the incident current for the downstream cylinder has speed

$$U_\infty - \frac{\Gamma}{l\sqrt{8}} < U_\infty$$

It means that this cylinder experiences a smaller drag than the upstream cylinder because the drag force goes as the square power of the involved current speed. This is an effect of wake interaction.

NB: Not always behind the body we see a vortex street and not always there is only one shedding frequency. In critical and supercritical conditions there is a spectrum of shedding frequencies.

In subcritical flow past a circular cylinder we can divide the wake in three parts:

1. a formation region (l_{fr}),
2. a stable region with uniform vortex sheet (l_{sr}) and
3. an unstable region (l_{ur}).

The lateral extension h increases as we move downstream and h/l may vary greatly: from 0.19 to 0.3.

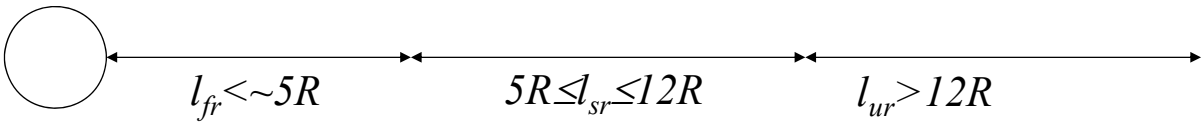

Oscillatory forces due to alternate vortex shedding:

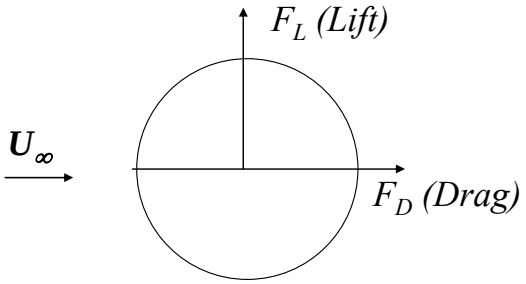

The alternate vortex shedding results in a force in the normal direction with respect to the current, i.e. a lift force

$$F_L(t) = |F_L| \cos(2\pi f_v t + \alpha) \quad \text{(F:6.21)}$$

The lift coefficient

$$C_L = \frac{|F_L|}{0.5\rho U_\infty{}^2 D} \quad \text{(F:6.22)}$$

is 1.35 in subcritical regime for a fixed cylinder.

In a 3D cylinder, one could think to estimate the total transverse (lift) force assuming that locally the flow is 2D and using a strip-theory approach, i.e. summing up the 2D lift-force contributions along the cylinder axis.

This would be a good approximation if the phase α was the same along the cylinder axis because this would mean that the body cross-sections are correlated with each other and the sum of the 2D force contributions gives the total force. In this ideal case the correlation length l_c, i.e. the length along the body where the phase α remains constant, is equal to the cylinder length.

In reality, α varies along the cylinder axis, this means that the correlation length of the vortex shedding is small and as a result

→ The total lift force on the cylinder is clearly reduced due to the cancellation effects.

The correlation length is l_c<5D in subcritical regime and reduces to 1D-2D in transcritical regime. The behaviour of l_c/D as a function of the Reynolds number is given in the figure below.

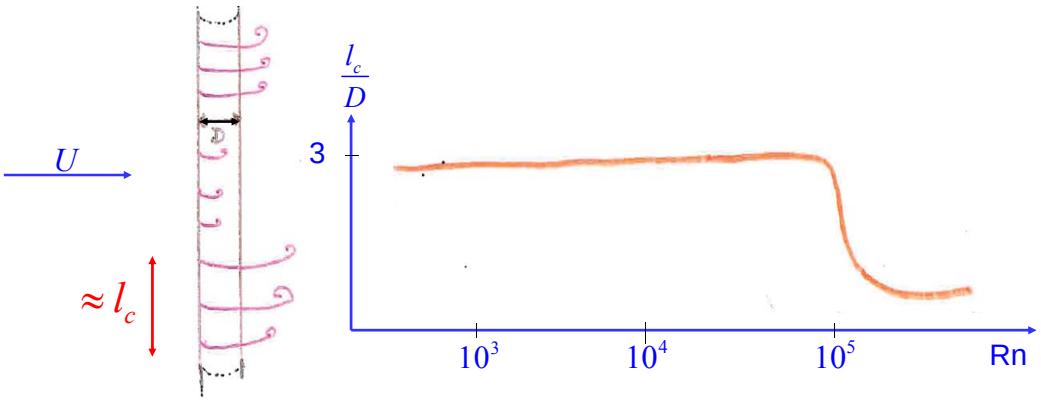

The drop of l_c/D when the flow becomes unstable and turbulent can be understood considering that a turbulent flow is not organized so it is more difficult to maintain a similar phase of the lift force, i.e. of the vortex shedding, as we move along the cylinder axis. One must also note that as the flow becomes turbulent the 3D effects become more important.

The alternate vortex shedding causes also an oscillatory drag force. In this case a mean (constant) value of the force exists due to the mean frictional terms and pressure losses around the cylinder, i.e.

$$F_D(t) = \bar{F}_D + A_D \cos(4\pi f_v t + \beta) \quad \text{(F:6.23)}$$

The amplitude A_D of the oscillatory part is typically the 20% of $\bar{F}_D$.

Also the phase β varies along the axis of a 3D cylinder which means that cancellation effects occur also for the drag as for the lift.

A vortex is shed every $1/2T_v$ alternatively from the two sides. From this it depends the oscillation period for the lift and drag forces:

1. For the lift, the change of the cylinder side where shedding occurs it matters, because the lift is sensitive to variations in the transverse direction. This means that
   → the lift oscillation period is T_v
2. For the drag, the change of the cylinder side where shedding occurs it does not matter, because the drag is only sensitive to variations in the current direction
   → the drag oscillation period is $T_v/2$

NB: The oscillatory forces may cause resonance phenomena, i.e. vortex-induced vibrations (VIV), as we will see later. In case of Vortex Induced Vibrations (VIV) the correlation length along the cylinder will be larger and this results in higher oscillatory forces.

Example from the sea: fishes

If we observe the motion of a fish tail, we see a shedding of vortices alternatively with opposite sign. They induce a speed on each other.

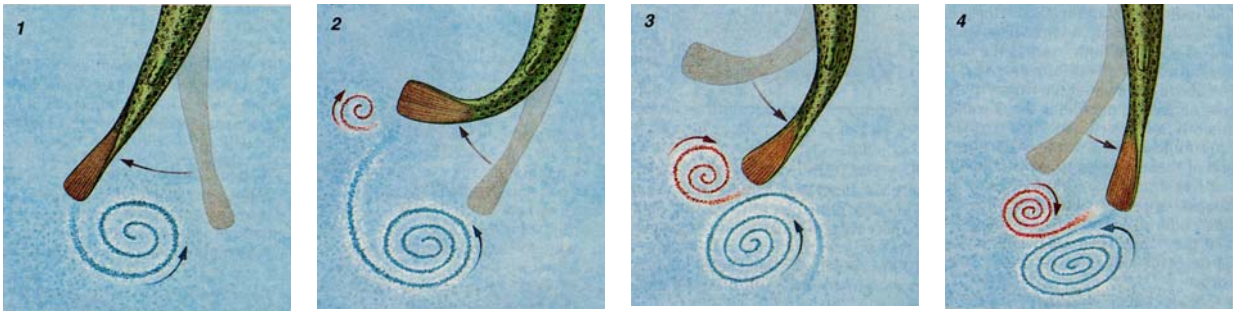

As for a fixed circular cylinder in a current also a moving fish is then associated with a vortex shedding but the sign of the vortices is reversed (see figure below).

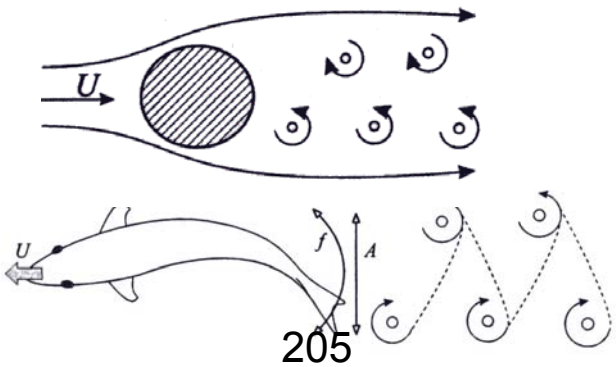

As a result: in the case of the cylinder, the vortex shedding causes drag and oscillatory forces; in the fish case, the vortex shedding leads to trust generation.
As for the circular cylinder, also for fishes the wake interaction can have positive effects. For example let's assume the case of a fish in the wake of two upstream fishes as in the figure below. The vortices shed by the upstream fishes cause a flow velocity in the motion direction on the downstream fish, so this one needs a lower trust to swim with the same velocity as the upstream fishes.

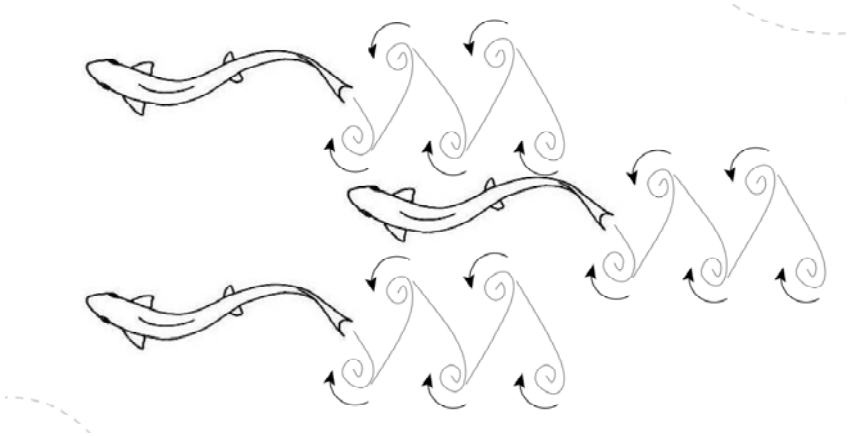

Triantifyllou et al. (1995) studied the Strouhal number for different fishes defining the parameters of an equivalent circular cylinder, as reported in the figure below.
From the results, the *St* varies in a range between 0.2 and 0.4. The smaller is this value the higher is the fish speed *U* relative to the product of the amplitude with frequency of tail motion, *fA*. It means that the fish locomotion is more efficient. On the other hand the capability of the fish to reach large accelerations and to manoeuvre reduces as *St* reduces because the frequency of tail motion *f* becomes small compared to *U/A*. In this framework the best range of *St* for fishes is considered around 0.25 and 0.35.

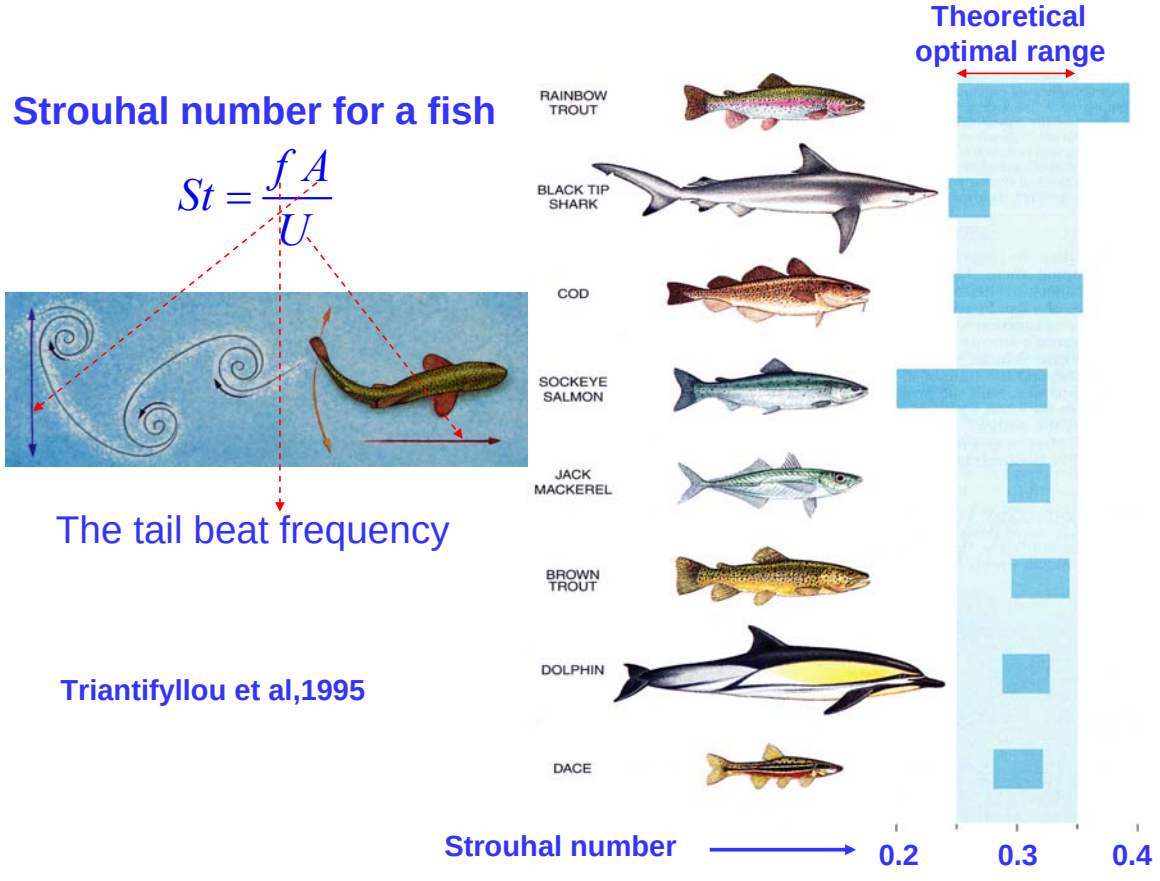

Current loads on ships (F:187-190)

We assume a current, with speed U_c, along the longitudinal axis of a ship long L, in calm water (i.e. no incident waves). In this case, the Froude number $Fn = U_c / \sqrt{Lg}$ is usually small, for example a typical design current in North Sea is U_c=1m/s, so for L>25m Fn<~0.06. This means that the wave resistance, i.e. due to the wave generation by the body, can be neglected and the resistance is dominated by viscous resistance. Viscous effects play then a dominant role for current loads and flow separation has in general relevance.

Assuming a current U_c with a direction β with respect to the ship longitudinal axis. The current loads can be obtained by decomposing the current and assuming that:

- the longitudinal component $U_c \cos\beta$ causes only a drag force
- the transverse component $U_c \sin\beta$ is responsible for flow separation and causes a transverse force and a yaw moment.

These assumptions allow to study separately the longitudinal (drag) force and the transverse loads. In the latter case we can apply the 'cross-flow' principle'.

These loads are often obtained using empirical formulas, i.e. from the experiments.

Drag current force:

The drag current force is mainly due to frictional resistance. The latter is connected with the tangential stresses along the vessel wetted surface, say S, and so is primarily dependent on S. It means that

→ an equivalent flat plate with the surface equal to the ship wetted surface S can be used to have a first approximation of the frictional resistance.

The 3D effects related to the shape of the vehicle contribute to an increase of the force with respect to the flat plate contribution, so

→ empirical form coefficients can be considered to account for this.

Using the assumptions above, in the case of a current along β, the resistance is caused by the longitudinal component (see figure below).

An empirical formula commonly used for the frictional resistance on ship hulls is given by ITTC (1957)

$$F_1^c = \underbrace{\frac{0.075}{(\log_{10} Rn - 2)^2}}_{C_F} \frac{1}{2} \rho S U_c^{\,2} \cos\beta \,|\cos\beta| \quad \text{(F:6.24)}$$

Here C_F is the frictional coefficient and agrees well with experimental results for the turbulent flow along a smooth flat plate. The absolute value in (F:6.24) is due to the fact that the force is in the direction of the current, so if $-\pi/2 < \beta < \pi/2$ the force is directed as x, otherwise it is directed as $-x$.

The Reynolds number in the formula is defined as

$$Rn = \frac{U_c \,|\cos\beta|\, L}{\nu}$$

NB: Other formulas exist for the C_F of a turbulent smooth flat plate.

To accounts for the 3D effects connected with the ship shape, the formula for the frictional coefficient in (F:6.24) can be modified as

$$C_F(1+k_f)$$

Here k_f is a form factor (usually indicated as k in the literature), found from experiments. Typical values for k_f are between 0.2 and 0.4 for β=0°. If the flow separates at the stern k_f may rise up to 0.8. This can be understood considering that when the flow separates, downstream of the separation line (a separation point in 2D becomes a separation line in 3D), the flow does not follow the body surface but another streamline, the separation streamline, which corresponds to a blunter 'body' → 3D effects become more important.

The roughness is an important parameter for the frictional resistance (see Faltinsen's book "Hydrodynamics of high-speed marine vehicles", pg. 232). There are many types of roughness. Schlichting (1979) presents the frictional coefficient C_F as a function the roughness height k in the case of sand roughness $k=k_s$ uniformly distributed on a plate long L. The results are shown in the figure below as a function of the Reynolds number of the plate $Rn=U_\infty L/\nu$ and of the parameters $U_\infty k/\nu$ and L/k.

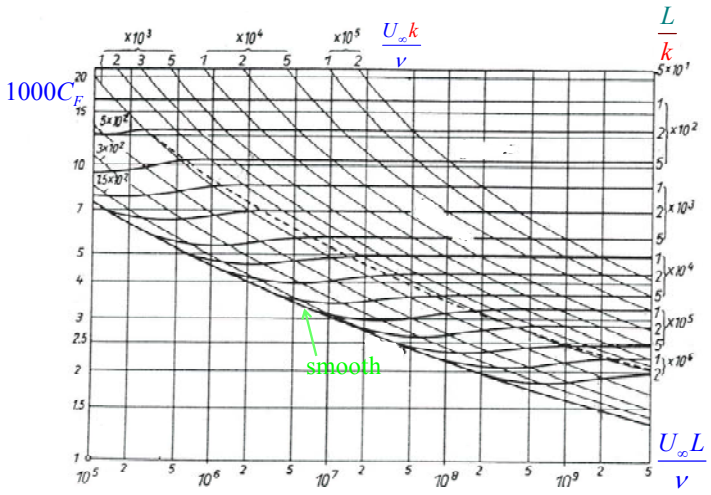

C_F increases when reducing the parameter L/k. Along curves with constant L/k, C_F becomes independent from Rn beyond the dashed line in the figure. This is because the flow becomes fully rough. For increasing values of $U_\infty k/\nu$ the frictional coefficient increases, as the roughness makes more turbulent the flow. The roughness has no effect on C_F if $U_\infty k/\nu$=100 (and <100)→$k_{adm}=100\,\nu/U_\infty$. This roughness value is called admissible and it means that if $k=k_{adm}$ it is like the plate was smooth. From the expression of k_{adm} we see that a ship can behave as smooth at model scale. At full scale, a smooth behaviour requires a very small admissible roughness due to the higher ship speed with respect to model tests and the fact that ν is the same at model and full scale.

There are different empirical formulas expressing the increase of the frictional coefficient ΔC_F due to the roughness with respect to the smooth plate. The formula by Bowden and Davison (1974)

$$10^3 \Delta C_F = 44\left[(AHR/L)^{1/3} - 10Rn^{-1/3}\right] + 0.125$$

accounts for the correlation between model tests and full scale and includes the effect of average hull roughness AHR (in the formula expressed in meters).

Transverse current force and current yaw moment:

If the current angle β is not small, in the meaning that the current has an important transverse component, then the transverse force and the yaw moment caused by the current are important and one can estimate them using the cross-flow principle. The basic assumptions are:

1) The flow separates due to the cross-flow past the ship
2) The longitudinal current component does not affect the transverse forces on a cross-section
3) The transverse forces on a cross-section are meanly due to the pressure loss connected with flow separation

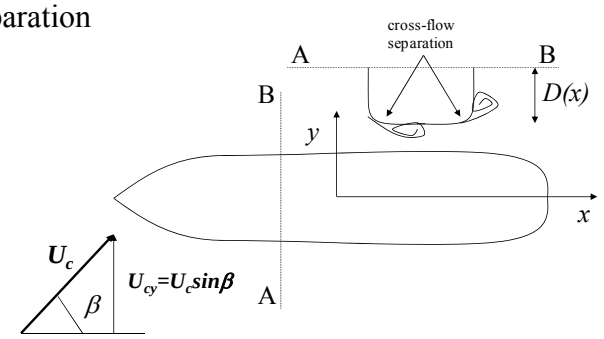

It means that we can express the transverse cross-section force as

$$dF_2^c(x) = \frac{1}{2}\rho C_D(x) D(x) U_c^2 \sin\beta\,|\sin\beta|\,dx$$

with $C_D(x)$ the drag coefficient for cross-flow past an infinitely long cylinder with the cross-sectional area equal to the one at location x along the ship and $D(x)$ the sectional draught.
We can then use the strip theory approach to get the loads on the vessel:

$$F_2^c = \frac{1}{2}\rho U_c^2 \sin\beta\,|\sin\beta| \int_L C_D(x) D(x) dx \qquad \text{(F:6.26)}$$

and

$$F_{6a}^c = \int_L x dF_2^c(x) = \frac{1}{2}\rho U_c^2 \sin\beta\,|\sin\beta| \int_L C_D(x) D(x) x dx \qquad \text{(F:6.27a)}$$

F_{6a}^c is only one of the two contributions to the ship yaw moment in a current. The other is the so-called Munk moment, which is associated with inviscid effects, i.e. it can be derived from non-separated potential flow theory (see figure below), and is a destabilizing moment. As we have seen, in general a body in an infinite potential steady flow is subjected to a moment (Munk moment) and to zero force (D'Alembert's paradox).
Because the force is zero, the Munk moment is a pure torque, i.e. it does not depend on a reference point, while the viscous moment does it. In the real case due to separation we will also have a force. Examples of pressure distribution along the body in potential and real flows are shown in the figure below.

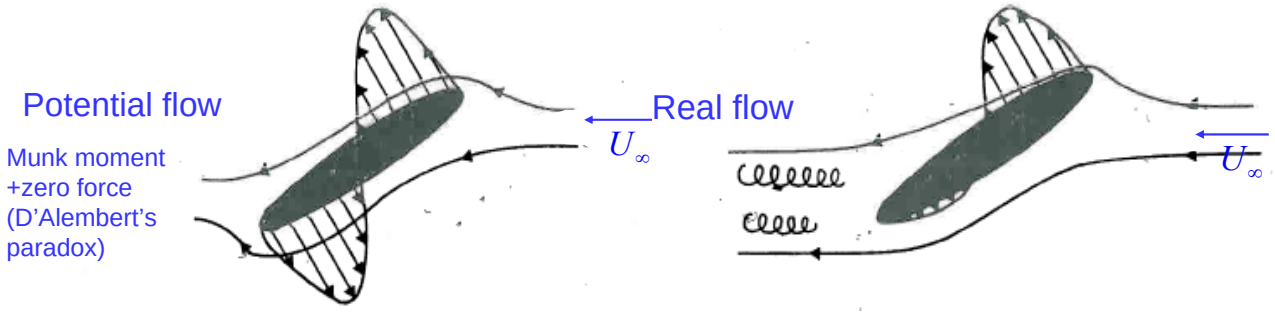

$$F_{6b}{}^{c} = \frac{1}{2} U_c{}^{2} (A_{22} - A_{11}) \sin 2\beta \qquad \text{(F:6.27b)}$$

with A_{11} and A_{22} the added masses in surge and sway.

The Munk moment is zero if
1). $A_{11} = A_{22}$, which is unlike to happen for a ship
2) β=0,π (longitudinal current) or π/2 (transverse current).

The two, viscous and inviscid, contributions to the yaw moment have then different angular dependence, see Fig. F:6.10. As the transverse force, also the viscous moment is zero when β=0,π, i.e. when the current is along x, but these load formulas connected with the current are valid far from this condition, i.e. when the transverse current component is important.

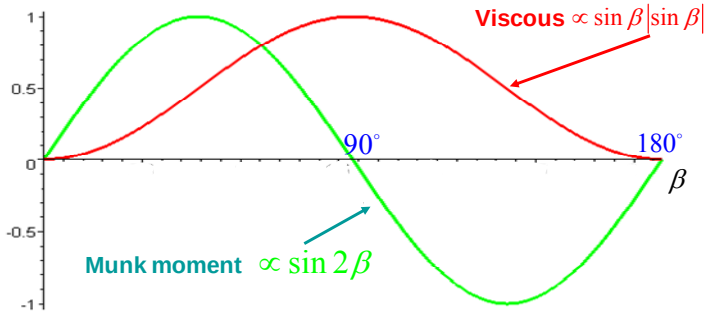

Fig. F:6.10

The comparison with experiments confirms that formulas (F:6.26) and (F:6.27=6.27a+6.27b) for the transverse force and yaw moment are good near β=90°, see figures F:6.11 and F:6.13. In figure F:6.13, the yaw moment is with respect to the vertical axis through the ship center of gravity and is assumed positive for a ship rotation toward larger β angles.

.

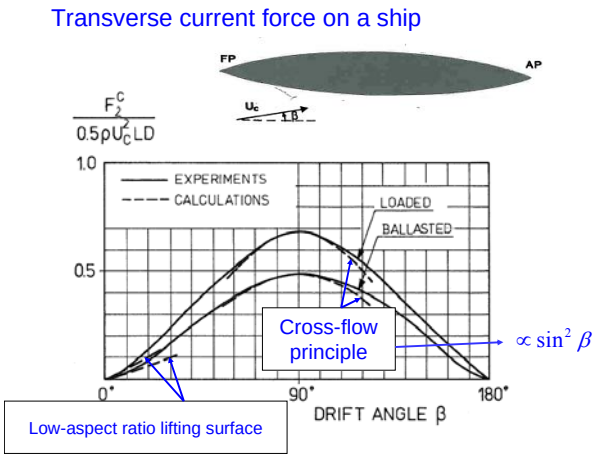

Fig. F:6.11

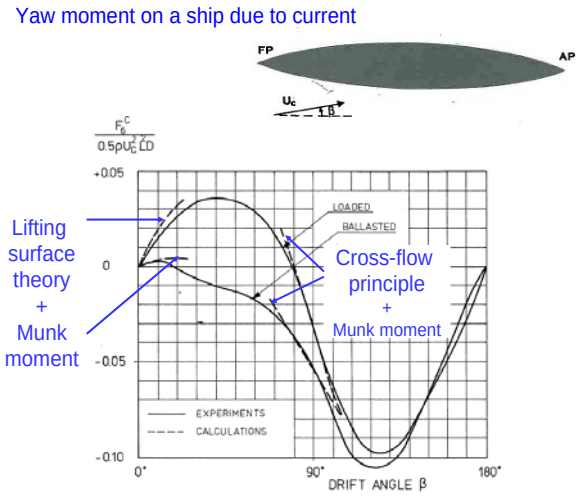

Fig. F:6.13

From experiments in Fig. 6.13, the viscous and Munk moments are of equal importance. This can be seen comparing the yaw moment at β=90° where $F_{6a}{}^{c}$ has maximum amplitude (and

negative value) and $F_{6b}{}^{c}$ is zero, with the yaw moment at β=45° where $F_{6b}{}^{c}$ has maximum amplitude (and positive value) and $F_{6a}{}^{c}$ is $1/\sqrt{2}$ times its value at β=90°.

For small angles (β close to 0°) a good approximation is obtained assuming the hull and rudder as low aspect-ratio lifting surfaces. An idea of what this means is given in the figure below for the hull and similarly could be considered for the rudder.

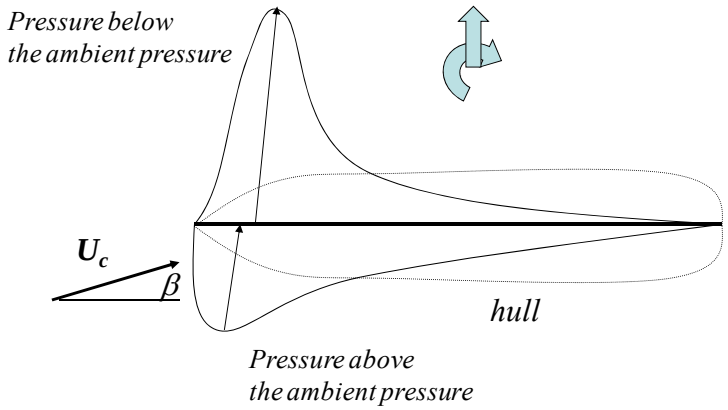

The ship and rudder are like flat plates in a current with an angle of attack. A pressure distribution is caused with suction pressure (below the ambient pressure) in one side and overpressure in the other. As a result a lift force and a yaw moment are caused.

Boundary layer along a 2D body

Hp: U_e = tangential velocity on the body from potential-flow solution

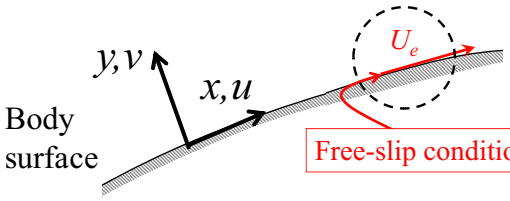

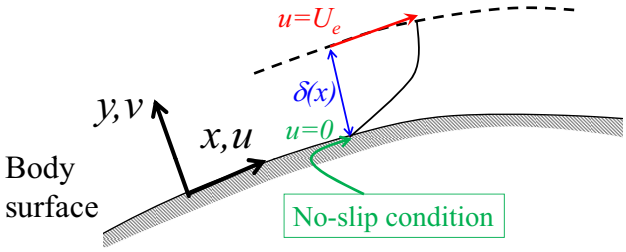

Tangential velocity u in the boundary layer: circular cylinder

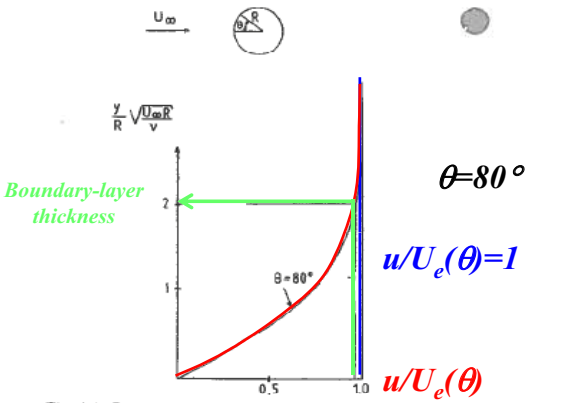

Fig. 6.4. Example of tangential velocity distribution u inside a steady laminar boundary layer flow around a circular cylinder. The results are for one angular position θ and are presented as a function of the y-coordinate normal to the body surface ($y = 0$ is at the body surface). $U_e(\theta)$ = tangential potential flow velocity just outside the boundary layer at the same angular position θ.

Velocity profiles and pressure along a 2D body

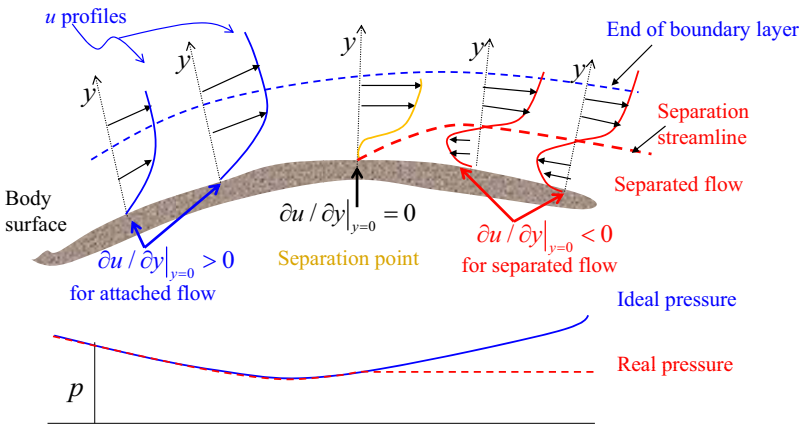

Condition for flow separation along a 2D body

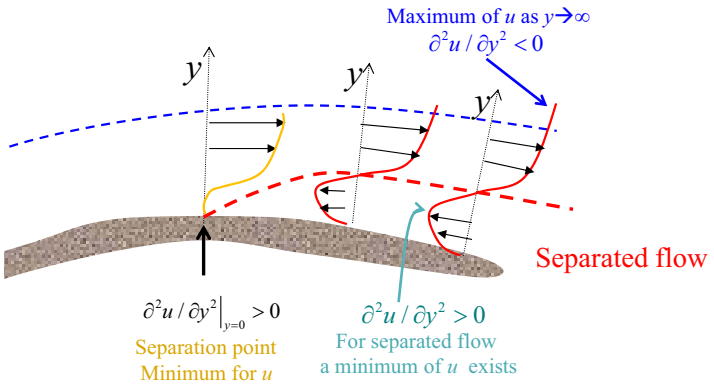

The instability and separation points depend on the Reynolds number and the boundary layer flow

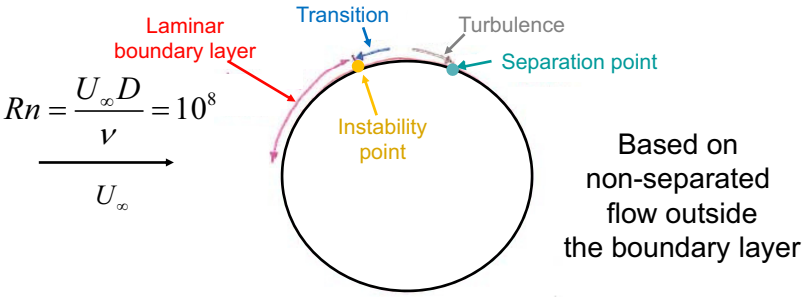

The instability and separation points depend on the Reynolds number and the boundary layer flow

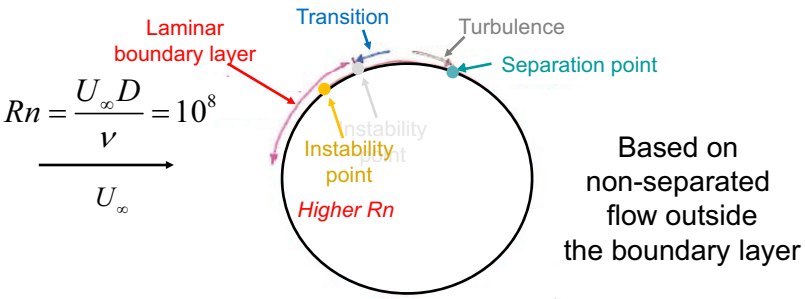

The instability and separation points depend on the Reynolds number and the boundary layer flow

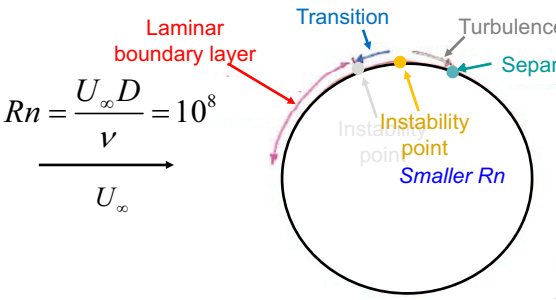

Based on non-separated flow outside the boundary layer

Laminar & turbulent velocity profiles: flat plate

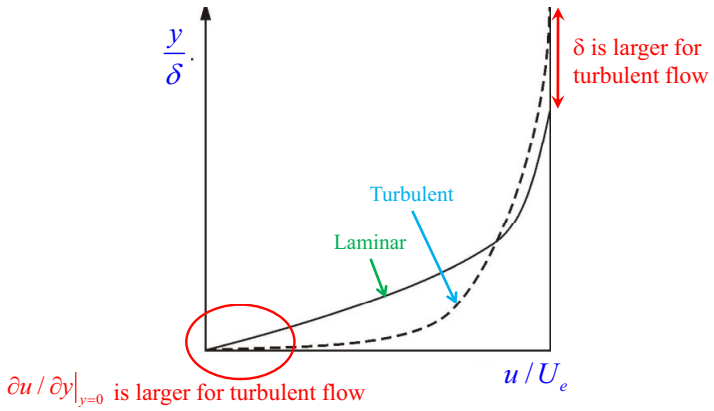

Flow regimes for steady ambient flow: circular cylinder

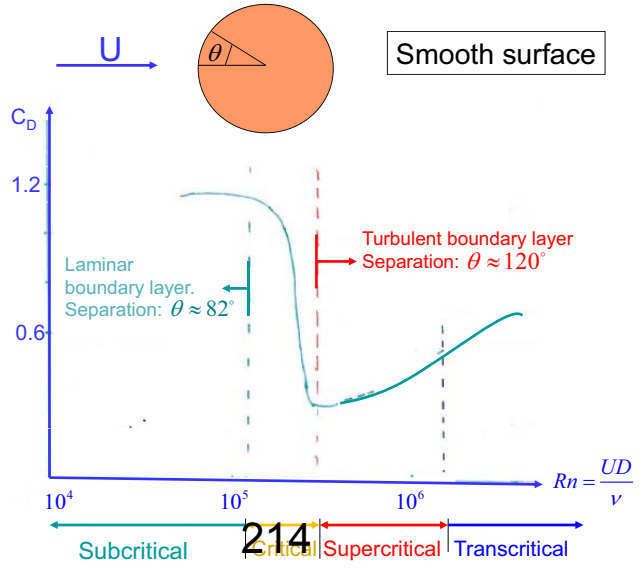

Drag coefficient for a circular cylinder in steady ambient flow

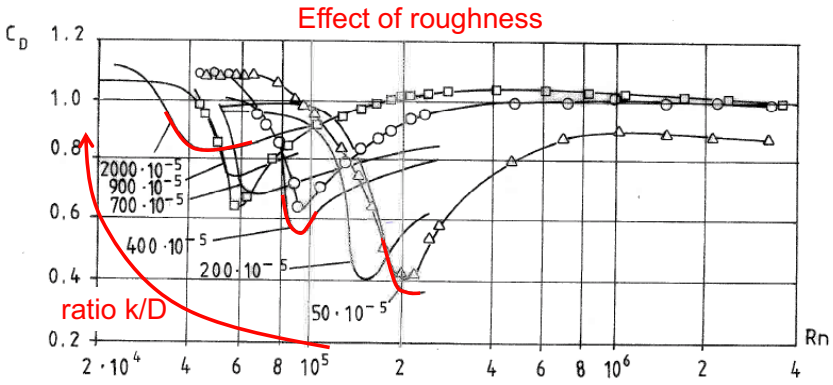

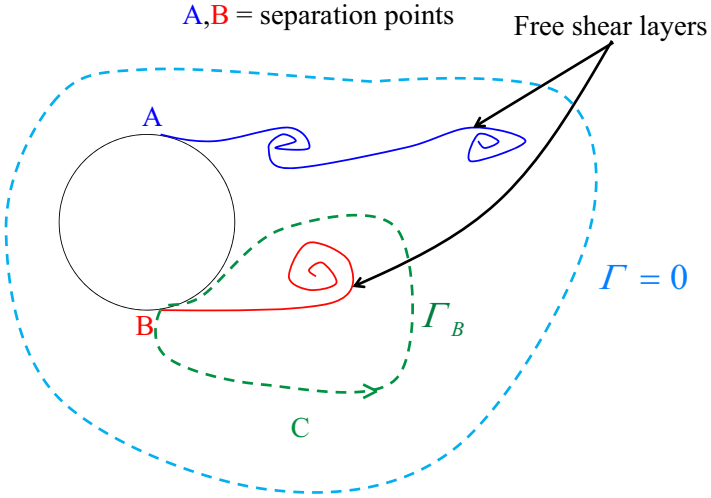

Von Karman wake for a blunt body

Unstable solution

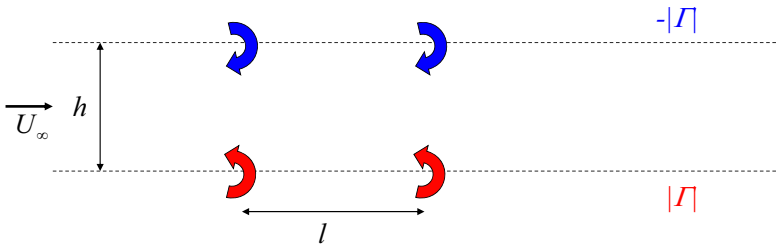

Von Karman wake for a blunt body

Stable solution if h/l=0.28

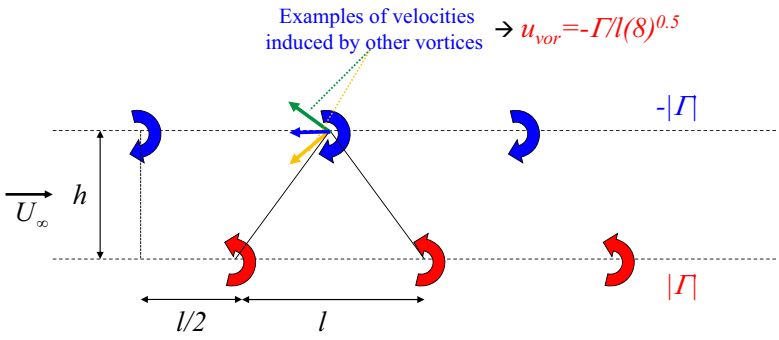

Wake in subcritical conditions: circular cylinder

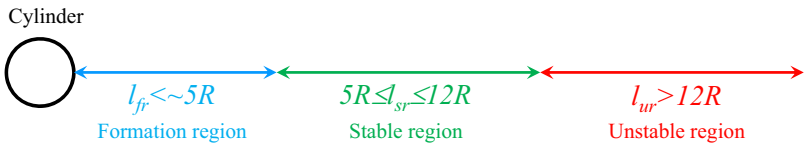

Oscillatory forces due to alternative vortex shedding
Circular cylinder

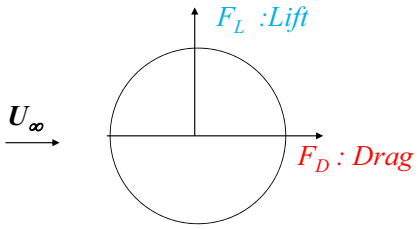

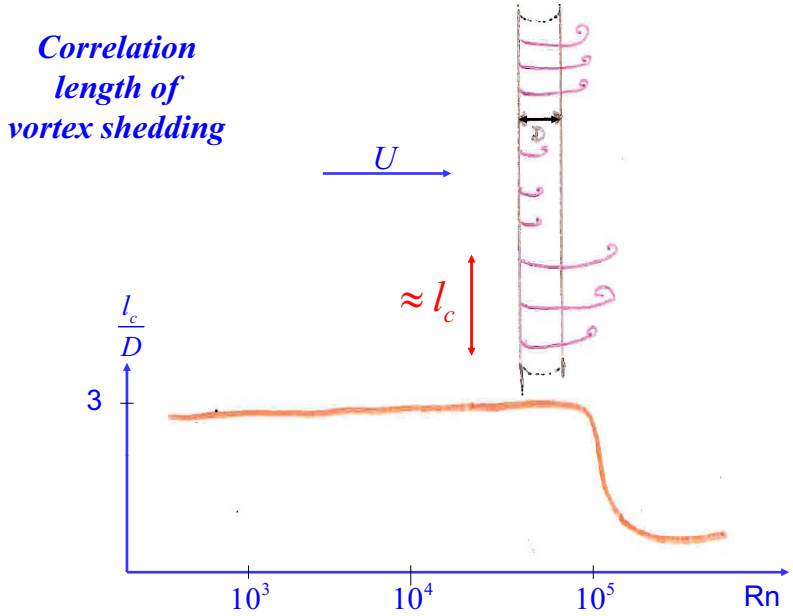

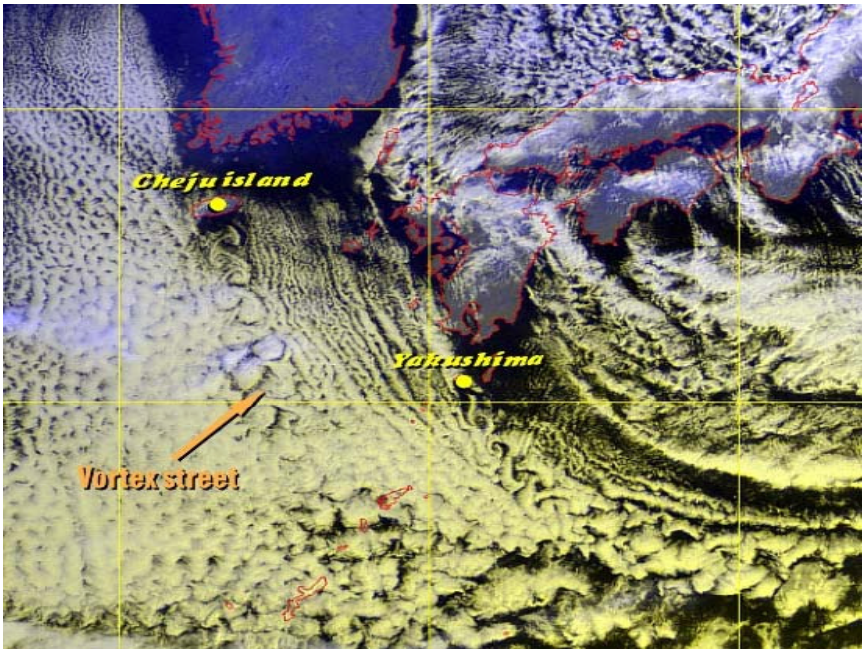

Wake interaction

Fish: tail motion

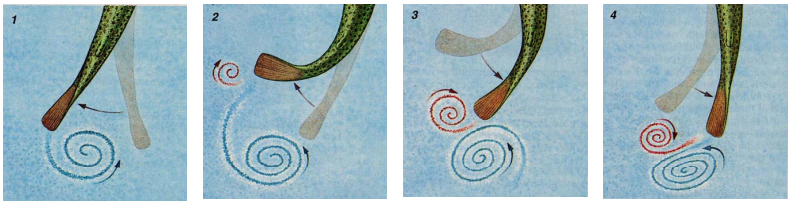

Fish encounters vortices

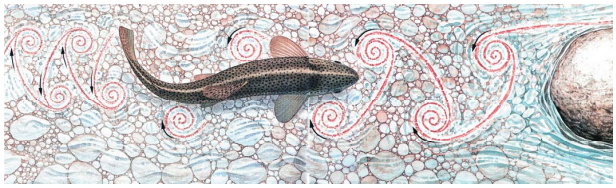

Wake structure and generation

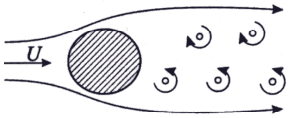

The flow separation causes drag and oscillatory forces associated with the vortex shedding

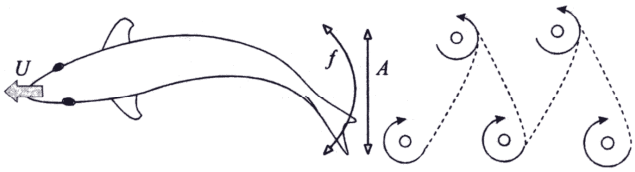

The wake of a swimming fish has reverse rotational direction, associated with thrust generation

The diamond pattern

- Forward flow velocity between two fish wakes
- Save energy by reducing thrust

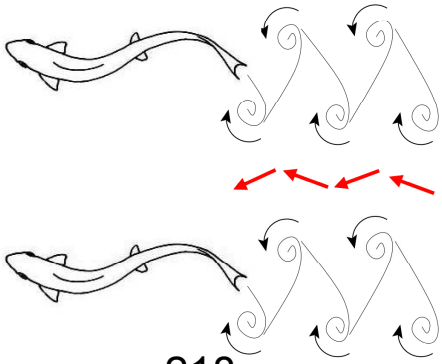

The diamond pattern

- Forward flow velocity between two fish wakes
- Save energy by reducing thrust

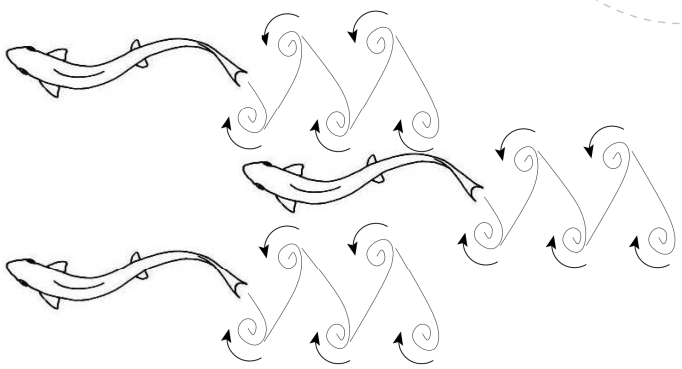

The diamond pattern

- Forward flow velocity between two fish wakes
- Save energy by reducing thrust

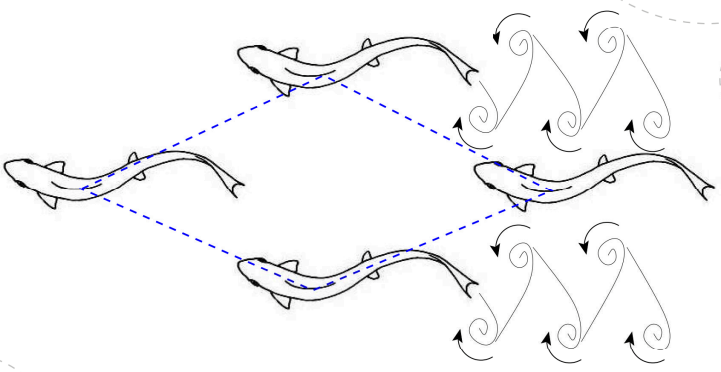

www.ntnu.no D. Kristiansen, Fish hydrodynamics

Strouhal number for a fish

$$St = \frac{Af}{U}$$

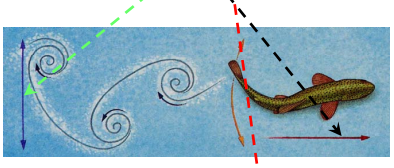

The tail beat frequency

Triantifyllou et al,1995

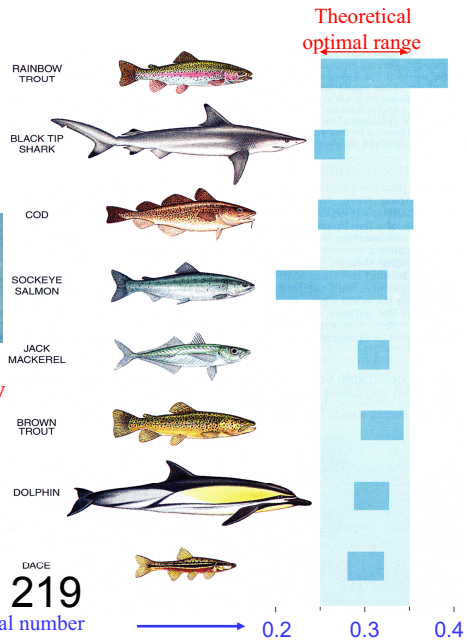

Current loads on a ship

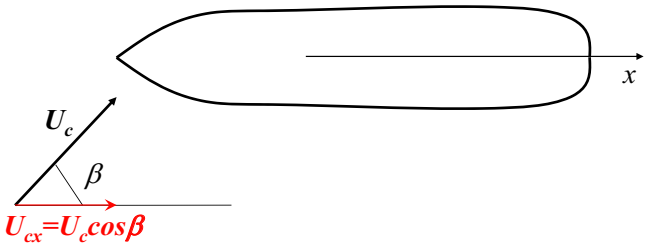

Resistance of sand - roughened plate with length L and roughness height k

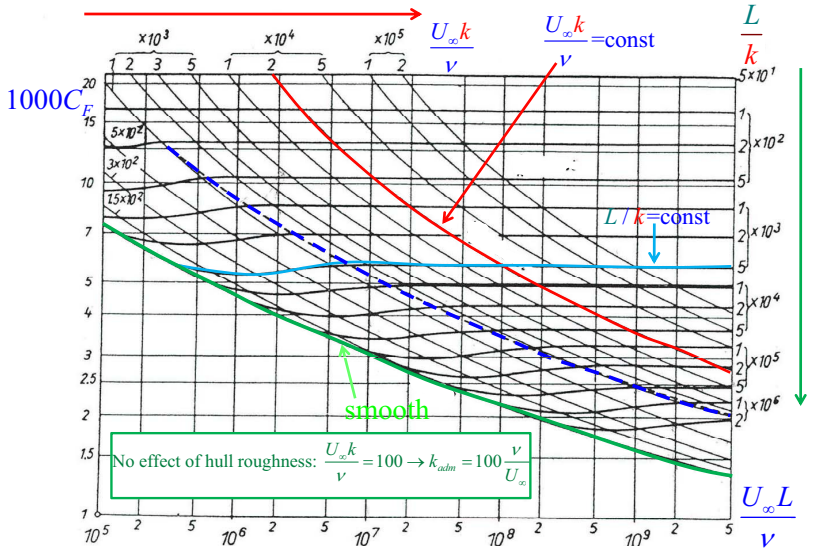

Smooth hull surface

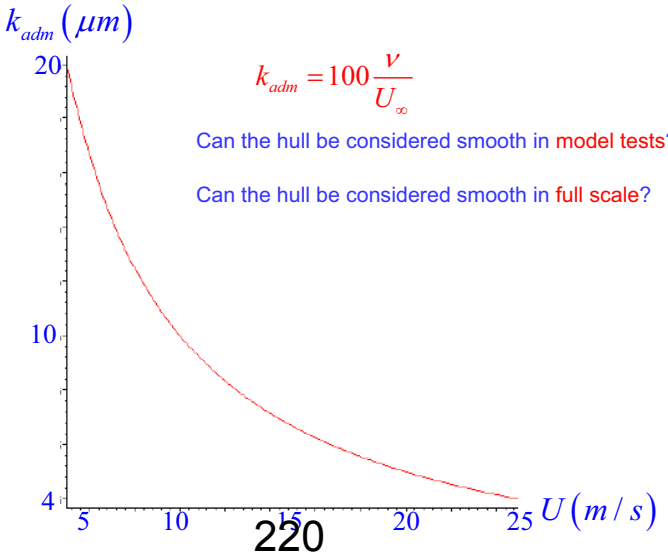

Roughness effects of submerged hull

Empirical formula by Bowden and Davison (1974):

$$10^3 \Delta C_F = 44\left[\left(AHR / L\right)^{1/3} - 10Rn^{-1/3}\right] + 0.125$$

It accounts for correlation between model and full scale as well as average hull roughness AHR (here in meters).

For newly built ships: $75\mu m < AHR < 150\mu m$

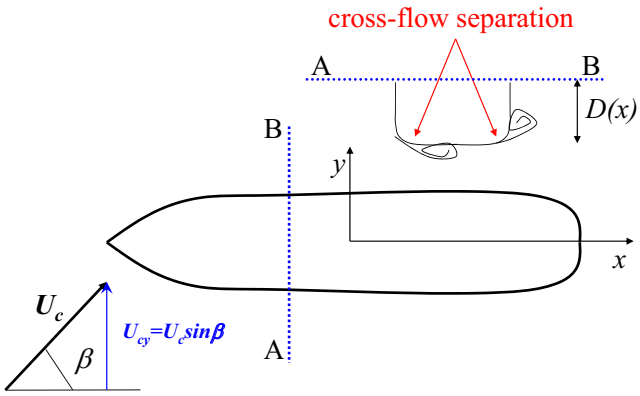

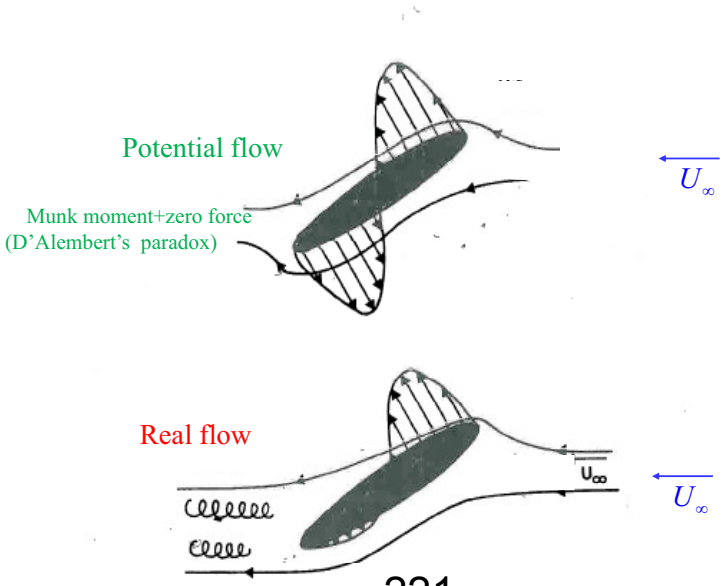

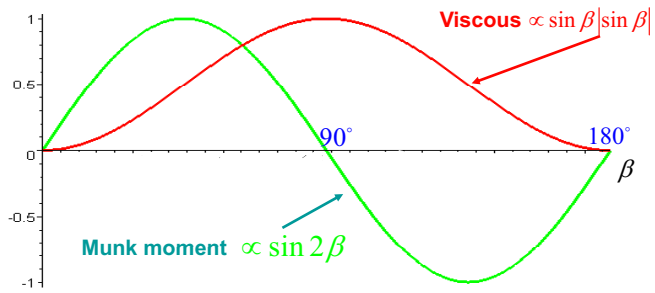

Transverse current force on a ship

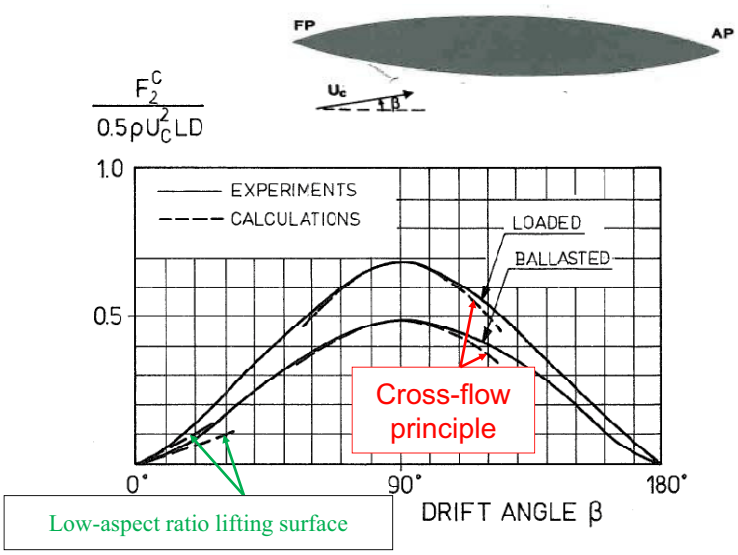

Yaw moment on a ship due to current

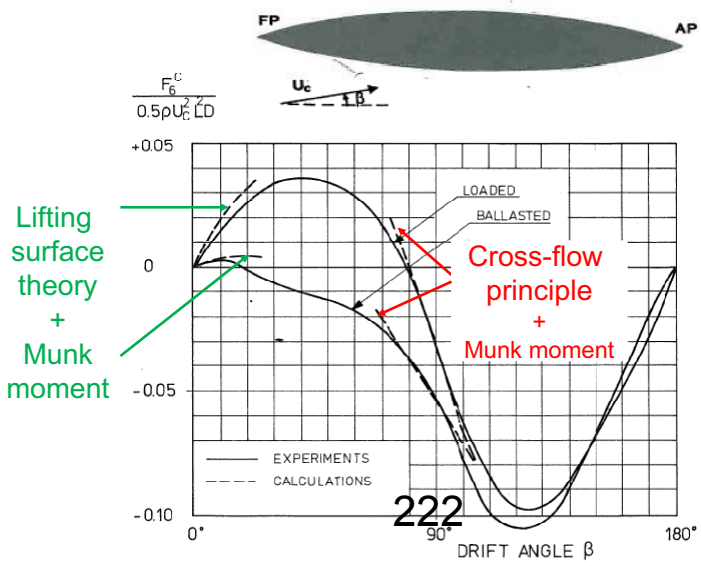

Yaw moment on a ship due to current

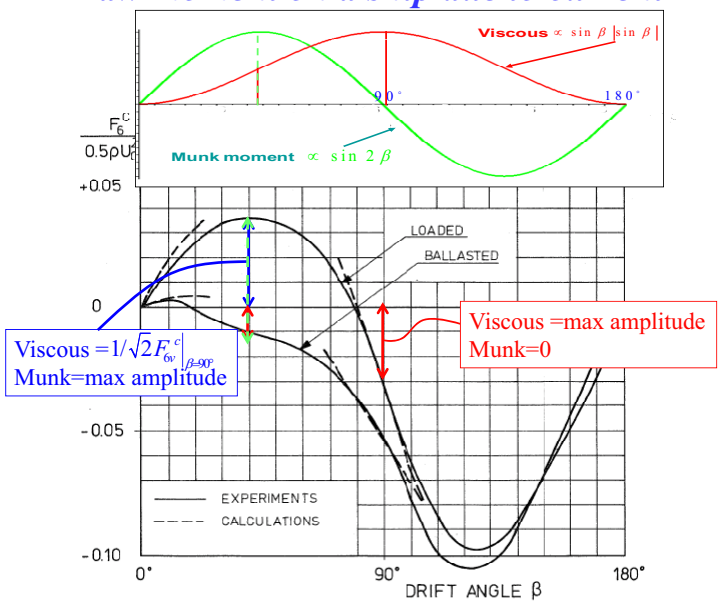

Application of low-aspect ratio lifting surface theory to the hull for small β

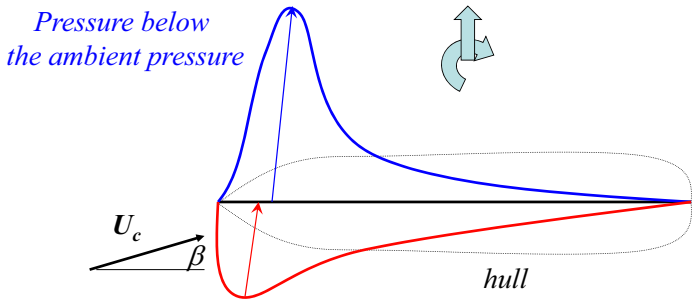

Zig-zag maneuvering of a ship from CFD

Axial vorticity due to cross-flow separation.

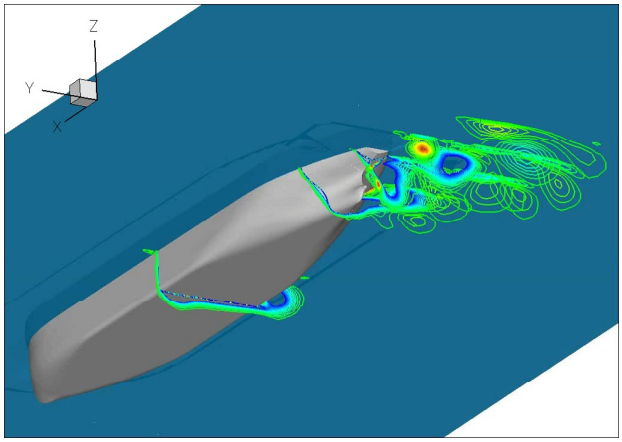

Reynolds number dependence

Broglia, Di Mascio & Muscari (2006)

44. Parameter analysis for C_D of ships. Current loads on offshore structures. Wind loads. Vortex-induced resonance oscillations. (F: 191-197,200-212)

Parameter analysis for C_D of ships (F:191-197)
Hp: A current U_c with a direction β with respect to the ship longitudinal axis, say x.

The sectional drag coefficient $C_D(x)$ in the expressions of the current viscous transverse force and yaw moment F_2^c and F_{6a}^c is affected by several factors:

1) free-surface effects
2) beam-draught ratio effects
3) bilge radius effects
4) bilge keel effects
5) Reynolds number effects, i.e. laminar or turbulent flow effects
6) 3D effects

To analyse factors 1 to 5 we will consider the 2D problem in the cross-sectional plane with uniform current U equal to the transverse current component $U_c \sin\beta$.

1. Free surface effects:
Hp: Calm water, i.e. no incident waves. Steady conditions. No viscous effects on the free-surface.

The combined free-surface boundary condition is

$$\left(\underbrace{\frac{\partial}{\partial t}}_{\text{steady conditions}} + \underbrace{U}_{=U_c \sin\beta} \frac{\partial}{\partial x} \right)^2 \phi + g \frac{\partial \phi}{\partial z} = 0 \quad \text{at } z = 0 \quad \underbrace{\Rightarrow}_{\substack{\text{nondimensional} \\ \text{variables}}} \quad Fn^2 \frac{\partial^2 \phi'}{\partial x'^2} + \frac{\partial \phi'}{\partial z'} = 0 \quad \text{at } z' = 0 \qquad (1)$$

As we have seen, $Fn = U/\sqrt{gL}$ associated with current is typically small, so
→ equation (1) leads to $\partial\phi/\partial z \cong 0$ at $z = 0$
→ the free surface acts as a rigid wall, i.e. as an infinitely long splitter plate
This leads to a smaller drag coefficient.

Why is this so?
Using the mirroring about the rigid wall in z=0, the problem is equivalent to a double body in infinite fluid with symmetric vortex shedding. Indeed the physical vortices shed from the body (below the free surface) are paired by 'image' vortices above the free surface and symmetric with respect to z=0. The image vortices have identical strength magnitude $|\Gamma(t)|$ as the physical vortices but with opposite sign (**NB:** the strength of the vortices corresponds to the circulation). This ensures zero vertical flow speed at $z=0$ as required by the rigid wall (see figure below).

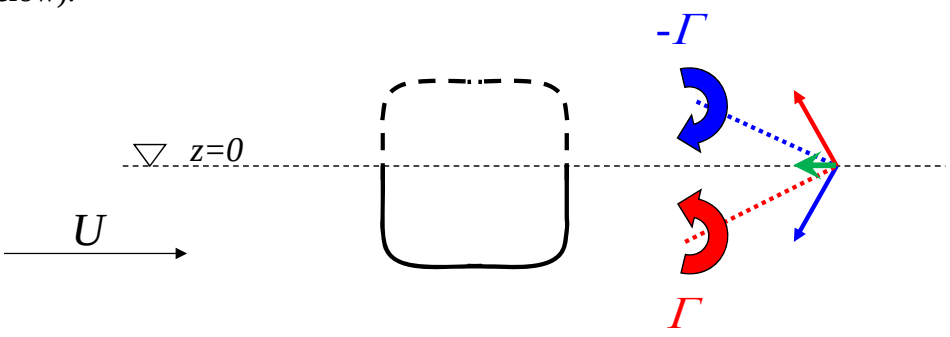

If the same double body geometry was in a steady current in a real infinite fluid, i.e. without free surface, the symmetric shedding would be unstable and a von Karman wake with alternate vortex shedding would occur. This means that the free surface has a strong influence because it is able to maintain stable a symmetric vortex shedding while without the free surface the vortex shedding would become alternate. This fact reduces the drag, because the symmetric vortex shedding leads to a smaller drag than an alternate vortex shedding.
→ All these aspects mean that the free-surface effects matter in the case of a steady current.

In this framework, the use of splitter plates to reduce the drag has been investigated. Hoerner (1965) examined the C_D-values for bodies with splitter plates of finite length in steady incident flow. His results confirm that a splitter plate causes a clear reduction of the drag coefficient.

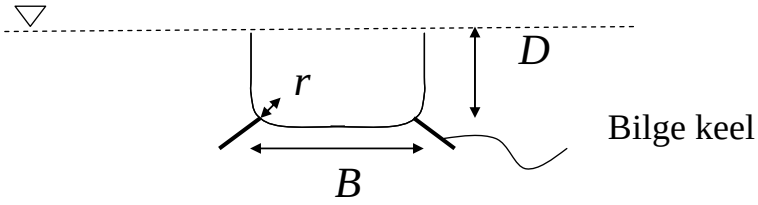

2. Beam-draught ratio effects:
Experiments by Tanaka et al. (1982) show a little effect of *B/D* with the exception of small *B/D.* In the case of a midship cross-section, this means a small effect if *B/D>0.8*, the reason is that as *B* increases relative to *D* is like going toward a flat plate geometry and shear stresses will play the main role while the presence of a draught will be less and less important.

3. Bilge radius effects:
Experiments by Tanaka et al. (1982) show a strong effect of the bilge radius. As *r* increases the drag coefficient decreases because the vortex shedding becomes less intense. The link is exponential

$$C_D = C_1 e^{-kr/D} + C_2$$

where C_1 and C_2 are two positive constants of similar magnitude and *D* is the draught. An example of *k* value is 6.

4. Bilge-keel effects:
These effects are strong due to the inviscid separation which always occurs and increases the drag coefficient with respect to the case without bilge keels. The drag coefficient is not very sensitive to the breadth of the bilge keel.

NB: The flow separation at the bilge keels occurs due to the geometric singularity, so the separation points are not scale dependent. Because the bilge keels are typically centered midships with a length half of the ship length, their presence avoids the serious problems connected with scaling of the transverse current force from model to full scale, while there is an uncertainty for the yaw moment.

5. Laminar/turbulent flow effects:
Where/if there are no bilge keels, the separation is usually dominated by viscous effects and depends on *Rn*. Aarnes (1984) has studied the 2D cross-flow past ship cross-sectional forms and calculated the drag coefficient. He showed that:

- C_D can be greatly different depending on laminar or turbulent separation. This is shown by figure F:6.16 in terms of the drag coefficient along the ship in subcritical (laminar separation) and transcritical (turbulent separation) flow. From the results, the transcritical flow regime leads to a lower drag coefficient.

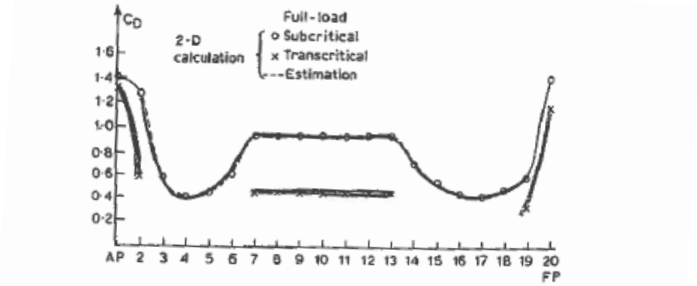

Fig. 6.16. Calculated and estimated drag coefficients C_D for two-dimensional cross-flow past cross-sections along the ship presented in Fig. 6.15. (Adapted from Aarsnes *et al.*, 1985.)

- The reason for the smaller drag coefficient in turbulent flow is analysed by figures F:6.17 and F:6.18 showing the time evolution of the flow separation at the midship cross-section.

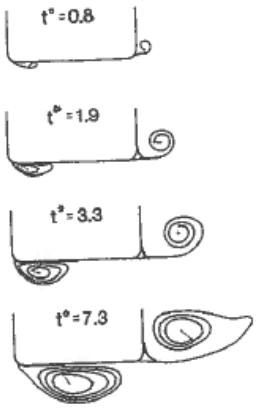

Fig. F:6.17 $Rn<Rn_{crit}$

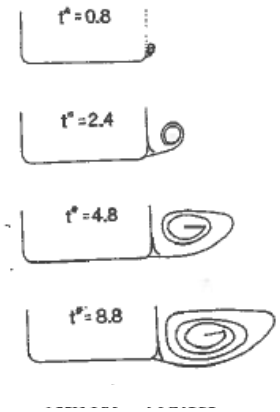

Fig. F:6.18 $Rn>Rn_{crit}$

In subcritical conditions: two large vortical structures detach from the leading and trailing edges. In transcritical conditions: the leading-edge vortical structure has disappeared. So, if the flow is laminar, the boundary layer (BL) tends to separate both at the leading and trailing edges of the ship cross-section. If the flow is turbulent the BL may sustain better adverse pressure gradients and remain attached at the leading edge due to the greater fluid-momentum exchange.

When flow separation occurs at the two corners roughly the drag coefficient is twice the drag coefficient obtained when flow separation occurs only at one corner.
These aspects lead to important scale effects if at model scale the flow is laminar while at full scale the flow is turbulent. When separation occurs from sharp corners one would expect less severe scale effects.
As already mentioned, the reason of the scale effects is that the examined flow separation depends on viscous effects and so on *Rn*. We have no scale effect if the Reynolds numbers at model and full scale are equal, i.e.

$$Rn_m = Rn_f \Rightarrow \frac{U_m L_m}{\nu_m} = \frac{U_f L_f}{\nu_f} \underbrace{\Rightarrow}_{\nu_f = \nu_m} U_m = U_f \frac{L_f}{L_m} \qquad (1)$$

Here the subscript 'f' stands for full scale and 'm' for model scale. In reality this does not occur because Froude scaling is used in the model tests, i.e.

$$Fn_m = Fn_f \Rightarrow \frac{U_m}{\sqrt{gL_m}} = \frac{U_f}{\sqrt{gL_f}} \Rightarrow U_m = U_f \sqrt{\frac{L_m}{L_f}} < U_f \quad (2)$$

and this implies

$$\frac{L_m U_m}{\nu} \underbrace{=}_{\text{using eq.(2)}} \frac{L_m U_f}{\nu} \sqrt{\frac{L_m}{L_f}} = \frac{U_p L_f}{\nu} \left(\frac{L_m}{L_f}\right)^{3/2} \Rightarrow Rn_m < Rn_f$$

It means that in the model tests *Rn* could be in the subcritical regime while in full scale it is typically in transcritical regime. This means that the experimental results could be qualitatively different than in full scale. To overcome this problem, turbulence stimulation is used in model tests.

6. 3D effects:

Aarnes (1984) pointed out that 3D effects associated with the edges of the ship reduce the drag coefficient with respect to the 2D cross-sectional estimations.

To see this let us consider the case with a transverse current U_c. The flow separation at the two edges causes two eddies. The shed vortical structures induce a velocity in x direction opposite to the incident current. The induced velocity is shown in the right plot of the figure below. The vortical structure at each edge of the ship is approximated as a vortex point centered.

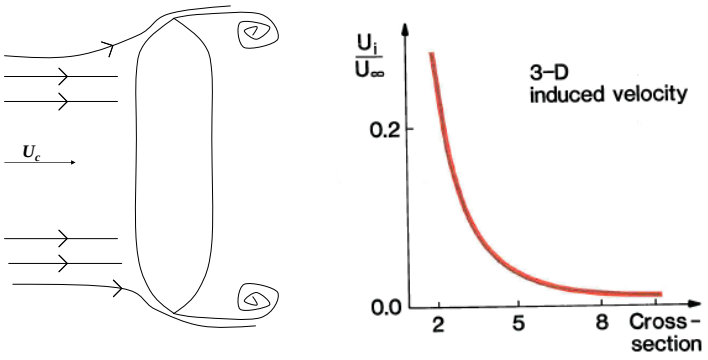

The velocity induced by the vortices is large only in their vicinity and goes to zero far from them. This means that near the edges we must consider a smaller effective inflow velocity, say $v < U_c$. This leads to a reduction of the drag force because the forces on the cross-sections near the ship edges are proportional to v^2. As a result, since the drag coefficient is made nondimensional by a term proportional to U_c^2, i.e. to the square of the incident-current speed, the reduction factor of the drag coefficient is v^2/U_c^2 (see figure F:6.20).

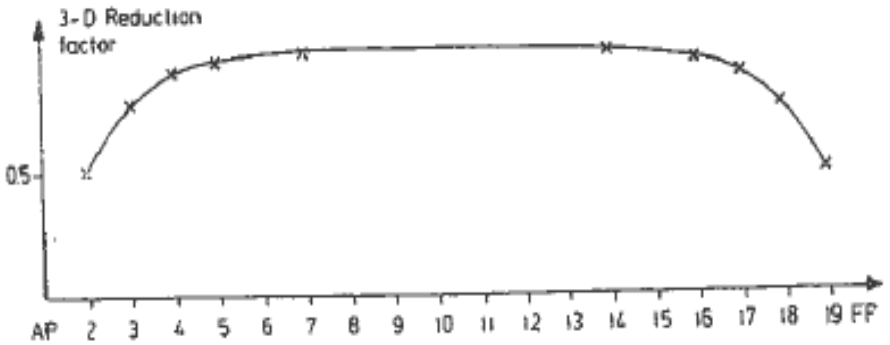

Fig. 6.20. Three-dimensional reduction factor of local drag coefficient due to the vertical vortex system at ship ends described in Fig. 6.19. (Adapted from Aarsnes *et al.*, 1985.)

Current loads on offshore structures (F:200-206)
What discussed for ships can be extended to offshore structures that consist of slender structural parts.
Examples are: risers, cables, columns and pontoons of semisubmersibles and TLPs.
We consider a current U_c and, also in this case, we can assume that:

- its longitudinal component causes only shear forces which can be calculated as done for the longitudinal drag forces on a ship.
- its transverse component causes flow separation. The forces in a cross-section due to flow separation can also be calculated similarly as done for the ship.

In the following we focus on the loads caused by the transverse current component U_N.

Hp: A slender structure and a steady incident current U_c, as in the figure below. The flow is assumed nearly 2D in the cross-sectional plane→strip theory can be applied

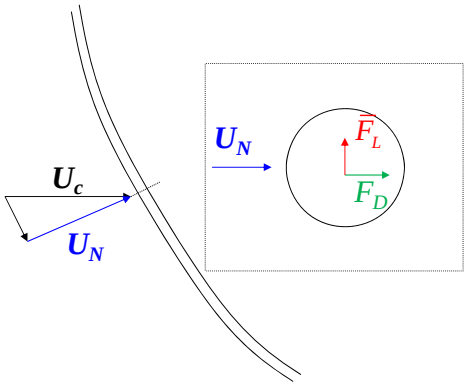

The mean (i.e. constant in time) force per unit length (i.e. the cross-section mean force) is in general characterized by two components: one in-lined and one orthogonal to U_N, which can be expressed, respectively, as

$$F_D = \frac{\rho}{2} C_D D U_N^2 \quad \text{(F:6.47)}$$

$$\bar{F}_L = \frac{\rho}{2} \bar{C}_L D U_N^2 \quad \text{(F:6.48)}$$

Here D is a characteristic cross-sectional length (e.g the diameter for a circular cylinder).
For a circular cylinder we have seen that $\bar{F}_L = 0$. In general, the mean lift force is zero in the case of any single body symmetric about the current direction and in infinite fluid. Otherwise $\bar{F}_L$ can be non-zero.
Coefficients C_D and $\bar{C}_L$ must be determined empirically. Major parameters affecting them are the same as for the drag coefficient for ships, in addition one must consider the influence of hydrodynamic interactions between structural elements.

Wake interaction effects:
Hp: A uniform current past a 2D circular cylinder centered at x=0 and y=0 (see figure below).

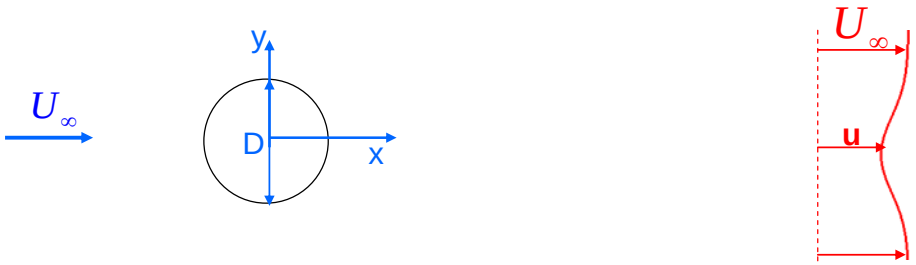

We briefly discussed the wake interaction effects using the von Karman wake, i.e. approximating the shed vortices as point vortices. Here we do not make this approximation but apply to the cylinder the wake solution downstream of a 2D body as given by Schlichting (1979). In this case, the mean wake velocity component u in the direction of the free stream U_∞ at a point (x,y), with x and y, respectively, the longitudinal and transversal distance from the cylinder, can be written as

$$u = U_\infty \left[1 - 0.95 \sqrt{\frac{C_D D}{x}} e^{-\eta^2/4} \right] \quad \text{(F:6.49)}$$

$$\eta = y / \sqrt{0.0222 C_D D x} \quad \text{(F:6.50)}$$

Here C_D is the drag coefficient of the cylinder. This expression is a good approximation of u if $x/(C_D D)>50$, i.e. it is a long-distance approximation. However, Blevins considered a fictitious origin placed $6D$ upstream of the cylinder and applied this formula for smaller distances x from the cylinder. He found good results.

Now let us place a second cylinder in the wake of the cylinder, i.e. centered at $x=l$ and $y=0$. Using expressions (F:6.49+6.50), the local inflow velocity of the downstream cylinder is

$$u = U_\infty \left[1 - 0.95 \sqrt{\frac{C_D D}{l}} \right] < U_\infty$$

and its drag coefficient $C_D^{(2)}$ is smaller than the drag coefficient C_D of the upstream cylinder, i.e.

$$C_D^{(2)} = C_D \left(\frac{u}{U_\infty} \right)^2 = C_D \left[1 - 0.95 \sqrt{\frac{C_D D}{l}} \right]^2 \approx C_D \left[1 - 2 \left(0.95 \sqrt{\frac{C_D D}{l}} \right) \right]$$

$$= C_D - 1.9 C_D^{3/2} \sqrt{\frac{D}{l}}$$

For example if C_D =1 and l/D=100→ $C_D^{(2)}$ = 0.81. We understand that $C_D^{(2)}$ may even become negative if the downstream cylinder is sufficiently close to the upstream cylinder, but one must note that strictly speaking the applied formula is valid for sufficiently large distances between the two cylinders.
In a more general framework, if a structural element is in the wake of another one, the loads on it are not the same as if this element was isolated in infinite fluid. The element will be subjected to a lower local current u and this leads to a smaller drag coefficient because $C_D^{(2)}$ goes as $(u/U_\infty)^2<1$.

NB: Because the discussed wake solution is the solution of a linear problem, one can apply the superposition principle in the case of clusters of bodies. As an example, if we have a series of side-by-side circular cylinders we can consider the wake behind each of them. This will give a velocity reduction as in expression (F:6.49) and we can sum up the effects of all wakes to estimate the local mean longitudinal wake velocity.

Zdravkovich (1985) has studied the interaction of pipe clusters in steady incident flow.
For the case of 2 cylinders we can have 3 different possible regimes:

- proximity interference (P)
- wake interference (W)
- no interference

Figure F:6.24(a) gives the existence plane of these regimes for cylinders with equal diameter *D*. Only one cylinder is shown in the figure centered at *(0,0)*. The location *(x/D,y/D)* represents the position of the center of the other cylinder, *x/D>0* means downstream location.

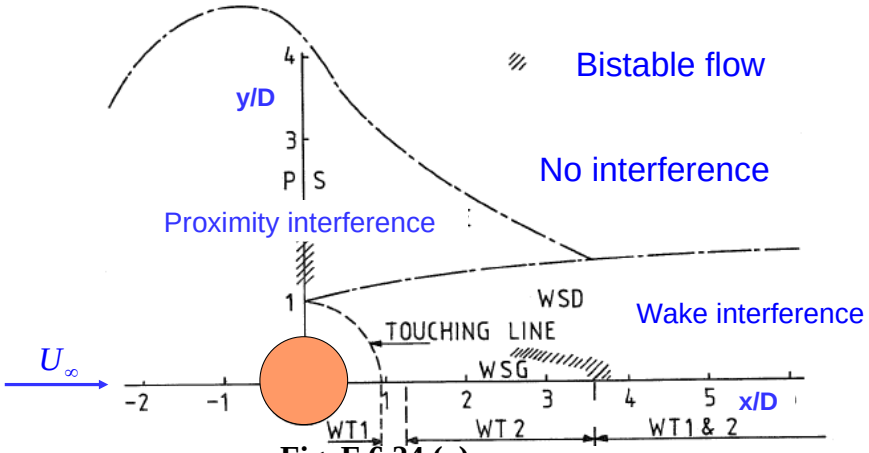

Fig. F.6.24 (a)

Wake interference occurs if one cylinder is in the wake of the other cylinder. Proximity interference occurs for sufficiently close cylinders but none in the wake of the other. No interference occurs when none of the cylinders is in the wake of the other and their distance is sufficiently large. In the figure, bistable flow indicates the positions of the second cylinder where two different vortex-shedding solutions could be stable.

Figure F:6.24(b) gives examples of flow features in the different regions. In a side-by-side set, i.e. the second cylinder is at *(0,y/D)*:

- If $1 < y/D < 1.1-1.2$ there is only a single vortex street for both cylinders
- If $2.7 < y/D < 4-5$ there are 2 vortex streams mirroring each other.
- If $y/D >\approx 5$ the mutual influence of the cylinders is small.

In a tandem set, i.e. the second cylinder is at *(x/D,0)*:

- If $1 \le x/D < 1.2-1.8$ the vortex street behind the cylinders is given by the free-shear layer detached from the upstream cylinder
- If $1.2-1.8 < y/D < 3.4-3.8$ the free-shear layer from the upstream cylinder reattaches to the cylinder downstream.

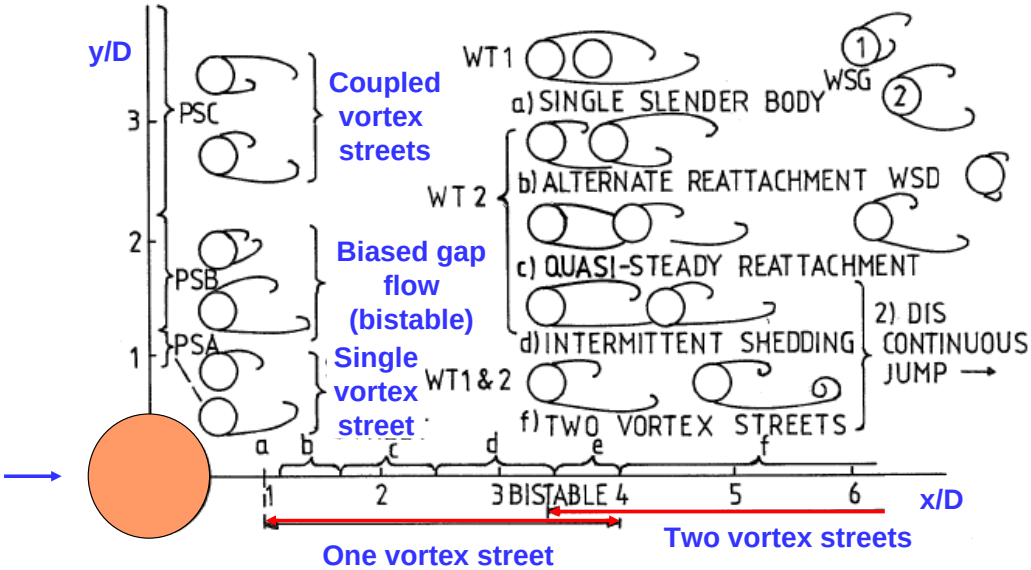

Fig. F.6.24 (b)

Figure 6.25 shows an experimental photo of vortex formation around two vertical cylinders in a close tandem arrangement in steady incident flow. The cylinders were towed in a model basin. The image shows that a vortex shed from the upstream cylinder can be trapped between the two cylinders.

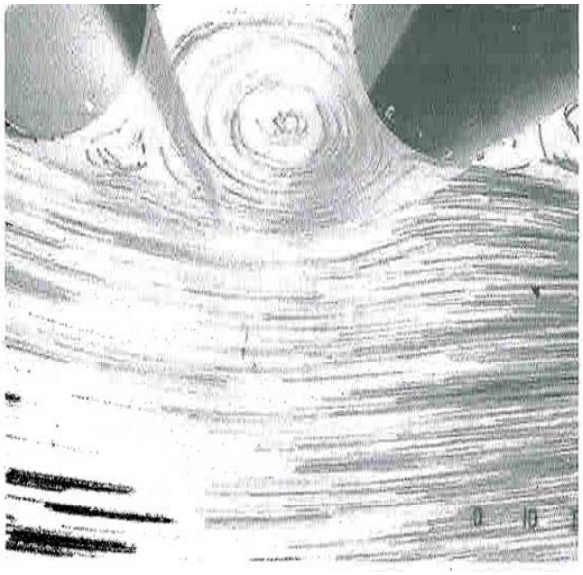

Fig. F.6.25

Zdravkovich (1985) studied the tandem configuration in subcritical and supercritical flow regimes. He found that if the cylinders are close, i.e. their distance is $x/D \lessapprox 4$, the drag coefficient may be negative on the second cylinder in a tandem position. The results depend on the Reynolds number, on the roughness ratio k/D and on the number of cylinders in the tandem configuration. The minimum drag coefficient reported is ≈-0.6.

These aspects are of practical importance in many contexts.

Example: fish farms.
The nets used in fish farms are similar to small cylinders, see figure below.

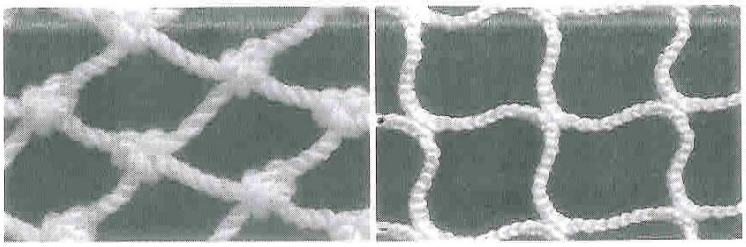

They can be placed in sequence in the case of a complex farm, as shown in the figure below.

In this case there is an inflow reduction when the current goes through successive nets. The reduction factor must be accounted for to ensure proper water exchange inside the nets. Figure above provides an estimation of the inflow reduction for the specific aquaculture-plant configuration using the long-distance approximation for the mean wake velocity in the longitudinal direction given by formula (F:6.49). This does not account for the effect of fishes inside the farm, e.g. the effect of fish schooling on the local current, but this could be important.

Wind loads (F:207)
Can be estimated similarly as for the current loads. Also in this case empirical/experimental data are necessary.

Vortex-induced resonance oscillations (F:207-212)
The current interaction with a blunt body causes alternate vortex shedding. For a circular cylinder the forces associated with alternate vortex shedding are

$$F_L(t) = |F_L| \cos(2\pi f_v t + \alpha) \quad \text{(lift)}$$
$$F_D(t) = \overline{F}_D + A_D \cos(4\pi f_v t + \beta) \quad \text{(drag)}$$

These forces may cause resonance problems: vortex induced oscillations. Strictly speaking, we talk about vortex induced motions (VIM) in case of rigid motions and about vortex induced vibrations (VIV) in case of elastic motions. In the following the VIV term is used to indicate both phenomena.
VIV is relevant for many slender marine structures: risers, spar platforms, pipelines, deep draft floaters, submerged bridges.

Important parameters for VIV are:

- Strouhal number $St = f_v D / U_c = D / (T_v U_c)$, which means the ratio of the characteristic length of the body (e.g. circular cylinder diameter) and the distance covered by the current during a vortex shedding period.
- Reduced velocity $U_R = U_c / (f_n D) = T_n U_c / D$, which means the ratio between the distance covered by the current during a natural period of the structure and the the characteristic length of the body (e.g. circular cylinder diameter).

NB: These definitions refer to the vortex-shedding and natural periods without VIV. As we will see, the occurrence of VIV changes in general T_n and T_v. To emphasize this, when necessary '0' will be used to indicate the variables in absence of VIV.

We can have VIV in two orthogonal directions, called respectively:

- cross-flow VIV, in the lift direction (transverse to the current, say *y*) and
- in-line VIV, in the drag direction (parallel to the current, say *x*)

Roughly speaking, we have cross-flow VIV when the oscillation period of the lift force, T_v, is equal to the transverse natural period. We have in-line VIV when the oscillation period of the drag force, $T_v/2$, is equal to the in-line natural period. These conditions are just indicative of where we are to have VIV. Actually VIV occurs in a broader range.

The cross-flow VIV is associated with larger oscillation amplitudes and larger reduced-velocity values than the in-line VIV. U_R is larger because the lift force oscillates with a period twice the oscillation period of the drag force. It means that cross-flow VIV is usually more critical and relevant for ultimate strength design.
In-line VIV is relevant for fatigue, because it involves smaller U_R which means higher natural frequencies, i.e. large number of oscillation cycles in time.
We discuss here the VIV phenomenon in terms of cross-flow VIV. All examples consider an academic uniform current.

1. Excitation of cross-flow VIV
Hp: A moored loading buoy in a current with speed U_c in x direction. The buoy is a vertical cylinder, long L, with diameter $D<<L$.

As rough condition we can say that cross-flow VIV occurs if T_v is equal to the sway ($y \perp U_c$) natural period, say T_n, of the structure. Again, this condition is only indicative, as we will discuss later, cross-flow VIV occurs in a broader range because it is able to change the vortex-shedding and natural periods. The consequences of cross-flow VIV are large vortex-induced sway oscillations and drag-forces.

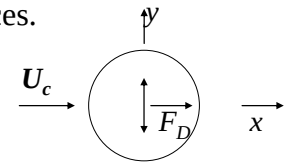

These aspects are of practical importance for instance for mooring systems. In particular anchor-line excursions and drag forces experienced due to interaction with a current are important for the correct design of the mooring system.

In our example, the vortex shedding period can be found from

$$T_v = \frac{1}{St}\frac{D}{U_c} \quad (1)$$

Let us assume U_c=1m/s and D=20m, while the Strouhal number can be obtained from Fig. F:6.26 in terms of the Reynolds number and of the roughness. The figure is for a fixed cylinder in steady incident flow.

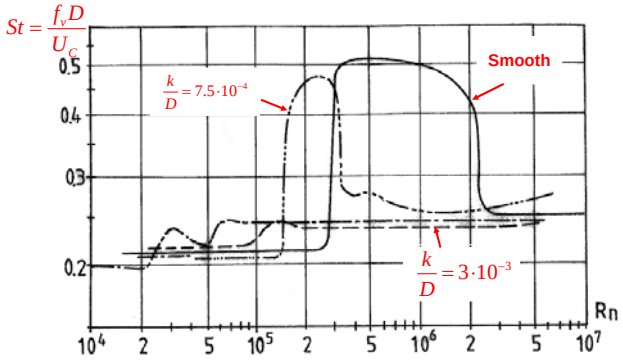

Fig. F:6.26

The Reynolds number in our case is $Rn \cong 2 \cdot 10^7$ and assuming a rough cylinder, for instance with $k/D \cong 3 \cdot 10^{-3}$, we obtain:
→ $St \cong 0.25$ from
→ T_v=80s.
This must be then compared with T_n.

NB: When performing model tests the Reynolds number is smaller. This leads to scale effects which affect the separation point location, the wake features, the body forces, the vortex-shedding frequency f_v. If the *Rn* is in the critical or supercritical flow regime and the cylinder behaves as smooth, the Strouhal number *St* will have a large variation depending on the roughness (see fig. F:6.26) but this is a false effect because at full scale the *Rn* number could be in transcritical flow regime. A model-scale *St* different than at full scale means a model-scale f_v different than at full scale. One way to avoid this effect is to use a greater roughness in model tests, i.e. larger than in reality, in this way *St* values are more reasonable.

Vortex-induced oscillations may cause elastic resonant oscillations of the 3D structure. Roughly speaking this occurs if the vortex-shedding period $T_v=f(St,D,U_c)$ is equal to an eigenperiod T_n of the structure.

Hp: A riser in a current with speed U_c.
Let us assume U_c=1m/s and D=1m. This leads to a Reynolds number $Rn \cong 8\cdot10^5$ and considering a rough cylinder so that St=0.25 we can then estimate the vortex-shedding period as T_v=5s.
The example in figure F:6.28 refers to a family of risers with the same features but for the length because they are attached to the sea floor at different water depths *h*. The same top tension 1250 kN is applied for all risers. The natural periods T_n (with n=1,2,..) of a riser depend on the riser length and so on the water depth. This leads to the curves in the figure. The horizontal dashed line represents T_v=5s.

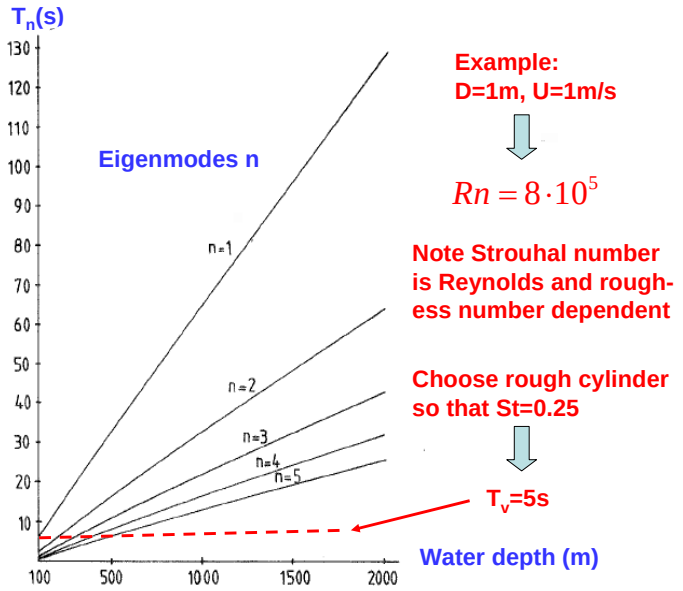

Fig. F:6.28

Resonance occurs at the intersection of this horizontal line with a natural-period curve. So, this value of the vortex-shedding period can cause resonance for certain modes at certain water depths. Other realistic current speeds could cause resonance on the same modes at different water depths and on different modes at the same water depth because would lead to different values of T_v.
In connection with such elastic resonance phenomena we talk about hydroelastic oscillations, because the elastic oscillations are affected by the flow and affect in return the flow, i.e. there is a coupling between structural and hydrodynamic problems. One must also note that VIV involves nonlinear behaviour of the system.

2. Cross-flow VIV affects the vortex-shedding frequency

Feng (1986) performed experiments for a current past a lightly damped 2D circular cylinder free to oscillate transversally in infinite fluid. The model tests were made in air.

We have three frequencies involved in this problem: the oscillation frequency of the cylinder f_c, the natural frequency of the cylinder f_n and the vortex-shedding frequency f_v.

Fig. F:6.29 shows f / f_n, with $f = f_c$ or $f = f_v$, and the transverse oscillation amplitude A as a function of the reduced velocity $U_R = U_c / (f_n D)$.

Due to the current-cylinder interaction vortex shedding is caused:

- If we assume small U_R, the vortex-shedding frequency of the cylinder f_v is equal to the value for a stationary cylinder $f_{v0} = StU_c / D = f_n StU_R$, which increases linearly with U_R. This remains true up to when f_{v0} becomes close to f_n, i.e. up to $U_R \approx 1/St \approx 5$ (in subcritical flow regime St=0.2).
- When f_{v0} becomes close to f_n, cross-flow VIV occurs, i.e. resonant vibrations of the cylinder caused by vortex shedding in the direction transverse to the current. Moreover, in this circumstance also the oscillation frequency of the cylinder, say f_c, is close to f_n. If we continue to increase U_R, f_v / f_n and f_c / f_n remain nearly constant and slightly less than unity. This occurs until an upper threshold value of the reduced velocity, say $U_R \approx 7$. For $U_R >\approx 7$, f_v jumps suddenly back to the value for the stationary cylinder f_{v0}.

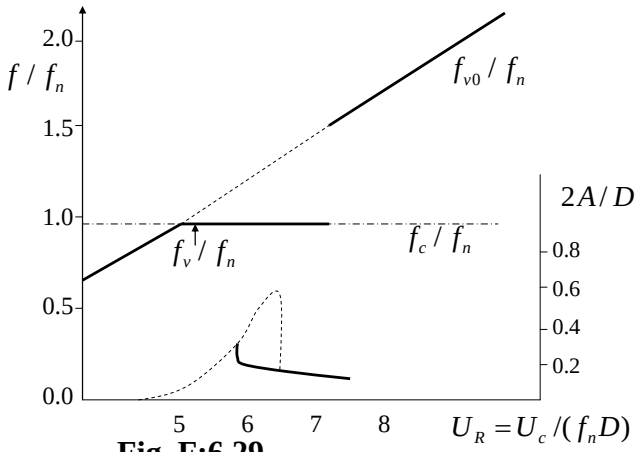

Fig. F:6.29

The region $5 \le U_R \le 7$ where cross-flow VIV occurs is referred to as lock-in region because the vortex shedding frequency locks on the natural frequency of the body. It is also called synchronization region, capture region, or resonance region. In the lock-in region, the amplitude A of transverse oscillations increases greatly with U_R until a maximum. For higher U_R it drops suddenly and then decreases with U_R. If we start from high values of U_R and decrease it down to the lock-in region, the amplitude A will follow the solid line in figure F:6.29 and then continue along the dashed line at the end of the solid line. This means that A increases less when starting from large U_R and decreasing it than when starting from small U_R and increasing it.

NB: This example confirms that **VIV affects** f_v and shows that $f_{v0} = f_n$ or $U_R = 1/St$ **is a rough condition for cross-flow VIV occurrence**. This must be just taken as an indication of where we are for VIV occurrence, especially in water, because in water the extension of lock-in region is larger than in air.

3. Cross-flow VIV in water affects the natural frequency

Hp: A current past a 2D circular cylinder in infinite water**.** The cylinder has a spring *C* and no structural damping. Free transverse oscillations of the cylinder.

The previous example was in air, when the fluid is water the added mass is relevant. This is analysed here.

The natural frequency without VIV is obtained from the one d.o.f. motion equation setting to zero the excitation force, i.e.

$$(m + A_{22}^{(noVIV)})\ddot{y} + Cy = 0$$

$$\Rightarrow f_{no} = \frac{1}{2\pi}\sqrt{\frac{C}{m + \rho\pi D^2/4}}$$

Hp: *St*=0.2 (subcritical regime).

A condition for VIV occurrence is given by $U_R = 1/St = 5$ which means $f_v = f_{n0}$. This gives an indication, because VIV will occur within a certain range of U_R, i.e. also for U_R<5.

NB: According to DNV rules, onset for VIV is U_R=3-5, the upper limit is U_R=16.

When VIV occurs, the amplitude of oscillations varies much, see figure below, leading to a variation in added mass.

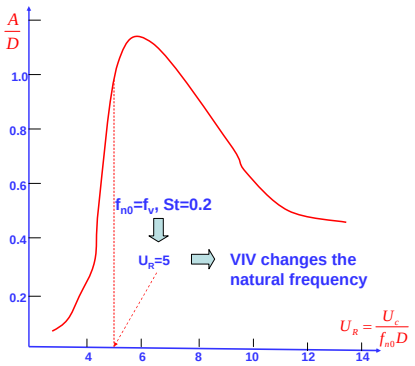

From the figure above, the lock-in region, corresponding to important increase of the amplitude, is wider than in fig. F:6.29. The reason is that in water the added mass plays an important role and will make broader the possibility of VIV excitation with respect to the case in air where the added-mass effects are negligible.

With VIV we may formally write the added mass as

$$A_{22} = C_a A_{22}^{(noVIV)}$$

C_a giving the variation of the added mass. This means that the natural frequency is now

$$f_n = \frac{1}{2\pi}\sqrt{\frac{C}{m + C_a A_{22}^{(noVIV)}}}$$

So, when VIV occurs, both f_v and f_n change. The constraint is that they remain roughly equal, i.e. $f_v = f_n$, during VIV, i.e.

$$\frac{f_n(=f_v)}{f_{n0}} = \sqrt{\frac{m + A_{22}^{(noVIV)}}{m + C_a A_{22}^{(noVIV)}}} \underset{\bar{M}=mass\ ratio=m/A_{22}^{(noVIV)}}{=} \sqrt{\frac{\bar{M}+1}{\bar{M}+C_a}} = \frac{StU_c}{Df_{n0}} = 0.2U_R$$

which means that $C_a = f(U_R)$.

These conditions could be reproduced (e.g. experimentally) to estimate the effect of VIV on the natural period.

4. Cross-flow VIV oscillation amplitude

Hp: A current past a 2D circular cylinder in infinite water**.** The cylinder has a spring *C* and no structural damping. Forced transverse oscillations of the cylinder.

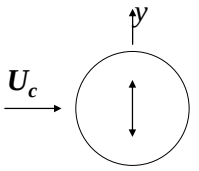

$$y = A\sin(\omega t) \quad \omega = 2\pi f$$

Due to the oscillations a lift force is caused. The lift coefficient can be written as

$$C_L = \frac{F_L}{0.5\rho U_c^{\,2} D} \underset{formally\ we\ may\ write}{=} C_{mh}\sin\omega t - C_{dh}\cos\omega t = -C_{mh}\frac{\ddot{y}}{A\omega^2} - C_{dh}\frac{\dot{y}}{A\omega}$$

C_{mh} and C_{dh} are proportional, respectively, to the added mass and damping and depend on *A/D* and *U/fD*.

If the oscillations were free instead of forced, the lift force would be the excitation force in the body motion equation, i.e.

$$(m + A_{22}^{(noVIV)})\ddot{y} + Cy = F_L = 0.5\rho D U_c^{\,2}\left(-C_{mh}\frac{\ddot{y}}{A\omega^2} - C_{dh}\frac{\dot{y}}{A\omega}\right)$$

$$\Rightarrow (m + C_a A_{22}^{(noVIV)})\ddot{y} + C_{dh}\rho D U_c^{\,2}\frac{\dot{y}}{2A\omega} + Cy = 0 \qquad (1)$$

with

$$C_a = 1 + \frac{0.5\rho D U_c^{\,2} C_{mh}}{A\omega^2 A_{22}^{(noVIV)}}.$$

According to the sign of C_{dh} in the motion equation (1) the damping can be positive (C_{dh}>0) or negative (C_{dh}<0).

Positive damping reduces the oscillation amplitude ←→ energy from the body to the fluid
Negative damping increases the oscillation amplitude ←→ energy from the fluid to the body
Zero damping gives resonance condition ←→ no energy exchange

NB: Using potential flow theory, we have seen that the radiation damping due to forced oscillations of the body will never be negative. Here we see an example where the interaction with a current can lead to negative damping.

The resonant steady-state condition gives:

$$f_n = \frac{1}{2\pi}\sqrt{\frac{C}{m + C_a A_{22}^{(noVIV)}}} \qquad C_{dh} = 0$$

This is the condition for lock-in/VIV because it means that the system energy remains constant.

We can identify the occurrence of VIV for instance reproducing these conditions experimentally:

1. We can study forced oscillations and vary the forced oscillation frequency and the forced oscillation amplitude ratio *A/D*.
2. For each combination we can measure C_L. Using its decomposition in sine and cosine functions, we can estimate C_{mh} and C_{dh}, respectively, from the component proportional to the acceleration and from the component proportional to the velocity, and then C_a.
3. In this way we can construct a family of C_{dh} iso-curves. The iso-curve $C_{dh} = 0$ gives the resonance condition, i.e. the forced oscillation frequency f is $f = f_n$. *A/D* measured along $C_{dh} = 0$ provides the oscillation amplitude ratio *A/D* due to VIV.

The figure below gives an example of how to find *A/D* at resonance as a function of U_R.

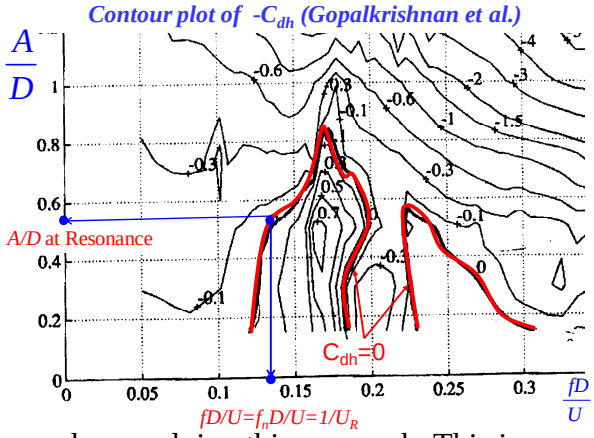

There is an error source when applying this approach. This is connected with the use of forced oscillations of the cylinder with a frequency of oscillation f in general $f \neq f_v$. This is the reason why the results of *A/D* obtained using forced and free oscillations may not coincide, as in the figure below (from C.M. Larsen's studies).

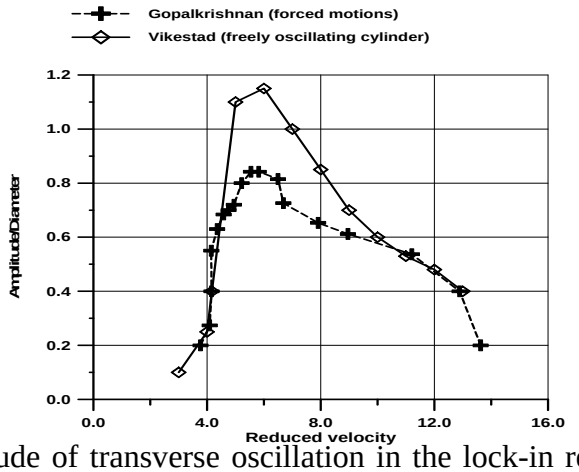

The maximum amplitude of transverse oscillation in the lock-in region depends also on the structure mode shapes. Sarpkaya (1978) studied the maximum amplitude A_{max} of the transverse oscillations in the lock-in range for both elastically-mounted and flexible cylinders. He wrote the maximum amplitude for any mode shape $\psi(z)$ as

$$\frac{A_{\max}}{D} = \frac{0.32\gamma}{\sqrt{0.06 + \Delta_r{}^2}} \quad \text{(F:6.54)} \;,\; \gamma = \psi_{\max}\sqrt{\frac{\int_L \psi^2(z)dz}{\int_L \psi^4(z)dz}} \quad \text{(F:6.55)} \;,\; \Delta_r = (2\pi St)^2 \frac{2m\zeta_s}{\rho D^2} \quad \text{(F:6.56)}$$

In this empirical formula, z is along the structure, L is the structure length and ζ_s is the fraction of the structural damping to critical damping, *St* is the Strouhal number for the non-oscillating cylinder, ρ is the fluid density and m is the sum of structural mass and added mass

per unit length. For marine applications Δ_r has small effect → we can set Δ_r=0. Once the mode shapes and A_{max} are known, we can estimate the stresses connected with cross-flow VIV. This is relevant for instance for risers.

5. Important consequences of Lock-in

Sarpkaya and Shoaff (1979) studied the lock-in region numerically using a discrete vortex method. According to their results, the lock-in consequences are

A. Correlation length of vortex shedding l_c increases → more relevant total loads on the 3D structure
B. Vortex strength increases
C. f_v locks onto f_n
D. The greater the amplitude A the wider the band width of lock-in in terms of reduced velocity
E. Oscillations are self-limiting, i.e. maximum relative amplitude $A/D \approx 1$
F. In-line (drag) force increases

Some of these consequences are linked:
- A and C are connected because, due to C, vortex shedding must be in phase with cylinder oscillations which can not vary rapidly along the cylinder for structural constraints. So the correlation length must increase.
- B and F are connected because the strength of vortices is linked to the circulation Γ in the wake and drag and lift forces are also linked to Γ (this can be shown using the Blasius theorem).

A rough estimate of the drag coefficient on a 2D circular cylinder during lock-in is:

$$C_D = C_{D0}[1 + 2A_{\max} / D]$$

which can be interpreted as the effect of an apparent projected area $D+2A_{max}$ (per unit length) with respect to D. See figure below:

Let assume A_{max} as the maximum oscillation amplitude in the cross-flow direction.

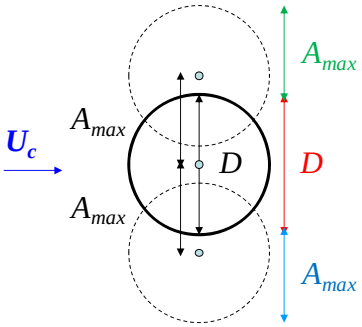

6. Cross-flow and in-line VIV

Cross-flow and in-line VIV can couple increasing the risks for the structure. It means that locally the cross-sections follow a '8' path with greater amplitude in the cross-flow direction.
Figure below gives an example of cross-flow and in-line VIV coupling, this application is relevant for instance for free-spanning pipelines.

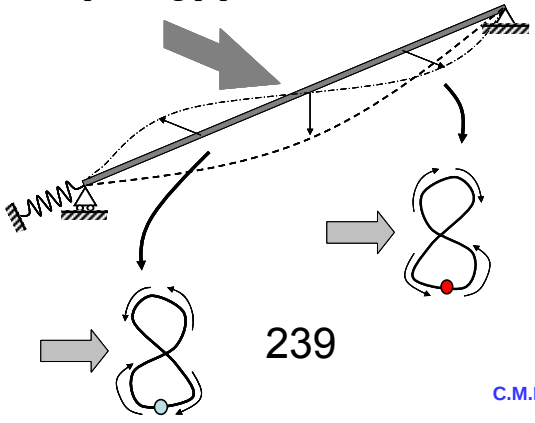

7. How to avoid VIV?

We can avoid VIV using spoilers which reduce the lift and increase the drag or by increasing the damping.

One can also try to ensure a reduced velocity outside the lock-in range. Taking the example of a submerged bridge. Cross-flow VIV could be avoided by design, enforcing that the reduced velocity $U_R = U_c / (f_{n0} D)$ is smaller than the threshold value to have lock-in. This means that in-line VIV can not be avoided because it occurs at smaller U_R than cross-flow VIV. However in-line VIV is connected with small oscillation amplitudes.

Common way to suppress VIV is to use helical strakes.
The optimal configuration it is said to be with three spirals and pitch equal to 5*D*, with *D* the structure diameter.
The height of the fins of the strakes should be 0.1-0.12 *D*.
A negative effect is that the fins increase the drag.

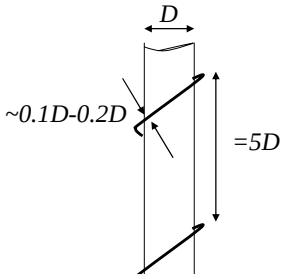

Munk moment versus Viscous moment

• The Munk moment is a pure torque, it comes from steady infinite potential flow with zero force from D'Alembert paradox
→It does not depend on a reference point
• It is destabilizing, i.e. It tends to increase the angle of attack β

For example, for the ship we studied in fig. F:6.13

• The viscous moment is a not pure torque
→It depends on the center of rotation
• It might be stabilizing or destabilizing depending on the body geometry

Current transverse viscous loads

$$F_2^c = \frac{1}{2}\rho U_c^2 \sin\beta\,|\sin\beta| \int_L C_D(x) D(x) dx$$

$$F_{6a}^{\ c} = \frac{1}{2}\rho U_c^2 \sin\beta\,|\sin\beta| \int_L C_D(x) D(x) x dx$$

Free-surface effects on C_D

Like a double body in infinite fluid with symmetric wake

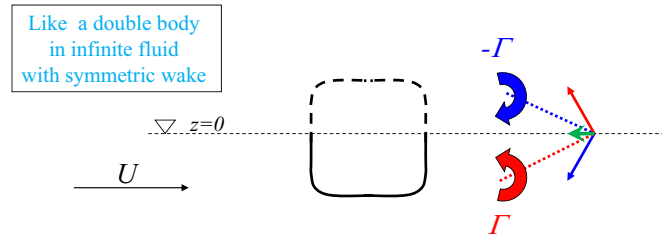

Hp: the double body in real infinite fluid, i.e. without free surface

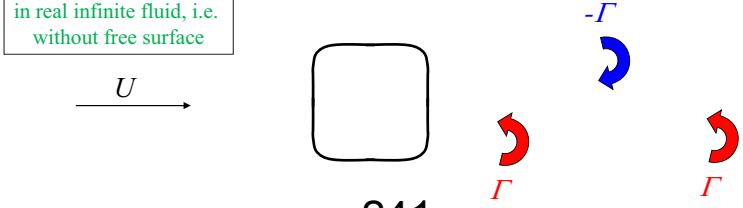

Effects of geometry on C_D

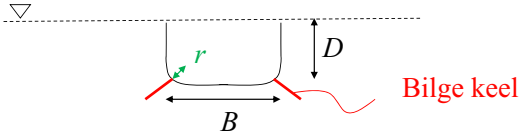

Effects of flow regime on C_D

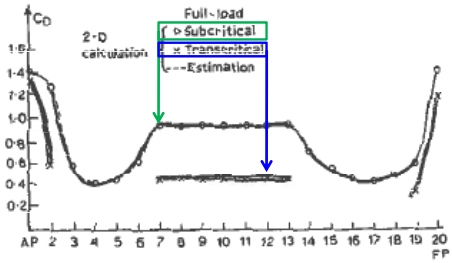

Fig. 6.16. Calculated and estimated drag coefficients C_D for two-dimensional cross-flow past cross-sections along the ship presented in Fig. 6.15. (Adapted from Aarsnes *et al.*, 1985.)

Vortex shedding at the midship cross-section

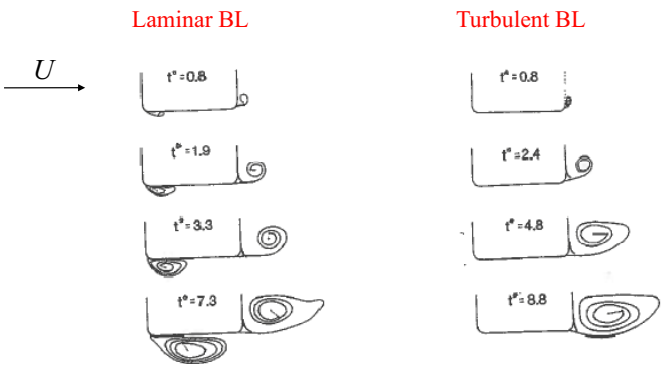

3D current effects on C_D

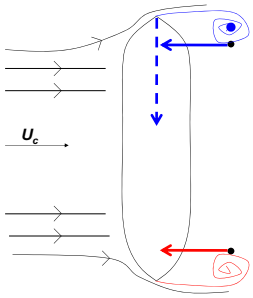

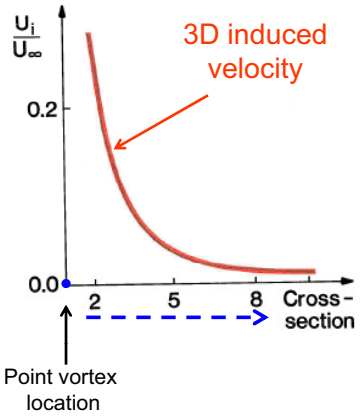

3D current effects on C_D

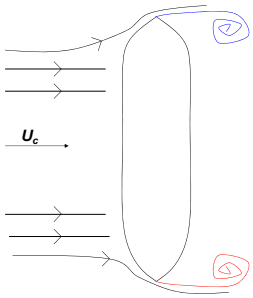

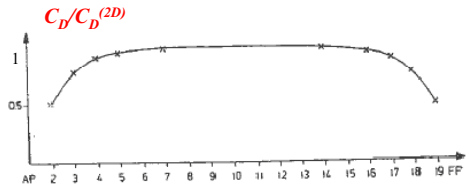

Fig. 6.20. Three-dimensional reduction factor of local drag coefficient due to the vertical vortex system at ship ends described in Fig. 6.19. (Adapted from Aarsnes *et al.*, 1985.)

Current loads on offshore slender structures

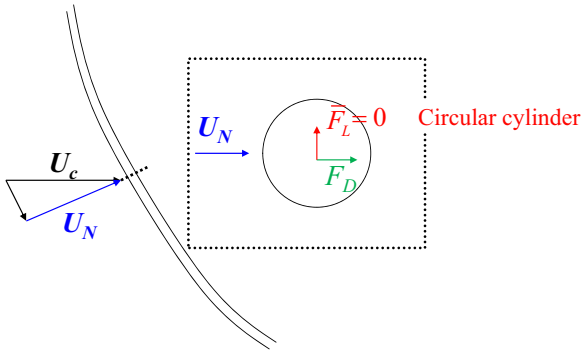

Normal drag force F_D=F_n for oblique flow (Ersdal)

From model tests

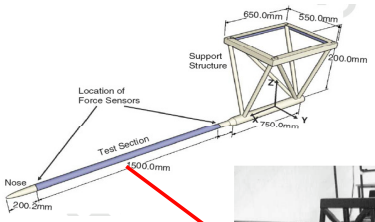

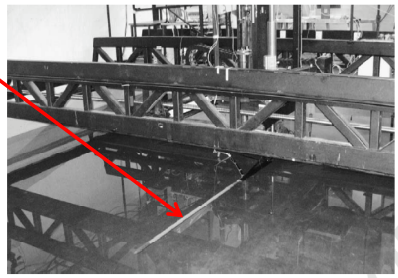

Oblique towing tests of very long submerged circular cylinder

Empirical formulas for F_D=F_n (Ersdal)

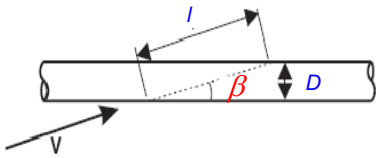

$$C_n(\beta) = \frac{F_n}{0.5\rho V^2 L_{cyl} D}$$

$\beta < 1^\circ : C_n = \pi C_f \sin\beta$ Friction important

$1^\circ < \beta < 6^\circ : C_n = C_{n1} \sin\beta$

$\beta > 6^\circ : C_n = C_d \sin\beta|\sin\beta|$ Flow separation important

Scale effect on normal drag force F_n for oblique flow

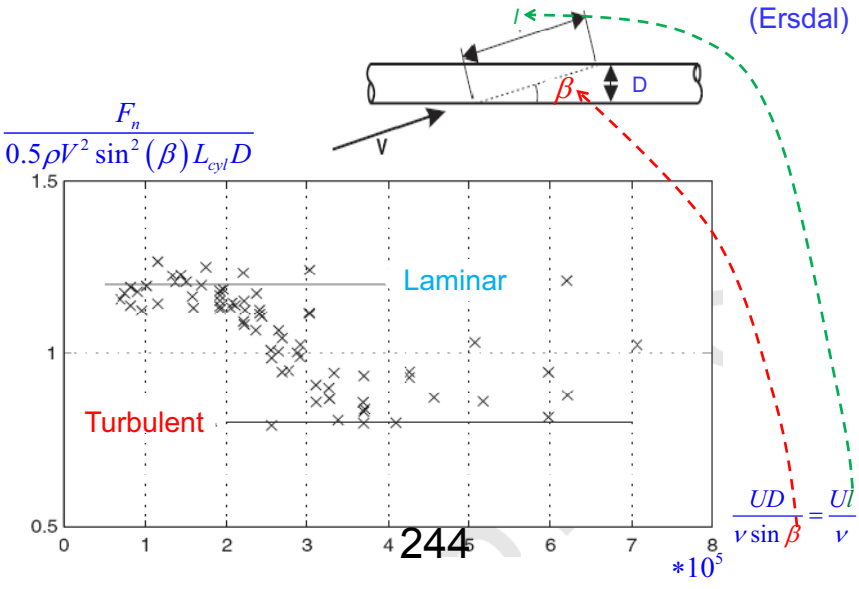

Drag coefficient of downstream cylinder

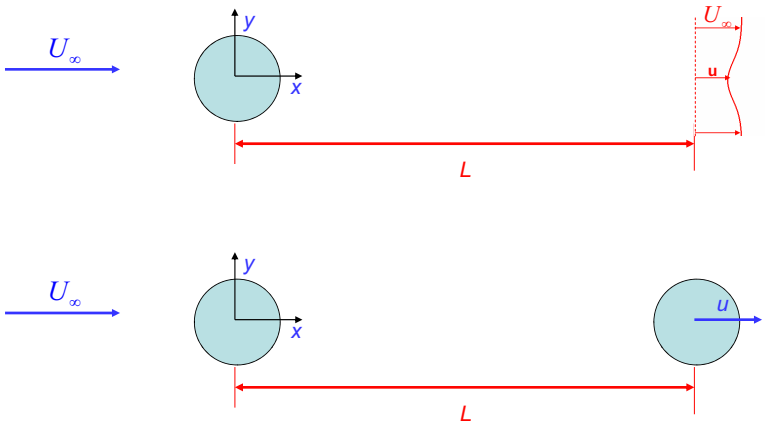

Hydrodynamic interaction between two cylinders in infinite fluid

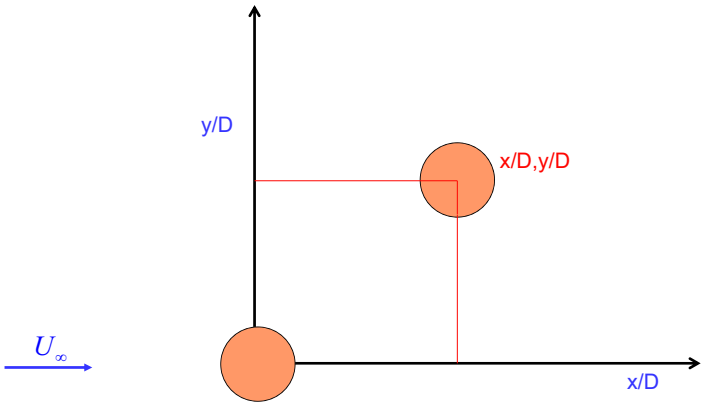

Hydrodynamic interaction between two cylinders in infinite fluid

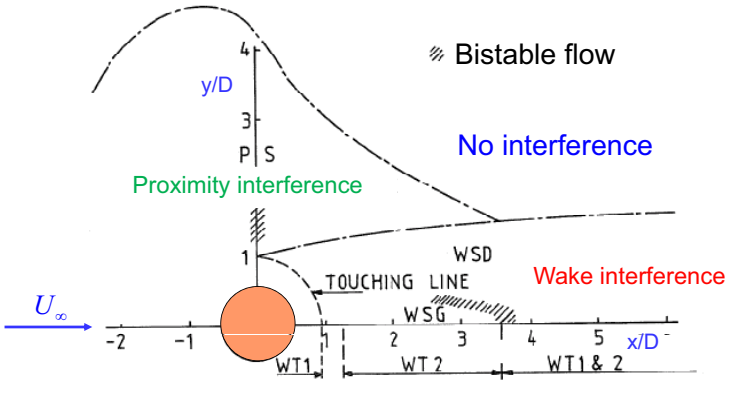

Interaction between two cylinders

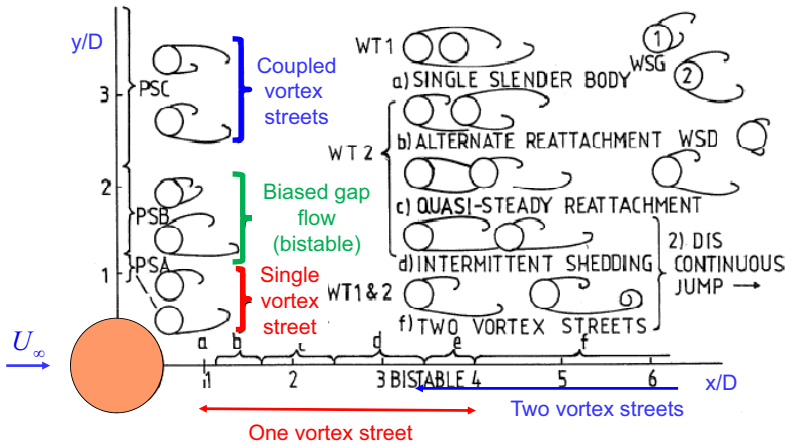

Interaction between two close tandem cylinders in steady ambient flow

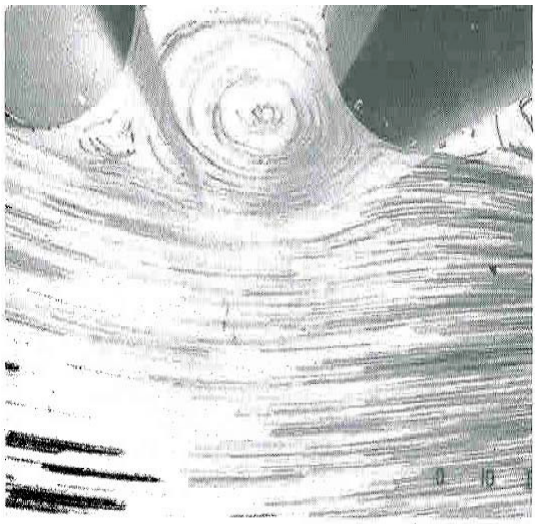

Viscous loads and flow through fishing nets

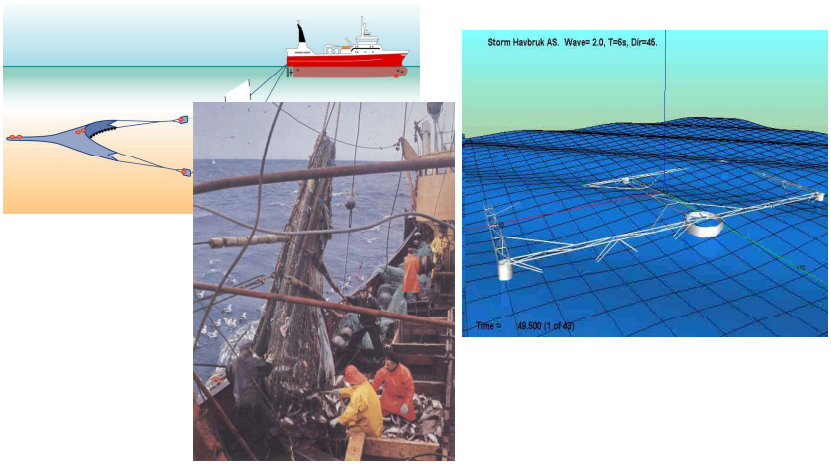

Fish farms

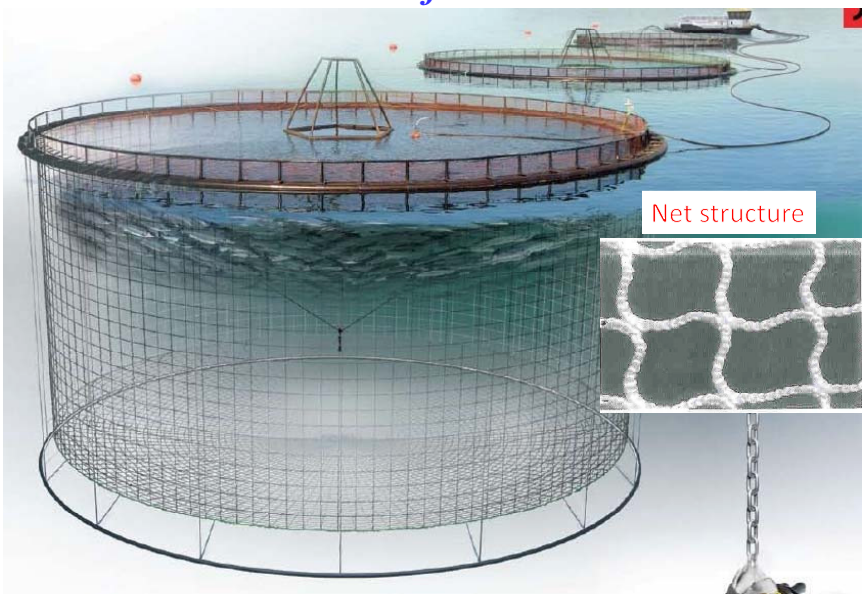

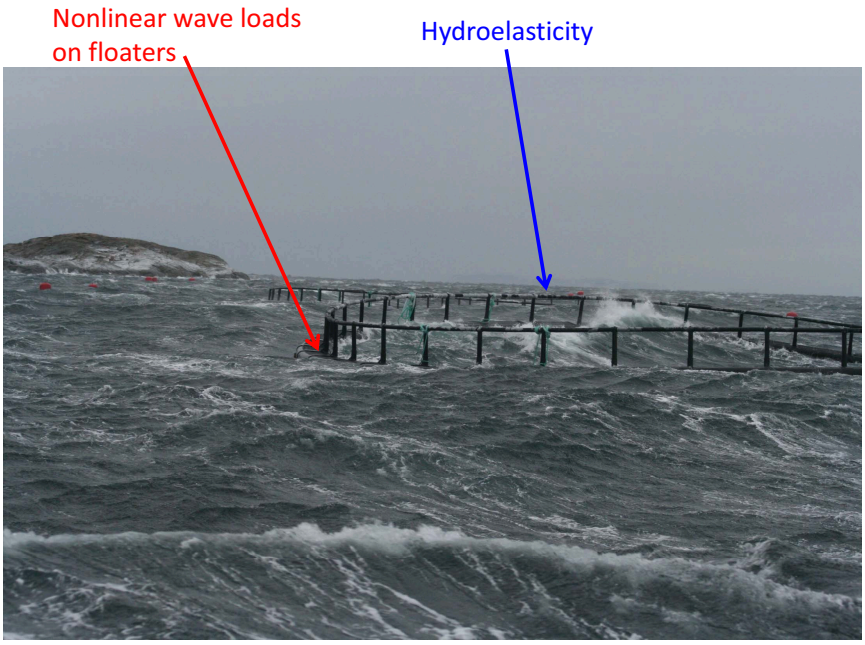

Damages

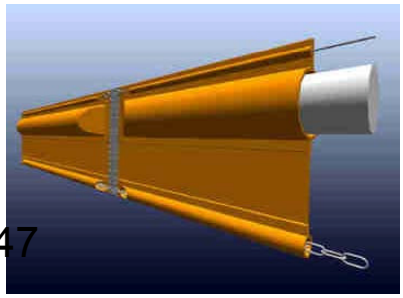

Sufficient water exchange inside the nets needed for the health and growth of a fish

Reduction of flow through nets of aquaculture plant

$$\frac{C_D D}{\lambda} = 0.15 \quad \text{with } \lambda \text{ the mesh size}$$

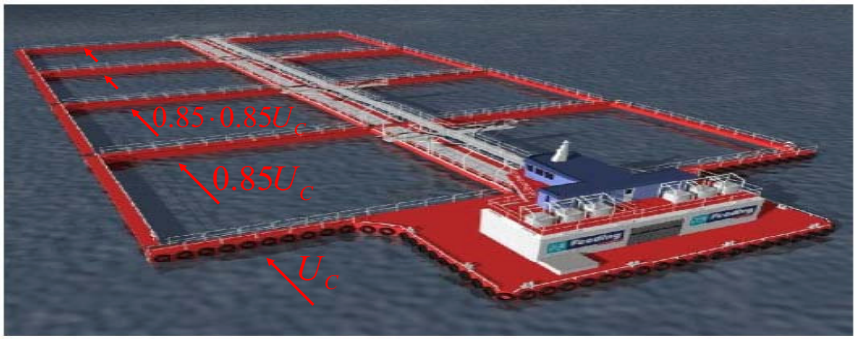

Does the fish have an influence?

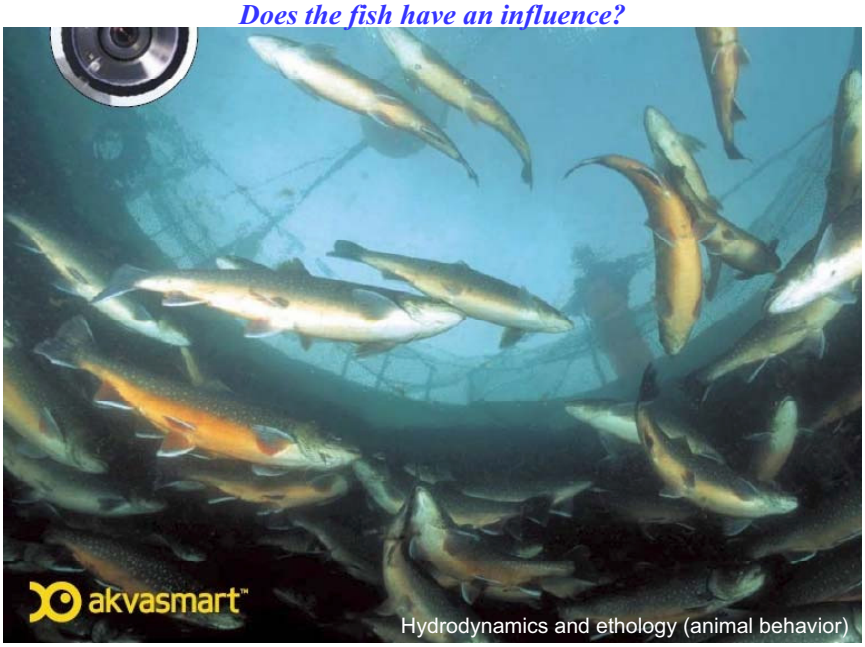

Schooling

Vortex Induced Vibrations (VIV)

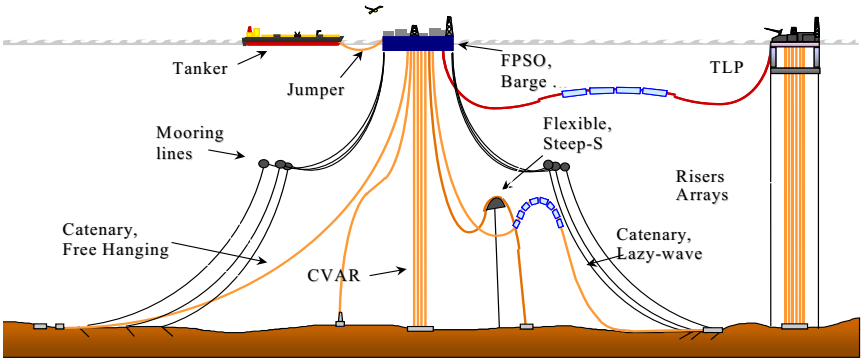

Cross-flow VIV

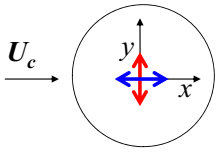

In-line VIV

Vortex shedding and Strouhal number St for circular cylinder

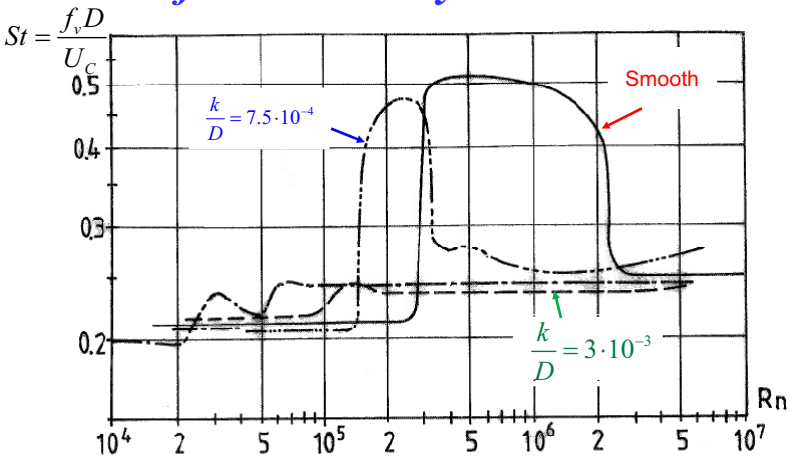

Riser data

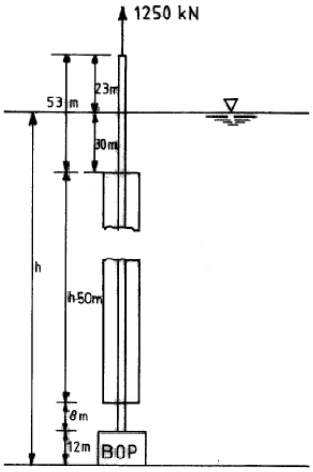

CROSS SECTION:

BUOYANCY DIAMETER
0.95 M
RISER DIAMETER
0.52 M

Natural periods for risers

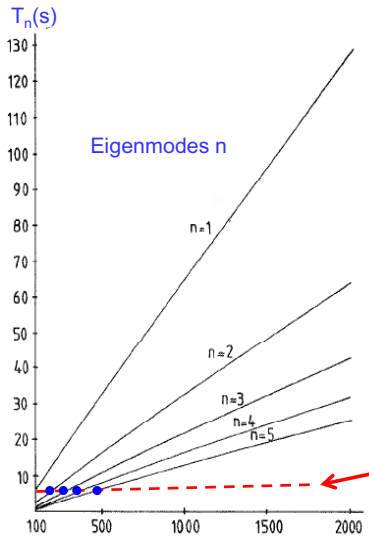

Example:
D=1m, U=1m/s

$Rn = 8 \cdot 10^5$

Note Strouhal number is Reynolds and rough-ess number dependent

Choose rough cylinder so that St=0.25

T_v=5s

Experiments for a circular cylinder free to oscillate transversally

In air, steady current

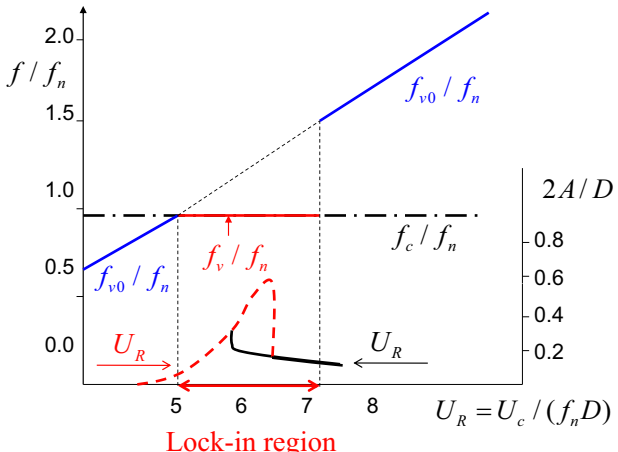

Lock-in region

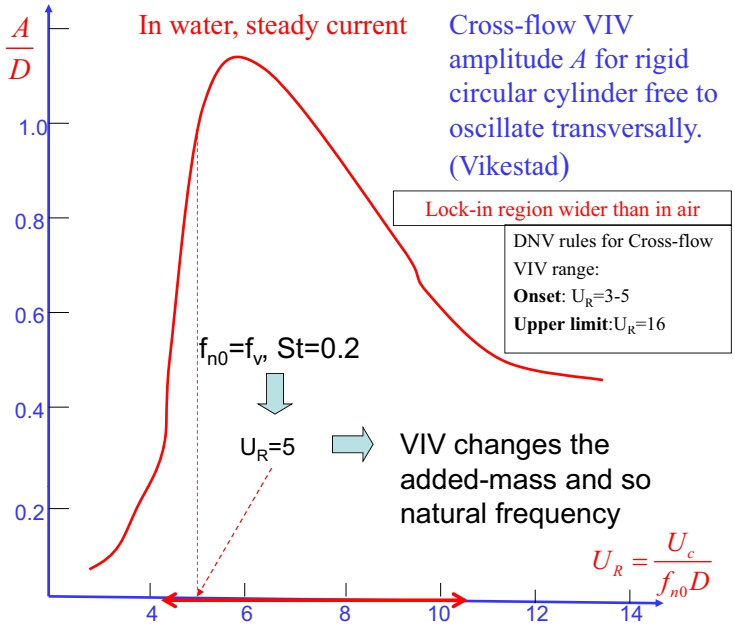

Example: Vikestad's experiments

$$m = 1.306\rho D^2$$

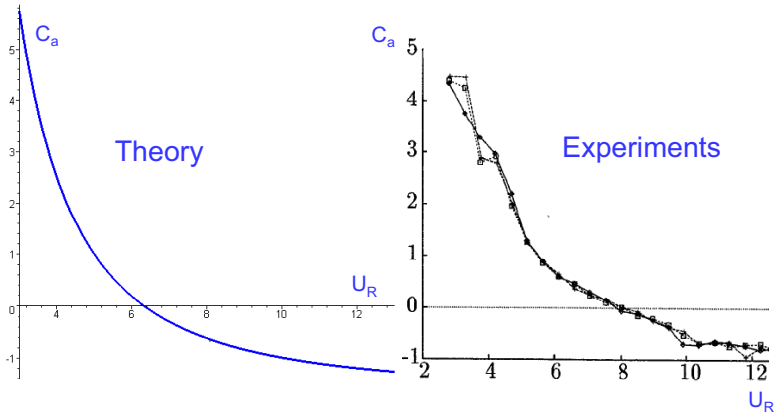

The theory does not account for the influence of VIV on the vortex shedding frequency

Forced transverse oscillation tests

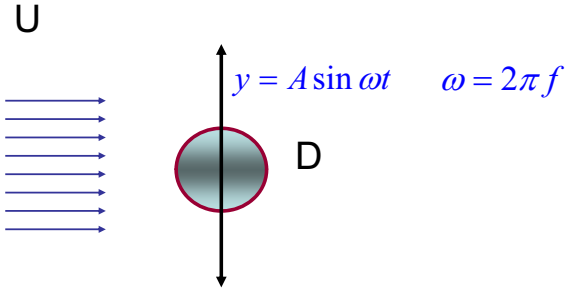

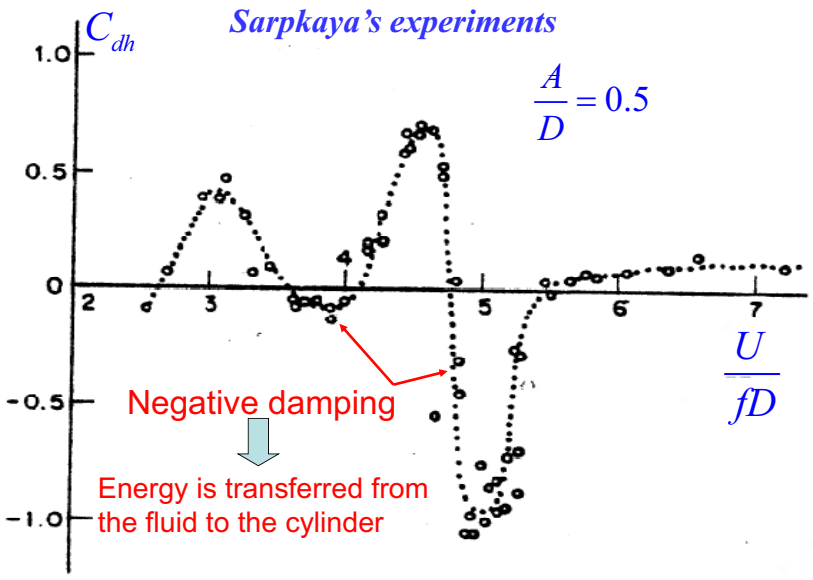

The lift coefficient varies with amplitude

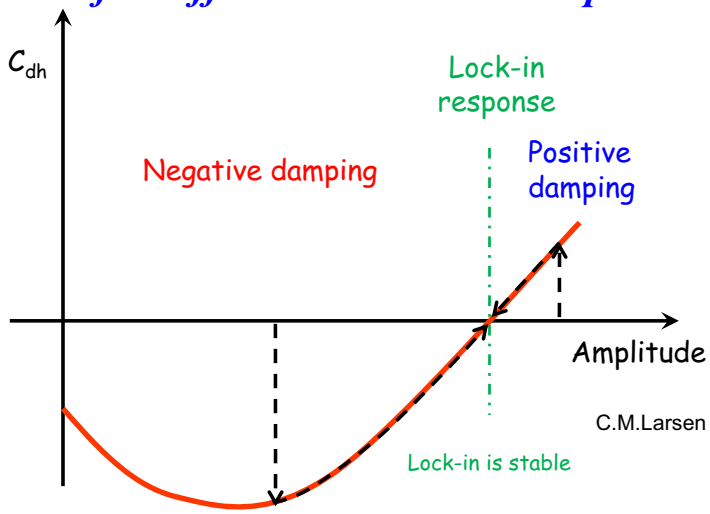

VIV experiment, no mechanical damping starting form zero

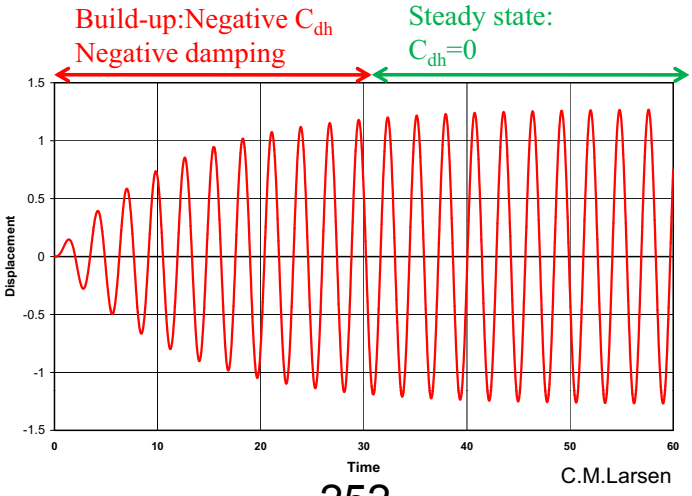

VIV experiment, no mechanical damping starting from large amplitude

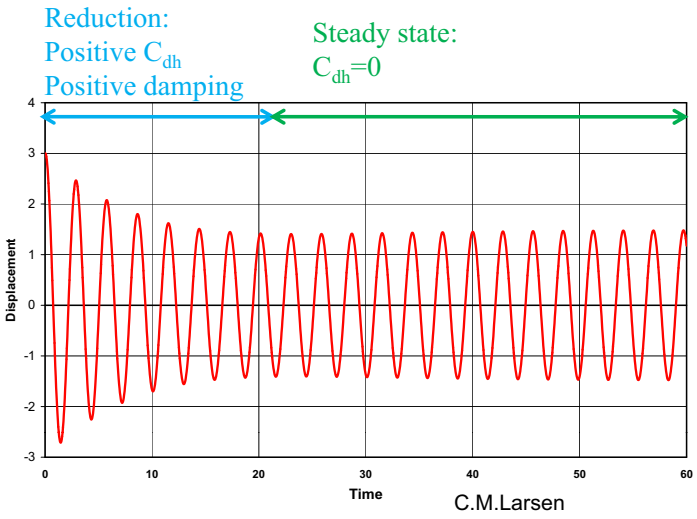

Contour plot of $-C_{dh}$ (Gopalkrishnan et al.)

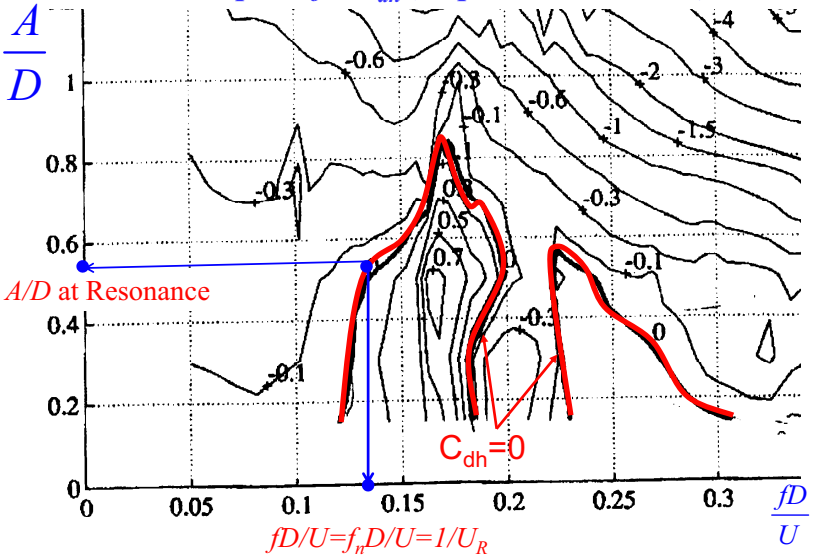

Results from forced motion tests and free oscillation tests

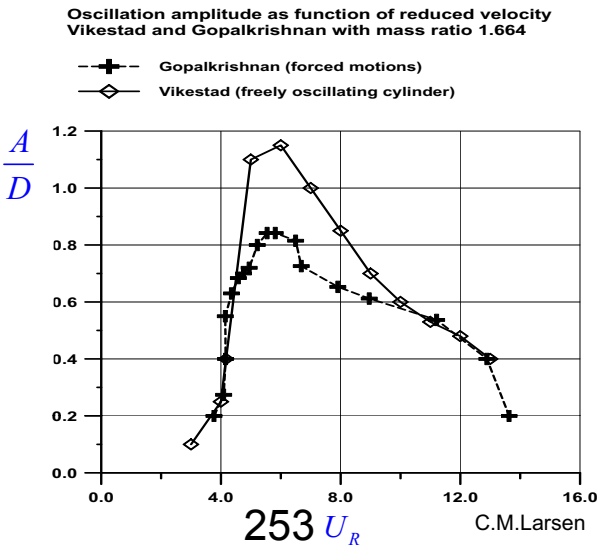

Empirical formula for the maximum transverse amplitude for a generic mode shape ψ (Sarpkaya 1978)

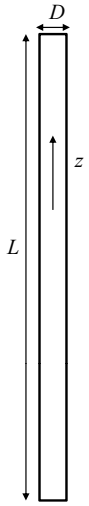

$$\frac{A_{max}}{D} = \frac{0.32\gamma}{\sqrt{0.06+\Delta_r^2}} \quad \text{(F:6.54)}$$

$$\gamma = \psi_{max}\sqrt{\frac{\int_L \psi^2(z)dz}{\int_L \psi^4(z)dz}} \quad \text{(F:6.55)}$$

Structural damping-to-critical damping ratio

$$\Delta_r = (2\pi St)^2 \frac{2m\zeta_s}{\rho D^2} \quad \text{(F:6.56)}$$

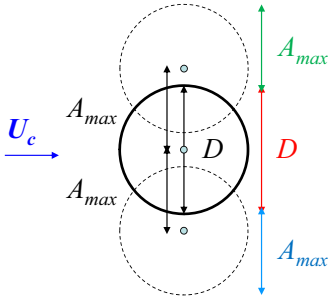

VIV example. Tow-out of monotower. U=1.3m/s

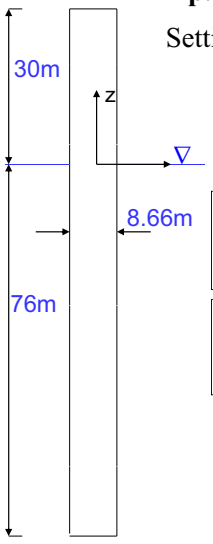

Hp: Coupled roll and sway. Zero damping.

Setting to zero the excitation loads:

$$\begin{Bmatrix} -\omega_n^2(M+\rho Ad) & \omega_n^2\rho Ad\overline{BG} \\ \omega_n^2\rho Ad\overline{BG} & -\omega_n^2(I_{44}+A_{44})+\rho g\nabla\overline{GM} \end{Bmatrix} \begin{Bmatrix} \eta_{2a} \\ \eta_{4a} \end{Bmatrix} = 0$$

Natural period:

$$T_n = \frac{2\pi}{\omega_n} = 89.8s$$

Eigenvalues:

$$\eta_{4a} = \frac{M+\rho Ad}{\rho Ad\overline{BG}}\eta_{2a} = 0.0225\eta_{2a}$$

Reduced velocity :

$$U_R = \frac{T_n U}{D} = 5.2, \text{ i.e. VIV}$$

Displacement: $s_2 = \eta_2 - \eta_4 z$

Eigenmode:

$$\psi(z) = 1 - 0.0225z(m)$$

NB: Center of roll at z=1/0.0225m≅44.5m

VIV example. Tow-out of monotower. U=1.3m/s

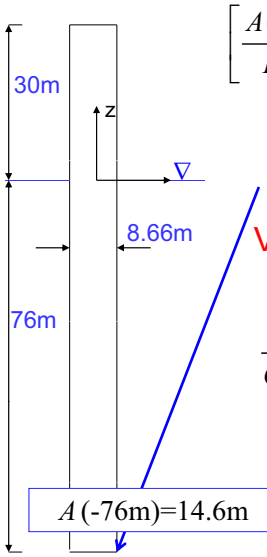

$$\left[\frac{A(z)}{D}\right]_{\max} = |\psi(z)|_{\max}\left[\frac{\int_{-76m}^{30m}\psi^2(z)\,dz}{\int_{-76m}^{30m}\psi^4(z)\,dz}\right]^{1/2}\frac{0.32}{\sqrt{0.06}}$$

$$\Downarrow$$

$$[A(z)] = 5.38\cdot(1-0.0225z)(m)$$

VIV increases the towing resistance

$$\frac{C_D}{C_{D0}} = 1 + 2\frac{\int_{-h}^{0}[A(z)]dz/h}{D} \quad \text{with } h\text{= draught}$$

$$\Downarrow$$

$$\frac{C_D}{C_{D0}} = 1 + 2\frac{5.38}{8.66}\cdot\frac{1}{76}\int_{-76}^{0}(1-0.0225z)dz = 3.3$$

Vortex induced vibrations

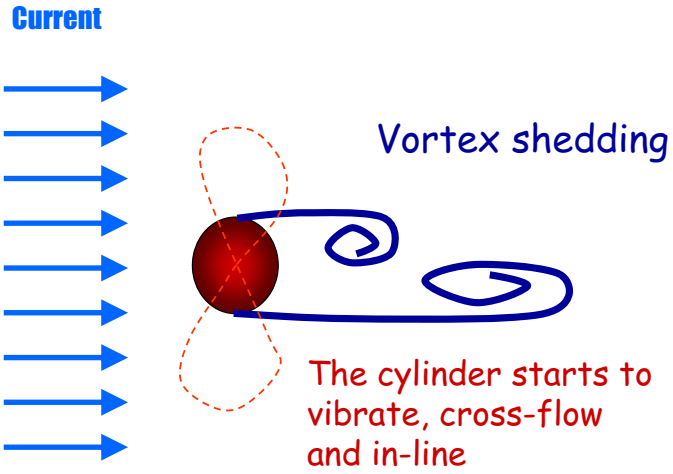

C.M.Larsen

Observations: Response amplitudes, frequency and drag amplification

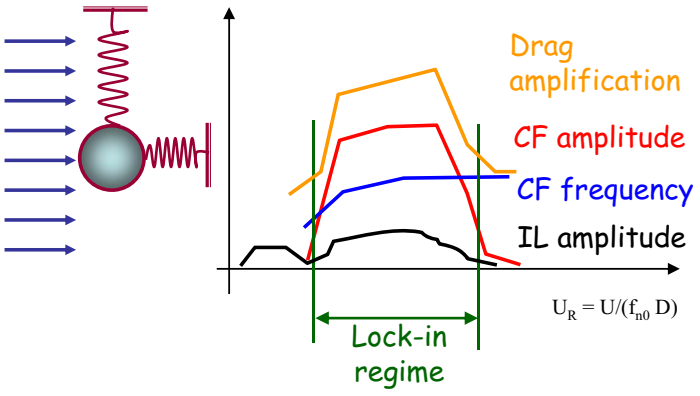

C.M.Larsen

Coupling between in-line and cross-flow oscillations

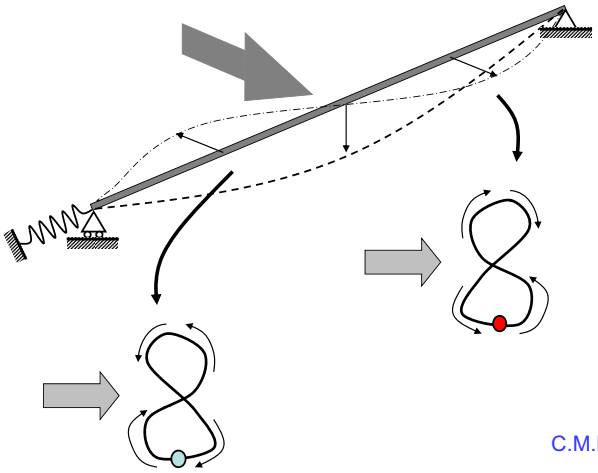

C.M.Larsen

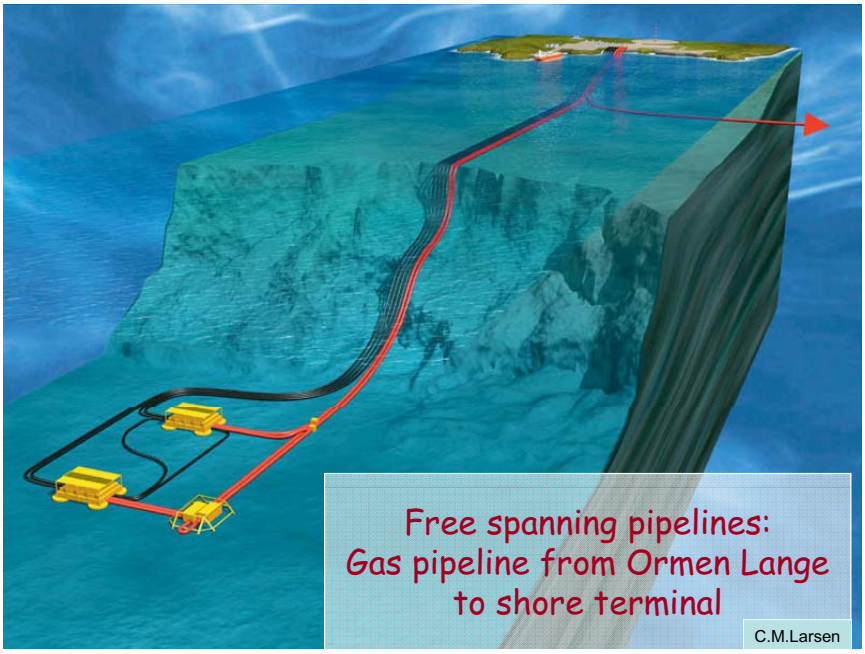

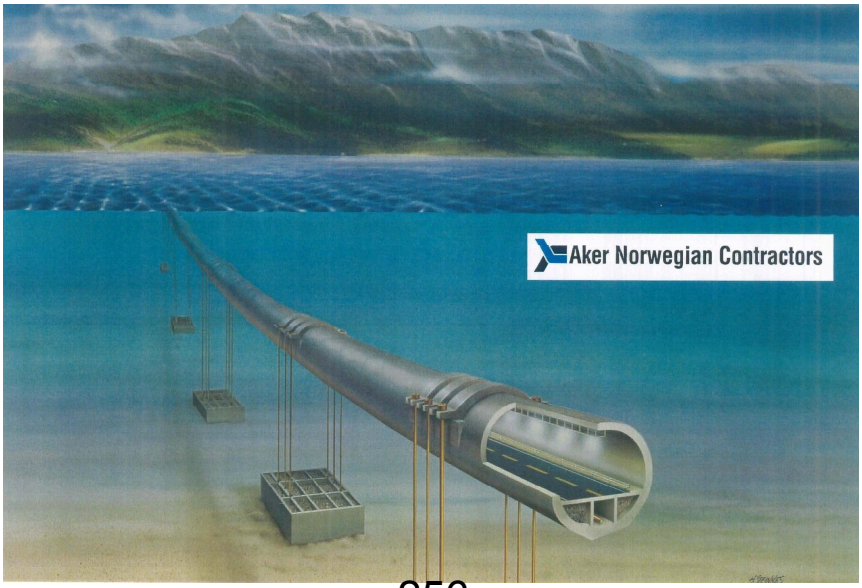

Cross-flow VIV must be avoided. In-line VIV cannot be avoided

Helical strakes for VIM-suppression on Spar platforms

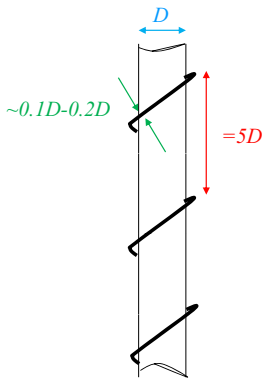

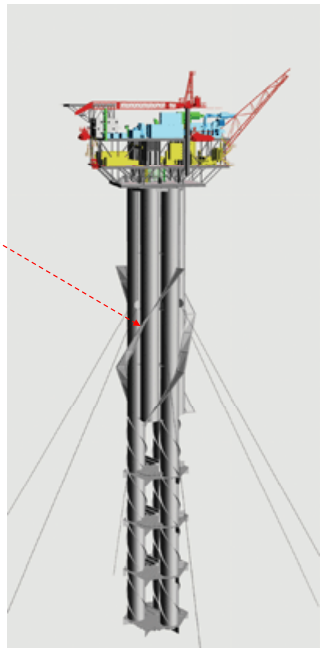

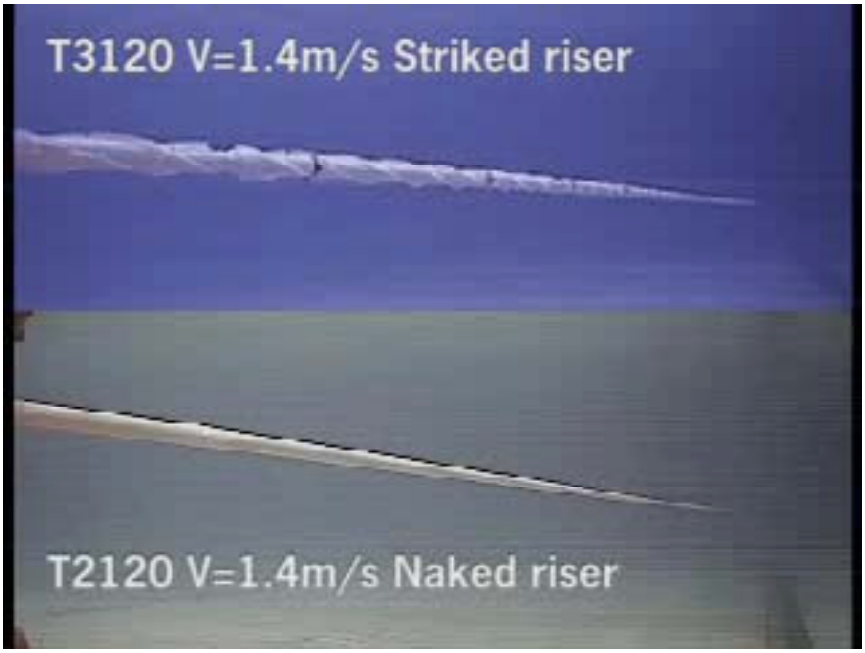

45. Galloping. Viscous wave loads and damping. Stationkeeping. Thrusters. (F:212-215,223-225,228-230,238-248,257-258,270-277)

Galloping (F:212-215)

Lock-in (cross-flow VIV): is a resonance phenomenon, connected with f_v close to f_n, zero damping of the system and self-limiting oscillation amplitudes.

Galloping: is a dynamic-instability phenomenon, implying negative damping of the system. When galloping occurs the system is unstable and unbounded oscillations can occur when perturbed. 'Unbounded' means that galloping motions are not self-limiting as lock-in oscillations. At high velocities the oscillation amplitude is proportional to the incident velocity. Luckily there are limitations on how large the inflow velocity U_c, and so the reduced velocity $U_R = U_c / (f_n D)$, can be. U_R represents an important parameter for galloping.

Let us discuss this phenomenon with an example.

Hp: - A long cylinder with uniform rectangular cross-section in a uniform current with speed U_c → We can study the problem as 2D in the (x,y) cross-section plane with x// U_c
- The body is symmetric about x axis of the current → No force in y without perturbation
- The fluid forces are quasi-steady, i.e. oscillating vortex-shedding forces are not important. This is approximately correct for reduced velocity U_R>10.
- The body is attached to linear springs and has natural (giro) frequency ω_n for y motion.

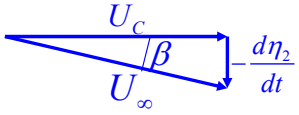

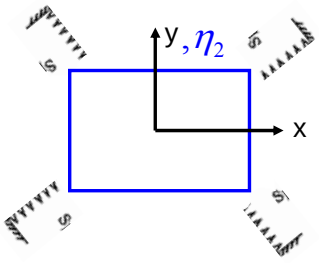

Galloping motion will occur if the hydrodynamic forces cause a sufficiently large negative damping of the transversal oscillations.

Let us assume that small perturbations cause an oscillatory body motion in y direction, η_2. The body oscillations result in a time-dependent angle of attack of the incident current in the body reference frame:

$$\beta(t) = -\text{arctg}(\dot{\eta}_2 / U_c) \underset{\dot{\eta}_2 << U_c}{\approx} -\dot{\eta}_2 / U_c \quad \text{(small)}$$

This results in a transverse current force F_y :

$$F_y = \frac{1}{2}\rho U_\infty{}^2 A C_y(\beta)$$

with ρ the fluid density, A the projected area along x, U_∞ the effective incident-flow velocity and the drag coefficient C_y is function of β. $C_y(\beta=0)=0$ because of the body symmetry about y. For small β, $U_\infty{}^2 \approx U_c{}^2$ and using a Taylor expansion about β=0, we find

$$F_y \approx \underbrace{\frac{1}{2}\rho U_c{}^2 A C_y(0)}_{=0} + \frac{1}{2}\rho U_c{}^2 A \left.\frac{\partial C_y}{\partial \beta}\right|_{\beta=0} \beta(t)$$

This will be an excitation force for the body motion, i.e. the 1D equation of motion is

$$(M + A_{22})\ddot{\eta}_2 + 2\zeta_s (M + A_{22})\omega_n \dot{\eta}_2 + C_{22}\eta_2 = F_y$$

with ζ_s the non-hydrodynamic damping as a fraction of the critical damping $2(M+A_{22})\omega_n$. The restoring coefficient C_{22} is given by the linear springs attached to the body. Substituting the expression of the transverse current force, we find

$$(M+A_{22})\ddot{\eta}_2+\underbrace{\left[2\zeta_s(M+A_{22})\omega_n+\rho\frac{1}{2}U_cA\left.\frac{\partial C_y}{\partial\beta}\right|_{\beta=0}\right]}_{B_{22}}\dot{\eta}_2+C_{22}\eta_2=0$$

Condition for a negative damping , i.e. B_{22} <0, is

$$\left.\frac{\partial C_y}{\partial\beta}\right|_{\beta=0}<-\frac{4\zeta_s(M+A_{22})\omega_n}{U_c\rho A}$$

If D is the characteristic length of the cross-section and $f_n=\omega_n/(2\pi)$, we can rewrite the condition for galloping in terms of the reduced velocity $U_R=U_c/f_nD$, i.e.

$$\left.\frac{\partial C_y}{\partial\beta}\right|_{\beta=0}<-\frac{8\pi\zeta_s(M+A_{22})}{U_R\rho AD}\quad\text{(F:6.64)}$$

In practice, galloping occurs at large U_R, typically higher than for VIV, e.g. U_R >10.

NB: - For a circular cylinder, due to the axial symmetry of the body, $\partial C_y/\partial\beta|_{\beta=0}=0$
→ Galloping can not occur
- Practical examples for which galloping is relevant are riser bundles and ships with a single-point mooring system or towed.

Challenges connected with currents: Deep and ultra-deep waters. Internal waves.

Currents play an important role in different parts of the World and in some circumstances the design current velocity in extreme conditions can be larger than 1m/s used for the North Sea, e.g. in Gulf of Mexico. Currents represent in general an important design parameter in deep and ultra-deep waters because they can act along the whole column of water while wave effects go to zero quickly with the depth. Currents in general have a spatial variation. This has not been accounted for in our examples, i.e. academic uniform currents were examined.

Internal waves, i.e. waves caused in stratified regions of the sea, travel along the interface between layers of sea with different density and are associated with large periods of oscillation, and therefore large wavelength. They are not relevant as dynamic excitation but act mostly as a steady current with features slowly varying in time. Similarly as free-surface waves, their disturbances may go to zero exponentially going far from the interface. In this case 'far' means far up and far down from the interface. In some cases the internal waves can be represent the main 'current' design parameter. An example is the Lufeng field in South of China. There, the currents vary typically between 0.2 and 0.4 m/s with maximum values between 1.0 and 1.2 m/s, the internal waves have period of oscillations of 20 min and behave as a steady current with a behaviour along the water depth like in the figure below, i.e. with a change in direction and maximum value much larger than for the true currents.

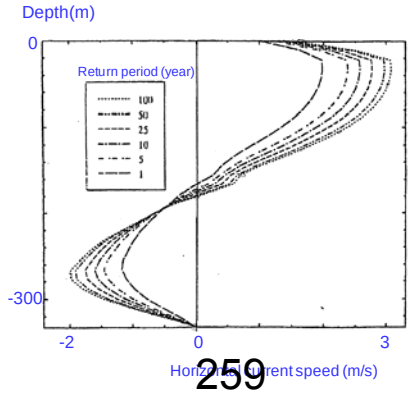

The figure shows the value of the horizontal velocity for different design criteria. Historically internal waves have been studied in connection with dead waters and with ships travelling with small forward speed in regions with stratification interface sufficiently close to the sea surface. Today they may be relevant for marine operations and may affect the acoustic propagation in the ocean.

Viscous wave loads and damping (F:223-225,228-230,238-248)
Viscous flow phenomena are important in several problems related with wave loads on ships and offshore structures. Examples are: wave loads on jackets, risers, tethers, pipelines, roll damping on ships and barges, slow-drift oscillation damping of moored structures in irregular sea and wind, anchor-line damping, 'springing' damping of TLPs.

The main parameters are the same as discussed for the current loads, i.e., *Rn*, *k/D*, body form, free-surface effects, sea-floor effects, nature and direction of ambient flow. In addition we have:

- Keulegan-Carpenter number $KC = U_M T / D$, for ambient oscillatory flow with velocity $U_M \sin(2\pi t/T + \varepsilon)$, which represents the ratio between the distance covered moving with the maximum velocity U_M during an oscillation period and the characteristic body length. From this, $KC \rightarrow \infty$ means steady ambient flow.
  If we assume that the oscillatory flow is given by an incident wave with amplitude A, in the linear case $U_M = \omega A = 2\pi A / T$. Then KC can be rewritten as $KC = 2\pi A / D$ and represents a measure of the importance of A relative to D. In this case large KC means high waves relative to the structure characteristic dimension.
- Relative current number$= U_c / U_M$, when there is a steady current velocity U_c parallel to the oscillatory velocity $U_M \sin(2\pi t/T + \varepsilon)$. This measures the importance of the current relative to the oscillatory ambient flow.

Morison's equation
It is used often to calculate wave loads in circular cylindrical structural members of fixed offshore structures when viscous forces matter, but it can also be applied for other cross-section shapes. It is a long-wave approximation, i.e. it assumes $\lambda/D > 5$.

Hp: Incident waves in *x* direction. A vertical rigid fixed circular cylinder with diameter *D*.

Morison's equation provides the horizontal force, i.e. normal to the cylinder axis, along the wave direction. The contribution *dF* from the strip *dz* is

$$dF = C_M \underbrace{\rho \overbrace{\frac{\pi D^2}{4}}^{=A}}_{=A_{11}=\text{added mass in infinite fluid}} a_1 dz + \frac{\rho}{2} C_D D \,|u|\, u dz = dF_{Mass} + dF_{Drag} \quad \text{(F:7.1)}$$

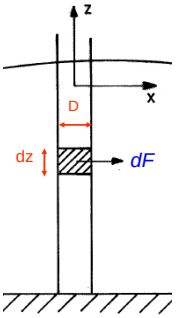

with a_1 and u the horizontal incident-wave acceleration and velocity at the midpoint of the strip. The positive direction is the incident-wave propagation direction. The two force components are called mass and drag force, respectively.

What are these forces?

The drag force is the in-line force, i.e. along the incident-wave direction and in the cross-sectional plane, due to flow separation and shear stresses along the body. The Morison's equation does not provide instead the oscillatory forces due to vortex shedding in the lift direction, i.e. orthogonal to the incident-wave propagation and in the cross-sectional plane.

Concerning the mass force, let us assume negligible viscous effects, in this case the Morison's equation gives

$$dF = \underbrace{dF_{Drag}}_{=0} + dF_{Mass} = \rho C_M (\pi D^2 / 4) a_1 dz.$$

Now, in potential-flow long wave approximation, the elementary excitation force is

$$dF = \underbrace{\rho A a_1 dz}_{dF_{FK}} + \underbrace{A_{11} a_1 dz}_{dF_D} = 2\rho(\pi D^2 / 4) a_1 dz.$$

It means that C_M =2 and C_D =0. So the Morison's equation gives the correct inviscid excitation force on the body in the asymptotic condition of large λ/D.

In general, the mass and drag coefficients C_M and C_D in equation (F:7.1) must be estimated empirically and depend on the parameters mentioned above about viscous wave loads. If the acceleration can be neglected, the Morison's equation is a good empirical formula for the time average force. Typical C_D and C_M values for transcritical flow past a smooth circular cylinder are 0.7 and 1.8 at $KC>\approx 40$, i.e. toward steady inflow conditions. A roughness number k/D=0.02 may increase more than 100% the C_D, implying a greater importance of the roughness in oscillatory ambient flow than in a steady incident flow.

Assuming deep-water linear incident wave solution in equation (F:7.1), we find that the mass and drag force per unit length are largest near the free surface and decrease with z, respectively, as e^{kz} and e^{2kz}. So the drag force is the most concentrated near the free surface. The application of Morison's equation near the free surface requires accurate estimate of the undisturbed velocity distribution under a wave crest because using the linear solution involves an error near the free surface. In this case the largest force per unit length is predicted at the free surface while in reality the force per unit length must go to zero as we approach the free surface because one must recover the fact that the pressure is atmospheric (see figure below).

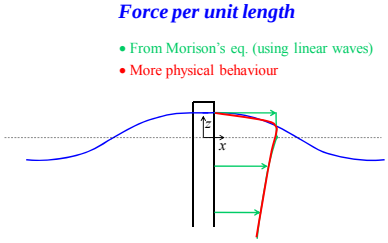

The vertical position of the maximum absolute value of the force is below the free surface and must to be found experimentally. As a rough estimate, it could be at z distant the 25% of the incident-wave amplitude from the free surface.

The force on the 3D cylinder can be obtained integrating equation (F:7.1) along the cylinder wetted surface. Because F_{Mass} and F_{Drag} on the structure are out of phase of 90 degrees, if the cylinder corresponds to a wave node the force is only given by the mass force which is also maximum, and if it corresponds to a wave crest the force is only given by the drag force which is also maximum (see figure below).

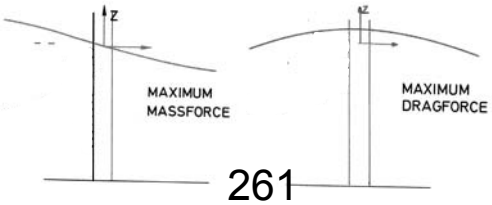

NB: As we have already mentioned for the Froude-Kriloff force, one must integrate along the correct wetted surface of the body. This is critical at the junctions of structural elements, e.g. at the junction between a pontoon and a column of a semisubmersible.

Morison's equation can be modified to account for the horizontal motion η_1 of the body in x direction.
Hp: Incident waves in x direction. A vertical rigid circular cylinder with diameter D and surge motion η_1.

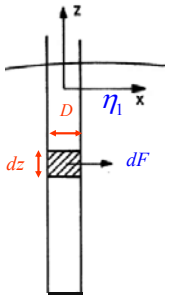

The Morison's equation states that the horizontal hydrodynamic force dF on the strip dz , in the body-fixed coordinate system, is

$$dF = \frac{\rho}{2} C_D D \,|u - \dot{\eta}_1|\,(u - \dot{\eta}_1)dz + \rho \frac{\pi D^2}{4} C_M a_1 dz - \rho \frac{\pi D^2}{4}(C_M - 1)\ddot{\eta}_1 dz \qquad \text{(F:7.2)}$$

From the formula, the drag-force contribution is connected with the relative velocity between incident waves and body while there is not a pure dependence on the relative acceleration for the remaining force contribution. This can be understood if we consider that in potential-flow theory the Froude-Kriloff force depends only on the incident-wave acceleration, i.e. not on the rigid-body acceleration.

NB: C_M and C_D in equation (F:7.2) can be different than for a fixed cylinder.

The Morison's equation can also be applied to inclined cylinders assuming that only the velocity and acceleration components normal to the cylinder axis will contribute to the force. The force direction will be normal to the cylinder axis. In the potential flow case this is the correct expression. In the viscous case it means that we use the 'cross-flow' principle. The method can also be generalized to the case when the cylinder axis is not in the incident-wave propagation plane. For example if the cylinder is horizontal and the waves propagate along x normally to the cylinder axis, a modified version of the Morison's equation provides the wave forces along x and z. In case of wave-current environment, the Morison's equation is usually applied by setting the velocity term in the equation as the vector addition of the wave and current velocities.

Flow separation

Oscillatory inflow reduces the possibility of flow separation in blunt bodies with no sharp corners because the incident velocity changes direction in time, so the flow can remain attached more easily to the body. In this case it is more difficult to set a criterion for flow separation. The criterion in steady ambient flow, which is zero shear stress on the body surface, i.e. in 2D: $\mu\,\partial u / \partial y\big|_{y=0} = 0$, is not generally accepted as criterion for flow separation in unsteady ambient flow. If this condition occurs one talks about 'detachment point' (Telionis 1981).
Let us assume a blunt-shaped marine structure without sharp corners.
• The flow does not separate in oscillatory ambient flow at very small KC numbers, which means when the inflow oscillation periods (or the wave amplitudes) are very small. As an indication we could say for $KC \lessapprox 2$ though flow separation has been reported for KC smaller than 2 (Sarpkaya 1986 for a circular cylinder).
• The flow separates always in a steady current.

• In the case of combined steady current and oscillatory inflow (in the same direction), the existence of a threshold KC number, say KC_{lim}, for flow separation depends on the relative current number U_c/U_M. Roughly speaking the flow may be able to not separate if the ambient flow velocity in the current direction changes sign in time. Flow separation always occurs if $U_c/U_M>1$ (see figure below) because in this case the flow does not return in time toward the body.

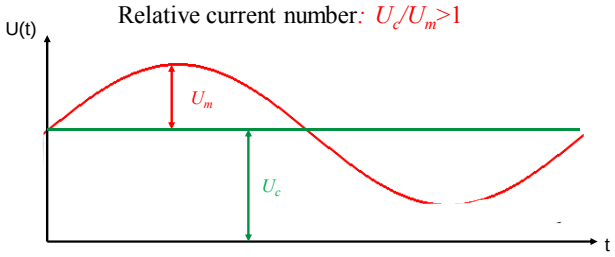

Example: flow separation around a hemisphere in waves and current.
The figure below gives experimental results for flow-separation occurrence. It confirms that for sufficiently small relative current number and small KC number, flow separation can be avoided. As the current velocity U_c increases relative to the amplitude of the oscillatory velocity U_M, then flow separation occurs even for very small KC numbers.

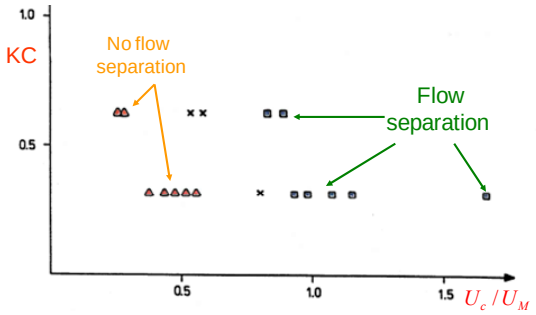

NB: There results are relevant also for large volume structures. Typically for them we neglect flow separation and assume potential flow theory. Now we see that flow separation can occur depending on KC and U_c/U_M. In this case, it is important to quantify how extended flow separation is, i.e. if it is very localized then the consequences can be limited in terms of loads.

Separated flow at small KC-numbers
Oscillatory inflows with small KC-numbers, are relevant for damping of slow-drift motions of moored structures and roll damping of ships and barges.
Using Berman's (1985) work for a circular cylinder in waves and without current, roughly speaking when flow separation occurs at $KC<7$ the flow is symmetric. This means zero lift force.
Graham (1980) found that at small KC-numbers the C_D is strongly dependent on the local flow at the separation point. His analysis considers only the effect of flow separation on the pressure along the body, i.e. viscous shear forces are not included. He assumed fixed separation point and found this empirical behaviour for the drag coefficient:

$$C_D \propto KC^{\eta}, \eta = (2\delta - \pi)/(3\pi - 2\delta) \quad (1)$$

with δ the body internal angle at the separation point. The larger is δ the smaller is the vortex-shedding intensity and then C_D. In particular we have

Flat plate: $\delta = 0 \rightarrow C_D = 8.0KC^{-1/3}$
Square section: $\delta = \pi/2 \rightarrow \eta$=0, i.e. no influence of KC (F:7.24)
Circular cylinder: $\delta = 0 \rightarrow C_D = 0.2KC$

For instance for the eddy making slow-drift damping: Graham's results for a rectangular cross-section indicate that the damping does not depend on *KC;* those for a flat plate can be used to find the damping connected with bilge keels and show a great influence of *KC* on the damping. The eddy-making slow-drift damping is important for slow-drift motions of moored structures. An exception is surge motion of a ship for which flow separation does not play a role. In this case the viscous damping is given by shear stresses (frictional forces) along the body.

Figure F:7.8 shows the experimental results of C_D for a circular cylinder in subcritical conditions at small *KC* numbers. When the laminar boundary layer is without flow separation, i.e. $KC<\approx 1$, the measurements show a decrease of C_D as *KC* increases and agree with the viscous formula by Wang (1968)

$$C_D = \frac{3\pi^3}{2KC}\left[\left(\frac{\pi Rn}{KC}\right)^{-1/2} + \left(\frac{\pi Rn}{KC}\right)^{-1} + \frac{1}{4}\left(\frac{\pi Rn}{KC}\right)^{-3/2}\right] \quad \text{(F:7.21)}$$

With flow separation the measurements show an increase of C_D as *KC* increases and agree with the formula by Graham. The latter is true up to *KC* about 10.

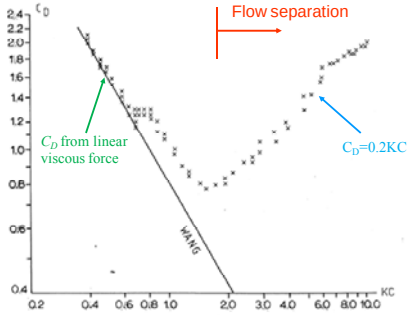

Fig. F:7.8

Separated flow at high *KC*-numbers

Flow separation at high KC-numbers is relevant for predicting wave loads on jackets and risers in extreme weather conditions. At $KC>10$, the oscillatory ambient flow is like a quasi-steady current that changes direction in large time. In a steady current we learned that the vortices released by the body induce in the wake locally a velocity against the inflow current. When the quasi-steady current changes sign the vortex induced velocity increases the inflow velocity, say of an average quantity $\bar{u}$ (at the center of the cylinder), and so the C_D. One talks about 'returning vortices' because the wake is like it was upstream of the body. This effect reduces as $KC\rightarrow\infty$, i.e. as we approach steady inflow conditions. It means that the increase of the drag coefficient with respect to steady conditions is formally given by

$$C_D \sim C_D\big|_{KC=\infty}(\bar{u}+U_M)^2 / U_M{}^2 \quad \text{(F:7.32a)}$$

and modelling the vortical structures as discrete vortices we find

$$C_D \sim (1+0.58e^{-0.064KC})^2 \quad \text{(F:7.32b)}$$

Parameter dependence of C_D

The drag coefficient in oscillatory ambient flow, and so the eddy-making damping, depends in general on, for instance: the free-surface effects, beam-to-draught ratio *B/D*, bilge keel dimensions, bilge radius *r*, current, Reynolds number *Rn*, roughness ratio *k/D* and Keulegan-Carpenter number *KC*. The free surface is relevant in waves as for in steady current and reduces C_D. An exception is for small *KC* because in this case, both with and without the free surface, i.e. double body in real infinite fluid, the vortex shedding is symmetric. *B/D* has a small effect but for small *B/D* especially at $KC<\approx 10$ (in this case *B/D* must be $<\approx 1$). *r* is

important and reduces C_D. Bilge keels are important especially at small KC and increase C_D. At high KC, C_D is not very sensitive to the bilge-keel breadth, i.e. as in steady current, while at small KC it increases enlarging the breadth. Concerning Rn, scale effects are small when flow separation occurs at sharp corners like bilge keels. Without sharp corners, scale effects are not severe for small KC and their relevance is also reduced when bilge radius is small, i.e. it becomes close to a sharp corner. Otherwise scale effects matter.

NB: Cross-flow VIV can also occur in ambient harmonic oscillatory flow for KC>7 (which means an asymmetric vortex shedding), as well as with combination of waves and current. In this case for vertical structures lock-in can not occur along the whole structure at the same time because wave effect attenuates with depth.
Waves can also mitigate the occurrence of VIV. An example is deep-draught floaters.This needs long and high waves→ the current velocity is smaller than wave velocity and the waves can work against the lock-in excitation by changing in time the direction of the inflow and may avoid VIV.

Stationkeeping (F:257-258)
Thrusters and mooring systems are used to ensure precise position and motion control of ships and floating structures. They must be designed properly to counteract the mean loads due to waves, current and wind. They also provide a damping and lead to a restoring for the motions in the horizontal plane, i.e. surge, sway and yaw motions, which do not have any restoring due to gravity.
Mooring systems provide a static positioning, while the thrusters give a dynamic positioning. The former are easier to design and realize, the latter are more flexible, both in terms of water depth and manoeuvring. Mooring lines and thrusters can be used separately or in combination. In the latter case one talks about thruster assisted position mooring (POSMOOR).
Here we briefly mention about the mooring systems and discuss more in detail about the thrusters.

Mooring systems
Mooring systems are made of sets of cables connecting the vessel to the sea floor (either laying or attached to the sea floor). An initial tension (or pre-tension) is used to keep the lines in place. System motion consequent to the environmental conditions modifies the lines geometry and so their tension. Thus the mooring cables have an effective stiffness, partially elastic and partially geometric. We have discussed the restoring force due to the anchor-lines in the case of surge motion, i.e. $C_{11}\eta_1 = (dT_H / dx)\eta_1$. They also contribute in terms of slow-drift damping to the system, which is a viscous damping, e.g. in surge: $B_{11}\dot{\eta}_1 \mid \dot{\eta}_1 \mid$.

Thrusters/dynamic positioning (F:270-277)
Thrusters can be used in set both on vessels and offshore structures. On vessels, bow and azimuth (can be rotated) thrusters are combined with the main (stern) thruster.

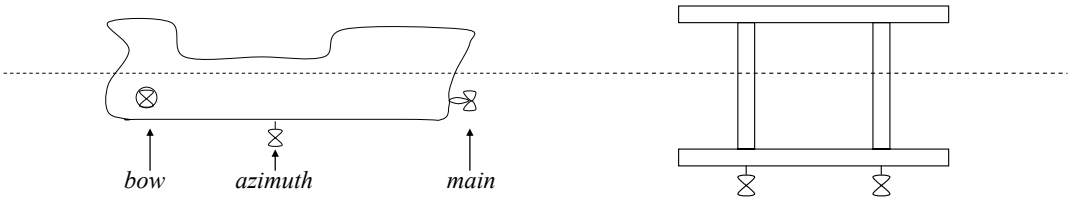

Thrusters are combined to provide restoring and damping through proper phasing of the forces (thrust) that they produce. The damping in this case is much larger than for mooring lines, as a rough estimate it can be about the 60% of the critical damping.

NB: The phasing of the thrusters forces is very important for the damping provided, both in terms of absolute level and sign (positive or negative) of damping.

To design the thrusters, for example to fix the propeller disk area A_0 and the number of revolutions per second n at which they should work, open-water tests are considered, i.e. the propeller is studied as isolated and in infinite fluid. This provides the thruster characteristics in terms of thrust T and torque Q. Corrections must then be considered to account for thrust losses connected with:

- interaction with other thrusters
- interaction with the hull/structure
- work near the free surface
- work in wave-current-wind environment

These factors can modify the inflow to the propeller and/or its jet flow. Let us discuss some of them.

Interaction with the hull/structure:
If there is a portion of the structure in the wake of the thruster, the slip stream of the thruster is attracted by the structure. This is known as **Coanda effect**.
To understand this let us first approximate the slip stream as a circular jet emerging from a circular opening and merging with the surrounding fluid at rest:

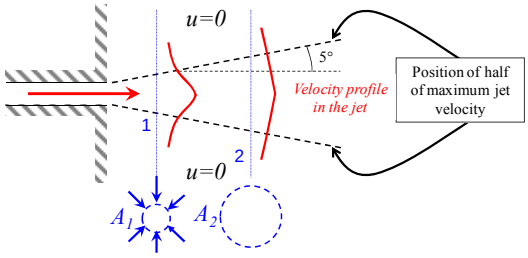

The jet is characterized by high speed and brings on its motion also part of the surrounding fluid. This means that the jet attracts the surrounding fluid, acting as a line of 'sinks' along its axis. As a result, the jet spreads outwards moving downstream and the cross-sectional area increases, i.e. $A_2>A_1$.

NB: An estimate of the jet widening is that the point with velocity half of the maximum sectional speed is deviated outwards of 5 degrees.

Moving downstream, as the jet spreads outwards, the velocity in the center of the jet (maximum velocity) reduces, i.e. $\left(V_{j,2}\right)_{\max} < \left(V_{j,1}\right)_{\max}$.

Let us approximate then the jet as a line of sink points along its axis and examine what happen if this distribution of sinks meets a wall parallel to its axis. Let us neglect the wall boundary layer for simplicity.

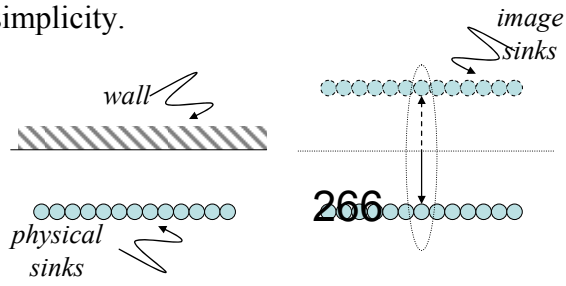

The wall is an obstruction to the flux toward the inner jet because it is impermeable, i.e. the normal velocity is zero there. It means that its presence is like to have another distribution of sink points symmetric about the wall.
The two sink lines attract each other → the wall attracts the jet and deviates the jet axis.
If the portion of the wall is sufficiently long, the jet may reach it, this leads to frictional forces and so to thrust losses. For a thin jet released at distance h from an infinitely long wall, it takes about $6h$ to reach the wall.

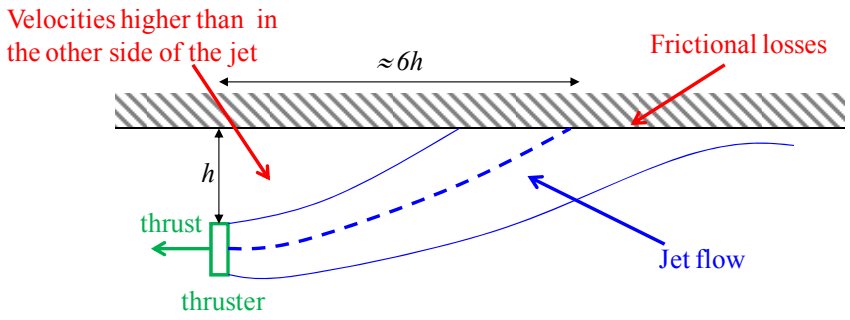

NB: For a ship, thrust losses due to Coanda effect can be up to 30%-40%. For a semisubmersible, if a thruster is aligned to a pontoon the loss of power could be 10-15%.

Loss of efficiency due to current/forward speed:
The forces generated by a tunnel thruster are affected by the flow of a current past the entrance and exit of the tunnel. For example, a current not in-lined with the thruster slip stream can reduce the thrust furnished by the thruster because can deviate the jet direction. In the case of a bow thruster on an advancing ship, thrust losses are partially due to the interaction with the hull and partially due to the deviation caused by the ‘ ahead current’ effect. Fig. F:8.11 shows experimental results and documents large trust reduction.

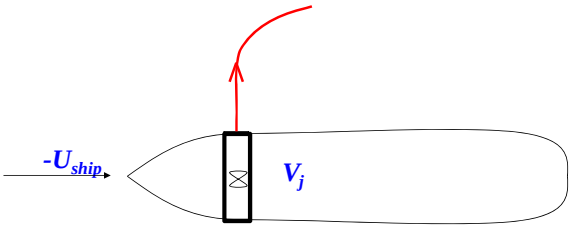

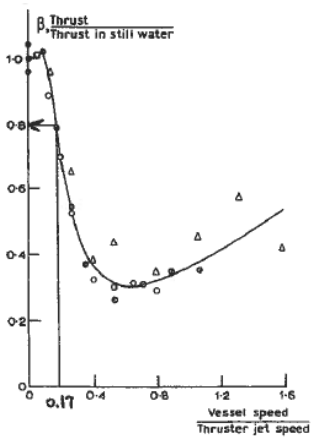

Fig. 8.11. Bow thruster performance. Effect of ahead current/vessel speed. (Chislett & Bjørheden, 1966.)

Example: If we assume a ship speed U_{ship}=1m/s, a thruster disk area A_0=3.5m^2 and a design thrust T_{sw}=130kN, the jet speed is

$$T_{sw} = \rho A_0 V_j^2 \Rightarrow V_j = \sqrt{\frac{T_{sw}}{\rho A_0}} \cong 6m/s \text{ and } U_{ship}/V_j \cong .17$$

Then from fig. F:8.11 we find that the thrust is 80% of the thrust in still water T_{sw}.
The thrust losses due to current, depend obviously on the current direction. This is examined in the figure below in terms of thrust-to-thrust in still water ratio for a bow thruster in a current with velocity equal to 0.2 times the thruster jet velocity.

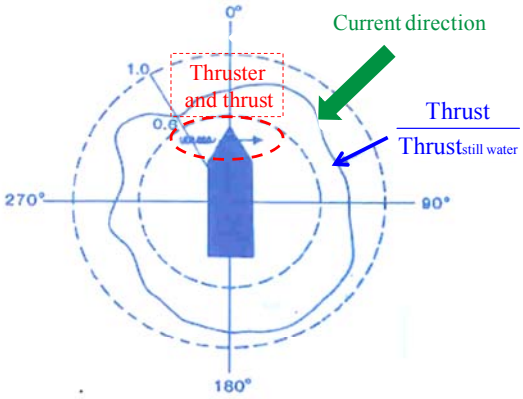

Influence of free-surface effects on thruster characteristics:

Wave-induced motion affects the thruster behaviour when the thruster is sufficiently close to the free surface.

Minsaas et al. (1986) studied wave effects using model tests in calm water. This approach is reasonable because the wave frequencies of practical interest are much smaller than propeller rotation frequencies →quasi-steady approximation can be applied.

The parameters studied in the tests by Minsaas et al. (1986) are:

- submergence of the propeller axis, *h*
- propeller radius, *R=D/2*
- number of revolutions/sec, *n*

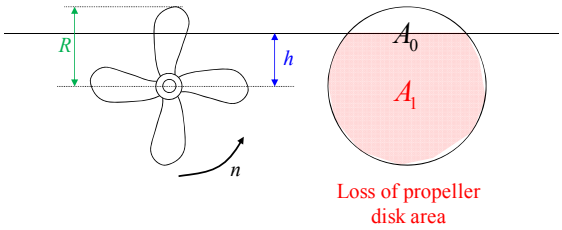

The experimental information can be transferred to the case with the waves, e.g. waves generated by ship motion, by interpreting *h* as the instantaneous submergence of the propeller axis *h(t)* under local wave surface (see Fig. F:8.12). This is possible on the basis of the quasi-steady assumption. Results are reported in figure F:8.12 in terms of the ratio between actual thrust and thrust in open-water conditions (i.e. with the propeller fully immersed), $\beta_T = K_T(h/R)/K_{T0}$ with $K_T = T/\rho n^2 D^4$, as a function of *h/R*.

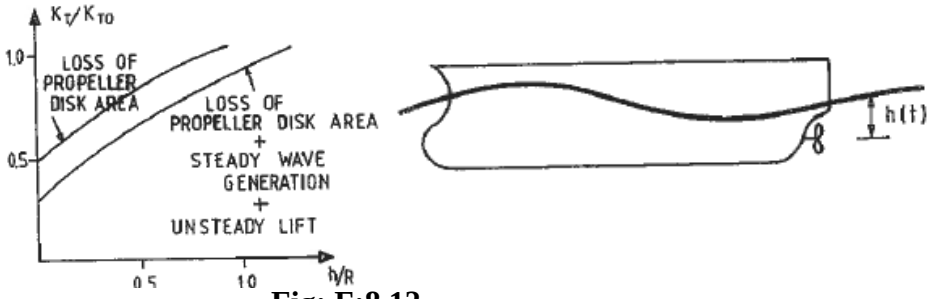

Fig: F:8.12

Figure F:8.13 documents an important effect on β_T of

- loss of effective propeller-disk area $\beta_0 = A_1 / A_{t0}$
- number of revolutions/sec *n*

For *h/R*>=1.5, β_T=1. For *h/R*<1.5, the loss of disk area leads to a reduction of thrust ratio. This effect becomes less important as *n* is sufficiently high because another stronger effect becomes visible in terms of a sudden drop of β_T. This is the ventilation effect. Higher *n*

means higher blade loading → higher suction pressure, i.e. higher dynamic pressure → lower static pressure. Thus, sufficiently close to the free surface, i.e. when the hydrostatic pressure is small, a large *n* can lead locally to pressure lower than the atmospheric pressure in the suction side of the blades. In this case, air can move toward the blades leading to propeller ventilation.

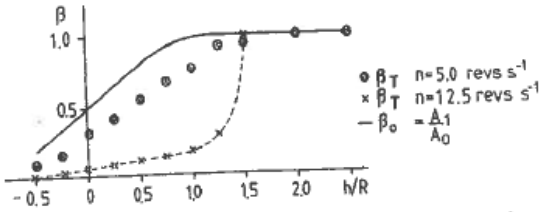

Fig. 8.13. Loss of thrust due to reduced immersion of a bow thruster in calm water. Model scale. (β_T = thrust divided by thrust for deeply submerged propeller. β_0 (see equation (8.39)), n = number of propeller revolutions per second, h = propeller axis submergence relative to the free surface, R = propeller radius.) (Minsaas *et al.*, 1986.)

The consequences of ventilation are:

- air is attracted and brought into the water during the blades rotation
- entrapped air means a reduction in the blade loading and thrust reduction

The amount of air on a blade will reduce as the blade moves at higher immersion because of the higher hydrostatic pressure. The result is a variation in time of the thrust reduction. It means that, in the case of ventilation, the calm-water tests are not reliable to describe the wave-induced effects, because the quasi-steady assumption in not valid.

Minsaas et al. (1986) tried to apply their experiments in regular waves for bow thrusters and ducted propellers to different ships and sea states. They found an influence of: *n, h, R,* propeller pitch and hull form and great reduction of β_T in rough sea states.

Thruster performance and dynamic positioning:

We want to determine the loads that thrusters in a dynamic positioning (DP) system must provide to ensure proper control in waves, current and wind. We can express the total thruster loads as

$$F_k = \overline{F}_k - \sum_{j=1}^{6}(B_{kj}{}^{DP}\dot{\eta}_j + C_{kj}{}^{DP}\eta_j) \qquad k = 1,..,6 \quad \text{(F:8.40)}$$

For a dynamically positioned ship we are interested to surge, sway and yaw (k=1,2,6).

The mean loads $\overline{F}_k$ must balance the mean wave, current and wind loads. The motions η_j are the slowly-varying motions of the structure obtained by filtering the high-frequency motions due to waves because these can not be controlled by a DP, i.e. they are too fast for the system to react effectively and the related loads are too high to be counteracted.

We have discussed the mean loads connected with waves (higher-order effects) and current (for wind they are similar to current). Let's see the procedure to estimate the damping and restoring that must be provided to a ship by a DP system:

1) As first step approximation the coupling can be neglected, i.e. $B_{kj}{}^{DP} = 0, C_{kj}{}^{DP} = 0$ if $k \neq j$
2) $C_{kk}{}^{DP}, k = 1,2,6,$ are chosen on the basis of the natural period that we want for our DP+ship system, for example in the range $T_{nk} = 100 - 200s$ in surge, sway and yaw.
3) $B_{kk,}{}^{DP}, k = 1,2,6,$ can be set equal to the ≈60% of the critical damping in mode k, i.e. $0.6[2(M_{kk} + A_{kk})2\pi / T_{nk}]$

Example: surge motion of a ship.
The equation for the slow-drift surge motion can be written as:

$$(M + A_{11})\ddot{\eta}_1 + (B_{11} + B_{11}{}^{DP})\dot{\eta}_1 + C_{11}{}^{DP}\eta_1 = F_1{}^{SW} + F_1{}^{wind} \quad \text{(F:8.41)}$$

In eq. (F:8.41): M=ship mass, A_{11}=surge added mass, B_{11}=hydrodynamic surge damping, $B_{11}{}^{DP} = 1.2\sqrt{(M + A_{11})C_{11}{}^{DP}}$ assuming 60% of the critical damping, $C_{11}{}^{DP} = (2\pi / T_{n1})^2 (M + A_{11})$ from the resonance condition (T_{n1} could be for instance 100s), $F_1{}^{SW}$=slowly-varying wave excitation force (with zero mean value), $F_1{}^{wind}$=slowly-varying gust excitation force (with zero mean value). In this case we have not included the viscous hull damping. If the ship has also a mooring system then an additional restoring term, say $C_{11}{}^{m}\eta_1$, must be added. The mooring lines will also provide damping, say $B_{11}{}^{m}\eta_1|\eta_1|$, but this is small compared to the damping given by the thrusters system.
An important parameter is the variance of the slow-drift motion. As we learned, this can be obtained as

$$\sigma_{\eta_1}{}^2 = \int_0^\infty \frac{S_{F_1}(\mu)}{[C_{11}{}^{DP} - (M + A_{11})\mu^2]^2 + [(B_{11} + B_{11}{}^{DP})\mu]^2} d\mu \qquad \text{as eq. (F:5.47)}$$

which gives a measure on how wide is the motion spectral density for a given force spectrum. Another important parameter is the variance for the total thruster surge force given by eq. (F:8.40). Here we discussed the total thruster forces, they must be distributed among the single thrusters of the DP system.
An example of dynamic positioning (DP) system is given in the figure below:

1. Measurements are made for position (with satellites, hydroacoustics, etc.), heading (with gyrocompass, GPS) and motions (accelerometers) of the vessel and for the wind (anemometers), typically by redundant methods, and processed (signal processing)
2. High-frequency components (also those connected with waves) are filtered out and variables of interest not measured are predicted (vessel observer)
3. Damping and restoring loads needed from thrusters are estimated on the basis of the desired control conditions and their thrust quantified (controller/power management system/thrust allocation)
4. The control model could need to be modified if the weather changes greatly (adaptive law), or if required by an operator or by a specific additional control criterion (reference model)

Dynamic Positioning Control Architecture

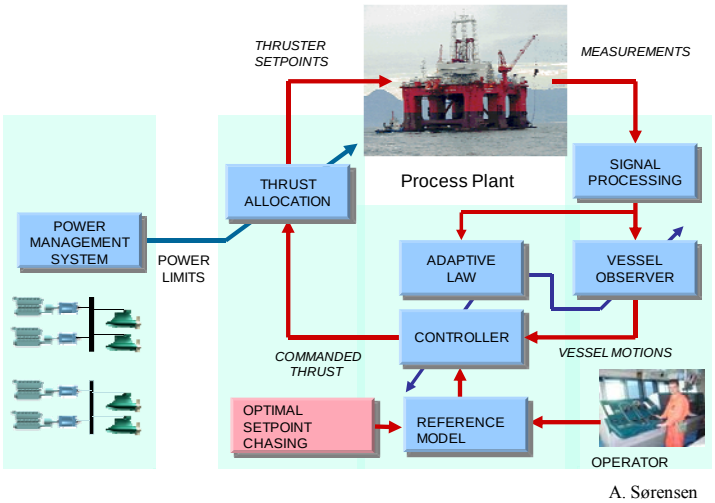

A. Sørensen

Additional remarks:

• There are circumstances when vertical motions must also be considered by the DP. An example is given by semisubmersibles for which vertical motions have large resonant periods (>20 s) which could be excited by the DP through the coupling between horizontal and vertical motions. This should be taken into account by the DP so that a proper damping for the vertical motions is provided.

• In extreme sea states the wave-frequency motion is not filtered out by the DP in the aim to behave as good as possible in such circumstances. In these conditions it is more appropriate to enforce a constant torque than a constant pitch/rpm (rotation per minutes) because the provided power is smoother (see figure below). Power with sharp changes could lead to the break up of the system. A constant torque can only be provided by electrically driven propellers.

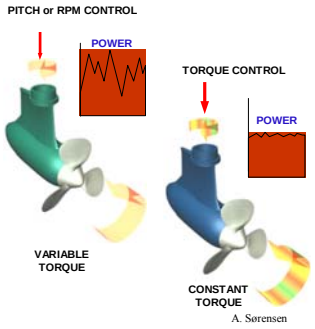

Summary: Current and wind loads. Viscous wave loads and damping. Stationkeeping.

Scale effects: Issue for VIV

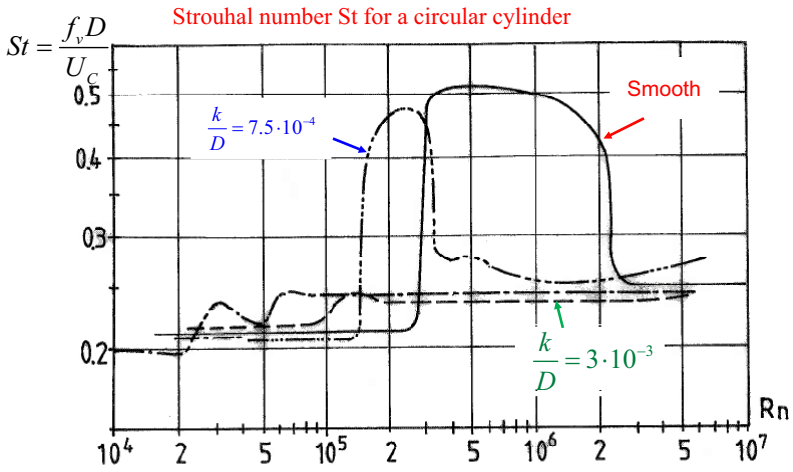

Galloping (Dynamic instability)

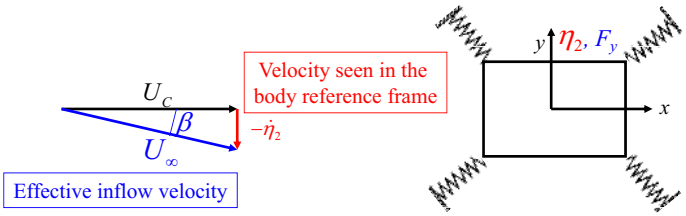

Riser bundle in a current (Overvik's model tests)

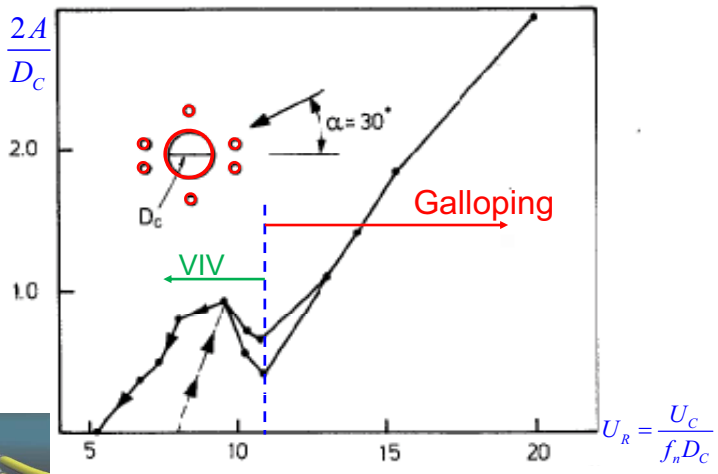

Pipe bundle

Stability of Single-Point Mooring System (Whichers 1988)

Stability criterion

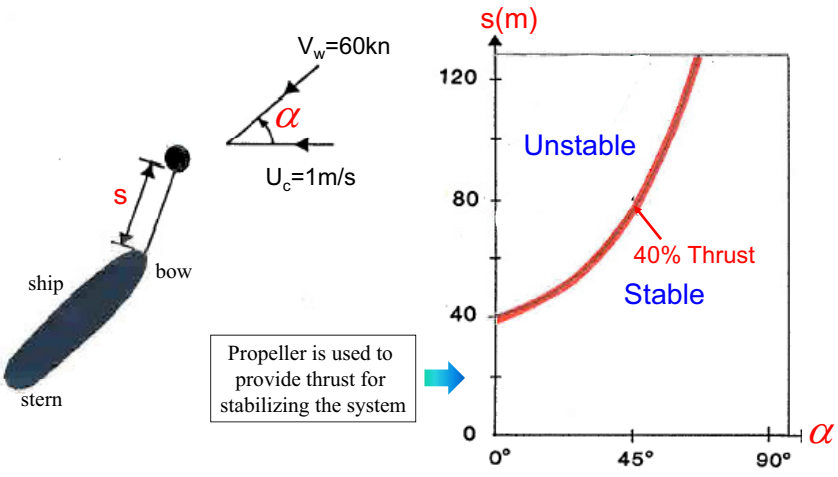

Stability of Single-Point Mooring System (Whichers 1988)

Stability criterion

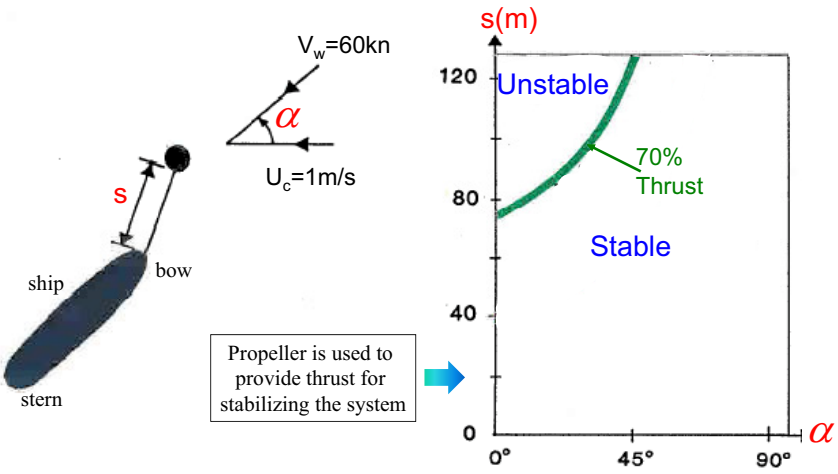

Stability of Single-Point Mooring System (Liapis 1979)

Configurations with better stability behavior

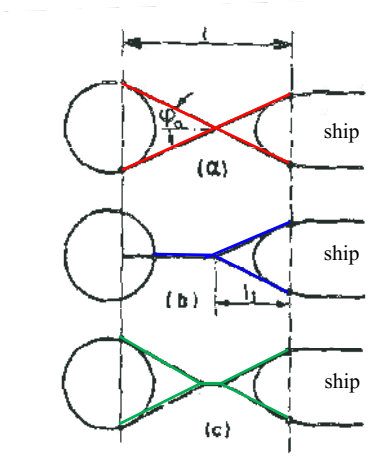

Currents are relevant for deep water development

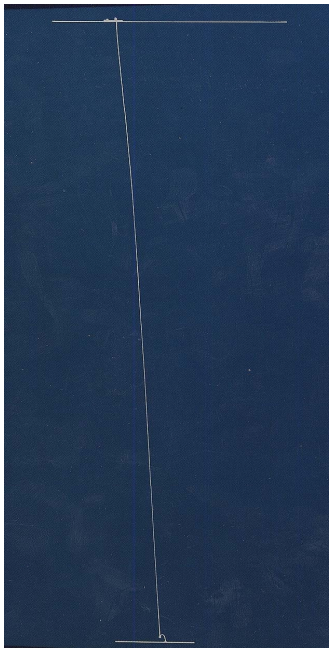

Oil and gas production in deep and ultra-deep water

Challenges

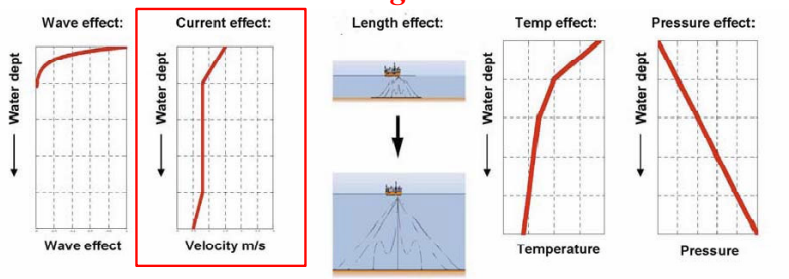

Current acting through the whole water column – increased importance

Strong and complex current profiles (x,t)

Internal waves

Increase importance of current loads & loads effects (VIV).

Increase weights and loads on sub systems.

May need buoyancy elements (increased drag)

Complex installation & retrieval operations.

Low ambient temperature, below 0° C may occur.

Increased risk of hydrate formation.

Increased external pressure – collapse of risers and pipelines.

Water intrusion in electrical and hydraulic systems.

Depressurisation access limited.

The loop current in the Gulf of Mexico

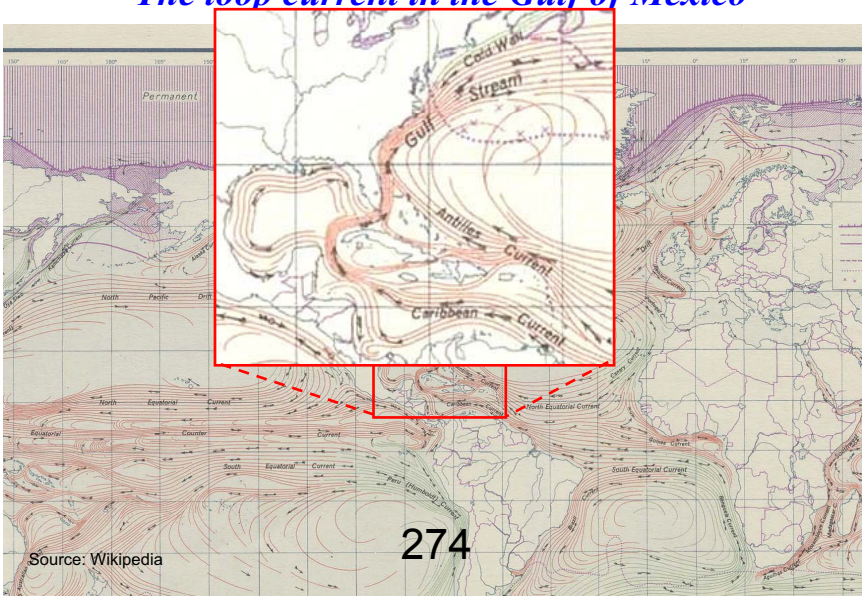

Source: Wikipedia

Loop current rings in the Gulf of Mexico on the Na Kika field

- Water depth 1770-2300 m
- Typical background current velocities is in the order of 0.2-0.5 m/s

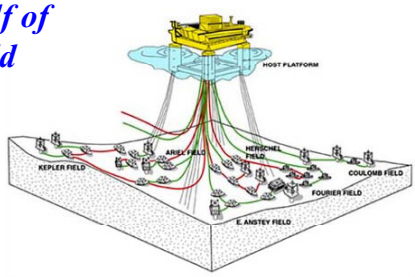

Condition	Free surface	At 500 m depth	At 750 m depth
100 year winter storm	0.46 m/s (0.9 kts)	0	0
100 year hurricane	1.75 m/s (3.4 kts)	0	0
100 year loop current ring event*	1.95 m/s (3.8 kts)	0.5 m/s (1.0 kts)	0.3 m/s (0.6 kts)

*The loop current ring extends down to about 1000 m

Internal waves

Internal waves may form if the water is stratified, i.e. contains layers with different density

We may see the internal waves on the free surface

Strait of Gibraltar. Internal waves (wavelength 2 km) Artificially colored

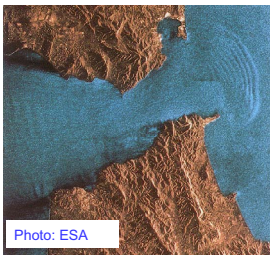

Act as a strong localized current with large loads on a typical riser or mooring system

Difficult to monitor and forecast

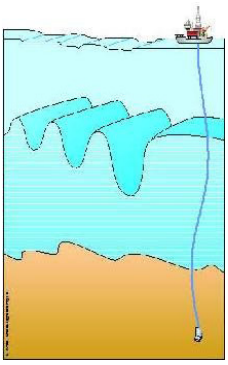

Examples of Present Challenges

- Internal waves may cause problems for marine operations
- Affect acoustic propagation in the ocean

Lufeng in the South China Sea

Internal waves are governing in design

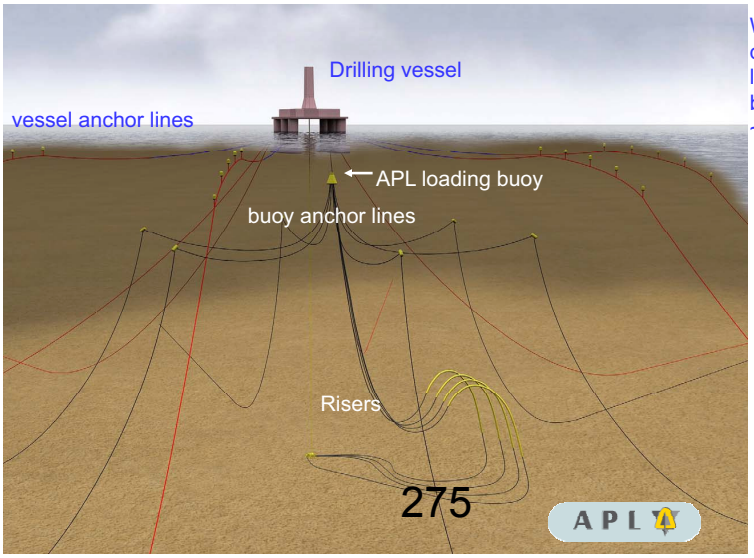

Water depth at loading buoy: ~300 m

Lufeng – Internal waves

- Characteristic time scale of internal waves in the South China Sea is 20 minutes
- Act as a static current

The typical ambient current velocity on the Lufeng field is in the order of 0.2-0.4 m/s, with maximum values up to 1.0-1.2 m/s.

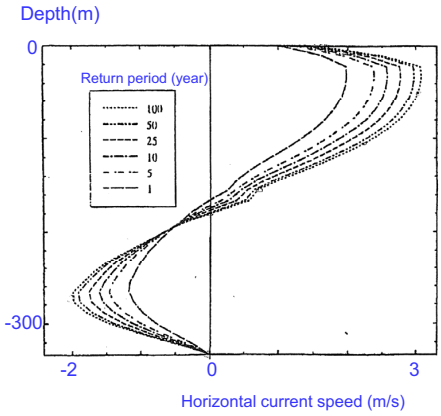

Morison's equation

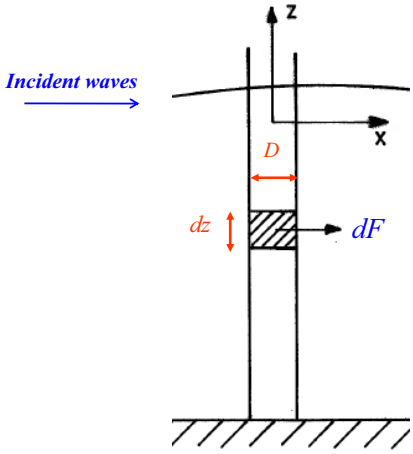

Force per unit length

- From Morison's eq. (using linear waves)
- More physical behaviour

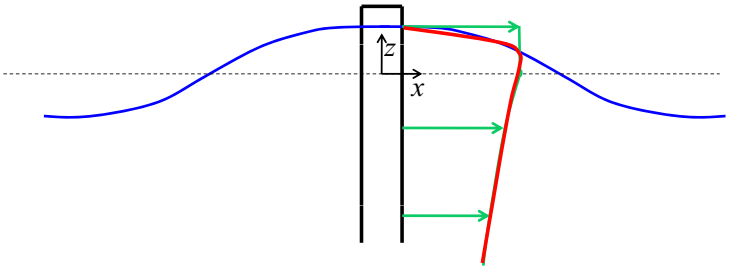

Time instants of maximum mass and drag force

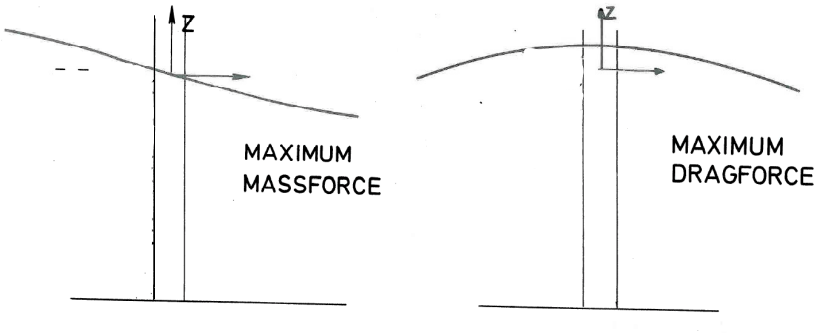

Intersection between two structural members

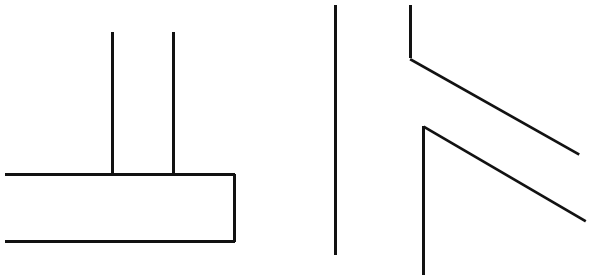

- Froude-Kriloff loads: One must integrate on the correct wetted surface
- The Froude-Kriloff force in Morison's equation can be associated with cancellations of large Froude-Kriloff pressures

Morison's equation for moving body

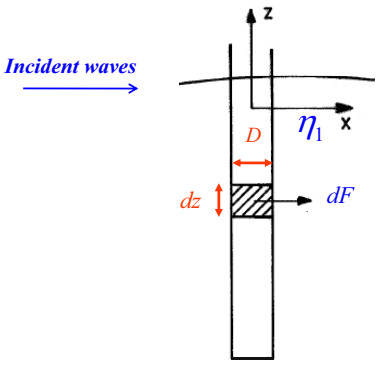

Other applications/generalizations of Morison's equation

Inclined cylinders

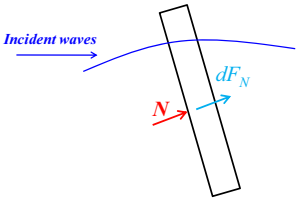

Inflow velocity & acceleration components along ***N*** are used in the Morison equation

Cylinders with axis not in the plane of wave propagation

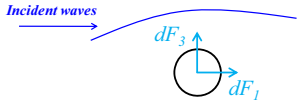

Relative current number

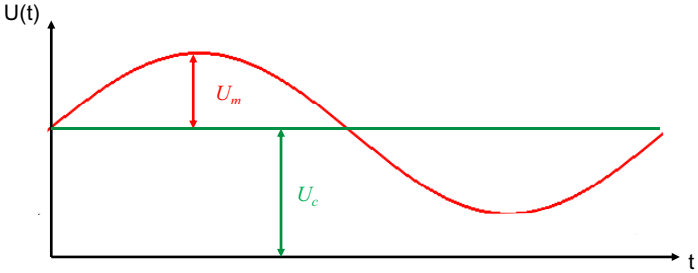

$U_c/U_m>1$

In this case, the flow will never return towards the body

⇩

Always flow separation

Flow separation around hemisphere: in current and waves

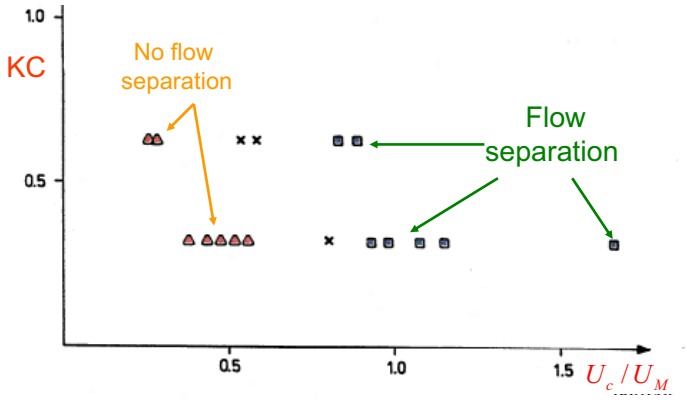

Small KC-number separated flow

Graham:

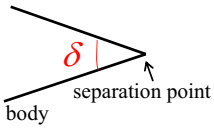

$$C_D \propto KC^{\eta}, \eta = \frac{2\delta - \pi}{3\pi - 2\delta}$$

Flat plate ↔ $\delta = 0$ ⇩ $\eta = -1/3$ ⇩ $C_D = 8.0KC^{-1/3}$

Rectangle ↔ $\delta = \pi/2$ ⇩ $\eta = 0$

Circle ↔ $\delta = \pi$ ⇩ $\eta = 1$ ⇩ $C_D = 0.2KC$ $(Subcritical, KC_{lim} < KC < 10)$

KC limit for flow separation

Drag coefficient of circular cylinder with subcritical flow: in waves

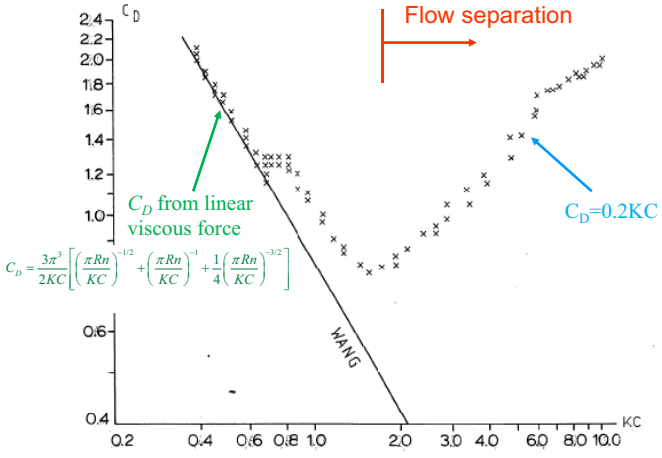

Oscillatory flow past a cylinder at high KC number

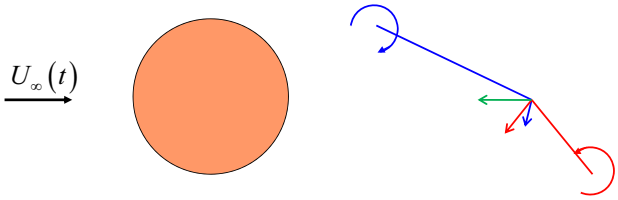

Oscillatory flow past a cylinder at high KC number

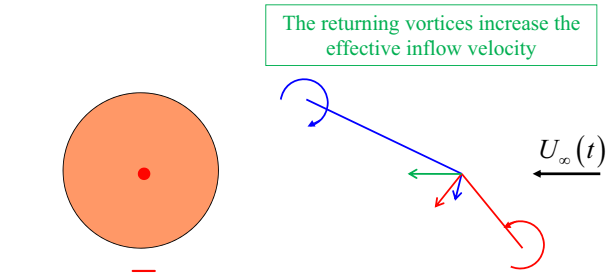

$\overline{u}$

Vortex-induced average velocity at the cylinder center

KC-dependence at high KC

Assuming discrete vortices

$$\frac{C_D}{C_D^\infty} \sim \left[\frac{\overline{u}+U_M}{U_M}\right]^2 \Downarrow = \left[1+0.58\exp\left(-0.064KC\right)\right]^2$$

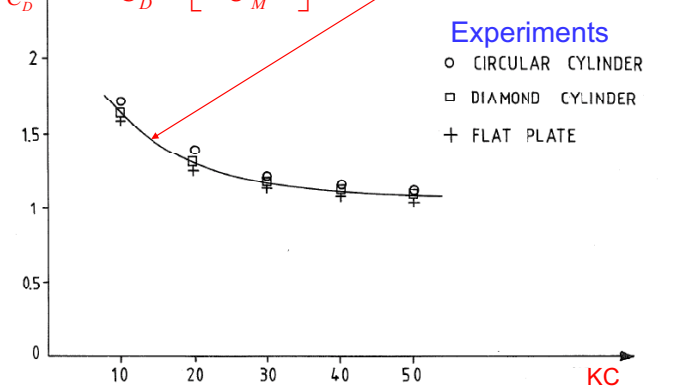

Wave and current loads on risers

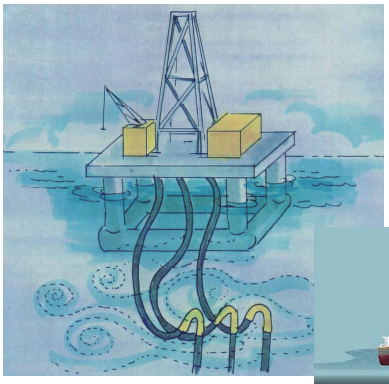

Fluid accelerations and velocities influenced by the platform

Slow-drift velocities comparable to current velocities

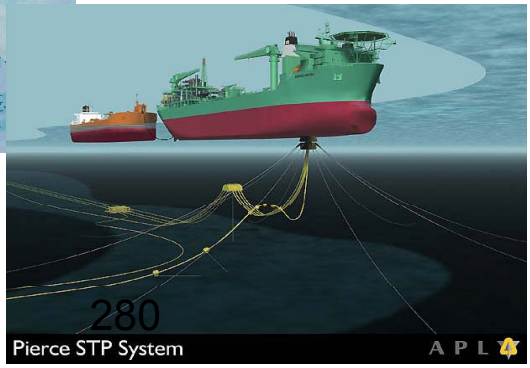

Current and waves are relevant for Marine Seismic Survey Systems

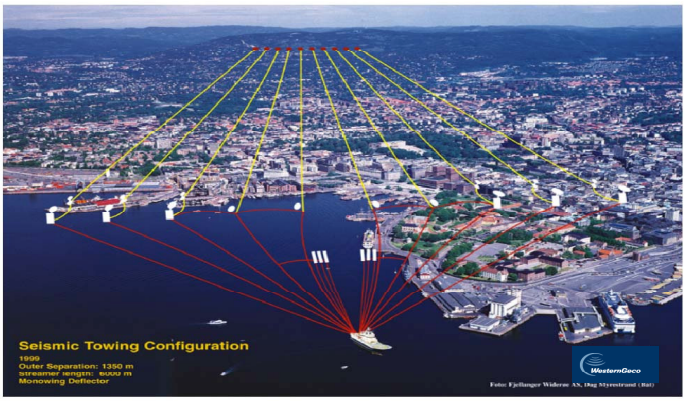

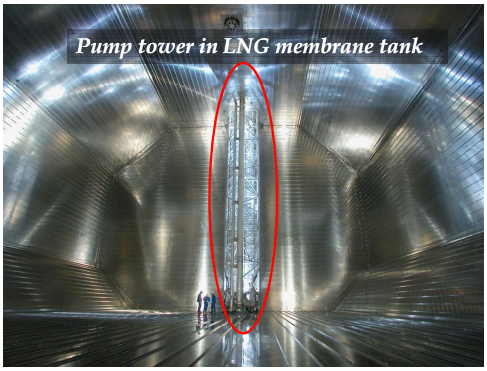

Which factors influence the C_M and C_D coefficients in Morison's equation?

1. Side wall effects
2. Interaction between structural members

Does VIV matter in the oscillatory flow of sloshing waves?

Vortex shedding frequency f_v must be in the vicinity of a structural natural frequency

Both cross-flow and in-line VIV must be considered

f_v ⇦

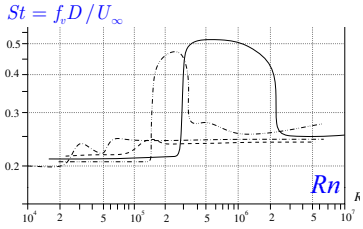

Example when waves can avoid lock-in: deep-draft floater

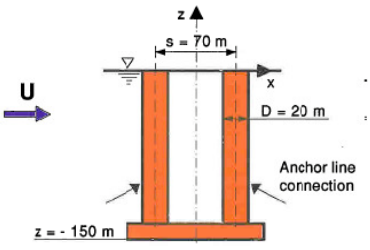

T_N (Sway) =176 sec

Hp: no incident waves

Strouhal number=0.13 for two cylinders in tandem (S/D=3.0)

⇩

T_v=154 sec when U=1 m/s

⇩

Cross-flow VIV dangerous for mooring-line safety

Long and high waves can avoid VIV because their velocities can be larger than current velocity and avoid lock-in excitation

Thrusters

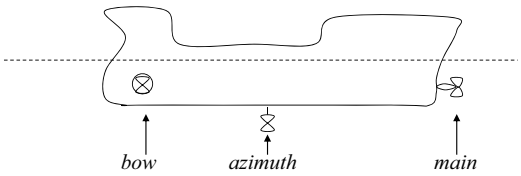

on ships

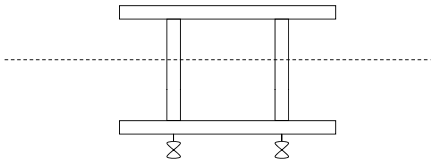

on offshore structures

Free-surface and wave effects on propeller performance

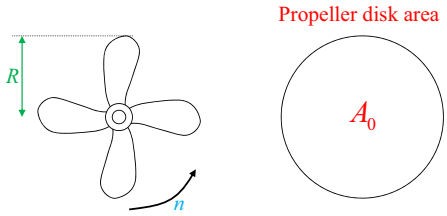

Number of propeller revolutions per second

Thrusters: slip stream as a circular jet

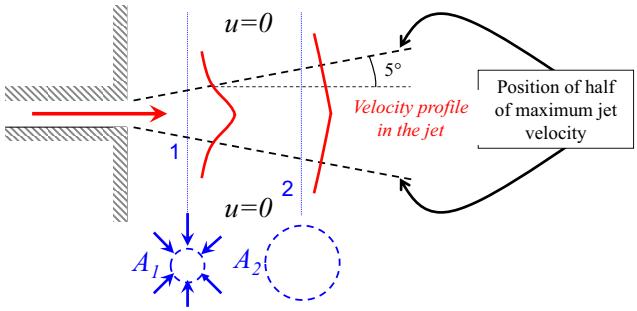

Flow toward the jet center
→ jet behaves as a sink

Thrusters: slip stream as a circular jet

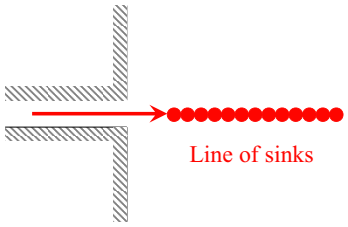

Thrusters: jet-wall interaction

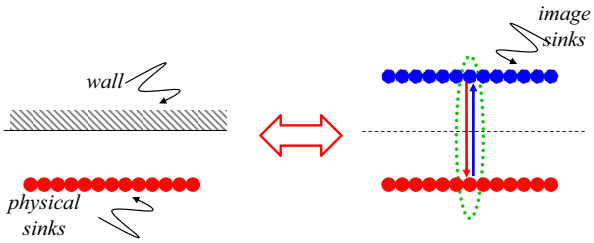

Thrusters: Coanda effect

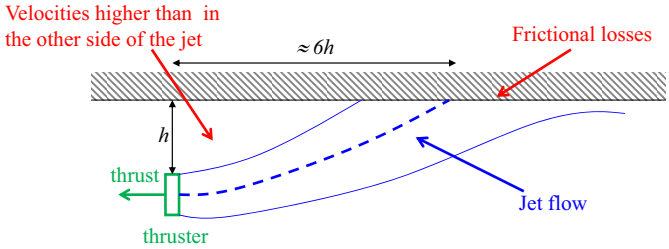

Bow Thrusters: thrust losses due to ahead current/ship speed

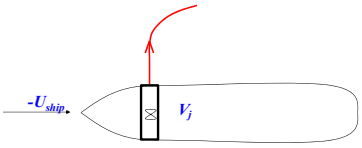

Hp: U_{ship}=1m/s, disc area A_0=3.5 m^2, thrust in still water T_{sw}= 130KN

$$T_{sw} = \rho A_0 V_j^2 \Rightarrow V_j = \sqrt{\frac{T_{sw}}{\rho A_0}} \cong 6m/s$$

$$\Rightarrow U_{ship} / V_j \cong 0.17$$

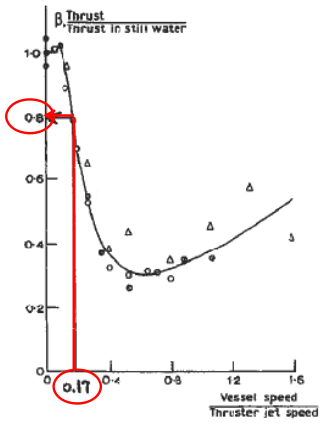

Fig. 8.11. Bow thruster performance. Effect of ahead current/vessel speed. (Chislett & Bjørheden, 1966.)

Effect of current velocity on thruster capacity

Current velocity=0.2Thruster jet velocity

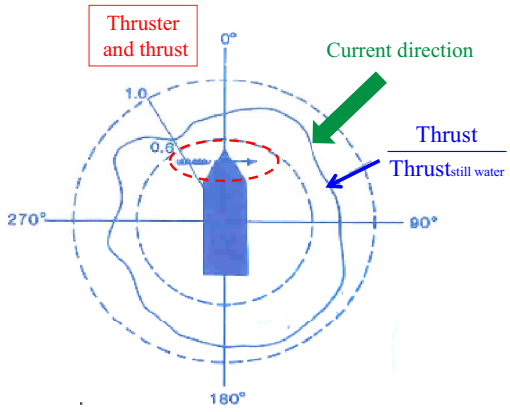

Free-surface and wave effects on propeller performance

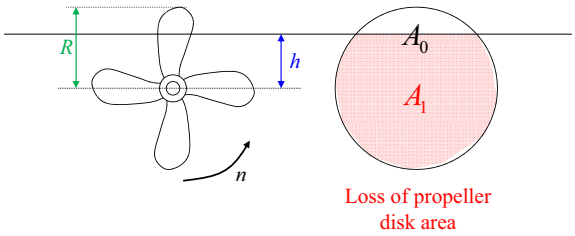

Loss of propeller disk area

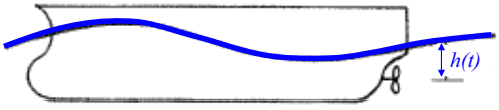

Free-surface and wave effects on propeller performance

$\beta_T = \dfrac{\text{Thrust}}{\text{Thrust}_{\text{open water}}}$

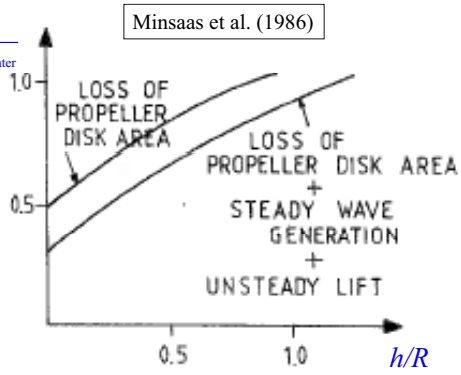

Thrusters: Thrust losses due to free-surface effects

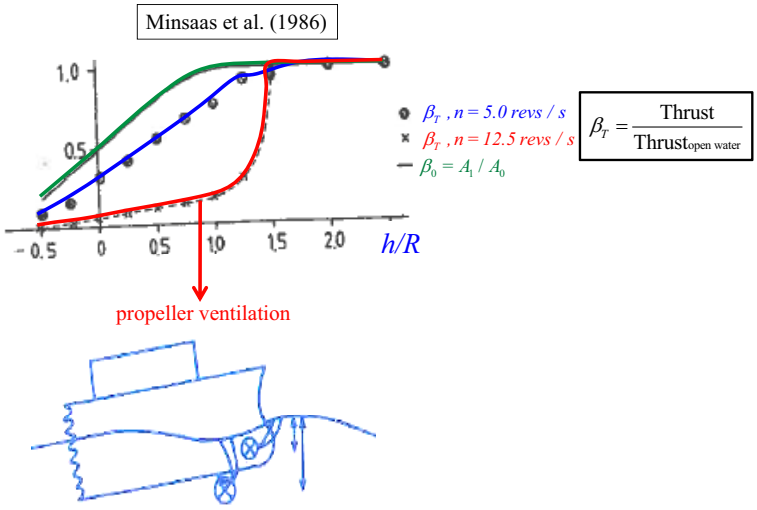

Propeller Ventilation
(Califano & Kozlowska, 2009)

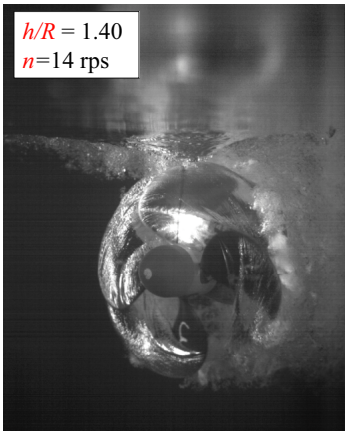

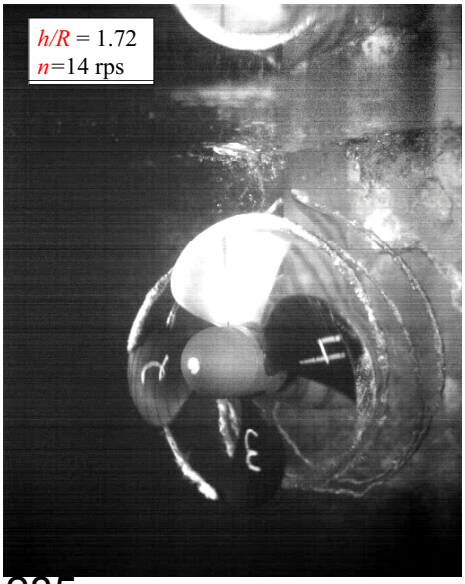

Surge equation of dynamically positioned ship

$$\left(M + A_{11}\right)\ddot{\eta}_1 + \left(B_{11} + B_{11}^{DP}\right)\dot{\eta}_1 + C_{11}^{DP}\eta_1 = F_1^{SW}(t) + F_1^{Wind}(t)$$

$$C_{11}^{DP} = \left(\frac{2\pi}{T_n}\right)^2 \left(M + A_{11}\right) \Longrightarrow \quad T_n = 100\text{s, for example}$$

$$B_{11}^{DP} = 1.2\sqrt{\left(M + A_{11}\right)C_{11}^{DP}} \Longrightarrow \quad \text{i.e. 60\% of critical damping, for example}$$

Dynamic Positioning Control Architecture

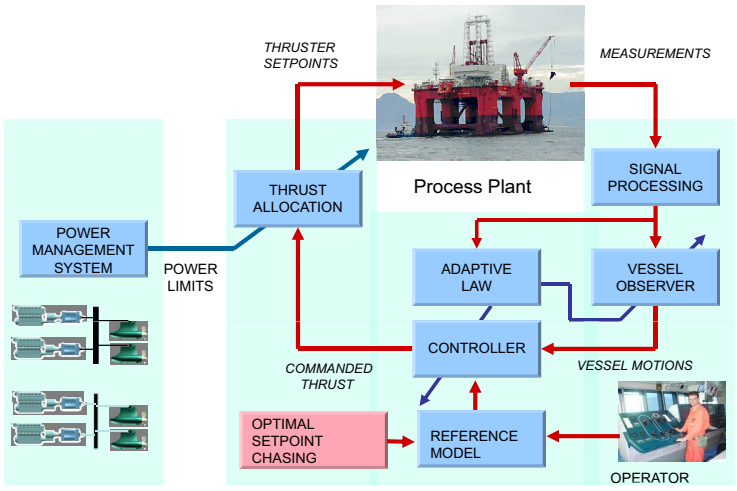

A. Sørensen

Dynamic positioning of ships and floating structures in extreme conditions

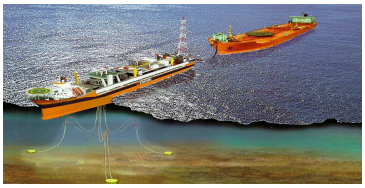

Nonlinear robust controllers for Extreme Sea Conditions

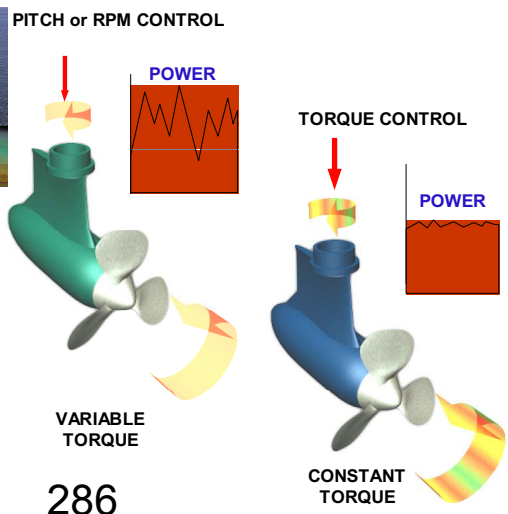

A. Sørensen

Position and motion control

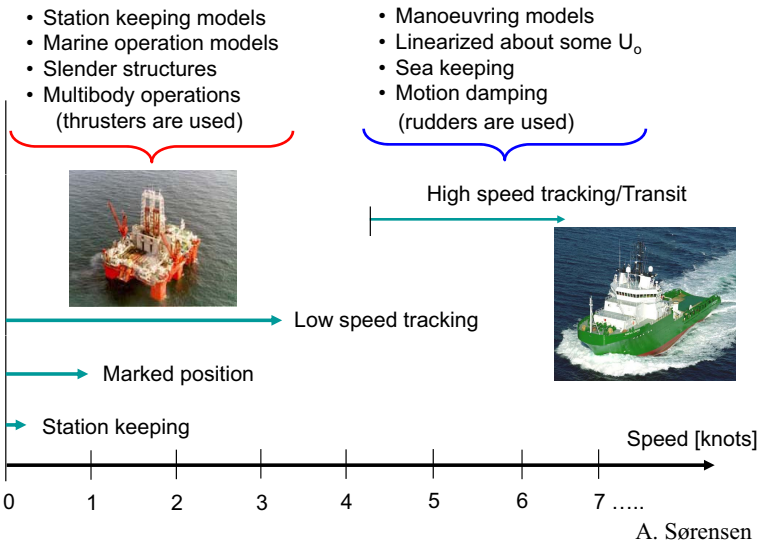

Summary

Current and wind loads. Viscous wave loads and damping. Stationkeeping.

Viscous loads

Relevant Parameters

Current & wind loads steady incident flow		Viscous wave loads oscillatory incident flow (also combined with current)
	$Rn = UD/\nu$ k/D Body form Free surface Sea floor Inflow nature & direction $U_R = U/f_n D$ $KC = U_M T/D$ Relative current n.$= U_c/U_M$	

Practical relevance: 'slender' marine structures

Risers, cables, jackets, pipelines, columns and pontoons of semisubmersibles and TLP, spar platforms, deep draft floaters, submerged bridges, ships,….

Steady uniform inflow past a blunt body

Boundary layer (BL):

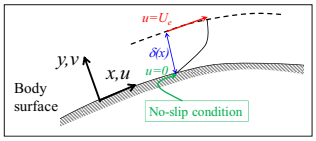

Criterion for flow separation:

- $\partial u / \partial y\big|_{y=0} = 0$
- $\partial^2 u / \partial y^2\big|_{y=0} > 0 \Rightarrow \partial p / \partial x\big|_{y=0} > 0$

Laminar vs turbulent flow:

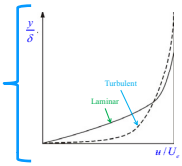

Turbulent flow leads to
- Larger fluid momentum exchange
- Larger δ
- Larger $\partial u / \partial y\big|_{y=0}$
- Spatial delay in flow separation

Flow regimes: subcritical, critical, supercritical, transcritical

Steady uniform inflow past a blunt body

Through the separation points vorticity is shed from the body in the form of vortices, i.e. wake

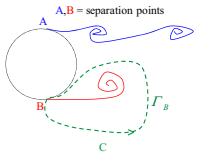

From Von Karman: only staggered vortex shedding is stable

→ Strouhal number $St = f_v D / U$

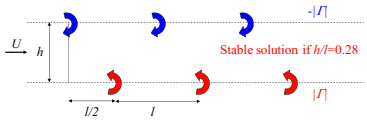

Wake interaction effects: fishes, fish farms, pipe clusters, etc.

Steady uniform inflow past a blunt body

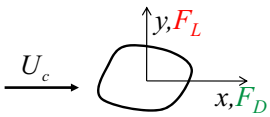

$$F_L(t) = \overline{F}_L + |F_L| \cos(2\pi f_v t + \alpha)$$
$$F_D(t) = \overline{F}_D + A_D \cos(4\pi f_v t + \beta)$$

Mean forces

Drag force $\overline{F}_D$:
- friction force (shear stresses)
- pressure force (flow separation)

Lift force $\overline{F}_L$:
Zero for a single body simmetric about inflow direction in infinite fluid, e.g. circular cylinder

Oscillatory forces

- α and β change along the 3D body
→Small correlation length
→ Cancellation effects for the total 3D loads
- They can cause resonance problems: VIM & VIV

⇩

Force coefficients to be found empirically

Mean Current loads on ships and offshore structures

To find the loads, it is usually assumed that:

- The longitudinal current component causes shear forces
→ Drag force
- The transversal current component causes flow separation
→ Transverse loads, from cross-flow principle

Ships

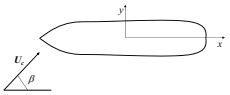

Offshore structures

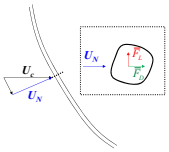

Long.: $F_1^c = f(C_f(Rn, k/D), \rho, U_c^2, S, \beta, k_f)$

Transv.: $F_2^c, F_{6a}^c = f(C_D(x), \rho, U_c^2, D(x), \beta)$

(Current causes also the Munk moment)

$\bar{F}_D = f(C_D, \rho, U_N^2, D)$

$\bar{F}_L = f(C_L, \rho, U_N^2, D)$

Parameter analysis for C_D, C_L

Vortex induced vibrations (VIV)

General features

- Resonance phenomenon caused by oscillatory forces due to vortex shedding
- Nonlinearities. Hydroelasticity.
- Relevant parameters:
  $St = f_v D / U_c \quad U_R = U_c / f_n D$

Lock-in's consequences:

- Greater correlation length
- Greater vortex strength
- f_v locks onto f_n : VIV changes f_v and in water also f_n
- The greater A the wider lock-in region
- Oscillations are self-limiting
- Greater in-line (drag force)

VIV types

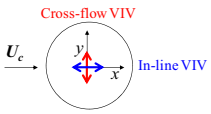

Roughly:
Cross-flow VIV: f_v close to f_n
In-line VIV: $2f_v$ close to f_n

Cross-flow VIV is associated with larger oscillation amplitudes A and larger U_R than in-line VIV. They can couple.

VIV studies

- VIV practical relevance
- How to estimate VIV (scale effects issue)
- How to suppress VIV

Galloping

- Dynamic-instability phenomenon → negative damping
- It occurs when forces are quasi-steady, i.e. oscillatory forces small (U_R>10)
- Oscillations are not self-limiting
- Relevant parameter: U_R

Oscillatory incident flow

Morison's equation

- It involves a mass and a drag force
- Applicability

Boundary layer

- Flow separation less easy than in a current
- No separation at very small KC
- Symmetric vortex shedding for KC<7
- Separated flow at small and large KC
- C_D parameter analysis

Wave and current environment

- Examples of when they are relevant
- VIV can be caused

Stationkeeping

- For position and motion control of ships and offshore structures
- Aimed to counteract mean wave-current-wind loads
- Provides damping and leads to restoring in the horizontal plane

Mooring systems (static positioning)

- Easier to realize

vs

Thrusters (dynamic positioning)

- More flexibles
- Provide larger damping

Parameter analysis of performances
How does a DP work